P-08-96

Oskarshamn site investigation

Confirmatory hydraulic interference test and tracer test in Laxemar

Anna Lindquist, Calle Hjerne, Rune Nordqvist,
Jan-Erik Ludvigson, Johan Harrström, Seje Carlsten
Geosigma AB

December 2008

Svensk Kärnbränslehantering AB
Swedish Nuclear Fuel
and Waste Management Co

Box 250, SE-101 24 Stockholm
Phone +46 8 459 84 00

ISSN 1651-4416
SKB P-08-96

Oskarshamn site investigation

Confirmatory hydraulic interference test and tracer test in Laxemar

Anna Lindquist, Calle Hjerne, Rune Nordqvist,
Jan-Erik Ludvigson, Johan Harrström, Seje Carlsten
Geosigma AB

December 2008

Keywords: KLX15A, HLX27, Tracer test, Dilution test, Sorption, Pumping test, Hydraulic interference test, Transport parameters, Hydrogeological model, AP PS 400-08-007.

Abstract

A cross-hole tracer test has been conducted between a packed-off section in KLX15A (260.0–272.0 metres borehole length (mbl)) and borehole HLX27 within the Oskarshamn site investigation. The straight-line distance between the two boreholes is c. 140 m. In combination with the tracer test a hydraulic interference test was carried out by measuring the pressure responses in several boreholes surrounding the pumping borehole HLX27. The aims of the tests were to verify transport parameters previously obtained using other methods and to, at least partly, verify the hydrogeological model of the Oskarshamn investigation area.

The main tracer test was preceded by a pre-test using only a non-sorbing tracer (Rhodamine WT). In the main tracer test, the non-sorbing tracers Uranine and Tb-DTPA and three sorbing tracers, lithium (Li^+), cesium (Cs^+) and rubidium (Rb^+), were injected simultaneously. The tracer tests were performed as weak dipoles, i.e. tracer was injected with a small excess pressure. Both tests were evaluated with two different transport models (advection–dispersion, AD, and advection–dispersion with matrix diffusion, AD-MD). Transport parameters were also evaluated.

No breakthrough was detected for Rb^+ or Cs^+ in HLX27. Tb-DTPA and Li^+ displayed high recoveries (c. 80%) despite that the concentration in the pumping borehole were significantly above background at the end of the test.

The AD model was considered to provide the most reliable and robust results with a mean residence time of 560 h and Peclet number of 3 for Tb-DTPA. The estimation of retardation factor for Li^+ was consistent around 1.1 in simulations with both the AD model and the AD-MD model. Since no breakthrough was detected for Rb^+ or Cs^+, only a minimum retardation factor could be estimated for the two elements. It was estimated to be higher than 20 based on simulations with the AD model and the results from Tb-DTPA. The mass balance aperture was evaluated to be about $4 \cdot 10^{-2}$ m.

Hydraulic responses to pumping were detected in 32 out of 75 observation sections. In 25 of these sections, clear responses were observed and also used for transient evaluation. The transmissivity of the pumping section in HLX27 was estimated to $3 \cdot 10^{-5}$ m^2/s. The responses from the hydraulic interference test were fairly evenly spread around the pumping hole with no clear directional preference.

The interpretation of the hydraulic interference test indicates that the zone ZSMNE942A enhances hydraulic pressure responses while ZSMNW042A do not. Furthermore, an interpretation of ZSMNS059A as a hydraulic boundary may have some support from the interference test results. However, the conclusions of the zone characteristics are rather uncertain and not unambiguous.

Sammanfattning

Ett spårförsök har utförts från den isolerade sektionen i KLX15A (260,0–272,0 mbl) till borrhålet HLX27 inom platsundersökningen i Oskarshamn. Avståndet mellan de både borrhålen är 140 m. Kombinerat med detta genomfördes ett interferenstest genom att tryckresponser registrerades i ett stort antal borrhål omkring pumphålet HLX27. Syftet med försöket var dels att verifiera transportparametrar som tidigare uppmätts på annat sätt samt att partiellt verifiera den hydrogeologiska modellen över Oskarshamns undersökningsområde.

Spårförsöket utfördes dels i form av ett förförsök med ett icke sorberande spårämne (Rhodamine WT), dels som ett huvudförsök där de icke sorberande spårämnena Uranin och Tb-DTPA injicerades samtidigt som med litium (Li^+), cesium (Cs^+) och rubidium (Rb^+), vilka är sorberande av olika grad. Spårförsöken genomfördes som svaga dipoler, dvs spårämnet injicerades med ett litet övertryck. Båda försöken utvärderades genom anpassning av två transportmodeller (advektion-dispersion, AD, och advektion-dispersion med matrisdiffusion, AD-MD) till uppmätta data. Dessutom beräknades transportparametrar.

Inget genombrott av Rb^+ eller Cs^+ kunde konstateras i HLX27. Tb-DTPA och Li^+ i huvudförsöket visade på hög återfångst (cirka 80%) trots att koncentrationen i pumphålet var betydligt över bakgrunden vid försökets avslutande.

AD-modellen ansågs ge mest tillförlitliga och robusta resultat vid utvärderingen med en uppehållstid av 560 h och peclet-tal av 3 för TB-DTPA. Retardationsfaktorn för Li^+ var cirka 1,1 i simuleringar med både AD-modellen och AD-MD-modellen. Eftersom inget genombrott kunde konstateras för Rb^+ eller Cs^+ var det endast möjligt att göra en minimi-uppskattning av retardationsfaktorn för dessa ämnen. Den uppskattades till att vara mer än 20 baserad på simuleringar med AD-modellen och resultat från TB-DTPA. Massbalansaperturen bestämdes till $4 \cdot 10^{-2}$ m.

Tryckresponser på pumpningen kunde ses i 32 av totalt 75 tryckregistrerade sektioner. 25 av dessa sektioner visade tydliga responser och utvärderades också transient. Transmissiviteten för den pumpade sektionen i HLX27 bestämdes till $3 \cdot 10^{-5}$ m^2/s. Responserna i interferenstestet var fördelade relativt jämnt geografisk runt pumphålet utan någon tydlig förskjutning åt någon riktning.

Tolkningen av interferenstestet visade på att ZSMNE942A underlättar tryckresponser medan inga sådana tecken fanns för ZSMNW042A. Vidare så stöder interferenstestet en tolkning av ZSMNS059A som en hydraulisk gräns. Dock, slutsatserna om zonernas egenskaper utifrån interferenstestet är osäkra och inte entydiga.

Contents

1	**Introduction**	9
2	**Objectives and scope**	13
2.1	Borehole data	13
2.1.1	Injection and withdrawal boreholes	13
2.1.2	Interference test boreholes	15
2.2	Tests performed	15
2.2.1	Interference tests	15
3	**Equipment**	19
3.1	General	19
3.2	Groundwater flow measurements	20
3.3	Tracer tests	21
3.3.1	Pre test and rinsing after tracer injections	22
3.3.2	Main tracer test	23
3.3.3	Tracers used	25
3.4	Pumping and interference test	26
3.5	Interpretation tools	26
3.5.1	Hydraulic evaluation	26
3.5.2	Transport models	26
3.5.3	Parameter estimation method	28
3.5.4	Handling of tracer injection data	29
3.5.5	Other derived transport parameters	29
4	**Execution**	31
4.1	General	31
4.2	Scoping calculations	31
4.2.1	Injection method	31
4.2.2	Pumping flow rate	31
4.2.3	Tracers	33
4.3	Preparations	35
4.3.1	Calibration and functionality checks	36
4.4	Execution of field work	36
4.4.1	Groundwater flow measurements	37
4.4.2	Pumping and interference test	37
4.4.3	Tracer tests	38
4.4.4	Water sampling	39
4.5	Data handling	39
4.6	Analysis and interpretation	39
4.6.1	Groundwater flow measurements	39
4.6.2	Pumping and interference test	40
4.6.3	Tracer test	41
4.7	Nonconformities	43
5	**Results**	45
5.1	Nomenclature and symbols	45
5.2	Groundwater flow measurements	45
5.3	Interference test in HLX27	47
5.3.1	General	47
5.3.2	Summary of the results of the interference test in HLX27	51
5.3.3	Response analysis and estimation of the hydraulic diffusivity	55
5.4	Water sampling	60
5.5	Tracer tests – general	60
5.6	Tracer breakthrough	63
5.6.1	Pre-test	63
5.6.2	Main tracer test	63
5.6.3	Tube sampling at two levels in HLX27	66

5.7 Model results and evaluated parameters 68
5.7.1 Pre-test 68
5.7.2 Main test 70
5.7.3 Transport parameters 80

6 Summary and discussion 81
6.1 Equipment and procedures 81
6.2 Errors and uncertainities 81
6.2.1 Outliers 81
6.2.2 Analyses or metals (Tb, Li, Cs, Rb) 81
6.2.3 Analyses of Uranine 82
6.3 Tracer test – general 82
6.3.1 Tube sampling 82
6.4 Model simulations 83
6.5 Transport parameters 84
6.5.1 Fracture minerals and geology 84
6.6 Comparision of results with scoping calculations 85
6.6.1 Comparision of pre-test with scoping calculations 85
6.6.2 Adjusted scoping calculations after the pre-test 86
6.6.3 Comparision of main test with predictions 86
6.7 Geohydraulic conditions 87
6.7.1 Comparision of different hydraulic tests 87
6.7.2 Flow regimes 88
6.7.3 The hydrogeological model 88

7 References 95

Appendix 1 Technical data of boreholes KLX15A and HLX27 99

Appendix 2 Borehole data for interference test boreholes 101

Appendix 3 Chemical composition of groundwater, tracer solution and sub flow of salt 105

Appendix 4 Calculation of normalised mass flux 107

Appendix 5 Transient evaluation of responses in the boreholes 109

Appendix 6 Test diagrams 147

Appendix 7 Correction of head and drawdown for natural decreasing trend 217

Appendix 8 Chemical composition of groundwater from HLX27. Samples taken during the tracer test 221

Appendix 9 Injection functions and breakthrough curves 223

1 Introduction

This document reports the results from the combined interference test and tracer test in the southern part of the Laxemar subarea. The test is one of the activities performed within the site investigation at Oskarshamn. One of the permanently installed sections in KLX15A (260.0–272.0 mbl) was used as injection section and pumping was conducted in HLX27. A map of the site investigation area in Oskarshamn is presented in Figure 1-1. The work was carried out in accordance with activity plan AP PS 400-08-007. In Table 1-1 the controlling documents for performing this activity are listed. The activity plan and the method descriptions are SKB's internal controlling documents. The obtained data from the activity are reported to the database Sicada, where they are traceable by the activity plan number.

The field work was performed during 15 weeks from March to July 2008. The field work involved groundwater flow measurements in KLX15A using the dilution method, pumping in HLX27 together with pressure registration in surrounding boreholes, a pre-test (tracer test) and the main tracer test.

Figure 1-1. *Map showing KLX15A and HLX27 in the southern part of the Laxemar subarea within the Oskarshamn Site investigation. The map also shows the hydrological observation point (PSM000364) in the small river "Laxemarån" where flow and electric conductivity were measured on-line and water samples were taken throughout the pumping period.*

Table 1-1. Controlling documents for performance of the activity.

Activity plan	Number	Version
Spårförsök med sorberande spårämnen mellan KLX15A och HLX27.	AP PS 400-08-007.	1.0
Method descriptions	**Number**	**Version**
Metodbeskrivning för flerhålsspårförsök.	SKB MD 530.006	1.0
Metodinstruktion för analys av injektions- och enhålspumptester.	SKB MD 320.004	1.0
Metodbeskrivning för interferenstester	**SKB MD 330.003**	**1.0**
System för hydrologisk och meterologisk datainsamling.	SKB MD 368.010	1.0
Vattenprovtagning och utspädningsmätning i observationshål.		

Pumping was conducted in the open borehole HLX27. A number of other boreholes as well as monitoring wells in soil surrounding the pumped borehole served as observation points and the pressure were monitored using HMS (Hydro Monitoring System) or miniTroll loggers. After about 4 weeks of pumping, the main tracer test begun by injecting five different tracers (Uranine, Tb-DTPA, lithium, cesium and rubidium) in a packed-off section (260.0.0–272.0 mbl) of borehole KLX15A, which is located near HLX27. The tracers were injected with a small excess pressure creating a weak dipole. The water in the section in KLX15A was circulated for mixing and samples were collected regularly to monitor the tracer injection concentrations. Water samples from HLX27 were also taken and analysed for tracer breakthrough. A schematic view of the layout of the tracer test is shown in Figure 3-5.

The pumped water was discharged into the stream “Laxemarån” at a point c. 100 m south of HLX27. Regulation and limits were set by County Administrative Board regarding tracer concentration and conductivity in the water discharged to the stream at the hydrological station (PSM000364), see Figure 1-1. The conductivity of the pumped water and in “Laxemarån” at the outlet point was also monitored during the test. When the flow rate in “Laxemarån” became too low the pumped water was instead infiltrated near KLX03, c. 600 m from HLX27.

KLX15A is a telescopic core-drilled borehole and HLX27 is a percussion-drilled borehole drilled for the site investigation in the Oskarshamn area. The cleaning procedures of the equipment in the boreholes were performed according to level 1 in the cleaning instructions in MD 600.004 (Instruktion för rengöring av borrhålsutrustning och viss markbaserad utrustning).

Several other tests have previously been performed in KLX15A, such as single-hole injection tests /Enaschescu et al. 2007a/, geophysical borehole logging /Nielsen and Ringgaard 2007/ and RAMAC, BIPS and deviation logging /Gustafsson and Gustafsson 2007/. Section KLX15A:6 (260.0.0–272.0 mbl), which is the tracer injection section, is included in the monitoring program where groundwater flow measurements and water sampling are regularly carried out.

Borehole HLX27 has also been investigated previously including, for example, flow logging /Rohs et al. 2007/, geophysical borehole logging /Nielsen et al. 2004/ and RAMAC, BIPS and deviation logging /Gustafsson and Gustafsson 2004/.

In HLX27 a deformation zone is interpreted at 156–164.7 mbl (metre borehole length) associated with a flow anomaly around 158 mbl /Hermanson et al. 2008/. The deformation zone NW042A (visible in Figure 1-2) is located near the pumping borehole HLX27, but HLX27 is not interpreted to intersect with the zone /Wahlgren et al. 2008/. However, HLX27 and some other percussion-drilled boreholes (HLX15, HLX28, HLX26 and HLX32) are interpreted to be associated with the zone NW042A /Wahlgren et al. 2008/. This interpretation is supported by a pattern of red staining. This pattern of red staining is consistent with the pattern associated with ZSMEW007A, i.e. a broad belt of oxidation (red staining) that contains a number of sub-parallel structures that together form a complex zone /Wahlgren et al. 2008/.

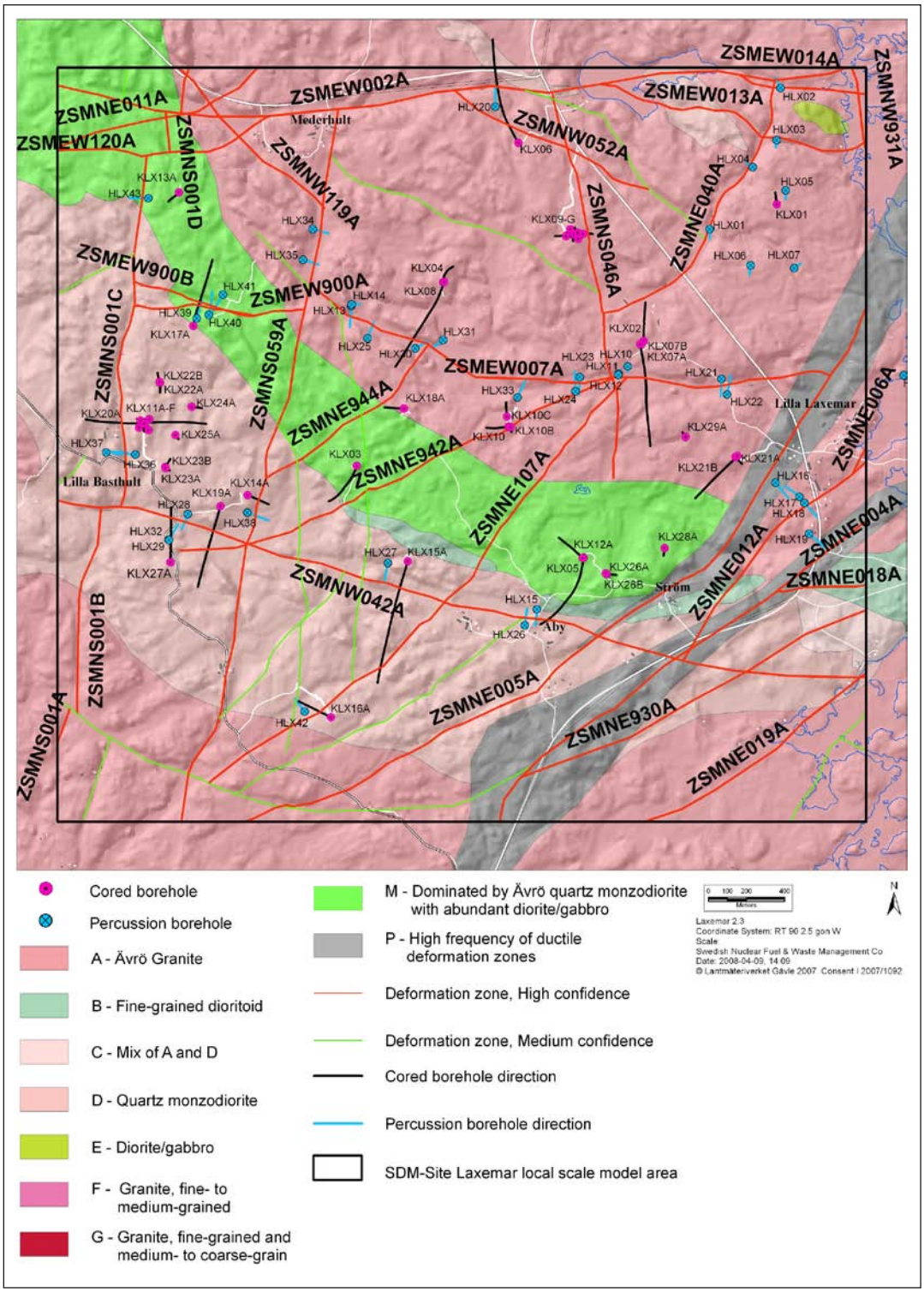

Figure 1-2. *An overview of the deformation zones and rock domains modelled deterministically in the Laxemar local model area /Wahlgren et al. 2008/.*

The interval 262.35–265.79 mbl in section KLX15A:6 (260–272 mbl) is interpreted as an uncertain brittle deformation zone. An interval (629.1–634.94 mbl) of the other circulation section (where ground water flow measurements were conducted), KLX15A:3 (623–640 mbl) is interpreted as a certain brittle deformation zone /Hermanson et al. 2008/.

In the vicinity of the tracer test location there is a high-confidence zone called NW042A, striking in the NW-SE direction through the southern part of the Laxemar area.. This zone is moderately southward dipping (55°), about 40 m thick and 10.8 km long. It has a dominantly brittle character although ductile precursors are present /Wahlgren et al. 2008/. NW042 is included in a group of E-W and NW-SE steep to moderately southward dipping deformation zones. The largest deformation zone in this group is ZSMEW002A (Mederhult zone) which is more or less parallel with the northern boundary of the local model area. All of the main deformation zones that have been investigated by drilling show an original ductile fabric that has been very heavily overprinted by brittle reactivation. Alteration, dominated by red staining, is also common in this group of deformation zones /Wahlgren et al. 2008/.

The zone NW042 is intersected by only two core-drilled boreholes, KLX27 and KLX15A. KLX27A was drilled at a late stage with the aim of further investigating the orientation and character of the zone and is interpreted to make a clear intercept with the zone between borehole length 210–250 mbl /Wahlgren et al. 2008/. KLX15A is interpreted to intersect with this zone but not penetrating the full width of the zone and is interpreted as ending within in the zone /Wahlgren et al. 2008/.

The model area and the modelled deformation zones together with the boreholes in the area are shown in Figure 1-2.

2 Objectives and scope

The objectives of the combined interference test and tracer test were to partially verify the hydrogeological model of the Oskarshamn candidate area and to verify transport characteristics that previously have been determined through laboratory tests of drill cores and other investigations. The activity also gives an opportunity to directly compare transport parameters acquired from single-hole tracer tests (SWIW-tests) that have been performed earlier in the Laxemar area.

During the pumping, the withdrawal rate (constant flow rate) and the pressure response in HLX27 were registered. Pressure responses to the pumping in surrounding boreholes were monitored using HMS (Hydro Monitoring System). Tracers were injected into a permanently installed section in KLX15A (260.0–272.0 mbl) and the pumped water from HLX27 was analysed for tracer breakthrough. Water samples from KLX15A were also collected and analysed in order to monitor the tracer concentration in the injection section. The experimental data were used to estimate transport parameters.

Prior to the tracer test, groundwater flow measurements were conducted in two sections in KLX15A (the planned injection section KLX15A:6 and also KLX15A:3). The measurements were started about a week before the pumping in HLX27 begun and continued during five days of pumping. This was done in order to investigate the effect on groundwater flow from the pumping.

The activity can be divided into two main parts; one part concerns the hydraulic parameters and the hydrogeological model (the pumping test and the interference test) and the second part concerns the transport characteristics (the tracer test). One of the aims is to combine the evaluation of these two parts as well as results from previous investigations in the area to make a combined interpretation.

2.1 Borehole data

The reference point of the boreholes is always top of casing (ToC). The Swedish National coordinate system (RT90 2.5 gon V 0:-15) is used in the x-y-plane together with RHB70 in the z-direction. Northing and Easting refer to the top of the boreholes at top of casing. All section positions are given as length along the borehole (not vertical distance from ToC).

2.1.1 Injection and withdrawal boreholes

Technical data for the injection borehole KLX15A and the withdrawal borehole HLX27 are given in Table 2-1. In Table 2-2, some data for the borehole sections in KLX15A involved in the tests and for HLX27 are presented. Technical data for boreholes KLX15A and HLX27 are also presented in Appendix 1.

According to flow logging in HLX27 /Rohs et al. 2007/ there are three inflows in the borehole located at 104.0–105.5 mbl, 157.5–158 mbl and at 158.0–159.0 mbl. The transmissivity of these inflows are $1.7 \cdot 10^{-5}$ m^2/s, $2.2 \cdot 10^{-5}$ m^2/s and $1.6 \cdot 10^{-5}$ m^2/s, respectively. In this report these anomalies are regarded as two dominating anomalies, one at 158 mbl (157.5–159.0 mbl) and one at 105 mbl (104.0–105.5 mbl).

Table 2-1. Selected technical data for boreholes KLX15A and HLX27 (from Sicada).

Borehole ID	Elevation of top of casing (ToC) (m.a.s.l.)	Borehole length from ToC (mbl)	Bh-diam. (below casing) (m)	Inclin.-top of bh (from horizontal plane) (º)	Dip-Direction-top of bh (º)	Northing (m)	Easting (m)
KLX15A	14.59	1,000.43	0.076	–54.42	198.83	6365614.17	1547987.47
HLX27	8.25	164.7	0.137	–59.41	191.00	6365605.07	1547882.69

Table 2-2. Data on section volumes and transmissivity (T) for the tested borehole sections in KLX15A and borehole HLX27.

Bh ID	Secup (mbl)	Seclow (mbl)	Section length (m)	Section volume (ml)	T_T (transient eval.) (m^2/s)	T (PFL) (m^2/s)
KLX15A:3	623.0	640.0	17	57,606.[1)]	$7.0\ 10^{-7}$ [2)]	$9.1\ 10^{-7}$ [3)]
KLX15A:6	260.0	272	12	29,384 [1)]	$1.1\ 10^{-5}$ [2)]	$3.7\ 10^{-6}$ [3)]
HLX27	6.03	164.7	–	–	$2.7\ 10^{-5}$ [4)] $5.0\ 10^{-5}$ [5)]	–

[1)] Including hoses and circulation equipment used in this test.

[2)] From PSS measurement (summation of T_T measured in 20 m sections (KLX15A:6) and in 5 m sections (KLX15A:3) within the interval) /Enachescu et al. 2007a/.

[3)] From PFL measurement (summation of T_f from detected fractures within the interval) /Pöllänen et al. 2007/.

[4)] From pumping test, transient evaluation (this report).

[5)] From HTHB measurement (transient evaluation of pumping test) /Rohs et al. 2007/.

The distance between KLX15A and HLX27 is c. 105 m at the ground surface level and c. 140 m between the midpoint of the tracer injection section (borehole length 266 mbl) and borehole length 131.5 mbl in HLX27 (which is between the dominating flow anomalies (158 mbl and 105 mbl) in the pumping borehole.

The transmissivity distribution according to PFL measurements in the interval used for tracer injection in KLX15A, given in Figure 2-1, indicate seven flowing fractures /Pöllänen et al. 2007/.

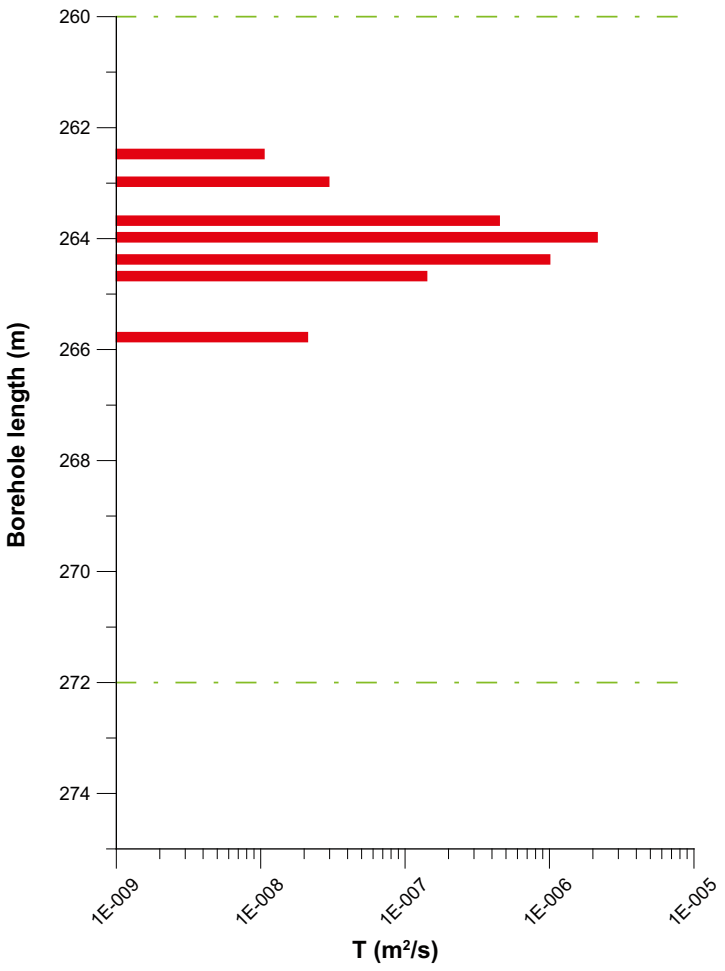

Figure 2-1. *Transmissivity distribution in the injection section KLX15A:6 (260–272 mbl). The dashed green lines represent the section limits. Data from difference flow logging /Pöllänen et al. 2007/.*

2.1.2 Interference test boreholes

The pressure responses caused by the pumping in HLX27 were measured in about 30 core drilled and 40 percussion drilled boreholes in the Laxemar area. In addition, a number of soil wells were measured. Boreholes within a radius of about 1 km from the pumping borehole HLX27 were monitored with higher sampling frequency. Technical data and coordinates of the boreholes are presented in Appendix 2.

In this report borehole responses are presented in alphabetic and numeric order, i.e. the percussion-drilled boreholes (HLX-boreholes) are presented first and then the core drilled-boreholes (KLX-boreholes); within each group boreholes are listed according to increasing borehole numbers

2.2 Tests performed

The tests performed within this activity comprise groundwater flow measurements (natural and stressed conditions), a preliminary tracer test (only with a non-sorbing tracer), and a main tracer test (with both sorbing and non-sorbing tracers) combined with a hydraulic interference test, see Table 2-3. The boreholes and sections involved in the interference test and the tests performed within this sub-activity are presented in Section 2.2.1.

2.2.1 Interference tests

The start and stop of pumping occurred on March 26 at 10:31 and June 26 at 10:05, respectively. The overall data acquisition was continued until August 6 in the pumping borehole. The data acquisition in the observation boreholes runs continuously, but for evaluation of the interference test only data until August 10 was included.

All borehole sections involved in the interference test in HLX27 are listed in Table A2-1 in Appendix 2 together with the start and stop times of the pumping and distances from the pumping section. The data extracted from HMS (Hydro Monitoring System) for the observation boreholes was selected to obtain sufficient data as well as adequate information about the hydraulic conditions prior to and after the interference test.

The test performance was according to the SKB internal documents presented in Table 1-1. However, no response matrix was prepared since only one major interference test was performed.

Interpreted points of application (mid-point of sections), length of sections, distances from the pumping borehole HLX27 as well as the estimated transmissivity range of the observation sections, based on previous single-hole tests, are presented in Table 2-4. The distances are calculated between the points of application in the pumping borehole and in the observation borehole sections. The point of application in the pumping borehole is selected as the midpoint between the two dominating flow anomalies, i.e. at 131.5 mbl.

Table 2-3. Tests performed within the activity.

Test	Borehole	Secup (mbl)	Seclow (mbl)	Start date and time	Stop date and time
Gw flow measurement (natural gradient)	KLX15A:3	623.0	640.0	2008-03-18 18:08	2008-03-26 10:31
Gw flow measurement (natural gradient)	KLX15A:6	260.0	272.0	2008-03-19 15:10	2008-03-26 10:31
Gw flow measurement (stressed gradient)	KLX15A:3	623.0	640.0	2008-03-26 10:31	2008-04-01 08:12
Gw flow measurement (stressed gradient)	KLX15A:6	260.0	272.0	2008-03-26 10:31	2008-04-01 08:15
Pre tracer test	KLX15A:6-HLX27			2008-04-02 11:45	2008-06-26 10:05
Main tracer test	KLX15A:6-HLX27			2008-04-23 09:10	2008-06-26 10:05
Pumping test	HLX27			2008-03-26 10:31	2008-06-26 10:05
Interference test [1)]	HLX27 (pumping borehole)			2007-03-26 10:31	2008-06-26 10:05

[1)] The interference test is presented separately in Section 2.2.1.

Table 2-4. Points of application, lengths of sections together with the distances from the pumping borehole HLX27 and the estimated transmissivities for the observation sections from previous investigations.

Bh ID	Test section (mbl)	Point of application (mbl below TOC)	Section length (m)	Distance to HLX27:131.5 (m)	Transmissivity from single-hole tests (m^2/s)
HLX15	12.04–151.90	81.97	139.9	822.0	2.5E–7 [1)]
HLX26	11.00–151.20	81.1	140.2	768.5	1.5E–7 [1)]
HLX38	15.02–199.50	107.3	184.5	738.2	1.2E–4 [2)]
HLX42:1	30.00–152.60	91.3	122.6	805.0	4.3E–5 [3)]
HLX42:2	9.10–29.00	19.05	19.9	822.9	
KLX03:1	965.50–971.50	968.5	6.0	958.2	4.5E–7–4.6E–7 [4)]
KLX03:2	830.50–964.50	897.5	134.0	898.8	below l.m.l. of PFL
KLX03:3	752.50–829.50	791	77.0	814.8	6.0E–7–1.2E–6 [4)]
KLX03:4	729.50–751.50	740.5	22.0	777.6	4.6–5.9E–6 [4)]
KLX03:5	652.50–728.50	690.5	76.0	742.9	2.5–4.9E–7 [4)]
KLX03:6	465.50–651.50	558.5	186.0	663.9	9.7E–9–1.3E–8 [4)]
KLX03:7	349.50–464.50	407	115.0	596.4	2.9E–7–1.6E–6 [4)]
KLX03:8	199.50–348.50	279	159.0	566.4	2.0–2.8E–6 [4)]
KLX03:9	193.50–198.50	196	5.0	564.8	9.2E–6–1.3E–5 [4)]
KLX03:10	100.05–192.50	146.3	92.5	570.1	3.0E–7–4.5E–7 [4)]
KLX05:1	721.00–1,000.00	860.5	279.0	1,107.8	6.2E–9–2.2E–8 [5)]
KLX05:2	634.00–720.00	677	86.0	1,057.9	1.0E–8–1.6E–8 [5)]
KLX05:3	625.00–633.00	629	8.0	1,047.7	5.6E–9–1.2E–8 [5)]
KLX05:4	501.00–624.00	562.5	123.0	1,036.7	below l.m.l. of PFL
KLX05:5	361.00–500.00	430.5	139.0	1,025.5	3.7E–9–2.1E–8 [5)]
KLX05:6	256.00–360.00	308	104.0	1,022.9	2.2E–8 [5)]
KLX05:7	241.00–255.00	248	14.0	1,024.4	1.9E–6–2.2E–6 [5)]
KLX05:8	220.00–240.00	230	20.0	1,025.1	1.6E–6–6.2E–7 [5)]
KLX05:9	128.00–219.00	173.5	91.0	1,028.2	1.5E–6—6.6E–6 [5)]
KLX05:10	111.30–127.00	71	112.0	1,039.5	9.2E–6–1.6E–5* [5)]
KLX10:1	711.00–1,001.00	856	290.0	1,201.1	1.6E–7–1.7E–7 [6)]
KLX10:2	689.00–710.00	699.5	21.0	1,121.9	4.5E–8–6.7E–7 [6)]
KLX10:3	465.00–688.00	576.5	223.0	1,071.9	4.8E–8–9.1E–8 [6)]
KLX10:4	369.00–464.00	416.5	95.0	1,026.8	3.2E–6–1.4E–5 [6)]
KLX10:5	351.00–368.00	359.5	17.0	1,016.4	7.4E–7–1.7E–6 [6)]
KLX10:6	291.00–350.00	320.5	59.0	1,014.8	1.0E–5–2.8E–4 [6)]
KLX10:7	131.00–290.00	210.5	159.0	1,011.0	5.4E–5–2.2E–4 [6)]
KLX10:8	12.10–130.00	71.05	117.9	1,003.8	(1.9E–5–2.8E–5)* [6)]
KLX10C:1	66.00–146.25	106.1	80.3	1,097.2	1.3E–6 [7)]
KLX10C:2	32.00–65.00	48.5	33.0	1,076.4	6.1E–6 [7)]
KLX10C:3	9.00–31.00	20	22.0	1,067.8	2.8E–8 [7)]
KLX12A:1	546.00–602.29	574.1	56.3	1,034.1	5.6E–10–5.3E–9 [8)]
KLX12A:2	535.00–545.00	540	10.0	1,025.6	1.3E–7–3.6E–7 [8)]
KLX12A:3	426.00–534.00	480	108.0	1,013.4	6.0E–9–4.3E–8 [8)]
KLX12A:4	386.00–425.00	405.5	39.0	1,003.1	2.0E–7–8.5E–7 [8)]
KLX12A:5	291.00–385.00	338	94.0	998.7	9.2E–10–1.6E–8 [8)]
KLX12A:6	160.00–290.00	225	130.0	1,004.2	4.0E–7–1.5E–6 [8)]
KLX12A:7	142.00–159.00	150.5	17.0	1,014.2	2.0E–6–2.6E–6 [8)]
KLX12A:8	104.00–141.00	122.5	37.0	1,019.3	2.0E–6–2.6E–6 [8)]
KLX12A:9	17.92–103.00	60.46	85.1	1,033.0	no data
KLX14A:1	123.00–176.27	149.6	53.3	739.1	1.9E–6 [9)]
KLX14A:2	77.00–122.00	99.5	45.0	774.5	6.1E–5 [9)]
KLX14A:3	6.45–76.00	41.2	69.6	816.4	6.2E–6 [9)]
KLX15A:1	902.00–1,000.43	951.2	98.4	798.3	below l.m.l.–8.3E–8 [10)]
KLX15A:2	641.00–901.00	771.0	260.0	619.4	2.5E–8–8.4E–8 [10)]
KLX15A:3	623.00–640.00	631.5	17.0	481.7	2.3E–7–9.0E–7 [10)]
KLX15A:4	481.00–622.00	551.5	141.0	403.2	1.3E–7–4.8E–7 [10)]

Bh ID	Test section (mbl)	Point of application (mbl below TOC)	Section length (m)	Distance to HLX27:131.5 (m)	Transmissivity from single-hole tests (m^2/s)
KLX15A:5	273.00–480.00	376.5	207.0	235.7	2.0E–6–4.3E–6 [10]
KLX15A:6	260.00–272.00	266.0	12.0	140.4	3.7E–6–1.1E–5 [10]
KLX15A:7	191.00–259.00	225.0	68.0	112.4	1.3E–6–1.6E–6 [10]
KLX15A:8	79.00–190.00	134.5	111.0	95.3	1.8E–5–1.1E–4 [10]
KLX15A:9	11.65–78.00	44.8	66.4	147.6	3E6 [11]
KLX16A:1	327.00–433.55	380.3	106.6	821.6	1.2E–7–3.7E–7 [12]
KLX16A:2	86.00–326.00	206.0	240.0	787.4	1.1E–4–2.8E–4 [12]
KLX16A:3	11.25–85.00	48.1	73.8	789.2	8.3E–6–3.4E–4 [12]
KLX18A:1	571.00–611.28	591.1	40.3	1,001.0	9.4E–7–1.9E–6 [13]
KLX18A:2	490.00–570.00	530.0	80.0	973.5	6.3E–7–7.7E–7 [13]
KLX18A:3	472.00–489.00	480.5	17.0	953.8	5.4E–8–1.1E–7 [13]
KLX18A:4	315.00–471.00	393.0	156.0	924.7	4.2E–6–3.6E–5 [13]
KLX18A:5	155.00–314.00	234.5	159.0	892.3	5.7E–8–2.7E–7 [13]
KLX18A:6	104.00–154.00	129.0	50.0	886.0	5.7E–6–3.5E–5 [13]
KLX18A:7	11.83–103.00	57.4	91.2	889.0	no data
KLX19A:1	661.00–800.07	730.5	139.1	1,091.9	4.9E–7–1.5E–6 [14]
KLX19A:2	518.00–660.00	589.0	142.0	1,026.9	below l.m.l. of PFL
KLX19A:3	509.00–517.00	513.0	8.0	998.0	1.0E–6–4.9E–6 [14]
KLX19A:4	481.50–508.00	494.8	26.5	991.8	below l.m.l. of PFL
KLX19A:5	311.00–480.50	395.8	169.5	963.0	3.8E–7–1.8E–6 [14]
KLX19A:6	291.00–310	300.5	19.0	933.7	1.1E–5–9.1E–4 [14]
KLX19A:7	136.00–290	213.0	154.0	944.2	1.4E–6–4.3E–6 [14]
KLX19A:8	92.75–135.00	113.9	42.3	935.0	1.2E–4–3.0E–4 [14]

* Below c. 100 mbl.

[1] T_M from single-hole pumping test in open borehole (from Sicada).

[2] T_T from pumping test during flow logging /Rohs 2006/.

[3] T_T from single-hole pumping test in open borehole /Thur et al. 2007b/.

[4] From PFL /Rouhiainen et al. 2005/ and PSS injection tests /Rahm and Enachescu 2005a/.

[5] From PFL /Sokolnicki and Rouhiainen 2005/ and PSS injection tests /Rahm and Enachescu 2005b/.

[6] From PFL /Sokolnicki 2006/ and PSS injection tests /Harrström et al. 2006a/.

[7] From PFL /Väisäsvaara et al. 2006a/.

[8] From PFL /Väisäsvaara et al. 2006b/ and PSS injection tests /Harrström et al. 2006b/.

[9] From PFL /Väisäsvaara 2007a/.

[10] From PFL /Pöllänen et al. 2007/ and PSS injection tests /Enachescu et al. 2007a/.

[11] Q/s_w from Wire Line Test.

[12] From PFL /Väisäsvaara 2007b/ and PSS injection tests /Enachescu et al. 2007b/.

[13] From PFL /Sokolnicki and Kristiansson 2006/ and PSS injection tests /Enachescu et al. 2006/.

[14] From PFL /Kyllönen et al. 2007/ and PSS injection tests /Enachescu et al. 2007c/.

The reported transmissivity ranges are in most cases derived from difference flow logging (flow anomalies) and injection tests in 5 m or 20 m borehole section. The ranges are only approximate since the estimated T-values may differ depending on test method: sequential and detailed difference flow logging, respectively, and injection tests with different section lengths. In some boreholes, only difference flow logging has been performed. For the uppermost (un-cased) borehole sections generally no data are available. In a few boreholes, some information can be derived from e.g. wire line tests (WLT) during drilling, difference flow logging etc.

3 Equipment

3.1 General

Borehole KLX15A and most of the surrounding boreholes where the pressure was measured during the interference test are permanently instrumented with 1–9 inflatable packers isolating 2–10 borehole sections in each borehole. In Figure 3-1 drawings of the instrumentation in core- and percussion-drilled boreholes are presented. One borehole, HLX38, was monitored using a logger in the open borehole (no packers).

All isolated borehole sections are connected to the HMS-system for pressure monitoring. In general, the sections planned to be used for tracer tests are equipped with three polyamide tubes. Two are used for injection, sampling and circulation in the borehole section and one is used for pressure monitoring.

The pressure monitoring is made using pressure transducers in standpipes connected to each section in the borehole (see Figure 3-1). All data are collected by means of pressure transducers connected to different types of data loggers. In order to calibrate registrations from the data loggers, manual levelling of all sections is made, normally once every month. The logger data are converted to water levels by means of a linear calibration equation. It is also necessary to subtract the air pressure since all transducers give the absolute pressure. The ground water levels are given in metres above sea level (m.a.s.l.).

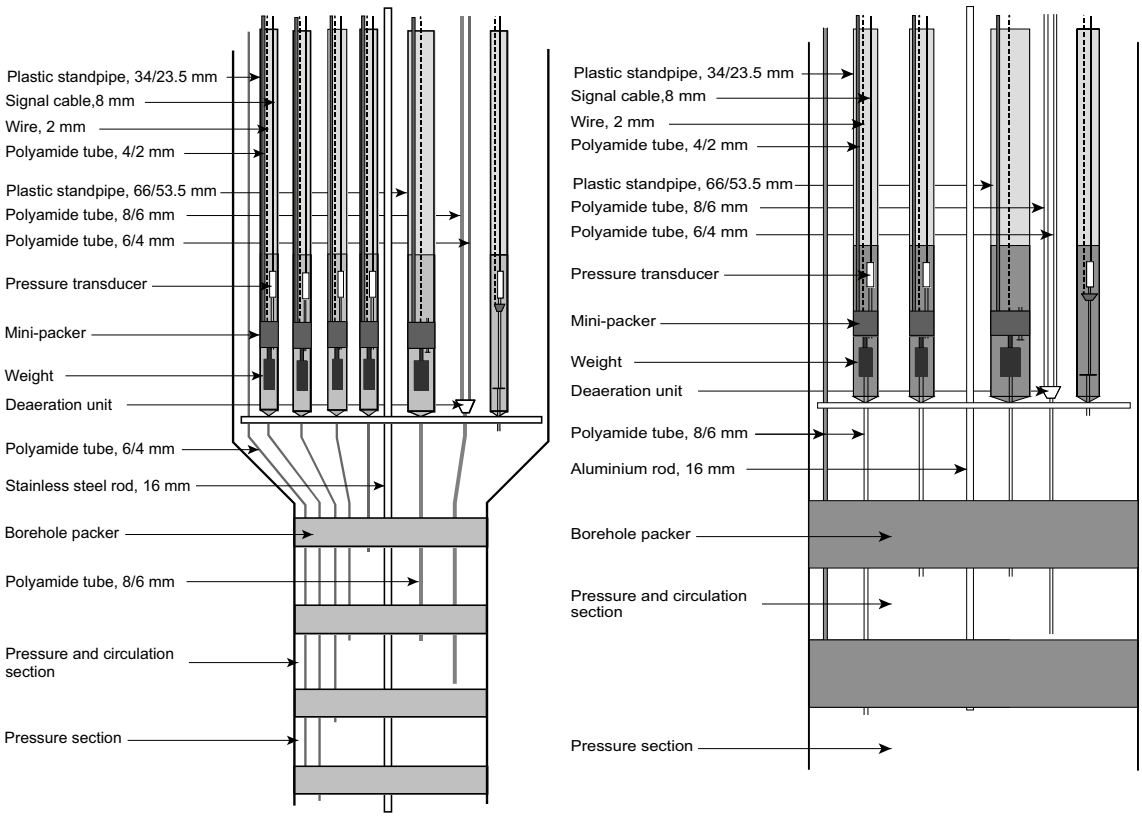

Figure 3-1. *Example of permanent instrumentation in core boreholes (left) and percussion boreholes (right) with circulation sections.*

3.2 Groundwater flow measurements

A schematic drawing of the dilution tracer test equipment is shown in Figure 3-2. The basic idea is to accomplish internal circulation in the borehole section. The circulation makes it possible to obtain a homogeneous tracer concentration in the borehole section and to sample the water and determine the tracer concentration in order to monitor the dilution of the tracer with time.

Circulation is controlled by a down-hole pump with variable speed and is measured using a flow meter. Tracer injections are made with a peristaltic pump and sampling is made by continuously extracting a small volume of water from the system through another peristaltic pump (constant leak) to a fractional sampler. The equipment and test procedure is described in detail in SKB MD 368.010, SKB internal document, see Table 1-1.

The tracer used in the groundwater flow measurements was the fluorescent dye Amino-G Acid, from Aldrich-Chemie.

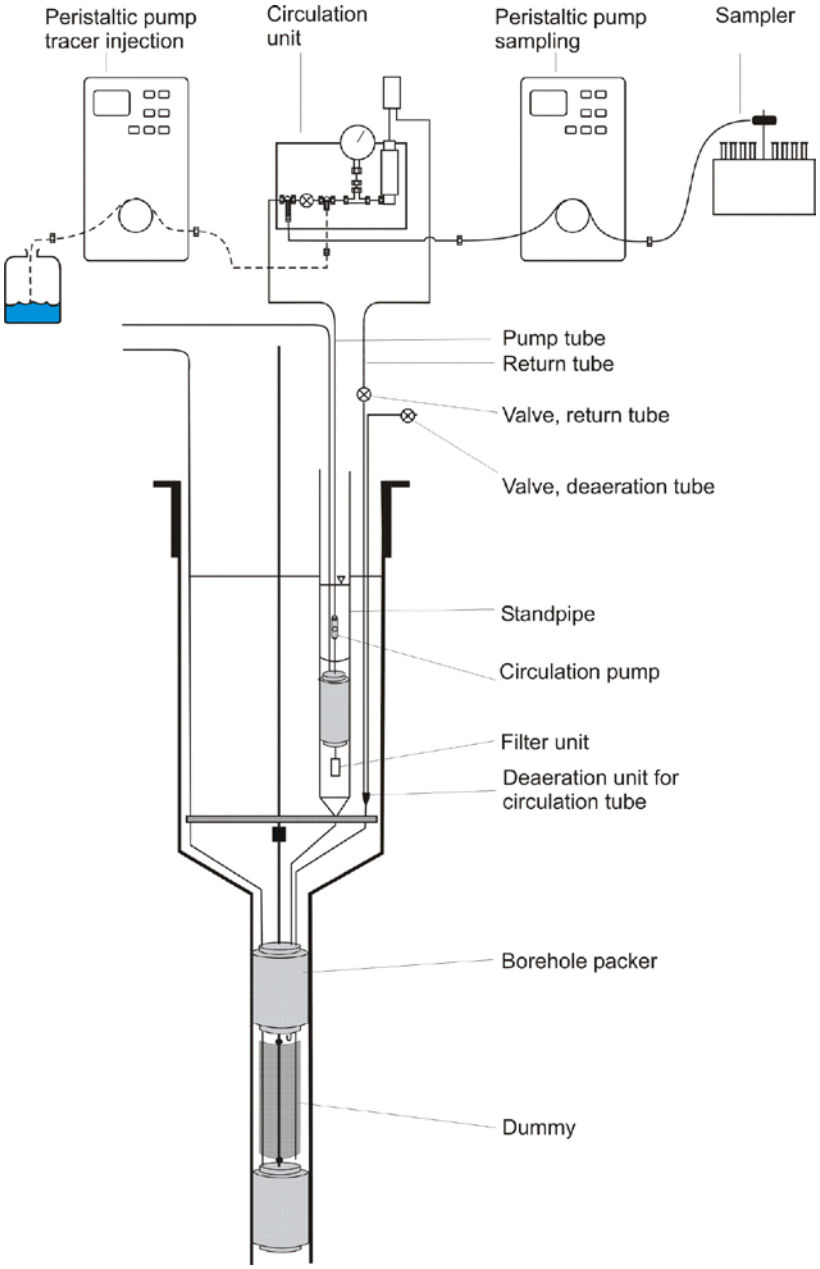

Figure 3-2. *Schematic drawing of the equipment used in tracer dilution measurements.*

3.3 Tracer tests

In this chapter the test set-up, equipment and tracers used are presented. The choices made and the designs of the experiments are based on the scoping calculations presented in Section 4.2.

The same equipment that was used for the dilution measurements (with a few additions and modifications) were used for sampling, injection and circulation in and at KLX15A during the tracer test. Samples from the injection section were continuously collected in sampling tubes using a peristaltic pump extracting a small sample volume to a fractional sampler, see Figure 3-3.

Samples were collected from the withdrawal borehole HLX27 using two different automatic samplers, see Figure 3-4. One of the samplers consists of 24 magnetic valves and a control unit allowing selection of time period between openings/samples and open time (to obtain the desired sample volume). Samples for analysis of metals (Tb, Li, Cs and Rb) were collected in 125 ml acid-washed plastic (HDPE) bottles. Samples for Rhodamine WT and Uranine analysis were collected using the other sampler providing 500 ml samples. This sampler also has 24 bottles and a portion of each sample was poured into 19 ml tubes kept for analyses and the rest was emptied and the bottles were re-used. The sampling frequency was equal for both samplers.

All samples intended for analysis of Rhodamine WT and Uranine was buffered with 1% Titrisol buffer solution (pH 9). Previous experience has shown that the buffer prevents decomposition of the dye. To all samples intended for analyses of metals (Tb, Li, Cs and Rb) 1% HNO_3 was added. The acid was added in order to keep the Tb-DTPA complex stable.

Both the pre-test and the main tracer test were performed as weak dipoles, i.e. the tracer was injected with a small excess pressure. Different equipment and set-ups were used for the injection of tracers during the pre-test and the rinsing, compared to the injection of tracers for the main tracer test. The reason for this is further discussed in Section 4.2. The equipment and injection procedures are presented below.

Figure 3-3. *Peristaltic pump and fraction sampling equipment used at the injection hole KLX15A.*

Figure 3-4. *The automatic sampling equipment (24 magnetic valves) used at the withdrawal hole HLX27.*

3.3.1 Pre test and rinsing after tracer injections

A part of the pumped water from HLX27 was re-circulated and injected into KLX15A. The flow rate was kept constant (500 ml/min) using a flow regulator. Because of the difference in salinity between the two boreholes (see Appendix 3), a sub-flow with a concentrated salt solution was added to the re-circulated water to increase the salinity. During the injection of tracer (RdWT) during the pre test, the tracer solution was added by a second sub-flow. An overview of the equipment is shown in Figure 3-5.

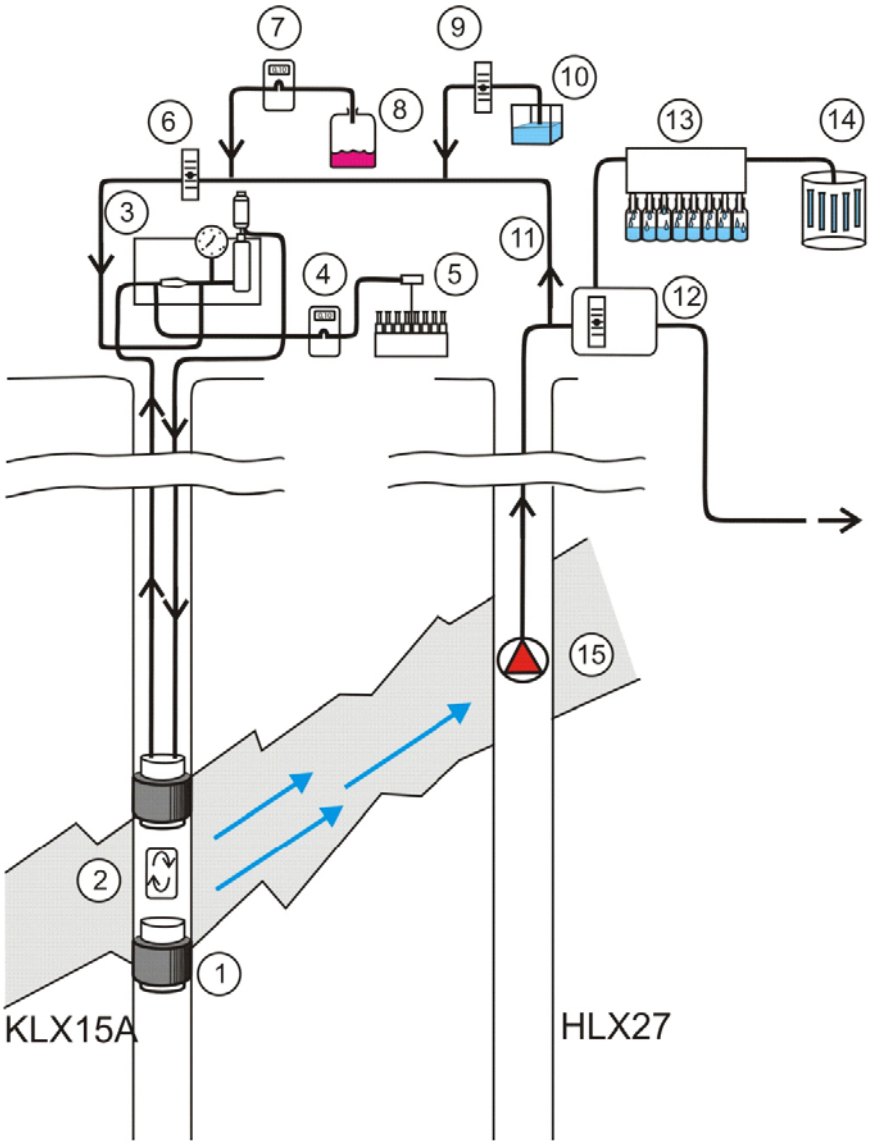

Figure 3-5. *Schematic overview of injection and sampling equipment used and tracer test layout during the pre-test and during rinsing (after tracer injection of the main test).*

3.3.2 Main tracer test

The method for tracer injection used during the pre-test was changed in the main test due to the large amounts of salt needed to be added, which would change the density and the ionic strength, see further Section 4.2. The tracers were mixed in a large (5 m^3) tank standing next to the borehole. The tracer solution in the tank was purged with nitrogen gas in order to remove oxygen. The injection of tracer was made by pumping the tracer solution, using a peristaltic pump, from the tank to the circulation loop. An overview of the equipment used is shown in Figure 3-6.

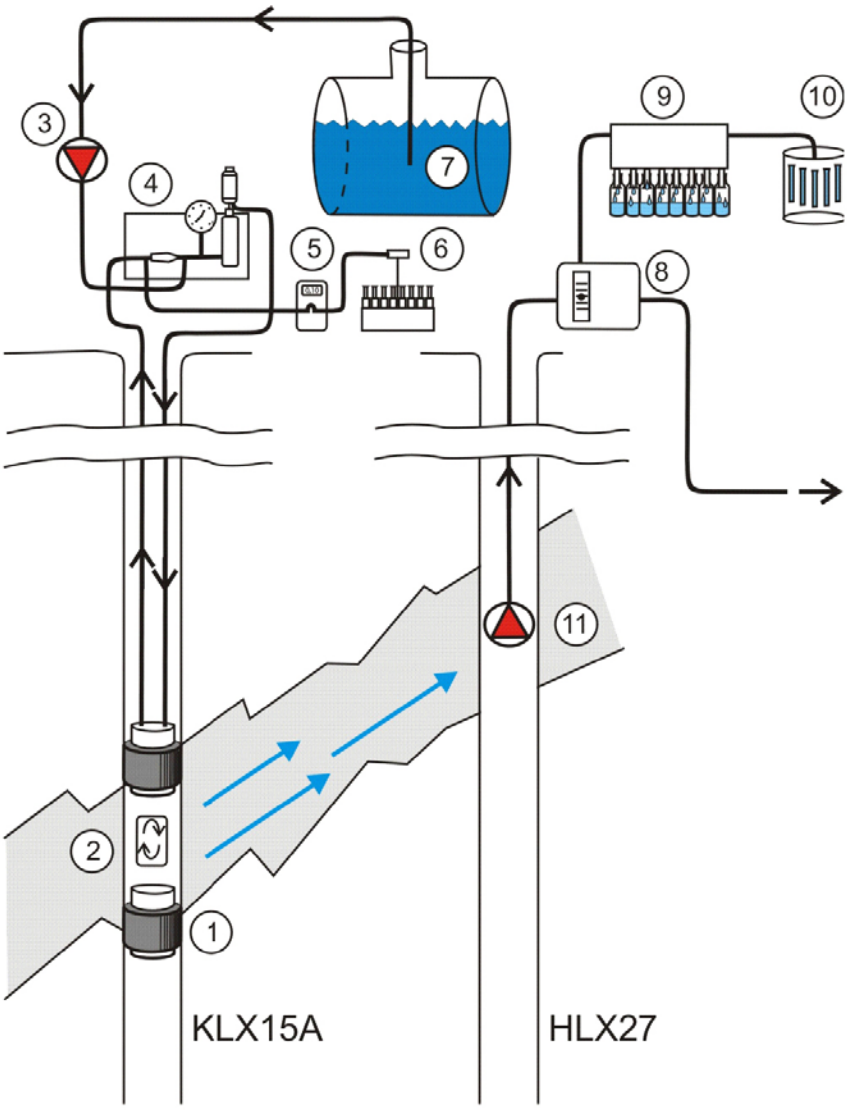

1. Packer
2. Circulation pump
3. Hose pump
4. Circulation unit
5. Peristaltic pump for sample withdrawal
6. Fractional sampler
7. Tracer tank
8. Flow meter connected to logger
9. Automatic sampler
10. Automatic sampler
11. Pump

Figure 3-6. *Schematic overview of injection and sampling equipment used and tracer test layout during the injection of tracers in the main tracer test.*

After the injection of tracers, rinsing by injecting re-circulated water from HLX27, in the same way as during the pre-test, continued throughout the whole test period.

Samples were also taken from HLX27 at two different depths (90 and 120 mbl) using a tube sampling equipment. This was done in order to find out which one of the dominating anomalies that contributes most to the tracer transport. The equipment consisted of a polyamide tube that was lowered until the lower end reached the desired depth. A valve at the surface was then opened allowing water to fill the tube after which the valve was closed and the tube was lifted. The sampled water was emptied into bottles and tubes by connecting nitrogen gas to one end of the tube. A schematic view of the equipment is seen in Figure 3-7.

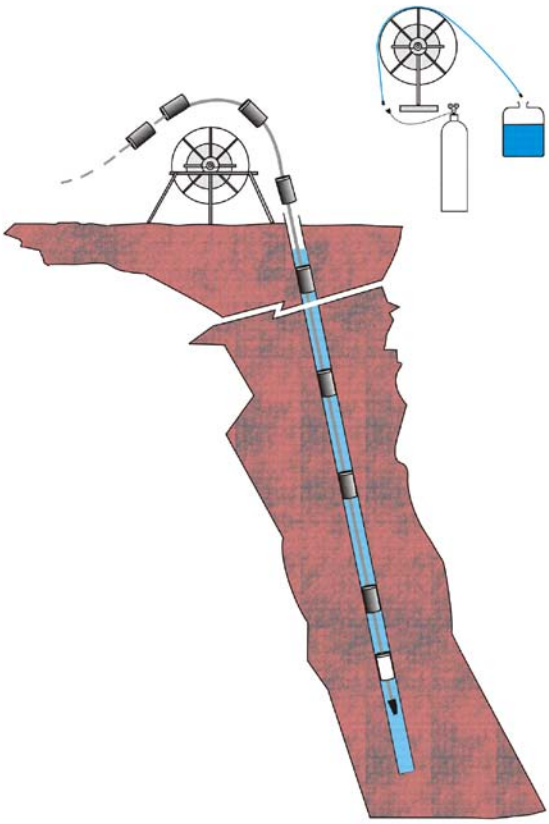

Figure 3-7. Schematic view of the tube sampling equipment used in HLX27. At the lower end of the tube there is a check valve and a weight connected.

3.3.3 Tracers used

In the pre-test, Rhodamine WT (RdWT) was used as non-sorbing tracer. Concentrated RdWT (24 g/l) was injected as a sub-flow (0.75 ml/min) into the injection flow of 500 ml/min leading to a dilution and expected concentration of 36 ppm in the section.

In the main test, Uranine, Tb, Li, Cs and Rb at the concentrations presented in Table 3-1 were used. Li, Cs and Rb were all added in the form of chloride salts and Tb was added as Tb-DTPA solution. Tb was only used in the form of Tb-DTPA, however in the analyses only the concentration of Tb is determined. The discrepancy between the concentration suggested by the scoping calculations and the theoretical concentration presented in Table 3-1 is due to uncertainty in the volume of the mixing tank. The actual volume was measured by analysis of the concentrated Tb-DTPA solution added to the tank and the Tb concentration after dilution in the tank. Since the volume showed to be somewhat smaller than intended, the actual concentration of tracers are slightly higher than suggested by the scoping calculations.

Table 3-1. Injection concentrations (C0) of the tracers.

Tracer	Conc. suggested from scoping (ppm)	Conc. Theoretical (ppm)	Conc. Measured in tank (ppm)	Conc. Maximum measured in KLX15A (ppm)	Comment
Rhodamine WT	50.0	36.0		34.2	No tank used in the pre-test
Uranine	25.0	32.6	22.0	23.5	
Tb	4.22	5.50	5.50	5.41	
Lithium	148	194	190	186	
Cesium	155	204	206	204	
Rubidium	271	356	375	390	

3.4 Pumping and interference test

The equipment in the pumping borehole, HLX27, consisted primarily of the following parts:

- A submersible pump at c. 45 mbl with a discharge pipe (PEM32) connected to the ground surface.
- Plastic hose for diverting the pumped water further away from the borehole.
- Pressure transducer in the borehole.
- Flow meter at the surface.
- Data logger to sample data from the flow meter and the pressure transducer.
- Flow rate control valve at the surface.
- An extra pipe passing the pump allowing water samples to be taken with tube-sampling equipment at two depths (90 and 120 mbl) below the pump.

All observation sections included in the interference test are part of the SKB hydro monitoring system (HMS), where pressure is recorded continuously.

3.5 Interpretation tools

3.5.1 Hydraulic evaluation

Transient evaluation of the hydraulic responses in the pumping borehole HLX27 and observation sections in surrounding boreholes was made using models included in the AQTESOLV software, cf. Section 4.6.2.

3.5.2 Transport models

The models used for evaluation of the tracer test and calculation of transport parameters are described below.

Advection-dispersion model with sorption in a single pathway

This model is described by the standard governing equation for one-dimensional advection-dispersive transport with linear equilibrium sorption:

$$D_L \frac{\partial^2 C}{\partial x^2} - v\frac{\partial C}{\partial x} = R\frac{\partial C}{\partial t} \qquad (3\text{-}1)$$

where C is concentration [e.g. M/L^3], x is distance along transport path [L], t is time [T], v is the average water velocity [L/T] along the flow path, D_L is the longitudinal dispersion coefficient [L^2/T] and R is the retardation factor.

The following initial and boundary conditions are applied:

$$C(x,0) = 0 \qquad (3\text{-}2)$$

$$\frac{\partial C(\infty,t)}{\partial x} = 0 \qquad (3\text{-}3)$$

$$-D_L \frac{\partial C}{\partial x} + vC = vC_0 \qquad x = 0 \qquad (3\text{-}4)$$

where C_0 is the concentrations of the in-flowing water across the inlet boundary. The above boundary and initial conditions result in a solution for a constant injection of tracer. For a tracer pulse with constant concentration of limited duration (t_{inj}), the resulting tracer concentration may be calculated as:

$$C(x,t) = M(x,t) \qquad 0 < t \leq t_{inj} \tag{3-5}$$

$$C(x,t) = M(x,t) - M(x,\, t - t_{inj}) \qquad t > t_{inj} \tag{3-6}$$

where $M(x,t)$ is the solution for a step-input injection with constant injection concentration. A more complex temporal variation in the tracer injection may be calculated in an analogous way by summation of a several such injection periods. A solution to the above equations, for a step input of constant concentration, is given by /Javandel et al. 1984/ as follows:

$$\begin{aligned} M(x,t) = {} & \frac{1}{2} erfc\left[\frac{Rx - vt}{2(D_L Rt)^{1/2}}\right] + \left[\frac{v^2 t}{\pi D_L R}\right]^{1/2} \exp\left[-\frac{(Rx - vt)^2}{4 D_L R t}\right] \\ & - \frac{1}{2}\left[1 + \frac{vx}{D_L} + \frac{v^2 t}{D_L R} + \right] \exp\left[\frac{vx}{D_L}\right] erfc\left[\frac{Rx + vt}{2(D_L Rt)^{1/2}}\right] \end{aligned} \tag{3-7}$$

where *erfc* is the complimentary error function.

The advection-dispersion model with sorption is herein referred to as the AD model.

The results from AD model evaluation are in this report presented using mean residence time, t_m (= x/v), Peclet number, Pe (= x/a_L) and retardation factor (R). Further, the proportionality factor, pf , which describes the fraction of the injected tracer mass that arrives at the sampling section, is obtained from the model fitting.

Advection-dispersion model in multiple pathways

This model is essentially the same as the preceding one (AD-1) except that tracer transport is assumed to occur in two, or more, separate pathways and mix in the pumping section. This is calculated by summing up the contribution from the different pathways as (for n pathways):

$$C(x,t) = \sum_{i=1}^{n} pf_i \cdot C_i(x,t) \tag{3-8}$$

where $C_i(x,t,)$ represents the partial tracer breakthrough from each individual pathway and pf_i is a proportionality factor that describes the contribution from each pathway.

It may here be noted that the pf parameter also represents dilution effects in the pumping section as well as other proportional tracer losses. Thus, this parameter is often relevant to include also when applying the advection-dispersion model for a single pathway.

Advection-dispersion model with matrix diffusion (one pathway)

In this model, the governing equation for the AD model is extended by adding a term that represents diffusion of tracer into a hydraulically stagnant matrix:

$$R\frac{\partial C}{\partial t} = - v\frac{\partial C}{\partial x} + D_L \frac{\partial^2 C}{\partial x^2} + \frac{2 D_e}{\delta}\frac{\partial C_p}{\partial y} \tag{3-9}$$

with the transport in the matrix given by:

$$\frac{\partial C_p}{\partial t} - \frac{D_e}{R_d n_p}\frac{\partial^2 C_p}{\partial y^2} = 0 \tag{3-10}$$

where n_p is the matrix porosity, D_e is the effective diffusion coefficient [L^2/T], δ is the fracture aperture [L] of the flowing fracture, $C_p\,(y)$ is the tracer concentration in the matrix, R_d is the matrix retardation factor and y is a spatial coordinate perpendicular to the direction of the flowing transport path. The matrix diffusion model used here is also presented by /Tang et al. 1981/ and /Moreno et al. 1983/. The model with advection-dispersion with sorption and matrix diffusion is herein referred to as the AD-MD model.

The boundary and initial conditions are:

$C(x,0) = 0$ (3-11)

$C(\infty,t) = 0$ (3-12)

$C(0,t) = C_0$ (3-13)

$C_p(0,x,t) = C(x,t)$ (3-14)

$C_p(\infty,x,t) = 0$ (3-15)

$C_p(y,x,0) = 0$ (3-16)

When this matrix diffusion model is employed for interpretation of tracer breakthrough curves, all unknown parameters in Equations 3-8 and 3-9 cannot be evaluated independently. Instead, it is common to use a lumped parameter, A, which describes the effect of matrix diffusion. The parameter A may be written as:

$$A = \frac{\delta \cdot R}{2\sqrt{n_p D_e R_d}} \quad (3\text{-}17)$$

With this definition, the matrix diffusion effect increases with decreasing values of A.

3.5.3 Parameter estimation method

Estimated parameter values are obtained by non-linear least-squares regression. The basic non-linear least-squares regression minimises the sum of squared differences between the modelled (Y^M) and the observed (Y^O) variables and may be formulated as:

$$\min S = \mathbf{E_R}^T \mathbf{W} \mathbf{E_R} \quad (3\text{-}18)$$

where $\mathbf{E_R}$ is a vector of residuals ($\mathbf{Y}^O - \mathbf{Y}^M$) and $\mathbf{W}$ is a vector of reliability weights on observations.

The specific method for carrying out the regression employed in this study is often referred to as the Marquardt-Levenberg method. This method is a Newton-type optimisation algorithm that finds the parameter values that minimises the sum of squared errors between model and measurement values in an iterative manner. A basic Newton-type search algorithm used may be written as:

$$\mathbf{B}_{r+1} = \mathbf{B}_r + (\mathbf{X}_r^T \mathbf{W} \mathbf{X}_r)^{-1} \mathbf{X}_r^T (\mathbf{Y}^O - \mathbf{Y}_r^M) \quad (3\text{-}19)$$

where $\mathbf{B}$ is a vector of parameter estimates, $\mathbf{X}$ is a parameter sensitivity matrix, and the subscripts r and r+1 refer to the iteration number. The Marquardt-Levenberg method is an extension that enhances the convergence properties of the search algorithm by restricting the search direction.

Given an initial parameter estimate (B_r), the model variable vector (Y^M) and the sensitivity matrix (X) are calculated and a new vector of estimates (B_{r+1}) is obtained. Equation 3-18 is then repeated until a local optimal solution is found. The local minimum is defined by some convergence criterion, for example when parameter estimates are essentially identical between iterations. Finding a local minimum does not guarantee that the global minimum is found. When this appears to be a problem, several sets of initial estimates may be tried. When some knowledge about the parameters to be estimated and the physical system is already available, the initial estimates are often good enough for ensuring that a global minimum is found.

An important element of the above procedure is the matrix containing the parameter sensitivities. Parameter sensitivity is defined as the partial derivative of the dependent (simulated) variable with respect to a parameter. A sensitivity matrix contains one row for each observation and one column for each estimated parameter, as in the following example with three observations and two parameters.

$$\mathbf{X} = \begin{pmatrix} \frac{\partial y_1}{\partial b_1} & \frac{\partial y_1}{\partial b_2} \\ \frac{\partial y_2}{\partial b_1} & \frac{\partial y_2}{\partial b_2} \\ \frac{\partial y_3}{\partial b_1} & \frac{\partial y_3}{\partial b_2} \end{pmatrix} \tag{3-20}$$

Parameter sensitivities may be used to determine the precision of the estimated parameter values. Two diagnostic measures are given below regarding parameter uncertainty that may be obtained as a result of regression /Cooley 1979/.

The *standard errors* of parameter estimates are obtained by taking the square roots of the diagonals in the parameter covariance matrix, which is given by:

$$s^2(\mathbf{X}^T\mathbf{W}\mathbf{X})^{-1} \tag{3-21}$$

with s^2 being the error variance:

$$s^2 = \frac{\sum_{i=1}^{N} w_i \, (y_i^O - y_i^M)^2}{N - P} \tag{3-22}$$

where N is the number of measurements, P the number of parameters to be estimated and w_i the weight on observation i.

The linear correlation $r(p_1,p_2)$ between two parameters with values of p_1 and p_2, respectively, is given by:

$$r(p_1, p_2) = \frac{Cov\,(p_1, p_2)}{\sqrt{Var(p_1)\,Var(p_2)}} \tag{3-23}$$

where the variance and covariance terms are elements of the $s^2(\mathbf{X}^T\mathbf{W}\mathbf{X})^{-1}$ matrix. The correlation is a measure of the inter-dependence between two parameter estimates, and correlation values range between –1 and 1. Values close to either –1 or 1 mean that a change in one parameter value may be compensated for by a similar change in another parameter value to maintain the same fit (sum of squares) between model and measurements. The standard errors and parameter correlation values are the main diagnostic measures used in this analysis when examining the parameter estimation results from evaluation of the tracer tests.

3.5.4 Handling of tracer injection data

Measured injection flows and tracer concentration in the injection section were used to calculate the tracer input function for the evaluation models. The input function was approximated by a number of step input periods that were superimposed as described in Equation 3-6. Each injection period is given an input value that is proportional to the injected tracer mass/time.

3.5.5 Other derived transport parameters

In accordance with the SKB method description for two-well tracer tests (SKB MD 530.006), some further transport parameters are derived, mainly based on the average residence time (t_m) determined from the model evaluation described above. The derived parameters are:

- fracture aperture (mass balance aperture),
- hydraulic fracture conductivity,
- flow porosity.

The fracture aperture, δ [L], is determined from:

$$\delta = \frac{Qt_m}{\pi(r^2 - r_w^2)} \tag{3-24}$$

where Q is the average pumping rate [L^3/T], r is the travel distance [L] and r_w is the borehole radius [L].

The hydraulic fracture conductivity, K_{fr} [L/T] is calculated using:

$$K_{fr} = \ln\left(\frac{r}{r_w}\right)\frac{\left(r^2 - r_w^2\right)}{2t_m \Delta h} \tag{3-25}$$

where Δh is the head difference [L] between the injection and pumping sections. The flow porosity, ε_f is determined from:

$$\varepsilon_f = \frac{K}{K_{fr}} \tag{3-26}$$

where K is the hydraulic conductivity of the packed-off section determined from a steady-state evaluation of the interference test /Moye 1967/.

4 Execution

4.1 General

The activity included planning and preparations, execution of field work and analyses and interpretation of data.

4.2 Scoping calculations

In order to optimize the test in terms of tracer injection method, injection times, pumping rates, tracers, etc, some scoping calculations were performed during the planning stage.

4.2.1 Injection method

Two main tracer injection methods were considered, with and without additional pressure in the injection section. The intention was that the selected injection method should minimize the dilution of tracer between KLX15A and HLX27 and provide a temporally well-defined injection period.

Injection without additional pressure is done by replacing the ambient water in the injection interval with a tracer solution. The tracer will then be injected simply by dilution with native water. The dilution from KLX15A to HLX27 with this method depends on the induced flow rate in KLX15A while pumping in HLX27. No such measurement had been performed at the time of the scoping calculations and therefore some assumptions had to be made. The groundwater flow was assumed to be radially converging while pumping in HLX27. Furthermore, the flow was assumed to converge/diverge to some extent around the injection section. With these assumptions a dilution of c. 3,000 times is expected if the distance is 140 m between the sections. The scoping calculations also indicated that the concentration decrease in the injection section would be rather slow without applying additional pressure.

If tracer injection with additional pressure is used, the dilution between the injection and pumping sections would be equal to ratio of the flow rates if the mass recovery is 100%, i.e. if the injection rate is 100 times lower than the pumping rate the dilution would be 100 times. When this injection method is used, the test is said to be carried out as an unequal dipole. Hence, a much smaller dilution is possible to achieve with this method compared to the one described above. Another benefit of this method is that the injection period is rather distinct, i.e. the concentration increases and decreases relatively fast at the start and stop of the injection. A disadvantage with the method is that water without tracer has to be injected both before and after the period of tracer injection in order to maintain stable hydraulic conditions during the test.

The recommended methodology was to inject tracer with an additional pressure due to the lower dilution and the more distinct injection period compared to the tracer injection without applying additional pressure.

4.2.2 Pumping flow rate

The duration of the test was originally planned to be 4–6 weeks. In order to ensure a tracer breakthrough in HLX27, a high flow rate in the section was preferable. On the other hand, the flow rate should be constrained so that the total expected drawdown in HLX27 would not exceed 30 m. The transmissivity, T, of HLX27 is $5.0 \cdot 10^{-5}$ m^2/s according to previous investigation /Rohs et al. 2007/.

An approximation of flow rate according to Equation 4-1 then results in a maximum flow rate of c. 90 l/min.

$$T \approx \frac{Q}{s} \tag{4-1}$$

where T is the transmissivity (m^2/s), Q is the flow rate (m^3/s) and s is the drawdown (m).

However, because flow rate changes during the test should be avoided, some safety margin should be used. In addition, at these relatively high flow rates the friction losses in the pump hose are significant.

As mentioned above, the pumping flow rate has significance for the residence time of the tracer. The residence time may be estimated according to Equation 4-2 (SKB MD 530.006):

$$t_m = \frac{\delta\pi(r^2 - r_w^2)}{Q} \tag{4-2}$$

where t_m is mean residence time (s), δ is fracture aperture (m), r is travel distance (m), r_w is borehole radius (m) and Q is mean pumping flow rate (m^3/s).

Equation 4-2 requires an assumption of the fracture aperture since no data was available during the scoping calculations. According to the cubic law and the transmissivities reported from the borehole sections the fracture aperture (one fracture) would be in the range of 0.2–0.4 mm. However, from experience it is commonly known that the cubic law underestimates the fracture aperture considerably. In Table 4-1 the mean residence time is calculated for a few values of the pumping flow rate and the fracture aperture, respectively. Since there is considerable uncertainty about the fracture aperture, there was an obvious risk that the experimental residence time would be rather large, especially for low flow rates.

The recommendation about pumping flow rate was therefore to maximize the flow rate. However, a high pumping flow rate also requires a high injection flow rate to achieve the desired 1/100 dipole. A high injection flow rate consequently requires a large volume of tracer solution and hence also a large quantity of tracers. A very large amount of tracer solution would be difficult to prepare and some of the tracers are very expensive. Also, the flow rate has to be adjusted to the chosen equipment and the expected friction losses in the pump hose. Hence, the selection of a suitable flow rate becomes a question of priority. After these considerations, the recommended initial pumping flow rate was 50 l/min.

Earlier experience from a similar tracer test in Forsmark /Lindquist et al. 2008a/, where the same type of scoping calculations and models were used, indicated that a fracture aperture of 25 times the cubic law estimate is reasonable. This corresponds to a fracture aperture of 5–10 mm in this test and to a mean residence time of 100–200 h with the recommended flow rate 50 l/min.

Table 4-1. Mean residence time (h) with different pumping flow rates and fracture apertures. The distance between the sections is assumed to be 140 m.

Mean residence time [h]		Pumping flow rate [l/min]				
		30	50	60	70	90
Fracture aperture [mm]	1	34	21	17	15	11
	5	171	103	86	73	57
	10	342	205	171	147	114
	20	684	411	342	293	228

4.2.3 Tracers

Several factors have to be considered for the selection of the sorbing tracer (preferably cations) in an *in situ* experiment of the present type:

- The injection concentration of the tracer should be high enough to allow detection in the withdrawal borehole where the dilution process often results in concentration several orders of magnitudes lower compared to the injection borehole.
- If the injection concentration is too high, some of the following problems may occur:
  - Full or partial saturation of the adsorption sites on the fracture walls leading to nonlinear adsorption giving lower retention compared to a realistic case of radionuclides dispersed in tracer concentrations.
  - Changes in water composition which may influence the competition for the cation exchange sorption sites.
  - Precipitation of less soluble compounds of the proposed cations, i.e. formation of e.g. carbonates, sulphates, fluorides and hydroxides.
  - Concentrations significantly higher than the natural salt content of the water may result in significantly increased density of the injection solution and thus poor mixing with the natural groundwater.
- The retention should be low enough to enable tracer breakthrough within the time frame of a tracer experiment (weeks-month) and preferably high enough to be able to distinguish the breakthrough from a simultaneously injected non-sorbing tracer.

The best type of tracers, given the above considerations, is radioactive tracers; there is no background signal to overcome and a large dynamic range is in most cases available without making any significant concentration increase, cf. e.g. /Andersson et al. 2002/. However, it was in the present tracer experiment, for various practical reasons, not possible to use radioactive tracers. Instead, increased concentrations of naturally occurring cations were used.

From the commonly used types of sorbing tracers (alkali metals and alkaline earth metals, cf. e.g. /Andersson et al. 2002/, it is obvious that the alkaline earth metals (Mg^{2+}, Ca^{2+}, Sr^{2+} and Ba^{2+}) cannot be used due to their limited solubility as e.g. carbonates (Mg^{2+} and Ca^{2+}) and sulphates (Sr^{2+} and Ba^{2+}). An increase of the natural concentrations of these species with 1–2 orders of magnitudes is predicted to cause precipitation problems. Regarding the alkali metals (i.e. Li^+, Na^+, K^+, Rb^+ and Cs^+), no compound with low solubility can be identified so there are no restrictions from this point of view. However, for Na^+ being present in the groundwater at a natural concentration of 1,090 ppm (0.05 M) it is obvious that an increase of the natural concentration in orders of magnitudes will lead to an increase of the density of the water. In addition, this will also make the solution approach the solubility limit of NaCl (~6 M). The ion K^+ is present in the natural groundwater in a concentration of 23.3 ppm ($6.0 \cdot 10^{-4}$ M), which also is comparatively high for the use of this cation as a tracer. The three best candidates are therefore Li^+, Rb^+ and Cs^+, present in the natural concentrations of about 130 ppb ($1.9 \cdot 10^{-5}$ M), 40.2 ppb ($4.7 \cdot 10^{-7}$ M) and 0.5 ppb ($3.8 \cdot 10^{-9}$ M), respectively.

Based on the considerations above and the results of the scoping calculation (see Section 4.2.3), the following strategy was outlined:

- Li^+, Rb^+ and Cs^+ should be used as sorbing tracers.
- Injection concentrations was, based on the scoping calculations, selected to be $2.2 \cdot 10^{-2}$ M for Li^+, $3.9 \cdot 10^{-2}$ M for Rb^+ and $2.3 \cdot 10^{-2}$ M for Cs^+, i.e. a concentration increase with a factor $1 \cdot 10^3$, $8.4 \cdot 10^4$ and $6 \cdot 10^6$ for the various tracers, respectively.
- To avoid increasing the ionic strength and thereby minimize density changes, it was decided that the injection solutions should be prepared on a synthetic groundwater basis. A groundwater with the same composition as the natural groundwater should therefore be prepared, except that some of the natural Na^+ concentration (0.05M) should be substituted with Li^+.

One should be aware of that a significant change of the water composition and increasing the tracer concentration may give retention characteristics that are not directly comparable to performance assessment cases, laboratory data and/or other *in situ* experiment. However, the objective of this work is more from a demonstration/confirmation perspective, i.e. to give a qualitative indication that tracer retardation can be observed *in situ*.

In addition to the injection phase of the tracer experiment, this tracer experiment also includes a pre-test phase and a rinsing phase (after the injection phase in the sorbing tracer experiment). In order to obtain stable flow conditions during the experiment, a water injection at the same flow rate had to be performed during the other two phases. In order to minimize any changes in the groundwater composition, this should be performed using water with a salt matrix identical to the natural groundwater. This can be done using three alternative methods:

1. Pump and store natural groundwater in large tanks and inject directly from them.
2. Inject a part of the pumped water directly into the injection section (re-circulation).
3. Prepare a synthetic groundwater with the same composition as the natural groundwater.

A general disadvantage with storing natural groundwater is that the pressure release combined with air contact may cause precipitation of e.g. iron and manganese hydroxides. On the other hand, preparation of synthetic groundwater is quite laborious. Since the execution of this test would demand very large quantities of synthetic groundwater (which was practically impossible) it was decided to use some of the pumped water from HLX27 and inject into KLX15A:6 for the other experimental phases. A sub-flow with concentrated salt solution was connected to attain the same chemical composition as the water in KLX15A:6. A summary of the chemical composition of the water in HLX27 and KLX15A:6 together with the composition of the sub-flow is given in Appendix 3.

For convenience, it was decided to prepare concentrated salt solutions in the laboratory and in the field subsequently dilute the concentrated solutions with tap water to obtain the correct water composition.

The preparation of the synthetic groundwater with tracers is further described in Appendix 3.

A very similar confirmatory tracer test has been performed successfully within the Forsmark site investigation /Lindquist et al. 2008a/. Prior to that test an investigation of possible tracers were made. A prerequisite for the main tracer test in Forsmark was that non-sorbing as well as sorbing tracers should be used. The investigation showed that Uranine and the ions Li^+, Cs^+ and Rb^+ were suitable. These tracers were used successfully in the test in Forsmark and it was decided to use them also in this test. Metal complexes (Ho-DTPA and Tb-DTPA) were also suggested as non sorbing tracers, but they were not used in Forsmark (Uranine was used instead). However, since the required amount of Uranine in the present test might be very large in order to reach concentrations of about 100 times the background concentration, it was decided to use Tb-DTPA as the non-sorbing tracer. Some Uranine was also used, but only as an indicator of tracer breakthrough.

A number of simulations were performed with the AD model in a single pathway, described in Section 3.5, in order to investigate the applicability of Uranine, RdWT, Tb-DTPA, Cs^+, Rb^+ and Li^+. Since there is uncertainty about residence time, dispersivity and sorption, several combinations of these parameters were simulated. Different injection schedules with regard to time and flow rate were also simulated. Because of the various uncertainties in the scoping simulations, it is only reasonable to discuss if a tracer is likely to be suitable or not in the test. In these scoping calculation, numerous simulated breakthrough curves were produced that will not be shown in this report. However, one example is shown in Figure 4-1.

Previously SWIW-tests in the Laxemar area resulted in retardation factors ranging from 66 to 850 for Cs and 104–2,700 for Rb. This can be compared to a SWIW test performed in KFM02A in Forsmark where R = 11 was reported for Cs. From the cross-hole tracer test performed between KFM02A and KFM02B in Forsmark in 2007, R = 3.4 for Cs and R = 2.7 for Rb was reported. Hence, the sorption in the present tracer test was expected to be higher compared with the results from Forsmark.

The simulations also showed that reasonable injection concentrations of Uranine, RdWT, Tb-DTPA, Li^+, Rb^+ and Cs^+, that would provide significant breakthrough in HLX27, may be attainable.

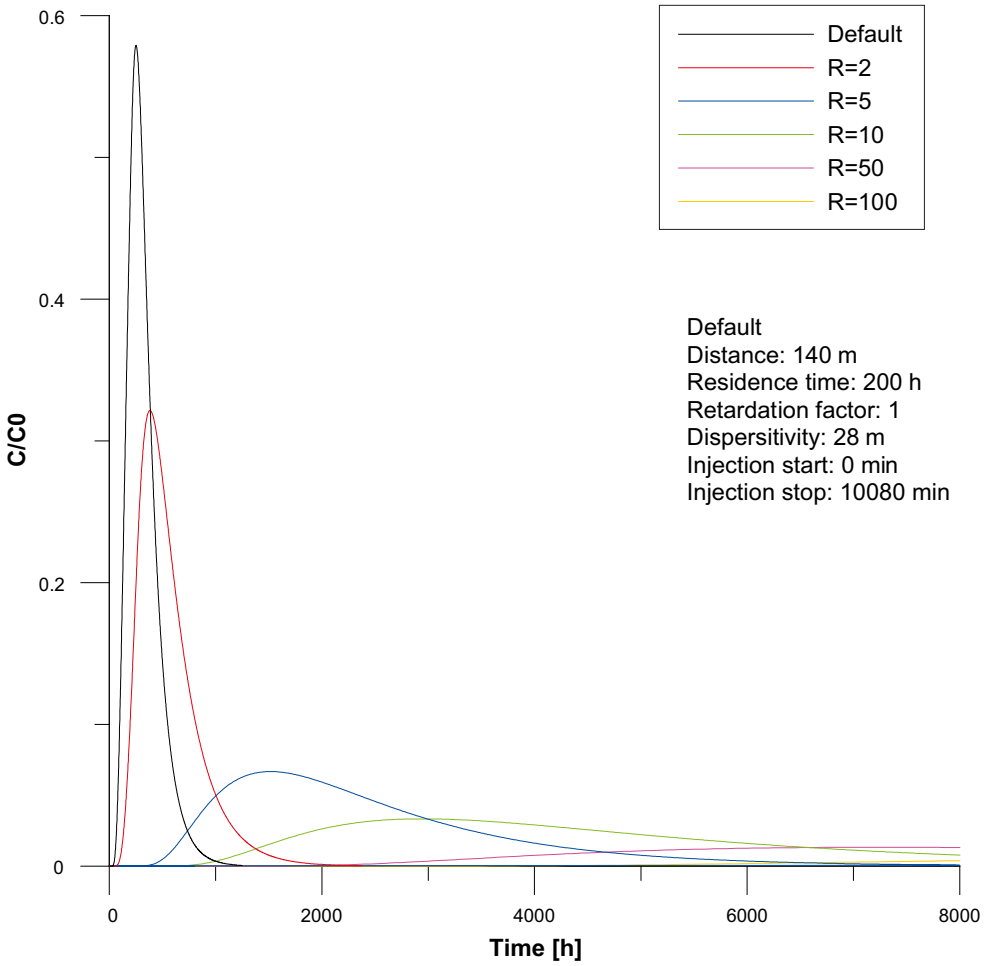

Figure 4-1. *Example of simulated breakthrough curves. The injection duration is one week with constant concentration. All curves assume a dispersivity of 28 m and a residence time of 200 h. The retardation factor varies from 1 to 100 in the example.*

If large quantities or high concentrations of Rb^+ and Cs^+ are used, the sorption sites in the fractures may become limited so that an assumption of a linear sorption isotherm would no longer be valid. However, the concentrations and amounts of Cs^+ and Rb^+ should not be too low since the concentration in the pumping section may be too low compared with the background level. Hence, the recommended total concentrations and amounts of Cs^+ and Rb^+ is a trade-off between the risk of non-linear sorption and the risk of too low concentration in the pumping section. Based on the scoping simulations, an injection period of one week was recommended since the highest concentration in the breakthrough is less dependent on the dispersivity when the injection period is longer.

Because of uncertainty about the residence time and therefore how long time the experiment should last to meet the objectives of the test, it was recommended to perform a short pre-test with RdWT. This would also be an opportunity to test the equipment prior to the main test.

4.3 Preparations

Other preparations involved calibrations, preparation of salt-solution to be added as sub-flow, preparation of synthetic ground water with tracers and preparation of concentrated RdWT for the pre-test. The following section describes this in more detail.

In addition, the groundwater flow measurements and the pre-test can be regarded as preparations for the main tracer test. However, they are treated as separate tests in this report and are therefore presented in Section 4.4.

4.3.1 Calibration and functionality checks

Functionality checks of the equipment were performed before starting the measurements. An equipment check was performed at the Geosigma engineering workshop in Uppsala as well as at the site as a simple and fast test to establish the operating status of the equipment.

To check the function of the pressure sensor, the air pressure was recorded and found to be as expected. Submerged in water, the pressure coincided well with the total head of water at all depths.

The pumps used for tracer injections of both RdWT and the tracer solution for the main test were calibrated and tested in the field under the actual conditions to give the desired flow rates. The flow regulator was also tested during the actual prevailing conditions before any tracer injections begun.

The preparation of the synthetic groundwater tracer solution and the sub-flow of salt solutions together with their chemical composition and amounts of salts added are further described in Appendix 3.

4.4 Execution of field work

The field work was performed during 15 weeks from March to July 2008. Table 4-2 lists the major field work events. Pumping was conducted in the open borehole HLX27. After about 4 weeks of pumping the main tracer test started by injecting five different tracers (Uranine, Tb-DTPA, Li^+, Cs^+ and Rb^+) into a packed-off section (260.0–272.0 mbl) of the permanently instrumented borehole KLX15A, which is located near HLX27. The water in the injection interval (KLX15A:6) was circulated for mixing and samples were continuously collected to monitor the tracer concentrations. Water samples from HLX27 were also taken and analysed for tracer breakthrough.

To optimize the design of the tracer test (to choose an appropriate withdrawal rate and concentrations of tracers), preparations consisting of scoping calculations, dilution measurements (to monitor the groundwater flow during both natural and stressed conditions) and a pre-test were performed. The pre-test resembled the main test but only one non-sorbing tracer (Rhodamine WT) was used. The pre-test resulted in tracer breakthrough and indicated that the flow rate should be increased before performing the main tracer test.

Pressure responses from the pumping in HLX27 were monitored in 78 observation sections in surrounding boreholes. All boreholes monitored for potential responses are part of HMS (SKB Hydro Monitoring System).

The relevant method descriptions (SKB internal documents) are presented in Table 1-1 in Section 1.

Water samples (SKB Class 3) were taken at three occasions during the thirteen week pumping period.

Table 4-2. Overview of field work events.

Activity	Borehole	Date
Dilution mesurements, natural conditions	KLX15A:3	2008-03-18 18:08–2008-03-26 10:31
Dilution mesurements, natural conditions	KLX15A:6	2008-03-19 15:10–2008-03-26 10:31
Start pumping (pressure registration, HMS)	HLX27	2008-03-26 10:31
Dilution mesurements, stressed conditions	KLX15A:3	2008-03-26 10:31–2008-04-01 08:12
Dilution mesurements, stressed conditions	KLX15A:6	2008-03-26 10:31–2008-04-01 08:15
Injection of Rhodamine Wt	KLX15A:6	2008-04-02 11:45–2008-04-08 11:48
Performance of pre-test	KLX15A:6 and HLX27	2008-04-02 11:45–2008-06-26 10:05
Flow rate increased from 50l/min to 75 l/min	HLX27	2008-04-21 17:45
Injection of tracers (Uranine, Li, Cs, Rb) for the main tracer test	KLX15A:6	2008-04-23 09:10–2008-04-29 08:22
Performance of main tracer test	KLX15A:6 and HLX27	2008-04-23 09:10–2008-06-26 10:05
Injection of re-circulated water (rinsing) to maintain the dipole	KLX15A:6	2008-04-01 16:02–2008-04-23 09:10 2008-04-29 08:22–2008-06-26 10:05
Stop pumping	HLX27	2008-06-26 10:05

4.4.1 Groundwater flow measurements

The groundwater flow measurements in KLX15A were performed before the start of the tracer test in order to measure the flow response due to pumping in HLX27. The time periods for the measurements are presented in Table 4-2. Two sections (section 3 and 6) were measured although section 6 was the only one intended for tracer injection. Section 3 was interpreted to intersect the major fracture zone NW042 and was therefore of interest to check the connectivity with HLX27.

The measurement period with natural gradient was 326 hours, and the corresponding time during the period with stressed gradient (during pumping) was 305 hours for both of the measured sections.

The pumping in HLX27 started at 10:31 on March 26 and the flow rate was kept at 50 l/min after an initial adjustment period to obtain a steady flow rate. The pumping is described in detail in Section 4.4.2

The groundwater flow measurements were made by injecting a slug of tracer (Amino G Acid, 1,000 mg/l) in the selected borehole sections and allowing the natural groundwater flow to dilute the tracer. The tracer was injected during a time period equivalent to the time it takes to circulate one section volume. The injection/circulation flow ratio was set to 1/1,000, implying that the initial concentration in the borehole section would be about 1.0 mg/l. The tracer solution was continuously circulated and sampled using the equipment described in Section 3.2.

The samples were analysed for dye tracer content at the Geosigma Laboratory using a Jasco FP 777 Spectrofluorometer.

4.4.2 Pumping and interference test

The pumping during the pre-test was performed as a constant flow rate pumping test with a flow rate of 50 l/min. Before the main tracer test started, the flow rate was increased and then kept at 75 l/min due to a somewhat slower tracer recovery than expected in the pre-test. The pumping was followed by a pressure recovery period. The data logger sampled data at a suitable frequency determined by the operator, see Table 4-3. The pressure interference was recorded in a total of 78 sections in 14 observation boreholes, both core- and percussion-drilled boreholes, all part of the HMS (SKB Hydro Monitoring System).

In HLX27, the absolute pressure transducer connected to the data logger was attached to the pump pipe at approximately 45 mbl. In both the observation boreholes and the pumping borehole, the hydro monitoring system was utilized for pressure registration.

Approximate sampling intervals for flow rate and pressure in the pumping borehole HLX27 are presented in Table 4-3. During the first hours of pumping the sampling frequency was adjusted manually and Table 4-3 shows only the changes of frequency intervals. After the stop of pumping, the sampling frequency was also changed in accordance with Table 4-3.

The observation sections have either permanently installed equipment or have removable miniTroll transducers equipped with an attached logger for measuring pressure in the various sections. The miniTroll transducers recorded a pressure value with the standard frequency of one reading every two hours. In addition, logging was done whenever there was a pressure change of at least 0.1 m since the last logging. The permanent installations were set to automatically measure once every 5 minutes and store a value every 30 minutes as well as at a pressure change of 0.01 m. During the first 24 hours in connection with pump start or stop, the logging frequency was further increased.

Table 4-3. Standard sampling intervals used for pressure registration during the pumping test.

Time interval (s) from start/stop of pumping	Sampling interval (s)
1–300	2
301–600	10
601–3,600	60
>3,600	300

4.4.3 Tracer tests

The tracer test was performed as a weak dipole implying that the tracer was injected with some excess pressure. Initially the dipole was 1/100 (i.e. the pumping flow rate was 100 times larger than the injection flow). The dipole was created in two different ways during the test:

1) Some of the pumped water from HLX27 was re-circulated and injected in KLX15A:6 at flow rate 500 ml/min.
2) Synthetic groundwater with tracers was injected from a tank at flow rate 400 ml/min (intended flow rate was 500 ml/min).

Prior to the main tracer test a pre-test was performed. The injection of water re-cycled from HLX27 started after 6 days of pumping in HLX27. After one more day of pumping a sub-flow of concentrated Rhodamine WT was added so that the concentration of RdWT in the injection section reached 36 ppm. The injection of Rhodamine WT lasted for six days and the injection of re-cycled water was continued in order to maintain steady-state hydraulic conditions.

The performance of the main tracer test (including the injection) was somewhat different. After the pre-test (26 days after pump start), the pumping rate was increased to 75 l/min but the re-circulated groundwater was still injected at 500 ml/min. This means the dipole was changed from 1/100 to 1/150. When the injection of tracers for the main test started the dipole was changed again, to about 1/200. This was however not deliberately, but an effect of the injection pump not providing the 500 ml/min it was set at but only 400 ml/min. The injection of tracers for the main tracer test was made by injecting a tracer solution with synthetic water from a large tank (5 m^3). The injection continued for 6 days and after that the re-cycled water from HLX27 was injected throughout the rest of the test period at flow rate 500 ml/min.

The reason the injection flow was kept at 500 ml/min (and not increasing it to 750 ml/min to maintain the 1/100 dipole) was mainly practical. All the equipment was tested and calibrated for 500 ml/min. Also, a higher injection flow rate would have required more tracer solution and hence additional amounts of tracers. Very large volumes of tracer solution are hard to handle, and the cost for some of the tracers are high. In addition, it was judged that the change of dipole conditions should not have a large impact on the results and that the amount of tracers should be sufficient for a tracer breakthrough.

During the main tracer test, samples were still analysed for Rhodamine WT to in order to obtain data for the whole breakthrough curve from the pre-test.

The injection pump worked well. However, since no flow meter was connected possible variations in injection flow was not possible to observe. It cannot be excluded that the small variations in concentrations in the injection section are due to injection flow rate variations.

A simple and reasonable assumption is that the amount of tracer that leaves the injection section (and into the transport path) is proportional to the tracer concentration in the injection section. Samples were continuously withdrawn from the injection section to monitor the tracer injection versus time. Samples were also continuously collected from HLX27 and analysed for tracer breakthrough.

The samples were analysed for dye tracer content at the Geosigma Laboratory using a Jasco FP 777 Spectrofluorometer. The samples to be analysed for metals (Tb, Li, Cs and Rb) were sent to ALS Scandinavia laboratory in Luleå for analysis (using ICP-AES and ICP-SFMS).

Samples were taken more frequently during the beginning of the test period and then with a gradually decreasing frequency as presented in Table 4-5.

Table 4-4. Injection rates and times.

	Unit	Pre-test	Main tracer test
Circulation rate	(l/h)	26	34
Injection rate (tracer solution)	(ml/min)	0.75 [1)]	400
Injection rate during rinsing	(ml/min)	500	500
Injection time (tracer solution)	(min)	8,643	8,592

[1)] Concentrated tracer solution as a sub-flow. Total injection flow rate was 500 ml/min.

Table 4-5. Sampling frequency during the tracer tests.

Pre-test			Main tracer test		
Time after injection start	Sample interval (min)		Time after injection start	Sample interval (min)	
	KLX15A	HLX27		KLX15A [1)]	HLX27
0–5 h	10		0–6 h	5	
5–48 h	60		6–24 h	60	
48–192 h	180		24–340 h	120	
0–2 h		10			
2–4 h		20	0–6 h		30
4–24 h		30	6–30 h		60
24–120 h		180	30–120 h		180
>120 h		360	>120 H		360

[1)] During the main tracer test every second tube was analysed for Uranine and the others for metals.

Samples were also taken from two depths in HLX27 using a tube sampling equipment as described in Section 3.3.2. The sampling was conducted at five occasions during the main tracer test period, once a week or every two weeks.

4.4.4 Water sampling

Water samples submitted for analyses according to SKB class 3 were taken during the pumping test. Four samples were collected, one immediately after pumping start, one after about three weeks of pumping and one at the end of the pumping, one day before the pumping was stopped. A fourth sample was taken prior to the test, after a short pumping. This sample was taken because there was little information about the chemical conditions in HLX27 and some data were needed for the planning of the test. Table 4-6 presents the date and time when the samples were taken together with the SKB sample number.

4.5 Data handling

Data from the pumping borehole (flow rate and pressure) was stored in the HMS system. All data from HMS (pumping and observation sections) was downloaded as .mio-files for further processing.

The results from the laboratory analyses were compiled in an Excel-file together with sample date for further processing, plotting and calculations.

4.6 Analysis and interpretation

4.6.1 Groundwater flow measurements

In the dilution method, a tracer is introduced and homogeneously distributed into a borehole test section. The tracer is subsequently diluted by the ambient groundwater, flowing through the borehole test section. The dilution of the tracer is proportional to the water flow through the borehole section and the groundwater flow is calculated from the rate with which the tracer concentration decreases with time, cf. /Gustafsson 2002/ and Figure 4-2.

Table 4-6. SKB class 3 water samples taken during the pumping test in HLX27.

Bh ID	Date and time of sample	Pumped section (mbl)	Sample type	Sample ID no	Remarks
HLX27	2008-03-18 16:40	6.03–164.7	WC080	15484	Short pumping
HLX27	2008-03-27 08:56	6.03–164.7	WC080	15485	
HLX27	2008-05-21 15:13	6.03–164.7	WC080	15486	
HLX27	2008-06-26 09:02	6.03–164.7	WC080	15487	

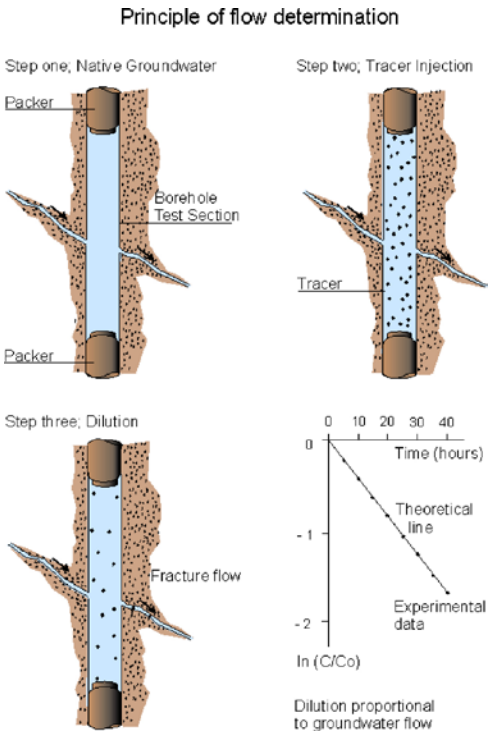

Figure 4-2. *General principles of dilution and flow determination.*

The so-called "dilution curves" were plotted as the natural logarithm of concentration versus time. Theoretically, a straight-line relationship exists between the natural logarithm of the relative tracer concentration (c/c_0, where c_0 is the initial concentration) and time, t (s):

$$\ln (c/c_0) = - (Q_{bh} /V) \cdot \Delta t \qquad (4\text{-}3)$$

where Q_{bh} (m^3/s) is the groundwater flow rate through the borehole section and V (m^3) is the volume of the borehole section. By plotting ln (c/c_0) or ln c versus t, and by knowing the borehole volume V, Q_{bh} may then be obtained from the straight-line slope.

The sampling procedure with a constant flow of 3–6 ml/h also creates a dilution of tracer. The sampling flow rate is therefore subtracted from the value obtained from Equation 4-3.

4.6.2 Pumping and interference test

Qualitative and quantitative evaluation have been carried out in accordance with the methodology description for interference tests, SKB MD 330.003, and reported in Section 5.3 below. Standard methods for constant flow rate tests in an equivalent porous medium were used for the evaluation of the responses in the test sections. The main objective of the interference test in HLX27 was to document how different fracture zones are connected hydraulically, to quantify their hydraulic properties and to clarify whether there are any major hydraulic boundaries in the area.

Data from all available observation sections were used in the primary qualitative analyses. The qualitative analysis of the responses in interference test in HLX27 was primarily based on linear time versus pressure diagrams together with corresponding diagrams of precipitation and any internal and/or external disturbances listed in Sicada data base. Linear diagrams of pressure versus time for all test sections are presented in Appendix 5.

For observation sections where unambiguous transient evaluation was possible the dominating flow regimes (pseudo-linear, pseudo-radial and pseudo-spherical flow, respectively) and possible outer boundary conditions were identified. In particular, pseudo-radial flow is reflected by a constant (horizontal) derivative in the diagrams, whereas no-flow and constant-head boundaries are characterized by a rapid increase and decrease of the drawdown derivative, respectively.

Quantitative evaluation was made in observation sections with a clear response to the pumping. A total of 25 sections were analysed with standard transient methods, mainly regarding transmissivity and storativity, described in e.g. /Kruseman and de Ridder 1990/. The tests were analysed as variable flow rate tests.

Other responding borehole sections included in the interference test were only qualitatively analysed, mainly by means of response analysis reported in Section 5.3.2 below. The borehole sections involved in the interference test that showed no or very weak and/or uncertain responses were not included in the response analysis. Sections with no or weak responses are presented in Table 5-2. In addition, the response in the pumping borehole HLX27 was evaluated as a single-hole pumping test according to the methods described in the instruction SKB MD 320.004 and /Moench 1985/.

The quantitative transient analysis was performed using the test analysis software AQTESOLV that enables both manual and automatic type curve matching. The transient evaluation was carried out as an iterative process of manual type curve matching and by employing automatic non-linear regression. The quantitative, transient interpretation of the hydraulic parameters of the observation sections (mainly transmissivity and storativity) is normally based on the identified pseudo-radial flow regime during the tests in log-log and lin-log data diagrams.

For the single-hole pumping test in HLX27 the storativity was calculated using an empirical regression relationship between storativity and transmissivity /Rhén et al. 1997/:

$$S = 0.0007 \cdot T^{0.5} \quad (4\text{-}4)$$

where S is the storativity (–) and T is transmissivity (m^2/s)

4.6.3 Tracer test

The concentration in the borehole at a certain time is reflected at the sampling point a short time later, since there is a delay caused by the transport time through the hoses from the section to the sample bottle/tube. Hence, the elapsed time must be corrected for the water residence time in the hoses. This can be done when the volume of the hoses and the flow rate is known. The corrected elapsed time was calculated for both KLX15A and HLX27 before plotting concentrations against elapsed time and evaluating the data. However, for HLX27 the delay was only about 30 seconds, hence this delay was neglected. The elapsed time is always referred to as the time since injection start.

For various reasons some of the data points were considered as outliers since they were obviously erroneous. Such data points were removed from the data set before any further calculations were made. No outliers were discovered in the Tb-DTPA and Cs^+ breakthrough curves. The reason for the diverging data points are in some cases easy to explain whereas others are more unclear. This is further described in Section 6.2. The outliers that were removed are marked with red ellipses in Figure 4-3. Also, the background level of concentration was determined and was subtracted from the concentration values for all tracers respectively.

A function of normalized mass flux against elapsed time was created as an input function for the model analysis. This takes into account the two different injection flow rates during the tracer injection period and the rinsing period. When normalising the mass flux it is also possible to plot the data from all tracers in the same scale. The data from the breakthrough curves were also calculated and presented as normalized mass flux. The procedure for calculating the normalized mass flux is further described in Appendix 4, where it is also explained how the total injected mass was calculated.

The total mass of tracer recovered was then calculated by integration of the breakthrough curves for mass flux in HLX27. Comparing the calculated total injected mass in KLX15A (M_{inj}) with the total mass detected in HLX27 (M_{pump}) gives the mass recovery.

$$Recovery\ (\%) = \frac{M_{pump}}{M_{inj}} \cdot 100 \quad (4\text{-}5)$$

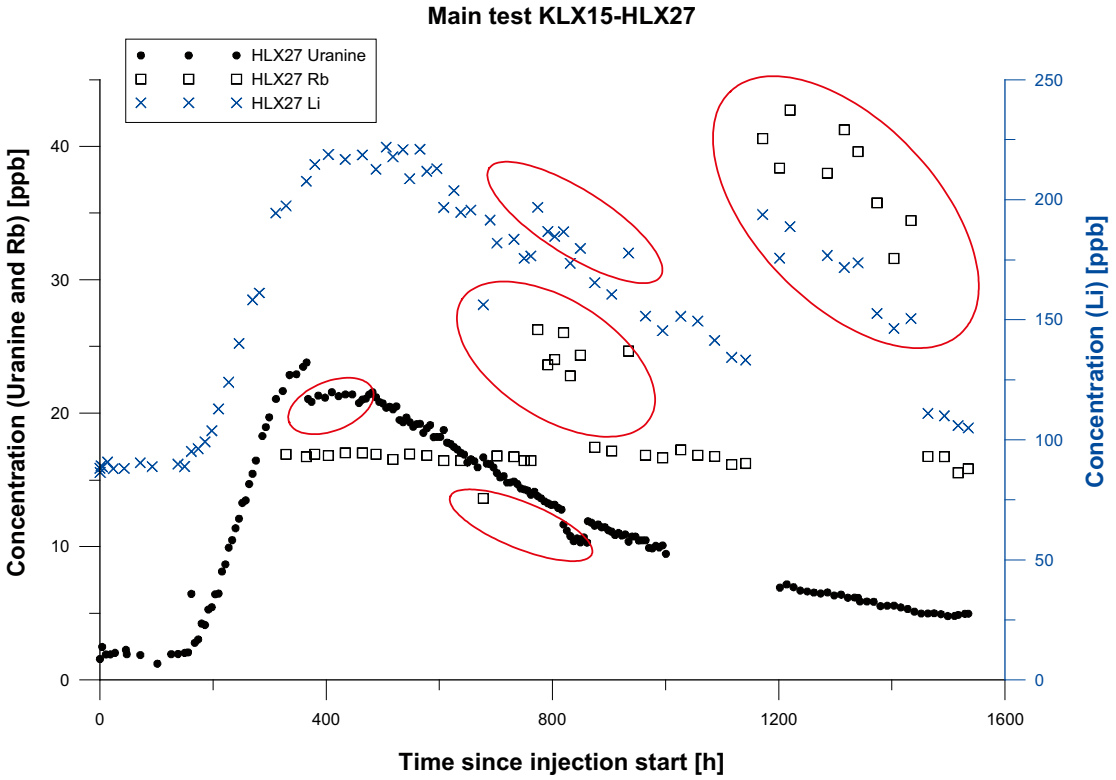

Figure 4-3. *Tracer concentration in HLX27 of Uranine, Li^+ and Rb^+. Outliers that were removed from the data set before any further calculations and evaluation are marked with red ellipses.*

Assumptions

- Complete mixing is assumed in the injection section, KLX15A:6.
- The flow out of section KLX15A:6 into the rock formation, is assumed to equal the injection flow rate (400 ml/min during the injection period of the main tracer test and 500 ml/min during rinsing with re-circulated water).
- Constant withdrawal rate from HLX27 (or for Rhodamine WT in the pre-test, two different constant flow rates).
- Constant injection flow rates are assumed (400 ml/min during the tracer injection period of the main test and 500 ml/min during rinsing with re-circulated water).

Modelling

The tracer breakthrough curves were evaluated using the one-dimensional transport models described in Section 3.5. Estimation of model parameters was accomplished by employing non-linear regression as outlined in Section 3.5.

Estimation parameters comprise tracer residence time (for non-sorbing tracers), dispersivity (or Peclet number) and a fracture retardation factor for sorbing tracers. For the matrix diffusion model, a composite matrix diffusion parameter (Equation 3-17) was estimated as well.

As a possible additional estimation parameter, a proportionality factor (*pf*) may be used. The parameter *pf* is simply a multiplying factor for the simulated tracer breakthrough curve. Alternatively, this parameter may be set a fixed value. With the assumptions made for calculation of normalized mass flux for injection and sampling, as described above, the value of *pf* is 1.0 at 100% tracer recovery.

Breakthrough curves for sorbing data may be estimated simultaneously with non-sorbing tracers or, alternatively, a sequential approach may be employed.

4.7 Nonconformities

- The pump in HLX27 stopped for about 24 hours during the injection of tracer for the main tracer test. The pump was replaced, but this pump was not powerful enough to provide the desired flow rate of 75 l/h. Hence, another short pump stop was made for a second pump replacement.
- The pump was deliberately stopped at one occasion to allow switching from diverting the pumped water in to the stream "Laxemarån" to an infiltration point near KLX03.
- There were some problems with the pump for the sub-flow of salt at a few occasions. Before the main tracer test begun it was discovered that the check valves did not work properly which caused water to leak into the tank instead. At another occasion it was discovered that the flow rate was too high due to a decreased pressure in the re-circulation hose.
- It was intended to take samples from two different depths in HLX27 during the whole test period to investigate if it was possible to determine which one of the two major inflows (105 mbl and 158 mbl) contributed to the tracer transport. However, the equipment could not be lowered deeper than to about 60 mbl due to a mistake during the installation. After the change of pumps this problem was corrected and samples could be taken during the main tracer test.
- A power failure occurred on May 25th. A diesel power generator was started after c. 30 minutes, hence the interruption was short. The use of the diesel power generator resulted in a somewhat higher pumping flow rate (80 l/min) for about 24 hours until the regular power supply was functioning again.
- A few other power failures also occurred (see Table 5-12). After the stops the flow rate was sometimes below the desired 75 l/min and sometimes higher for a day until manual adjustments were made.
- When the groundwater flow measurements during natural conditions were made, the pressure had not fully recovered from an earlier pumping in HLX27. Hence the data from this period cannot be regarded as representative for natural gradient conditions.
- For some of the observation sections in percussion boreholes the logging interval of pressure data was 10 minutes in connection with pump start, although the plan was to log and store data every 10 second.
- HLX38 was monitored using a logger in open borehole until June 2nd and only this period was evaluated. Then work with instrumentation of the boreholes started. At the end of the test period, four sections were installed. However, there are doubts about the quality of the data from this period, therefore it was not evaluated.

None of the above mentioned non-conformities are judged to have an impact on the results and conclusions of the performed tests.

5 Results

Original data from the reported activity are stored in the primary database Sicada. Data are traceable in Sicada by the Activity Plan number (AP PS 400-08-007). Only data in databases are accepted for further interpretation and modelling. The data presented in this report are regarded as copies of the original data. Data in the databases may be revised, if needed. However, such revision of the database will not necessarily result in a revision of this report, although the normal procedure is that major data revisions entail a revision of P-reports. Minor data revisions are normally presented as supplements, available at www.skb.se.

5.1 Nomenclature and symbols

The nomenclature and symbols used for the results of the single-hole and interference test are according to the Instruction for analysis of single-hole injection- and pumping tests (SKB MD 320.004) and the method description for interference tests (SKB MD 330.003), respectively (both are SKB internal controlling documents). The same applies for nomenclature and symbols used for the results from groundwater flow measurements and tracer tests which are carried out according to the method descriptions SKB MD 368.010 and SKB MD 530.006 respectively (SKB internal controlling documents. Additional symbols used are explained in the text.

Since the pressure in the boreholes are given in terms of groundwater levels in HMS both the terms pressure and groundwater level are used to explain the hydraulic conditions in the boreholes. Also, the term (hydraulic) “head” is used synonymous to groundwater level.

5.2 Groundwater flow measurements

The results obtained are presented in Table 5-1 including measured groundwater flow rates together with transmissivity and section volume. In Figure 5-1 and Figure 5-2, the tracer dilution curves from KLX15A:3 and KLX15A:6 are shown. The flow rate is calculated from the slope of the straight-line fit.

No clear influence of the pumping in HLX27 is observed in any of the two tested sections. The natural period is however affected by an earlier short pumping performed in HLX27. The groundwater levels during the test period are not fully recovered during the measurement of groundwater flow with natural gradient, as seen in Figure 5-3. Hence, it is likely that the direction of the groundwater flow measured during this period is influenced by the pumping and does not fully represent undisturbed conditions. Earlier groundwater flow measurements during natural gradient in these two sections were conducted just a few months earlier. The results are shown in Figure 5-4 and they demonstrate groundwater flow of 18.2 ml/min and 3.0 ml/min for sections 3 and 6 respectively /Thur 2008/. When this is considered the flow rate is significantly increased in both sections when pumping in HLX27.

Table 5-1. Measured groundwater flow in KLX15A:3 and KLX15A:6.

Borehole/ section	Borehole length (mbl)	Transmissivity (m^2/s)	Volume (l)	Measured flow (ml/min) Natural gradient	Measured flow (ml/min) Stressed gradient [3]
KLX15A:3	623–640	2.3E–07 [1]	57.61	48	27/52
		9.0E–07 [2]		18 [4]	
KLX15A:6	260–272	1.1E–05 [1]	29.38	43	31
		3.4E–06 [2]		3 [4]	

[1] From PSS measurements 20 m section, transient evaluation, /Enachescu et al. 2007a/.

[2] From PFL measurements /Pöllänen et al. 2007/.

[3] Where two flows are given, the first occurs early and the other one later. See tracer dilution graph, Figure 5-1.

[4] From earlier groundwater flow measurements /Thur 2008/.

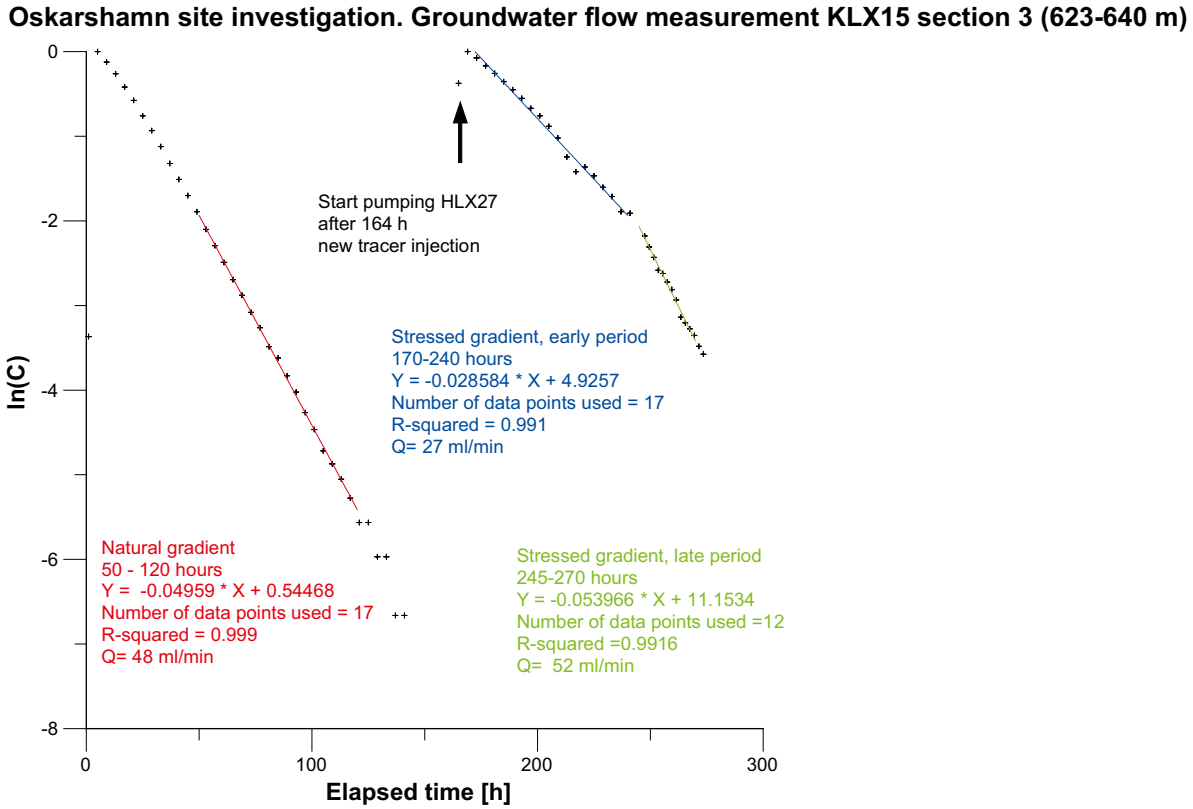

Figure 5-1. *The tracer dilution graph (logarithm of concentration versus time) for borehole KLX15A section 3, including straight-line fits during both natural and pumped conditions.*

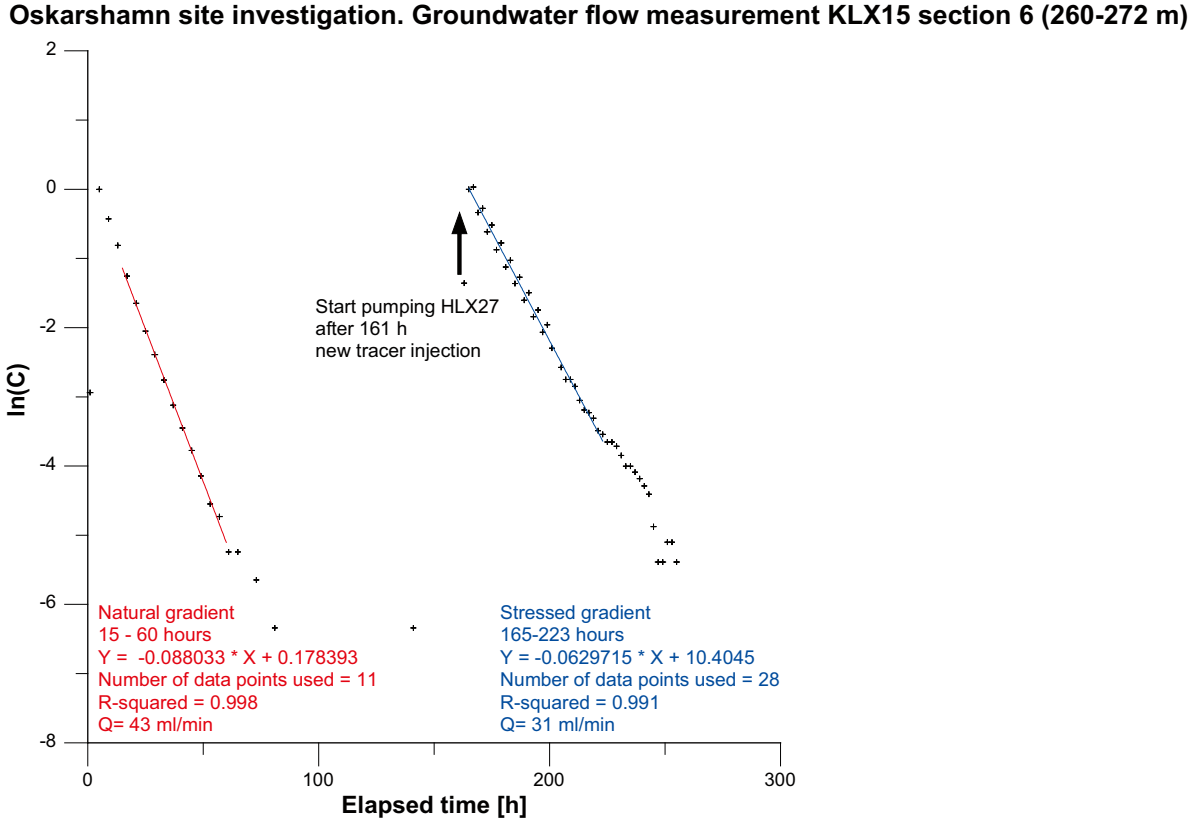

Figure 5-2. *The tracer dilution graph (logarithm of concentration versus time) for borehole KLX15A section 6, including straight-line fits during both natural and pumped conditions.*

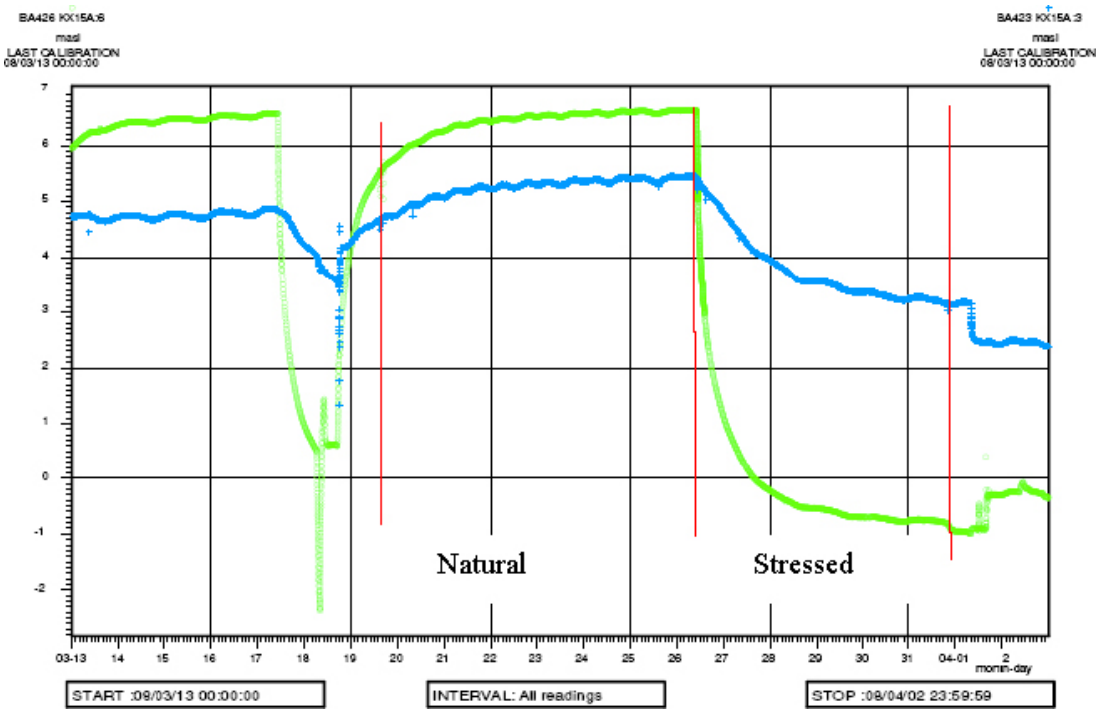

Figure 5-3. *Groundwater levels in sections 3 (blue) and 6 (green) in borehole KLX15A during the groundwater flow measurement periods (natural and stressed).*

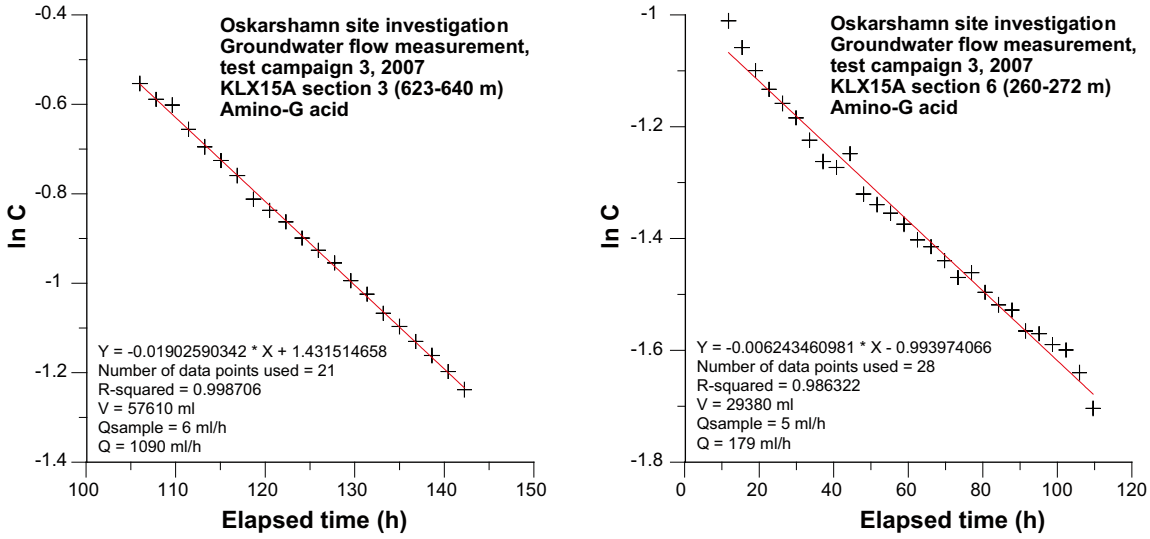

Figure 5-4. *Earlier groundwater flow measurements during natural conditions in KLX15A:3 (left) and KLX15A:6 (right) /Thur 2008/.*

5.3 Interference test in HLX27

5.3.1 General

The flow period during the interference test in HLX27 lasted from March 26th to June 26th, 2008. The subsequent recovery period analysed ended July 20th . The exact start and stop times of the flow and recovery period are given in Table A5-1 in Appendix 5. The observed precipitation, air pressure and sea water level during the interference test period are shown in Figure A5-1. The flow rate and pressure in the pumping borehole are shown in Figures A5-2. Linear diagrams of the groundwater level versus time in all observation boreholes are presented in Figures A5-3 through A5-18 in Appendix 5.

The locations of boreholes in the Laxemar area, including the pumping borehole HLX27, are shown in Figure 5-5. Observation borehole KLX10B, originally intended to be included in the interference test, did not provide any pressure data and was therefore excluded.

In Table 5-2, all observation sections included in the interference test are listed together with an assessment of the type of responses, distances to HLX27 and estimated transmissivity from previous single-hole tests in the observation sections. Visual inspection of the pressure responses in the observation sections in linear diagrams indicates that presumed responses were registered in 32 sections, i.e. c. 40% of the totally 75 observation borehole sections included in the interference test. Clear responses were observed in 25 sections and transient evaluation was made of the responses from these sections. Seven sections showed some response to the pumping but the data were either too uncertain or of such poor quality that no transient evaluation was possible to conduct.

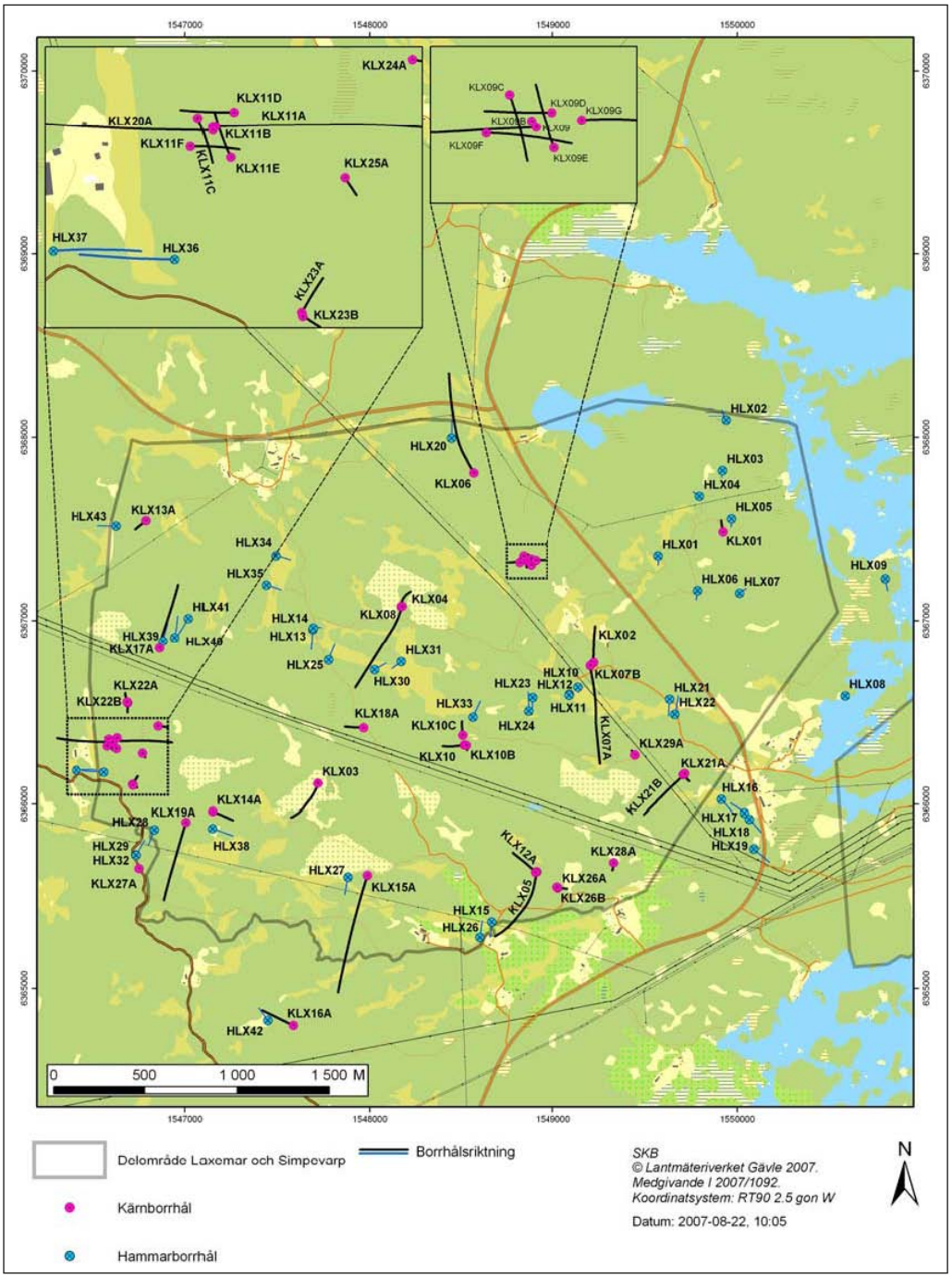

Figure 5-5. *Locations of boreholes in the Laxemar investigation area. The pumping borehole HLX27 is located in the southern central part of the map.*

Table 5-2. Observation sections used, type of responses, distances to HLX27, estimated transmissivity from previous single-hole tests in the interference test in HLX27 at Laxemar.

Bh ID	Test section (mbl)	Type of response [1)]	Distance to HLX27:131.5 (m)	Transmissivity from single-hole tests (m^2/s)	Comments
HLX15	12.04–151.90	1	822.0	2.5E–7	
HLX26	11.00–151.20	1	768.5	1.5E–7	
HLX38	15.02–199.50	1	738.2	1.2E–4	
HLX42:1	30.00–152.60	1	805.0	4.3E–5	
HLX42:2	9.10–29.00	4	822.9		
KLX03:1	965.50–971.50	3	958.2	4.5E–7–4.6E–7	Missing or defect data
KLX03:2	830.50–964.50	1	898.8	below l.m.l. of PFL	
KLX03:3	752.50–829.50	1	814.8	6.0E–7–1.2E–6	
KLX03:4	729.50–751.50	1	777.6	4.6–5.9E–6	
KLX03:5	652.50–728.50	1	742.9	2.5–4.9E–7	
KLX03:6	465.50–651.50	1	663.9	9.7E–9–1.3E–8	
KLX03:7	349.50–464.50	1	596.4	2.9E–7–1.6E–6	
KLX03:8	199.50–348.50	1	566.4	2.0–2.8E–6	
KLX03:9	193.50–198.50	1	564.8	9.2E–6–1.3E–5	
KLX03:10	100.05–192.50	1	570.1	3.0E–7–4.5E–7	
KLX05:1	721.00–1,000.00	3	1,107.8	6.2E–9–2.2E–8	
KLX05:2	634.00–720.00	3	1,057.9	1.0E–8–1.6E–8	
KLX05:3	625.00–633.00	3	1,047.7	5.6E–9–1.2E–8	
KLX05:4	501.00–624.00	3	1,036.7	below l.m.l. of PFL	
KLX05:5	361.00–500.00	3	1,025.5	3.7E–9–2.1E–8	
KLX05:6	256.00–360.00	3	1,022.9	2.2E–8	Missing or defect data
KLX05:7	241.00–255.00	3	1,024.4	1.9E–6–2.2E–6	Missing or defect data
KLX05:8	220.00–240.00	3	1,025.1	1.6E–6–6.2E–7	Missing or defect data
KLX05:9	128.00–219.00	3	1,028.2	1.5E–6—6.6E–6	Missing or defect data
KLX05:10	15.00–127.00	3	1,039.5	9.2E–6–1.6E–5*	Missing or defect data
KLX10:1	711.00–1,001.00	3	1,201.1	1.6E–7–1.7E–7	Missing or defect data
KLX10:2	689.00–710.00	3	1,121.9	4.5E–8–6.7E–7	Missing or defect data
KLX10:3	465.00–688.00	3	1,071.9	4.8E–8–9.1E–8	
KLX10:4	369.00–464.00	3	1,026.8	3.2E–6–1.4E–5	
KLX10:5	351.00–368.00	3	1,016.4	7.4E–7–1.7E–6	Missing or defect data
KLX10:6	291.00–350.00	2	1,014.8	1.0E–5–2.8E–4	
KLX10:7	131.00–290.00	2	1,011.0	5.4E–5–2.2E–4	
KLX10:8	12.10–130.00	2	1,003.8	(1.9E–5–2.8E–5)*	
KLX10C:1	66.00–146.25	4	1,097.2	1.3E–6	
KLX10C:2	32.00–65.00	3	1,076.4	6.1E–6	
KLX10C:3	9.00–31.00	3	1,067.8	2.8E–8	
KLX12A:1	546.00–602.29	2	1,034.1	5.6E–10–5.3E–9	
KLX12A:2	535.00–545.00	2	1,025.6	1.3E–7–3.6E–7	
KLX12A:3	426.00–534.00	2	1,013.4	6.0E–9–4.3E–8	
KLX12A:4	386.00–425.00	3	1,003.1	2.0E–7–8.5E–7	
KLX12A:5	291.00–385.00	3	998.7	9.2E–10–1.6E–8	
KLX12A:6	160.00–290.00	3	1,004.2	4.0E–7–1.5E–6	
KLX12A:7	142.00–159.00	4	1,014.2	2.0E–6–2.6E–6	
KLX12A:8	104.00–141.00	4	1,019.3	2.0E–6–2.6E–6	
KLX12A:9	17.92–103.00	4	1,033.0	no data	
KLX14A:1	123.00–176.27	1	739.1	1.9E–6	
KLX14A:2	77.00–122.00	1	774.5	6.1E–5	
KLX14A:3	6.45–76.00	2	816.4	6.2E–6	
KLX15A:1	902.00–1,000.43	4	798.3	below l.m.l.–8.3E–8	
KLX15A:2	641.00–901.00	1	619.4	2.5E–8–8.4E–8	
KLX15A:3	623.00–640.00	1	481.7	2.3E–7–9.0E–7	
KLX15A:4	481.00–622.00	1	403.2	1.3E–7–4.8E–7	

Bh ID	Test section (mbl)	Type of response [1)]	Distance to HLX27:131.5 (m)	Transmissivity from single-hole tests (m^2/s)	Comments
KLX15A:5	273.00–480.00	1	235.7	2.0E–6–4.3E–6	
KLX15A:6	260.00–272.00	1	140.4	3.7E–6–1.1E–5	
KLX15A:7	191.00–259.00	1	112.4	1.3E–6–1.6E–6	
KLX15A:8	79.00–190.00	1	95.3	1.8E–5–1.1E–4	
KLX15A:9	11.65–78.00	1	147.6	3E6	
KLX16A:1	327.00–433.55	3	821.6	1.2E–7–3.7E–7	
KLX16A:2	86.00–326.00	1	787.4	1.1E–4–2.8E–4	
KLX16A:3	11.25–85.00	1	789.2	8.3E–6–3.4E–4	
KLX18A:1	571.00–611.28	3	1,001.0	9.4E–7–1.9E–6	
KLX18A:2	490.00–570.00	3	973.5	6.3E–7–7.7E–7	
KLX18A:3	472.00–489.00	3	953.8	5.4E–8–1.1E–7	
KLX18A:4	315.00–471.00	3	924.7	4.2E–6–3.6E–5	
KLX18A:5	155.00–314.00	3	892.3	5.7E–8–2.7E–7	
KLX18A:6	104.00–154.00	3	886.0	5.7E–6–3.5E–5	
KLX18A:7	11.83–103.00	3	889.0	no data	
KLX19A:1	661.00–800.07	3	1,091.9	4.9E–7–1.5E–6	
KLX19A:2	518.00–660.00	3	1,026.9	below l.m.l. of PFL	
KLX19A:3	509.00–517.00	3	998.0	1.0E–6–4.9E–6	Missing or defect data
KLX19A:4	481.50–508.00	3	991.8	below l.m.l. of PFL	
KLX19A:5	311.00–480.50	3	963.0	3.8E–7–1.8E–6	
KLX19A:6	291.00–310	3	933.7	1.1E–5–9.1E–4	
KLX19A:7	136.00–290	3	944.2	1.4E–6–4.3E–6	Missing or defect data
KLX19A:8	92.75–135.00	3	935.0	1.2E–4–3.0E–4	Missing or defect data

[1)] 1 = clear response, 2 = some response but not evaluated, 3 = response can neither be confirmed nor rejected, 4 = no response.

* Below c. 100 mbl.

Eight of the observation sections were considered as unaffected by the pumping during the interference test. Finally, in as many as 35 sections it cannot be confirmed if the sections were affected or not by the pumping. The reasons for this are small drawdowns at long distances in combination with natural disturbances (e.g. precipitation, tidal effects), external disturbances (e.g. other pumping or drilling activities) or defect or missing data.

In Appendix 5, observed test data in linear diagrams together with comments on the test data are presented section by section, whereas the test diagrams showing the transient evaluations are shown in Appendix 6.

Before the analyses of the test responses, all pressure data from the observation boreholes presented in this report have been corrected for atmospheric pressure changes by subtracting the latter pressure from the measured (absolute) pressure. In addition, corrections for the naturally decreasing head trend have been done in all observation sections as discussed below. No other corrections of the measured drawdown due to e.g. precipitation, tidal effects etc have been made.

During the interference test, approximately 125 mm of total precipitation (of which c. 50 mm during the flow period) was reported at two stations in the vicinity of the boreholes included in the test, see Figure A5-1 in Appendix 5. The rain that fell just before stop of pumping and during the recovery period may in some boreholes have influenced the pressure in the observation boreholes. In Figure A5-1, the air pressure together with the sea-water level during the interference test period, as recorded from a station in the vicinity of the investigation area, are also included.

There are strong indications of a natural trend of decreasing groundwater levels during the entire interference test period. At the end of the recovery period analysed, the pressure in most observation sections had not returned to the levels that prevailed prior to start of pumping and the decreasing natural trend continued at the end of this period. An example of this effect can be observed in Figure 5-6.

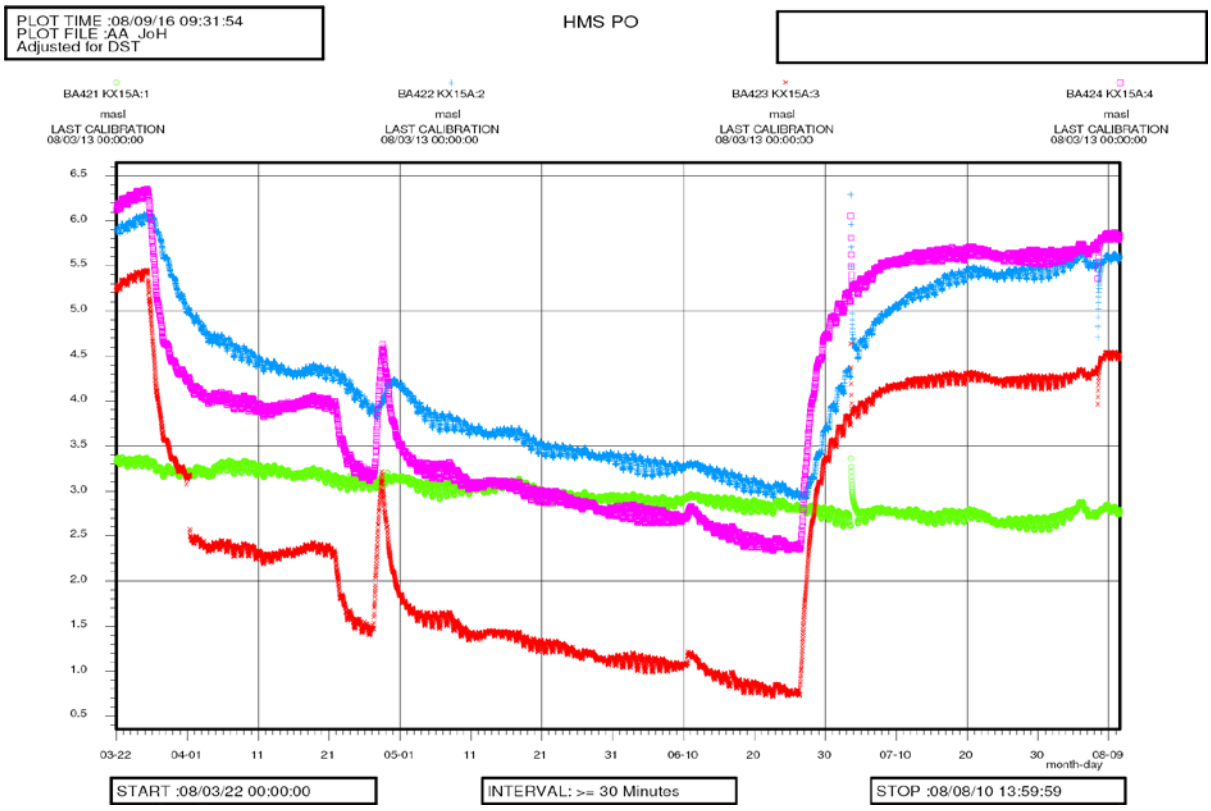

Figure 5-6. *Linear plot of observed head versus time in observation borehole KLX15A, sections 1 to 4 during pumping in HLX27 illustrating the natural decreasing head trend. KLX15A:1 is considered unaffected by the pumping test and only affected by the decreasing natural head trend. Section 1 = green, section 2 = blue, section 3 = red, section 4 = pink.*

Observed and corrected head for the naturally decreasing trend together with corrected drawdown and recovery data are presented in the test diagrams in Appendix 6. The correction procedure is described in Appendix 7. The magnitude of the natural trend generally varies from section to section.

In several of the observation sections, the head showed an oscillating behaviour. This is believed to be caused by so called tidal fluctuations or earth tides in combination with changes of the sea water level. These phenomena have, to some extent, been investigated previously at Forsmark by /Ludvigson et al. 2004/.

The observed and corrected maximal drawdown (s_p) during the flow period of the interference test in HLX27 together with the estimated response time lags (dt_L) in all responding observation sections are shown in Tables 5-9 and 5-10 in Section 5.3.2. The response time is here defined as the time lag after start of pumping until a drawdown response of 0.1 m was observed in the observation section.

5.3.2 Summary of the results of the interference test in HLX27

A compilation of measured test data from the pumping borehole HLX27 and the observation boreholes are shown in Tables 5-3 and 5-4, respectively. In Tables 5-5 and 5-6, calculated hydraulic parameters for the pumping borehole and the responding observation sections are presented. The evaluation of the pumping borehole HLX27 is also presented in the Test Summary Sheet in Table 5-7.

Table 5-3. Summary of test data from the pumping borehole during the interference test in HLX27 in the Laxemar area.

Section (mbl)	Test Type[1)]	p_i (m)	Q_m (m^3/s)	p_F (m)	p_i (m) Corr	p_p (m) Corr	p_F (m) Corr	Q_p (m^3/s)	V_p (m^3)
6.03–164.70	1B	37.93	$1.11 \cdot 10^{-3}$	37.46	37.93	16.79	37.93	$1.25 \cdot 10^{-3}$	$8.79 \cdot 10^{3}$

[1)] 1B: Pumping test-submersible pump.

p_i = Pressure in test section before start of the flow period.

p_p = Pressure in test section before stop of the flow period.

p_F = Pressure in test section at end of the recovery period.

Q_p = Flow in test section immediately before stop of flow period.

Q_m = Arithmetical mean flow rate during the flow period.

V_p = Total water volume pumped out during the flow period.

Table 5-4. Summary of test data from the responding observation borehole sections involved in the interference test in HLX27 in the Laxemar area.

Pumping borehole ID	Borehole ID	Section (mbl)	Test Type[1)]	h_i (m)	h_p (m)	h_F (m)	h_i corrected (m)	h_p corrected (m)	h_F corrected (m)
HLX27	HLX15	12.04–151.90	2	5.7	3.72	5.19	5.7	4.13	5.71
HLX27	HLX26	11.00–151.20	2	4.04	2.82	3.68	4.04	3.1	4.04
HLX27	HLX38	15.02199.50	2	5.63	5.20[2)]	–	5.63	5.20[2)]	–
HLX27	HLX42:1	30.00–152.60	2	9.63	7.41	8.93	9.63	7.95	9.62
HLX27	KLX03:2	830.50–964.50	2	10.15	8.51	9.58	10.15	8.96	10.15
HLX27	KLX03:3	752.50–829.50	2	10.33	8.56	9.59	10.32	9.14	10.32
HLX27	KLX03:4	729.50–751.50	2	10.15	8.47	9.54	10.15	8.95	10.15
HLX27	KLX03:5	652.50–728.50	2	10.33	9.07	9.63	10.33	9.62	10.33
HLX27	KLX03:6	465.50–651.50	2	9.91	8.57	9.17	9.91	9.15	9.91
HLX27	KLX03:7	349.50–464.50	2	9.62	8.36	8.97	9.62	8.88	9.62
HLX27	KLX03:8	199.50–348.50	2	10.25	8.86	9.98	10.25	9.07	10.25
HLX27	KLX03:9	193.50–198.50	2	10.28	8.9	10.04	10.28	9.09	10.28
HLX27	KLX03:10	100.05–192.50	2	10.02	8.47	9.78	10.02	8.66	10.02
HLX27	KLX14A:1	123.00–176.27	2	6.07	5.33	5.66	6.07	5.65	6.07
HLX27	KLX14A:2	77.00–122.00	2	5.32	4.68	4.82	5.32	5.07	5.31
HLX27	KLX14A:3	6.45–76.00	2	10.79	10.5	10.59	10.79	10.66	10.79
HLX27	KLX15A:2	641.00–901.00	2	6.04	3.37	5.49	6.04	2.94	6.04
HLX27	KLX15A:3	623.00–640.00	2	5.41	0.74	4.32	5.41	1.6	5.41
HLX27	KLX15A:4	481.00–622.00	2	6.31	2.36	5.71	6.31	2.82	6.3
HLX27	KLX15A:5	273.00–480.00	2	6.75	2.63	6.23	6.75	3.06	6.76
HLX27	KLX15A:6	260.00–272.00	2	6.6	–4.63	6.15	6.6	–4.27	6.6
HLX27	KLX15A:7	191.00–259.00	2	7.01	–4.72	6.58	7.01	–4.31	7
HLX27	KLX15A:8	79.00–190.00	2	6.96	–4.16	6.49	6.97	–3.75	6.96
HLX27	KLX15A:9	11.65–78.00	2	7.14	–1.88	6.68	7.15	–1.52	7.14
HLX27	KLX16A:2	86.00–326.00	2	8.44	6.25	7.77	8.44	6.77	8.44
HLX27	KLX16A:3	11.25–85.00	2	11.09	9.03	9.79	11.09	10.06	11.09

[1)] 1B: Pumping test-submersible pump, 2: Interference test (observation borehole during pumping in another borehole).

[2)] Mean value at the end of the data series from HLX38 which was stopped 080602.

h_i = Water level above reference level in test section before start of flow period.

h_p = Water level above reference level in test section before stop of flow period.

h_F = Water level above reference level in test section at the end of recovery period.

Table 5-5. Summary of calculated hydraulic parameters from the single-hole test in HLX27 in the Laxemar area.

Pumping borehole ID	Section (mbl)	Test type	Q/s (m^2/s)	T_M (m^2/s)	T_T (m^2/s)	ζ (–)	C (m^3/Pa)	S* (–)
HLX27	6.03–164.70	1B	$5.80 \cdot 10^{-5}$	$4.81 \cdot 10^{-5}$	$2.74 \cdot 10^{-5}$	–6.05	$2.05 \cdot 10^{-6}$	$3.66 \cdot 10^{-6}$

Q/s = specific flow for the pumping borehole (m^2/s).

T_M = steady state transmissivity from Moye´s equation (m^2/s).

T_T = transmissivity from transient evaluation of single-hole test (m^2/s).

S* = assumed/calculated storativity by estimation of the skin factor (–).

C = wellbore storage coefficient (m^3/Pa).

ζ = skin factor (–).

Table 5-6. Summary of calculated hydraulic parameters from the responding observation boreholes during the interference test in HLX27 in the Laxemar area.

Pumping borehole ID	Observation borehole ID	Section (mbl)	Test type	T_o (m^2/s)	S_o (–)	T_o/S_o (m^2/s)	K'/b' (s^{-1})
HLX27	HLX15	12.04–151.90	2	3.76E–05	1.16E–04	0.32	4.87E–11
HLX27	HLX26	11.00–151.20	2	1.66E–04	1.13E–04	1.47	8.95E–11
HLX27	HLX38	15.02–199.50	2	3.73E–05	5.12E–05	0.73	4.47E–10
HLX27	HLX42:1	30.00–152.60	2	1.09E–04	7.19E–05	1.52	2.43E–11
HLX27	KLX03:2	830.50–964.50	2	3.50E–05	5.85E–05	0.60	8.08E–11
HLX27	KLX03:3	752.50–829.50	2	6.69E–05	1.49E–04	0.45	7.75E–11
HLX27	KLX03:4	729.50–751.50	2	5.53E–05	1.46E–04	0.38	1.01E–10
HLX27	KLX03:5	652.50–728.50	2	3.17E–05	2.17E–04	0.15	2E–10
HLX27	KLX03:6	465.50–651.50	2	1.51E–05	1.59E–04	0.09	2.17E–10
HLX27	KLX03:7	349.50–464.50	2	2.31E–05	2.53E–04	0.09	3E–10
HLX27	KLX03:8	199.50–348.50	2	1.11E–04	1.73E–04	0.64	1.5E–10
HLX27	KLX03:9	193.50–198.50	2	1.24E–04	1.53E–04	0.81	1.39E–10
HLX27	KLX03:10	100.05–192.50	2	3.72E–05	1.32E–04	0.28	2.03E–10
HLX27	KLX14A:1	123.00–176.27	2	2.76E–05	5.31E–05	0.52	4.17E–10
HLX27	KLX14A:2	77.00–122.00	2	1.40E–04	6.07E–05	2.31	3.75E–10
HLX27	KLX15A:2	641.00–901.00	2	3.44E–05	8.80E–05	0.39	1.95E–11
HLX27	KLX15A:3	623.00–640.00	2	8.06E–05	2.50E–05	3.22	5.05E–11
HLX27	KLX15A:4	481.00–622.00	2	7.07E–05	4.90E–05	1.44	1.4E–10
HLX27	KLX15A:5	273.00–480.00	2	6.72E–05	1.17E–04	0.57	7.53E–12
HLX27	KLX15A:6	260.00–272.00	2	5.45E–05	4.77E–06	11.43	1.64E–11
HLX27	KLX15A:7	191.00–259.00	2	5.05E–05	8.67E–06	5.82	4E–11
HLX27	KLX15A:8	79.00–190.00	2	4.78E–05	1.89E–05	2.53	–
HLX27	KLX15A:9	11.65–78.00	2	3.61E–05	3.12E–05	1.16	2.17E–11
HLX27	KLX16A:2	86.00–326.00	2	1.14E–04	7.46E–05	1.53	–
HLX27	KLX16A:3	11.25–85.00	2	5.26E–05	2.70E–04	0.19	4.87E–11

T_o = transmissivity from transient evaluation of observation section (m^2/s).

S_o = storativity from transient evaluation of observation section (–).

T_o/S_o = hydraulic diffusivity (m^2/s).

K'/b' = leakage coefficient from transient evaluation (s^{-1}).

Table 5-7. Test Summary Sheet – Pumping test in HLX27 during the interference test.

Test Summary Sheet – Pumping section HLX27: 6.03–164.70 mbl			
Project:	PLU	Test type:	1B
Area:	Laxemar	Test no:	1
Borehole ID:	HLX27	Test start:	2008-03-26 10:31:02
Test section (mbl):	6.03–164.70	Responsible for test performance:	GEOSIGMA AB
Section diameter, 2·rw (m):	0.137	Responsible for test evaluation:	GEOSIGMA AB J-E Ludvigson

Linear plot pressure – Entire test period

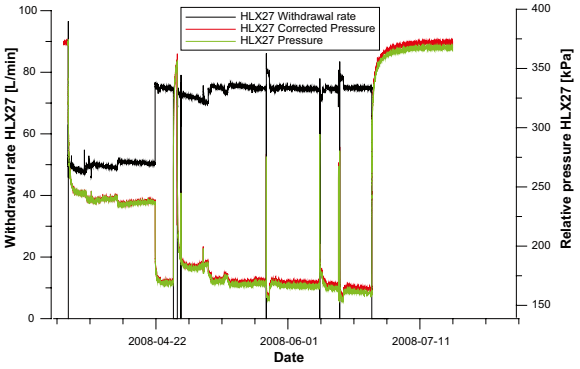

Flow period		**Recovery period**	
Indata		Indata	
p_0 (kPa)			
p_i (kPa)	372.21		
p_p(kPa)	164.79*	p_F (kPa)	372.21*
Q_p (m^3/s)	$1.25 \cdot 10^{-3}$		
tp (s)	7,947,240	t_F (s)	2,115,300
S*	$4.65 \cdot 10^{-6}$	S*	$3.66 \cdot 10^{-6}$
EC_w (mS/m)			
Te_w(gr C)			
Derivative fact.	0.3	Derivative fact.	0.2
Results		**Results**	
Q/s (m^2/s)	$5.8 \cdot 10^{-5}$		

Log-Log plot incl. derivate – Flow period – early phase

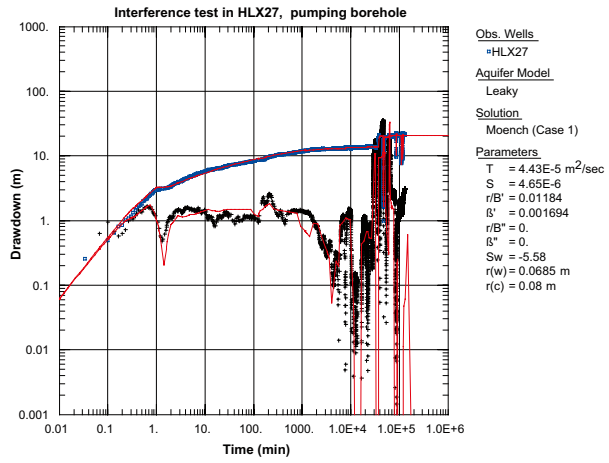

T_{Moye}(m^2/s)	$4.81 \cdot 10^{-5}$		
Flow regime:	WBS-> PRF->PSF	Flow regime:	WBS-> PRF->PSF
t_1 (s)	3	dt_{e1} (s)	100
t_2 (s)	1,000	dt_{e2} (s)	1,000
T_w (m^2/s)	$4.43 \cdot 10^{-5}$	T_w (m^2/s)	$2.74 \cdot 10^{-5}$
S_w (–)		S_w (–)	
K_{sw} (m/s)		K_{sw} (m/s)	
S_{sw} (1/m)		S_{sw} (1/m)	
C (m^3/Pa)	$2.05 \cdot 10^{-6}$	C (m^3/Pa)	$2.05 \cdot 10^{-6}$
C_D (–)		C_D (–)	
ξ (–)	–5.58	ξ (–)	–6.05
T_{GRF}(m^2/s)		T_{GRF}(m^2/s)	
S_{GRF}(–)		S_{GRF}(–)	
D_{GRF} (–)		D_{GRF} (–)	

Log-Log plot incl. derivative – Recovery period

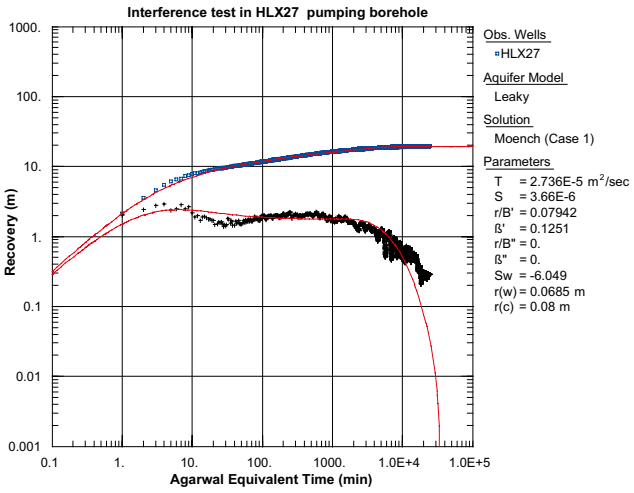

Interpreted formation and well parameters.

Flow regime:	WBS-> PRF->PSF	C (m^3/Pa)	$2.05 \cdot 10^{-6}$
t_1 (s)	100	C_D (–)	
t_2 (s)	1,000	ξ (–)	–6.05
T_T (m^2/s)	$2.74 \cdot 10^{-5}$		
S (–)	3.66e–06		
K_s (m/s)			
S_s (1/m)			

Comments: After initial wellbore storage, pseudo-radial flow occurred during c. 3–1,000 min transitioning to slightly pseudo-spherical (leaky) flow during the first part of the flow period. After the change of flow rate a transition to a new flow regime occurs. During the recovery period, initial wellbore storage effects dominated followed by a transition to pseudo-radial flow between c. 100–1,000 min and pseudo-spherical (leaky) flow by the end of the period. The evaluation of the flow period was made on the first phase. The agreement in evaluated parameter values between the flow and recovery period is good. The parameter values from the recovery period are selected as the most representative.

* Corrected pressure for naturally decreasing pressure trend.

5.3.3 Response analysis and estimation of the hydraulic diffusivity

A response analysis according to the method description for interference tests was made. All responding sections are included in the response analysis. However, since only one interference test was performed, no response matrix was made. The response time lags (dt_L) in the responding observation sections during pumping in HLX27 are shown in Table 5-9. The lag times were derived from the corrected drawdown curves in the observation borehole sections at the actual drawdown of 0.1 m.

Because of disturbances, e.g. oscillating head or responses to other activities in the area, see for instance Figure 5-2, it was sometimes difficult to determine the exact time lag for a drawdown of 0.1 m. It was possible, however, to make approximate estimates of the lag times from the drawdown curves. The estimated time lag for many of the responding observation sections must thus be considered as rough estimates. The corrected drawdown during the flow period was used in the response analysis.

The following response parameters are used in the response analysis presented below:

$dt_L[s = 0.1\ m]$ = time after start of pumping (s) at a drawdown s = 0.1 m in the observation section. Drawdown data should be corrected for the naturally decreasing head trend.

r_s = euclidian distance between the hydraulic point of application (hydr. p.a.) in the pumping borehole and observation borehole (m).

s_p = maximal drawdown in the observation borehole/section (m).

s_{p_corr} = maximal drawdown in the observation borehole/section (m) corrected for the naturally decreasing head trend.

Q_p = pumping flow rate by the end of the flow period (m^3/s).

From the above response parameters the following response indices are defined according to SKB MD 330.003:

Index 1 = $r_s^2/dt_L[s = 0.1\ m]$ = normalized distance with respect to the lag time (m^2/s).

Index 2 = s_p/Q_p = normalized drawdown with respect to the pumping flow rate (s/m^2).

Index 2_new = $s_p/Q_p * \ln(r_s/r_0)$ = same as above but including a weight factor for the distance to the pumping borehole ($r_0 = 1$).

Index 2 has been used in previous response analyses. However, in this investigation Index 2 was not calculated but instead, Index 2_new.

In Tables 5-9 and 5-10 the 25 sections with clear responses (denoted "1" in Table 5-2) are included. Index 1 and Index 2_new were calculated, based on the corrected head data from the flow period. Index 1 is directly related to the hydraulic diffusivity (T/S) of the formation and Index 2_new reflects the strength of the response. The numerical values of the indices are presented in Table 5-9 and 5-10, respectively together with a classification of the indices. The classification of the response indices is shown below in Table 5-8.

Table 5-8. Classification of the response indices. The lag time dt_L is based on a drawdown s = 0 .1 m.

Index 1 (r_s^2/dt_L)	Response	Code
$r_s^2/dt_L > 100\ m^2/s$	Excellent	E
$10 < r_s^2/dt_L \le 100\ m^2/s$	High	H
$1 < r_s^2/dt_L \le 10\ m^2/s$	Medium	M
$0.1 < r_s^2/dt_L \le 1\ m^2/s$	Low	L
Index 2-new (s_p/Q_p) · ln(r_s/r_0)	**Response**	**Code**
$(s_p/Q_p)*\ln(r_s/r_0) > 5\cdot10^5\ s/m^2$	Excellent	E
$5\cdot10^4 < (s_p/Q_p)*\ln(r_s/r_0) \le 5\cdot10^5\ s/m^2$	High	H
$5\cdot10^3 < (s_p/Q_p)*\ln(r_s/r_0) \le 5\cdot10^4\ s/m^2$	Medium	M
$(s_p/Q_p)*\ln(r_s/r_0) \le 5\cdot10^3\ s/m^2$	Low	L
$s_p < 0.1\ m$	No response	N

Table 5-9. Calculated response lag times corresponding to a drawdown of 0.1 m and distances together with Index 1 for the responding observation sections in the interference test in HLX27.

Pumping borehole	Observation borehole	Section (mbl)	dt_L(s) [s=0.1 m]	r_s (m)	Index 1: r_s^2/dt_L (m^2/s) [s=0.1 m]	Index 1 classification
HLX27	HLX15	12.04–151.90	54,232	822	12.5	H
HLX27	HLX26	11.00–151.20	99,390	768.5	5.9	M
HLX27	HLX38	15.20–199.50	151,800	738.2	3.6	M
HLX27	HLX42:1	30.00–152.60	96,000	805	6.7	M
HLX27	KLX03:2	830.50–964.50	170,940	899	4.7	M
HLX27	KLX03:3	752.50–829.50	96,540	815	6.9	M
HLX27	KLX03:4	729.50–751.50	98,340	777.6	6.1	M
HLX27	KLX03:5	652.50–728.50	212,900	743	2.6	M
HLX27	KLX03:6	465.50–651.50	240,000	664	1.8	M
HLX27	KLX03:7	349.50–464.50	174,540	596.4	2.0	M
HLX27	KLX03:8	199.50–348.50	92,340	566.4	3.5	M
HLX27	KLX03:9	193.50–198.50	85,740	564.8	3.7	M
HLX27	KLX03:10	100.05–192.50	146,940	570	2.2	M
HLX27	KLX14A:1	123.00–176.27	172,740	739.1	3.2	M
HLX27	KLX14A:2	77.00–122.00	79,200*	774.5	7.6	M
HLX27	KLX15A:2	641.00–901.00	91,140	619.4	4.2	M
HLX27	KLX15A:3	623.00–640.00	4,320	481.7	53.7	H
HLX27	KLX15A:4	481.00–622.00	14,100	403.2	11.5	H
HLX27	KLX15A:5	273.00–480.00	10,800	235.7	5.1	M
HLX27	KLX15A:6	260.00–272.00	162	140.4	121.7	E
HLX27	KLX15A:7	191.00–259.00	120	112.4	105.3	E
HLX27	KLX15A:8	79.00–190.00	288	95.3	31.5	H
HLX27	KLX15A:9	11.65–78.00	1,800	147.6	12.1	H
HLX27	KLX16A:2	86.00–326.00	93,540	787.4	6.6	M
HLX27	KLX16A:3	11.25–85.00	350,940	789.2	1.8	M

* Very uncertain due to tidal effects.

Table 5-10. Observed and corrected drawdown together with Index 2_new for the responding observation sections in the interference test in HLX27. Flow rate $Q_p = 1.25 \cdot 10^{-3}$ m^3/s.

Pumping borehole	Observation borehole	Section (mbl)	$s_{p\_}$ (m)	s_{p_corr} (m)	Index 2_new: $s_{p\_corr}/Q_p * \ln(r_s/r_0)$ (s/m^2)	Index 2_new classification
HLX27	HLX15	12.04–151.90	1.98	1.57	8,430	M
HLX27	HLX26	11.00–151.20	1.22	0.94	4,997	L
HLX27	HLX38	15.02–199.50	0.58	0.46	2,430	L
HLX27	HLX42:1	30.00–152.60	2.22	1.68	8,992	M
HLX27	KLX03:2	830.50–964.50	1.64	1.19	6,475	M
HLX27	KLX03:3	752.50–829.50	1.77	1.18	6,328	M
HLX27	KLX03:4	729.50–751.50	1.68	1.2	6,390	M
HLX27	KLX03:5	652.50–728.50	1.26	0.71	3,755	L
HLX27	KLX03:6	465.50–651.50	1.34	0.76	3,951	L
HLX27	KLX03:7	349.50–464.50	1.26	0.74	3,783	L
HLX27	KLX03:8	199.50–348.50	1.39	1.18	5,984	M
HLX27	KLX03:9	193.50–198.50	1.38	1.19	6,032	M
HLX27	KLX03:10	100.05–192.50	1.55	1.36	6,904	M
HLX27	KLX14A:1	123.00–176.27	0.74	0.42	2,219	L
HLX27	KLX14A:2	77.00–122.00	0.64	0.25	1,437	L
HLX27	KLX15A:2	641.00–901.00	3.1	2.67	13,886	M
HLX27	KLX15A:3	623.00–640.00	4.67	3.81	18,828	M
HLX27	KLX15A:4	481.00–622.00	3.95	3.49	16,750	M
HLX27	KLX15A:5	273.00–480.00	4.12	3.69	16,125	M
HLX27	KLX15A:6	260.00–272.00	11.23	10.87	42,997	M
HLX27	KLX15A:7	191.00–259.00	11.72	11.32	42,763	M
HLX27	KLX15A:8	79.00–190.00	11.13	10.72	39,081	M
HLX27	KLX15A:9	11.65–78.00	9.03	8.67	34,642	M
HLX27	KLX16A:2	86.00–326.00	2.19	1.67	8,909	M
HLX27	KLX16A:3	11.25–85.00	2.06	1.03	5,497	M

Figure 5-7 shows a response diagram for the responding observation sections with Index 2_new versus Index 1. The figure is based on time lags of 0.1 m during the flow period. The basic idea with the response diagram is to group the responses according to their strength and time lag. Observation sections represented by data points towards the upper right corner in the diagram generally indicate better connectivity to the pumping borehole with higher hydraulic diffusivities whereas sections located towards the bottom left corner in the diagram generally represent sections with low connectivity to the pumping borehole and weak responses.

Figure 5-7 indicates that the most distinct responses were found in the upper part of borehole KLX15A (sections 6-9). The two sections in borehole KLX14A show the weakest responses. All sections in borehole KLX03 show similar and intermediate responses to the pumping in HLX27.

Some of the sections towards the upper right corner of Figure 5-7 may represent sections with more or less direct responses along potential fracture zones or other hydraulic structures between borehole HLX27 and the actual observations sections. Sections 6, 7, 8 and 9 in KLX15A are responding most strongly. Alternatively, some of the sections may also be hydraulically connected via interconnecting fractures in the upper part of the bedrock.

The hydraulic diffusivity T/S of the observation sections, which is assumed to reflect the hydraulic connection between the section and the pumping borehole, can also be estimated from the response time lag dt_L in the sections according to /Streltsova 1988/:

$$T/S = r_s^2 / [4 \cdot dt_L \cdot (1+dt_L/t_p) \cdot ln(1+t_p/dt_L)] \qquad (5\text{-}1)$$

The distance r_s is defined above and t_p is the duration of the flow period of the test. The estimated lag times based on the corrected drawdown in the responding sections are shown in Table 5-9. The estimated hydraulic diffusivity T/S of the sections from the lag times are shown in Table 5-11. For comparison, the ratio of the estimated transmissivity and storativity, T_o/S_o, from the transient evaluation (see Table 5-6) of the responses in these sections are also presented.

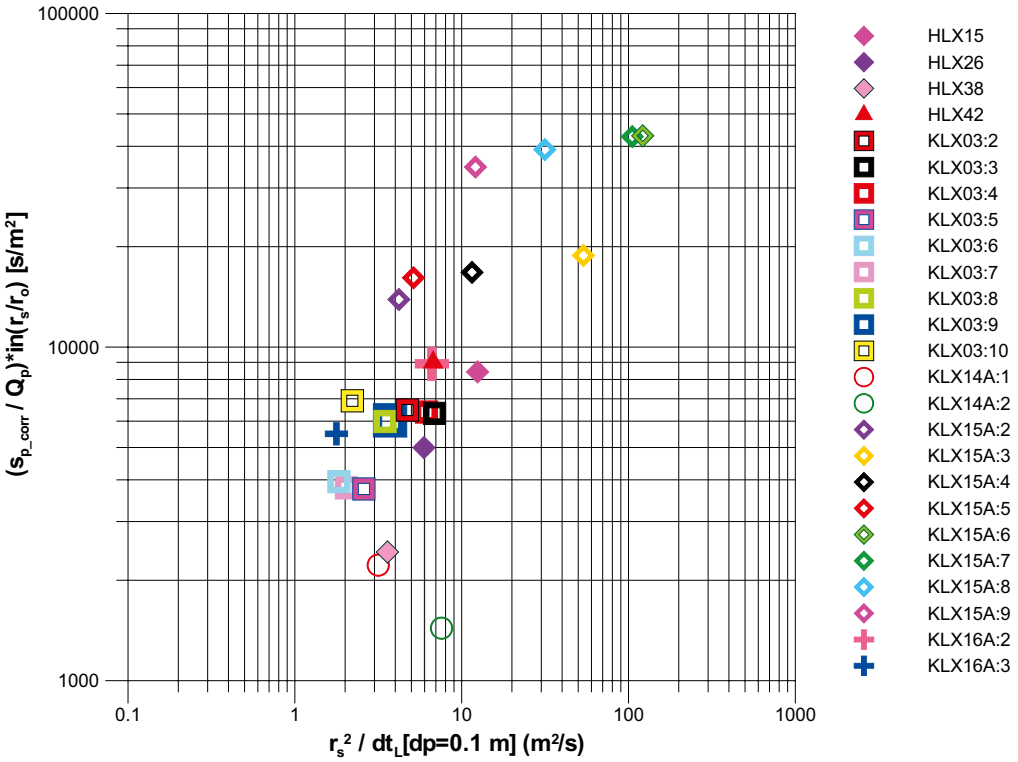

Figure 5-7. *Response diagram showing the responses in the presumed responding observation sections during the interference test in HLX27. Lag time based on a drawdown of 0.1 m (drawdown corrected for the natural head trend).*

Table 5-11. Estimated hydraulic diffusivity for the responding observation sections from the interference test in HLX27 at Laxemar.

Pumping borehole	Observation borehole	Section (mbl)	r_s (m)	T/S (m^2/s)	T_o/S_o (m^2/s)
HLX27	HLX15	12.04–151.90	822	0.62	0.32
HLX27	HLX26	11.00–151.20	768.5	0.33	1.47
HLX27	HLX38	15.20–199.50	738.2	0.22	0.73
HLX27	HLX42:1	30.00–152.60	805	0.38	1.52
HLX27	KLX03:2	830.50–964.50	899	0.30	0.60
HLX27	KLX03:3	752.50–829.50	815	0.38	0.45
HLX27	KLX03:4	729.50–751.50	777.6	0.34	0.38
HLX27	KLX03:5	652.50–728.50	743	0.17	0.15
HLX27	KLX03:6	465.50–651.50	664	0.13	0.09
HLX27	KLX03:7	349.50–464.50	596.4	0.13	0.09
HLX27	KLX03:8	199.50–348.50	566.4	0.19	0.64
HLX27	KLX03:9	193.50–198.50	564.8	0.20	0.81
HLX27	KLX03:10	100.05–192.50	570	0.14	0.28
HLX27	KLX14A:1	123.00–176.27	739.1	0.20	0.52
HLX27	KLX14A:2	77.00–122.00	774.5	0.41	2.31
HLX27	KLX15A:2	641.00–901.00	619.4	0.23	0.39
HLX27	KLX15A:3	623.00–640.00	481.7	1.79	3.22
HLX27	KLX15A:4	481.00–622.00	403.2	0.45	1.44
HLX27	KLX15A:5	273.00–480.00	235.7	0.19	0.57
HLX27	KLX15A:6	260.00–272.00	140.4	2.82	11.43
HLX27	KLX15A:7	191.00–259.00	112.4	2.37	5.82
HLX27	KLX15A:8	79.00–190.00	95.3	0.77	2.53
HLX27	KLX15A:9	11.65–78.00	147.6	0.36	1.16
HLX27	KLX16A:2	86.00–326.00	787.4	0.37	1.53
HLX27	KLX16A:3	11.25–85.00	789.2	0.13	0.19

Table 5-11 and Figure 5-8 show that there is a fair agreement between the estimated hydraulic diffusivity of the sections based on the response time lags and from the results of the transient evaluation, respectively, also at long distances from the pumping borehole. Thus, the results from the response analysis are consistent with the results of the hydraulic evaluation. The results from the response time lag are in general, however, somewhat lower than the results from the transient evaluation.

In Figure 5-9 the discrepancies between the estimated transmissivities from the interference tests and the results of previous single-hole tests in the responding observation sections are shown. The latter values were generally selected from the difference flow logging (flow anomalies) or from the PSS injection tests in a few cases, cf. Section 2.2.1.

It can be noted that the interference test generally provides significantly higher transmissivity values than from the single-hole tests. This fact is assumed to be due to the inherent differences between single-hole tests and interference tests regarding test scale, duration of pumping and investigated volume of rock. In this case, the estimated transmissivities from the interference test are assumed to be dominated by the transmissivity near the pumping borehole and intersecting hydraulic structures. The estimated transmissivity of the pumping borehole HLX27 ranged from $2–4 \cdot 10^{-5}$ m^2/s, see Table 5-7.

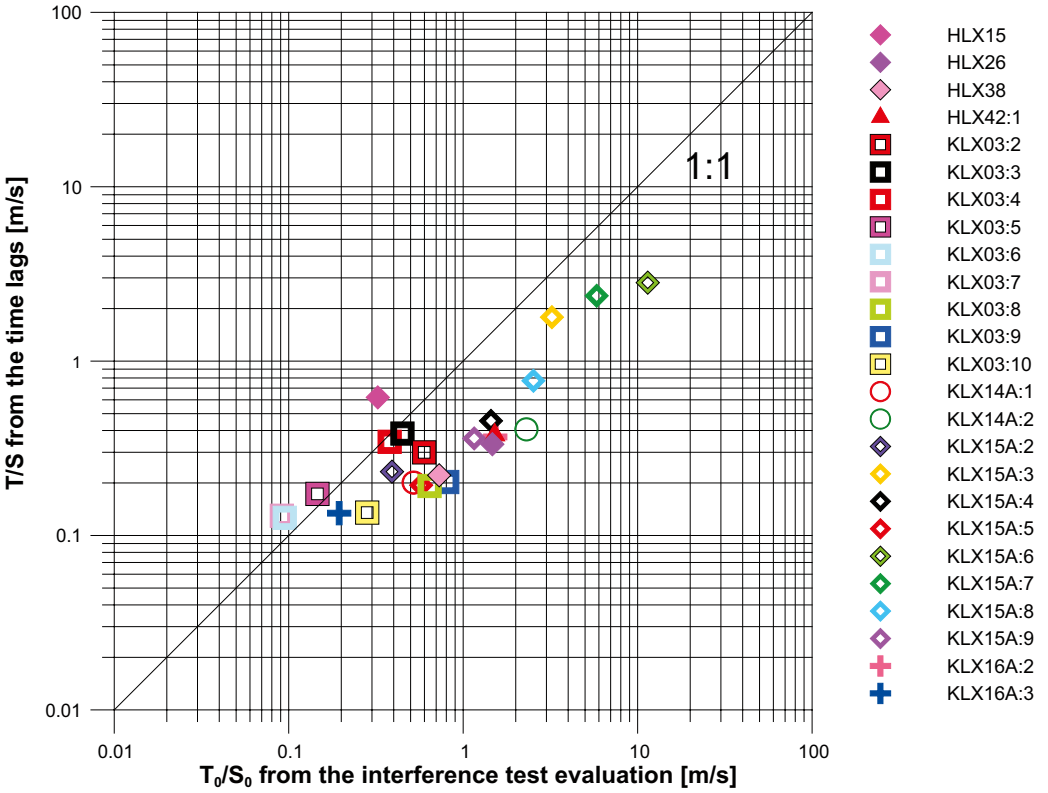

Figure 5-8. *Comparison of estimated hydraulic diffusivity, of the responding observation sections from the lag times and test evaluations, respectively in the interference test in HLX27.*

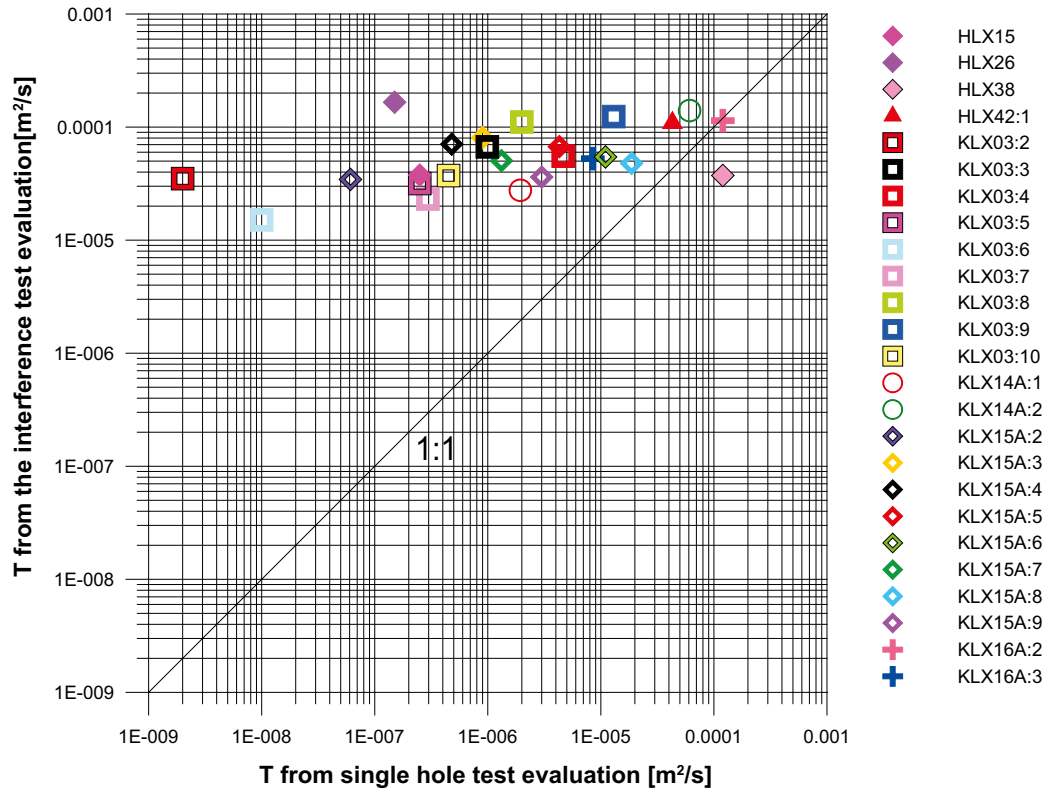

Figure 5-9. *Comparison of estimated transmissivities of the responding observation sections from the interference test in HLX27 and previous single-hole tests in the observation sections. The estimated transmissivity of the pumping borehole HLX27 ranged from 2–4·10^{-5} m^2/s.*

5.4 Water sampling

Water samples according to SKB Class 3 (with Cs and Rb as additional parameters) were taken at four occasions. The first one was taken during a short pumping before the start of the actual pumping period, the second one just after pump start, the third after three weeks of pumping and the last one just before pump stop. The sampling was done in order to monitor the chemical composition during the test period. If the chemical composition changes significantly during the experiment period, there is a risk that the sorption characteristics are changed. The results show a stable chemical composition during the test period. Some of the main constituents are plotted in Figure 5-10. The results of all the parameters analysed are presented in Appendix 8.

5.5 Tracer tests – general

During the pumping period the flow rate was kept at 50 l/min during the pre-test and at 75 l/min during the main tracer test. However, due to a pump failure and some power failures the stable flow rate was sometimes disturbed see Figure 5-11. The pump stops were often short, but one lasted for 24 hours. Also, just after the pump stops the flow rate varied for a while until stable conditions prevailed again. The pump stops and some other events are seen as pressure responses in KLX15A:6. These events are marked in Figure 5-12 and are also described in Table 5-12. The effects can also be seen in some of the other sections in this borehole (see Figure A5-15 in Appendix 5).

The water and tracer injection procedure generally worked well. In connection with a power failure the regulating equipment used for injecting water at 500 ml/min also stopped. However, when the power was back again some water was still injected, although the regulation did not function. In order to start the regulating unit again, a manual re-start of the equipment was needed.

During the pre-test the injection flow rate was 500 ml/min water with a sub-flow of tracer with flow rate 0.75 ml/min. The flow rate of the sub-flow of tracer was checked after the injection by weighing. It was intended to be 1 ml/min, but it was found out that the actual flow rate had only been 0.75 ml/min. During the main tracer test the injection flow rate was 400 ml/min during the time when the tracers were injected. It was intended to be 500 ml/min, but afterwards it was observed that the actual flow rate had been 400 ml/min. After the tracers were injected, water from HLX27 was re-circulated and the injection flow rate during the rinsing time was 500 ml/min.

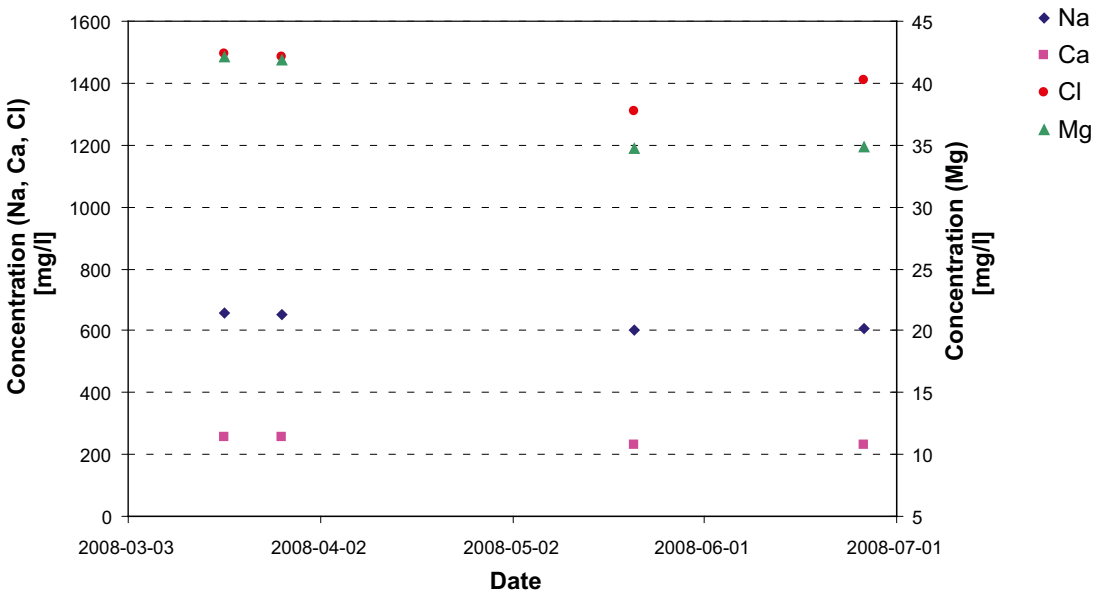

Figure 5-10. *Variation of some main chemical constituents in HLX27 during the experiment time.*

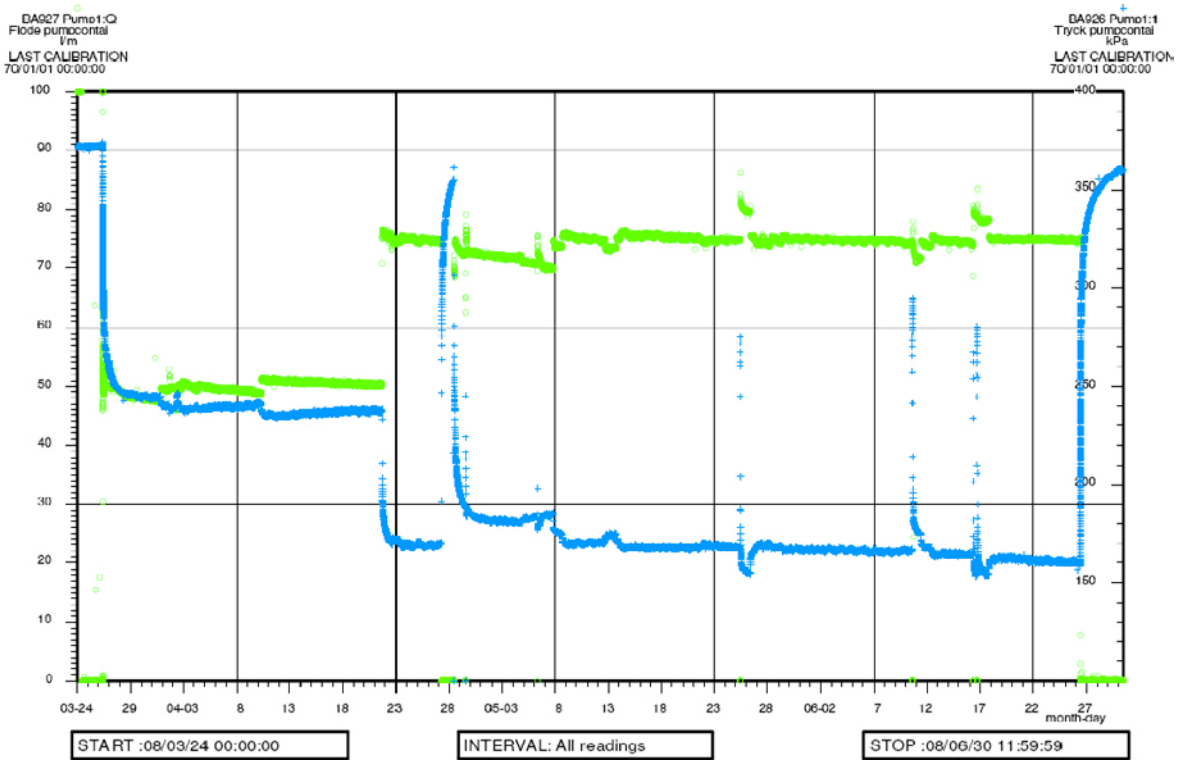

Figure 5-11. *Pumping flow rate, l/min (green) and pressure (compensated for atmospheric pressure), kPa (blue) in the pumping borehole HLX27.*

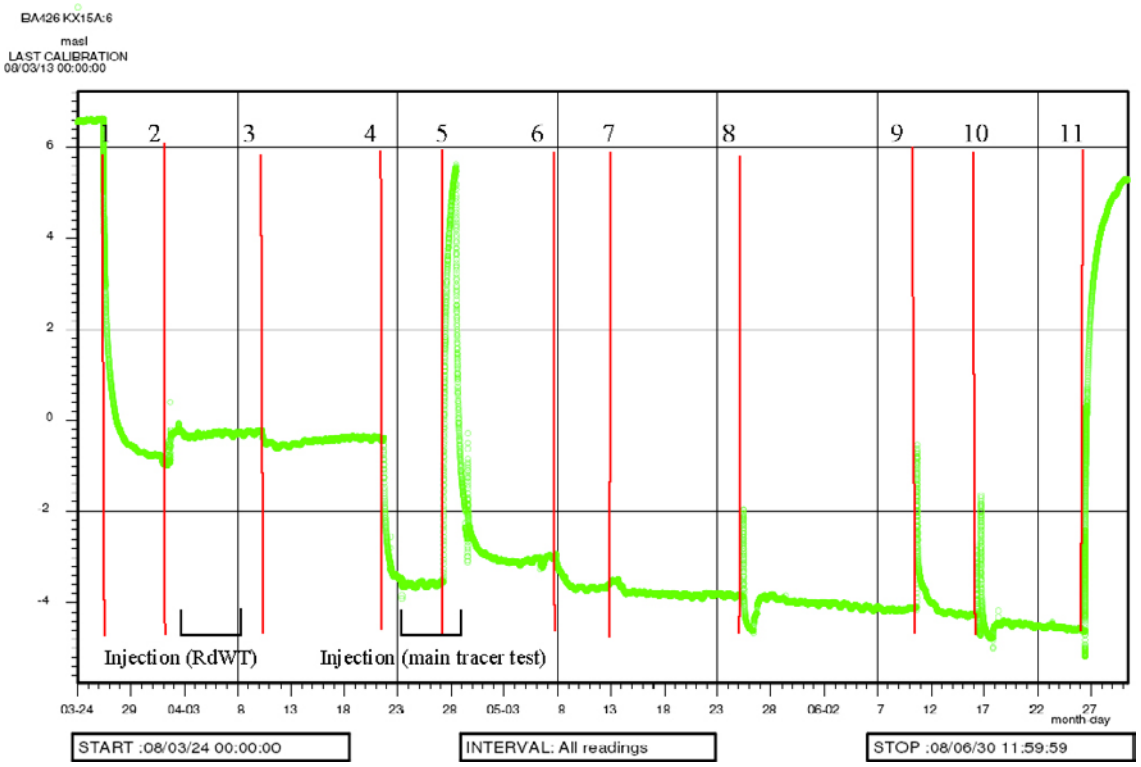

Figure 5-12. *Hydraulic head (m.a.s.l.) in the injection section KLX15A:6 during the test. The numbers refer to events listed in Table 5-12.*

Table 5-12. Pump stops and other major events during the tracer test.

Event	Date and time	Duration of stop (min)	Number in Figure 5-12
Start pumping HLX27	2008-03-26 10:31		1
Injection start (water)	2008-04-01 16:02		2
Injection start (RdWT)	2008-04-02 11:45		
Injection stop (RdWT)	2008-04-08 11:48		
Minor flow rate adjustment	2008-04-10 07:58		3
Withdrawal rate increase (from 50 l/min to 75 l/min)	2008-04-21 17:45		4
Pump failure	2008-04-27 06:42	1,716	5
Injection start (main test)	2008-04-23 09:10		
Injection stop (main test)	2008-04-29 08:22		
Minor flow rate adjustment	2008-05-07 20:30		6
Minor flow rate adjustment	2008-05-13 17:45		7
Power failure	2008-05-25 10:12	30	8
Power failure	2008-06-10 14:23	99	9
Power failure	2008-06-16 07:20	20	10
Power failure	2008-06-16 15:52	54	10
Stop pumping HLX27	2008-06-26 10:05		11

The first stop of the pump in HLX27 was a pump failure, which unfortunately occurred during the end of the injection period of the main tracer test. During this time the injection pump was still injecting the tracer solution at the same rate. When studying the concentration in the injection section it can be seen that an increase coincides with the pump stop (Figure 5-17). When evaluating the data using the various transport models, this variation in input concentration was accounted for.

The effects of the variations in flow rate and the pump stops in the pumping borehole was examined by comparing calculations of the normalized mass flux assuming constant flow rate and no pump stops with calculations accounting variations in flow rate and pump stops. When plotting the normalized mass flux against elapsed time for the pre-test it is obvious that the pump stops and varying flow rate have very little effect on the breakthrough curve (Figure 5-13). Hence, in the following evaluation and calculations, constant flow rate is assumed.

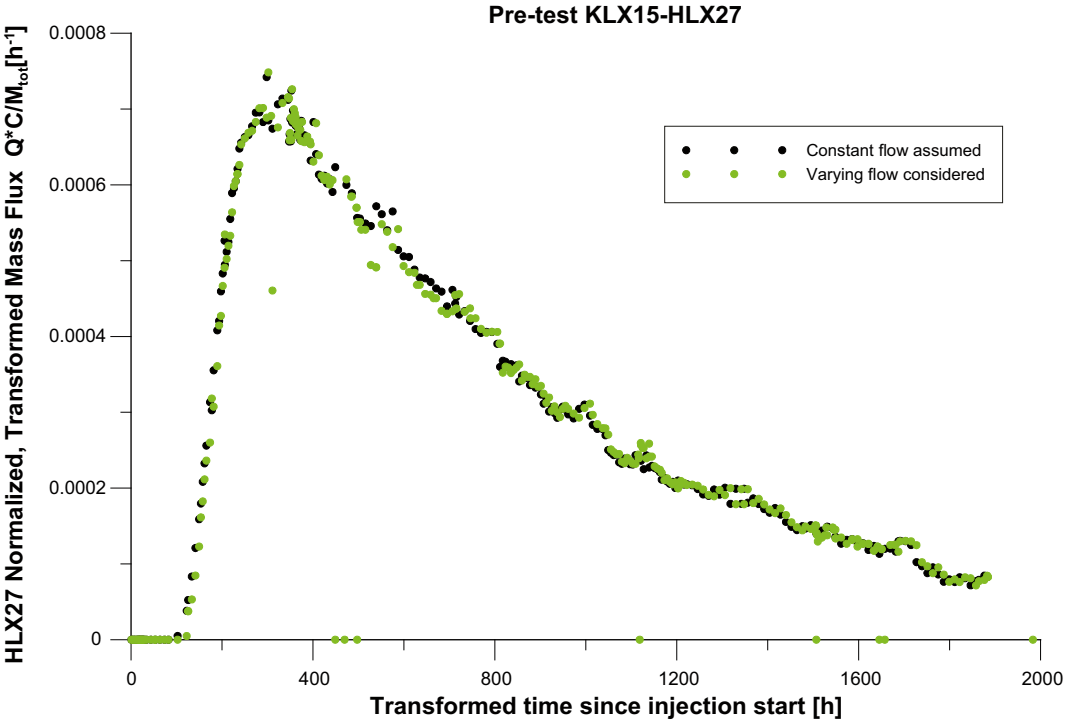

Figure 5-13. *Transformed normalized mass flux against transformed elapsed time. Comparison of considering the pump stops and varying flow rate to assuming constant flow rates (50 l/min and 75 l/min) and no stops.*

The total volume of injected tracer solution was measured in the following way in the main tracer test. The volume of tracer in the tank was determined by measuring the dilution of the concentrated Tb-DTPA solution added to the tank and calculating the total volume. The volume of tracer solution remaining after injection was then measured. In the pre-test the vessel with concentrated tracer solution was weighed before and after the injection to calculate the injected volume. The volumes injected during the tests are shown in Table 5-13.

5.6 Tracer breakthrough

Tracer breakthrough was obtained for RdWT in the pre-test and for three of the five tracers used in the main tracer test. No breakthrough was obtained for the sorbing tracers Cs^+ and Rb^+ within the experimental time frame. The time for first arrival is c. 165 h for Uranine and 174 h for Li^+ and Tb-DTPA. In the pre-test, the time for first arrival of Rhodamine WT was 154 h (pumping rate 50 l/min) which corresponds to 102 h in transformed time (pumping rate 75 l/min). However, this apparently faster transport during the pre-test may be incorrect since the time for first arrival also depends on the background level of the tracer. For example, a small increase of the tracer concentration may not be noticed if the variation of background level is large. The difference in dipole strength may also have played a role in the difference of the first arrival.

5.6.1 Pre-test

The results from the pre-test showed a longer residence time than predicted. Since there was only a limited time for completing the test it was decided to increase the pumping flow rate before the start of the main test to shorten the travel times. Some further scoping calculations were performed to find a new suitable pumping flow rate. For practical reasons the flow could not be increased to more than 75 l/min.

In Figure 5-14 the normalized mass flux in the injection and the withdrawal sections are plotted against transformed time since injection start. The pumping flow rate in HLX27 was increased in the middle of the test period from 50 l/min to 75 l/min. In order to facilitate a comparison between the main test and the pre-test, the time of the pre-test was transformed so that the volume pumped per time unit (i.e. pumping flow rate) was constant (75 l/ transformed minute) throughout the pre-test. The consequence for the breakthrough curve is that the first part is somewhat compressed since one real hour is longer than one transformed hour for this period. Since the time is affected by this transformation so is also the normalized mass flux as plotted on the y-axis in Figure 5-14.

5.6.2 Main tracer test

The breakthrough curves are shown in Figure 5-11 and the concentration for all tracers in injection section KLX15A:6 are plotted against time since injection in Figure 5-12. In these two plots all data including outliers are presented. Explanations for the outliers and other erroneous data are further discussed in Section 6.2. The higher injection concentrations at the end of the injection period (see Figure 5-16 and 5-17) are correlated to the pump stop in HLX27 that occurred during the tracer injection.

After removing outliers and erroneous data and subtracting the background concentration the normalized mass flux was calculated, cf. Figure 5-18 (pumping borehole) and 5-17 (injection section). In Appendix 9, the corresponding curves are also presented for each tracer separately.

The total mass injected for each tracer and their mass recovery at the end of the breakthrough curve are shown in Table 5-14.

Table 5-13. Volume of tracer solution injected.

Test	Volume (l)
Main tracer test	3,427
Pre-test	6.50

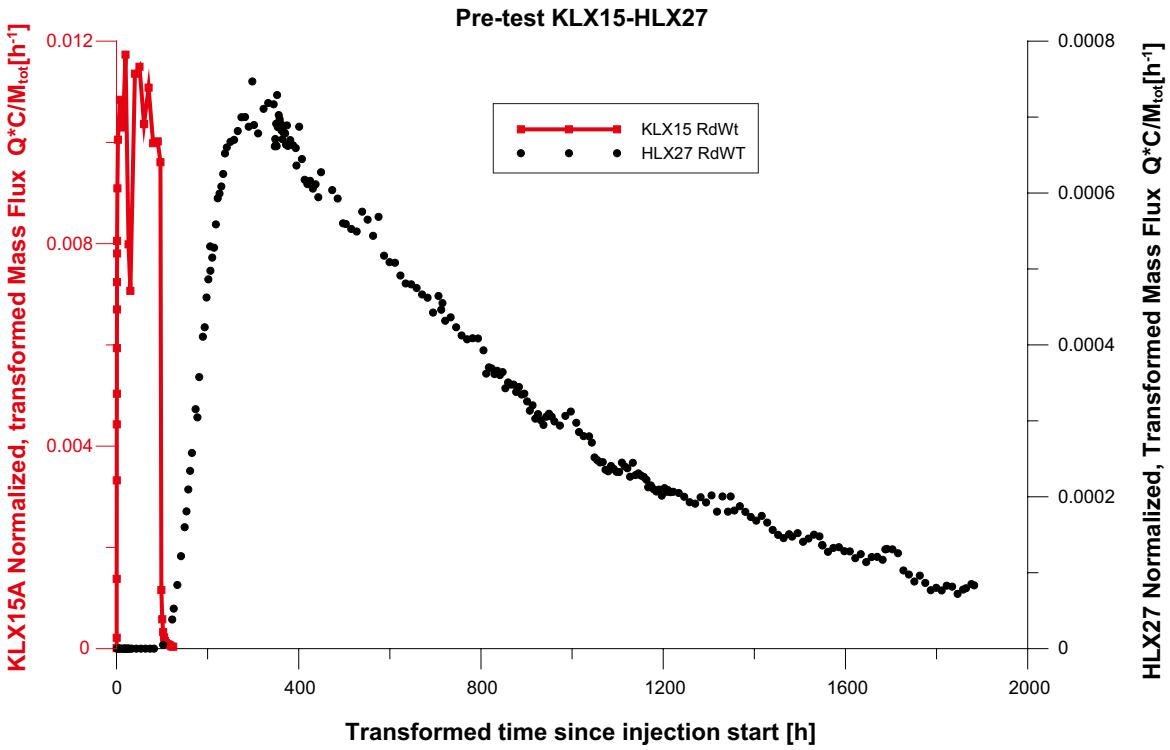

Figure 5-14. *Tracer (Rhodamine WT) breakthrough in HLX27 and injection in KLX15A:6 from the pre-test. Normalized transformed mass flux against transformed elapsed time.*

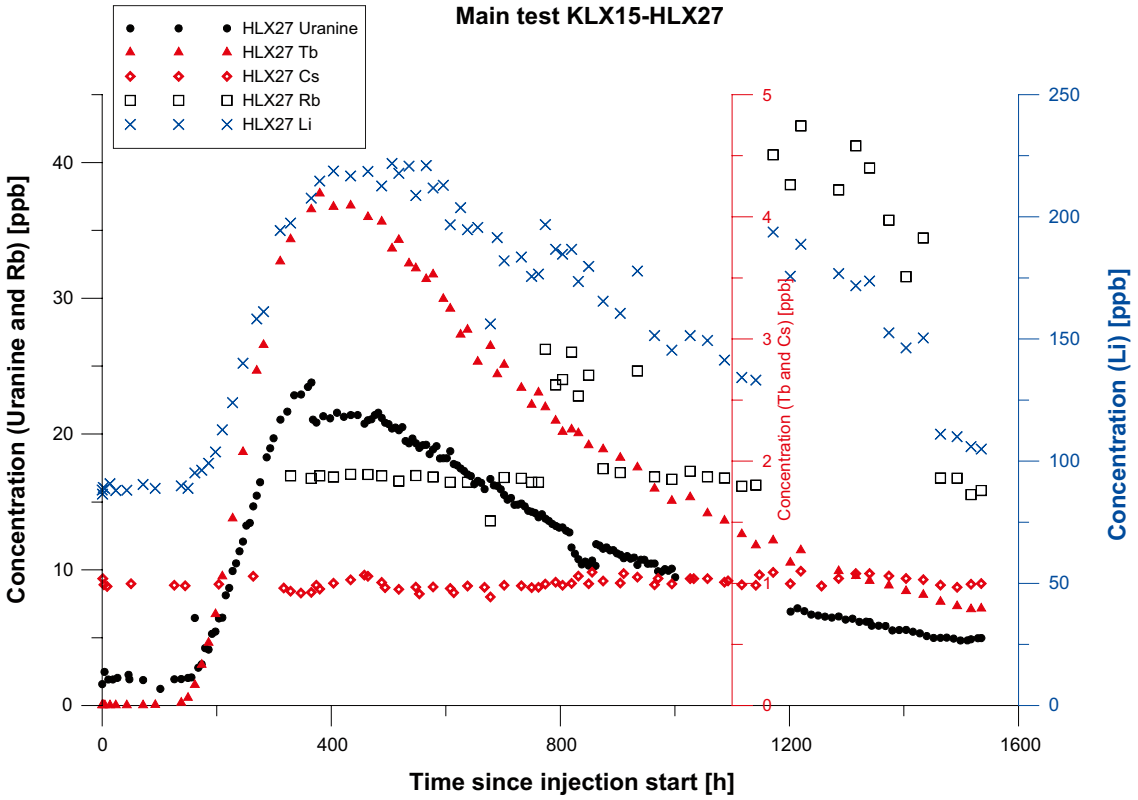

Figure 5-15. *Tracer breakthrough in HLX27 from injection in KLX15A:6 from the main tracer test. Concentration (ppb) versus elapsed time (hours).*

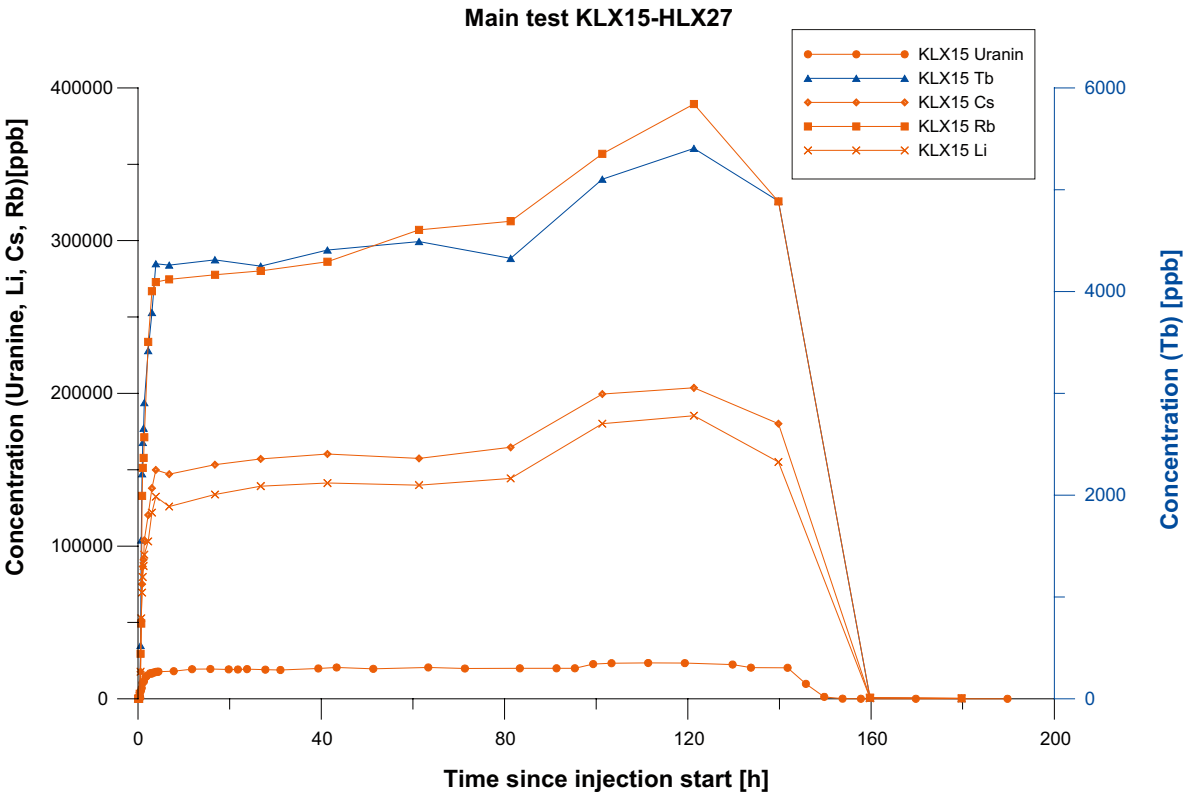

Figure 5-16. *Tracer concentration in the injection section (KLX15A:6). Concentration (ppb) in the injection section versus elapsed time (hours).*

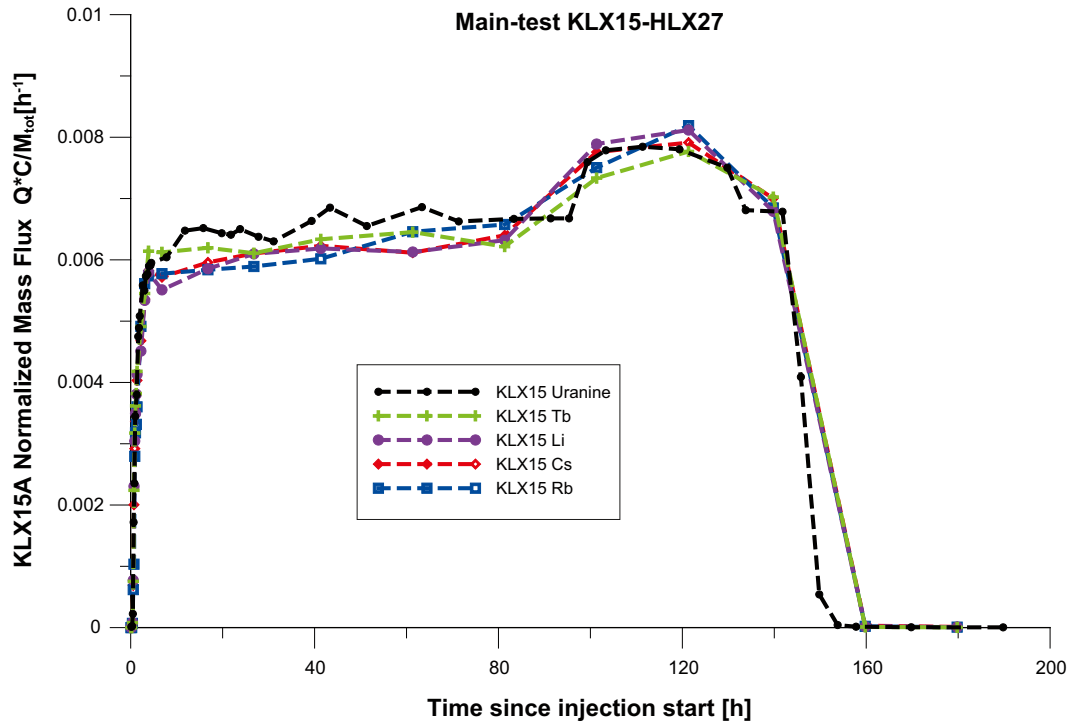

Figure 5-17. *Tracer concentration in the injection section (KLX15A:6). Normalized mass flux versus elapsed time.*

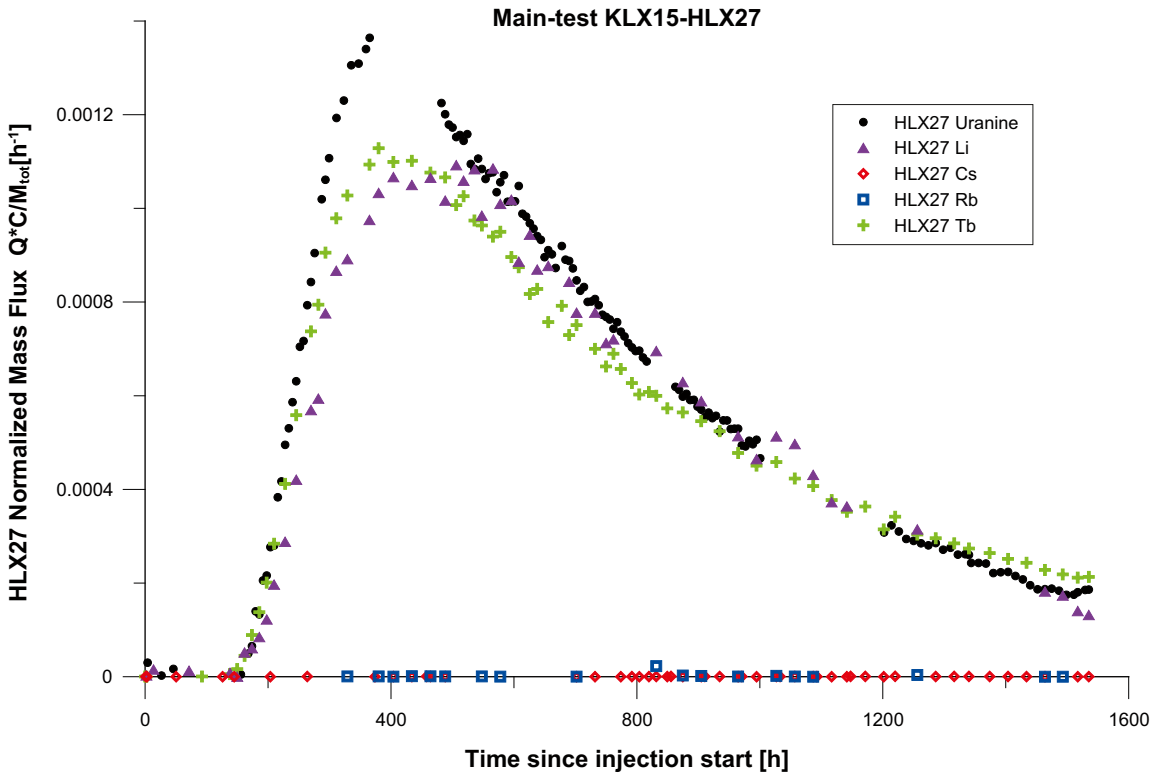

Figure 5-18. *Tracer breakthrough in HLX27. Normalized mass flux versus elapsed time.*

Table 5-14. Total injected mass and mass recoveries of different tracers at pump stop (1,540 hours after injection start).

	Total injected mass (g)	Mass Recovery (%)
Rhodamine WT [1)]	131	57
Uranine	72	88
Tb-DTPA	17	80
Li^+	548	80
Cs^+	618	–
Rb^+	1,141	–

[1)] Time since the injection for Rhodamine WT is 500 h longer than for the other tracers.

5.6.3 Tube sampling at two levels in HLX27

During the main tracer test samples were taken from two different levels in HLX27 using a tube sampling equipment (described in Section 3.3.2). The samples from the 90 mbl level contain water transported from both major water conducting fractures in the borehole, whereas the samples from 120 mbl only represent the lower fracture. The concentration in the samples from the 120 mbl level is generally higher for all samples. Only one sample of Tb-DTPA at the 90 mbl level shows higher concentration than the 120 mbl level, and one of the RdWT samples show the same concentration at both levels (Figure 5-19 to 5-21). On average the concentration at 120 mbl is 1.1 times higher than the concentration at 90 mbl for Tb-DTPA. The corresponding number for Uranine and RdWT is 1.3 and 1.2, respectively. The results indicate that the lower fracture has higher concentration of tracer than the upper one. However, the difference in tracer concentration at the two levels does not exclude that also the upper fracture is involved in the tracer transport. The concentrations in the samples differ considerably from the concentrations of the breakthrough curves. Reasons for this and the interpretation of the results are further discussed in Section 6.3.1.

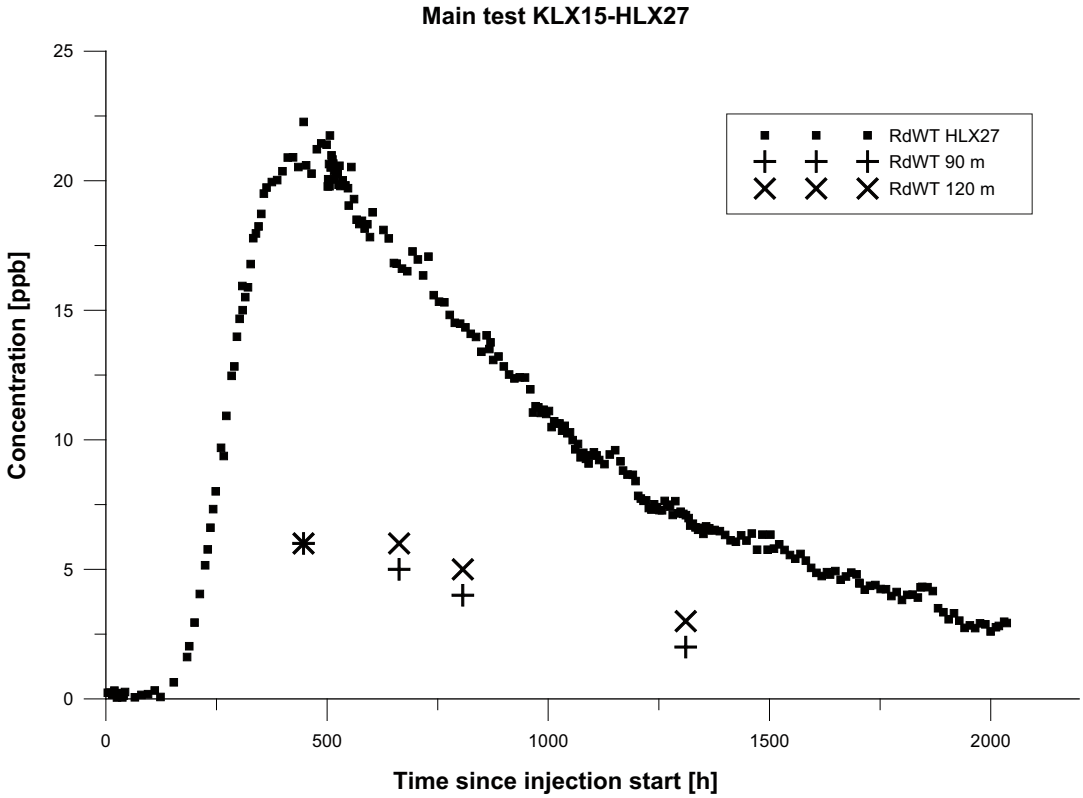

Figure 5-19. *Concentration of RdWT during the continuous sampling in HLX27 compared to the samples taken at 90 and 120 mbl borehole length in HLX27 at five occasions.*

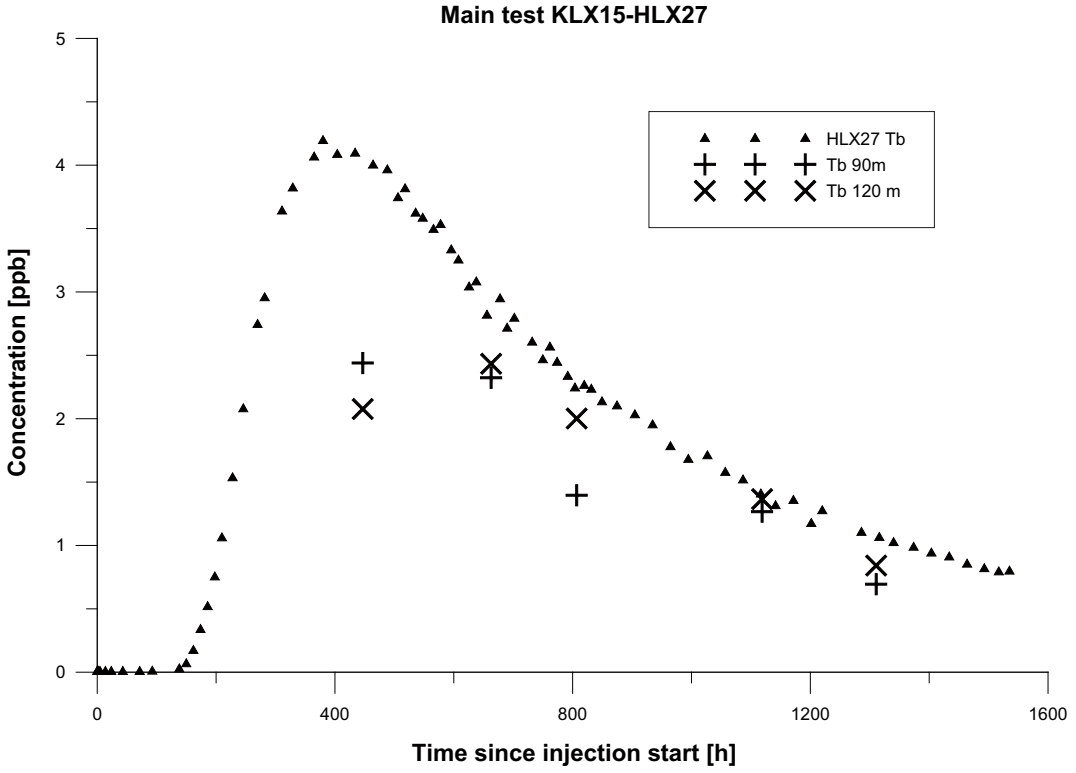

Figure 5-20. *Concentration of Tb (as Tb-DTPA) during the continuous sampling in HLX27 compared to the samples taken at 90 and 120 mbl borehole length in HLX27 at five occasions.*

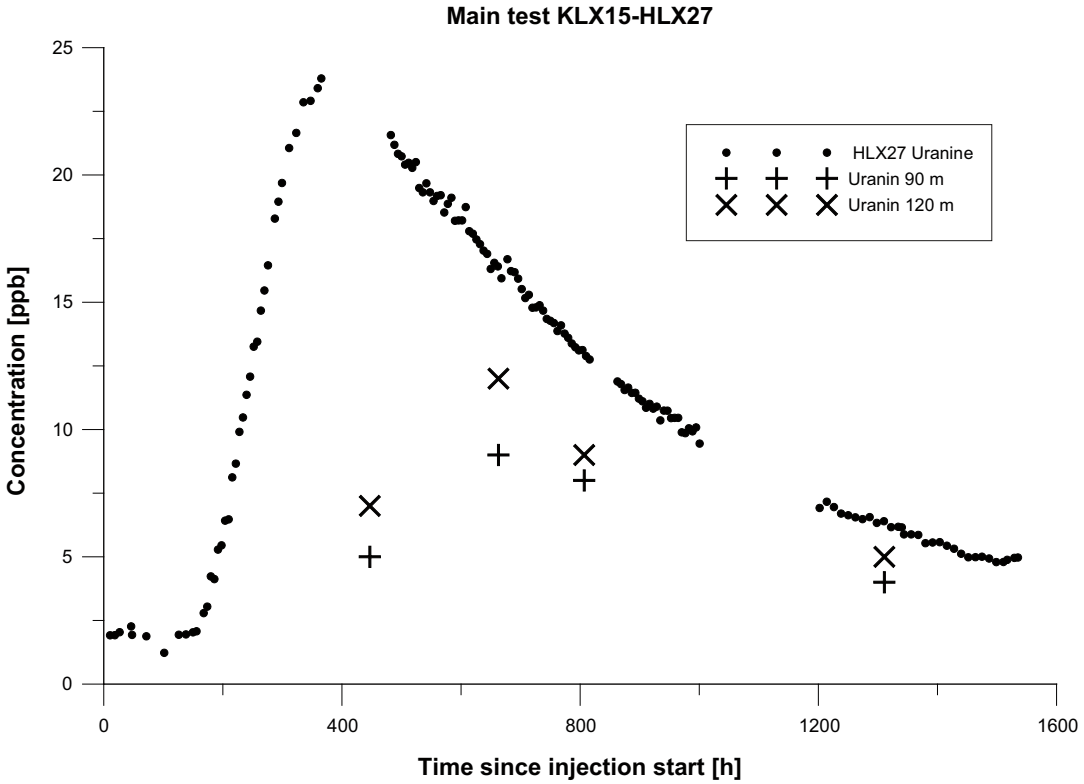

Figure 5-21. *Concentration of Uranine during the continuous sampling in HLX27 compared to the samples taken at 90 and 120 mbl borehole length in HLX27 at five occasions.*

5.7 Model results and evaluated parameters

The models used in the evaluation of the tracer tests are presented in Section 3.5. The simulation procedure was to choose suitable starting values, then to run the selected model and finally examine the results mainly by considering the reasonableness, standard errors and correlation of the parameters as well as visual inspection of the model fit. The model used first was the AD model for a single pathway. After that, further simulations were tried with multiple pathways and finally the AD-MD model.

The results from the model simulations are presented below in Figures 5-22 to 5-37, where estimated parameter values also are presented. The transport parameters that are extracted from the models are the proportionality factor (*pf*), longitudinal dispersivity in terms of Peclet number (*Pe*), mean residence time (t_m), retardation factor for the fracture (R) and the lumped matrix diffusion parameter (A). For further description of the parameters see Section 3.5.

The data used in the simulations are normalized mass flux (h^{-1}) and time (h). By using these units, the value of *pf* directly indicates the recovery in the simulation as *pf* = 1 implies 100% recovery in the simulation.

Generally, the AD and AD-MD models were both found to be useful in the evaluation.

5.7.1 Pre-test

As described in Section 5.4.2, the data from the pre-test were transformed in order to facilitate simulations and a comparison to the main test.

To begin with, the AD model was used in the simulations. Since RdWT is assumed to be non-sorbing, R was fixed to 1.0. It resulted in a rather good model fit to the experimental data. Next, the AD model with 2 pathways was applied, and also this model provided a good fit to field data. However, a view at the simulation results revealed that the parameters had a high correlation which implicates that a change in one parameter may be compensated by a change in some other parameter with the solution close to intact. Hence, no unambiguous solution for a two way AD-model may be found for

the tracer. Finally the AD-MD model was also used. When all parameters were allowed to be free, the recovery was estimated to more than 100%, which is unreasonable. Hence, another simulation was conducted, this time *pf* was fixed to 1.0. This resulted in a rather good fit, although the tail is somewhat high in the simulation.

Since *pf* had to be fixed to 1.0 in order to get a reasonable simulation with the AD-MD model, the AD model was also tested with a fixed *pf* to 1.0. However, this simulation with the AD model resulted in too low top and too high tail compared to the field data and was therefore not considered to be a good simulation.

The fits from the AD and AD-MD model for one pathway are presented in Figure 5-22 (linear) and Figure 5-23 (logarithmic) together with evaluated parameters. The parameters are also presented in Table 5-15.

When considering the parameters extracted from the models it is evident that the recovery at infinite time is rather low, 63% with the AD model. However, the assumption of recovery of 100% for the AD-MD model provides a good fit to experimental data. This assumption does however also affect the mean residence time, t_m, which is quite different in the two models as the AD model indicates 580 h while AD-MD model indicates 330 h. These observations are further discussed in Section 6.

Table 5-15. Parameters as a result of the simulations with the AD model and the AD-MD model RdWT in the pre-test

Model	Parameter	Results
AD model	t_m	580
	Pe	2.0
	pf	0.63
AD-MD model	t_m	330
	Pe	5.7
	pf	1.0 (fixed)
	A	610

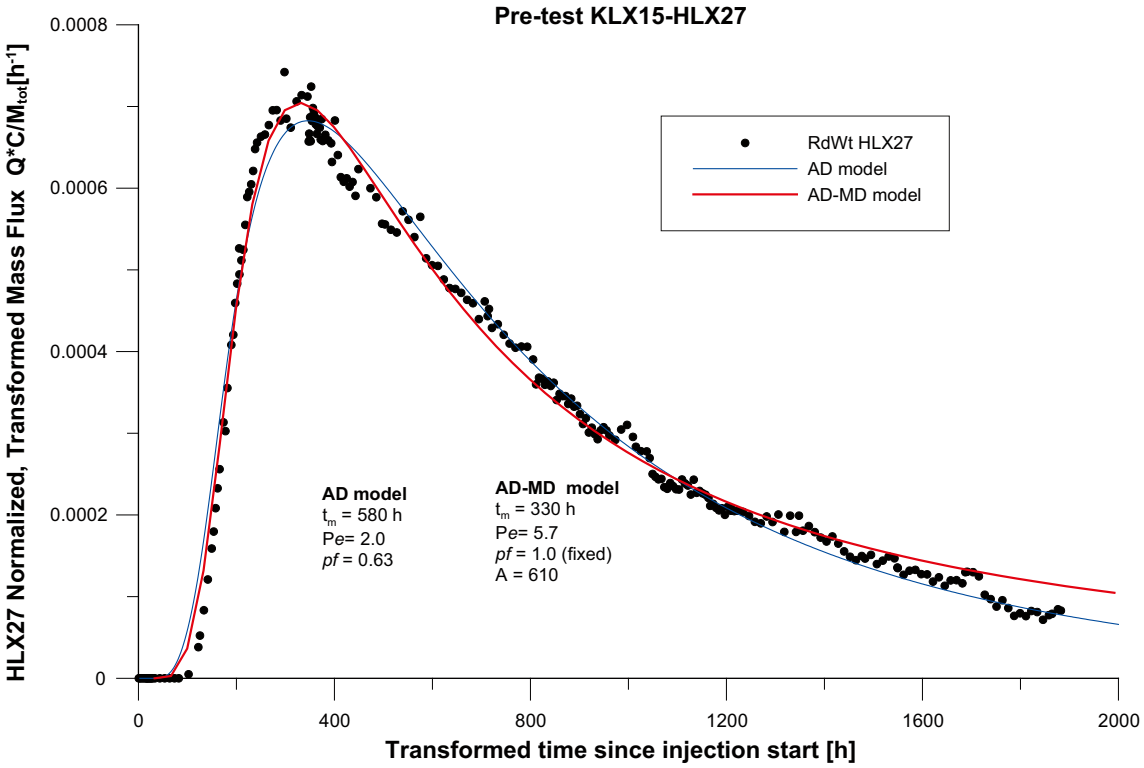

Figure 5-22. *Linear plot of model fits using the AD model and the AD-MD model to experimental data for the pre-test (Rhodamine WT). Note the transformed units on the axes.*

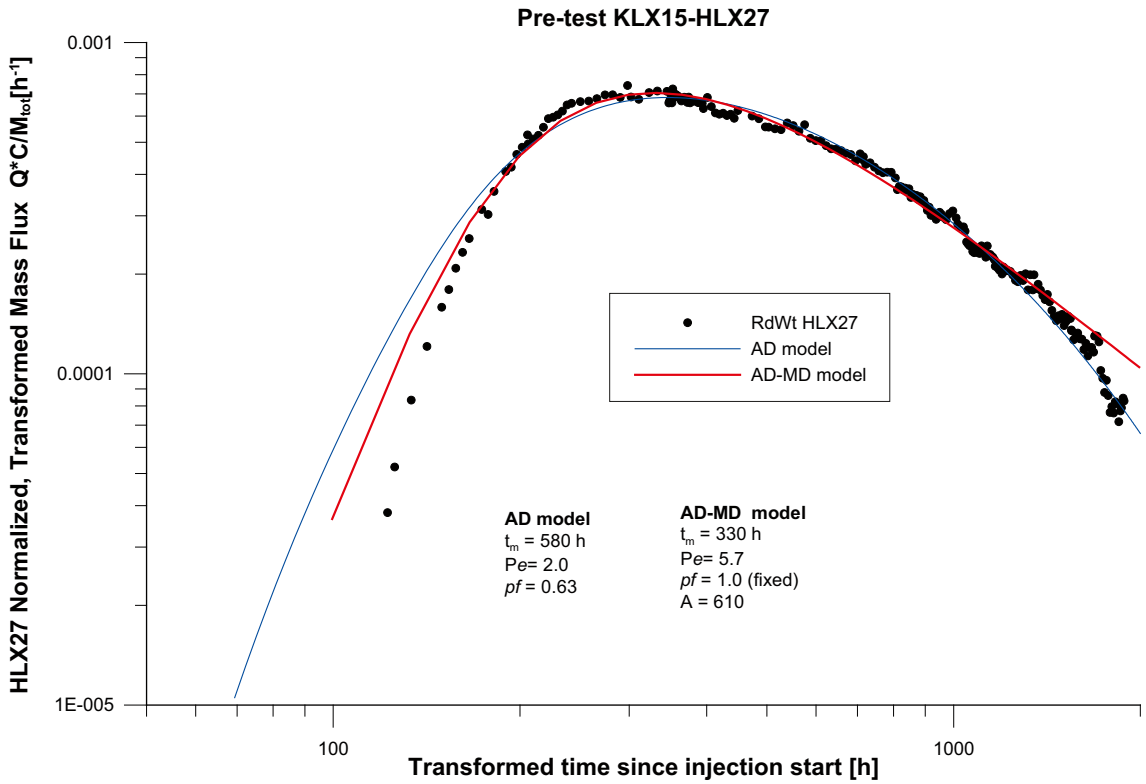

Figure 5-23. *Logarithmic plot of model fits using the AD model and the AD-MD model to experimental data for the pre-test (Rhodamine WT). Note the transformed units on the axes.*

5.7.2 Main test

To begin with, it is important to point out that the simulations of Uranine presented here are only used to support the results from the other simulations. The concentration of Uranine used in this test is to low to guarantee sufficient quality of the data. The reasons for this are further discussed in Section 6.2.3

The modelling was performed in three different steps:

1) Each tracer was modelled separately and assumed to be non-sorbing (R = 1.0).
2) Li^+ was modelled as a sorbing tracer together with the non-sorbing tracer Tb-DTPA.
3) Estimation of lowest possible retardation factor, R, was estimated for Cs^+ and Rb^+.

The AD models for one and two pathways as well as the AD-MD model for one pathway were used in the simulations of the main test except for the estimation of the retardation factor for Cs^+ and Rb^+ where only the AD models were used.

Modelling with assumption of non-sorbing tracers

Each tracer (Uranine, Tb-DTPA and Li^+) was simulated separately under the assumption that they were non-sorbing, hence R was fixed to 1.0. The results from these simulations are displayed in Figure 5-24 to 5-31 below.

The AD model for one pathway with all parameters (t_m, Pe and pf) free was used initially. The result is shown in Figure 5-24 to 5-29 as a black line. Generally, the model fits the data quite well although the maximum values are not quite matched by the model for Tb-DTPA and Uranine and the tails are low in the simulations (especially for Tb-DTPA). The results of the simulations are also presented in Table 5-15.

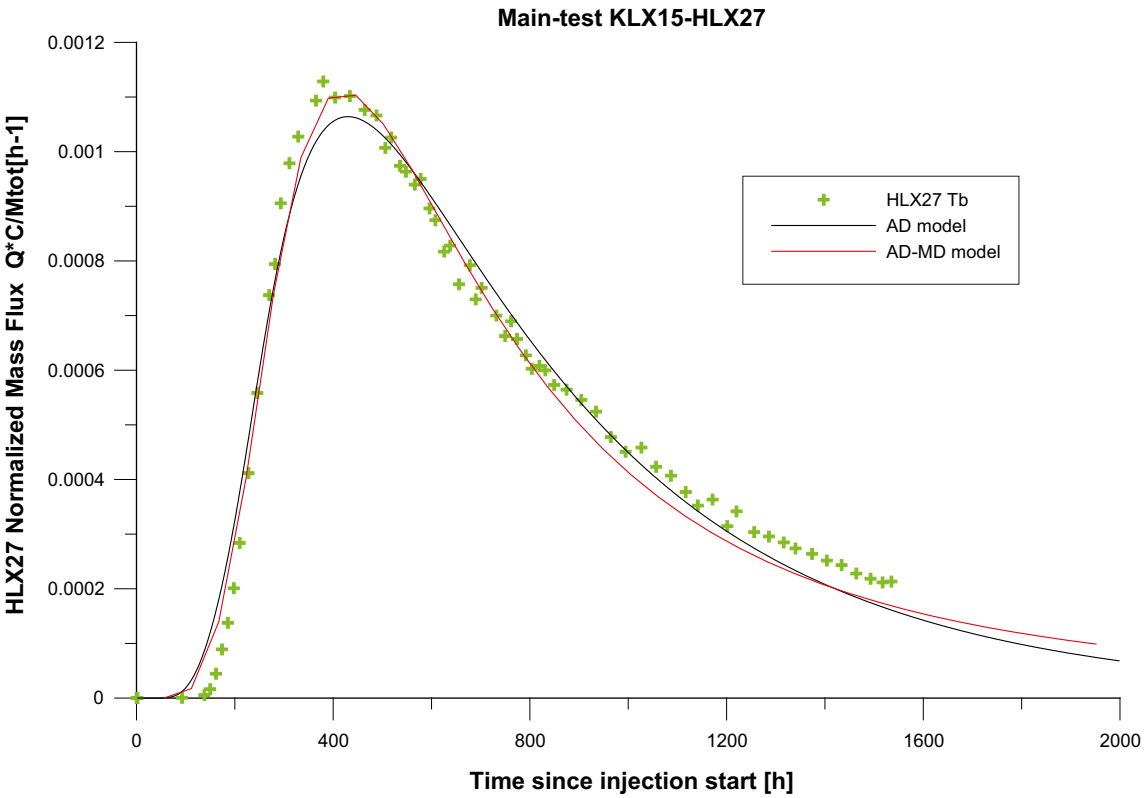

Figure 5-24. *Linear plot of model fit using the AD model (all parameters free) and the AD-MD model (pf = 1) to experimental data for Tb-DTPA from the main test.*

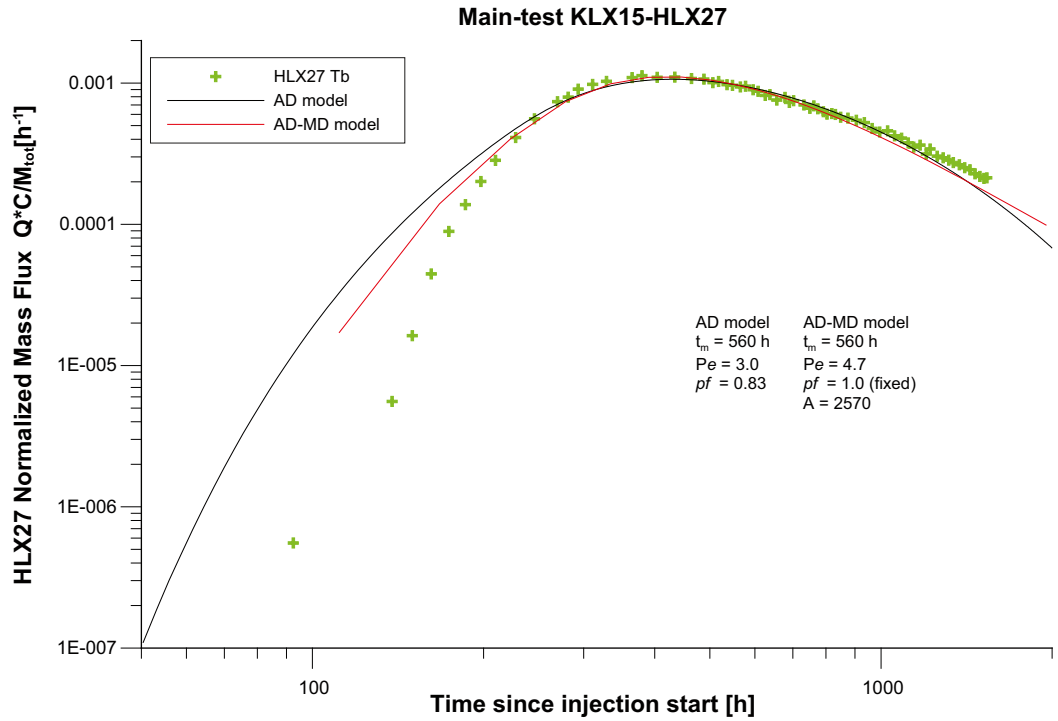

Figure 5-25. *Logarithmic plot of model fit using the AD model (all parameters free) and the AD-MD model (pf = 1) to experimental data for Tb-DTPA from the main test.*

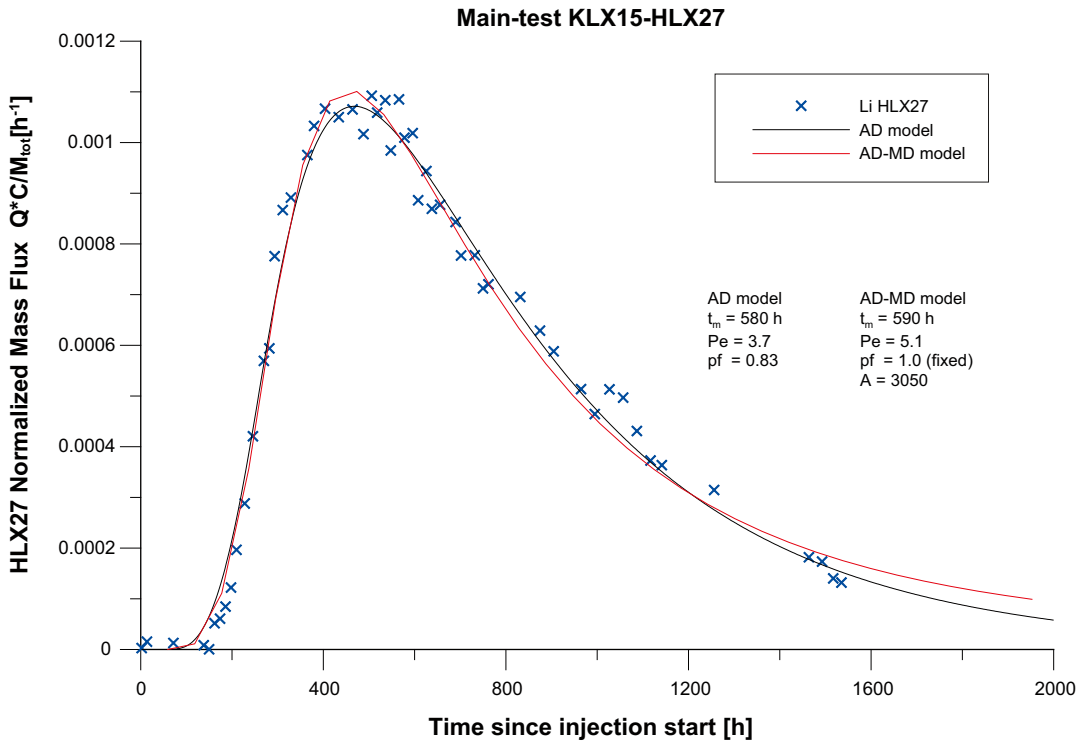

Figure 5-26. *Linear plot of model fit using the AD model (all parameters free) and the AD-MD model (pf = 1) to experimental data for Li^+ from the main test.*

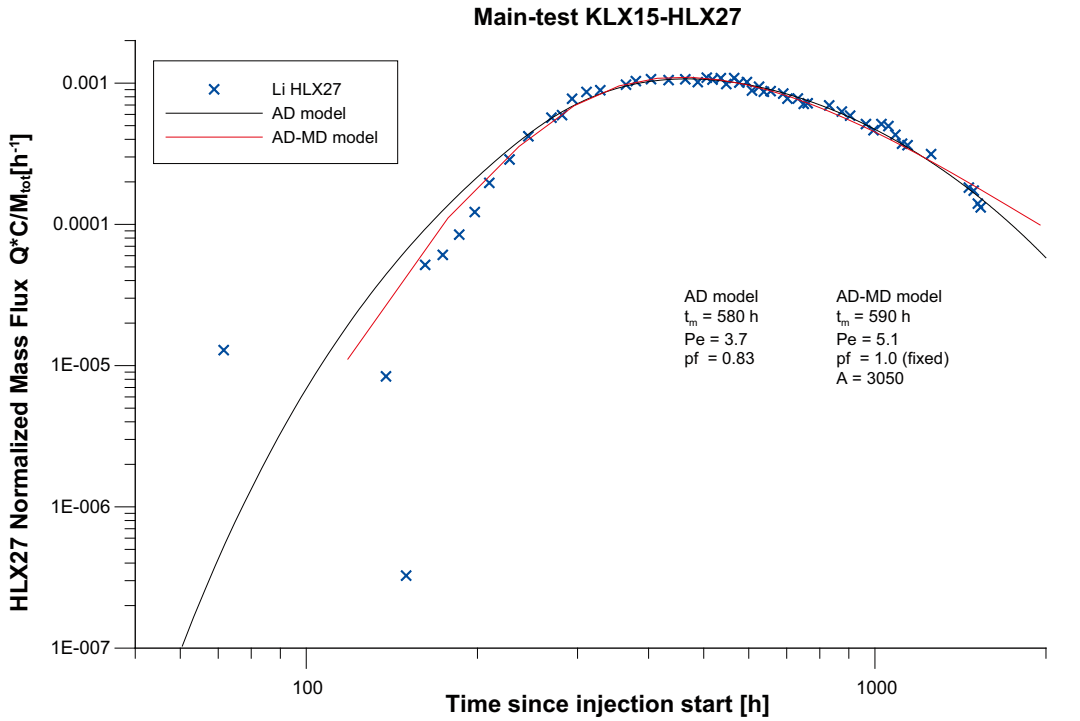

Figure 5-27. *Logarithmic plot of model fit using the AD model (all parameters free) and the AD-MD model (pf = 1) to experimental data for Li^+ from the main test.*

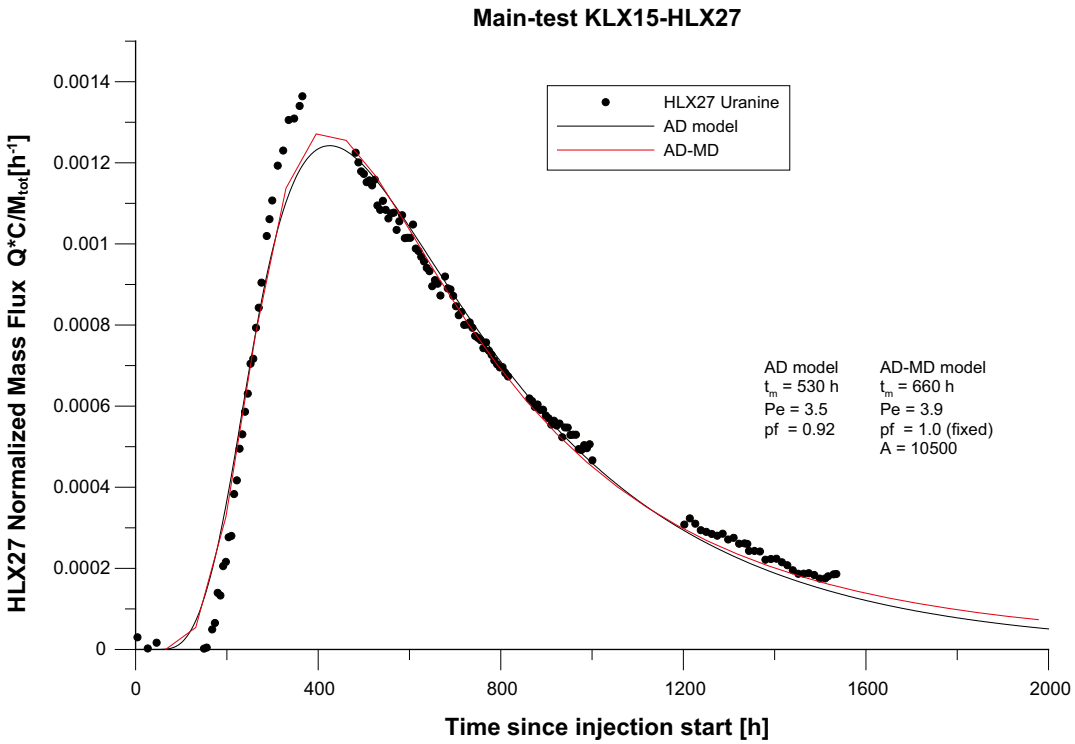

Figure 5-28. *Linear plot of model fit using the AD model (all parameters free) and the AD-MD model (pf = 1) to experimental data for Uranine from the main test.*

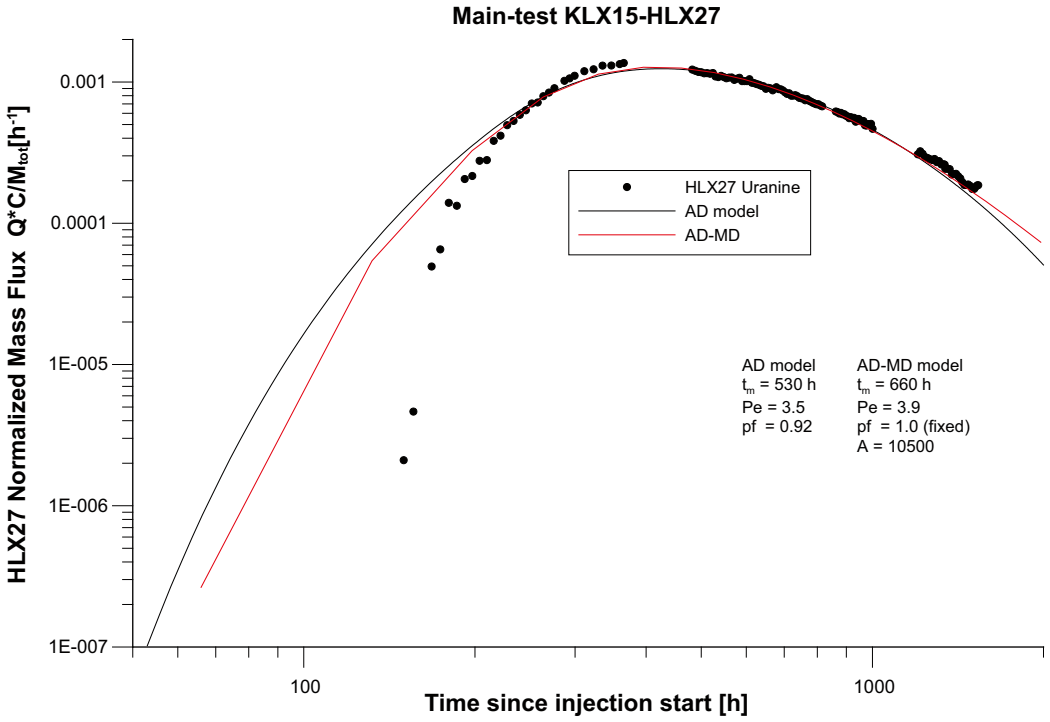

Figure 5-29. *Logarithmic plot of model fit using the AD model (all parameters free) and the AD-MD model (pf = 1) to experimental data for Uranine from the main test.*

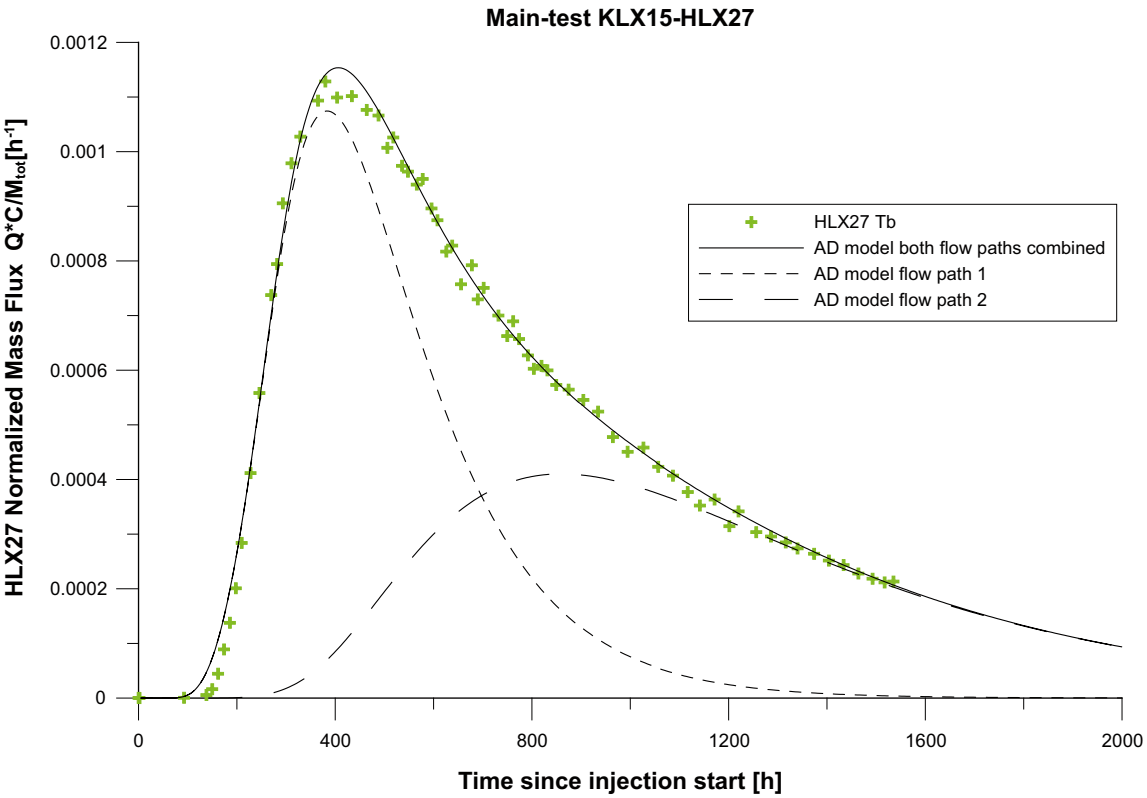

Figure 5-30. *Linear plot of a model fit using the AD model with 2 pathways to experimental data for Tb from the main test. Note that this model fit is only one of many possible for the AD model with two pathways and is only displayed as an example.*

The next step was to add another pathway in the AD-model. Also in this case were all parameters free. This model also fits the data quite well, and is able to simulate the peak very well and at the same time not become too low at the tail. However, for different choices of starting values, the model converged to different solutions that fit the data equally well. A closer look at the simulation results also reveals that some parameters are strongly correlated with each other, which implicates that a change in one parameter may be compensated by a change in some other parameter with the solution close to intact. Hence, no unambiguous solution for a two-way AD-model may be found for the tracers. The two-way AD-model is therefore excluded from presented results. Still, since the tube sampling indicates a possible two-way flow path an example for a two-way model for Tb-DTPA is shown in Figure 5-30 as one of many possibilities for a two-way flow path.

Finally, the AD-MD model was also used. When all parameters were free (except R) pf became unreasonable large ($pf > 1$) for all three tracers. Hence, another simulation was performed restricting pf to be 1.0. This restriction provided better fits to experimental data. The results of the simulations are shown in Figure 5-24 to 5-29 as a red line.

Since pf in the AD-MD-model had to be fixed to 1.0 to provide a good fit and reasonable parameters, the corresponding simulations (with $pf = 1.0$) were performed also with the AD-model as a comparison. The results from these simulations did not differ much from the results obtained with free pf. The result resembles that from the pre-test when the same method was used i.e. that the tail for simulations with pf fixed to 1.0 is somewhat high.

The default for regression weights on observations (see Section 3.5.3) is to give all observations equal weight, which gives more importance to higher values in the regression analysis. This may be altered by assigning different weight for different parts of the breakthrough curve and was also tested. However, when weighting the data so a better fit to the tail was obtained, the fit to the peak was worse. It was therefore judged that the overall fit to the breakthrough curves was not significantly improved by adjusting regression weights.

The parameters extracted from the model runs are presented in Table 5-16 (AD model), and Table 5-17 (AD-MD model).

Table 5-16. Result of the simulations with the AD-model assuming all tracers are non-sorbing (each tracer simulated separately).

Parameter	Free *pf* Tb-DTPA	Li^+	Uranine
t_m	560	580	530
Pe	3.0	3.7	3.5
pf	0.83	0.83	0.92

Table 5-17. Result of the simulations with the AD-MD-model assuming all tracers are non-sorbing (each tracer simulated separately).

Parameter	Fixed *pf* (*pf* = 1.0) Tb-DTPA	Li^+	Uranine
t_m	560	590	660
Pe	4.7	5.1	3.9
pf	1.0 (fixed)	1.0 (fixed)	1.0 (fixed)
A	2,570	3,050	10,500

The results from the simulations are consistent. When using the AD-MD model the dispersivity becomes lower (higher Pe-numbers). The mean residence time for Tb-DTPA and Li^+ agrees very well between the best fit with the AD model (single pathway) and the AD-MD model.

The recoveries from the different simulations (where *pf* is allowed to vary) are also consistent. The slightly shorter residence time for Tb-DTPA compared to Li^+ indicates that Li^+ is weakly sorbing. Figure 5-31 shows the breakthrough curves and the fits to the AD-model for all three tracers in the same plot. In this figure it is also indicated that Li^+ is weakly sorbing compared to Tb-DTPA.

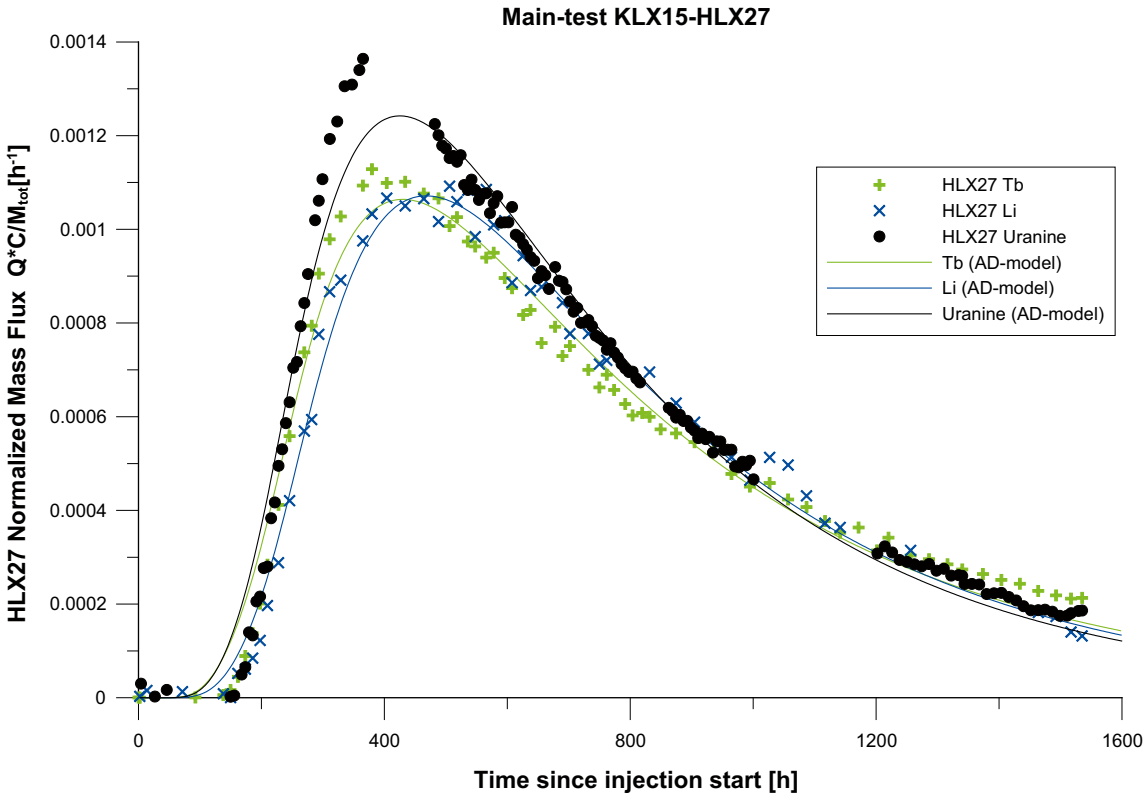

Figure 5-31. *Linear plot of model fit using the AD model to experimental data for the main test. All three tracers are simulated separately.*

Estimation of R for Li⁺

Besides the indications above Li^+ is also earlier reported to be weakly sorbing in similar tracer tests in Forsmark /Lindquist et al. 2008a/. To determine the retardation factor (R) for Li^+ it was simulated together with Tb-DTPA (which is assumed to be a non-sorbing tracer). First, this was done with the AD model by simultaneous estimation, with t_m, *Pe* and *pf* as free parameters. However, the proportionality factor *pf* for Li^+ was restricted to be the same as for Tb-DTPA. Another simulation was then carried out where some parameters (t_m and P*e*) were fixed from the simulation of Tb-DTPA only, and *pf* for Li^+ was restricted to equal *pf* for Tb_DTPA. These two simulations both resulted in good fits, and there is not much difference between the values of the estimated parameters, R = 1.06 in the first case and 1.07 in the second. The simulated curves are presented in Figure 5-32 (linear) and Figure 5-33 (logarithmic). The resulting parameter values are presented in Table 5-18.

Table 5-18. Result of the simulations with the AD model, the AD model with two pathways and the AD-MD model for Tb-DTPA together with the sorbing tracer Li^+.

Model	Parameter setup	Parameter	Tb-DTPA	Li^+
AD model	Free parameters, but ($pf_{Li} = pf_{Tb}$)	t_m	550	550
		Pe	3.3	3.3
		pf	0.82	0.82
		R	1 (fixed)	1.06
AD model	t_m, Pe fixed and ($pf_{Li} = pf_{Tb}$)	t_m	560 (fixed)	560 (fixed)
		Pe	3.0 (fixed)	3.0 (fixed)
		pf	0.86	0.86
		R	1 (fixed)	1.06
AD-MD model	t_m, Pe and *pf* fixed and ($pf_{Li} = pf_{Tb}$)	t_m	560 (fixed)	560 (fixed)
		Pe	4.7 (fixed)	4.7 (fixed)
		pf	1.00 (fixed)	1.00 (fixed)
		A	2,570	3,670
		R	1 (fixed)	1.13

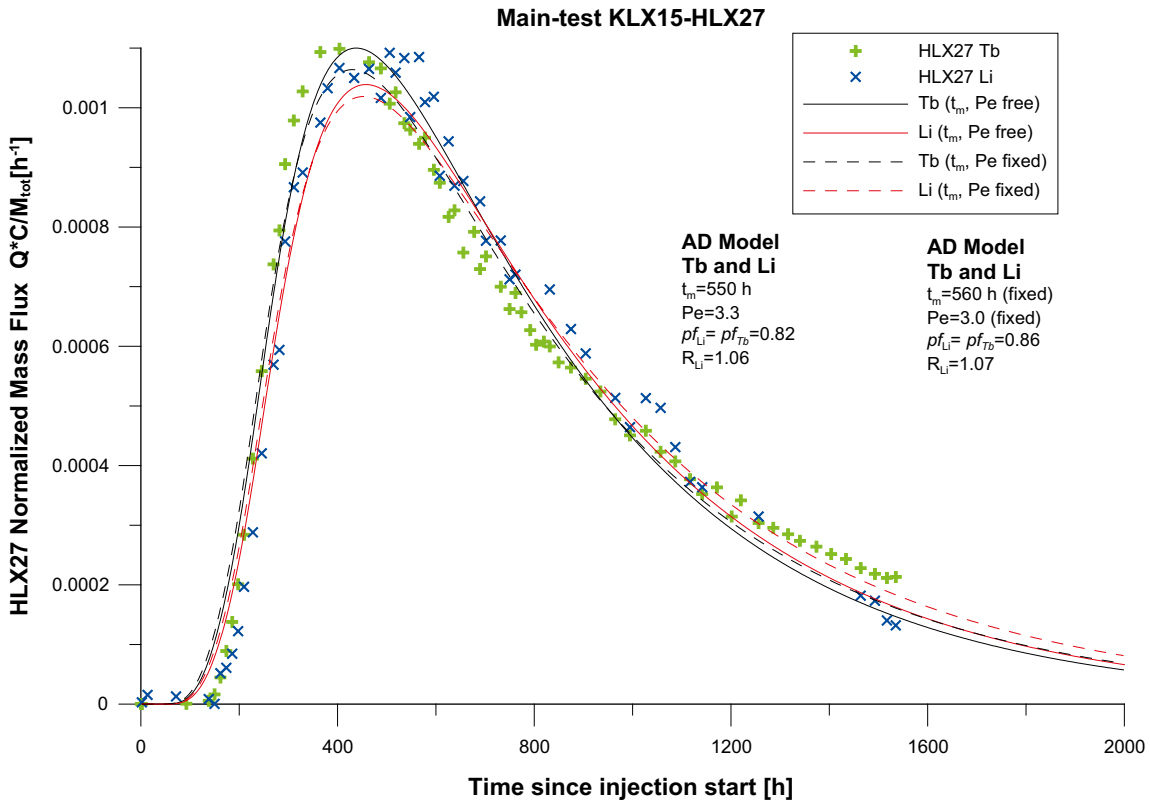

Figure 5-32. *Linear plot of model fits using the AD model to experimental data for the main test. Tb-DTPA is the non-sorbing tracer and Li^+ is weakly sorbing.*

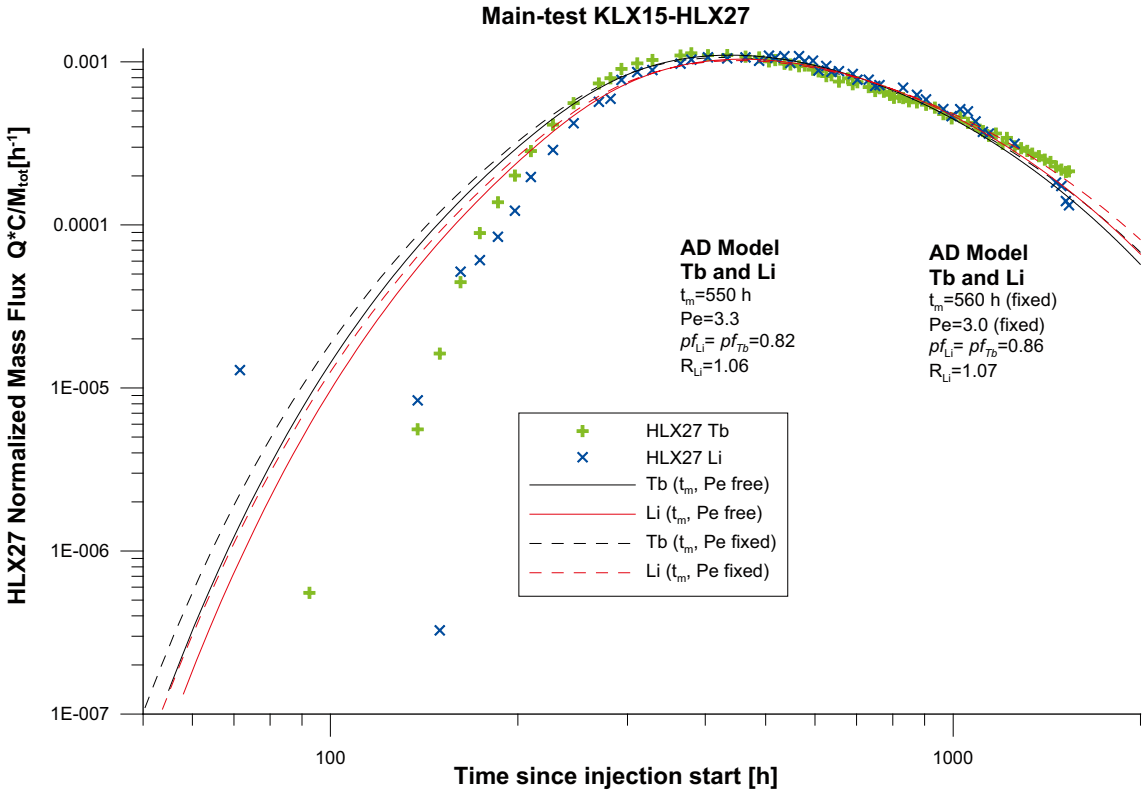

Figure 5-33. *Logarithmic plot of model fit using the AD model to experimental data for the main test. Tb-DTPA is the non-sorbing tracer and Li^+ is weakly sorbing.*

Since the AD model with two pathways did not give satisfying results for one tracer it was not used in the simulations with Tb-DTPA and Li^+ together. Instead, the AD-MD model was tested, but it resulted in $pf > 1$, as in all other simulations with AD-MD model and free *pf*. When *pf* was fixed ($pf = 1$ for both tracers) the model did not converge. A number of simulations were performed combining various parameters to be fixed or free. The only simulation that provided reasonable parameters and a good model fit to experimental data was obtained when the parameters t_m and P*e* and *pf* were fixed from the simulation of Tb-DTPA only and *pf* was restricted to be the same for both tracers. This simulation resulted in R = 1.13 for Li^+. The simulated curves are presented in Figure 5-34 (linear) and Figure 5-35 (logarithmic). The resulting parameter values can be found in Table 5-18.

Retardation of Cs^+ and Rb^+

Since no breakthrough was obtained for Cs^+ and Rb^+, the retardation factor cannot be determined. However, a lowest possible retardation factor can be evaluated by assuming different values of *R* and plot together with experimental data. The same values of the parameters t_m, P*e* and *pf* obtained from the modelling of Tb-DTPA were used and different values of *R* were tested. The AD model with a single path way was used for both Cs^+ and Rb^+. Figure 5-36 shows an overview of the Tb-DTPA, Cs^+ and Rb^+ breakthrough curve as well as simulations for different values of *R* in the AD model. It is clear in the figure that the simulations of Cs^+ and Rb^+ for $R = 20$ gives almost the exact same result which is expected due to the very similar injection function for the two tracers. Therefore, only Cs^+ is shown for the other values of *R*. Figure 5-37 shows the same as Figure 5-36 but in a logarithmic scale. It is obvious from the two figures that a retardation factor of 10 is too low. Otherwise a tracer breakthrough would be visible in the test result during the experiment time. Instead, when considering the rather poor fit for Tb-DTPA to the first arrival, a minimum estimate of *R* should be about 20 for both Cs^+ and Rb^+.

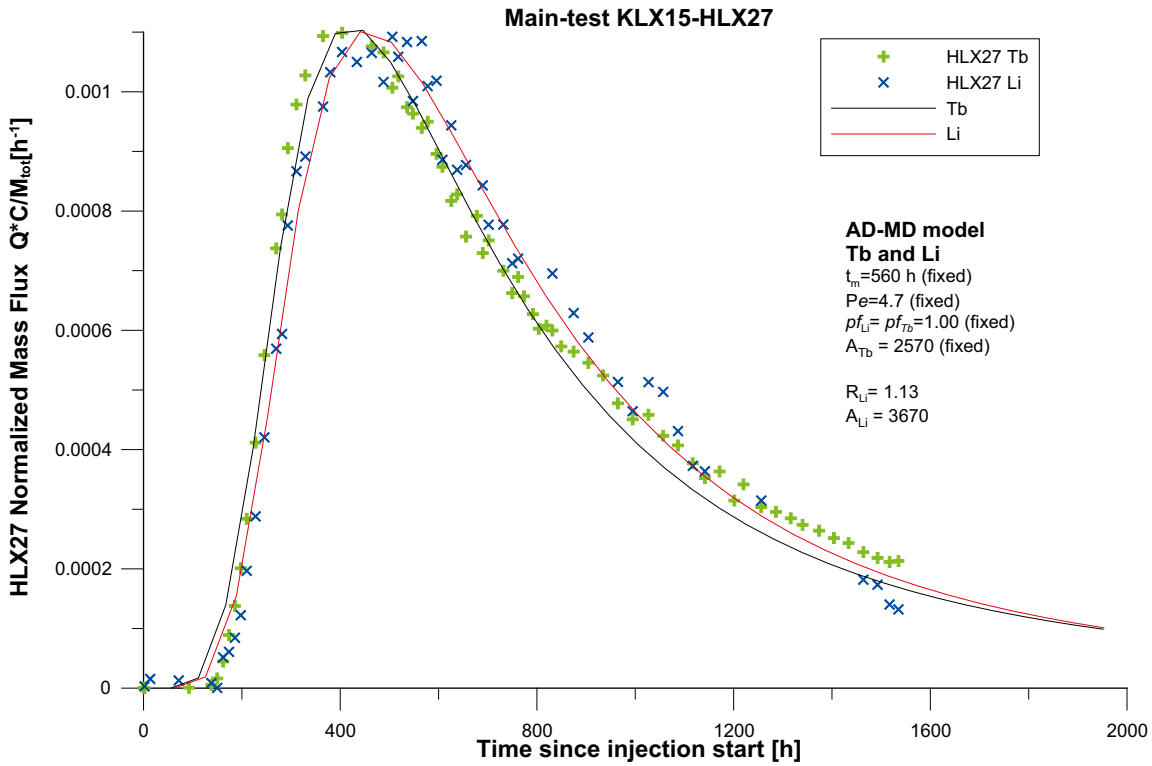

Figure 5-34. *Linear plot of model fit using the AD-MD model to experimental data for the main test. Tb-DTPA is the non-sorbing tracer and Li^+ is weakly sorbing.*

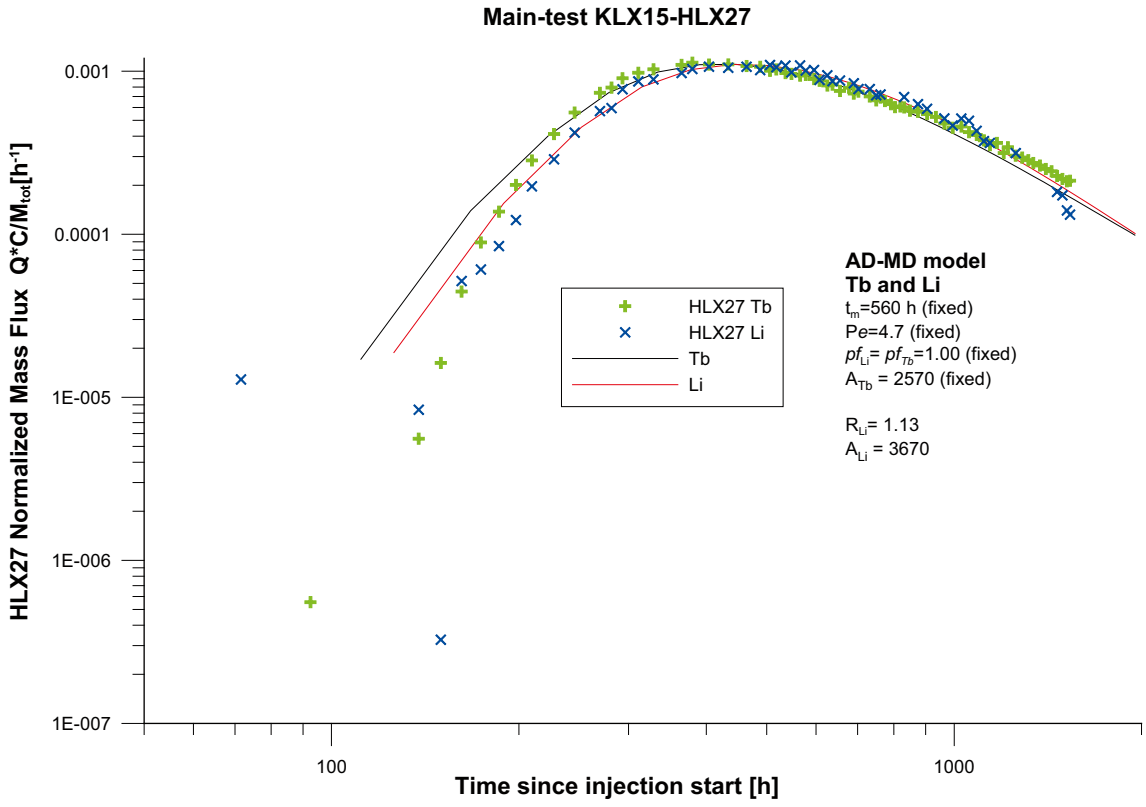

Figure 5-35. *Logarithmic plot of model fit using the AD-MD model to experimental data for the main test. Tb-DTPA is the non-sorbing tracer and Li^+ is weakly sorbing.*

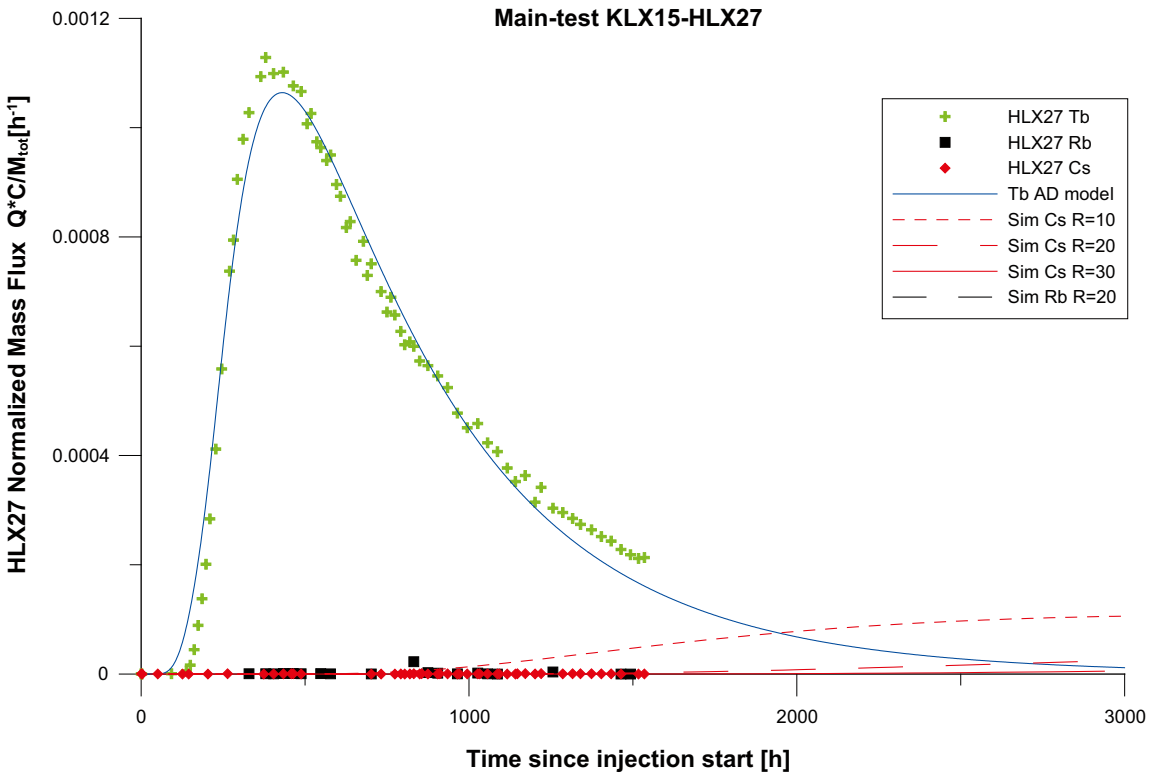

Figure 5-36. *Linear plot of simulations using the AD model and experimental data for Tb-DTPA (non-sorbing), Cs^+ (R = 10, 20, 30) and Rb^+ (R = 20) during the main test.*

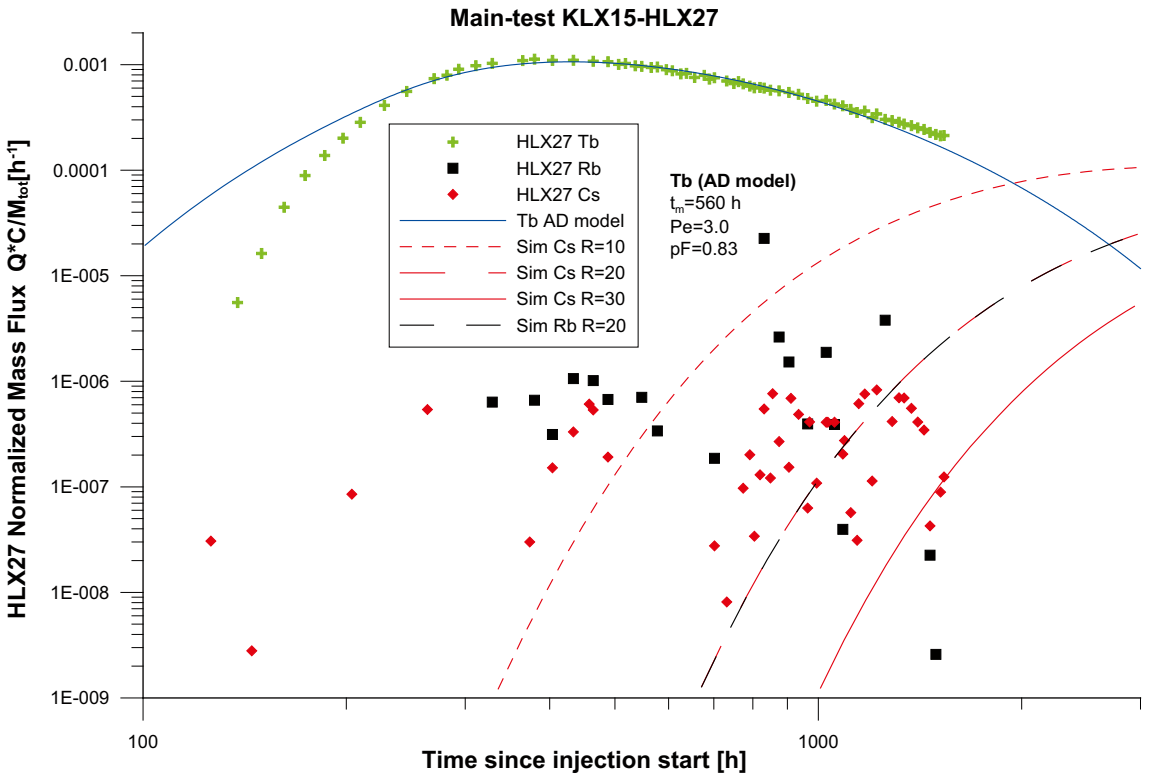

Figure 5-37. *Logarithmic plot of simulations using the AD model and experimental data for Tb-DTPA (non-sorbing), Cs^+ (R = 10, 20, 30) and Rb^+ (R = 20) during the main test.*

Calculations and simulations were made to check that the injection concentration used really should be able to result in a detectable concentration increase in HLX27. If the injection concentration is too low and the residence time very high the breakthrough might not occur due to a too large dilution along the pathway. For R = 20 a concentration of 24 times the background is expected for Cs^+ and 3.7 times background for Rb^+ after 9,744 h. Hence, the absence of Rb^+ and Cs above the background level during the experimental time frame does not depend on a too low injection concentration or too large dilution along the pathway.

Summary

Both the AD and AD-MD model for one pathway could fit the test results for Tb-DTPA, Li^+ and Uranine relatively well. In the AD-MD model the parameter *pf* had to be fixed in order to obtain a good fit. The AD model for two pathways could fit the test results very well. However, the fit was not unambiguous meaning that several setups of parameter values resulted in similar fits. Due to these results, the AD model with one pathway without fixed *pf* was considered to provide the best and robust simulation results and was therefore used in subsequent calculations of transport parameters (see below).

The estimation of R for Li^+ was consistent around 1.1 in simulations with both the AD as well as the AD-MD model.

The minimum estimation of R for both Cs^+ and Rb^+ was judged to be around 20.

5.7.3 Transport parameters

A number of other transport parameters may be derived from the modelling results. The simulation with the AD model for one pathway for Tb-DTPA in the main test presented in Figure 5-24 and 5-25 was considered to provide the most reliable result and is therefore used for the following results. Fracture conductivity (K_{fr}), equivalent fracture aperture (δ) and flow porosity (ε_f) were calculated according to SKB's method description (SKB MD 530.006). These calculated parameters are presented in Table 5-19 together with the background data used for the calculations.

In order to calculate the additional transport parameters the mean head difference, Δh (m) between injection- and pumping section has to be determined. The mean head differences were determined from head readings (pressure registrations) in both boreholes just before pump stop. The width of the flow anomalies given in Table 5-19 is based on the flow logging results as reported in /Rohs et al. 2007/.

The additional transport parameters were not calculated for the pre-test since the mean residence time t_m is in transformed time units corresponding to flow rate 75 l/min and the ground water levels used to calculate the head difference, Δh corresponds to the drawdown caused by the lower flow rate (50 l/min).

Table 5-19. Evaluated transport parameters and background data for calculation of transport parameters.

Input for calculation of transport parameters	
Tracer	Tb-DTPA
Model	AD
t_m (h)	560
Pumping flow, Q (l/min)	75
Distance (m)	140
Width of flow anomaly (m)	3
Head difference (m)	10.00
Evaluated transport parameters	
Fracture conductivity, K_{fr} (m/s)	4.0E–03
Mass balance aperture, δ (m)	4.1E–02
Flow porosity, ε_f (–)	3.6E–03

6 Summary and discussion

6.1 Equipment and procedures

The performance of this tracer test included a rather complicated chain of methods and procedures in order to maintain and control of both chemical and hydraulic boundary conditions. Synthetic water was manufactured in large quantities and three different chemical solutions were added simultaneously and with constant flow rates to maintain a steady flow field. Overall this worked quite well. The major technical problem was a number of pump stops in HLX27 caused by pump failure and power failures creating a somewhat varying pumping flow rate. However, this is considered not to have any significant impact on the results and evaluation of the test.

6.2 Errors and uncertainities

6.2.1 Outliers

Obvious outliers in the measured tracer concentration data were deleted before further calculations were made and before analyzing data with transport models. No outliers had to be removed from the Cs^+ and Tb-DTPA data sets.

The reason for the anomalous results of Li^+ and Rb^+ for some samples (see Figure 5-15) has been investigated. The anomalous results appear in the same samples for both Li^+ and Rb^+. Several aspects have been considered e.g. different staff handling samples, pH measurement to exclude suspicion that some samples were not acidificated, the sample position in the sampler, time for restart of sampler but no correlations of these events and the diverging samples can be found.

Li^+ and Rb^+ are much more abundant in nature resulting in more severe contamination risks. This might partly explain why some samples show diverging results for Li^+ and Rb^+, but not for Cs^+ and Tb-DTPA. Also, since the samples were not filtrated before acidification, contribution from leaching of particulates will result in increase of concentration over storage time which will be more pronounced for more abundant elements (Rb^+ and Li^+).

Directly after the peak concentration of Uranine the breakthrough curve makes a leap down to a lower level. Some low values are also seen just after 800 h. Each jump is correlated to the collection of a new sample batch made in the field. It is possible that the samples in these batches were not buffered, or were exposed to sunlight. Hence, these sample points are regarded as outliers and are removed from the data set. Another gap is seen around 1,000–1,200 h, and in this case it can be verified that exposure to sunlight occurred, and these results are not considered reliable. They were also removed from the data set.

6.2.2 Analyses or metals (Tb, Li, Cs, Rb)

The accuracy of the analyses performed by ALS Scandinavia is ±15% and depends on several factors such as:

a). Uncertainty in concentration of calibration standard.

b). Dilution variations.

c). Drift allowance.

d). Instrumental spread.

e). Uncertainty associated with blank correction.

However, short-term reproducibility (within single analytical run) can be much better (3–4%) as many variation contributions will be the same for all samples within the run.

6.2.3 Analyses of Uranine

Uranine was used in this test only as a rough indicator of tracer breakthrough since it can be easily and quickly analysed. If it had been used as a real tracer, very large amounts of tracer would have been needed. In groundwater flow measurements using the dilution technique a peak concentration of 500 ppb is normally used and in earlier cross-hole tracer tests the peak concentrations have been around 300 ppb /Lindquist et al. 2008a/ and /Lindquist et al. 2008b/. The concentration of Uranine in the pumping borehole of this tracer test is considered to be too low to be certain. In this test the peak concentration is 24 ppb which is only a factor 10 above the background at the start of pumping. Given the fact that Uranine is used as marker of the drilling fluid in all boreholes, it is likely that the background will vary as pumping goes on. Hence, a correction for background will be probably be highly speculative.

The normalized breakthrough curves of Uranine and Tb-DTPA show a higher peak of Uranine, which might lead to the assumption that Tb-DTPA is weakly sorbing. However, because of the large uncertainties of the Uranine analysis, such a conclusion is doubtful.

Tb (in the form Tb-DTPA used here) is earlier reported as a non-sorbing tracer /Byegård et al. 1999/. In order to evaluate the retardation of Li^+, Tb-DTPA was therefore regarded as the non-sorbing tracer. Also, Tb-DTPA and Li^+ are analysed by the same analytical method, hence it is more reasonable to compare these two elements. The evaluation of the Uranine breakthrough curve should only be seen as supportive to the evaluations of Li^+ and Tb-DTPA.

6.3 Tracer test – general

Both the simulated recovery at infinite time as well as calculated recovery at pump stop is lower for RdWT than for Tb-DTPA and Uranine, despite the longer time of pumping for RdWT. This likely depends on the lower flow rate during the pre-test. When a lower flow rate is used, the risk that tracer is transported in other directions than to the pumping borehole increases.

The recovery of tracers from the main tracer test could have been affected by the fact that there was a 24 h long pump stop during the injection period. It is reasonable to suspect that the spreading around the injection section increased during the stop, which also might result in lower tracer recovery than otherwise.

It is reasonable to believe that the recovery of tracer in the experiment (main test) is near 100% at infinite time. The models indicate recoveries of 83% for both Tb-DTPA and Li^+ although the tails are obviously a little too low, at least for Tb-DTPA. Recovery at pump stop is also rather high, c. 80% for both of the tracers.

During planning and design of the tracer test, the risk of saturating sorption sites was considered. The test was designed to avoid saturation of sorption sites, and the scoping calculations implied that the sorption sites should not be saturated using the present concentrations of the sorbing tracers. However, it may still be possible that some part of the flow-path might be partly saturated. A saturation of sorption sites would result in a shorter residence time than if no saturation occurred. Since no breakthrough was obtained neither for Cs^+ nor for Rb^+, conclusions of whether any saturation of flow paths occurred or not cannot be drawn.

6.3.1 Tube sampling

Since it turned out that the results for Li^+ and Rb^+ can be somewhat uncertain due to different storage time (and possible contamination) it was decided not to consider the Li^+ and Rb^+ results for analysing the tube sampling activity. Also, since no breakthrough was obtained for Cs^+, these results are not useful either. When plotting the results from the tube sampling for Tb-DTPA, Uranine and RdWT together with the breakthrough curves, it is obvious that the single tube samples show

lower concentration than the continuous breakthrough curve and the agreement between the two is rather poor. Two possible explanations for the lower concentration in the tube sampling than in the discharge water from the pumping may be found. The first possible explanation is leakage of water from shallower depths into the tube during lowering of the tube. The second possible explanation is that the tracer does not enter the borehole evenly in the flow anomalies and the mixing from the flow anomaly to the point of sampling with tube in the borehole is poor.

The flow logging in HLX27 prior to the tracer test /Rohs et al. 2007/ suggests two major areas of inflow at 157.5–159.0 mbl and 104.0–105.5 mbl. Furthermore, the transmissivity of the lower anomaly is twice the transmissivity of the upper anomaly. Consequently, if all tracers would enter HLX27 in the lower anomaly and no tracers enters in the upper anomaly the concentration at the 120 mbl level would ideally be 1.5 times the concentration at the 90 mbl level assuming that the inflow of water is proportional to the transmissisivity. However, since the concentration at the 120 mbl level is on average 1.1 times the concentration at the 90 mbl level for Tb, 1.2 for RdWt and 1.3 for Uranine, it may not be excluded that the upper anomaly at 104.0–105.5 mbl also transports tracers, however with a lower concentration than at 157.5–159.0 mbl.

The possible uncertainties about the mixing of water in the borehole and leakage of water into the tube makes the conclusion about tracer transport in the upper flow anomaly very uncertain. Anyway, it is clear that the lower anomaly transport tracer in this test.

6.4 Model simulations

The consistency between the pre-test and the main test is very good regarding the estimate of mean residence time in the simulations with the AD-model. However, using the AD-MD model ($pf = 1$), the mean residence time is significantly lower in the pre-test (330 h) compared to the main test (560 h and 590 h for Tb-DTPA and Li^+ respectively).

The Peclet number and *pf* factor are quite similar for the different models and tracers. The exception is the low recovery for RdWt as discussed earlier and a slightly lower Peclet number for RdWt during the pre test. The Peclet numbers are higher for the AD-MD model than the AD model for both of the tests. This is expected since the Peclet number in the AD model also has to account for any spreading in the breakthrough curve caused by diffusion effects while this is handled by the separate parameter *A* in the AD-MD model.

Consistency between the results from the two tests was expected since they were performed with basically the same set-up. The small differences that still may be observed can, for example, depend on the differences in pumping flow rate during the two tests. Also, there is a difference in the relation between injection flow rate and pumping flow rate (the dipole). During the beginning of the tracer test the relative strength of the dipole was 1/100, but during the main tracer test it varied between 1/150 and 1/190. A stronger dipole may increase the risk that tracer is pushed away and spread more around the injection section. Some of the tracer may then spread in the wrong direction and the recovery in the pumping borehole becomes lower.

A control of the regression statistics from the simulations with the AD-MD model show that there is a high correlation between some of the parameters when *pf* is free. This explains why it is difficult to obtain a well-defined fit. Choosing other initial values results in totally different estimation of t_m, P*e*, *pf* and A. Normally, the fit ought to be better with more free parameters, but in this case, since the fit with the AD model is already quite good, too many free parameters lead to instability.

Since the combined results of the flow logging in HLX27 prior to the tracer test /Rohs et al. 2007/ and the tube sampling during the tracer suggests tracer transport in two separate flow paths, the AD model with two flow paths would be appealing to use. However, as described in Section 5.7.2, the AD model with two flow paths did not give unambiguous results.

6.5 Transport parameters

Since no breakthrough of Cs^+ and Rb^+ was obtained within the experimental time frame, the only conclusion that can be drawn from the tracer experiment is that the value of R for Cs^+ and Rb^+ is at least 20 (see Section 5.7.2). This is higher than the retardation factors evaluated from the similar tracer test performed at the Forsmark site investigations 2007 between KFM02A (section 411.0–441.0 mbl) and KFM02B which was R = 3.4 for Cs^+ and R = 2.7 for Rb^+ /Lindquist et al. 2008a/.

The retardation factor for Li^+ is rather low according to the simulations which is consistent with similar tracer test performed in 2007 at Forsmark /Lindquist et al. 2008a/.

Single-Well Injection-Withdrawal (SWIW) tests have previously been performed in four different boreholes in the Laxemar area (KLX03, KLX02, KLX11 and KLX18). The estimated values of R for Cs^+ and Rb^+ in these tests varies from R = 66 to R = 850 for Cs^+ and from R = 104 to R = 2,700 for Rb^+ /Gustafsson and Nordqvist 2005a, Gustafsson et al. 2005b, Thur et al. 2006/ and /Thur et al. 2007a/. R-values for Cs^+ have been also been reported from other cross-hole tracer tests using similar transport models (advection-dispersion and linear sorption). For example, /Winberg et al. 2000/, reported R = 69, whereas R = 140 was reported by /Andersson et al. 1999/. The lowest retardation factor obtained for Cs^+ in all SWIW-tests conducted within the Oskarshamn and the Forsmark site investigations are reported from section 414.7–417.7 mbl in KFM02A, where R = 11 was reported /Gustafsson et al. 2005c/. The tracer experiment performed between KFM02A and KFM02B in 2007 also resulted in low retardation factors as pointed out above /Lindquist et al. 2008a/.

The relatively high values of the parameter *A* indicate that the effect of diffusion is low. This is consistent with the fact that the AD model provides rather good fits.

The time for first arrival differs between Uranine, Tb-DTPA and Li^+ (all non-sorbing or weakly sorbing) and RdWT. Time for first arrival is shorter for RdWT although the pumping rate at this time was only 50 l/min compared to 75 l/min when the other tracers were injected. A possible explanation for this is that the injection flow was higher during the injection of RdWT (500 ml/min) leading to an increased velocity close to the injection section. During the one week period when the tracers for the main tracer test were injected the injection flow was only 400 ml/min. The pump stop cannot have effected the first arrival since it occurred after the time of first arrival.

The interpreted dispersion in the pre-test was slightly higher than during the main test. This may also depend on the stronger dipole during the pre-test compared to the main test causing the tracer to spread more around the injection section than during the main test.

6.5.1 Fracture minerals and geology

Investigation of fracture minerals in the section 260.0–272.0 mbl in KLX15A showed that all open fractures, which according to PFL– and PSS measurements are dominating in the investigated section of KLX15A (260.0–272.0 mbl), have visible mineral coating or filling, see Table 6-1. The pre-dominant fracture minerals in the interval are chlorite and calcite. As third fracture mineral occurs pyrite and hematite. The open fractures are generally slightly altered. The dominating rock type in the interval is quartz monzodiorite (rock code 501036) /Carlsten et al. 2008/. Subordinate rock types also occur within the investigated section and comprise fine-grained diorite-gabbro (rock code 505102) and fine-grained granite (rock code 511058). The section 262.35–265.79 mbl is characterized as a brittle deformation zone with increased frequency of open and sealed fractures /Carlsten et al. 2008/.

No laboratory tests of sorption characteristics have been made previously on core material from 260.0–272.0 mbl in KLX15A. A direct comparison of the tracer test results to laboratory results will therefore not be possible. However, no unusual fracture minerals or rock types for the Laxemar area are found in the section. Instead, they are all rather frequently occurring in the area. Sorption characteristics for the Laxemar site investigation area in general are described in the retardation model /Selnert et al. 2008, in prep/.

Table 6-1. Occurrence of fracture minerals in the hydraulically dominating fractures in borehole interval 260.0–272.0 mbl in KLX15A (Data from Sicada).

Length to fracture (PFL) (mbl)	Length to fracture (geology) (mbl)	T_f (PFL) (m^2/s)	% of section transmissivity (%)	Fracture mineral	Fracture interpretation	Aperture (mm)	Surface	Fracture alteration
262.40	262.350	1.0E–08	0.3%	Chlorite	Open	0.5	Rough	Slightly Altered
	262.444			Chlorite, Calcite, Pyrite	Open	0.5	Slickensided	Slightly Altered
262.90	262.822	2.9E–08	0.8%	Calcite, Chlorite	Open	0.5	Smooth	Slightly Altered
	262.851			Calcite, Chlorite	Open	0.5	Rough	Slightly Altered
	262.931			Calcite, Chlorite	Open	0.5	Rough	Slightly Altered
	262.960			Calcite, Chlorite	Open	2	Rough	Slightly Altered
263.60	263.529	4.4E–07	11.8%	Chlorite, Calcite	Open	1	Rough	Slightly Altered
	263.543			Chlorite, Calcite	Open	1	Smooth	Slightly Altered
	263.589			Chlorite, Calcite, Hematite	Open	0.5	Rough	Slightly Altered
	263.671			Calcite, Chlorite, Hematite	Open	2	Rough	Slightly Altered
263.90	263.821	2.1E–06	56.4%	Chlorite, Calcite, Hematite	Open	0.5	Slickensided	Slightly Altered
	263.888			Chlorite, Calcite	Open	10	Rough	Slightly Altered
264.30	264.370	9.9E–07	26.5%	Chlorite, Calcite	Open	0.5	Slickensided	Slightly Altered
264.60	264.584	1.4E–07	3.7%	Calcite, Chlorite	Open	2	Rough	Slightly Altered
	264.601			Chlorite	Open	1	Rough	Slightly Altered
265.70	265.643	2.1E–08	0.6%	Chlorite, Calcite, Pyrite	Open	0.5	Rough	Slightly Altered
	265.704			Chlorite, Calcite, Pyrite	Open	1	Rough	Slightly Altered
Total		3.7E–06	100%					

6.6 Comparision of results with scoping calculations

6.6.1 Comparision of pre-test with scoping calculations

The original plan was to use tracers in concentrations high enough to obtain a maximum concentration in HLX27 of about 100 times the background concentration. The scoping calculations, as presented in Section 4.2, predicted a mean residence time of 100–200 h with a pumping rate of 50 l/min. The mean residence time was based on the assumption of a fracture aperture of 5–10 mm (which corresponds to c. 25 times the aperture according to the cubic law, see Section 4.2.2). When a breakthrough of RdWT was detected in HLX27, the result was evaluated using the AD model to obtain an approximate mean residence time (t_m). Note that this evaluation was made when only an early part of the breakthrough from the pre-test was available since it had to be done prior to the main test. The maximum concentration in the pre-test occurred the same day as the flow rate increase prior to the main test injection. The early evaluation of the pre-test indicated a travel time of about 800 h (non-transformed time). Hence, the original scoping calculations obviously underestimated the fracture aperture.

6.6.2 Adjusted scoping calculations after the pre-test

Because of the rather long mean residence time indicated by the pre-test, it was decided to increase the flow rate to shorten the mean residence time in the main test. New scoping calculations were made assuming a mean residence time of 400 h (as a result of approximately doubling the flow rate to 90 l/min). The tracers had to be ordered a few weeks in advance because of the tight time schedule. Hence, the total amount of tracers could not be increased, as would have been preferred because of the increased flow rate. Instead, the possibility of using the amount already ordered was investigated. Some of the tracers were already ordered in excess to be prepared for a flow increase. However, RbCl is an expensive chemical and due to economic reasons the amount had to be decreased. The use of Li^+ was restricted by regulations prohibiting a concentration higher than 200 ppb in the pumped water.

The following table (Table 6-1) shows the expected ratio $C_{max}/C_{background}$ and time for concentration maximum to occur for an increased pumping rate (90 l/min).The table shows the concentrations used in the simulation, the concentration possible to achieve (based on the amounts of tracers already bought and in the case of Li^+ restrictions of allowed concentration) and as comparison the actual concentrations as they were in the test performance. The concentration actually used was higher than intended due to an underestimation of the volume in the tank used for preparation of the injection solution. The simulation assumed a dispersivity of 28 m (P*e* = 5), a residence time of 400 h and a dilution factor of 200 due to a 1/200 dipole. One hundred percent recovery was also assumed.

Table 6-1 shows that breakthrough is possible for all tracers within the experimental time frame (about 1,500 h) unless the retardation for Cs^+ and Rb^+ is not too great (> 5).

6.6.3 Comparision of main test with predictions

The actual flow rate used during the main test was 75 l/min instead of the 90 l/min as suggested in the above calculations since it was the practical maximum flow rate for the pump. Since the injection concentrations and the pumping flow rate actually used differed from the planned during the scoping it is difficult to compare the parameters in Table 6-1 with the results. Hence, a new prediction was done assuming the actual injection concentrations used, a travel time of 530 h (corresponding to flow rate of c. 75 l/min), P*e* = 5 and dipole 1/200. The new prediction is presented together with the actual results in Table 6-2.

The results in Table 6-2 show that the new prediction was quite good, especially for the mean residence time. The maximum levels are a little lower than predicted due to the slightly higher dispersivity (lower Peclet number) and lower recovery in the results than assumed in the scoping and prediction, see Table 6-3.

Finally, as pointed out above, the equivalent fracture aperture in the original scoping calculations was too low (5–10 mm) compared to the actual results (39–42 mm). This has been a challenge also in scoping calculations prior to tracer tests performed earlier /Lindquist et al. 2008a/.

Table 6-1. Pump flow 90 l/min (assuming t_m = 400 h). Prediction of breakthrough with the available amount of tracers.

		Cs^+	Rb^+	Li^+	Uranine [2)]	Tb-DTPA
C_{00} (simulated)		150,000	270,000	440,000	50,000	4,200
C_{00} (possible to use)		204,000	271,000	149,000	25,000	4,200
Actual conc. used (measured in the tank) [3)]		206,000	375,000	190,000	22,000	5,500
Time to C_{max} [4)]	**C_{max}/C_{backgr} [4)]**					
384 h	R=1			12 [1)]	7	136
1,520 h	R=5	51	7			
2,940 h	R=10	26	4			

[1)] Gives 774 ppb, maximum allowed is 200 ppb which is only 3 times background.

[2)] Assumed background of Uranine 13 ppb. Amount was decreased and Tb was used as the main-non-sorbing tracer.

[3)] The actual concentration and concentration possible to use differ because the actual volume used was smaller than intended.

[4)] From simulated C_{00}.

Table 6-2. Results compared with predictions assuming Peclet number = 5, t_m = 530 h, dipole 1/200 and 100% recovery.

Tracer	Time to C_{max} (h)		t_m (predicted 530 h) (h) result	C_{max} (times background)	
	Result	Predicted		Result	Predicted
Tb-DTPA	380	475	560	1,097	1,777
Li^+	506	475	580	2	3.6
Uranine	365	475	530	12	15
Cs^+ (R=20)	–	7,728		–	14
Cs^+ (R=10)	–	3,890		–	27

Table 6-3. Model results compared with assumptions in scoping calculations with the AD model.

Tracer	Mass recovery	Peclet number	Mass balance aperture, δ (mm)
RdWt in pre test	63%	2.0	42
Tb-DTPA in main test	83%	3.0	41
Li^+ in main test	83%	3.7	42
Uranine in main test	92%	3.5	39
Assumed in scoping	100%	5.0	5–10

6.7 Geohydraulic conditions

6.7.1 Comparision of different hydraulic tests

The estimated transmissivity for the pumping borehole HLX27 from transient evaluation ($T = 2.7 \cdot 10^{-5}$ m^2/s) is in good agreement with that of previous flow logging ($T = 5.0 \cdot 10^{-5}$ m^2/s) in this borehole /Rohs et al. 2007/. However, the estimated transmissivities for several observation sections in the interference test are significantly higher than the T-values obtained from single-hole tests in these sections from previous investigations, cf. Figure 5-9. This fact is assumed to be due to that the calculated T-values from interference tests represent a larger volume of rock than single-hole tests since the pumping duration is much longer, resulting in a larger radius of influence. Furthermore, during large-scale interference tests the more transmissive hydraulic units dominate and the less transmissive rock may be disguised by units of higher transmissivities. In addition, estimated transmissivities from interference tests may be dominated by the hydraulic conditions close to the pumping borehole in heterogeneous rock.

The estimated transmissivity of observation sections from interference tests in heterogeneous rock may sometimes be overestimated (or not representative) due to poor hydraulic connection to the pumping borehole, cf. Figure 5-9. Hence, estimated T-values from single-hole tests in a certain observation section cannot directly be compared with corresponding T-values from an interference test. In addition, transmissivity and storativity may only be adequately separated for observation sections having good hydraulic connection to the pumping borehole. In other sections, the hydraulic diffusivity (T/S) may be more representative of the specific hydraulic conditions of the observation sections and corresponding pathways in interference tests.

Difference flow logging and injection tests in the injection section KLX15A:6 (260.0–272.0 mbl) indicated transmissivities ranging from $3.4 \cdot 10^{-6}$ to $1.1 \cdot 10^{-5}$ m^2/s in this section /Pöllänen et al. 2007, Enachescu et al. 2007a/. For a recommended transmissivity of $1.1 \cdot 10^{-5}$ m^2/s and an assumed storativity of $1.0 \cdot 10^{-6}$ the radius of influence during the injection test (duration 20 min) in this section was estimated to c. 143 m. From HLX27, the distance to KLX15A:6 is c. 140 m at the actual depth used in the interference test. The interference test evaluation of KLX15A:6 indicated a transmissivity of $5.4 \cdot 10^{-5}$ m^2/s, which is in accordance with the pumping test in HLX27 ($T = 2.7 \cdot 10^{-5}$ m^2/s).

6.7.2 Flow regimes

The single-hole injection test interpretation in KLX15A included evaluation of flow regimes /Enachescu et al. 2007a/. During the injection period of the test in section KLX15A: 260–280 mbl (covering the present injection section KLX15A: 260–272 mbl) the derivative showed a downward slope at middle and late times but did not reach horizontal stabilisation (i.e. radial flow). The injection period was analysed using a two shell composite radial flow model with increasing transmissivity at some distance from the borehole. Alternatively, a radial flow model with transition to pseudo-spherical (leaky) flow by the end might have been used. During the recovery period, the pressure derivative showed a continuous downward trend at middle and late times, which is indicative for transition from wellbore storage and skin dominated flow to pure formation (radial) flow. However, no pure radial flow was reached during this period. A homogenous radial flow model with wellbore storage and skin was chosen for the analysis of the recovery period.

The analyses of the injection and recovery period respectively showed inconsistency regarding the chosen flow model. This inconsistency was attributed to positive skin (+4.2) estimated from the analysis of the recovery period /Enachescu et al. 2007a/. During the injection period the skin factor was estimated to –1.6. The results from the recovery period were chosen as representative for the test.

The pumping test in HLX27 indicated a first PRF (pseudo-radial flow) transitioning to a PSF (pseudo-spherical flow) during the first phase of the test before the increase of flow rate. The same flow regimes were observed in observation section KLX15A:6 during the interference test, cf. Appendix 5.

6.7.3 The hydrogeological model

The results of the hydraulic interference test and tracer test may be compared to the hydrogeological model for the Laxemar area. This model is currently under development, so it may be altered at later occasions. The references used in this report for the hydrogeological model are /Rhén et al. 2008 in prep/, /Wahlgren et al. 2008 in prep/ and /Hermanson et al. 2008/.

Regarding the hydraulic interference test, the main tools for comparison are the response type presented in Table 5-2, Index 1 in Table 5-9 and Index 2_new in Table 5-10. These results are compiled in Table 6-4 together with interpreted deformation zones according to the references mentioned above. The responses listed in Table 6-4 are also displayed visually in Figure 6-1. Each symbol in the figure represents an observation section during the interference test, where the shape of the symbol represents the response type in Table 6-4. For response type 1, the colour represents Index 1 and the size of the circle represents Index 2_new according to the legend in Figure 6-1. The position of the symbols represents the order of sections in the borehole correctly, but is not accurate according to the length scale. The exception is KLX18A where only one grey square is shown, although it should be seven grey squares.

Table 6-4. Hydraulic response and interpreted deformation zone for observation sections used in the interference test. Type: 1 = clear response, 2 = some response but not evaluated, 3 = response can neither be confirmed nor rejected, 3* = as 3 but with missing or detected data, 4 = no response. Index 1 and 2_new: E = Excellent, H = High, M = Medium, L = Low.

Bh ID	Test section (mbl)	Deformation zone	Distance to HLX27: 131.5 mbl (m)	Response Type	Index 1 (r_s^2/dt_L)	Index 2_new $(s_p/Q_p) \cdot \ln(r_s/r_0)$
HLX15	12.04–151.90		822	1	H	M
HLX26	11.00–151.20	ZSMNW042A	769	1	M	L
HLX38	15.02–199.50	ZSMNS059A	738	1	M	L
HLX42:1	30.00–152.60	ZSMNS947A	805	1	M	M
HLX42:2	9.10–29.00		823	4	–	–
KLX03:1	965.50–971.50	DZ8	958	3*	–	–
KLX03:2	830.50–964.50	DZ7	899	1	M	M
KLX03:3	752.50–829.50	KLX03_DZ1b, KLX03_DZ1c	815	1	M	M
KLX03:4	729.50–751.50	ZSMEW946A (DZ1)	778	1	M	M
KLX03:5	652.50–728.50	ZSMEW946A (DZ1), DZ4 – DZ6	743	1	M	L
KLX03:6	465.50–651.50		664	1	M	L
KLX03:7	349.50–464.50	DZ3	596	1	M	L

Bh ID	Test section (mbl)	Deformation zone	Distance to HLX27: 131.5 mbl (m)	Response Type	Index 1 (r_s^2/dt_L)	Index 2_new ($s_p/Q_p) \cdot \ln(r_s/r_0$)
KLX03:8	199.50–348.50	DZ2	566	1	M	M
KLX03:9	193.50–198.50		565	1	M	M
KLX03:10	100.05–192.50		570	1	M	M
KLX05:1	721.00–1,000.00	DZ13	1,108	3	–	–
KLX05:2	634.00–720.00	DZ12	1,058	3	–	–
KLX05:3	625.00–633.00	DZ11	1,048	3	–	–
KLX05:4	501.00–624.00	DZ8 – DZ10	1,037	3	–	–
KLX05:5	361.00–500.00	DZ6, DZ7	1,026	3	–	–
KLX05:6	256.00–360.00	DZ4, DZ5	1,023	3*	–	–
KLX05:7	241.00–255.00		1,024	3*	–	–
KLX05:8	220.00–240.00		1,025	3*	–	–
KLX05:9	128.00–219.00	DZ2, DZ3	1,028	3*	–	–
KLX05:10	15.00–127.00	DZ1	1,040	3*	–	–
KLX10:1	711.00–1,001.00		1,201	3*	–	–
KLX10:2	689.00–710.00	ZSMEW946A (DZ9)	1,122	3*	–	–
KLX10:3	465.00–688.00		1,072	3	–	–
KLX10:4	369.00–464.00	DZ8	1,027	3	–	–
KLX10:5	351.00–368.00		1,016	3*	–	–
KLX10:6	291.00–350.00	ZSMNE942A (DZ7)	1,015	2	–	–
KLX10:7	131.00–290.00	ZSMNE942A (DZ2–DZ6)	1,011	2	–	–
KLX10:8	12.10–130.00	ZSMNE942A (DZ1)	1,004	2	–	–
KLX10C:1	66.00–146.25	KLX10C_DZ7, DZ4 – DZ6	1,097	4	–	–
KLX10C:2	32.00–65.00	KLX10C_DZ3	1,076	3	–	–
KLX10C:3	9.00–31.00	DZ1, DZ2	1,068	3	–	–
KLX12A:1	546.00–602.29	DZ12	1,034	2	–	–
KLX12A:2	535.00–545.00		1,026	2	–	–
KLX12A:3	426.00–534.00	DZ9 – DZ11	1,013	2	–	–
KLX12A:4	386.00–425.00		1,003	3	–	–
KLX12A:5	291.00–385.00	DZ6 – DZ8	999	3	–	–
KLX12A:6	160.00–290.00	DZ1 – DZ5	1,004	3	–	–
KLX12A:7	142.00–159.00		1,014	4	–	–
KLX12A:8	104.00–141.00		1,019	4	–	–
KLX12A:9	17.92–103.00		1,033	4	–	–
KLX14A:1	123.00–176.27	DZ5, DZ6	739	1	M	L
KLX14A:2	77.00–122.00	ZSMNS059A (DZ4)	775	1	M	L
KLX14A:3	6.45–76.00	DZ1 – DZ3	816	2	–	–
KLX15A:1	902.00–1,000.43	ZSMNW042A (DZ19), DZ20	798	4	–	–
KLX15A:2	641.00–901.00	ZSMNE107A (DZ16), DZ13 – DZ15, DZ17, DZ18	619	1	M	M
KLX15A:3	623.00–640.00	DZ12	482	1	H	M
KLX15A:4	481.00–622.00	DZ10, DZ11	403	1	H	M
KLX15A:5	273.00–480.00	DZ5 – DZ9	236	1	M	M
KLX15A:6	260.00–272.00	DZ4, DZ5	140	1	E	M
KLX15A:7	191.00–259.00	DZ2, DZ3	112	1	E	M
KLX15A:8	79.00–190.00	DZ1	95	1	H	M
KLX15A:9	11.65–78.00		148	1	H	M
KLX16A:1	327.00–433.55	ZSMNE107A (DZ12)	822	3	–	–
KLX16A:2	86.00–326.00	ZSMNE107A (DZ9–DZ11), DZ3–DZ8	787	1	M	M
KLX16A:3	11.25–85.00	DZ1, DZ2	789	1	M	M
KLX18A:1	571.00–611.28	ZSMEW946A	1,001	3	–	–
KLX18A:2	490.00–570.00		974	3	–	–
KLX18A:3	472.00–489.00	KLX18_DZ9	954	3	–	–
KLX18A:4	315.00–471.00	DZ4 – DZ8	925	3	–	–
KLX18A:5	155.00–314.00	ZSMNE944A (DZ3)	892	3	–	–
KLX18A:6	104.00–154.00	DZ1, DZ2	886	3	–	–
KLX18A:7	11.83–103.00		889	3	–	–
KLX19A:1	661.00–800.07	DZ9, DZ10	1,092	3	–	–
KLX19A:2	518.00–660.00	klx19_dz5–8_dolerite (DZ7, DZ8)	1,027	3	–	–
KLX19A:3	509.00–517.00	klx19_dz5–8_dolerite (DZ6)	998	3*	–	–
KLX19A:4	481.50–508.00	klx19_dz5–8_dolerite (DZ5)	992	3	–	–
KLX19A:5	311.00–480.50	ZSMNE942A (DZ4), DZ3	963	3	–	–
KLX19A:6	291.00–310	DZ2	934	3	–	–
KLX19A:7	136.00–290		944	3*	–	–
KLX19A:8	92.75–135.00	DZ1	935	3*	–	–

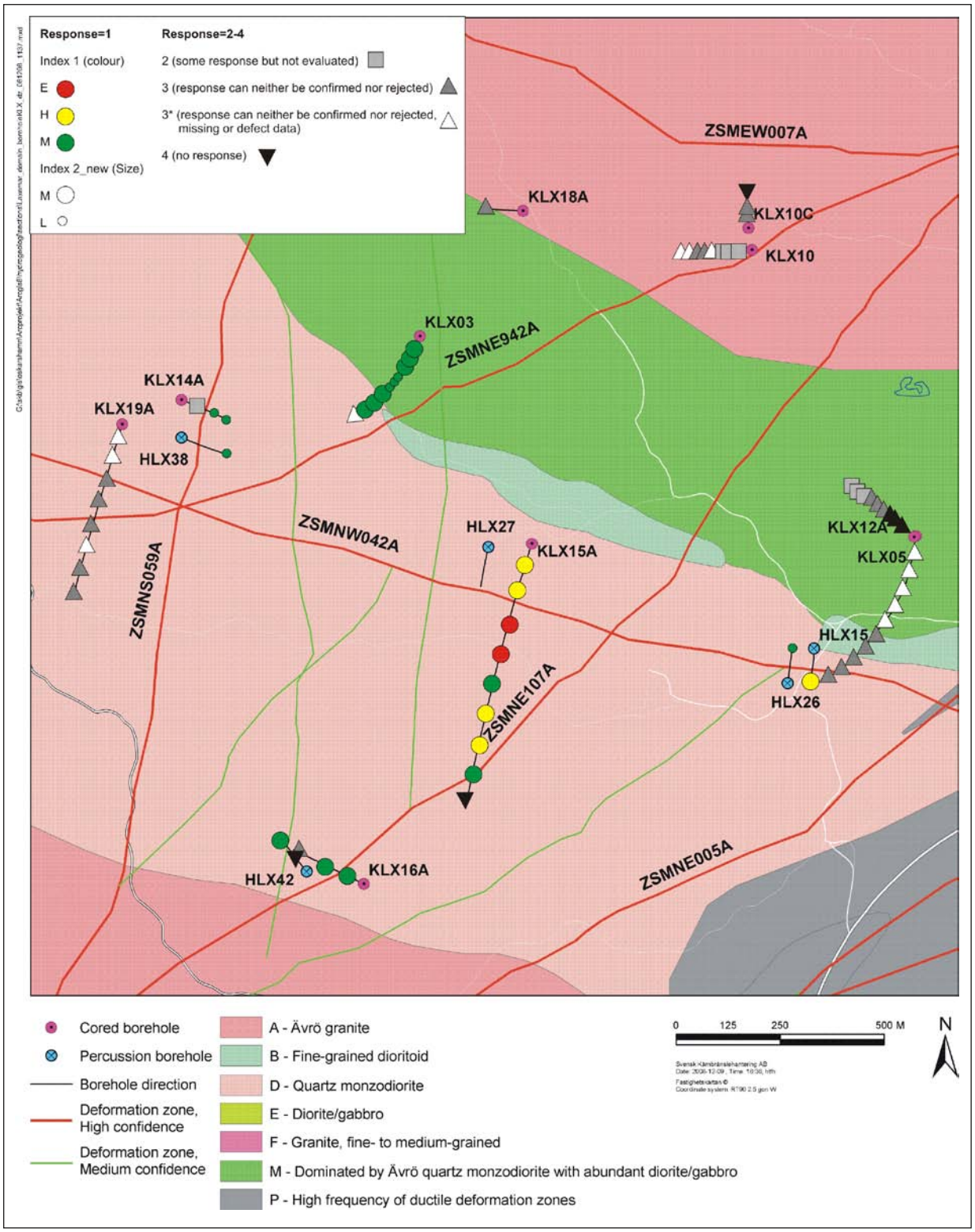

Figure 6-1. *Map of boreholes used in the interference test. The pumping hole was HLX27 in the centre of the map. The shape, size and colour indicate the hydraulic response according to Table 6-4. Where there is more than one dot, each dot represents a section in the borehole. The pink circles with a black dot represent core-drilled boreholes and the blue circles with a black cross percussion-drilled boreholes.*

It is important to remember that the responses shown in Figure 6-1 and Table 6-4 only are based on pressure responses and not flow responses. A good pressure response is likely to also indicate a good connectivity from the pumping section to the observation point. Vice versa, no pressure response is likely to indicate a bad connectivity. However, a good connectivity to a zone with high transmissivity (and good access to water) may also result in a small or no response. The extreme example of this would be a zone with excellent connectivity to a lake or the sea. It is therefore important to also consider the transmissivity values from single hole tests as presented in Table 2-4 when discussing the responses.

Figure 6-1 shows that the responses of type 1 are located rather evenly distributed around the pumping hole in all directions, while the responses of type 2, 3 and 4 generally are located further away from the pumping hole. However, some interesting observations can be made.

Borehole section KLX15A:1 displays no response even though it is considered to intersect ZSMNW042A and the straight line distance from HLX27 is shorter (798 m) than to other sections with better responses (e.g. HLX15, HLX42, KLX03). This may partly depend on the rather low single hole transmissivity for KLX15A:1. HLX26 is also interpreted to intersect ZSMNW042A. However, the response in the rather closely situated borehole HLX15 is better than in HLX26, even though the straight line distance from HLX27 is longer to HLX15 and does not include any interpreted zones. The single hole transmissivity of the two holes are also rather similar. This may also indicate that ZSMNW042A does not facilitate good hydraulic responses. The other boreholes east of HLX27 (KLX05 and KXL12A) does not display any large responses (only response type 2, 3 or 4). This is not unexpected since the straight line distance from HLX27 is rather long and no larger deformation zones are interpreted to intersect the boreholes according to Table 6-4.

In KLX16A and HLX42 (located south of HLX27) the larger responses seem to be present in the borehole sections with higher transmissivity (KLX16A:2 and KLX16A:3) or sections with major deformation zones (HLX42:1 intersects ZSMNS947A). The exception is KLX16A:1 which is interpreted to intersect the lower part of ZSMNE107A. However, it seems like the more transmissive part of ZSMNE107A is located in KLX16A:2.

All sections in KLX03 display relatively good responses, except for KLX03:1, no matter if a major zone is interpreted in the sections or not. Other boreholes north of HLX27 do not display any response type 1. Still, an interesting observation may be made for KLX10, where the three upper most sections, which also intersects ZMNE942A, show response type 2 while the other show response type 3 or 4. Other boreholes to the north of HLX27 do not show any good responses. This could indicate that ZMNE942A enhances hydraulic responses in the area.

KLX14A (located west of HLX27) display better responses in KLX14A:2 and KLX14A:3, which intersects or is located east of ZSMNS059A, than in KLX14A:1, which is located west of ZSMN059A. HLX38, which also intersects ZSMNS059A, displays a good response. KLX19A, on the other hand only display response type 3, even though KXL19A:5 includes ZSMNE952A, which to the north of HLX27 seems to enhance good hydraulic responses. The apparently better responses in the sections that intersect or are located east of ZSMNS059A, may indicate that the zone acts as a hydraulic boundary. However, this conclusion is vague since the reason for differences in the responses may be that the sections with less response west of HLX27 are located further from pumping hole than sections with better response (according to the straight line distance).

The results from the tracer test may also be compared to the hydrogeological model. However, the model does not suggest any major zone going straight from the tracer injection section (KLX15A:6) to the pumping hole HLX27. Therefore, the possible fractures for the tracer transport were investigated in more detail.

The section 262.35 to 265.79 mbl in KLX15A ,which coincides with the flow anomalies in the tracer injection section (cf. Figure 2-1) is described in /Carlsten et al. 2005/ as possible deformation zone DZ4. In /Hermanson et al. 2008/ the DZ4 has been interpreted having the strike and dip 302/14. However, DZ4 with this orientation, never intersects HLX27. DZ4 is indicated as the green coloured plane in Figure 6-2.

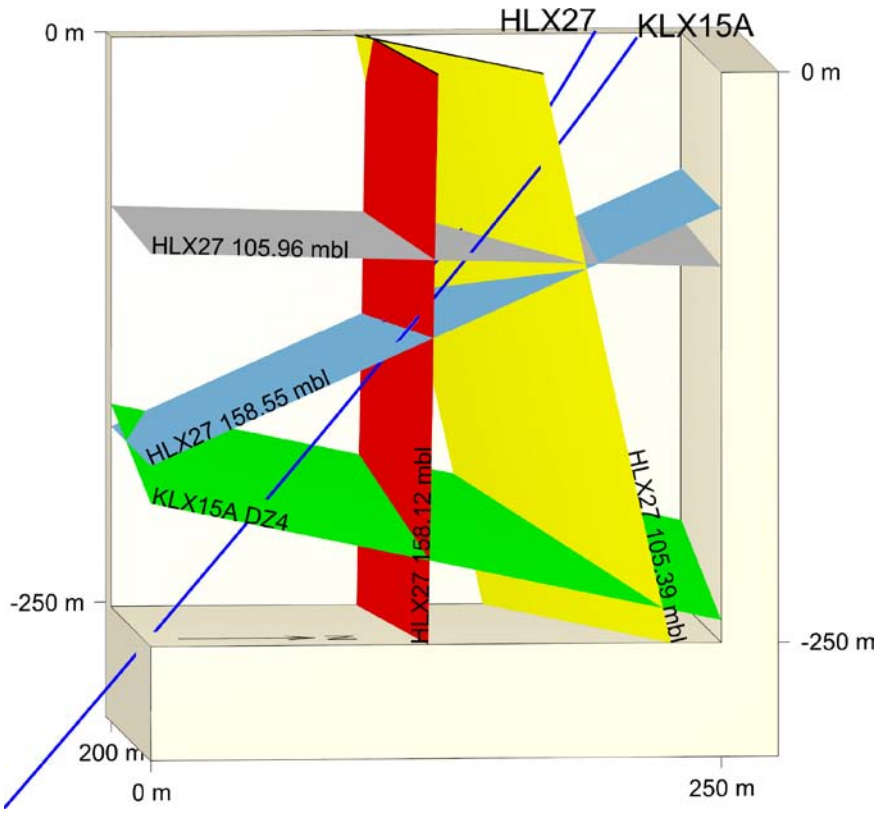

Figure 6-2. *Extrapolation of identified fractures possibly involved in the tracer transport from KLX15A:6 to HLX27.*

As discussed in Section 6.3, none of the flow anomalies at 104.0–105.5 mbl and 157.5–159.0 mbl in HLX27 may be excluded as an entering point for the tracers, however the lower anomaly (157.5–159.0 mbl) is likely to correspond to the majority of the tracer transport in the test. Boremap data was used for identification of possible fractures for tracer transport in HLX27. The Boremap-file /Boremap39_3_HLX27_20081119.mbd/ was used for interpretation of fractures and orientations in HLX27. The Boremap-file /Boremap39_3_KLX15A_20081211.mbd/ was used for interpretation of fractures and orientations in KLX15A. The end of Boremap mapping in HLX27 is at 158.654 mbl.

Investigation of Boremap data from HLX27 shows two open fractures in the section 104.0–105.5 mbl which are shown in Table 6-5. One open fracture occurs at 105.39 mbl with the orientation 252/78, fracture width 3 mm and aperture 0.5 mm, and the other open fracture occurs at 105.96 mbl with the orientation 301/02, fracture width 7.7 mm and aperture 0.5 mm. The fracture with sub horizontal orientation is shown as the grey coloured plane and the sub vertical fracture as the yellow plane in Figure 6-2.

The interval HLX27:157.5–159.0 mbl contains six open fractures. The three fractures at 158.116 mbl, 158.221 mbl and 158.223 mbl have similar directions and could be involved in the tracer transport since they intersect KLX15A:DZ4 rather close to the tracer injection point. The fracture with the largest width and aperture of them is shown as the red coloured plane in Figure 6-2. Also the fracture at 158.551 mbl has a direction that makes it a possible transport path for the tracer test. It is shown in Figure 6-2 as a light blue plane. The two uppermost fractures in the interval may also intersect KLX15A:DZ4 but further away from the tracer injection points. They are therefore considered as less likely transport paths and are not shown in Figure 6-2.

Table 6-5. Structures in HLX27 from Boremap data.

Borehole	Borehole length (mbl)	Character	Strike	Dip	Fracture width (mm)	Fracture aperture (mm)
HLX27	105.391	Open	252	78	3	0.5
HLX27	105.961	Open	301	02	7.7	0.5
HLX27	158.001	Open	122	24	4	2
HLX27	158.010	Open	284	74	3	1
HLX27	158.116	Open	086	89	3	1
HLX27	158.221	Open	070	72	3	1
HLX27	158.223	Open	089	84	2	0.5
HLX27	158.551	Open	090	24	10	10

Figure 6-2 display the extrapolation of the possible fractures involved in the tracer transport from KLX15A:6 to HLX27 as discussed above. The tracer injection point is located where the green plane intersects KLX15A. The entering point of tracer into HLX27 is located where the red or light-blue intersects HLX27 and/or where the yellow and grey plane intersects HLX27. According to previous hydraulic tests in the boreholes it is reasonable to assume that the transmissivity of the fractures in Figure 6-2 would be in the same range. An interpretation of the tracer transport based on Figure 6-2 would therefore be a major transport path starting in KLX15A:DZ4 (green plane) transitioning to HLX27:158.12 mbl (red) or HLX27:158.55 mbl (blue) to finally end in HLX27 at c. 158 mbl. However, several secondary transport paths could be possible where the tracer would enter HLX27 at c. 105 mbl. For example, KLX15A:DZ4 (green) to HLX27:105.39 mbl (yellow) or KLX15A:DZ4 (green) to HLX27:158.12 mbl (red) and finally HLX27:105.96 mbl (grey) or KLX15A:DZ4 (green) to HLX27:158.55 mbl (blue) and finally HLX27:105.39 mbl (yellow). These possible flow paths for the tracer from KLX15A:6 to HLX27 are summarized in Table 6-6 together with the estimated minimum travel distances for the different flow paths. It is clear that the flow paths ending in HLX27 at c. 105 mbl are longer than flow paths ending at c. 158 mbl in HLX27. This also points to a major transport from KLX15A:6 to HLX27 with an entering point at c. 158 mbl in HLX27.

Hence, the interpretation of the tracer test results with the major tracer entering point in HLX27 157.5–159.0 mbl and a possible minor tracer entering point in HLX27 104.0–105.5 mbl is not contradicted by Figure 6-2. If anything, Figure 6-2 provides support for the interpretation of the tracer test transport paths.

Table 6-6. Alternative flow paths from KLX15A:6 to HLX27. The given colour within parentheses corresponds to the colours in Figure 6-2.

Fracture #1	Fracture #2	Fracture #3	Estimated minimum travel distance [m]	Entering point in HLX27 [mbl]
KLX15A:DZ4 264 mbl (green)	HLX27:158.12 mbl (red)		158	158
KLX15A:DZ4 264 mbl (green)	HLX27:158.55 mbl (blue)		210	158
KLX15A:DZ4 264 mbl (green)	HLX27:105.39 mbl (yellow)		271	105
KLX15A:DZ4 264 mbl (green)	HLX27:158.12 mbl (red)	HLX27:105.96 mbl (grey)	225	105
KLX15A:DZ4 264 mbl (green)	HLX27:158.55 mbl (blue)	HLX27:105.39 mbl (yellow)	275	105

7 References

Andersson P, Wass E, Byegård J, Johansson H, Skarnemark G, 1999. Äspö Hard Rock Laboratory. True 1st stage tracer programme. Tracer test with sorbing tracers. Experimental description and preliminary evaluation. SKB IPR-99-15, Svensk Kärnbränslehantering AB.

Andersson P, Byegård J, Winberg A, 2002. Final report of the TRUE Block Scale project 2. Tracer tests in the block scale. SKB TR-02-14, Svensk Kärnbränslehantering AB.

Byegård J, Skarnemark G, Skålberg M, 1999. The stability of some metal EDTA, DTPA and DOTA complexes: Application as tracers in groundwater studies. Journal of Radioanalytical and Nuclear Chemistry, Vol 241, No. 2 (1999) 281–290.

Carlsten S, Hultgren P, Mattsson H, Stanfors R, Wahlgren C-H, 2005. Oskarshamn site investigation – Geological single-hole interpretation of KLX03, HLX26 and HLX27. SKB P-05-38, Svensk Kärnbränslehantering AB.

Carlsten S, Mattson K-J, Stråhle A, Hultgren P, Mattsson H, Wahlgren C-H, 2008. Oskarshamn site investigation. Geological single-hole interpretation of KLX15A, HLX30, HLX31 and HLX33. SKB P-08-05, Svensk Kärnbränslehantering AB.

Cooley R L, 1979. A method of estimating parameters and assessing reliability for models of steady ground water flow. 2. Applications of statistical analyses. Water Resourses Reaserch, 15:318–324.

Enaschescu C, Rohs S, van der Wall R, 2006. Oskarshamn site investigation. Hydraulic injection tests in borehole KLX18A. Subarea Laxemar. SKB P-06-225, Svensk Kärnbränslehantering AB.

Enaschescu C, Rohs S, van der Wall R, Wolf P, 2007a. Oskarshamn site investigation. Hydraulic injection tests in borehole KLX15A .Subarea Laxemar. SKB P-07-192, Svensk Kärnbränslehantering AB.

Enaschescu C, Rohs S, Wolf P, 2007b. Oskarshamn site investigation. Hydraulic injection tests in borehole KLX16A. Subarea Laxemar. SKB P-07-120, Svensk Kärnbränslehantering AB.

Enaschescu C, Böhner J, Wolf P, 2007c. Oskarshamn site investigation. Pumping tests and hydraulic injection tests in borehole KLX19A. Subarea Laxemar. SKB P-07-90, Svensk Kärnbränslehantering AB.

Gustafsson E, 2002. Bestämning av grundvattenglödet med utspädningsteknik – Modifiering av utrustning och kompletterande mätningar. SKB R-02-31, Svensk Kärnbränslehantering AB.

Gustafsson, J, Gustafsson C, 2004. Oskarshamn site investigation. RAMAC and BIPS logging in boreholes HLX10, HLX26, HLX27 and HLX28. SKB P-04-297, Svensk Kärnbränslehantering AB.

Gustafsson E, Nordqvist R, 2005a. Oskarshamn site investigation. Ground water flow measurements and SWIW-tests in boreholes KLX02 and KSH02. SKB P-05-28, Svensk Kärnbränslehantering AB.

Gustafsson E, Nordqvist R, Thur P, 2005b. Oskarshamn site investigation. Ground water flow measurements and SWIW-tests in borehole KLX03. SKB P-05-246, Svensk Kärnbränslehantering AB.

Gustafsson E, Nordqvist R, Thur P, 2005c. Forsmark site investigation. Groundwater flow measurements in boreholes KFM01A, KFM02A, KFM03A, KFM03B and SWIW tests in KFM02A, KFM03A. SKB P-05-77, Svensk Kärnbränslehantering AB.

Gustafsson J, Gustafsson C, 2007. Oskarshamn site investigation. RAMAC, BIPS and deviation logging in borehole KLX15A. SKB P-07-117, Svensk Kärnbränslehantering AB.

Harrström J, Ludvigson J-E, Hjerne C, 2006a. Oskarshamn site investigation. Single-hole injection tests in borehole KLX10. SKB P-06-182, Svensk Kärnbränslehantering AB.

Harrström J, Ludvigson J-E, Hjerne C, 2006b. Oskarshamn site investigation. Hydraulic injection tests in borehole KLX12A. SKB P-06-148, Svensk Kärnbränslehantering AB.

Hermanson J, Fox A, Öhman J, Rhén I, 2008. Compilation of data used for the analysis of the geological and hydrogeological DFN models. Site descriptive modelling. SDM-Site Laxemar. SKB R-08-56, Svensk Kärnbränslehantering AB.

Javandel I, Doughty C, Tsang C F, 1984. Groundwater transport: Handbook of mathematical models. American Geophysical Union, Washington, D.C.

Kruseman G P, de Ridder N A, 1990. Analysis and Evaluation of Pumping Test Data. ILRI publication 47, The Netherlands, Int. Inst. For Land Reclamation and Improvement.

Kyllönen H, Leppänen H, Kristiansson S, 2007. Oskarshamn site investigation. Difference flow logging in borehole KLX19A. Subarea Laxemar. SKB P-07-20, Svensk Kärnbränslehantering AB.

Lindquist A, Hjerne C, Nordqvist R, Byegård J, Walger E, Ludvigson J-E, Wass E, 2008a. Forsmark site investigation. Confirmatory hydraulic interference test and tracer test at drillsite 2. SKB P-08-13, Svensk Kärnbränslehantering AB.

Lindquist A, Hjerne C, Nordqvist R, Wass E, 2008b. Forsmark site investigation. Large scale confirmatory multiple hole tracer test. SKB P-08-59, Svensk Kärnbränslehantering AB.

Ludvigsson J-E, Jönsson S, Levén J, 2004. Forsmark site investigation. Hydraulic evaluation of pumping activities prior to hydro-geochemical sampling in vorehole KFM03A – Comparision with results from difference flow logging. SKB P-04-96, Svensk Kärnbränslehantering AB.

Moench A F, 1985. Transient flow to a large-diameter well in an aquifer with storative semiconfining layers, Water Resources Research, vol. 21, no. 8, pp. 1121–1131.

Moreno L, Neretnieks I, Klockars C-E, 1983. Evaluation of some tracer tests in the granitic rock at Finnsjön. SKB TR 83-38, Svensk Kärnbränslehantering AB.

Moye D G, 1967. Diamond drilling for foundation exploration. Civ. Eng. Trans. 7th.Inst. Eng. Australia.

Nielsen U T, Ringgaard J, Horn F, 2004. Oskarshamn site investigation. Geophysical borehole logging in boreholes KLX04, HLX26, HLX27 and HLX28. SKB P-04-306, Svensk Kärnbränslehantering AB.

Nielsen U T, Ringgaard J, 2007. Oskarshamn site investigation. Geophysical borehole logging in borehole KLX15A. SKB P-07-152, Svensk Kärnbränslehantering AB.

Pöllänen J, Sokolnicki M, Väisäsvaara J, 2007. Oskarshamn site investigation. Difference flow logging in borehole KLX15A. Subarea Laxemar. SKB P-07-176, Svensk Kärnbränslehantering AB.

Rahm N, Enachescu C, 2005a. Oskarshamn site investigation. Hydraulic injection tests in borehole KLX03, 2005. Subarea Laxemar. SKB P-05-192, Svensk Kärnbränslehantering AB.

Rahm N, Enachescu C, 2005b. Oskarshamn site investigation. Hydraulic injection tests in borehole KLX05, 2005. Subarea Laxemar. SKB P-05-222, Svensk Kärnbränslehantering AB.

Rhen I (ed), Gustafson G, Stanfors R, Wikberg P, 1997. Äspö HRL – Geoscientific evaluation 1997/5. Models based on site characterization 1986–1995. SKB TR 97-06, Svensk Kärnbränslehantering AB.

Rhén I, Forsmark T, Hartley L, Jacksson P, Roberts D, Swan D, Gylling B, 2008, in prep (draft 2008-07-18). Hydrogeological conceptualisation and parameterisation. Site Descriptive modelling, SDM-Site Laxemar. SKB R-08-78, Svensk Kärnbränslehantering AB.

Rohs S, 2006. Oskarshamn site investigation. Flow logging in boreholes HLX21, HLX35 and HLX38. Subarea Laxemar. SKB P-06-147, Svensk Kärnbränslehantering AB.

Rohs S, van der Wall R, Wolf P, 2007. Oskarshamn site investigation. Flow logging in boreholes HLX14, HLX20, HLX27, HLX28, HLX32, HLX33, HLX37, HLX39 and HLX43. Subarea Laxemar. SKP P-06-319, Svensk kärnbränslehantering AB.

Rouhiainen P, Pöllänen J, Sokolnicki M, 2005. Oskarshamn site investigation. Difference flow logging of borehole KLX03. Subarea Laxemar. SKB P-05-67, Svensk Kärnbränslehantering AB.

Selnert E, Byegård J, Widestrand H, Carlsten S, Döse C, Tullborg E-L, 2008 (in prep). Bedrock transport properties. Data evaluation and retardation model. Site Descriptive modelling, SDM-Site Laxemar. SKB R-08-100, Svensk kärnbränslehantering AB.

Sokolnicki M, Rouhiainen P, 2005. Oskarshamn site investigation. Difference flow logging of borehole KLX05. Subarea Laxemar. SKB P-05-160, Svensk Kärnbränslehantering AB.

Sokolnicki M, 2006. Oskarshamn site investigation. Difference flow logging of borehole KLX10. Subarea Laxemar. SKB P-06-58, Svensk Kärnbränslehantering AB.

Sokolnicki M, Kristiansson S, 2006. Oskarshamn site investigation. Difference flow logging of borehole KLX18A. Subarea Laxemar. SKB P-06-184, Svensk Kärnbränslehantering AB.

Streltsova T D, 1988. Well testing in heterogeneous formations. Exxon Monograph. John Wiley and sons.

Tang G H, Frind E O, Sudicky E A, 1981. Contaminant transport in fractured porous media. An analytical solution for a single fracture. Water Resources Research, Vol 17, 555.

Thur P, Nordqvist R, Gustafsson E, 2006. Oskarshamn site investigation. Ground water flow measurements and SWIW-tests in borehole KLX11A. SKB P-06-287, Svensk Kärnbränslehantering AB.

Thur P, Nordqvist R, Gustafsson E, 2007a. Oskarshamn site investigation. Ground water flow measurements and SWIW-tests in borehole KLX11A. SKB P-07-180, Svensk Kärnbränslehantering AB.

Thur P, Walger E, Ludvigson J-E, Morosini M, 2007b. Oskarshamn site investigation. Hydraulic interference tests in HLX34, HLX37 and HLX42. SKB P-07-185, Svensk Kärnbränslehantering AB.

Thur P, 2008. Oskarshamn site investigation. Groundwater flow measurements in permanently installed boreholes. Test campaign no. 3 2007. SKB P-08-31, Svensk Kärnbränslehantering AB.

Wahlgren C-H, Curtis P, Hermansson J, Forsberg O, Öhman J, Drake H, Fox A, La Pointe P, Triumf C-A, Mattsson H, Thunehed H, 2008, in prep (draft 2008-08-18). Geology Laxemar Site descriptive modelling, SDM-site Laxemar. SKB R-08-54, Svensk Kärnbränslehantering AB.

Winberg A, Andersson P, Hermansson J, Byegård J, Cvetkovic V, Birgersson L, 2000. Äspö Hard Rock Laboratory. Final report of the first stage of the tracer retention understanding experiment. SKB TR-00-07, Svensk Kärnbränslehantering AB.

Väisäsvaara J, Leppänen H, Kristiansson S, Pöllänen J, 2006a. Oskarshamn site investigation. Difference flow logging of boreholes KLX9G, KLX10B and KLX10C. Subarea Laxemar. SKB P-06-229, Svensk Kärnbränslehantering AB.

Väisäsvaara J, Heikkinen P, Kristiansson S, Pöllänen J, 2006b. Oskarshamn site investigation. Difference flow logging of borehole KLX12A. Subarea Laxemar. SKB P-06-185, Svensk Kärnbränslehantering AB.

Väisäsvaara J, 2007a. Oskarshamn site investigation. Difference flow logging of borehole KLX14A. Subarea Laxemar. SKB P-06-318, Svensk Kärnbränslehantering AB.

Väisäsvaara J, 2007b. Oskarshamn site investigation. Difference flow logging of borehole KLX16A. Subarea Laxemar. SKB P-07-87, Svensk Kärnbränslehantering AB.

Technical data of boreholes KLX15A and HLX27

Technical data

Borehole KLX15A

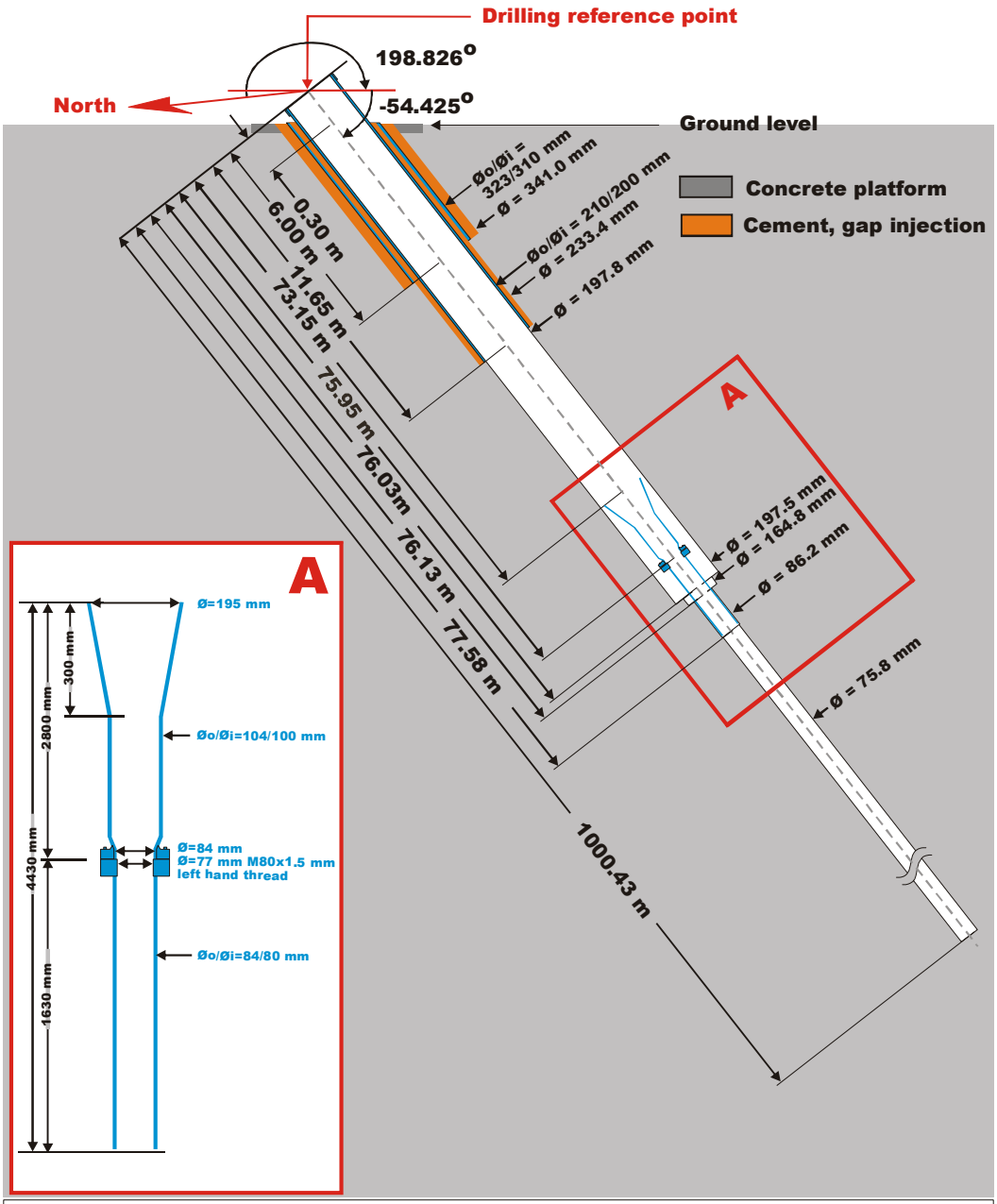

Drilling reference point

Northing: 6365614.168 (m), RT90 2,5 gon V 0:-15
Easting: 1547987.466 (m), RT90 2,5 gon V 0:-15
Elevation: 14.590 (m), RHB 70

Drilling period

Drilling start date: 2006-12-21
Drilling stop date: 2007-02-25

Ver 2007-04-24

Technical data

Borehole HLX27

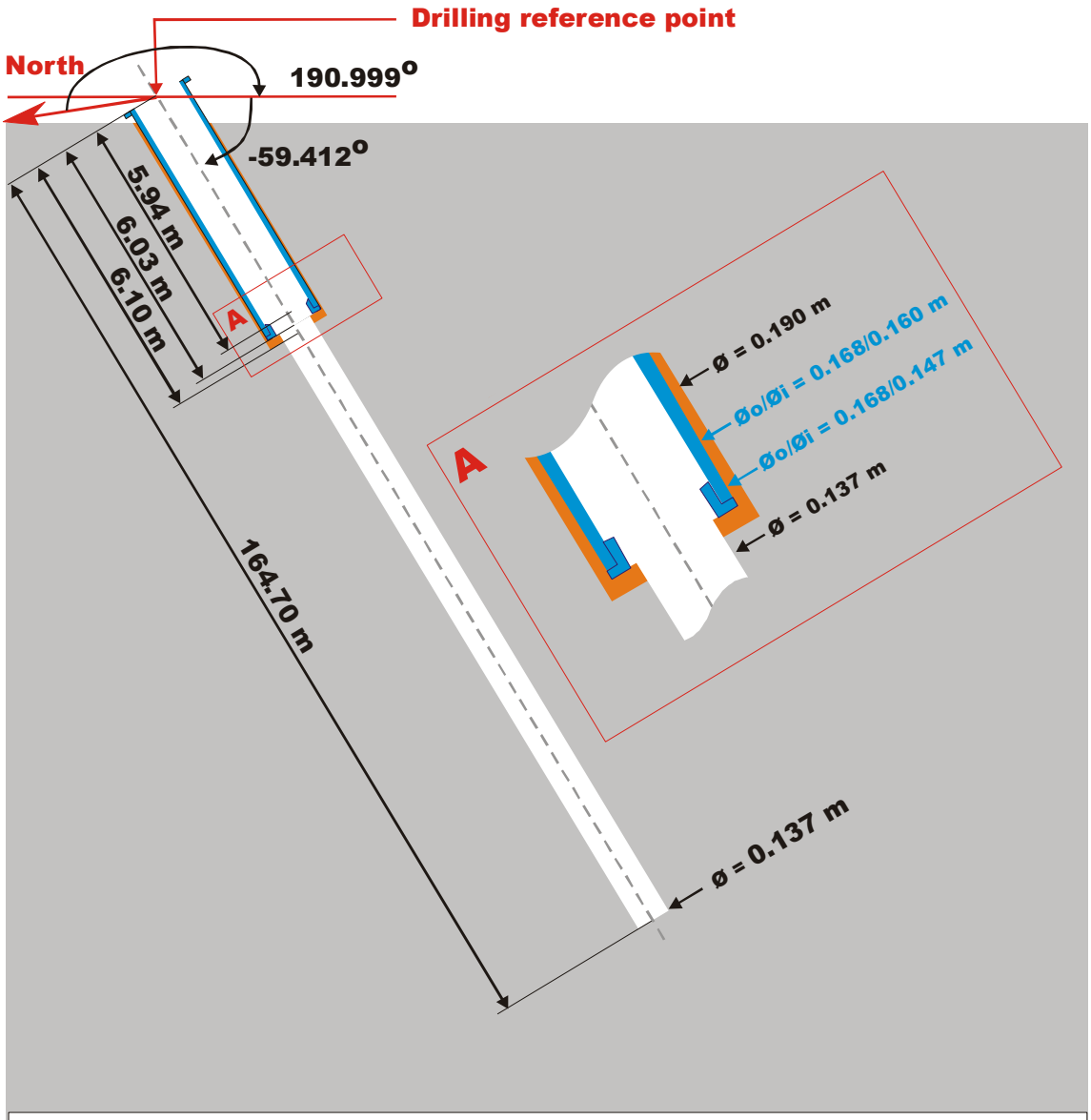

Drilling reference point

Northing: 6365605.073 (m), RT90 2,5 gon V 0:-15
Easting: 1547882.686 (m), RT90 2,5 gon V 0:-15
Elevation: 8.248 (m), RHB 70

Drilling period

Drilling start date: 2004-09-20
Drilling stop date: 2004-09-22

Appendix 2

Borehole data for interference test boreholes

The column "Test section" in Table A2-1 reports the length of the test sections. In sections "Above packers" and in "Open boreholes" the lengths of the open intervals are shown. Hence, the casing length is not included in the test section. The casing length of each borehole that showed any response in the interference test can be found in Table A2-2.

Table A2-1. Data for all observation sections involved in the interference test in HLX27.

Bh ID	Test section (mbl)	Test type[1]	Test config.	Distance to HLX27 (m) (at 131.5 mbl)	Test start date and time (YYYY-MM-DD tt:mm)	Test stop date and time (YYYY-MM-DD tt:mm)
HLX27	6.03–164.70	1B	Open borehole		2008-03-26 10:31	2008-06-26 10:04
HLX15	12.04–151.90	2	Below packer	822	2008-03-26 10:31	2008-06-26 10:04
HLX26	11.00–151.20	2	Below packer	768.5	2008-03-26 10:31	2008-06-26 10:04
HLX38	15.02–199.50	2	Open borehole	738.2	2008-03-26 10:31	2008-06-02 08:45[2)]
HLX42:1	30.00–152.60	2	Below packer	805	2008-03-26 10:31	2008-06-26 10:04
HLX42:2	9.10–29.00	2	Above packer	822.9	2008-03-26 10:31	2008-06-26 10:04
KLX03:1	965.50–971.50	2	Below packer	958.2	2008-03-26 10:31	2008-06-26 10:04
KLX03:10	100.05–192.50	2	Above packer	570.1	2008-03-26 10:31	2008-06-26 10:04
KLX03:2	830.50–964.50	2	Between packers	898.8	2008-03-26 10:31	2008-06-26 10:04
KLX03:3	752.50–829.50	2	Between packers	814.8	2008-03-26 10:31	2008-06-26 10:04
KLX03:4	729.50–751.50	2	Between packers	777.6	2008-03-26 10:31	2008-06-26 10:04
KLX03:5	652.50–728.50	2	Between packers	742.9	2008-03-26 10:31	2008-06-26 10:04
KLX03:6	465.50–651.50	2	Between packers	663.9	2008-03-26 10:31	2008-06-26 10:04
KLX03:7	349.50–464.50	2	Between packers	596.4	2008-03-26 10:31	2008-06-26 10:04
KLX03:8	199.50–348.50	2	Between packers	566.4	2008-03-26 10:31	2008-06-26 10:04
KLX03:9	193.50–198.50	2	Between packers	564.8	2008-03-26 10:31	2008-06-26 10:04
KLX05:1	721.00–1,000.00	2	Below packer	1,107.8	2008-03-26 10:31	2008-06-26 10:04
KLX05:10	15.00–127.00	2	Above packer	1,039.5	2008-03-26 10:31	2008-06-26 10:04
KLX05:2	634.00–720.00	2	Between packers	1,057.9	2008-03-26 10:31	2008-06-26 10:04
KLX05:3	625.00–633.00	2	Between packers	1,047.7	2008-03-26 10:31	2008-06-26 10:04
KLX05:4	501.00–624.00	2	Between packers	1,036.7	2008-03-26 10:31	2008-06-26 10:04
KLX05:5	361.00–500.00	2	Between packers	1,025.5	2008-03-26 10:31	2008-06-26 10:04
KLX05:6	256.00–360.00	2	Between packers	1,022.9	2008-03-26 10:31	2008-06-26 10:04
KLX05:7	241.00–255.00	2	Between packers	1,024.4	2008-03-26 10:31	2008-06-26 10:04
KLX05:8	220.00–240.00	2	Between packers	1,025.1	2008-03-26 10:31	2008-06-26 10:04
KLX05:9	128.00–219.00	2	Between packers	1,028.2	2008-03-26 10:31	2008-06-26 10:04
KLX10:1	711.00–1,001.00	2	Below packer	1,201.1	2008-03-26 10:31	2008-06-26 10:04
KLX10:2	689.00–710.00	2	Between packers	1,121.9	2008-03-26 10:31	2008-06-26 10:04
KLX10:3	465.00–688.00	2	Between packers	1,071.9	2008-03-26 10:31	2008-06-26 10:04
KLX10:4	369.00–464.00	2	Between packers	1,026.8	2008-03-26 10:31	2008-06-26 10:04
KLX10:5	351.00–368.00	2	Between packers	1,016.4	2008-03-26 10:31	2008-06-26 10:04
KLX10:6	291.00–350.00	2	Between packers	1,011	2008-03-26 10:31	2008-06-26 10:04
KLX10:7	131.00–290.00	2	Between packers	1,003.8	2008-03-26 10:31	2008-06-26 10:04
KLX10:8	12.10–130.00	2	Above packer	1,014.8	2008-03-26 10:31	2008-06-26 10:04
KLX10C:1	66.00–146.25	2	Below packer	1,097.2	2008-03-26 10:31	2008-06-26 10:04
KLX10C:2	32.00–65.00	2	Between packers	1,076.4	2008-03-26 10:31	2008-06-26 10:04
KLX10C:3	9.00–31.00	2	Above packer	1,067.8	2008-03-26 10:31	2008-06-26 10:04
KLX12A:1	546.00–602.29	2	Below packer	1,034.1	2008-03-26 10:31	2008-06-26 10:04
KLX12A:2	535.00–545.00	2	Between packers	1,025.6	2008-03-26 10:31	2008-06-26 10:04
KLX12A:3	426.00–534.00	2	Between packers	1,013.4	2008-03-26 10:31	2008-06-26 10:04
KLX12A:4	386.00–425.00	2	Between packers	1,003.1	2008-03-26 10:31	2008-06-26 10:04
KLX12A:5	291.00–385.00	2	Between packers	998.7	2008-03-26 10:31	2008-06-26 10:04
KLX12A:6	160.00–290.00	2	Between packers	1,004.2	2008-03-26 10:31	2008-06-26 10:04
KLX12A:7	142.00–159.00	2	Between packers	1,014.2	2008-03-26 10:31	2008-06-26 10:04

Bh ID	Test section (mbl)	Test type[1]	Test config.	Distance to HLX27 (m) (at 131.5 mbl)	Test start date and time (YYYY-MM-DD tt:mm)	Test stop date and time (YYYY-MM-DD tt:mm)
KLX12A:8	104.00–141.00	2	Between packers	1,019.3	2008-03-26 10:31	2008-06-26 10:04
KLX12A:9	17.92–103.00	2	Above packer	1,033	2008-03-26 10:31	2008-06-26 10:04
KLX14A:1	123.00–176.27	2	Below packer	739.1	2008-03-26 10:31	2008-06-26 10:04
KLX14A:2	77.00–122.00	2	Between packers	774.5	2008-03-26 10:31	2008-06-26 10:04
KLX14A:3	6.45–76.00	2	Above packer	816.4	2008-03-26 10:31	2008-06-26 10:04
KLX15A:1	902.00–1,000.43	2	Below packer	798.3	2008-03-26 10:31	2008-06-26 10:04
KLX15A:2	641.00–901.00	2	Between packers	619.4	2008-03-26 10:31	2008-06-26 10:04
KLX15A:3	623.00–640.00	2	Between packers	481.7	2008-03-26 10:31	2008-06-26 10:04
KLX15A:4	481.00–622.00	2	Between packers	403.2	2008-03-26 10:31	2008-06-26 10:04
KLX15A:5	273.00–480.00	2	Between packers	235.7	2008-03-26 10:31	2008-06-26 10:04
KLX15A:6	260.00–272.00	2	Between packers	140.4	2008-03-26 10:31	2008-06-26 10:04
KLX15A:7	191.00–259.00	2	Between packers	112.4	2008-03-26 10:31	2008-06-26 10:04
KLX15A:8	79.00–190.00	2	Between packers	95.3	2008-03-26 10:31	2008-06-26 10:04
KLX15A:9	11.65–78.00	2	Above packer	147.6	2008-03-26 10:31	2008-06-26 10:04
KLX16A:1	327.00–433.55	2	Below packer	821.6	2008-03-26 10:31	2008-06-26 10:04
KLX16A:2	86.00–326.00	2	Between packers	787.4	2008-03-26 10:31	2008-06-26 10:04
KLX16A:3	11.25–85.00	2	Above packer	789.2	2008-03-26 10:31	2008-06-26 10:04
KLX18A:1	571.00–611.28	2	Below packer	1,001	2008-03-26 10:31	2008-06-26 10:04
KLX18A:2	490.00–570.00	2	Between packers	973.5	2008-03-26 10:31	2008-06-26 10:04
KLX18A:3	472.00–489.00	2	Between packers	953.8	2008-03-26 10:31	2008-06-26 10:04
KLX18A:4	315.00–471.00	2	Between packers	924.7	2008-03-26 10:31	2008-06-26 10:04
KLX18A:5	155.00–314.00	2	Between packers	892.3	2008-03-26 10:31	2008-06-26 10:04
KLX18A:6	104.00–154.00	2	Between packers	886	2008-03-26 10:31	2008-06-26 10:04
KLX18A:7	11.83–103.00	2	Above packer	889	2008-03-26 10:31	2008-06-26 10:04
KLX19A:1	661.00–800.07	2	Below packer	1,091.9	2008-03-26 10:31	2008-06-26 10:04
KLX19A:2	518.00–660.00	2	Between packers	1,026.9	2008-03-26 10:31	2008-06-26 10:04
KLX19A:3	509.00–517.00	2	Between packers	998	2008-03-26 10:31	2008-06-26 10:04
KLX19A:4	481.50–508.00	2	Between packers	991.8	2008-03-26 10:31	2008-06-26 10:04
KLX19A:5	311.00–480.50	2	Between packers	963	2008-03-26 10:31	2008-06-26 10:04
KLX19A:6	291.00–310	2	Between packers	944.2	2008-03-26 10:31	2008-06-26 10:04
KLX19A:7	136.00–290	2	Between packers	935	2008-03-26 10:31	2008-06-26 10:04
KLX19A:8	92.75–135.00	2	Above packer	933.7	2008-03-26 10:31	2008-06-26 10:04

[1)] 1B: Pumping test-submersible pump, 2: Interference test.

[2)] Test stopped due to installations in the borehole.

Table A2-2. Pertinent technical data of the pumping borehole and the observation boreholes with a detected response from the pumping in HLX27. (From Sicada).

Borehole data							
Bh ID	**Elevation of top of casing (ToC) (m.a.s.l.)**	**Borehole interval from ToC (mbl)**	**Casing/ Bh-diam. (m)**	**Inclination-top of bh (from horizontal plane) (º)**	**Dip-direction-top of borehole (from local N) (º)**	**Remarks**	**Drilling finished Date (YYYY-MM-DD)**
HLX27	8.25	0.000–6.100	0.19	–59.41	191.00	Borehole	2004-09-22
”		6.100–164.700	0.137			Borehole	
”		0.000–5.940	0.160			Casing ID	
”		5.940–6.030	0.147			Casing ID	
HLX15	4.810	0.000–12.240	0.190	–58.370	184.65	Borehole	2004-04-29
		12.240–151.900	0.137			Borehole	
		0.000–11.950	0.160			Casing ID	
		11.950–12.040	0.147			Casing ID	
HLX26	6.48	0.000–9.100	0.190	–60.420	12.37	Borehole	2004-09-28
”		9.100–151.200	0.137			Borehole	
”		0.000–8.940	0.160			Casing ID	

Borehole data

Bh ID	Elevation of top of casing (ToC) (m.a.s.l.)	Borehole interval from ToC (mbl)	Casing/ Bh-diam. (m)	Inclination-top of bh (from horizontal plane) (º)	Dip-direction-top of borehole (from local N) (º)	Remarks	Drilling finished Date (YYYY-MM-DD)
”		8.940–9.030	0.147			Casing ID	
HLX38	11.53	0.000–15.100	0.190	–59.39	110.04	Borehole	2006-04-24
”		15.100–103.200	0.140			Borehole	
”		103.200–199.500	0.139			Borehole	
”		0.000–14.930	0.160			Casing ID	
		14.930–15.020	0.143			Casing ID	
HLX42	12.88	0.300–9.100	0.180	–57.11	321.51	Borehole	2006-11-16
”		9.100–152.600	0.139			Borehole	
		0.000–9.010	0.160			Casing ID	
”		9.010–9.100	0.143			Casing ID	
KLX03	18.49	0.100–11.950	0.347	–74.93	199.04	Borehole	2004-09-07
”		11.950–100.350	0.253			Borehole	
”		100.350–101.400	0.243			Borehole	
”		101.400–1,000.420	0.076			Borehole	
”		0.000–100.000	0.200			Casing ID	
”		0.100–11.650	0.311			Casing ID	
”		100.000–100.050	0.170			Casing ID	
KLX12A	17.74	0.150–15.100	0.343	–75.07	315.29	Borehole	2006-03-04
		15.100–17.920	0.248			Borehole	
		17.920–100.400	0.197			Borehole	
		100.400–100.570	0.161			Borehole	
		100.570–102.130	0.086			Borehole	
		102.130–602.290	0.076			Borehole	
		0.000–17.920	0.200			Casing ID	
		0.150–15.100	0.310			Casing ID	
KLX14A	16.35	0.300–3.200	0.116	–49.96	111.95	Borehole	2006-09-04
”		3.200–6.450	0.096			Borehole	
		6.450–176.270	0.076			Borehole	
”		0.000–6.450	0.077			Casing ID	
KLX15A	14.59	0.300–6.000	0.341	–54.42	198.83	Borehole	2007-02-25
”		6.000–11.650	0.233			Borehole	
”		11.65–76.030	0.198			Borehole	
		76.030–76.130	0.165			Borehole	
		76.130–77.580	0.086			Borehole	
		77.580–1,000.430	0.076			Borehole	
		0.000–11.650	0.200			Casing ID	
		0.300–6.000	0.310			Casing ID	
KLX16A	18.85	0.300–11.250	0.096	–64.98	294.37	Borehole	2007-01-09
”		11.250–433.550	0.076			Borehole	
”		0.000–11.250	0.077			Casing ID	
KLX19A	16.87	0.200–6.300	0.339			Borehole	2006-09-20
		6.300–70.000	0.254			Borehole	
		70.000–99.330	0.253			Borehole	
		99.330–100.730	0.086			Borehole	
		100.730–800.070	0.076			Borehole	
		520.300–522.500	0.084			Borehole	
		0.000–92.750	0.200			Casing ID	
		0.200–6.200	0.310			Casing ID	
		6.200–6.300	0.280			Casing ID	
		92.750–98.700	0.200			Casing ID	
		98.700–98.750	0.170			Casing ID	
		520.400–522.400	0.082			Casing ID	

Table A2-3. Coordinates of the observation boreholes with a detected response from the pumping in HLX27. (From Sicada).

Borehole data Bh ID	Northing (m)	Easting (m)
HLX15	6365361.97	1548664.02
HLX26	6365278.71	1548600.52
HLX38	6365868.86	1547146.08
HLX42	6364827.04	1547446.73
KLX03	6366112.59	1547718.93
KLX12A	6365630.78	1548904.44
KLX14A	6365959.69	1547146.87
KLX15A	6365614.17	1547987.47
KLX16A	6364797.69	1547584.06
KLX19A	6365901.42	1547004.62

Appendix 3

Chemical composition of groundwater, tracer solution and sub flow of salt

Table A3-1. Chemical composition of the groundwater in the injection section (KLX15A:6) and in the pumping borehole HLX27 (samples taken before tracer test start).

	KLX15:6	HLX27
SKB sample no.	**15334**	**15484**
pH (pH unit)	7.82	7.85
Conductivity (mS/m)	850	489
Constituent	**(mg/l)**	**(mg/l)**
Na	1,090	657
K	23.3	8.46
Ca	569	254
Mg	75.9	42.1
HCO_3	60	147.3
Cl	2,775	1,497
SO_4_S	19.3	26.8
Br	11.7	5.90
F	1.40	2.15
Fe	0.565	0.112
Mn	0.428	0.488
Li	0.13	0.0656
Sr	11	4.50
Cs	0.000508	0.000975
Rb	0.0402	0.0146

Table A3-2. Chemical composition of the sub-flow of salt added to the re-circulated water from HLX27.

Salt	Amount to be added per liter (g/l)	Upconc. solution (g/l)	Comments
LiCl	3.93E-04	0.020	
NaCl	1.09E+00	55.6	
KCl	2.83E-02	1.44	
$MgCl_2 * 6H_2O$	2.82E-01	14.4	
$CaCl_2 * 2H_2O$	1.15E+00	58.6	
$SrCl_2 * 6H_2O$	1.98E-02	1.01	
HCl	8.79E-03	0.448	100% HCl
NaBr	7.38E-03	0.377	
RbCl	3.62E-05	0.0018	

The concentrated solution was injected at rate 10 ml/min into the injection flow of 500 ml/min.

Table A3-3. Chemical composition of tracer solution for main tracer test. The table shows both planned concentrations and actual concentrations due to a smaller volume than intended.

Volume in tank Salt	Planned conc. 5,040 l (g/l)	Actual conc. 3,867 l (g/l)	Comments
LiCl	1.186	0.910	
NaCl	1.273	0.977	
KCl	0.050	0.038	
$MgCl_2 * 6H_2O$	0.782	0.600	
$CaCl_2 * 2H_2O$	2.653	2.036	
$SrCl_2 * 6H_2O$	0.043	0.033	
CsCl	0.259	0.198	
RbCl	0.504	0.387	
HCl	0.060	0.046	100% HCl
Na_2SO4	0.009	0.007	
NaBr	0.019	0.015	
$TbCl_3 * 6H_2O$	0.013	0.010	

Appendix 4

Calculation of normalised mass flux

Calculation of total mass

In order to compare the injection and breakthrough of tracers easily in e.g. figures and simulations the concentration measurements are transformed into normalised mass flux. The first step is to calculate the total mass for each tracer. The mass flux (m_t) at time, t, was calculated by multiplying the measured concentration (c_t) by the flow rate at that time (Q_t). The flow rate and concentration are known from measurements.

$$m_t = Q_t \times c_t \qquad \text{(A4-1)}$$

The total mass of the different tracers (M_{tot}) were calculated by numerical integration of the calculated mass flux assuming that the mass flux calculated in one point valid half a time step before and half a time step after the measurement time according to Figure A4-2. The total mass if then calculated according to Equation A4-2.

$$M_{tot} = \sum \Delta M_t = \sum (m_t \times \Delta t_t) \qquad \text{(A4-2)}$$

Normalizing mass flux

After calculating the total mass (for each tracer respectively) the mass flux over time for both the injection and pumping may be normalized by dividing with the total mass from the injection. The normalized mass flux was then used in the model tools.

Injection borehole (KLX15A)

The representative injection flow used in the calculations above was determined to 400 ml/min during the injection of tracers in the main test, and 500 ml/min during the pre-test and the rinsing period during the main test.

Withdrawal borehole (HLX27)

The breakthrough curve from HLX27 was also transformed into mass flux against elapsed time by dividing with the total injected mass. The withdrawal rate in HLX27 was determined to 75 l/min during the entire main test and was also used when calculating the mass flux. However, during the pre-test the flow rate was only 50 l/min. Hence, in order to facilitate the comparison between the main test and the pre-test, the time of the pre-test was transformed so that the volume pumped per time unit (i.e. pumping flow rate) was constant (75 l/transformed minute) throughout the pre-test. The consequence is that the breakthrough curve before the flow rate increase is somewhat compressed since one real hour is longer than one transformed hour for this period.

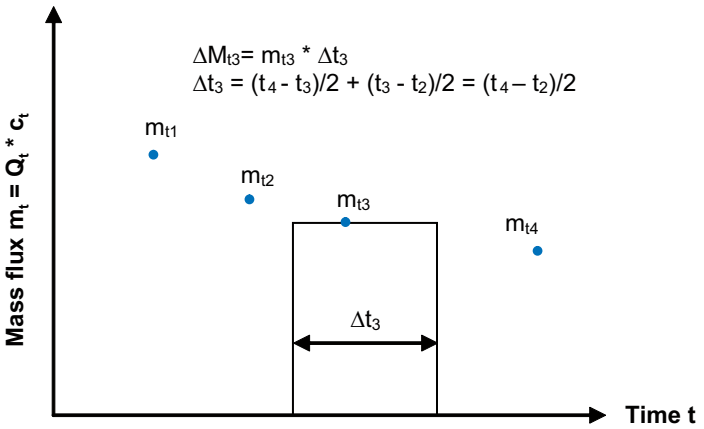

Figure A4-1. *Principle for calculation of total mass in a breakthrough curve.*

Appendix 5

Transient evaluation of responses in the boreholes

Standard transient evaluation was made for the pumping borehole HLX27 and most observation sections in which pressure interference was detected. However, in some borehole sections the responses were very small (≤0.1 m) and transient evaluation was considered to be too uncertain and thus no hydraulic parameters are presented.

Transient analysis of the pressure responses during the drawdown and recovery periods in the pumping borehole as well as in all observation borehole sections with a detectable response was made by the software AQTESOLV. Before the analysis, the observed head during the flow and recovery period in all responding observation sections was corrected for the naturally decreasing head trend during the test period. A linear correction was applied individually to each section during the entire test period, based on the linear head versus time diagrams for each section presented below. The correction procedure is described in Appendix 8.

During the entire test period, the precipitation (the last 24 h), air pressure and the sea water level were recorded at a climatic station near the experimental site, see Figure A5-1.

Abbreviations of flow regimes and hydraulic boundaries that may appear in the text below are as follows:

WBS = Wellbore storage

PRF = Pseudo-radial flow regime

PLF = Pseudo-linear flow regime

PSF = Pseudo-spherical (leaky) flow regime

PSS = Pseudo-stationary flow regime

NFB = Apparent no-flow boundary

CHB = Apparent constant-head boundary

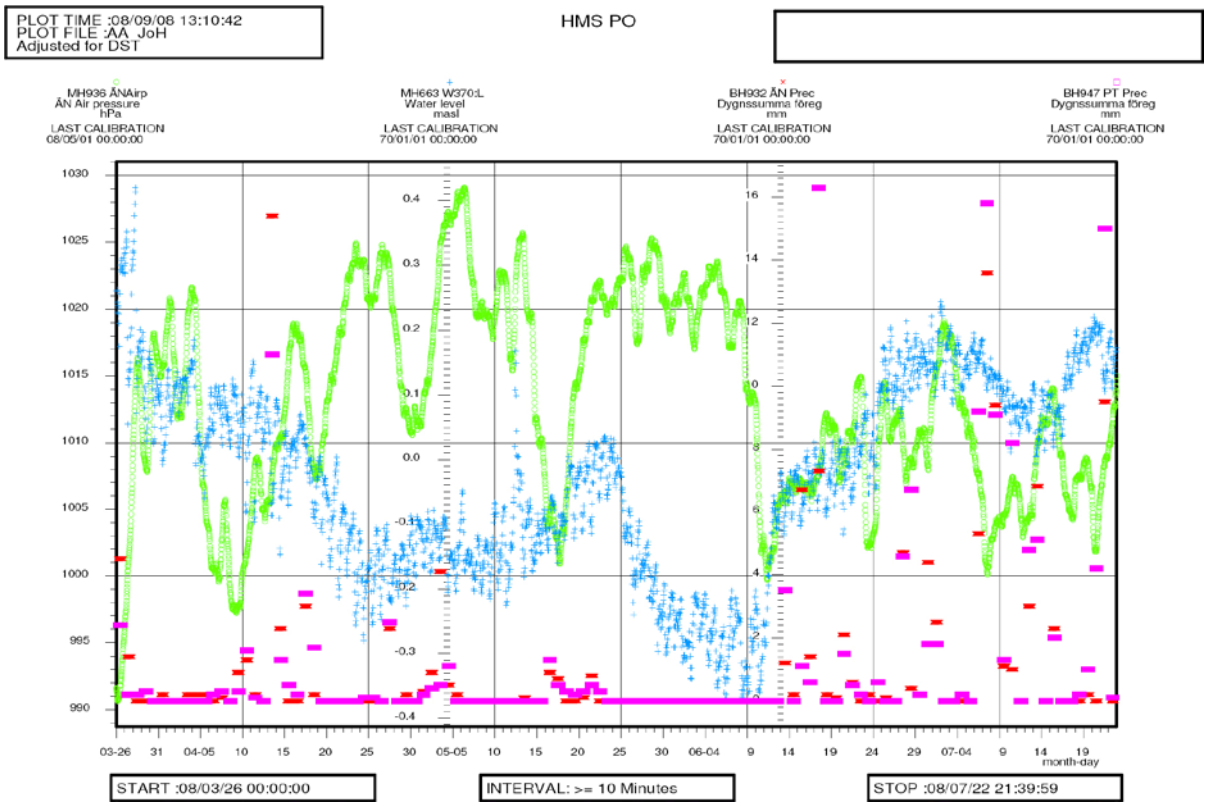

Figure A5-1. *Precipitation [mm] (pink and red), air pressure [mBar] (green) and sea water level [m.a.s.l.] (blue) recorded at a climatic station near the experimental site during the measurement period.*

A5.1 Pumping borehole

A5.1.1 HLX27

General test data for the pumping test in HLX27 are presented in Table A5-1. The open borehole interval is 6.03–164.70 m.

Table A5-1. General test data for the pumping test in HLX27: 6.03–164.70 m.

General test data			
Pumping borehole	HLX27		
Test type[1)]	Constant Rate withdrawal and recovery test		
Test section (open borehole/packed-off section):	open borehole		
Test No	1		
Field crew	Geosigma AB		
Test equipment system			
General comment	Interference test		
	Nomenclature	**Unit**	**Value**
Borehole length	L	m	164.70
Casing length	L_c	m	6.03
Test section – secup	Secup	m	6.03
Test section – seclow	Seclow	m	164.70
Test section length	L_w	m	158.67
Test section diameter[2)]	$2 \cdot r_w$	mm	137
Test start (start of flow period)		yymmdd hh:mm	080326 10:31:02
Packer expanded		yymmdd hh:mm:ss	
Start of flow period		yymmdd hh:mm:ss	080326 10:31:02
Stop of flow period		yymmdd hh:mm:ss	080626 10:04:58
Test stop (stop of recovery registration)		yymmdd hh:mm	080720 21:40:00
Total flow time	t_p	min	132,454
Total recovery time	t_F	min	35,255
Pressure data			
Relative pressure in test section before start of flow period	p_i	kPa	372.21 [3)]
Relative pressure in test section before stop of flow period	p_p	kPa	164.79 [3)]
Relative pressure in test section at stop of recovery period	p_F	kPa	372.21 [3)]
Pressure change during flow period (p_i–p_p)	dp_p	kPa	207.42
Flow data			
Flow rate from test section just before stop of flow period	Q_p	m^3/s	$1.25 \cdot 10^{-3}$
Mean (arithmetic) flow rate during flow period	Q_m	m^3/s	$1.11 \cdot 10^{-3}$
Total volume discharged during flow period	V_p	m^3	$8.79 \cdot 10^3$

Manual groundwater level measurements in HLX27			**GW level**	
Date YYYY-MM-DD	**Time tt:mm**	**Time (min)**	**(m b. ToC)**	**(m.a.s.l.)**
2008-03-26	10:25	10:25	1.31	6.94
2008-04-23	14:40	14:40	21.99	–13.74
2008-06-26	10:04	10:04	22.87	–14.62
2008-06-360	17:45	17:45	2.51	5.74

[1)] Constant Head injection and recovery or Constant Rate withdrawal and recovery.

[2)] Nominal diameter.

[3)] Pressure values corrected for the naturally decreasing head trend.

Comments on the test

The test was planned as a constant-flow rate pumping test but the flow rate was changed during the flow period. The average flow rate was c. 66.4 L/min and the duration of the flow period was c. 92 days. During the first 26 days of the flow period the flow rate was c. 49.8 L/min. The flow rate was then increased to an average of c. 73.0 L/min. The final flow rate was about 75 L/min. The final drawdown in HLX27 was approximately 21 m. The pressure recovery in HLX27 was, as well as in the observation boreholes, measured until 080720 or about 24 days. Overviews of the flow rate and pressure responses in HLX27 are presented in Figure A5-1.

The pressure data have been corrected for the naturally decreasing pressure trend before transient evaluation of the response. Several pump stops and variations of the flow rate occurred during the flow period due to power cuts and malfunctions which are seen in Figure A5-1 as peaks in the pressure curve (see also Section 4.7 in the main report for non-conformities). Heavy precipitation occurred on the 13th of April, see Figure A5-1. A major increase of the flow rate occurred on the 21st of April.

The pressure responses during the drawdown and recovery periods in HLX27 were evaluated. For the flow period, separate analyses were made on the early and late parts of the drawdown curve respectively. Log-log and lin-log plots of the evaluation of the flow and recovery periods from HLX27 are presented in Figures A7-3 to A7-8 in Appendix 6.

Interpreted flow regimes

During the flow period, after initial wellbore storage during the first minute, pseudo-radial flow occurred during c. 3–1,000 min transitioning to pseudo-spherical (leaky) flow at intermediate times. After the increase of flow rate at c. 37, 400 min a transition towards new flow conditions, reflected by an apparent, short late pseudo-radial flow regime is indicated, transitioning to a new pseudo-spherical (leaky) flow regime at the end of the flow period. During the recovery period, wellbore storage effects dominated to c. 1 min followed by a transition to pseudo-radial flow between c. 100–1,000 min and pseudo-spherical (leaky) flow by the end of the period.

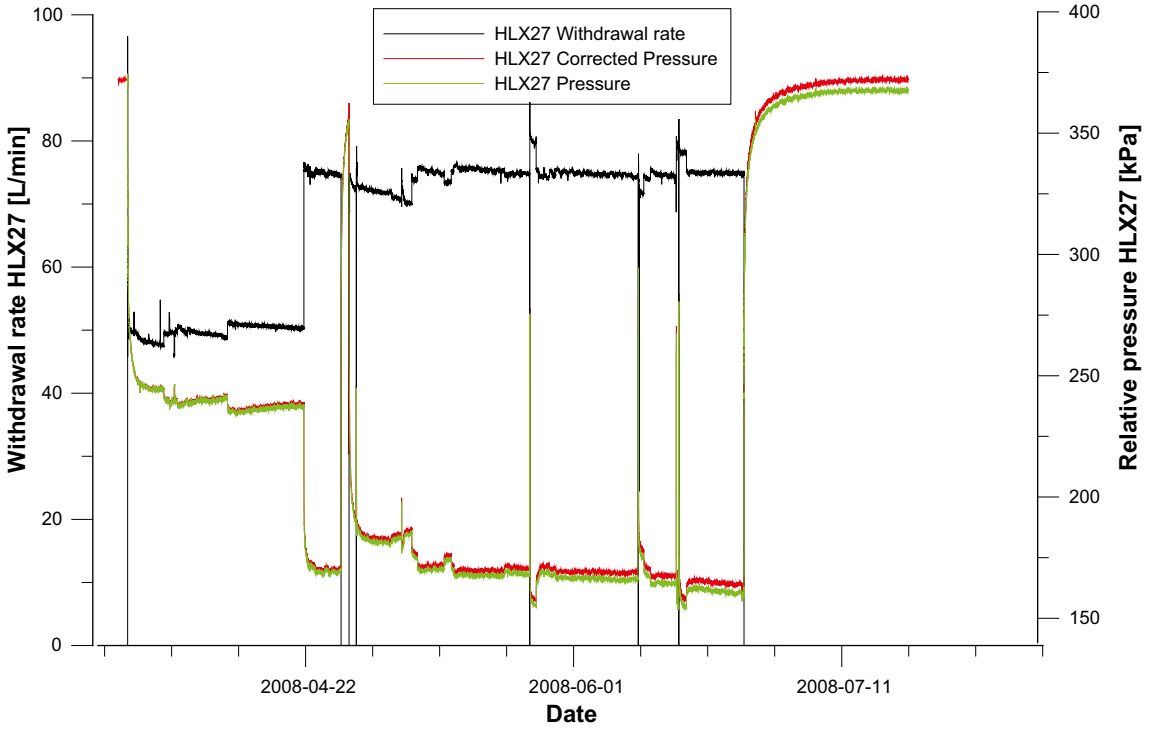

Figure A5-2. *Linear plot of flow rate (Q) and pressure (p) versus time in the pumping borehole HLX27 during the interference test in HLX27. The pressure data have been compensated for the naturally decreasing pressure trend.*

Interpreted parameters

The transient evaluation was based on variable flow rate. Due to the changed flow conditions after the flow rate change it is not possible to make a complete transient evaluation of the entire flow period with uniform values on the hydraulic (and leakage) parameters in this case (even if variable flow rates are accounted for). Transient evaluation of the flow period was made on the first part of the flow period before the disturbing effects using a leaky aquifer model for the actual flow (and leakage) conditions corresponding to the lower flow rate. A separate transient analysis was also made on the late time response after the increase of the flow rate. The estimated parameter values from the first part of the flow period are assumed to be representative for the flow period. Transient evaluation of the entire recovery period was made using a leaky aquifer model with uniform parameters.

The agreement in evaluated parameter values between the flow and recovery period is rather good. The pressure response during the flow period is more complex due to variable flow rate and pump stops. The parameter values from the recovery period are selected as the most representative for the test. The representative transmissivity is estimated to $2.7 \cdot 10^{-5}$ m^2/s for an assumed storativity of $3.7 \cdot 10^{-4}$.

Transient interpretation of the flow period is shown in log-log and lin-log diagrams in Figures A7-3 to A7-6 and of the recovery period in Figures A7-7 and A7-8, all in Appendix 6. The results from the transient evaluation of the pumping test in HLX27 are summarized in Table 5-5 and in the Test Summary Sheet (Table 5-7) in the main report.

A5.2 Observation boreholes

A5.2.1 Discussion of transient responses in the boreholes

The transient responses in the observation boreholes are rather complex during the flow period in this case due to precipitation, the major increase of flow rate and several pump stops in the pumping borehole (particularly after c. 50,0000 min). The transient responses in the observation sections in KLX03 (except KLX03:1) during the flow period together with the response in the pumping borehole HLX27 are shown in Figure A5-3. The responses in all sections are clearly affected by tidal effects during the entire period. The tidal effects are more exaggerated in the beginning of the period due to the logarithmic drawdown and time scales. The effects of the heavy precipitation on the 13th of April (after c. 26,000 min) and the increase of flow rate on the 21st of April (after c. 37,000 min) can be seen in most sections. Finally, the effects of the long pump stop after c. 50, 000 min can also be seen in most sections.

The transient responses in KLX03 can be divided in two groups. In the uppermost sections (KLX:8 to :10), which shows the most distinct responses, the effects of the above disturbances can clearly be seen whereas in sections with more delayed responses (KLX:5 to :7) these effects are more subdued. In the remaining sections the responses are intermediate between these two groups.

Sections with the most distinct responses are dominated by a pseudo-spherical (leaky) flow regime during early to intermediate times before the onset of the disturbing effects discussed above. In some sections this flow regime was preceded by a short period of pseudo-radial flow. After the increase of flow rate a transition towards new flow conditions, reflected by an apparent late pseudo-radial flow regime is indicated, eventually followed by a new pseudo-spherical (leaky) flow regime at the end of the flow period. In sections with the most distinct responses only an apparent pseudo-radial flow regime is indicated by the end and no pseudo-spherical flow regime has yet developed.

Due to the changed flow conditions after the flow rate change it is in general not possible to make a transient evaluation of the entire flow period with uniform values on the hydraulic (and leakage) parameters in this case (even if variable flow rates are accounted for). Thus, the transient evaluation of the flow period was in most cases based on the first part of the flow period before the disturbing effects using a leaky aquifer model for the actual flow (and leakage) conditions corresponding to the lower flow rate. This fact implies that the estimated parameters (in particular the parameter r/B representing the leakage conditions) from the first part in general are not representative for the response during late times due to the change of flow regimes. Only in sections with subdued and delayed responses transient evaluation may be performed on the entire drawdown curve with uniform parameters. The parameter values estimated from the early part are assumed to be representative for the flow period.

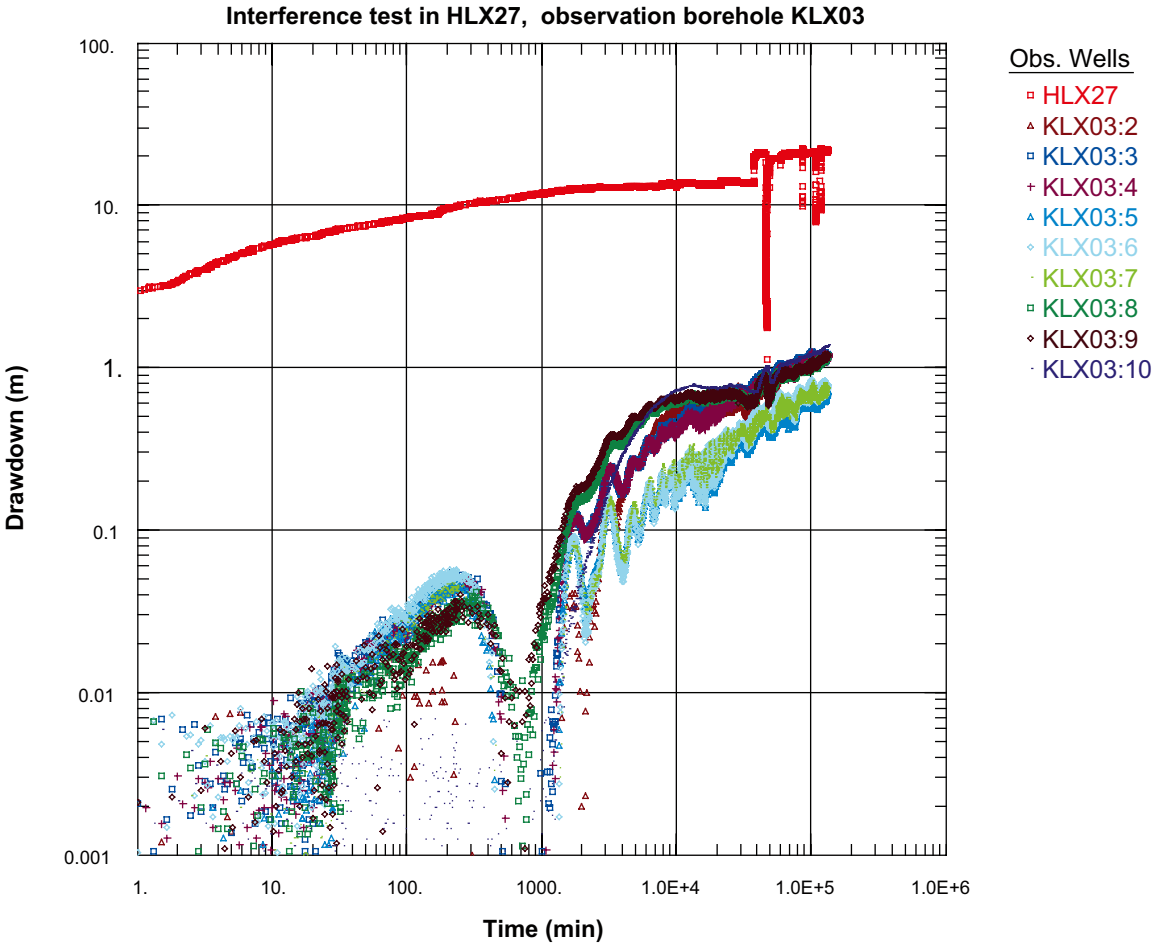

Figure A5-3. *Logarithmic plot of drawdown versus time in observation borehole KLX03 and the pumping borehole HLX27 during the interference test in HLX27. The drawdown data have been compensated for the naturally decreasing trend.*

In some of the sections with the most distinct responses a separate transient evaluation was made on the later part of the flow period after the increase of flow rate. An example is shown for section KLX03:10 in the test diagrams in Appendix 6. In this section an apparent pseudo-radial flow regime was developed at late times (corresponding to a very low value on the leakage coefficient r/B). The estimated transmissivity from the later part of the flow period is significantly higher than those estimated from the early part in this case, possibly representing major hydraulic structures within the radius of influence of the test.

In the sections with delayed responses the effects of the increase in flow rate (and the effects of the disturbing factors) are less pronounced. In these sections a fair transient evaluation may be performed on the entire flow period with uniform hydraulic parameter values if variable flow rates are accounted for, cf. Sections KLX03:5 to :7 in Appendix 6.

The transient responses in the observation sections in KLX15A (except KLX15A:1) during the flow period together with the response in the pumping borehole HLX27 are shown in Figure A5-4. In KLX15A all responses (except KLX15A:2) were distinct and similar to the type of responses in sections KLX03:8 to :10. Only section KLX15A:2 was significantly affected by tidal effects. In all sections (except KLX15A:2) the effects of the increase of flow rate and the disturbing effects discussed for KLX03 were clearly seen.

Evaluation of the late time response during the flow period was also made for some sections in KLX15A. An example is shown for the uppermost section KLX15A:9 in the test diagrams for this borehole in Appendix 6. In this section an apparent pseudo-radial flow regime transitioning to slightly leaky flow is developed at late times. The estimated transmissivity from the later part of the flow period is slightly higher than those estimated from the early part.

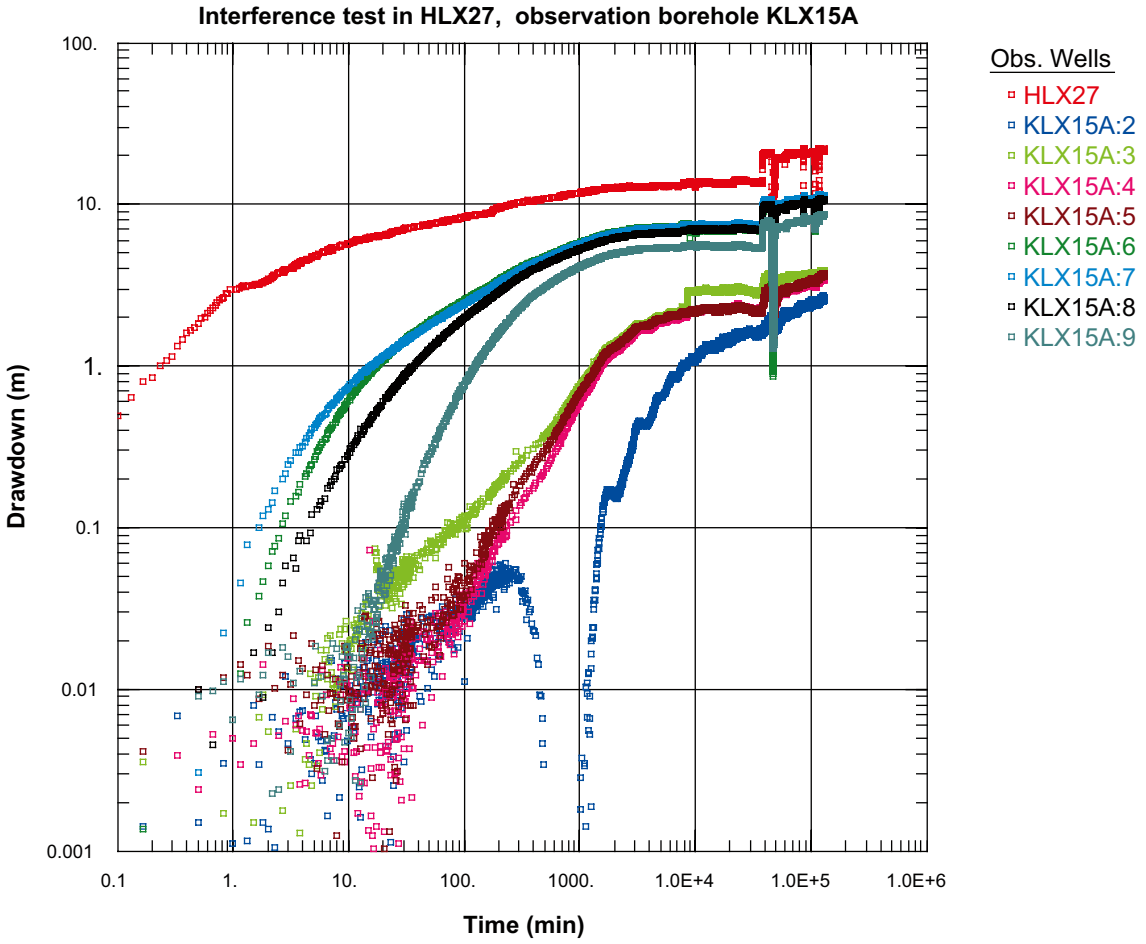

Figure A5-4. *Logarithmic plot of drawdown versus time in observation borehole KLX15A and the pumping borehole HLX27 during the interference test in HLX27. The drawdown data have been compensated for the naturally decreasing trend.*

During the recovery period, most sections in KLX03 and KLX15A exhibited a dominating pseudo-spherical (leaky) flow regime, eventually preceded by a short period of pseudo-radial flow in sections with the most distinct responses, cf. Appendix 6. Transient evaluation of the entire recovery period was in most cases readily made using a leaky aquifer model with uniform parameters. Thus, the estimated hydraulic parameters from the recovery period were selected as representative in these boreholes.

The type of transient responses in the other cored boreholes and percussion boreholes are similar to those in KLX03 and KLX15A. In observation boreholes located relatively close to the pumping borehole distinct responses occurred but in a few distant boreholes small and delayed responses were observed. The responses in the other boreholes were analysed and reported in the same manner as described above for KLX03 and KLX15A. The first part of the flow period was analysed in all sections. In some boreholes the late time response was also analysed. The estimated hydraulic parameters from the recovery period were in most cases selected as representative and reported in the Sicada data base from this interference test. Below, the responses in each observation borehole section are presented and discussed.

A5.2.2 Observation borehole HLX15

The open interval of HLX15 is 12.04–151.90 m. In Figure A5-5 an overview of the observed head versus time in observation borehole HLX15 is shown. A clear response of the pumping in HLX27 is seen. The pressure is affected by precipitation which fell on the 13th of April as well as a few pump stops during the flow period. General test data are presented in Table A5-2.

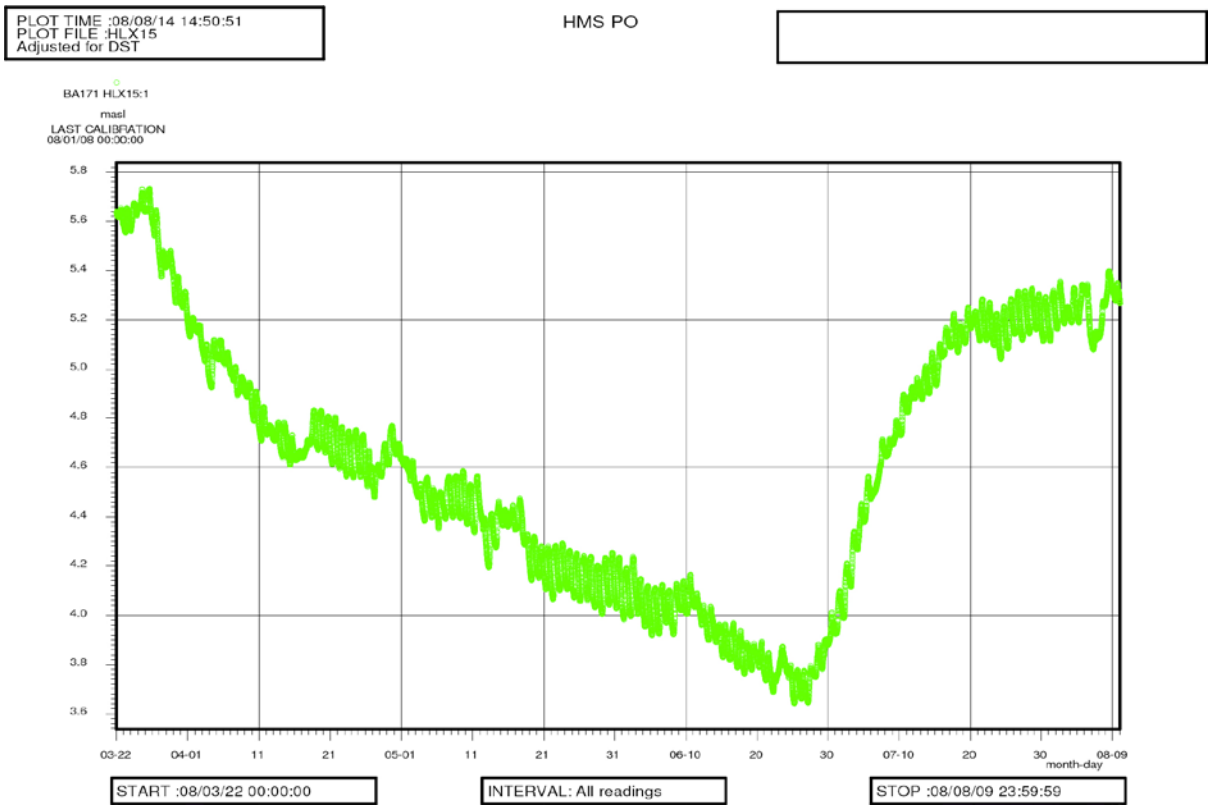

Figure A5-5. *Linear plot of observed (uncorrected) head versus time in observation borehole HLX15 during pumping in HLX27.*

Table A5-2. General test data from observation section HLX15 during pumping in HLX27.

Pressure data	Nomenclature	Unit	Value	Corrected Value[1)]
Hydraulic head in test section before start of flow period	h_i	m.a.s.l.	5.7	5.7
Hydraulic head in test section before stop of flow period	h_p	m.a.s.l.	3.72	4.13
Hydraulic head in test section at stop of recovery period	h_F	m.a.s.l.	5.19	5.71
Hydraulic head change during flow period (h_i–h_p)	dh_p	m	1.98	1.57

[1)] Head corrected for the naturally decreasing head trend.

Comments on the test

A clear response to the pumping in HLX27 is indicated in this section. The corrected drawdown during the flow period was c. 1.6 m. A (corrected) drawdown of 0.1 m was reached approximately 900 minutes (c. 15 hours) after start of pumping in HLX27. There was a (corrected) recovery of c. 1.58 m during the recovery period, lasting for approximately 24 days. A linear plot of the corrected and uncorrected head versus time is presented in Appendix 6.

Interpreted flow regimes and calculated parameters

During the flow period, pseudo-radial flow occurred between c. 2,000–20,000 min, transitioning to temporary pseudo-spherical (leaky) flow at intermediate times. After the change of flow rate at c. 37,000 min and major pump stop at c. 50,000 min in the pumping borehole, a transition towards a new pseudo-radial flow regime is indicated at the end of the period.

The transient evaluation was based on variable flow rate. For the flow period, transient evaluation was made on the first part of the drawdown curve before the effects of the flow rate change reached this borehole causing a change of flow regime. The estimated parameters (in particular r/B) from the

first part are not representative for the response during late times due to the change of flow regimes. During the recovery period approximate pseudo-radial flow occurred between c. 10,000–25,000 min with an anticipated transition to pseudo-spherical (leaky) flow at longer times.

The agreement in evaluated parameter values between the flow and recovery period is rather good. The parameter values from the recovery period are selected as the most representative. The representative transmissivity is estimated to $3.8 \cdot 10^{-5}$ m^2/s and the storativity to $1.2 \cdot 10^{-4}$.

Transient interpretation of the flow and recovery period is shown in log-log diagrams in Appendix 6. The results from the transient evaluation are summarized in Table 5-6 in the main report.

A5.2.3 Observation borehole HLX26

The open interval of HLX26 is 9.03–151.20 m. In Figure A5-6 an overview of the observed head responses in observation borehole HLX26 is shown. A clear response from the pumping in HLX27 was observed in the open borehole. General test data are presented in Table A5-3.

Table A5-3. General test data from observation section HLX26 during pumping in HLX27.

Pressure data	Nomenclature	Unit	Value	Corrected Value[1)]
Hydraulic head in test section before start of flow period	h_i	m.a.s.l.	4.04	4.04
Hydraulic head in test section before stop of flow period	h_p	m.a.s.l.	2.82	3.10
Hydraulic head in test section at stop of recovery period	h_F	m.a.s.l.	3.68	4.04
Hydraulic head change during flow period (h_i–h_p)	dh_p	m	1.22	0.94

[1)] Head corrected for the naturally decreasing head trend.

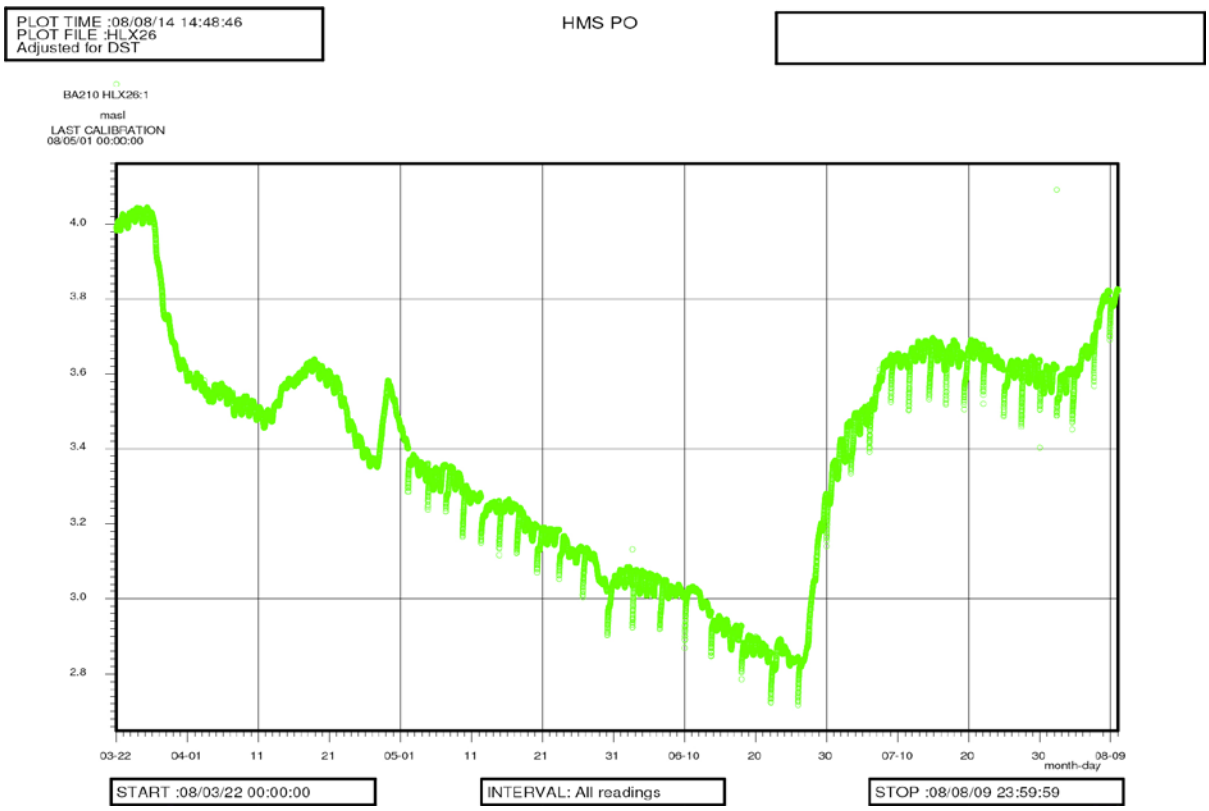

Figure A5-6. *Linear plot of observed (uncorrected) head versus time in observation borehole HLX26 during pumping in HLX27.*

Comments on the test

A clear response to the pumping in HLX27 is indicated in this section. The corrected drawdown during the flow period was c. 0.94 m. A (corrected) drawdown of 0.1 m was reached approximately 1,656 minutes (c. 28 hours) after start of pumping in HLX27. There was a corrected recovery of c. 0.94 m during the recovery period lasting for approximately 24 days.

A rainfall on the 13th of April clearly affected the pressure in HLX26. The pump stop on the 27th of April is seen as a sharp peak in the pressure. A linear plot of the corrected and uncorrected head versus time is presented in Appendix 6.

Interpreted flow regimes and calculated parameters

During the first part of the flow period temporary pseudo-spherical (leaky) flow dominated at intermediate times. After the change of flow rate at c. 37,000 min and major pump stop at c. 50,000 min in the pumping borehole, a transition towards a pseudo-radial flow regime is indicated at the end of the period.

The transient evaluation was based on variable flow rate. For the flow period, transient evaluation was made on the first part of the drawdown curve before the effects of the flow rate change reached this borehole causing a change of flow regimes and before the effects of the precipitation on the 13th of April. The estimated parameters (in particular r/B) from the first part are not representative for the response during late times due to the change of flow regimes. During the recovery period approximate pseudo-radial flow occurred between c. 2,000–10,000 min with a transition to pseudo-spherical (leaky) flow at longer times.

The agreement in evaluated parameter values between the flow and recovery period is rather good. The parameter values from the recovery period are selected as the most representative. The representative transmissivity is estimated to $1.7 \cdot 10^{-4}$ m^2/s and the storativity to $1.1 \cdot 10^{-4}$.

Transient interpretation of the flow and recovery periods is shown in log-log diagrams in Appendix 6. The results from the transient evaluation are summarized in Table 5-6 in the main report.

A5.2.4 Observation borehole HLX38

The open interval of HLX38 is 15.02–199.50 m. In Figure A5-7 an overview of the observed head responses in observation borehole HLX38 is shown. During this interference test, in the beginning of June, borehole HLX38 had four test sections installed. Since the data from these sections are considered as uncertain only pressure registered for the open borehole during the relatively short flow period which ended the 2nd of June, 2008 is used for evaluation of the response in HLX38. No pressure recovery was registered in the open borehole. General test data are presented in Table A5-4.

Comments on the test

A small but clear response is indicated in this section due to pumping in HLX27. A corrected drawdown during the flow period of c. 0.6 m was registered, but this value is registered at 080602 and the total drawdown should have been larger. A (corrected) drawdown of 0.1 m was reached approximately 2,530 minutes (c. 42 hours) after start of pumping in HLX27. No recovery was registered as explained above. Substantial precipitation around the 13th of April, as well as the pump stop at the 27th of April caused clear peaks in the head values. A linear plot of the corrected and uncorrected head versus time is presented in Appendix 6.

Table A5-4. General test data from observation section HLX38 during pumping in HLX27.

Pressure data	Nomenclature	Unit	Value	Corrected Value[1)]
Hydraulic head in test section before start of flow period	h_i	m.a.s.l.	5.63	5.63
Hydraulic head in test section before stop of flow period	h_p	m.a.s.l.	5.05 [2)]	5.17 [2)]
Hydraulic head in test section at stop of recovery period	h_F	m.a.s.l.	–	–
Hydraulic head change during flow period (h_i–h_p)	dh_p	m	0.58 [2)]	0.46 [2)]

[1)] Head corrected for the naturally decreasing head trend.

[2)] Mean value from the end of the data series from HLX38 at 080602.

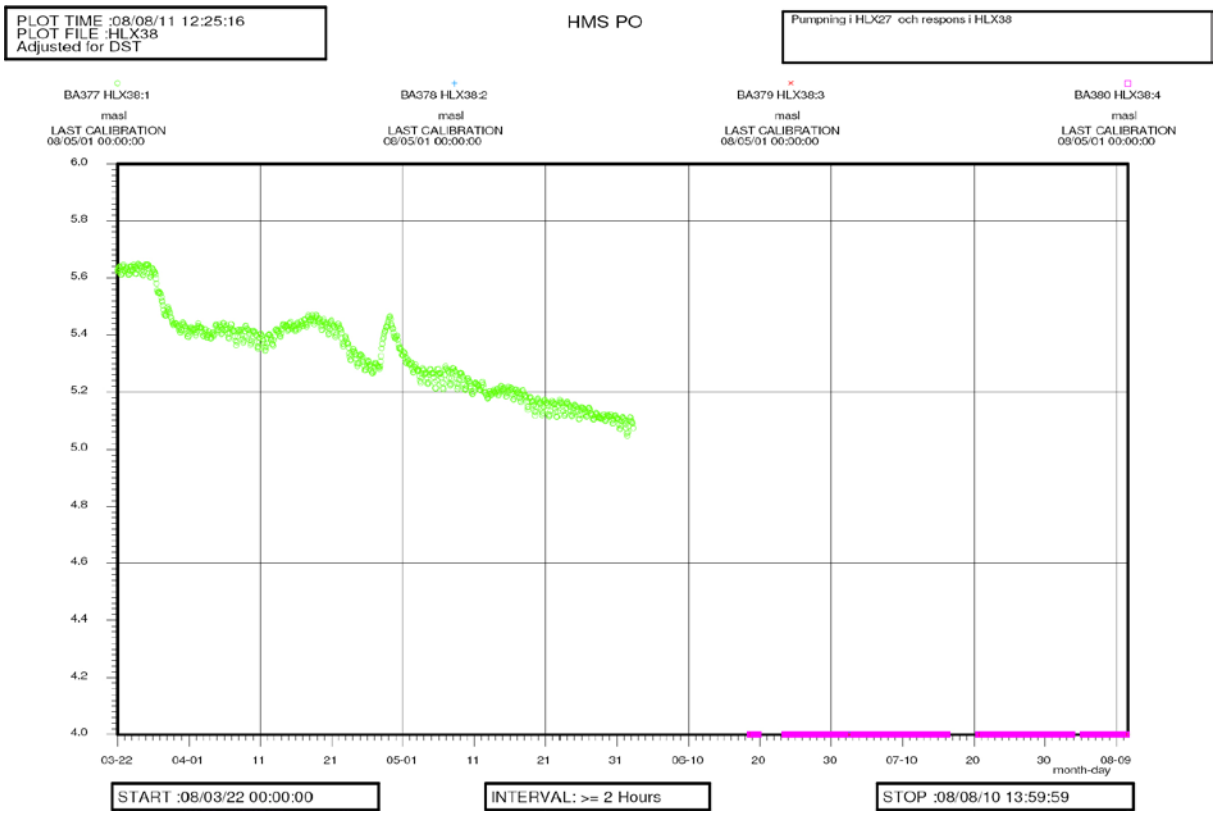

Figure A5-7. *Linear plot of observed (uncorrected) head versus time in HLX38 during pumping in HLX27. The registration of pressure is shortened in this borehole.*

Interpreted flow regimes and calculated parameters

During the first part of the flow period temporary pseudo-spherical (leaky) flow dominated at intermediate times. After the change of flow rate at c. 37,000 min and major pump stop at c. 50,000 min in the pumping borehole, a transition towards a pseudo-radial flow regime is indicated at the end of the period.

The transient evaluation was based on variable flow rate. For the flow period, transient evaluation was made on the first part of the drawdown curve before the effects of the flow rate change reached this borehole causing a change of flow regime and before the effects of the precipitation on the 13th of April. The estimated parameters (in particular r/B) from the first part are not representative for the response during late times due to the change of flow regimes. No evaluation was made on the recovery period.

The parameter values from the (first part of the) flow period are selected as the most representative. The representative transmissivity is estimated to $3.7 \cdot 10^{-5}$ m^2/s and the storativity to $5.1 \cdot 10^{-5}$.

Transient interpretation of the flow period is shown in log-log diagrams in Appendix 6. The results from the transient evaluation are summarized in Table 5-6 in the main report.

A5.2.5 Observation borehole HLX42

In Figure A5-8 an overview of the observed head responses in observation borehole HLX42 is shown. A clear response was observed in the lower of the two sections (HLX42:1) and is presented below. Section HLX42:2 is assumed to be virtually unaffected by the pumping in HLX27.

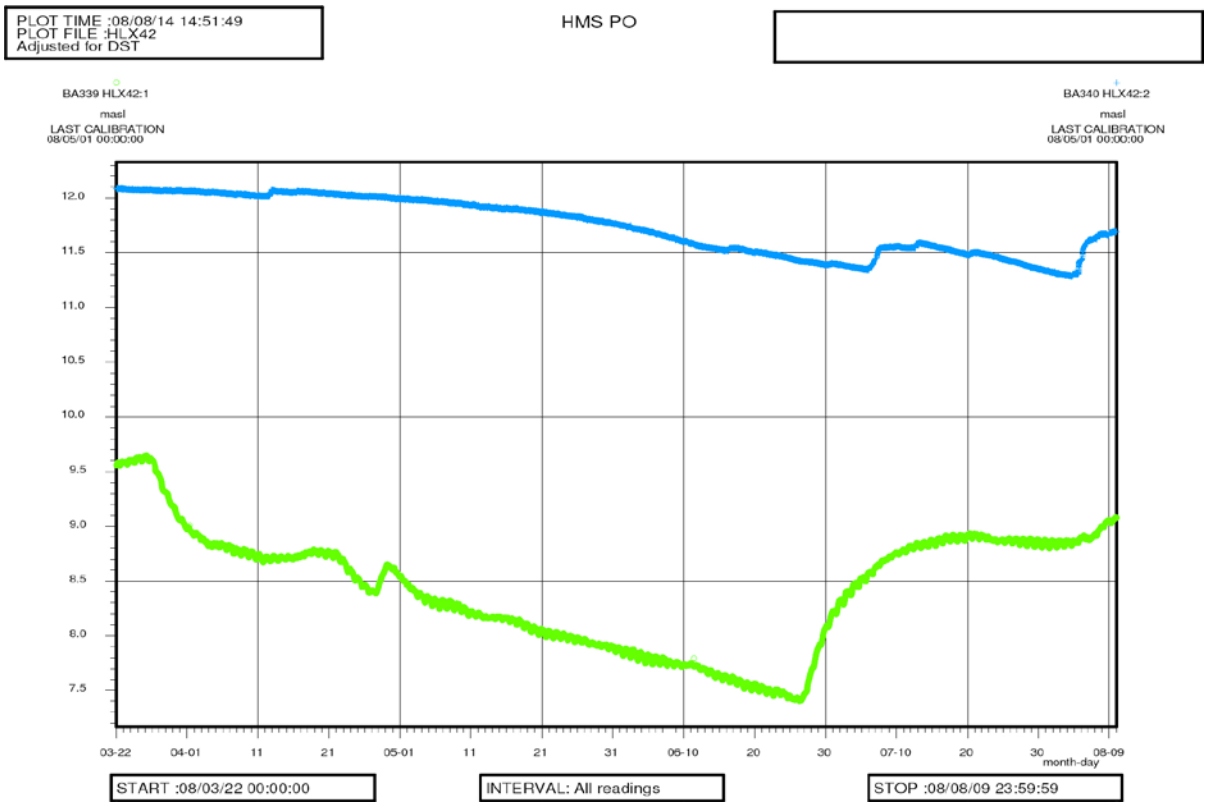

Figure A5-8. *Linear plot of observed (uncorrected) head versus time in observation borehole HLX42 during pumping in HLX27.*

A5.2.5.1 Observation section HLX42:1 30.0–152.6 m

General test data from the observation section HLX42:1 is presented in Table A5-5.

Comments on the test

A clear response to the pumping in HLX27 is indicated in this section. The corrected drawdown during the flow period was c. 1.68 m. A (corrected) drawdown of 0.1 m was reached approximately 1,600 min (c. 53 hours) after start of pumping in HLX27. There was a corrected recovery of c. 1.67 m during the recovery period lasting for approximately 24 days.

Heavy precipitation around the 13th of April, as well as the pump stop at the 27th of April caused clear peaks in the head values. A linear plot of the corrected and uncorrected head versus time is presented in Appendix 6.

Table A5-5. General test data from observation section HLX42:1 during pumping in HLX27.

Pressure data	Nomenclature	Unit	Value	Corrected Value[1)]
Hydraulic head in test section before start of flow period	h_i	m.a.s.l.	9.63	9.63
Hydraulic head in test section before stop of flow period	h_p	m.a.s.l.	7.41	7.95
Hydraulic head in test section at stop of recovery period	h_F	m.a.s.l.	8.93	9.62
Hydraulic head change during flow period (h_i–h_p)	dh_p	m	2.22	1.68

[1)] Head corrected for the naturally decreasing head trend.

Interpreted flow regimes and calculated parameters

During the first part of the flow period temporary pseudo-spherical (leaky) flow dominated at intermediate times. After the change of flow rate at c. 37,000 min and major pump stop at c. 50,000 min in the pumping borehole, a transition towards a pseudo-radial flow regime is indicated at the end of the period.

The transient evaluation was based on variable flow rate. For the flow period, transient evaluation was made on the first part of the drawdown curve before the effects of the flow rate change reached this borehole causing a change of flow regime and before the effects of the precipitation on the 13th of April. The estimated parameters (in particular r/B) from the first part are not representative for the response during late times due to the change of flow regimes. During the recovery period approximate pseudo-radial flow occurred between c. 4,000–20,000 min with a transition to pseudo-spherical (leaky) flow at longer times.

The agreement in evaluated parameter values between the flow and recovery period is rather good. The parameter values from the recovery period are selected as the most representative. The representative transmissivity is estimated to $1.1 \cdot 10^{-4}$ m^2/s and the storativity to $7.2 \cdot 10^{-5}$.

Transient interpretation of the flow period is shown in log-log diagrams in Appendix 6. The results from the transient evaluation are summarized in Table 5-6 in the main report.

A5.2.6 Observation borehole KLX03

In Figure A5-9 an overview of the observed head responses in observation borehole KLX03 is shown. Responses were observed in all sections. However, the pressure response in the deepest section KLX03:1 is too disturbed and uncertain to make any firm conclusions regarding the response. No evaluation of the response in this section was made. The most distinct responses occurred in the uppermost sections KLX03:8 to :10.

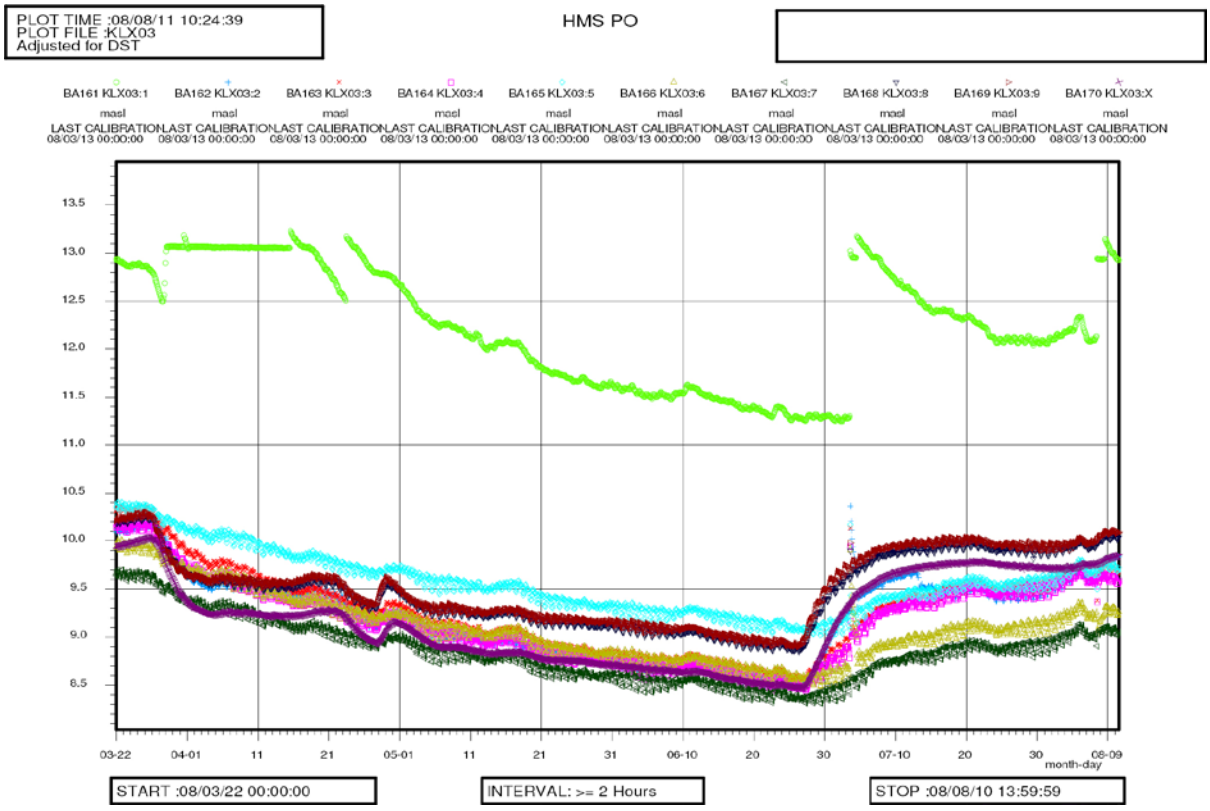

Figure A5-9. *Linear plot of observed (uncorrected) head versus time in observation borehole KLX03 during pumping in HLX27.*

Effects from the increased precipitation around the 13th of April as well as effects from the pump stop at the 27th of April caused distortions in the head values in most of the sections. Manual water levelling of KLX03, involving a short release of the packers in the boreholes is conducted at the 3rd of July and is seen as a short peak in the pressures in all sections (except in the uppermost section KLX03:10).

The transient evaluation in KLX03 is also discussed in Section A5.2.1.

A5.2.6.1 Observation section KLX03:2 830.50–964.50 m

General test data from the observation section KLX03:2 are presented in Table A5-6.

Comments on the test

A clear response to the pumping in HLX27 is indicated in this section. The corrected drawdown during the flow period was c. 1.19 m. A corrected drawdown of 0.1 m was reached approximately 2,800 min (c. 47 hours) after start of pumping in HLX27. There was a corrected recovery of c. 1.19 m during the recovery period lasting for approximately 24 days.

At the 13th of July the pressure in this section drops a bit but the reason to this is not clear. A linear plot of the corrected and uncorrected head versus time is presented in Appendix 6.

Interpreted flow regimes and calculated parameters

During the first part of the flow period temporary pseudo-spherical (leaky) flow dominated at intermediate times. After the change of flow rate at c. 37,000 min and major pump stop at c. 50,000 min in the pumping borehole, a transition towards a pseudo-radial flow regime is indicated at the end of the period.

The transient evaluation was based on variable flow rate. For the flow period, transient evaluation was made on the first part of the drawdown curve before the effects of the flow rate change reached this borehole causing a change of flow regime and before the effects of the precipitation on the 13th of April. The estimated parameters (in particular r/B) from the first part are not representative for the response during late times due to the change of flow regimes. During the recovery period approximate pseudo-radial flow occurred between c. 5,000–10,000 min with a transition to pseudo-spherical (leaky) flow at longer times. At the end of the recovery period the pressure is disturbed.

The agreement in evaluated parameter values between the flow and recovery period is rather good. The parameter values from the recovery period are selected as the most representative. The representative transmissivity is estimated to $3.5 \cdot 10^{-5}$ m^2/s and the storativity to $5.8 \cdot 10^{-5}$.

Transient, quantitative interpretation of the flow and recovery period is shown in log-log diagrams in Appendix 6. The results from the transient evaluation are summarized in Table 5-6 in the main report.

A5.2.6.2 Observation section KLX03:3 752.50–829.50 m

In Figure A5-9 an overview of the observed head responses in observation borehole KLX03 is shown. General test data from the observation section KLX03:3 are presented in Table A5-7.

Table A5-6. General test data from observation section KLX03:2 during pumping in HLX27.

Pressure data	Nomenclature	Unit	Value	Corrected Value[1)]
Hydraulic head in test section before start of flow period	h_i	m.a.s.l.	10.15	10.15
Hydraulic head in test section before stop of flow period	h_p	m.a.s.l.	8.51	8.96
Hydraulic head in test section at stop of recovery period	h_F	m.a.s.l.	9.58	10.15
Hydraulic head change during flow period (h_i–h_p)	dh_p	m	1.64	1.19

[1)] Head corrected for the naturally decreasing head trend.

Table A5-7. General test data from observation section KLX03:3 during pumping in HLX27.

Pressure data	Nomenclature	Unit	Value	Corrected Value[1)]
Hydraulic head in test section before start of flow period	h_i	m.a.s.l.	10.33	10.32
Hydraulic head in test section before stop of flow period	h_p	m.a.s.l.	8.56	9.14
Hydraulic head in test section at stop of recovery period	h_F	m.a.s.l.	9.59	10.32
Hydraulic head change during flow period (h_i–h_p)	dh_p	m	1.77	1.18

[1)] Head corrected for the naturally decreasing head trend.

Comments on the test

A rather clear response to the pumping is indicated in this section. The corrected drawdown during the flow period was c. 1.18 m. A (corrected) drawdown of 0.1 m was reached approximately 1,600 minutes (c. 27 hours) after start of pumping in HLX27. There was a corrected recovery of c. 1.18 m during the recovery period lasting for approximately 24 days.

The rainfall on the 13th of April and the pump stop at the 27th of April affected the pressure in KLX03:3. A linear plot of the corrected and uncorrected head versus time is presented in Appendix 6.

Interpreted flow regimes and calculated parameters

During the first part of the flow period approximate pseudo-radial flow occurred between c. 5,000–20,000 min. Then temporary pseudo-spherical (leaky) flow prevailed at intermediate times. After the change of flow rate at c. 37,000 min and major pump stop at c. 50,000 min in the pumping borehole, a transition towards a new pseudo-radial flow regime followed by pseudo-spherical (leaky) flow is indicated at the end of the period.

The transient evaluation was based on variable flow rate. For the flow period, transient evaluation was made on the entire drawdown curve in this case since the effects of the flow rate change and precipitation on the 13th of April were not very pronounced in this section. During the recovery period approximate pseudo-radial flow occurred between c. 8,000–20,000 min with a transition to pseudo-spherical (leaky) flow at longer times.

The agreement in evaluated parameter values between the flow and recovery period is rather good. The parameter values from the recovery period are selected as the most representative. The representative transmissivity is estimated to $6.7 \cdot 10^{-5}$ m^2/s and the storativity to $1.5 \cdot 10^{-4}$.

Transient, quantitative interpretation of the flow and recovery period is shown in log-log diagrams in Appendix 6. The results from the transient evaluation are summarized in Table 5-6 in the main report.

A5.2.6.3 Observation section KLX03:4 729.50–751.50 m

In Figure A5-9 an overview of the observed head responses in observation borehole KLX03 is shown. General test data from the observation section KLX03:4 are presented in Table A5-8.

Table A5-8. General test data from observation section KLX03:4 during pumping in HLX27.

Pressure data	Nomenclature	Unit	Value	Corrected Value[1)]
Hydraulic head in test section before start of flow period	h_i	m.a.s.l.	10.15	10.15
Hydraulic head in test section before stop of flow period	h_p	m.a.s.l.	8.47	8.95
Hydraulic head in test section at stop of recovery period	h_F	m.a.s.l.	9.54	10.15
Hydraulic head change during flow period (h_i–h_p)	dh_p	m	1.68	1.2

[1)] Head corrected for the naturally decreasing head trend.

Comments on the test

A rather clear response to the pumping in HLX27 is indicated in this section. The corrected drawdown during the flow period was c. 1.2 m. A (corrected) drawdown of 0.1 m was reached approximately 1,600 min (c. 27 hours) after start of pumping in HLX27. There was a corrected recovery of c. 1.2 m during the recovery period lasting for approximately 24 days.

The rainfall on the 13th of April and the pump stop at the 27th of April affected the pressure in KLX03:4. A linear plot of the corrected and uncorrected head versus time is presented in Appendix 6.

Interpreted flow regimes and calculated parameters

During the first part of the flow period approximate pseudo-radial flow occurred between c. 5,000–20,000 min. Then temporary pseudo-spherical (leaky) flow prevailed at intermediate times. After the change of flow rate at c. 37,000 min and major pump stop at c. 50,000 min in the pumping borehole, a transition towards a new pseudo-radial flow regime followed by pseudo-spherical (leaky) flow is indicated at the end of the period.

The transient evaluation was based on variable flow rate. For the flow period, transient evaluation was made on the entire drawdown curve in this case since the effects of the flow rate change and precipitation on the 13th of April were not very pronounced in this section. During the recovery period approximate pseudo-radial flow occurred between c. 8,000–20,000 min with a transition to pseudo-spherical (leaky) flow at longer times.

The agreement in evaluated parameter values between the flow and recovery period is rather good although the estimated transmissivity from the flow period is higher than that from the recovery period. The parameter values from the recovery period are selected as the most representative. The representative transmissivity is estimated to $5.5 \cdot 10^{-5}$ m^2/s and the storativity to $1.5 \cdot 10^{-4}$.

Transient, quantitative interpretation of the flow and recovery period is shown in log-log diagrams in Appendix 6. The results from the transient evaluation are summarized in Table 5-6 in the main report.

A5.2.6.4 Observation section KLX03:5 652.50–728.50 m

In Figure A5-9 an overview of the observed head responses in observation borehole KLX03 is shown. General test data from the observation section KLX03:5 are presented in Table A5-9.

Comments on the test

A rather clear but delayed response to the pumping in HLX27 is indicated in this section. The corrected drawdown during the flow period was c. 0.71 m. A (corrected) drawdown of 0.1 m was reached approximately 3,550 min (c. 59 hours) after start of pumping in HLX27. There was a corrected recovery of c. 0.71 m during the recovery period lasting for approximately 24 days.

The rainfall on the 13th of April and the pump stop at the 27th of April affected the pressure in KLX03:5. A linear plot of the corrected and uncorrected head versus time is presented in Appendix 6.

Table A5-9. General test data from observation section KLX03:5 during pumping in HLX27.

Pressure data	Nomenclature	Unit	Value	Corrected Value[1)]
Hydraulic head in test section before start of flow period	h_i	m.a.s.l.	10.33	10.33
Hydraulic head in test section before stop of flow period	h_p	m.a.s.l.	9.07	9.62
Hydraulic head in test section at stop of recovery period	h_F	m.a.s.l.	9.63	10.33
Hydraulic head change during flow period (h_i–h_p)	dh_p	m	1.26	0.71

[1)] Head corrected for the naturally decreasing head trend.

Interpreted flow regimes and calculated parameters

During the first part of the flow period approximate pseudo-radial flow occurred between c. 10,000–30,000 min. After the change of flow rate at c. 37,000 min and major pump stop at c. 50,000 min in the pumping borehole, a transition towards a new pseudo-radial flow regime followed by pseudo-spherical (leaky) flow is indicated at the end of the period.

The transient evaluation was based on variable flow rate. For the flow period, transient evaluation was made on the entire drawdown curve in this case since the effects of the flow rate change and precipitation on the 13th of April were not very pronounced in this section. During the recovery period approximate pseudo-radial flow occurred between c. 10,000–20,000 min with a transition to pseudo-spherical (leaky) flow at longer times.

The agreement in evaluated parameter values between the flow and recovery period is rather poor in this case. The estimated transmissivity from the flow period is significantly higher than that from the recovery period. The parameter values from the recovery period are selected as the most representative. The representative transmissivity is estimated to $3.2 \cdot 10^{-5}$ m^2/s and the storativity to $2.2 \cdot 10^{-4}$. According to the single-hole tests with PSS and PFL this section has a low transmissivity.

Transient, quantitative interpretation of the flow and recovery period is shown in log-log diagrams in Appendix 6. The results from the transient evaluation are summarized in Table 5-6 in the main report.

A5.2.6.5 Observation section KLX03:6 465.50–651.50 m

In Figure A5-9 an overview of the observed head responses in observation borehole KLX03 is shown. General test data from the observation section KLX03:6 are presented in Table A5-10.

Comments on the test

A rather clear but delayed response to the pumping in HLX27 is indicated in this section. The corrected drawdown during the flow period was c. 0.76 m. A (corrected) drawdown of 0.1 m was reached approximately 4,000 min (c. 67 hours) after start of pumping in HLX27. There was a corrected recovery of c. 0.76 m during the recovery period lasting for approximately 24 days.

The rainfall on the 13th of April and the pump stop at the 27th of April affected the pressure in KLX03:6. A linear plot of the corrected and uncorrected head versus time is presented in Appendix 6.

Interpreted flow regimes and calculated parameters

During the first part of the flow period approximate pseudo-radial flow occurred between c. 10,000–30,000 min. After the change of flow rate at c. 37,000 min and major pump stop at c. 50,000 min in the pumping borehole, a transition towards a new pseudo-radial flow regime followed by pseudo-spherical (leaky) flow is indicated at the end of the period.

The transient evaluation was based on variable flow rate. For the flow period, transient evaluation was made on the entire drawdown curve in this case since the effects of the flow rate change and precipitation on the 13th of April were not very pronounced in this section. During the recovery period pseudo-spherical (leaky) flow dominated.

Table A5-10. General test data from observation section KLX03:6 during pumping in HLX27.

Pressure data	Nomenclature	Unit	Value	Corrected Value[1)]
Hydraulic head in test section before start of flow period	h_i	m.a.s.l.	9.91	9.91
Hydraulic head in test section before stop of flow period	h_p	m.a.s.l.	8.57	9.15
Hydraulic head in test section at stop of recovery period	h_F	m.a.s.l.	9.17	9.91
Hydraulic head change during flow period (h_i–h_p)	dh_p	m	1.34	0.76

[1)] Head corrected for the naturally decreasing head trend.

The agreement in evaluated parameter values between the flow and recovery period is rather poor in this case. The estimated transmissivity from the flow period is significantly higher than that from the recovery period. The parameter values from the recovery period are selected as the most representative. The representative transmissivity is estimated to $1.5 \cdot 10^{-5}$ m^2/s and the storativity to $1.6 \cdot 10^{-4}$. According to the single-hole tests with PSS and PFL this section has a very low transmissivity.

Transient, quantitative interpretation of the flow and recovery period is shown in log-log diagrams in Appendix 6. The results from the transient evaluation are summarized in Table 5-6 in the main report.

A5.2.6.6 Observation section KLX03:7 m 349.50–464.50 m

In Figure A5-9 an overview of the observed head responses in observation borehole KLX03 is shown. General test data from the observation section KLX03:7 are presented in Table A5-11.

Comments on the test

A rather clear but delayed response to the pumping in HLX27 is indicated in this section. The corrected drawdown during the flow period was c. 0.74 m. A (corrected) drawdown of 0.1 m was reached approximately 2,900 min (c. 48 hours) after start of pumping in HLX27. There was a corrected recovery of c. 0.74 m during the recovery period lasting for approximately 24 days.

The rainfall on the 13th of April and the pump stop at the 27th of April affected the pressure in KLX03:7. A linear plot of the corrected and uncorrected head versus time is presented in Appendix 6.

Interpreted flow regimes and calculated parameters

During the first part of the flow period approximate pseudo-radial flow occurred between c. 10,000–30,000 min. After the change of flow rate at c. 37,000 min and major pump stop at c. 50,000 min in the pumping borehole, a transition towards a new pseudo-radial flow regime followed by pseudo-spherical (leaky) flow is indicated at the end of the period.

The transient evaluation was based on variable flow rate. For the flow period, transient evaluation was made on the entire drawdown curve in this case since the effects of the flow rate change and precipitation on the 13th of April were not very pronounced in this section. During the recovery period pseudo-spherical (leaky) flow dominated.

The agreement in evaluated parameter values between the flow and recovery period is rather poor in this case. The estimated transmissivity from the flow period is significantly higher than that from the recovery period. The parameter values from the recovery period are selected as the most representative. The representative transmissivity is estimated to $2.3 \cdot 10^{-5}$ m^2/s and the storativity to $2.5 \cdot 10^{-4}$. According to the single-hole tests with PSS and PFL this section has a low transmissivity.

Transient, quantitative interpretation of the flow and recovery period is shown in log-log diagrams in Appendix 6. The results from the transient evaluation are summarized in Table 5-6 in the main report.

Table A5-11. General test data from observation section KLX03:7 during pumping in HLX27.

Pressure data	Nomenclature	Unit	Value	Corrected Value[1)]
Hydraulic head in test section before start of flow period	h_i	m.a.s.l.	9.62	9.62
Hydraulic head in test section before stop of flow period	h_p	m.a.s.l.	8.36	8.88
Hydraulic head in test section at stop of recovery period	h_F	m.a.s.l.	8.97	9.62
Hydraulic head change during flow period (h_i–h_p)	dh_p	m	1.26	0.74

[1)] Head corrected for the natural decreasing head trend.

A5.2.6.7 Observation section KLX03:8 199.50–348.50 m

In Figure A5-9 an overview of the observed head responses in observation borehole KLX03 is shown. General test data from the observation section KLX03:8 are presented in Table A5-12.

Comments on the test

A clear response to the pumping in HLX27 is indicated in this section. The corrected drawdown during the flow period was c. 1.18 m. A (corrected) drawdown of 0.1 m was reached approximately 1,540 min (c. 26 hours) after start of pumping in HLX27. There was a corrected recovery of c. 1.18 m during the recovery period lasting for approximately 24 days.

Increased precipitation around the 13th of April, as well as the major pump stop at the 27th of April caused clear distortions of the head values. A linear plot of the corrected and uncorrected head versus time is presented in Appendix 6.

Interpreted flow regimes and calculated parameters

The first part of the flow period is dominated by pseudo-spherical (leaky) flow at intermediate times. After the change of flow rate at c. 37,000 min and major pump stop at c. 50,000 min in the pumping borehole, a transition towards a pseudo-radial flow regime is indicated at the end of the period.

The transient evaluation was based on variable flow rate. For the flow period, transient evaluation was made on the first part of the drawdown curve before the effects of the flow rate change reached this borehole causing a change of flow regimes and before the effects of the precipitation on the 13th of April. The estimated parameters (in particular r/B) from the first part are not representative for the response during late times due to the change of flow regimes. During the recovery period approximate pseudo-radial flow occurred between c. 5,000–10,000 min with a transition to pseudo-spherical (leaky) flow at longer times.

The agreement in evaluated parameter values between the flow and recovery period is rather good. The parameter values from the recovery period are selected as the most representative. The representative transmissivity is estimated to $1.1 \cdot 10^{-4}$ m^2/s and the storativity to $1.7 \cdot 10^{-4}$.

Transient, quantitative interpretation of the flow and recovery period is shown in log-log diagrams in Appendix 6. The results from the transient evaluation are summarized in Table 5-6 in the main report.

A5.2.6.8 Observation section KLX03:9 193.50–198.50 m

In Figure A5-9 an overview of the observed head responses in observation borehole KLX03 is shown. General test data from the observation section KLX03:9 are presented in Table A5-13.

Table A5-12. General test data from observation section KLX03:8 during pumping in HLX27.

Pressure data	Nomenclature	Unit	Value	Corrected Value[1)]
Hydraulic head in test section before start of flow period	h_i	m.a.s.l.	10.25	10.25
Hydraulic head in test section before stop of flow period	h_p	m.a.s.l.	8.86	9.07
Hydraulic head in test section at stop of recovery period	h_F	m.a.s.l.	9.98	10.25
Hydraulic head change during flow period (h_i–h_p)	dh_p	m	1.39	1.18

[1)] Head corrected for the naturally decreasing head trend.

Table A5-13. General test data from observation section KLX03:9 during pumping in HLX27.

Pressure data	Nomenclature	Unit	Value	Corrected Value[1)]
Hydraulic head in test section before start of flow period	h_i	m.a.s.l.	10.28	10.28
Hydraulic head in test section before stop of flow period	h_p	m.a.s.l.	8.90	9.09
Hydraulic head in test section at stop of recovery period	h_F	m.a.s.l.	10.04	10.28
Hydraulic head change during flow period (h_i–h_p)	dh_p	m	1.38	1.19

[1)] Head corrected for the naturally decreasing head trend.

Comments on the test

A clear response to the pumping in HLX27 is indicated in this section. The corrected drawdown during the flow period was c. 1.19 m. A (corrected) drawdown of 0.1 m was reached approximately 1,430 min (c. 24 hours) after start of pumping in HLX27. There was a corrected recovery of c. 1.19 m during the recovery period lasting for approximately 24 days.

Increased precipitation around the 13th of April, as well as the major pump stop at the 27th of April caused clear distortions of the head values. A linear plot of the corrected and uncorrected head versus time is presented in Appendix 6.

Interpreted flow regimes and calculated parameters

The first part of the flow period is dominated by pseudo-spherical (leaky) flow at intermediate times. After the change of flow rate at c. 37,000 min and major pump stop at c. 50,000 min in the pumping borehole, a transition towards a pseudo-radial flow regime is indicated at the end of the period.

The transient evaluation was based on variable flow rate. For the flow period, transient evaluation was made on the first part of the drawdown curve before the effects of the flow rate change reached this borehole causing a change of flow regime and before the effects of the precipitation on the 13th of April. The estimated parameters (in particular r/B) from the first part are not representative for the response during late times due to the change of flow regime. During the recovery period approximate pseudo-radial flow occurred between c. 5,000–10,000 min with a transition to pseudo-spherical (leaky) flow at longer times.

The agreement in evaluated parameter values between the flow and recovery period is rather good. The parameter values from the recovery period are selected as the most representative. The representative transmissivity is estimated to $1.2 \cdot 10^{-4}$ m^2/s and the storativity to $1.5 \cdot 10^{-4}$.

Transient, quantitative interpretation of the flow and recovery period is shown in log-log diagrams in Appendix 6. The results from the transient evaluation are summarized in Table 5-6 in the main report.

A5.2.6.9 Observation section KLX03:10 100.05–192.50 m

In Figure A5-9 an overview of the observed head responses in observation borehole KLX03 is shown. General test data from the observation section KLX03:10 are presented in Table A5-14.

Comments on the test

A clear response to the pumping in HLX27 is indicated in this section. The corrected drawdown during the flow period was c. 1.36 m. A (corrected) drawdown of 0.1 m was reached approximately 2,450 minutes (c. 41 hours) after start of pumping in HLX27. There was a corrected recovery of c. 1.36 m during the recovery period lasting for approximately 24 days.

Increased precipitation around the 13th of April, as well as the pump stop at the 27th of April caused clear distortions of the head values. A linear plot of the corrected and uncorrected head versus time is presented in Appendix 6.

Table A5-14. General test data from observation section KLX03:10 during pumping in HLX27.

Pressure data	Nomenclature	Unit	Value	Corrected Value[1)]
Hydraulic head in test section before start of flow period	h_i	m.a.s.l.	10.02	10.02
Hydraulic head in test section before stop of flow period	h_p	m.a.s.l.	8.47	8.66
Hydraulic head in test section at stop of recovery period	h_F	m.a.s.l.	9.78	10.02
Hydraulic head change during flow period (h_i–h_p)	dh_p	m	1.55	1.36

[1)] Head corrected for the naturally decreasing head trend.

Interpreted flow regimes and calculated parameters

The first part of the flow period is dominated by pseudo-spherical (leaky) flow at intermediate times. After the change of flow rate at c. 37,000 min and major pump stop at c. 50,000 min in the pumping borehole, a transition towards a pseudo-radial flow regime is indicated at the end of the period.

The transient evaluation was based on variable flow rate. For the flow period, transient evaluation was made on the first part of the drawdown curve before the effects of the flow rate change reached this borehole causing a change of flow regime and before the effects of the precipitation on the 13th of April. The estimated parameters (in particular r/B) from the first part are not representative for the response during late times due to the change of flow regime. During the recovery period approximate pseudo-radial flow occurred between c. 5,000–10,000 min with a transition to pseudo-spherical (leaky) flow at longer times.

The agreement in evaluated parameter values between the flow and recovery period is rather poor in this case. The estimated transmissivity from the flow period is significantly lower than that from the recovery period. The parameter values from the recovery period are selected as the most representative. The representative transmissivity is estimated to $3.7 \cdot 10^{-5}$ m^2/s and the storativity to $1.3 \cdot 10^{-4}$.

Transient, quantitative interpretation of the flow and recovery period is shown in log-log diagrams in Appendix 6. The results from the transient evaluation are summarized in Table 5-6 in the main report.

A5.2.7 Observation borehole KLX05

In Figure A5-10 an overview of the observed head responses in observation borehole KLX05 is shown. All ten sections in KLX05 are more or less affected by a minor pumping in KLX05:7 for water sampling in this section. The packers in KLX05 were released four times during the pumping for levelling of the sections and are seen as peaks in the pressure curves. The rainfall on the 13th of April also affected the pressure in the upper sections in KLX05.

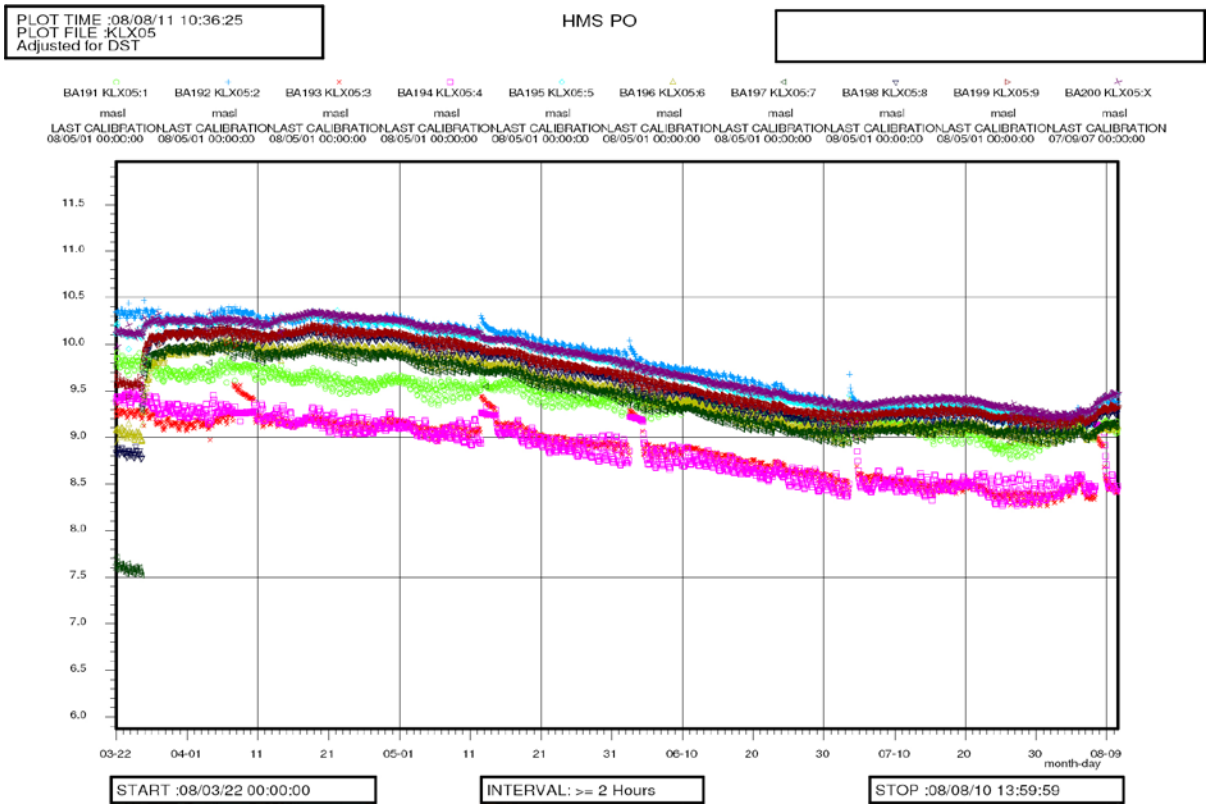

Figure A5-10. *Linear plot of observed (uncorrected) head versus time in the observation sections in KLX05 during pumping in HLX27.*

Comments on the test

Most sections in KLX05 are probably unaffected by the pumping in HLX27 since no or little reaction is observed on stop of pumping on June 26. However, in some sections a small response cannot be excluded. No evaluation is made of the responses in this borehole.

A5.2.8 Observation borehole KLX10

In Figure A5-11 an overview of the observed head responses in observation borehole KLX10 is shown. The drop of pressure in all eight sections in KLX10 around the 20th of July is caused by a logger breakdown. Sections 1, 2 and 5 are more or less affected by pumping for water sampling in these sections. The rainfall on the 13th of April may have affected the pressure in the upper sections in KLX10.

Comments on the test

Most sections in KLX10 are probably unaffected by the pumping in HLX27 since no or little reaction is observed on stop of pumping on June 26. However, in sections :6–:8 a small response probably occurred. No evaluation is made of the responses in this borehole.

A5.2.9 Observation borehole KLX10C

In Figure A5-12 an overview of the observed head responses in observation borehole KLX10C is shown. The drop of pressure in all sections in KLX10C around the 20th of July is caused by a logger break down. The rainfall on the 13th of April has affected the pressure in all three sections in KLX10C.

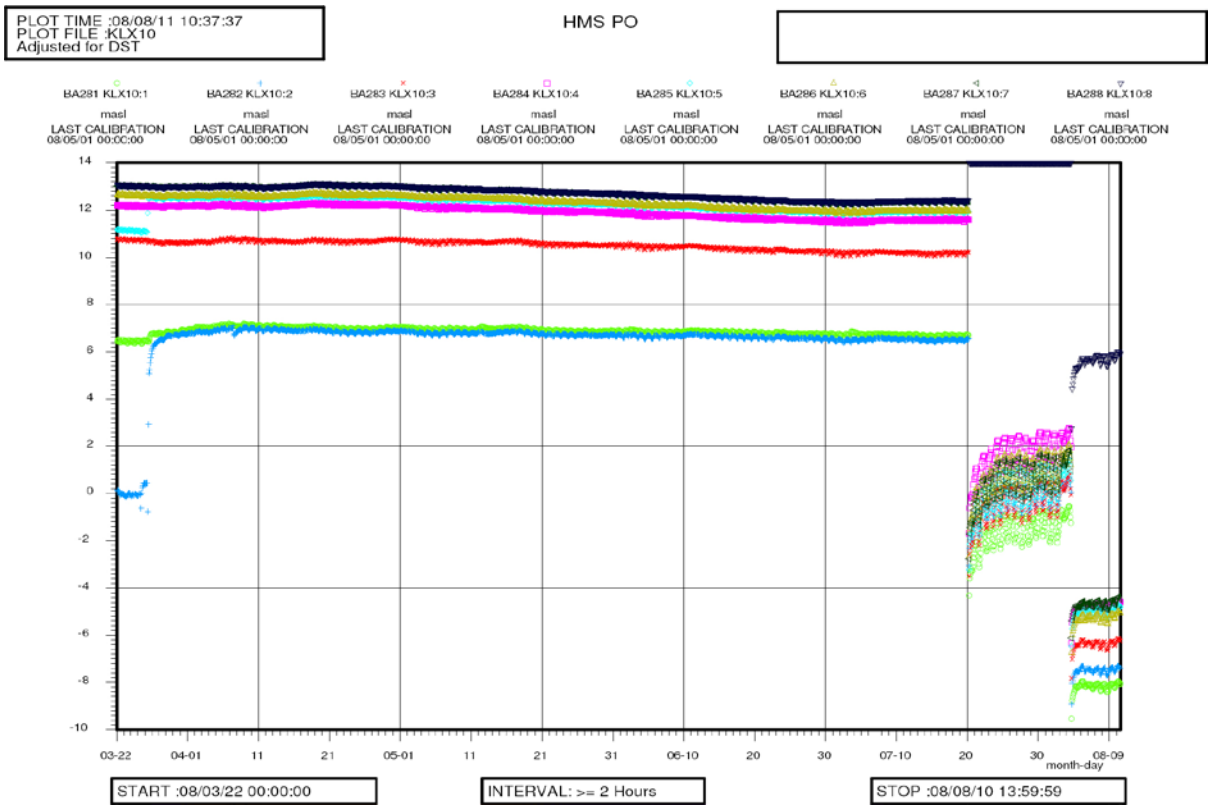

Figure A5-11. *Linear plot of observed (uncorrected) head versus time in the observation sections in KLX10 during pumping in HLX27.*

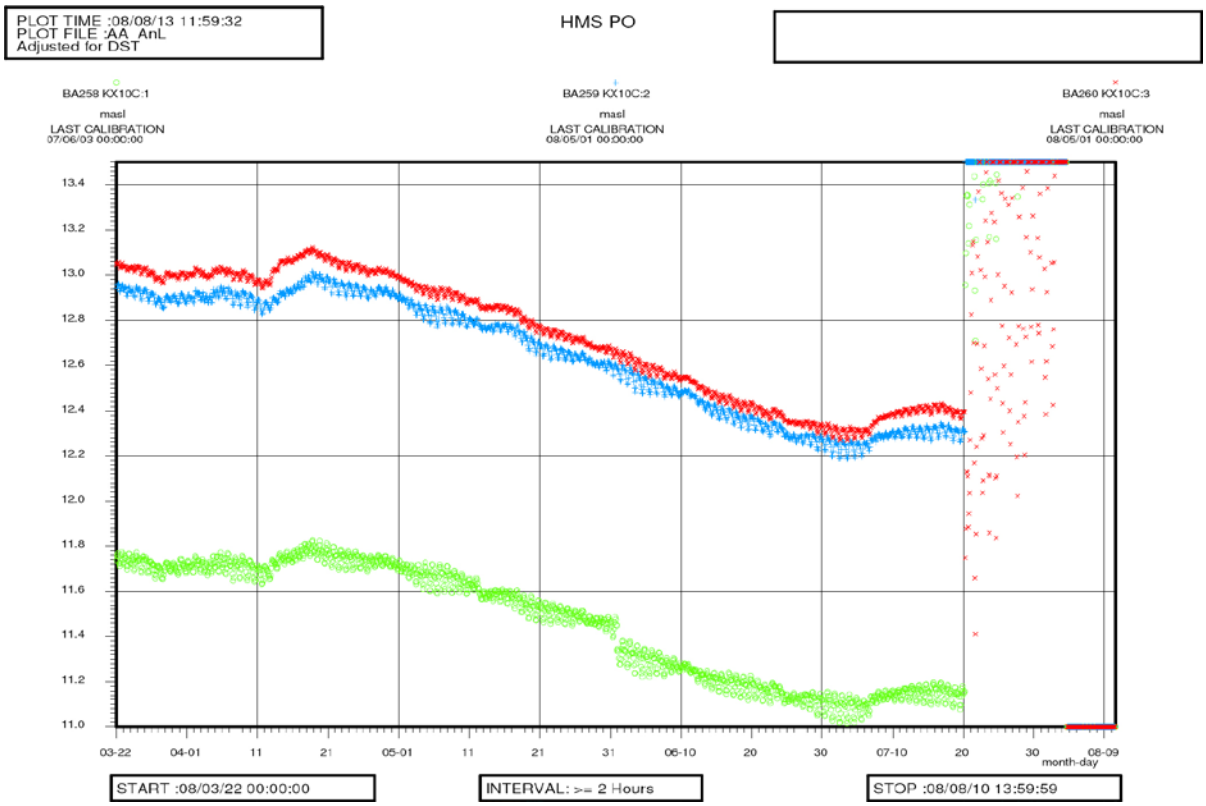

Figure A5-12. *Linear plot of observed (uncorrected) head versus time in the observation sections in KLX10C during pumping in HLX27.*

Comments on the test

All sections in KLX10C are probably unaffected by the pumping in HLX27 since no or little reaction is observed on stop of pumping on June 26. No evaluation is made of the responses in this borehole.

A5.2.10 Observation borehole KLX12A

In Figure A5-13 an overview of the observed head responses in all of the sections of the observation borehole KLX12A is shown. The three lowest sections are strongly affected by a pumping in section 2 made for water sampling. Peaks in the pressure for sections 1–3 at the 12th of May and 2nd of June is caused by levelling of the borehole. The drop of pressure in all sections in KLX12AC around the 20th of July is caused by a logger break down. The rainfall on the 13th of April has affected the pressure in some of the upper sections in KLX12A.

Comments on the test

The deepest sections in KLX12A (:1–:3) seem to be slightly affected by the pumping in HLX27. In sections :4–:6, a small response can neither be confirmed nor rejected whereas sections :7–:9 are virtually unaffected since no or little reaction is observed on stop of pumping on June 26. No evaluation is made of the responses in this borehole.

A5.2.11 Observation borehole KLX14A

In Figure A5-14 an overview of the observed head responses in observation borehole KLX14A is shown. Clear responses were observed in all three sections in KLX14A. The responses were clearer in sections 1 and 2 while the response in section 3 is more unclear.

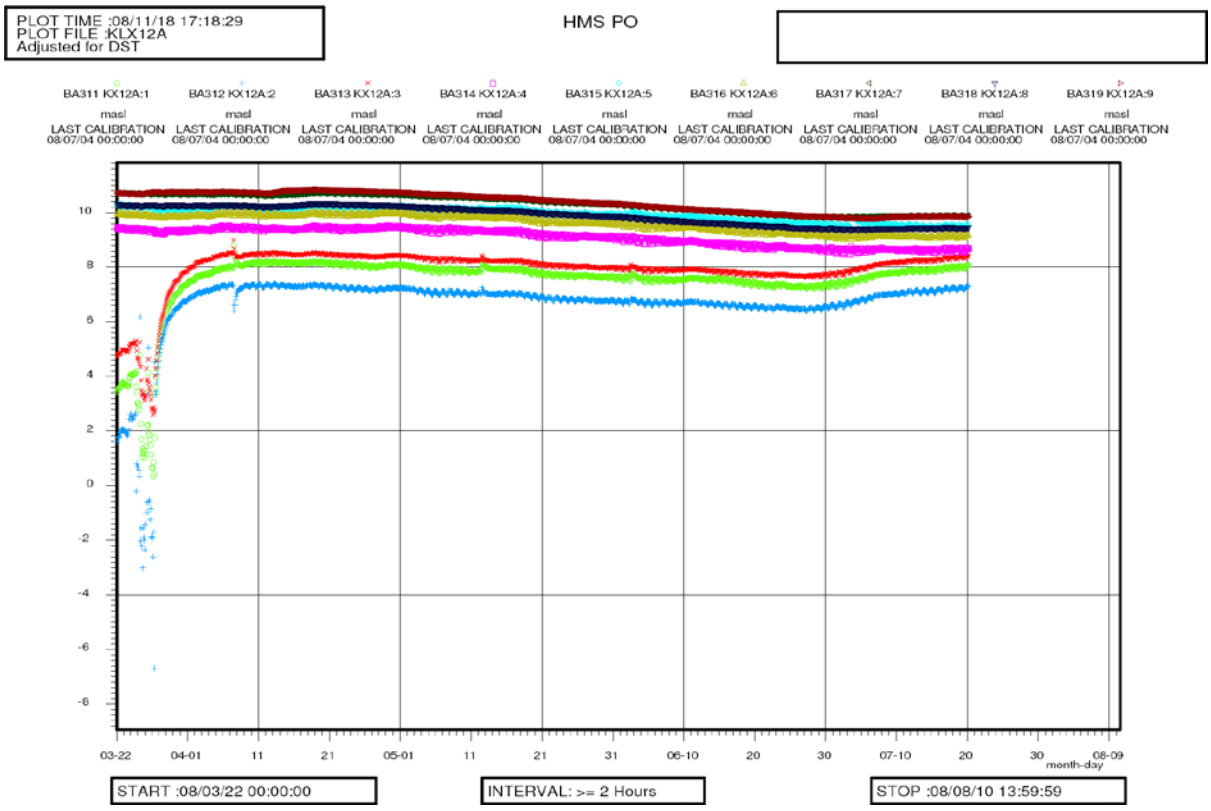

Figure A5-13. *Linear plot of observed (uncorrected) head versus time in the observation sections in KLX12A during pumping in HLX2-7.*

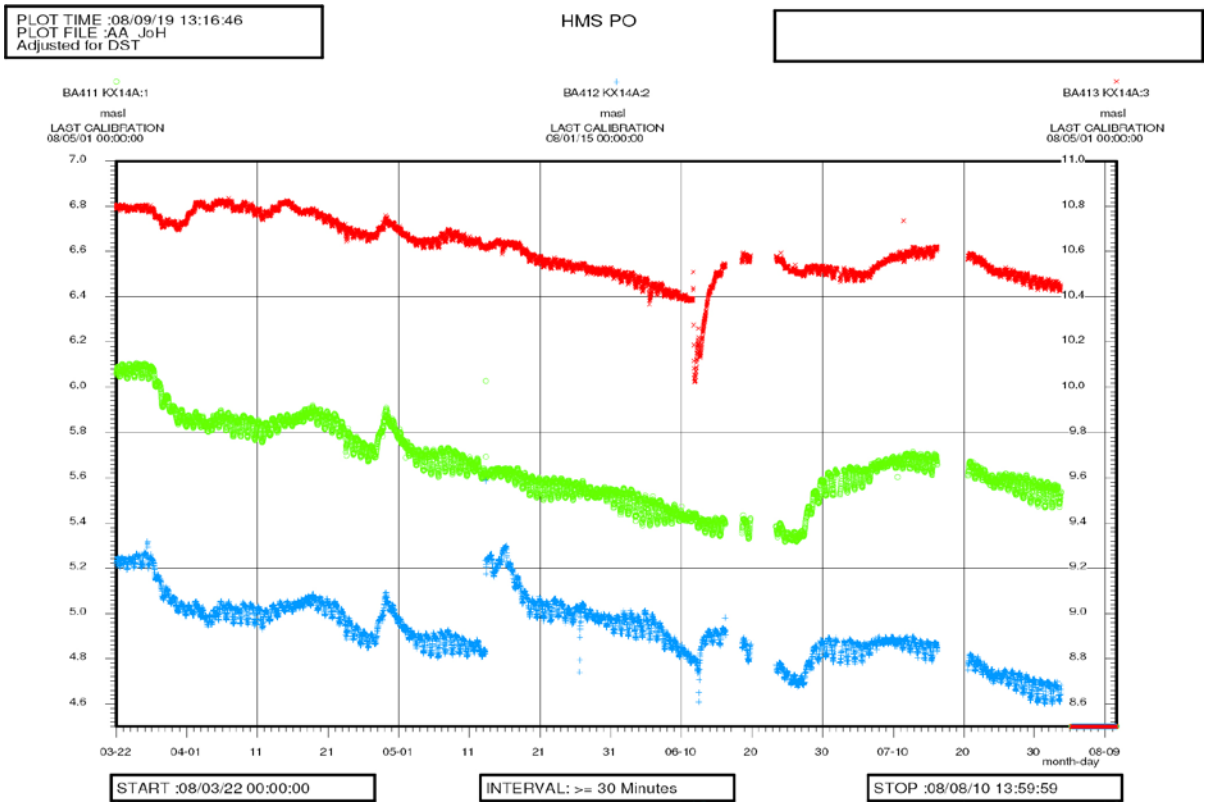

Figure A5-14. *Linear plot of observed (uncorrected) head versus time in the observation sections in KLX14A during pumping in HLX27.*

All three sections in KLX14A are missing data from three different periods during this pumping test. Times and causes were as follows: 16–19 of June due to communication error, 20–24 of June due to a thunderstorm which disrupted the logging and 17–20 of July due to that the logger malfunctioned. As seen in Figure A5-10, another thunderstorm at the 4th of August broke the data logger but this period is not part of the test. Section 3 is also affected by another pumping in HLX28 conducted on the 11th of June.

The rainfall on the 13th of April and the pump stop at the 27th of April also affected the pressure in KLX14A.

A5.2.11.1 Observation section KLX14A:1 123.0–176.27 m

In Figure A5-14 an overview of the pressure responses in observation borehole KLX14A is shown. General test data from the observation section KLX14A:1 is presented in Table A5-15.

Comments on the test

A small response is indicated in this section due to pumping in HLX27. A corrected drawdown during the flow period of c. 0.42 m was registered. A (corrected) drawdown of 0.1 m was reached approximately 2,900 min (c. 48 hours) after start of pumping in HLX27. There was a corrected recovery of c. 0.42 m during the recovery period of approximately 24 days.

At the pump stop on the 27th of April a clear peak in the head value can be seen in this section. A linear plot of the corrected and uncorrected head versus time is presented in Appendix 6.

Interpreted flow regimes and calculated parameters

The first part of the flow period is dominated by pseudo-spherical (leaky) flow at intermediate times. After the major change of flow rate at c. 37,000 min and major pump stop at c. 50,000 min in the pumping borehole, a transition towards a pseudo-radial flow regime is indicated at the end of the period.

The transient evaluation was based on variable flow rate. For the flow period, transient evaluation was made on the first part of the drawdown curve before the effects of the flow rate change reached this borehole causing a change of flow regime and before the effects of the precipitation on the 13th of April. The estimated parameters (in particular r/B) from the first part are not representative for the response during late times due to the change of flow regime. The recovery period is dominated by pseudo-spherical (leaky) flow.

The agreement in evaluated parameter values between the flow and recovery period is poor in this case. The estimated transmissivity from the flow period is significantly lower than that from the recovery period. The recovery curve is considered as uncertain due to interruptions of the data. The parameter values from the flow period are selected as the most representative. The representative transmissivity is estimated to $2.8 \cdot 10^{-5}$ m^2/s and the storativity to $5.3 \cdot 10^{-5}$.

Transient, quantitative interpretation of the flow and recovery period is shown in log-log diagrams in Appendix 6. The results from the transient evaluation are summarized in Table 5-6 in the main report.

Table A5-15. General test data from observation section KLX14A:1 during pumping in HLX27.

Pressure data	Nomenclature	Unit	Value	Corrected Value[1)]
Hydraulic head in test section before start of flow period	h_i	m.a.s.l.	6.07	6.07
Hydraulic head in test section before stop of flow period	h_p	m.a.s.l.	5.33	5.65
Hydraulic head in test section at stop of recovery period	h_F	m.a.s.l.	5.66	6.07
Hydraulic head change during flow period (h_i–h_p)	dh_p	m	0.74	0.42

[1)] Head corrected for the naturally decreasing head trend.

A5.2.11.2 Observation section KLX14A:2 77.0–122.0 m

In Figure A5-14 an overview of the observed head responses in observation borehole KLX14A is shown. General test data from the observation section KLX14A:2 are presented in Table A5-16.

Comments on the test

A small response is indicated in this section due to pumping in HLX27. A corrected drawdown during the flow period of c. 0.25 m was registered. A (corrected) drawdown of 0.1 m was reached approximately 1,320 min (c. 22 hours) after start of pumping in HLX27. There was a corrected recovery of c. 0.24 m during the recovery period of approximately 24 days.

In KLX14A:2 there is a sudden jump in pressure on the 13th of May, lifting it to a higher level. The reason to this is still unknown. The pump stop on the 27th of April is seen as a clear peak in the head for this section. Another pumping test in HLX28 at the 11th of June also affects the pressure. A linear plot of the corrected and uncorrected head versus time is presented in Appendix 6.

Interpreted flow regimes and calculated parameters

The first part of the flow period is dominated by pseudo-spherical (leaky) flow at intermediate times. After the major change of flow rate at c. 37,000 min and major pump stop at c. 50,000 min in the pumping borehole, a transition towards a pseudo-radial flow regime is indicated at the end of the period. The jump in the drawdown curve at c. 70,000 min is caused by the pressure jump mentioned above.

The transient evaluation was based on variable flow rate. For the flow period, transient evaluation was made on the first part of the flow period before the effects of the major flow rate change reached this borehole causing a change of flow regime and before the effects of the precipitation on the 13th of April and the pressure jump on the 13th of May. The estimated parameters (in particular r/B) from the first part are not representative for the response during late times due to the change of flow regime. The recovery period is dominated by pseudo-spherical (leaky) flow. The recovery curve may possibly also be affected by the pressure jump on the 13th of May (change of reference level for pressure).

The agreement in evaluated parameter values between the flow and recovery period is rather good in this case. The parameter values from the flow period are selected as the most representative. The representative transmissivity is estimated to $1.4 \cdot 10^{-4}$ m^2/s and the storativity to $6.1 \cdot 10^{-5}$.

Transient, quantitative interpretation of the flow and recovery period is shown in log-log diagrams in Appendix 6. The results from the transient evaluation are summarized in Table 5-6 in the main report.

A5.2.11.3 Observation section KLX14A:3 6.45–76.0 m

In Figure A5-14 an overview of the observed head responses in observation borehole KLX14A is shown. General test data from the observation section KLX14A:3 are presented in Table A5-17.

Table A5-16. General test data from observation section KLX14A:2 during pumping in HLX27.

Pressure data	Nomenclature	Unit	Value	Corrected Value[1)]
Hydraulic head in test section before start of flow period	h_i	m.a.s.l.	5.32	5.32
Hydraulic head in test section before stop of flow period	h_p	m.a.s.l.	4.68	5.07
Hydraulic head in test section at stop of recovery period	h_F	m.a.s.l.	4.82	5.31
Hydraulic head change during flow period (h_i–h_p)	dh_p	m	0.64	0.25

[1)] Head corrected for the naturally decreasing head trend.

Table A5-17. General test data from observation section KLX14A:3 during pumping in HLX27.

Pressure data	Nomenclature	Unit	Value	Corrected Value[1)]
Hydraulic head in test section before start of flow period	h_i	m.a.s.l.	10.79	10.79
Hydraulic head in test section before stop of flow period	h_p	m.a.s.l.	10.50	10.66
Hydraulic head in test section at stop of recovery period	h_F	m.a.s.l.	10.59	10.79
Hydraulic head change during flow period (h_i–h_p)	dh_p	m	0.29	0.13

[1)] Head corrected for the naturally decreasing head trend.

Comments on the test

A very small, slow and uncertain response is indicated in this section due to pumping in HLX27. A corrected drawdown during the flow period of c. 0.13 m was registered. A (corrected) drawdown of 0.1 m was reached approximately 75,000 min (c. 1,250 hours) after start of pumping in HLX27. There was a corrected recovery of c. 0.13 m during the recovery period of approximately 24 days.

The pump stop on the 27th of April is seen as a small peak in the head value for this section. Another pumping test in HLX28 on the 11th of June affects the pressure during a certain time. A linear plot of the corrected and uncorrected head versus time is presented in Appendix 6.

Interpreted flow regimes and calculated parameters

Due to the small response and the distortions of data described above no representative transient evaluation could be made on neither the flow nor the recovery period for this section.

A5.2.12 Observation borehole KLX15A

In Figure A5-15 an overview of the observed head responses in observation borehole KLX15A is shown. Strong responses from the pumping in HLX27 are seen in all sections (except in section 1) in this borehole. The most distinct responses occur in the upper sections (:8–:10). Section 1 is assumed to be virtually unaffected by the pumping in HLX27. No evaluation is made of the response in this section.

On the 2nd of April, a short release of packers caused a decrease in head in section 3. At the same time, start of injection of tracer in section :6 caused an increase in head in this section throughout the flow period. The increased precipitation around the 13th of April also caused distortions in the head values in all borehole sections.

The effects of the increased flow rate on the 21th of April from 50 to 75 L/min are clearly seen in the observed pressures in all sections of KLX15 as well as the pump stops (see Section 4.7 in the main report), especially the long pump stop on the 27th of April. The transient evaluation of the responses in KLX15A is also discussed in Section A5.2.1.

A5.2.12.1 Observation section KLX15A:2 641.0–901.0 m

In Figure A5-15 an overview of the observed head responses in observation borehole KLX15A is shown. General test data from the observation section KLX15A:2 are presented in Table A5-18.

Table A5-18. General test data from observation section KLX15A:2 during pumping in HLX27.

Pressure data	Nomenclature	Unit	Value	Corrected Value[1)]
Hydraulic head in test section before start of flow period	h_i	m.a.s.l.	6.04	6.04
Hydraulic head in test section before stop of flow period	h_p	m.a.s.l.	3.37	2.94
Hydraulic head in test section at stop of recovery period	h_F	m.a.s.l.	5.49	6.04
Hydraulic head change during flow period (h_i–h_p)	dh_p	m	3.10	2.67

[1)] Head corrected for the naturally decreasing head trend.

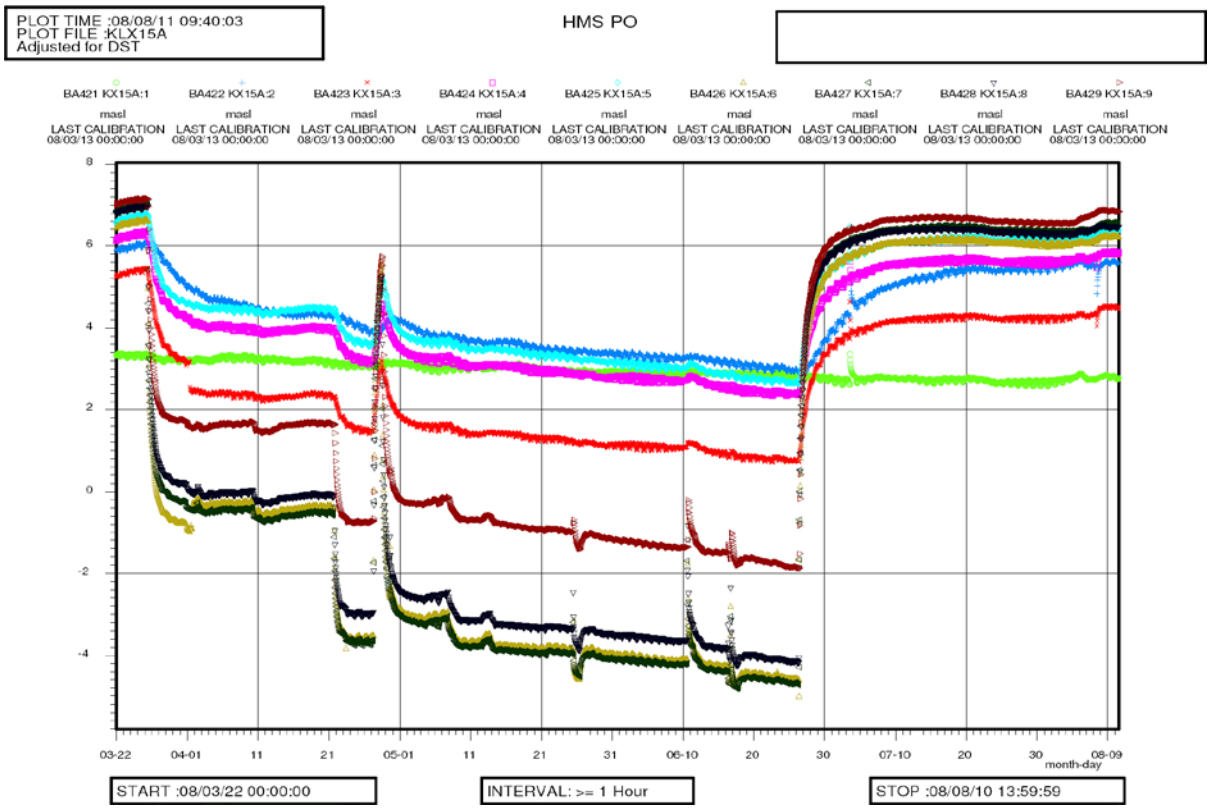

Figure A5-15. *Linear plot of observed (uncorrected) head versus time in the observation sections in KLX15A during pumping in HLX27.*

Comments on the test

A clear response is indicated in this section due to pumping in HLX27. A corrected drawdown during the flow period of c. 3.10 m was registered. A corrected drawdown of 0.1 m was reached approximately 1,500 min (c. 25 hours) after start of pumping in HLX27. There was a corrected recovery of c. 3.10 m during the recovery period of approximately 24 days.

A linear plot of the corrected and uncorrected head versus time is presented in Appendix 6.

Interpreted flow regimes and calculated parameters

During the first part of the flow period pseudo-radial flow occurred between c. 5,000–10,000 min transitioning to pseudo-spherical (leaky) flow at intermediate times. After the change of flow rate at c. 37,000 min and major pump stop at c. 50,000 min in the pumping borehole, a transition towards a new pseudo-radial flow regime is indicated at the end of the period.

The transient evaluation was based on variable flow rate. For the flow period, transient evaluation was made on the first part of the drawdown curve before the effects of the flow rate change reached this borehole causing a change of flow regime and before the effects of the precipitation on the 13th of April. The estimated parameters (in particular r/B) from the first part are not representative for the response during late times due to the change of flow regime. During the recovery period approximate pseudo-radial flow occurred between c. 5,000–10,000 min with a transition to pseudo-spherical (leaky) flow at longer times.

The agreement in evaluated parameter values between the flow and recovery period is very good. The parameter values from the recovery period are selected as the most representative. The representative transmissivity is estimated to $3.4 \cdot 10^{-5}$ m^2/s and the storativity to $8.8 \cdot 10^{-5}$.

Transient, quantitative interpretation of the flow and recovery period is shown in log-log diagrams in Appendix 6. The results from the transient evaluation are summarized in Table 5-6 in the main report.

A5.2.12.2 Observation section KLX15A:3 623.0–640.0 m

In Figure A5-15 an overview of the observed head responses in observation borehole KLX15A is shown. General test data from the observation section KLX15A:3 are presented in Table A5-19.

Comments on the test

A clear and fast response is indicated in this section due to pumping in HLX27. A corrected drawdown during the flow period of c. 3.81 m was registered. A corrected drawdown of 0.1 m was reached approximately 72 min (c. 1.2 hours) after start of pumping in HLX27. There was a corrected recovery of c. 3.81 m during the recovery period of approximately 24 days.

The pressure jump on the 2nd of April is caused by a short release of packers in this section.

A linear plot of the corrected and uncorrected head versus time is presented in Appendix 6.

Interpreted flow regimes and calculated parameters

During the first part of the flow period pseudo-radial flow occurred between c. 1,000–5,000 min transitioning to pseudo-spherical (leaky) flow at intermediate times before the pressure jump discussed above after c. 8,000 min. After the major change of flow rate at c. 37,000 min and major pump stop at c. 50,000 min in the pumping borehole, a transition towards a new pseudo-radial flow regime is indicated at the end of the period.

The transient evaluation was based on variable flow rate. For the flow period, transient evaluation was made on the first part of the drawdown curve before the effects of the pressure jump and the flow rate change reached this borehole causing a change of flow regime and finally, before the effects of the precipitation on the 13th of April. The estimated parameters (in particular r/B) from the first part are not representative for the response during late times due to the change of flow regime. During the recovery period approximate pseudo-radial flow occurred between c. 1,000–5,000 min with a transition to pseudo-spherical (leaky) flow at longer times.

The agreement in evaluated parameter values between the flow and recovery period is good. The parameter values from the recovery period are selected as the most representative. The representative transmissivity is estimated to $8.1 \cdot 10^{-5}$ m^2/s and the storativity to $2.5 \cdot 10^{-5}$.

Transient, quantitative interpretation of the flow and recovery period is shown in log-log diagrams in Appendix 6. The results from the transient evaluation are summarized in Table 5-6 in the main report.

A5.2.12.3 Observation section KLX15A:4 481.0–622.0 m

In Figure A5-15 an overview of the observed head responses in observation borehole KLX15A is shown. General test data from the observation section KLX15A:4 are presented in Table A5-20.

Table A5-19. General test data from observation section KLX15A:3 during pumping in HLX27.

Pressure data	Nomenclature	Unit	Value	Corrected Value[1)]
Hydraulic head in test section before start of flow period	h_i	m.a.s.l.	5.41	5.41
Hydraulic head in test section before stop of flow period	h_p	m.a.s.l.	0.74	1.60
Hydraulic head in test section at stop of recovery period	h_F	m.a.s.l.	4.32	5.41
Hydraulic head change during flow period (h_i–h_p)	dh_p	m	4.67	3.81

[1)] Head corrected for the naturally decreasing head trend.

Table A5-20. General test data from observation section KLX15A:4 during pumping in HLX27.

Pressure data	Nomenclature	Unit	Value	Corrected Value[1)]
Hydraulic head in test section before start of flow period	h_i	m.a.s.l.	6.31	6.31
Hydraulic head in test section before stop of flow period	h_p	m.a.s.l.	2.36	2.82
Hydraulic head in test section at stop of recovery period	h_F	m.a.s.l.	5.71	6.30
Hydraulic head change during flow period (h_i–h_p)	dh_p	m	3.95	3.49

[1)] Head corrected for the naturally decreasing head trend.

Comments on the test

A clear and large response is indicated in this section due to pumping in HLX27. A corrected drawdown during the flow period of c. 3.49 m was registered and a corrected drawdown of 0.1 m was reached approximately 235 min (c. 4 hours) after start of pumping in HLX27. There was a corrected recovery of c. 3.48 m during the recovery period of approximately 24 days.

A linear plot of the corrected and uncorrected head versus time is presented in Appendix 6.

Interpreted flow regimes and calculated parameters

During the first part of the flow period pseudo-radial flow occurred between c. 1,000–3,000 min transitioning to pseudo-spherical (leaky) flow at intermediate times. After the change of flow rate at c. 37,000 min and major pump stop at c. 50,000 min in the pumping borehole, a transition towards a new pseudo-radial flow regime is indicated at the end of the period.

The transient evaluation was based on variable flow rate. For the flow period, transient evaluation was made on the first part of the drawdown curve before the effects of the flow rate change reached this borehole causing a change of flow regime and finally, before the effects of the precipitation on the 13th of April. The estimated parameters (in particular r/B) from the first part are not representative for the response during late times due to the change of flow regime. During the recovery period approximate pseudo-radial flow occurred between c. 1,000–5,000 min with a transition to pseudo-spherical (leaky) flow at longer times.

The agreement in evaluated parameter values between the flow and recovery period is rather good. The parameter values from the recovery period are selected as the most representative. The representative transmissivity is estimated to $7.1 \cdot 10^{-5}$ m^2/s and the storativity to $4.9 \cdot 10^{-5}$.

Transient, quantitative interpretation of the flow and recovery period is shown in log-log diagrams in Appendix 6. The results from the transient evaluation are summarized in Table 5-6 in the main report.

A5.2.12.4 Observation section KLX15A:5 273.0–480.0 m

In Figure A5-15 an overview of the observed head responses in observation borehole KLX15A is shown. General test data from the observation section KLX15A:5 are presented in Table A5-21.

Table A5-21. General test data from observation section KLX15A:5 during pumping in HLX27.

Pressure data	Nomenclature	Unit	Value	Corrected Value[1)]
Hydraulic head in test section before start of flow period	h_i	m.a.s.l.	6.75	6.75
Hydraulic head in test section before stop of flow period	h_p	m.a.s.l.	2.63	3.06
Hydraulic head in test section at stop of recovery period	h_F	m.a.s.l.	6.23	6.76
Hydraulic head change during flow period (h_i–h_p)	dh_p	m	4.12	3.69

[1)] Head corrected for the naturally decreasing head trend.

Comments on the test

A clear response is indicated in this section due to pumping in HLX27. A corrected drawdown during the flow period of c. 3.69 m was registered and a corrected drawdown of 0.1 m was reached approximately 180 min (c. 3 hours) after start of pumping in HLX27. There was a corrected recovery of c. 3.7 m during the recovery period of approximately 24 days. Substantial precipitation around the 13th of April provides a peak in the head. The pump stop at the 27th of April also caused a large peak in the head values for KLX15A:5.

A linear plot of the corrected and uncorrected head versus time is presented in Appendix 6.

Interpreted flow regimes and calculated parameters

During the first part of the flow period pseudo-radial flow occurred between c. 1,000-3,000 min transitioning to pseudo-spherical (leaky) flow at intermediate times. After the change of flow rate at c. 37,000 min and major pump stop at c. 50,000 min in the pumping borehole, a transition towards a new pseudo-radial flow regime is indicated at the end of the period.

The transient evaluation was based on variable flow rate. For the flow period, transient evaluation was made on the first part of the drawdown curve before the effects of the flow rate change reached this borehole causing a change of flow regime and finally, before the effects of the precipitation on the 13th of April. The estimated parameters (in particular r/B) from the first part are not representative for the response during late times due to the change of flow regime. During the recovery period approximate pseudo-radial flow occurred between c. 1,000–5,000 min with a transition to pseudo-spherical (leaky) flow at longer times.

The agreement in evaluated parameter values between the flow and recovery period is rather good. The parameter values from the recovery period are selected as the most representative. The representative transmissivity is estimated to $6.7 \cdot 10^{-5}$ m^2/s and the storativity to $1.2 \cdot 10^{-4}$.

Transient, quantitative interpretation of the flow and recovery period is shown in log-log diagrams in Appendix 6. The results from the transient evaluation are summarized in Table 5-6 in the main report.

A5.2.12.5 Observation section KLX15A:6 260.0–272.0 m

In Figure A5-15 an overview of the observed head responses in observation borehole KLX15A is shown. General test data from the observation section KLX15A:6 are presented in Table A5-22.

Comments on the test

The response for this section due to pumping in HLX27 was very fast and distinct. A corrected drawdown during the flow period of c. 10.87 m was registered and a corrected drawdown of 0.1 m was reached approximately 3 min after start of pumping in HLX27. There was a corrected recovery of c. 10.87 m during the recovery period of approximately 24 days.

Substantial precipitation around the 13th of April provides a peak in the head. The pump stop at the 27th of April also caused a large peak in the head values for KLX15A:6 but other short stops of the pump are also clearly seen on the pressure.

Table A5-22. General test data from observation section KLX15A:6 during pumping in HLX27.

Pressure data	Nomenclature	Unit	Value	Corrected Value[1)]
Hydraulic head in test section before start of flow period	h_i	m.a.s.l.	6.60	6.60
Hydraulic head in test section before stop of flow period	h_p	m.a.s.l.	–4.63	–4.27
Hydraulic head in test section at stop of recovery period	h_F	m.a.s.l.	6.15	6.60
Hydraulic head change during flow period (h_i–h_p)	dh_p	m	11.23	10.87

[1)] Head corrected for the naturally decreasing head trend.

On the 2nd of April, start of injection of tracer in this section caused a slightly increased head throughout the flow period.

A linear plot of the corrected and uncorrected head versus time is presented in Appendix 6.

Interpreted flow regimes and calculated parameters

During the first part of the flow period pseudo-radial flow occurred between c. 200–1,000 min transitioning to pseudo-spherical (leaky) flow at intermediate times. An increase of head occurred after c. 8,000 min due to tracer injection in this section as mentioned above. After the change of flow rate at c. 37,000 min and major pump stop at c. 50,000 min in the pumping borehole, a transition towards a new pseudo-radial flow regime is indicated at the end of the period.

The transient evaluation was based on variable flow rate. For the flow period, transient evaluation was made on the first part of the drawdown curve before the effects of the pressure jump on the 2nd of April and the major flow rate change reached this borehole causing a change of flow regime and finally, before the effects of the precipitation on the 13th of April. The estimated parameters (in particular r/B) from the first part are not representative for the response during late times due to the change of flow regime. During the recovery period approximate pseudo-radial flow occurred between c. 200–2,000 min with a transition to pseudo-spherical (leaky) flow at longer times.

The agreement in evaluated parameter values between the flow and recovery period is good. The parameter values from the recovery period are selected as the most representative. The representative transmissivity is estimated to $5.5 \cdot 10^{-5}$ m^2/s and the storativity to $4.8 \cdot 10^{-6}$.

Transient, quantitative interpretation of the flow and recovery period is shown in log-log diagrams in Appendix 6. The results from the transient evaluation are summarized in Table 5-6 in the main report.

A5.2.12.6 Observation section KLX15A:7 191.0–259.0 m

In Figure A5-15 an overview of the observed head responses in observation borehole KLX15A is shown. General test data from the observation section KLX15A:7 are presented in Table A5-23.

Comments on the test

The response for this section due to pumping in HLX27 was very fast and distinct. A corrected drawdown during the flow period of c. 11.32 m was registered and a corrected drawdown of 0.1 m was reached approximately 2 min after start of pumping in HLX27. There was a corrected recovery of c. 11.31 m during the recovery period of approximately 24 days. Substantial precipitation around the 13th of April provides a peak in the head. The pump stop at the 27th of April also caused a large peak in the head values for KLX15A:7 but other short stops of the pump are clearly seen on the pressure as well.

A linear plot of the corrected and uncorrected head versus time is presented in Appendix 6.

Table A5-23. General test data from observation section KLX15A:7 during pumping in HLX27.

Pressure data	Nomenclature	Unit	Value	Corrected Value[1)]
Hydraulic head in test section before start of flow period	h_i	m.a.s.l.	7.01	7.01
Hydraulic head in test section before stop of flow period	h_p	m.a.s.l.	–4.72	–4.31
Hydraulic head in test section at stop of recovery period	h_F	m.a.s.l.	6.58	7.00
Hydraulic head change during flow period (h_i–h_p)	dh_p	m	11.72	11.32

[1)] Head corrected for the naturally decreasing head trend.

Interpreted flow regimes and calculated parameters

During the first part of the flow period pseudo-radial flow occurred between c. 200–1,000 min transitioning to pseudo-spherical (leaky) flow at intermediate times. After the change of flow rate at c. 37,000 min and major pump stop at c. 50,000 min in the pumping borehole, a transition towards a new pseudo-radial flow regime is indicated at the end of the period.

The transient evaluation was based on variable flow rate. For the flow period, transient evaluation was made on the first part of the drawdown curve before the effects of the major flow rate change reached this borehole causing a change of flow regime and before the effects of the precipitation on the 13th of April. The estimated parameters (in particular r/B) from the first part are not representative for the response during late times due to the change of flow regime. During the recovery period approximate pseudo-radial flow occurred between c. 200–2,000 min with a transition to pseudo-spherical (leaky) flow at longer times.

The agreement in evaluated parameter values between the flow and recovery period is good. The parameter values from the recovery period are selected as the most representative. The representative transmissivity is estimated to $5.0 \cdot 10^{-5}$ m^2/s and the storativity to $8.7 \cdot 10^{-6}$.

Transient, quantitative interpretation of the flow and recovery period is shown in log-log diagrams in Appendix 6. The results from the transient evaluation are summarized in Table 5-6 in the main report.

A5.2.12.7 Observation section KLX15A:8 79.0–190.0 m

In Figure A5-15 an overview of the observed head responses in observation borehole KLX15A is shown. General test data from the observation section KLX15A:8 are presented in Table A5-24.

Comments on the test

The response for this section due to pumping in HLX27 was very fast and distinct. A corrected drawdown during the flow period of c. 10.72 m was registered and a corrected drawdown of 0.1 m was reached approximately 5 min after start of pumping in HLX27. There was a corrected recovery of c. 10.71 m during the recovery period of approximately 24 days. Substantial precipitation around the 13th of April provides a clear peak in the head. The pump stop at the 27th of April also caused a large peak in the head values for KLX15A:8 but other short stops of the pump are clearly seen as responses on the pressure as well.

A linear plot of the corrected and uncorrected head versus time is presented in Appendix 6.

Interpreted flow regimes and calculated parameters

During the first part of the flow period pseudo-radial flow occurred between c. 200–1,000 min transitioning to pseudo-spherical (leaky) flow at intermediate times. After the change of flow rate at c. 37,000 min and major pump stop at c. 50,000 min in the pumping borehole, a transition towards a new pseudo-radial flow regime is indicated at the end of the period.

Table A5-24. General test data from observation section KLX15A:8 during pumping in HLX27.

Pressure data	Nomenclature	Unit	Value	Corrected Value[1)]
Hydraulic head in test section before start of flow period	h_i	m.a.s.l.	6.96	6.97
Hydraulic head in test section before stop of flow period	h_p	m.a.s.l.	–4.16	–3.75
Hydraulic head in test section at stop of recovery period	h_F	m.a.s.l.	6.49	6.96
Hydraulic head change during flow period (h_i–h_p)	dh_p	m	11.13	10.72

[1)] Head corrected for the naturally decreasing head trend.

The transient evaluation was based on variable flow rate. For the flow period, transient evaluation was made on the first part of the drawdown curve before the effects of the major flow rate change reached this borehole causing a change of flow regime and before the effects of the precipitation on the 13th of April. The estimated parameters (in particular r/B) from the first part are not representative for the response during late times due to the change of flow regime. During the recovery period approximate pseudo-radial flow occurred between c. 200–2,000 min with a transition to pseudo-spherical (leaky) flow at longer times.

The agreement in evaluated parameter values between the flow and recovery period is good. The parameter values from the recovery period are selected as the most representative. The representative transmissivity is estimated to $4.8 \cdot 10^{-5}$ m^2/s and the storativity to $1.9 \cdot 10^{-5}$.

Transient, quantitative interpretation of the flow and recovery period is shown in log-log diagrams in Appendix 6. The results from the transient evaluation are summarized in Table 5-6 in the main report.

A5.2.12.8 Observation section KLX15A:9 11.65–78.0 m

In Figure A5-15 an overview of the observed head responses in observation borehole KLX15A is shown. General test data from the observation section KLX15A:9 are presented in Table A5-25.

Comments on the test

The response in this section due to pumping in HLX27 was fast and distinct. A corrected drawdown during the flow period of c. 8.67 m was registered and a corrected drawdown of 0.1 m was reached approximately 30 min after start of pumping in HLX27. There was a corrected recovery of c. 8.66 m during the recovery period of approximately 24 days.

Substantial precipitation around the 13th of April provides a peak in the head. The major pump stop at the 27th of April also caused a large peak in the head values for KLX15A:9 but other short stops of the pump are clearly seen as responses on the pressure as well.

A linear plot of the corrected and uncorrected head versus time is presented in Appendix 6.

Interpreted flow regimes and calculated parameters

During the first part of the flow period pseudo-radial flow occurred between c. 200–1,000 min transitioning to pseudo-spherical (leaky) flow at intermediate times. After the change of flow rate at c. 37,000 min and major pump stop at c. 50,000 min in the pumping borehole, a transition towards a new pseudo-radial flow regime is indicated at the end of the period.

The transient evaluation was based on variable flow rate. For the flow period, transient evaluation was made on the first part of the drawdown curve before the effects of the flow rate change reached this borehole causing a change of flow regime and before the effects of the precipitation on the 13th of April. The estimated parameters (in particular r/B) from the first part are not representative for the response during late times due to the change of flow regime. During the recovery period approximate pseudo-radial flow occurred between c. 400–2,000 min with a transition to pseudo-spherical (leaky) flow at longer times.

Table A5-25. General test data from observation section KLX15A:9 during pumping in HLX27.

Pressure data	Nomenclature	Unit	Value	Corrected Value[1)]
Hydraulic head in test section before start of flow period	h_i	m.a.s.l.	7.14	7.15
Hydraulic head in test section before stop of flow period	h_p	m.a.s.l.	–1.88	–1.52
Hydraulic head in test section at stop of recovery period	h_F	m.a.s.l.	6.68	7.14
Hydraulic head change during flow period (h_i–h_p)	dh_p	m	9.03	8.67

[1)] Head corrected for the naturally decreasing head trend.

The agreement in evaluated parameter values between the flow and recovery period is good. The parameter values from the recovery period are selected as the most representative. The representative transmissivity is estimated to $3.6 \cdot 10^{-5}$ m^2/s and the storativity to $3.1 \cdot 10^{-5}$.

Transient, quantitative interpretation of the flow and recovery period is shown in log-log diagrams in Appendix 6. The results from the transient evaluation are summarized in Table 5-6 in the main report.

A5.2.13 Observation borehole KLX16A

In Figure A5-16 an overview of the observed head responses in observation borehole KLX16A is shown. Clear responses from the pumping in HLX27 are observed in sections :2 and :3. In KLX16A:1 the response is however very uncertain and no pressure recovery is observed. Hence, no evaluation is made in this section.

At the 8th, 9th and 10–12th of May some pressure data is missing since the batteries in the logger were discharged.

A5.2.13.1 Observation section KLX16A:2 86.0–326.0 m

In Figure A5-16 an overview of the pressure responses in observation borehole KLX16A is shown. General test data from the observation section KLX16A:2 are presented in Table A5-26.

Comments on the test

A clear response is indicated in this section due to pumping in HLX27. A corrected drawdown during the flow period of c. 1.67 m was registered. A corrected drawdown of 0.1 m was reached approximately 1,560 min (c. 26 hours) after start of pumping in HLX27. There was a corrected recovery of c. 1.67 m during the recovery period of approximately 24 days. Substantial precipitation around the 13th of April increases the pressure for a while. The pump stop at the 27th of April also caused a peak in the head values for KLX16A:2.

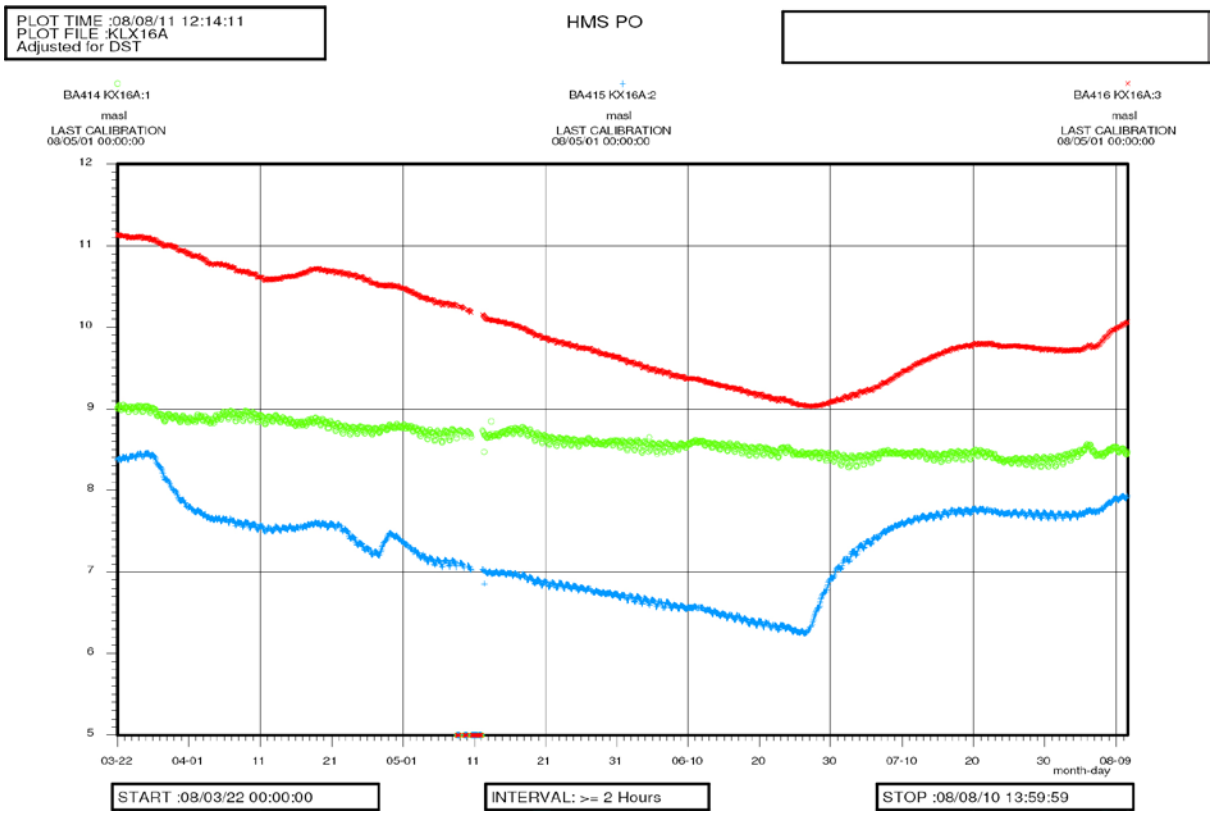

Figure A5-16. *Linear plot of observed (uncorrected) head versus time in the observation sections in KLX16A during pumping in HLX27.*

Table A5-26. General test data from observation section KLX16A:2 during pumping in HLX27.

Pressure data	Nomenclature	Unit	Value	Corrected Value[1)]
Hydraulic head in test section before start of flow period	h_i	m.a.s.l.	8.44	8.44
Hydraulic head in test section before stop of flow period	h_p	m.a.s.l.	6.25	6.77
Hydraulic head in test section at stop of recovery period	h_F	m.a.s.l.	7.77	8.44
Hydraulic head change during flow period (h_i–h_p)	dh_p	m	2.19	1.67

[1)] Head corrected for the naturally decreasing head trend.

A linear plot of the corrected and uncorrected head versus time is presented in Appendix 6.

Interpreted flow regimes and calculated parameters

The first part of the flow period is dominated by pseudo-radial flow. After the change of flow rate at c. 37,000 min and major pump stop at c. 50,000 min in the pumping borehole, a transition towards a new pseudo-radial flow regime is indicated at the end of the period.

The transient evaluation was based on variable flow rate. For the flow period, transient evaluation was made on the first part of the drawdown curve before the effects of the flow rate change reached this borehole causing a change of flow regime and before the effects of the precipitation on the 13th of April. The estimated parameters from the first part are not representative for the response during late times due to the change of flow regime. During the recovery period approximate pseudo-radial flow occurred between c. 8,000–20,000 min with a transition to pseudo-spherical (leaky) flow at longer times.

The agreement in evaluated parameter values between the flow and recovery period is rather good. The parameter values from the recovery period are selected as the most representative. The representative transmissivity is estimated to $1.1 \cdot 10^{-4}$ m^2/s and the storativity to $7.5 \cdot 10^{-5}$.

Transient, quantitative interpretation of the flow and recovery period is shown in log-log diagrams in Appendix 6. The results from the transient evaluation are summarized in Table 5-6 in the main report.

A5.2.13.2 Observation section KLX16A:3 11.25–85.0 m

In Figure A5-16 an overview of the observed head responses in observation borehole KLX16A is shown. General test data from the observation section KLX16A:3 are presented in Table A5-27.

Comments on the test

A clear response is indicated in this section due to pumping in HLX27. A corrected drawdown during the flow period of c. 1.03 m was registered and a corrected drawdown of 0.01 m was reached approximately 5,800 min (c. 97 hours) after start of pumping in HLX27. There was a corrected recovery of c. 1.03 m during the recovery period of approximately 24 days. Substantial precipitation around the 13th of April increases the pressure during a certain time period.

A linear plot of the corrected and uncorrected head versus time is presented in Appendix 6.

Table A5-27. General test data from observation section KLX16A:3 during pumping in HLX27.

Pressure data	Nomenclature	Unit	Value	Corrected Value[1)]
Hydraulic head in test section before start of flow period	h_i	m.a.s.l.	11.09	11.09
Hydraulic head in test section before stop of flow period	h_p	m.a.s.l.	9.03	10.06
Hydraulic head in test section at stop of recovery period	h_F	m.a.s.l.	9.79	11.09
Hydraulic head change during flow period (h_i–h_p)	dh_p	m	2.06	1.03

[1)] Head corrected for the naturally decreasing head trend.

Interpreted flow regimes and calculated parameters

During the first part of the flow period approximate pseudo-radial flow occurred between c. 8,000–20,000 min. After the change of flow rate at c. 37,000 min and major pump stop at c. 50,000 min in the pumping borehole, a transition towards a new pseudo-radial flow regime is indicated at the end of the period.

The transient evaluation was based on variable flow rate. For the flow period, transient evaluation was made on the first part of the drawdown curve before the effects of the flow rate change reached this borehole causing a change of flow regime and before the effects of the precipitation on the 13th of April. The estimated parameters from the first part are not representative for the response during late times due to the change of flow regime. During the recovery period a transition to pseudo-radial flow occurred.

The agreement in evaluated parameter values between the flow and recovery period is rather poor in this case. The transmissivity from the flow period was significantly higher than that from the recovery period. The parameter values from the recovery period are selected as the most representative. The representative transmissivity is estimated to $5.3 \cdot 10^{-5}$ m²/s and the storativity to $2.7 \cdot 10^{-4}$. The pressure recovery is more delayed in this section.

Transient, quantitative interpretation of the flow and recovery period is shown in log-log diagrams in Appendix 6. The results from the transient evaluation are summarized in Table 5-6 in the main report.

A5.2.14 Observation borehole KLX18A

In Figure A5-17 an overview of the observed head responses in all of the sections of the observation borehole KLX18A is shown.

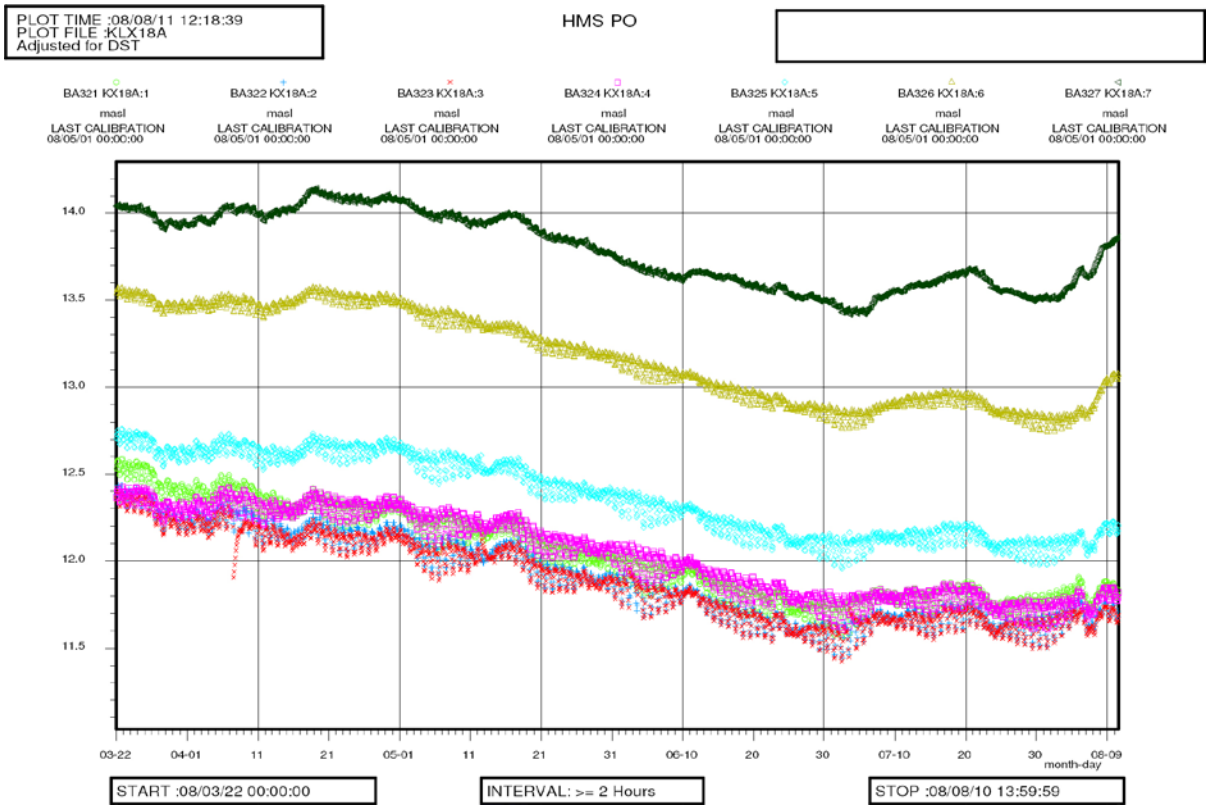

Figure A5-17. *Linear plot of observed (uncorrected) head versus time in the observation sections in KLX18A during pumping in HLX27.*

Comments on the test

The uppermost two sections (:6 and :7) in KLX18A are probably unaffected by the pumping in HLX27 since no or little reaction is observed on stop of pumping on June 26. However, in the lower sections a small response cannot be excluded. No evaluation is made of the responses in this borehole.

A5.2.15 Observation borehole KLX19A

In Figure A5-18 an overview of the observed head responses in all of the sections of the observation borehole KLX19A is shown. Sections :3 to :8 are strongly affected by another pumping in HLX28 on the 11th of June for water sampling. The peaks in the pressure for some sections at the 1st of April, 15th of May, 5th of June and 10th of July are caused by water levelling of the borehole. The losses of pressure data in all sections in KLX19A on the 16th–19th of June, 20th–24th of July and the 17th–20th of July are caused by, in order, a thunderstorm, communication problems and logger breakdown. The rainfall on the 13th of April may have affected the pressure in the uppermost section in KLX19A.

Comments on the test

Most sections in KLX19A are probably unaffected by the pumping in HLX27 since no or little reaction is observed on stop of pumping on June 26. However, in some sections a small response cannot be excluded. No evaluation is made of the responses in this borehole.

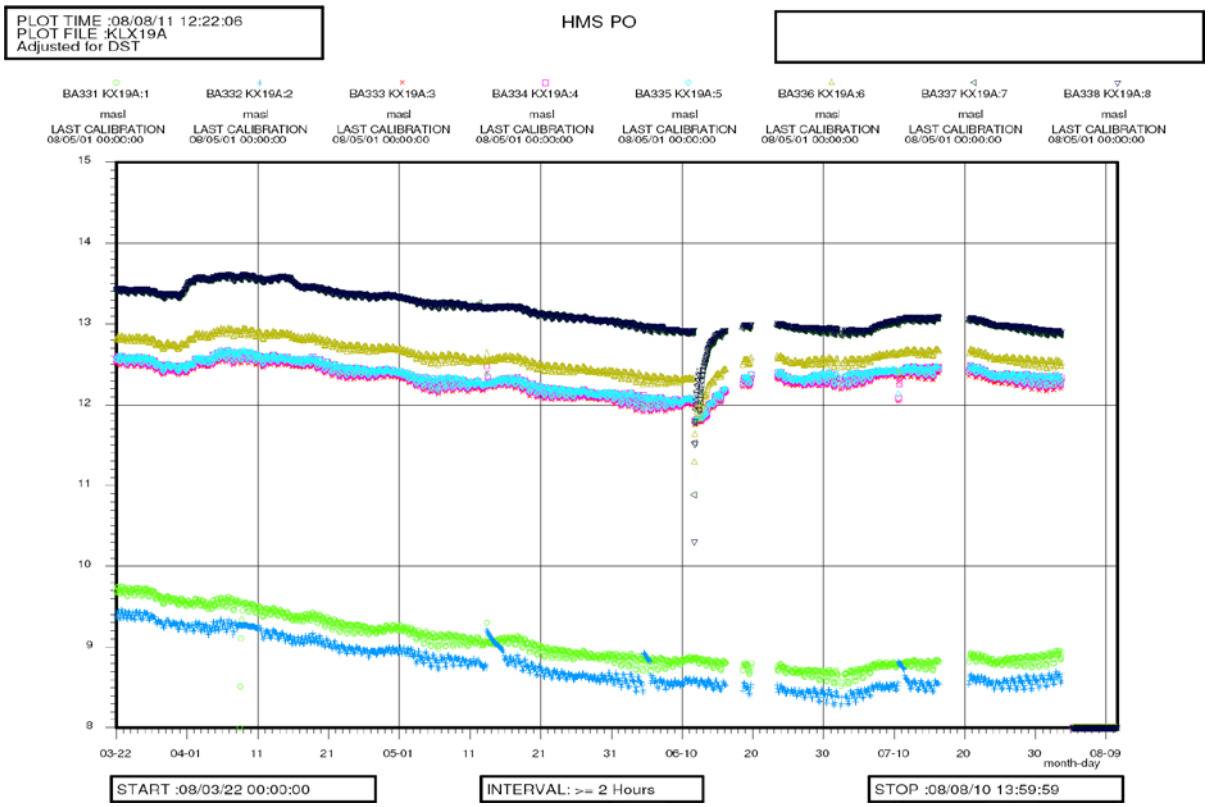

Figure A5-18. *Linear plot of observed (uncorrected) head versus time in the observation sections in KLX19A during pumping in HLX27.*

Appendix 6

Test diagrams

Nomenclature for AQTESOLV:

T = transmissivity (m^2/s)

S = storativity (–)

K_Z/K_r = ratio of hydraulic conductivities in the vertical and radial direction (set to 1)

Sw = skin factor

r(w) = borehole radius (m)

r(c) = effective casing radius (m)

r/B = leakage coefficient (s^{-1})

b = thickness of formation (m)

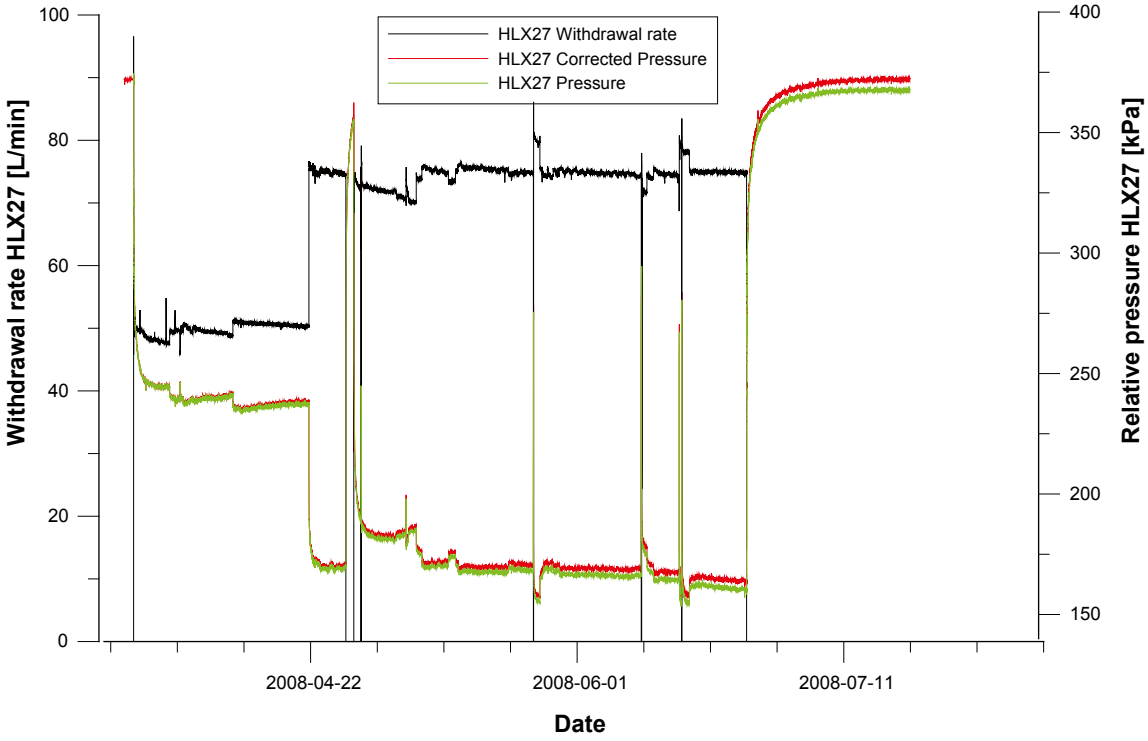

Figure A6-1. *Linear plot of measured and corrected pressure and flow versus time in the pumping borehole HLX27, 6.03–164.70 m during the interference test in HLX27.*

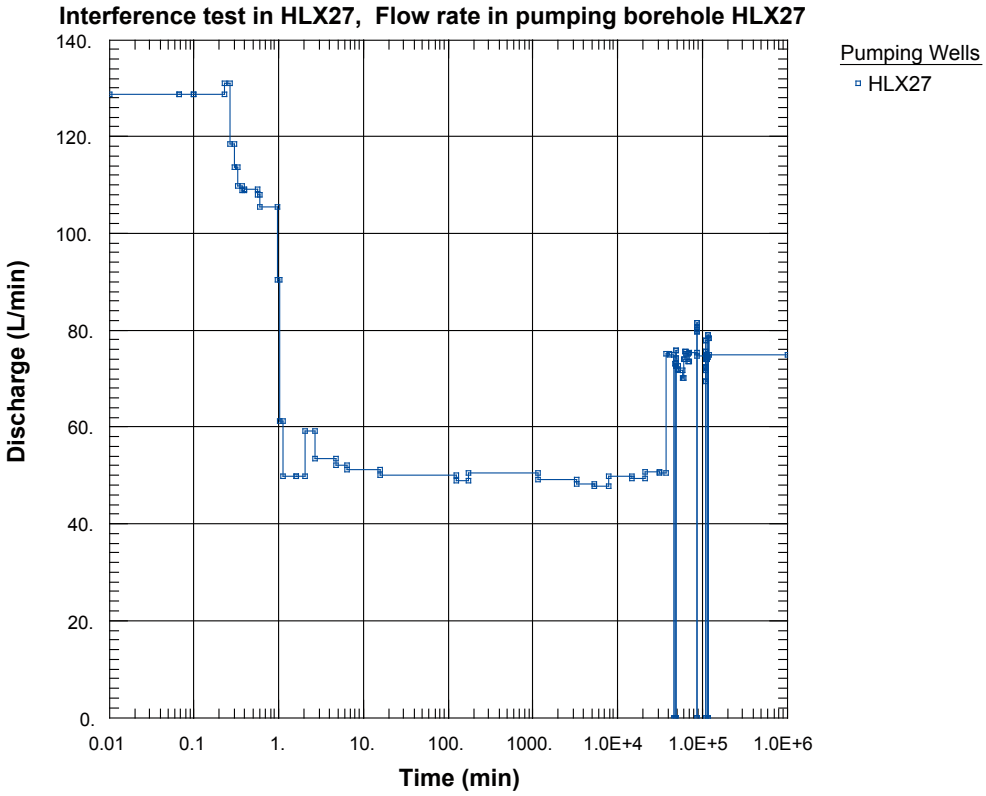

Figure A6-2. *Lin-log plot of flow rate (▫) versus time in the pumping borehole HLX27 during the interference test in HLX27.*

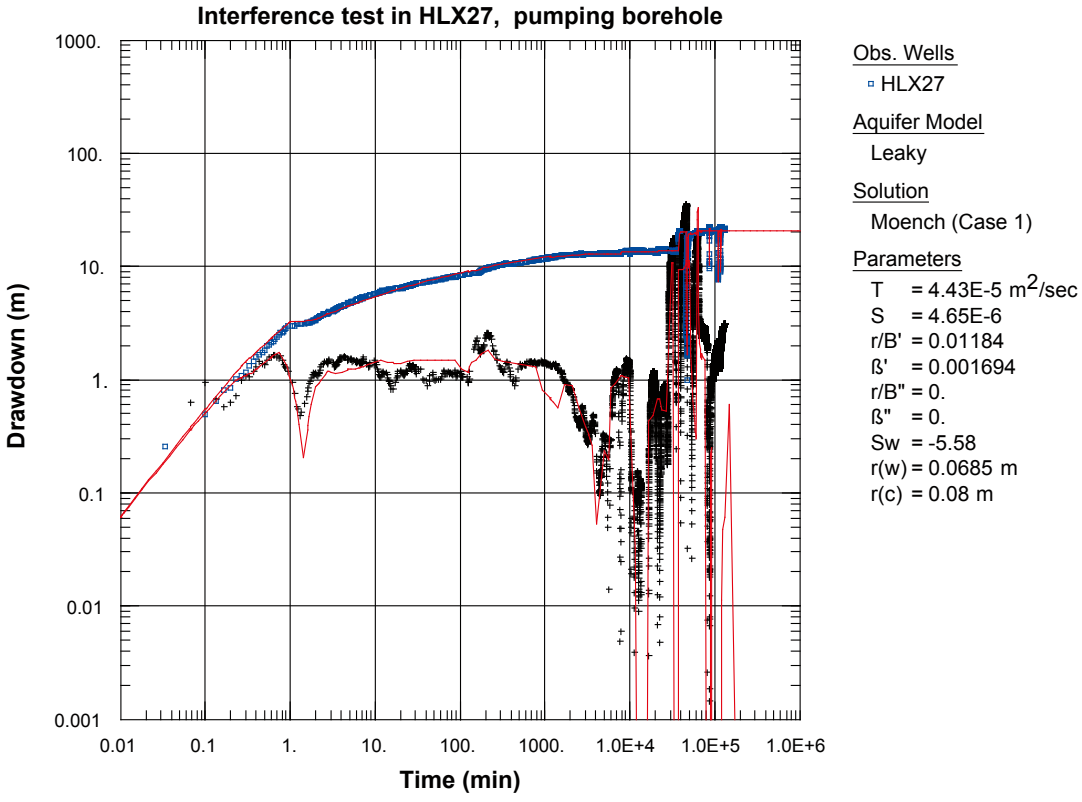

Figure A6-3. *Log-log plot of drawdown (▫) and drawdown derivative, ds/d(ln t) (+), versus time in the pumping borehole HLX27 during the interference test in HLX27. Transient evaluation is based on the early part of the flow period.*

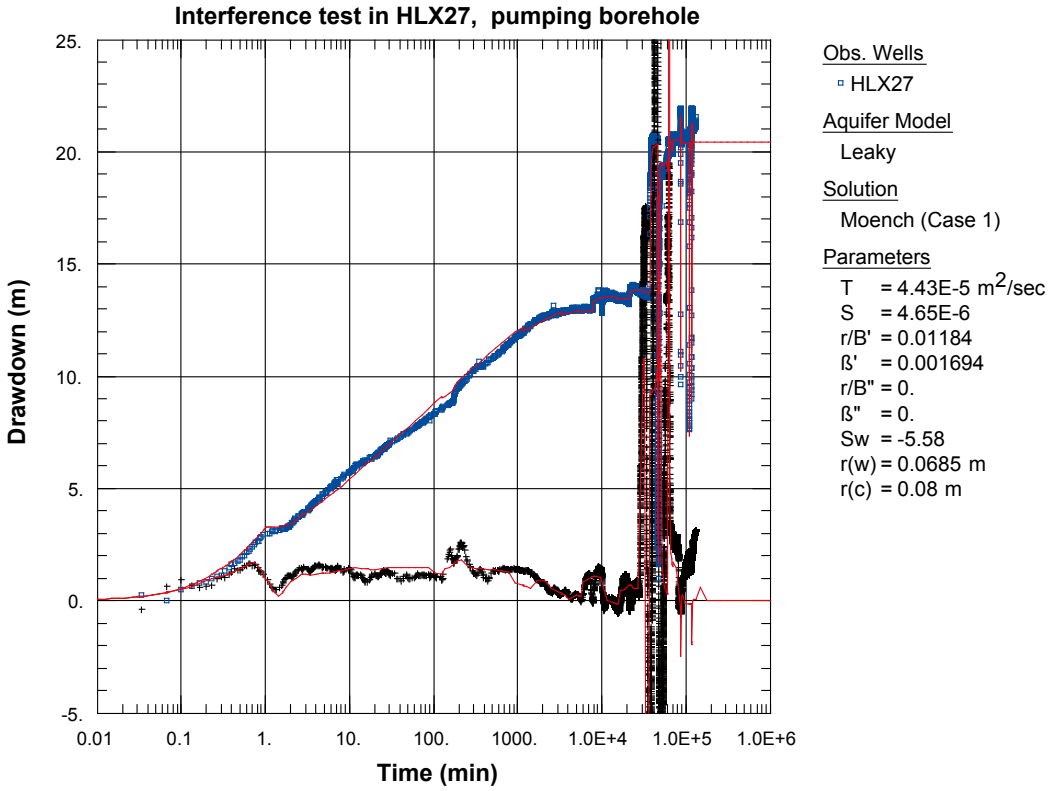

Figure A6-4. *Lin-log plot of drawdown (▫) and drawdown derivative, ds/d(ln t) (+), versus time in the pumping borehole HLX27 during the interference test in HLX27. Transient evaluation is based on the early part of the flow period.*

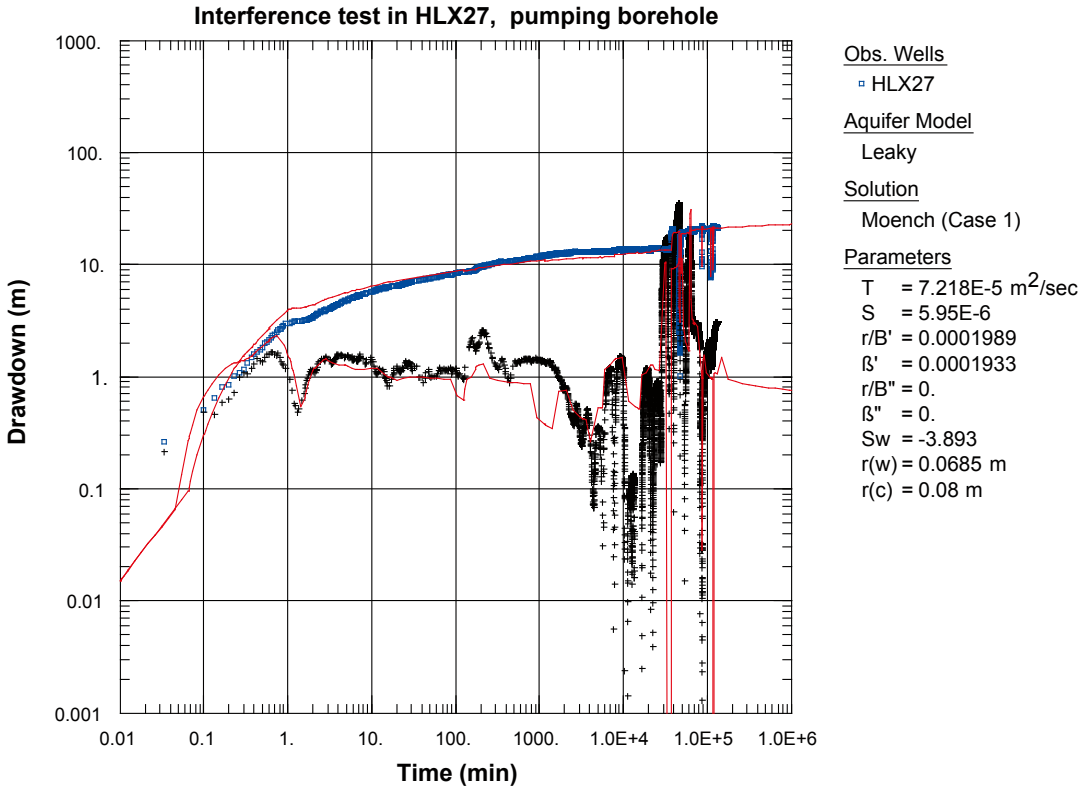

Figure A6-5. *Log-log plot of drawdown (▫) and drawdown derivative, ds/d(ln t) (+), versus time in HLX27 during the interference test in HLX27. Transient evaluation is based on the later part of the flow period.*

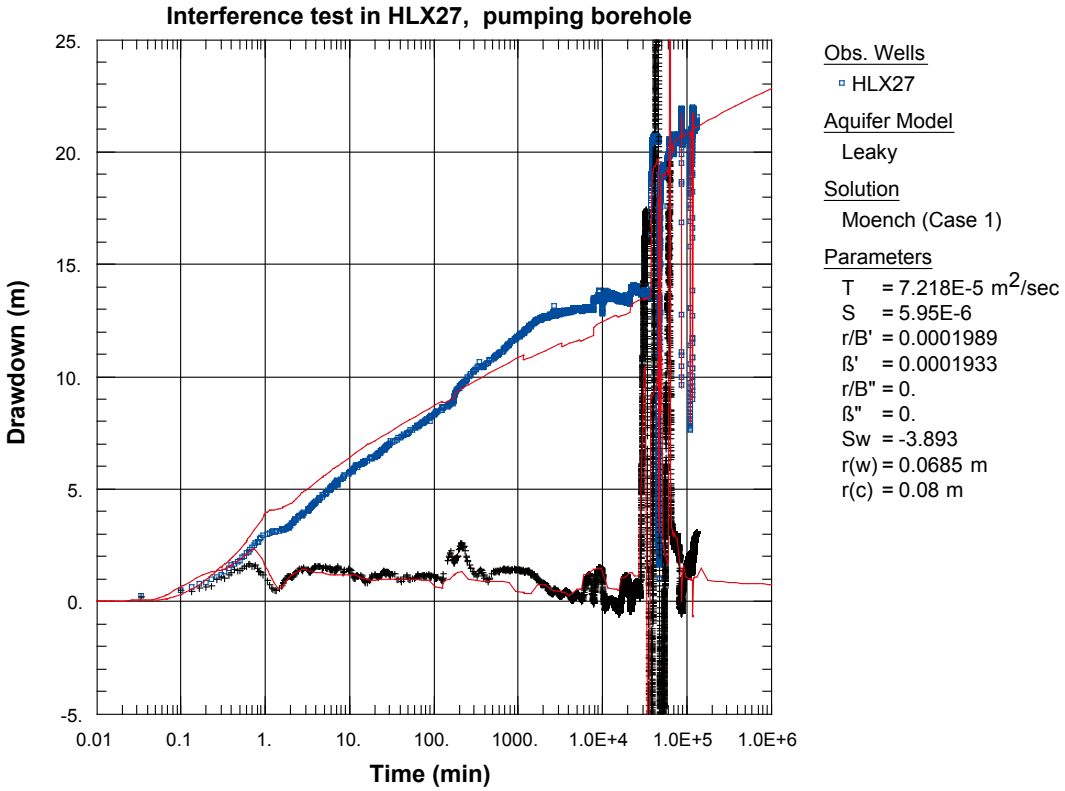

Figure A6-6. *Lin-log plot of drawdown (▫) and drawdown derivative, ds/d(ln t) (+), versus time in HLX27 during the interference test in HLX27. Transient evaluation is based on the later part of the flow period.*

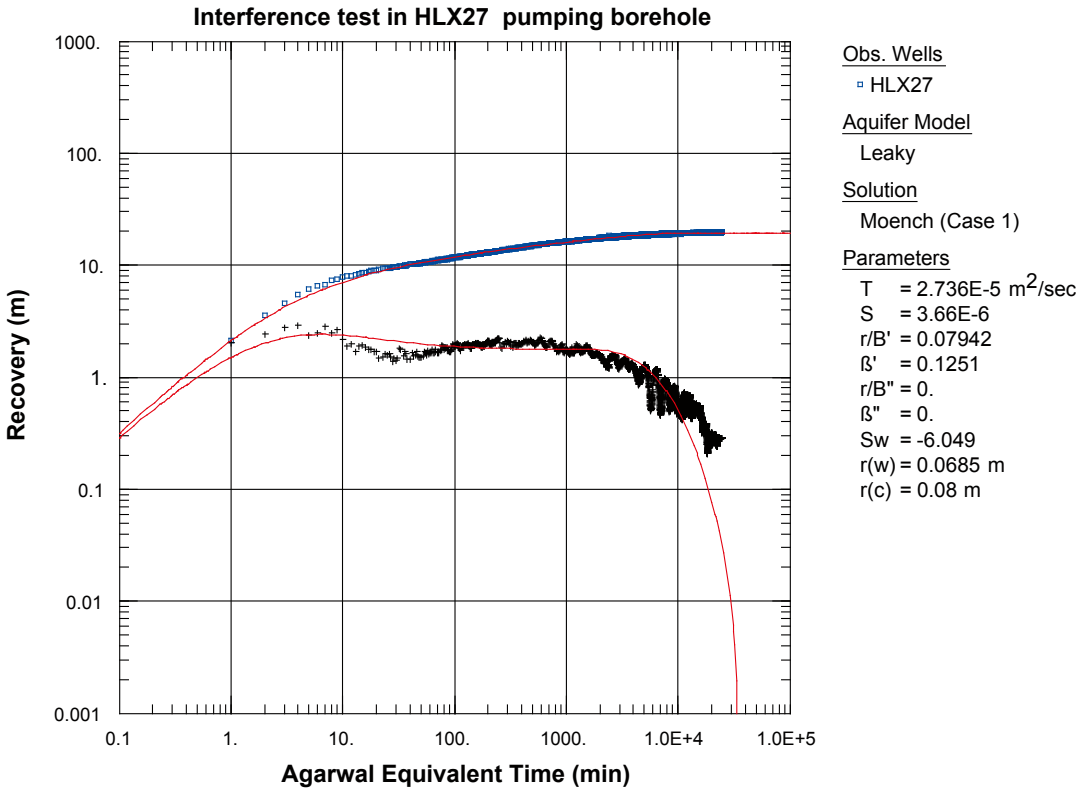

Figure A6-7. *Log-log plot of recovery (▫) and recovery derivative, ds/d(ln t) (+), versus time in the pumping borehole HLX27 during the interference test in HLX27.*

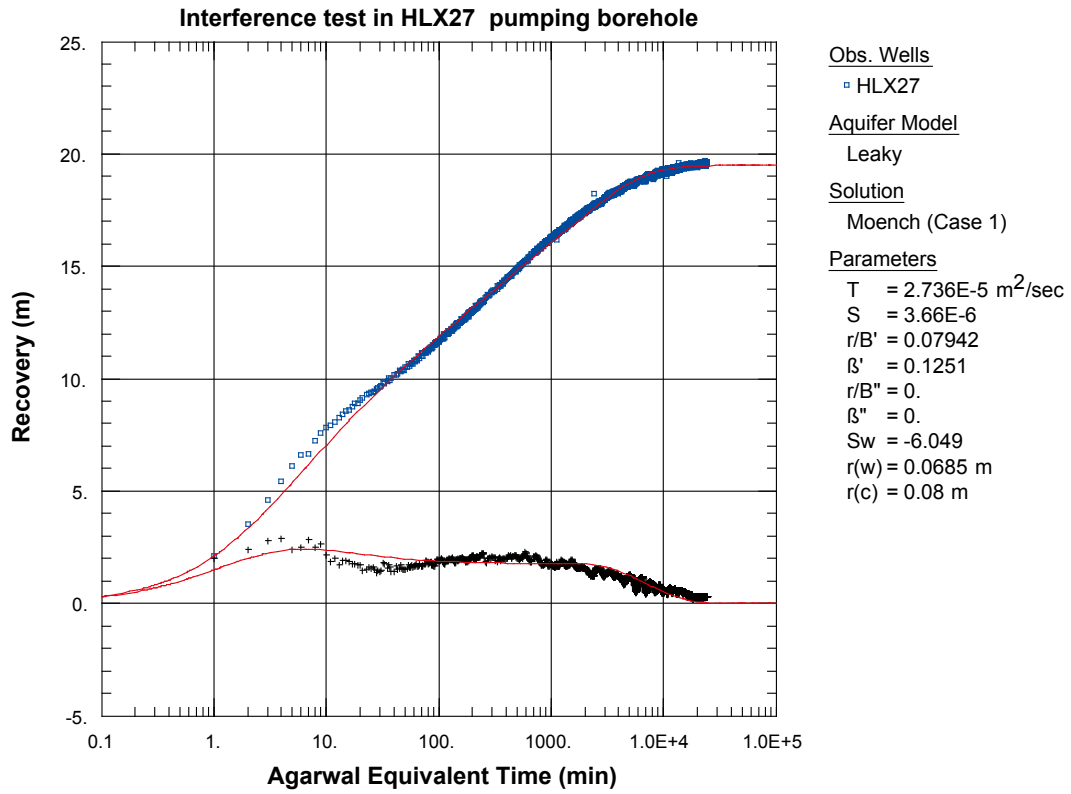

Figure A6-8. *Lin-log plot of recovery (▫) and recovery derivative, ds/d(ln t) (+), versus time in the pumping borehole HLX27 during the interference test in HLX27.*

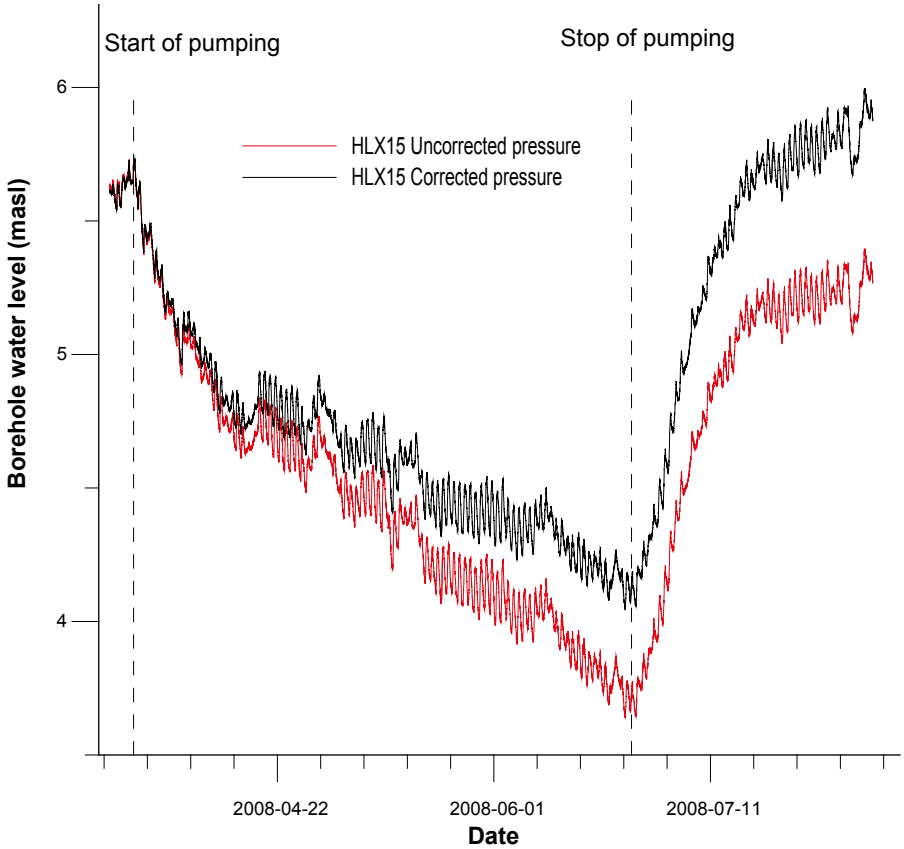

Figure A6-9. *Linear plot of observed pressure and pressure corrected for the naturally decreasing pressure trend versus time in the observation borehole HLX15 during the interference test in HLX27.*

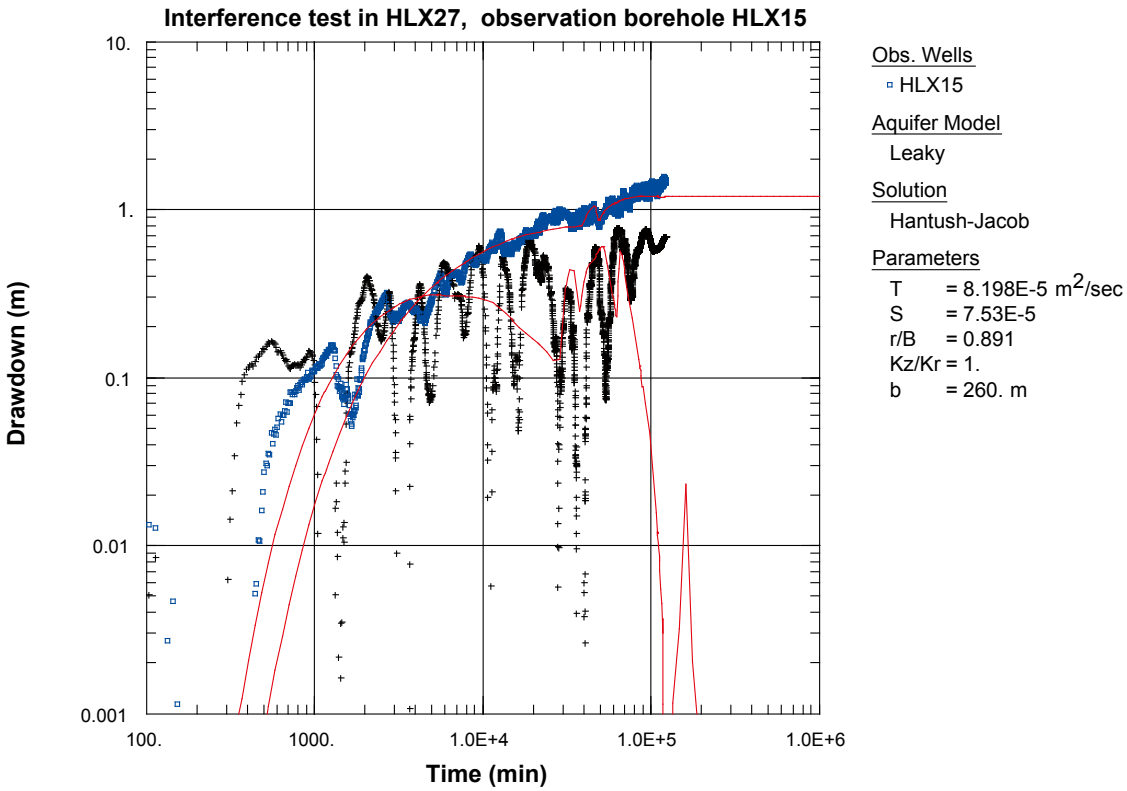

Figure A6-10. *Log-log plot of drawdown (▫) and drawdown derivative, ds/d(ln t) (+), versus time in HLX15 during the interference test in HLX27. Transient evaluation is based on the first part of the drawdown period.*

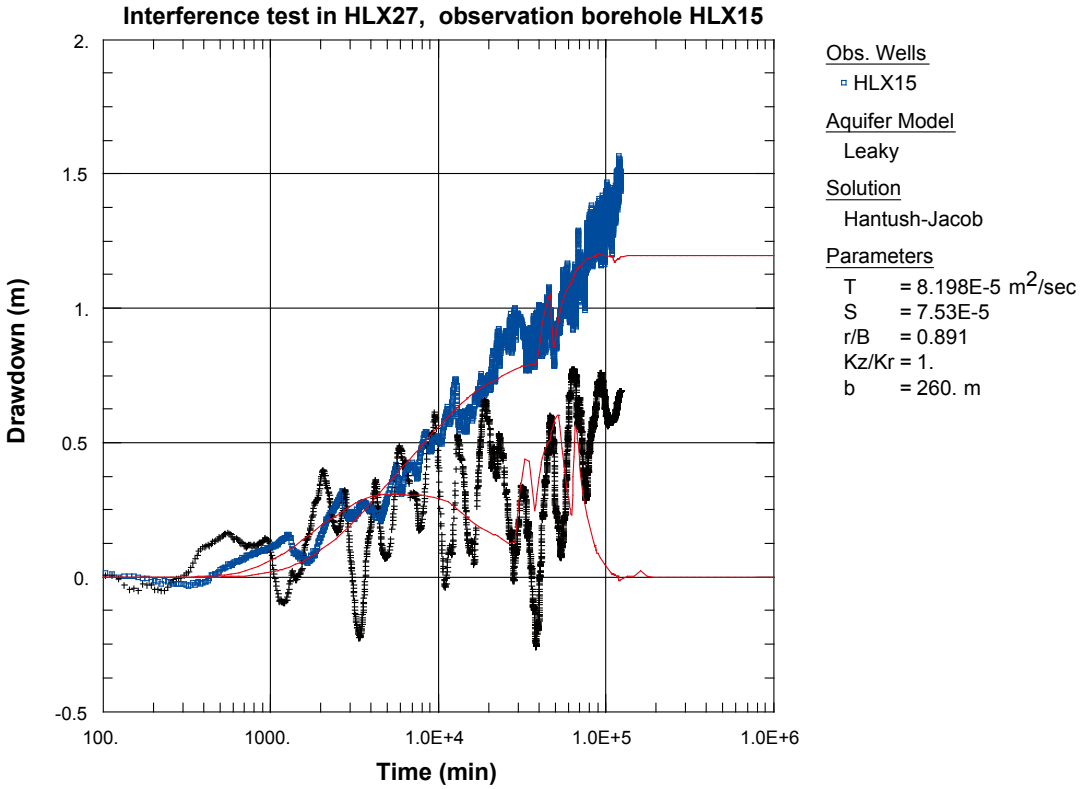

Figure A6-11. *Lin-log plot of drawdown (▫) and drawdown derivative, ds/d(ln t) (+), versus time in HLX15 during the interference test in HLX27. Transient evaluation is based on the first part of the drawdown period.*

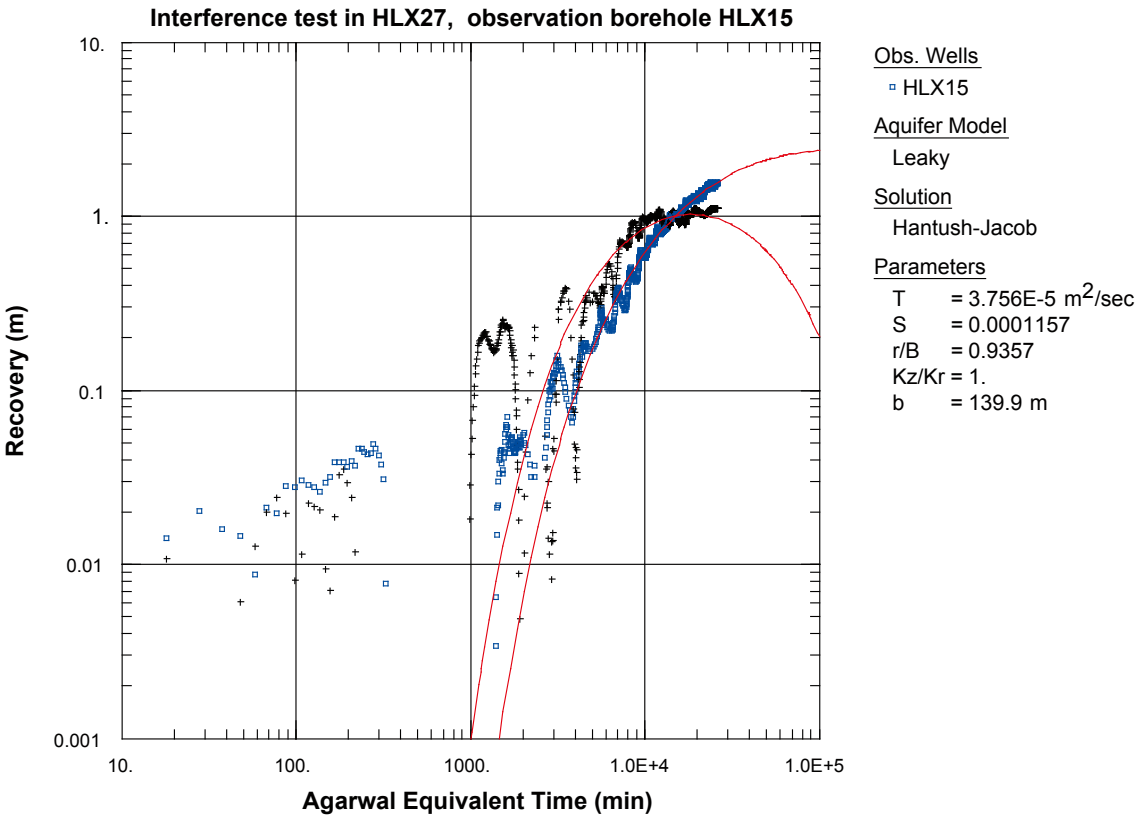

Figure A6-12. *Log-log plot of recovery (▫) and recovery derivative, ds/d(ln t) (+), versus time in HLX15 during the interference test in HLX27.*

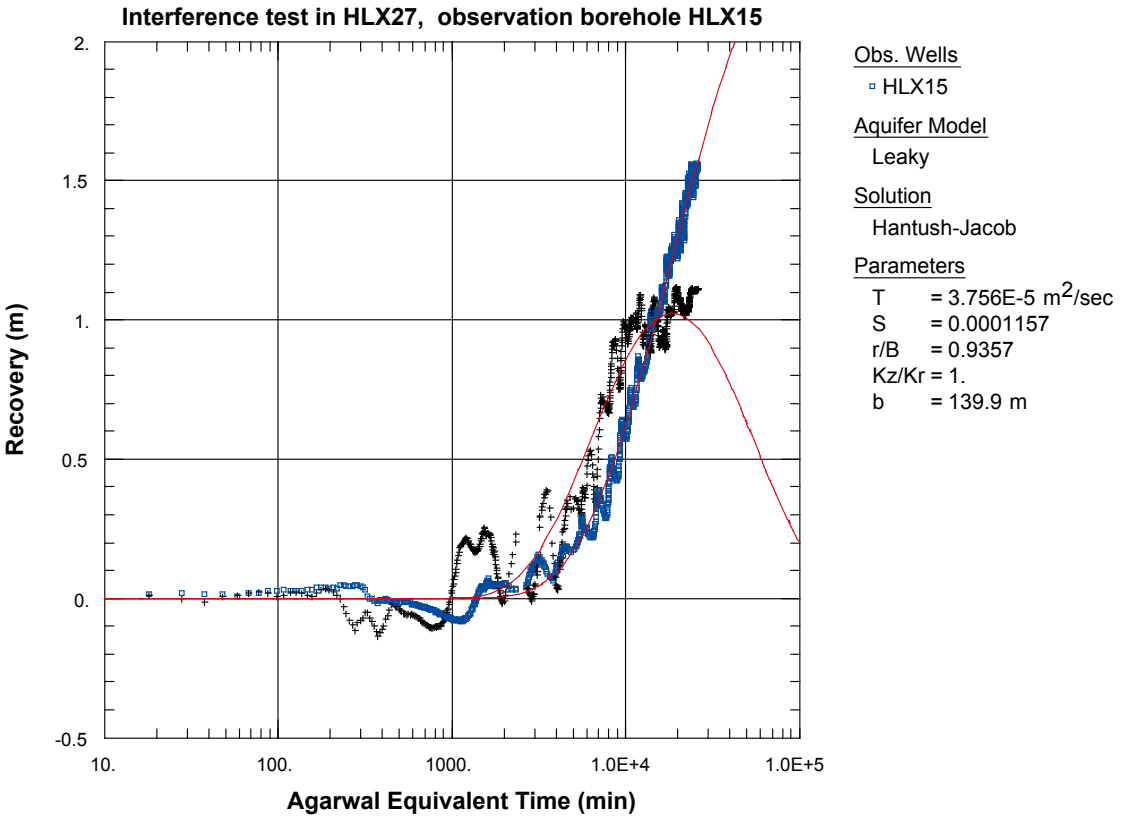

Figure A6-13. *Lin-log plot of recovery (▫) and recovery derivative, ds/d(ln t) (+), versus time in HLX15 during the interference test in HLX27.*

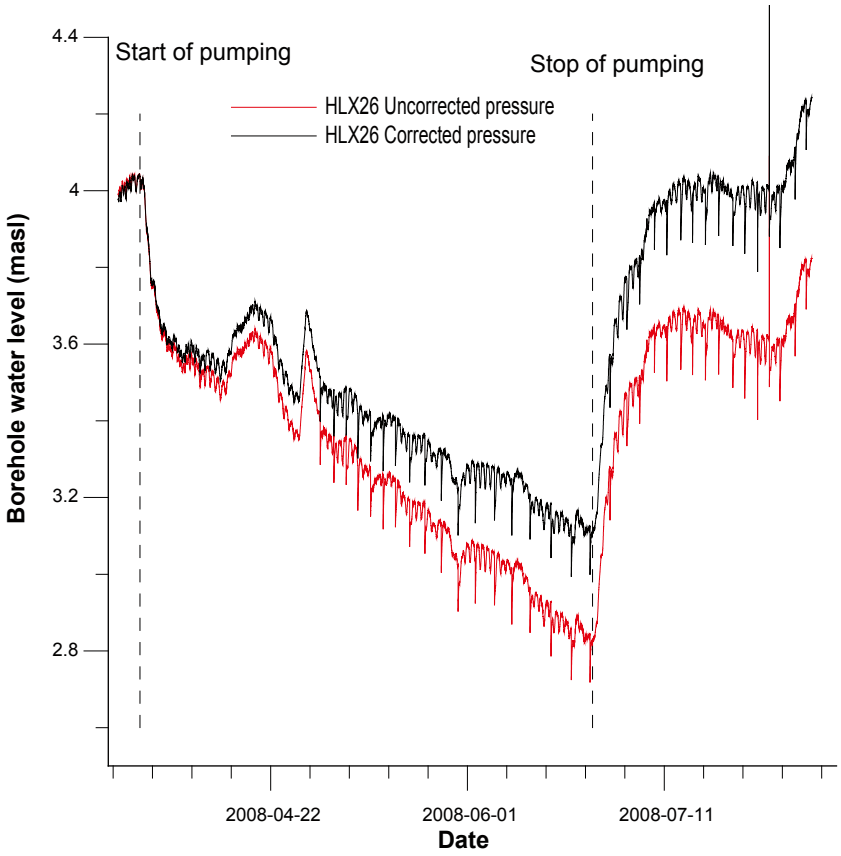

Figure A6-14. *Linear plot of observed pressure and pressure corrected for the naturally decreasing pressure trend versus time in the observation borehole HLX26 during the interference test in HLX27.*

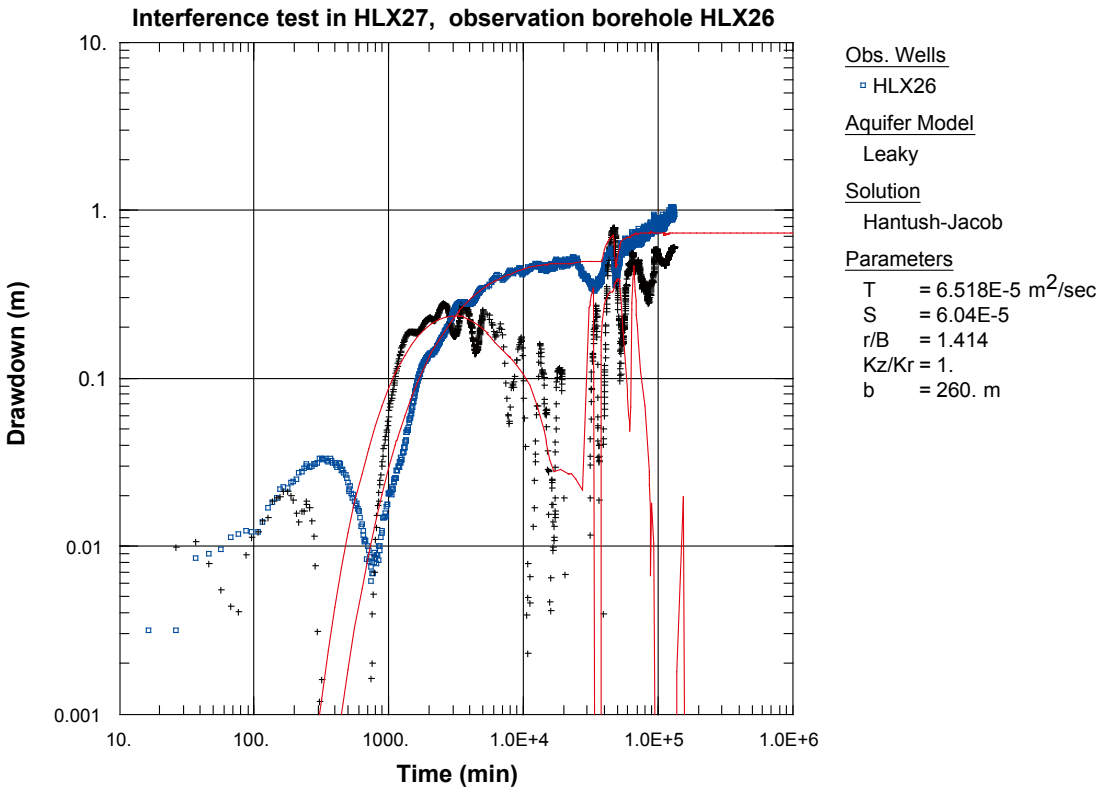

Figure A6-15. *Log-log plot of drawdown (▫) and drawdown derivative, ds/d(ln t) (+), versus time in HLX26 during the interference test in HLX27. Transient evaluation is based on the first part of the drawdown period.*

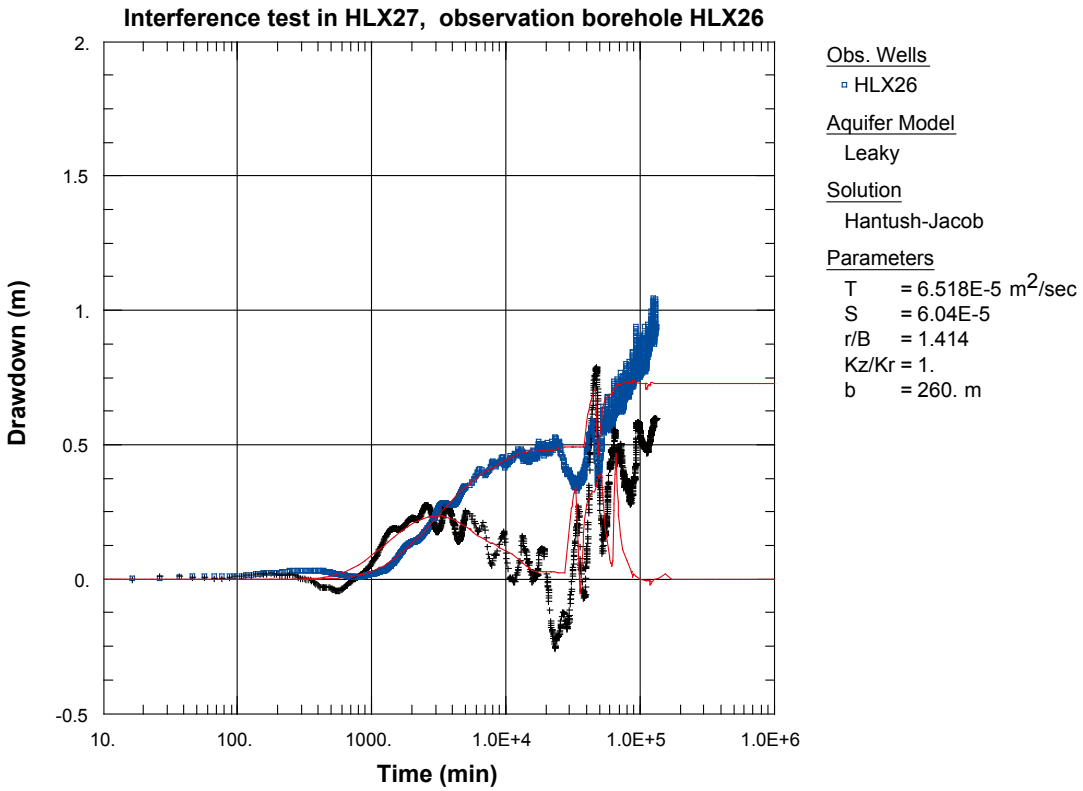

Figure A6-16. *Lin-log plot of drawdown (▫) and drawdown derivative, ds/d(ln t) (+), versus time in HLX26 during the interference test in HLX27. Transient evaluation is based on the first part of the drawdown period.*

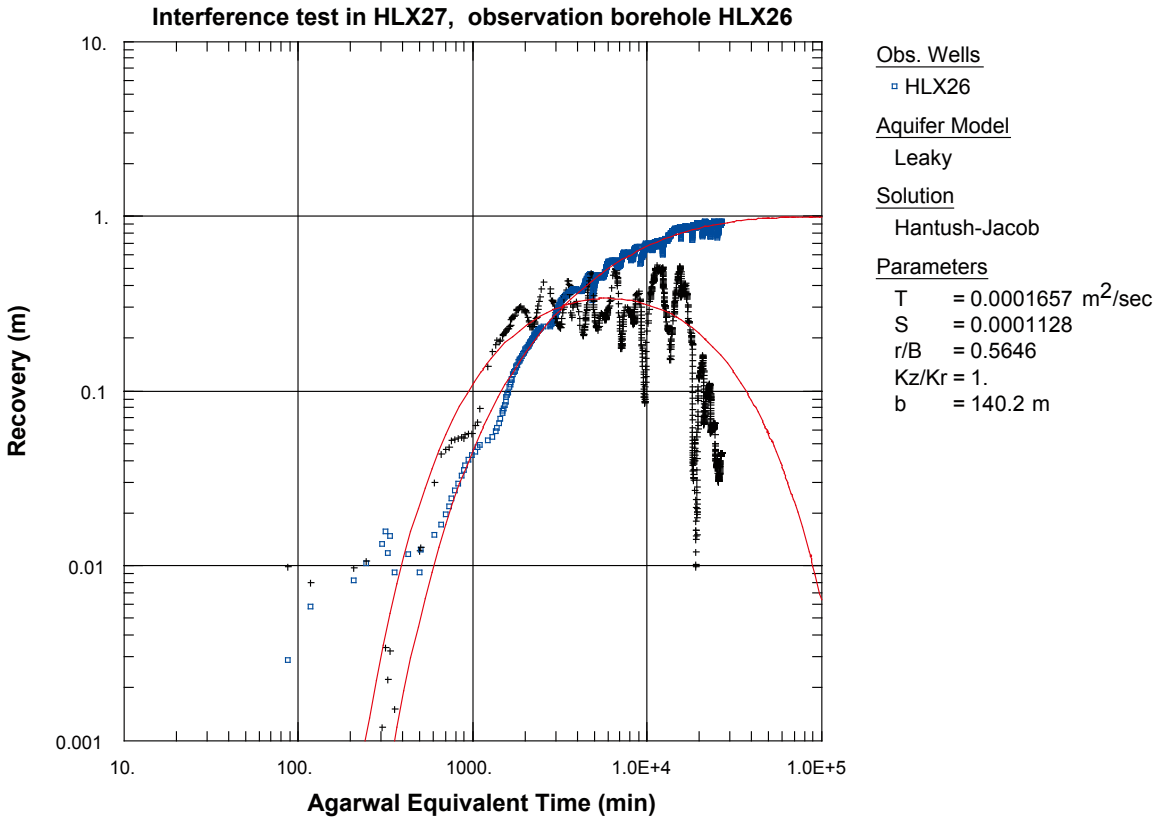

Figure A6-17. *Log-log plot of recovery (▫) and recovery derivative, ds/d(ln t) (+), versus time in HLX26 during the interference test in HLX27.*

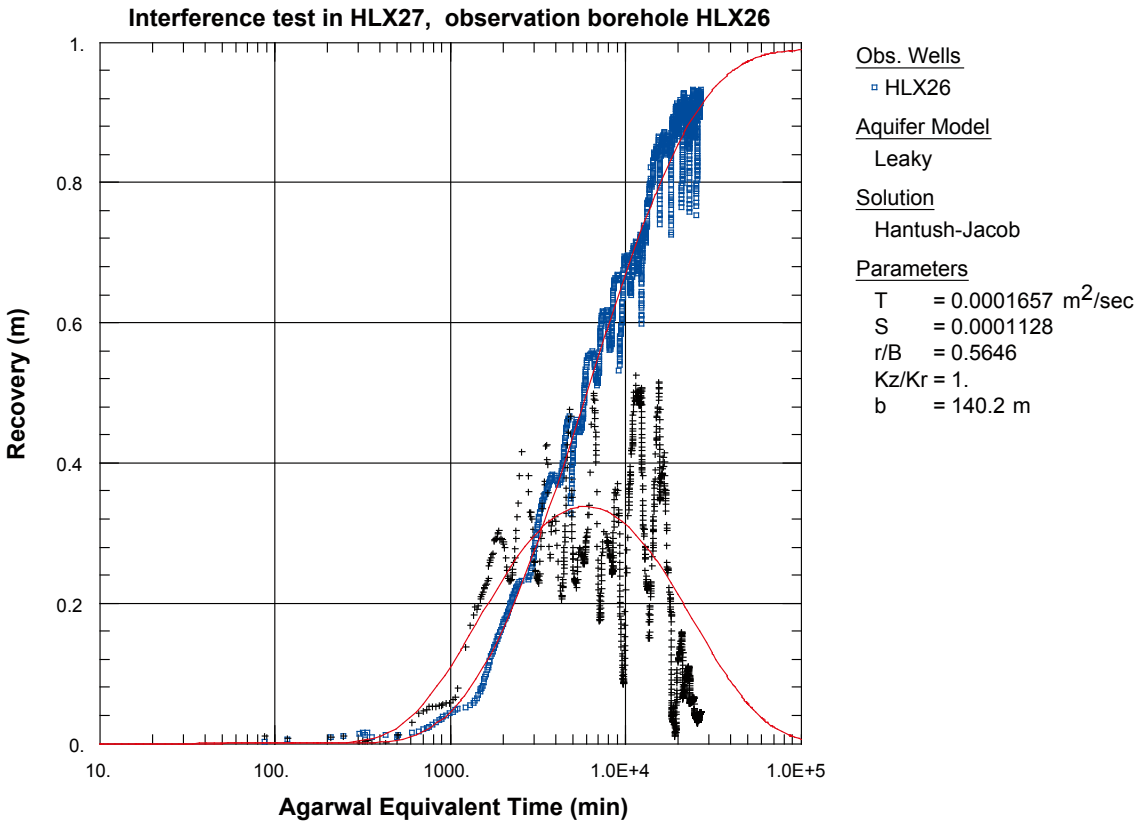

Figure A6-18. *Lin-log plot of recovery (▫) and recovery derivative, ds/d(ln t) (+), versus time in HLX26 during the interference test in HLX27.*

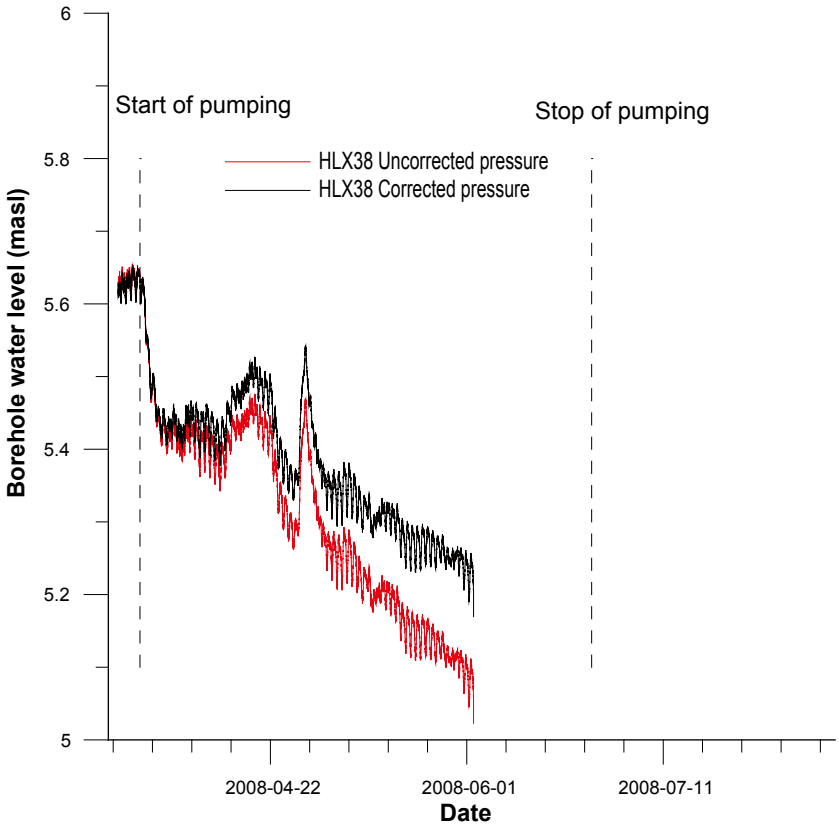

Figure A6-19. *Linear plot of observed pressure and pressure corrected for the naturally decreasing pressure trend versus time in the observation borehole HLX38 during the interference test in HLX27.*

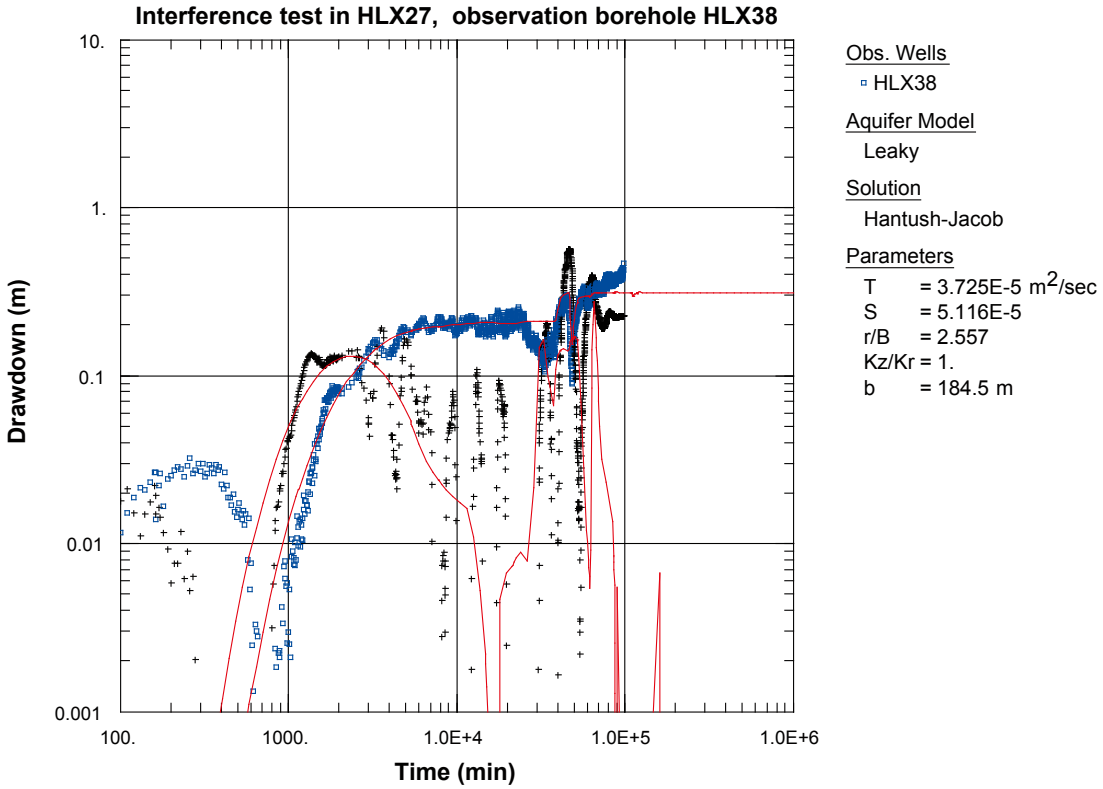

Figure A6-20. *Log-log plot of drawdown (▫) and drawdown derivative, ds/d(ln t) (+), versus time in HLX38 during the interference test in HLX27. Transient evaluation is based on the first part of the drawdown period.*

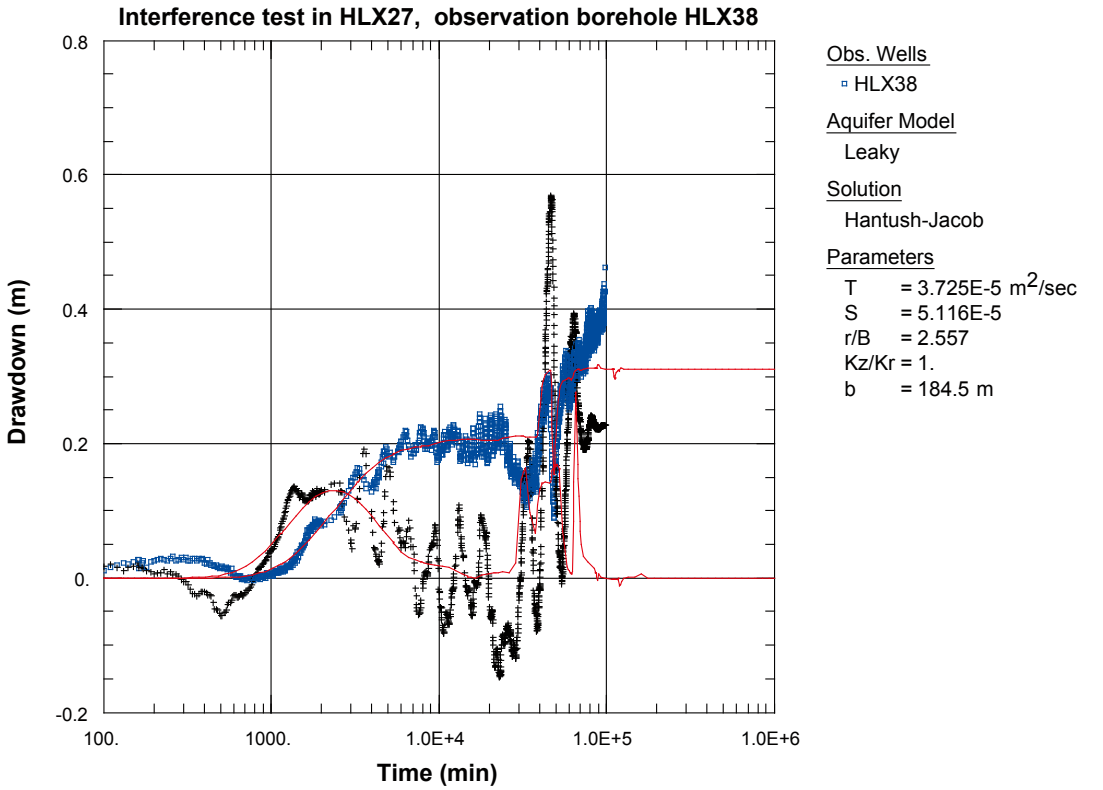

Figure A6-21. *Lin-log plot of drawdown (▫) and drawdown derivative, ds/d(ln t) (+), versus time in HLX38 during the interference test in HLX27. Transient evaluation is based on the first part of the drawdown period.*

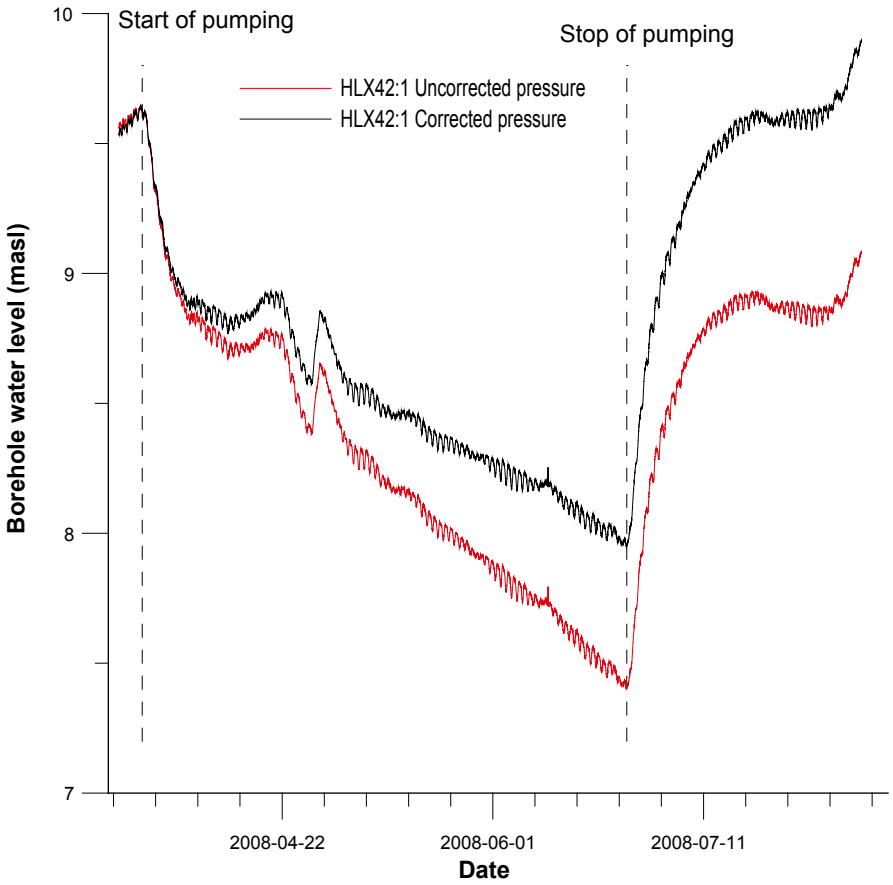

Figure A6-22. *Linear plot of observed pressure and pressure corrected for the naturally decreasing pressure trend versus time in the observation borehole HLX42:1 during the interference test in HLX27.*

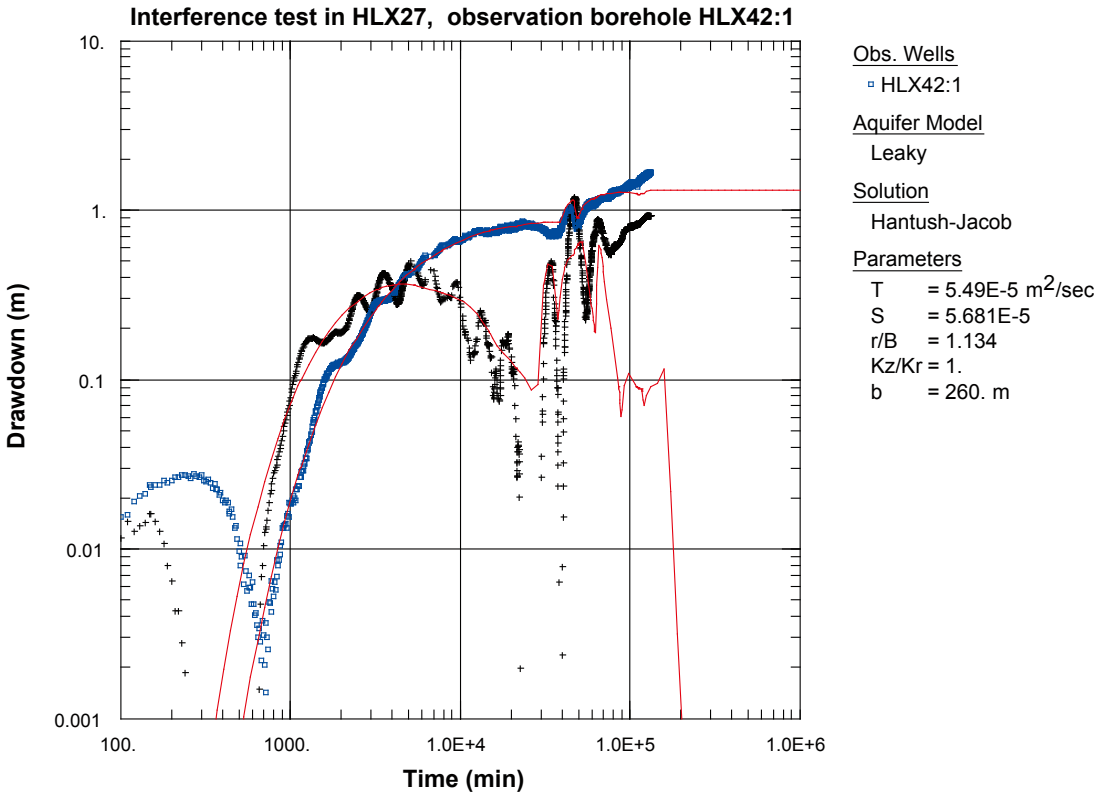

Figure A6-23. *Log-log plot of drawdown (▫) and drawdown derivative, ds/d(ln t) (+), versus time in HLX42:1 during the interference test in HLX27. Transient evaluation is based on the first part of the flow period.*

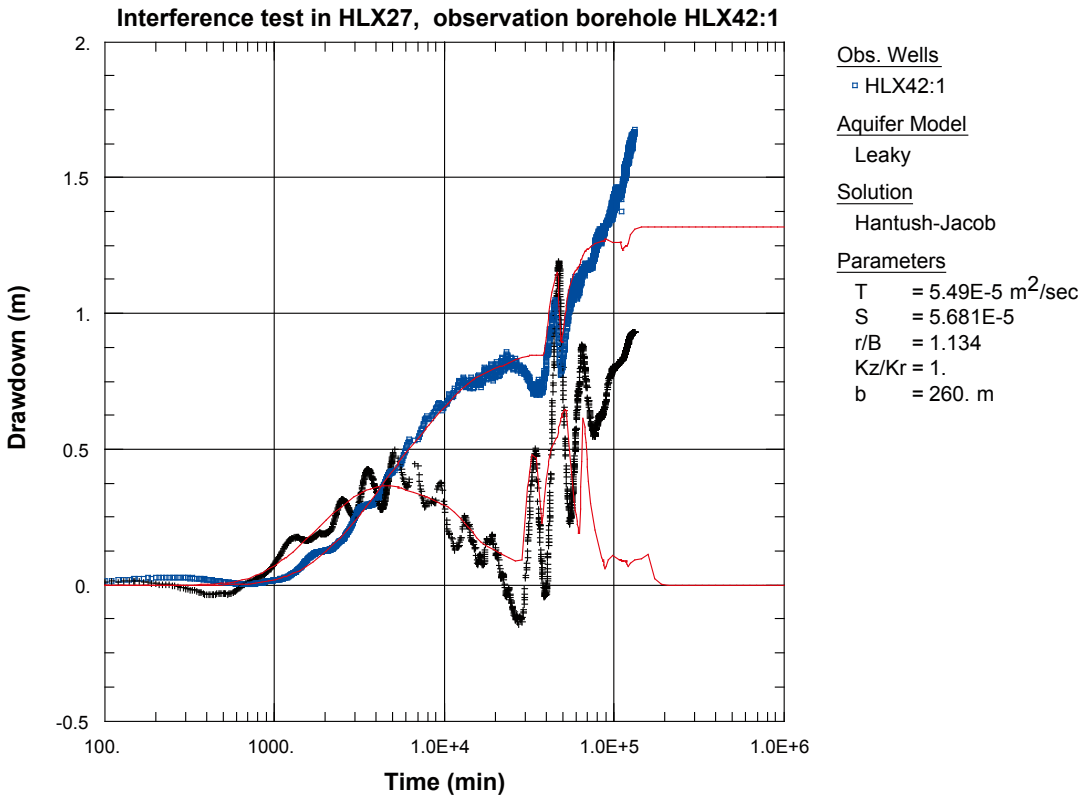

Figure A6-24. *Lin-log plot of drawdown (▫) and drawdown derivative, ds/d(ln t) (+), versus time in HLX42:1 during the interference test in HLX27. Transient evaluation is based on the first part of the flow period.*

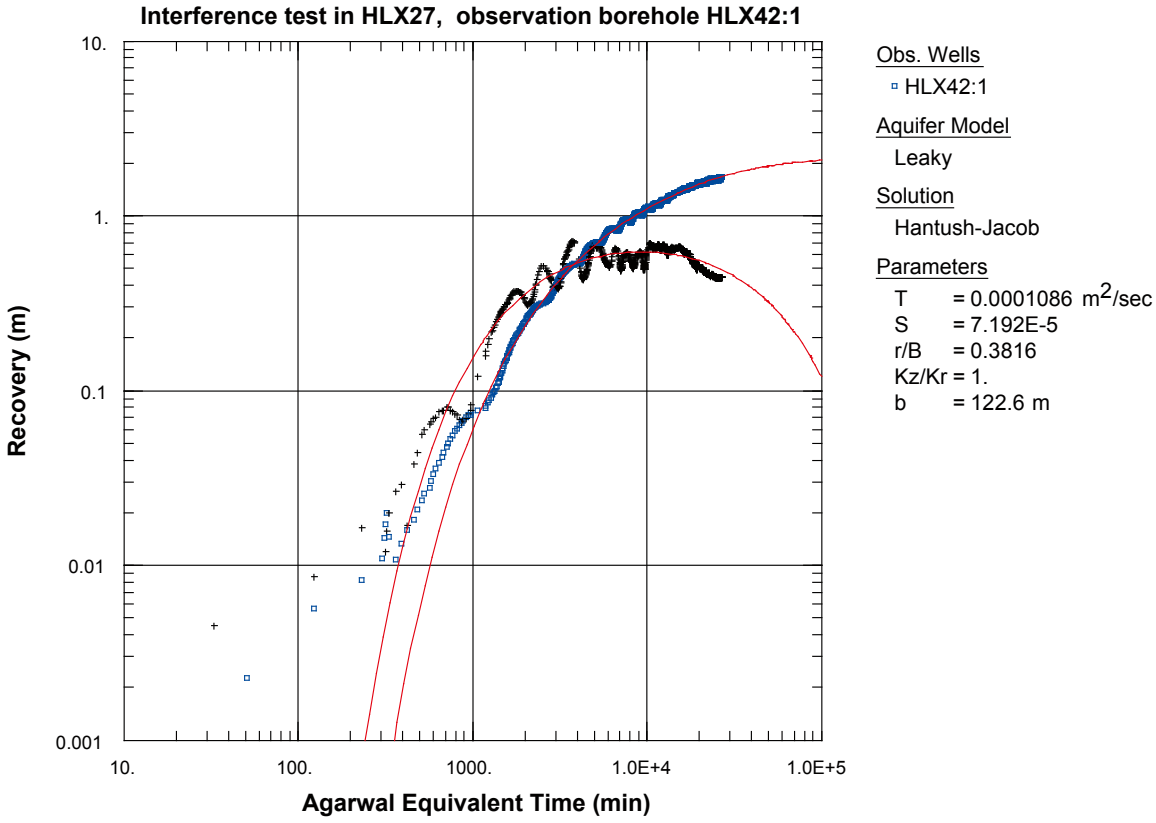

Figure A6-25. *Log-log plot of recovery (▫) and recovery derivative, ds/d(ln t) (+), versus time in HLX42:1 during the interference test in HLX27.*

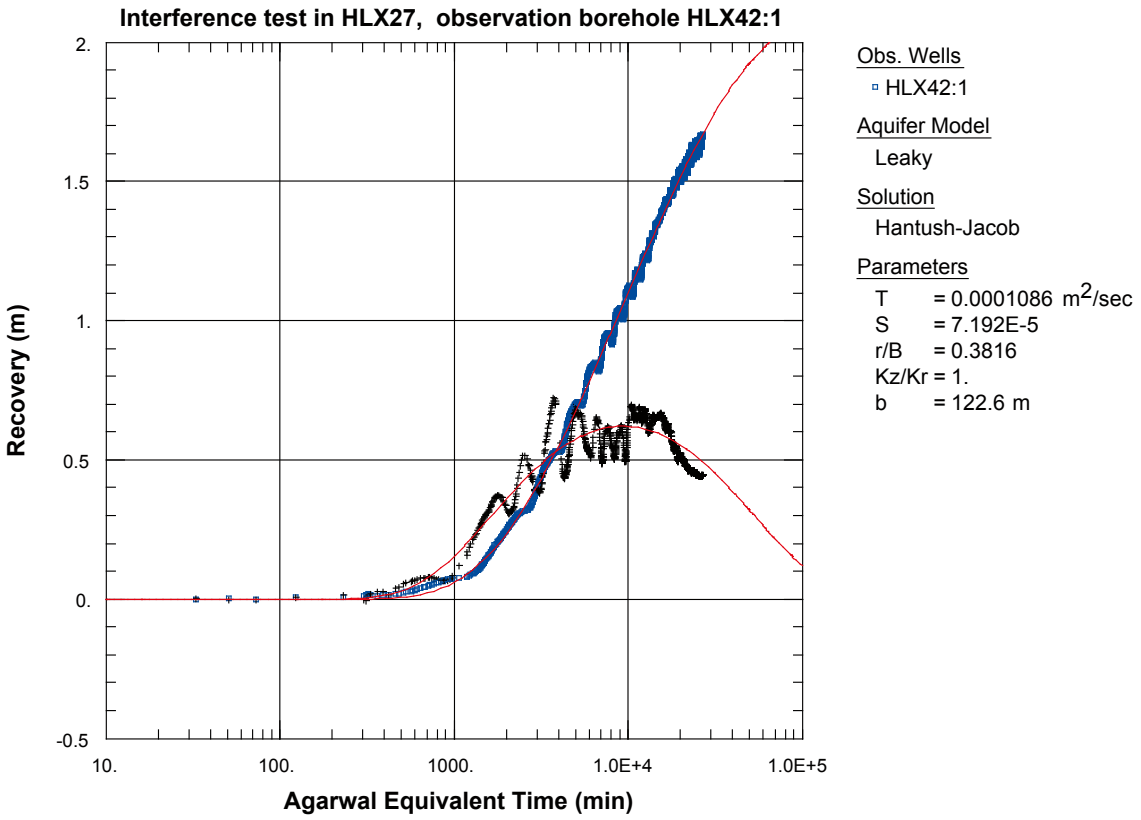

Figure A6-26. *Lin-log plot of recovery (▫) and recovery derivative, ds/d(ln t) (+), versus time in HLX42:1 during the interference test in HLX27.*

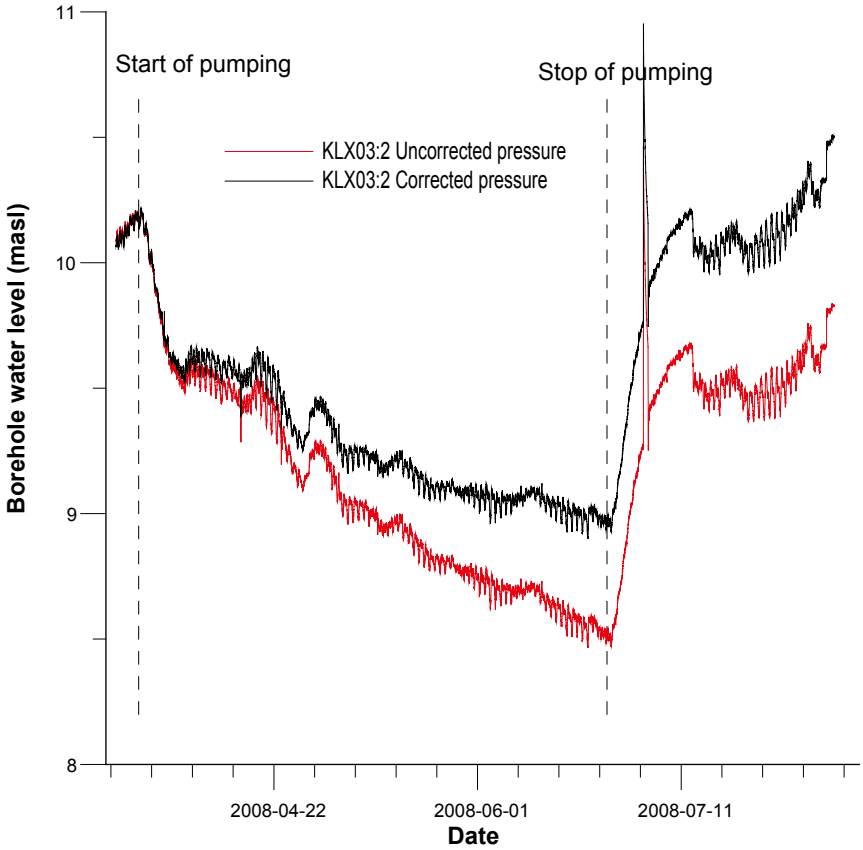

Figure A6-27. *Linear plot of observed pressure and pressure corrected for the naturally decreasing pressure trend versus time in the observation borehole KLX03:2 during the interference test in HLX27.*

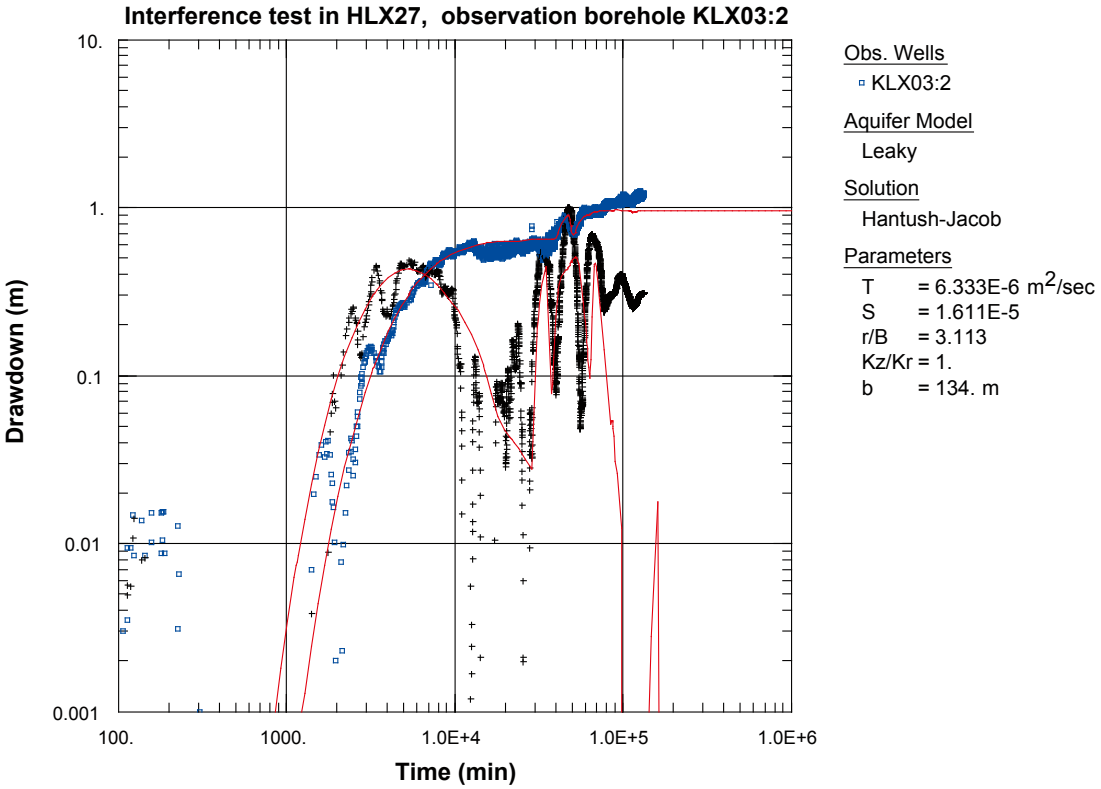

Figure A6-28. *Log-log plot of drawdown (▫) and drawdown derivative, ds/d(ln t) (+), versus time in KLX03:2 during the interference test in HLX27. The transient evaluation is based on the first part of the drawdown period.*

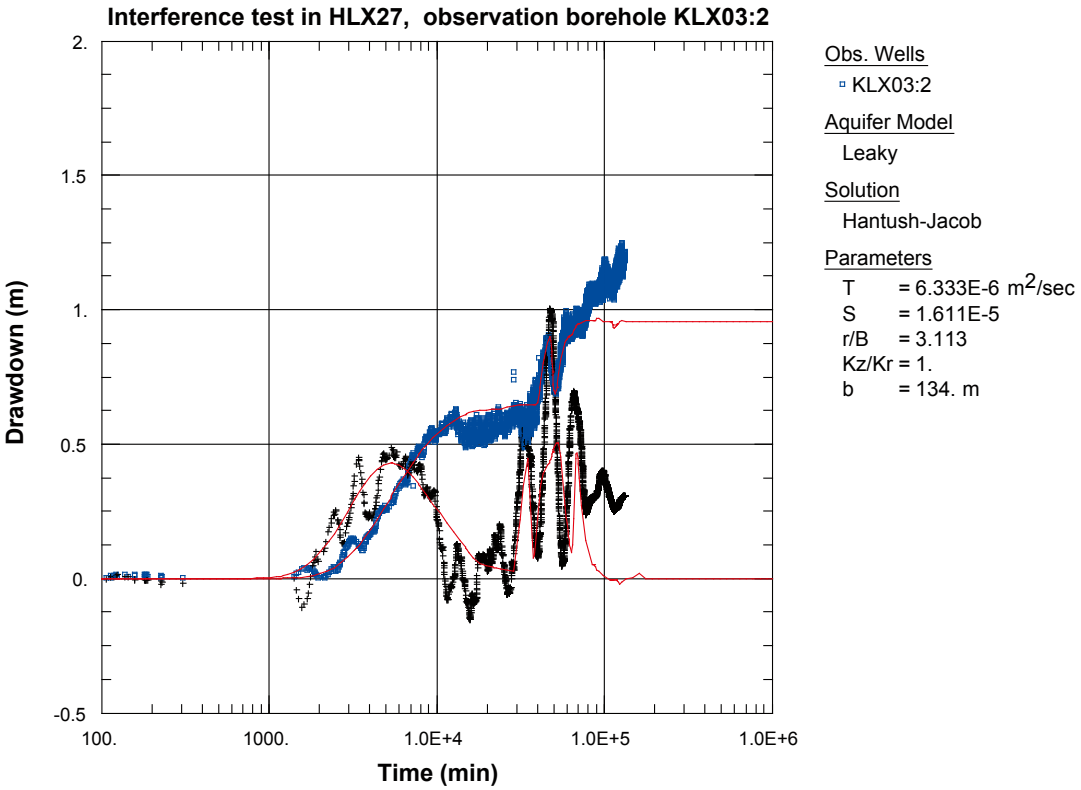

Figure A6-29. *Lin-log plot of drawdown (▫) and drawdown derivative, ds/d(ln t) (+), versus time in KLX03:2 during the interference test in HLX27. The transient evaluation is based on the first part of the flow period.*

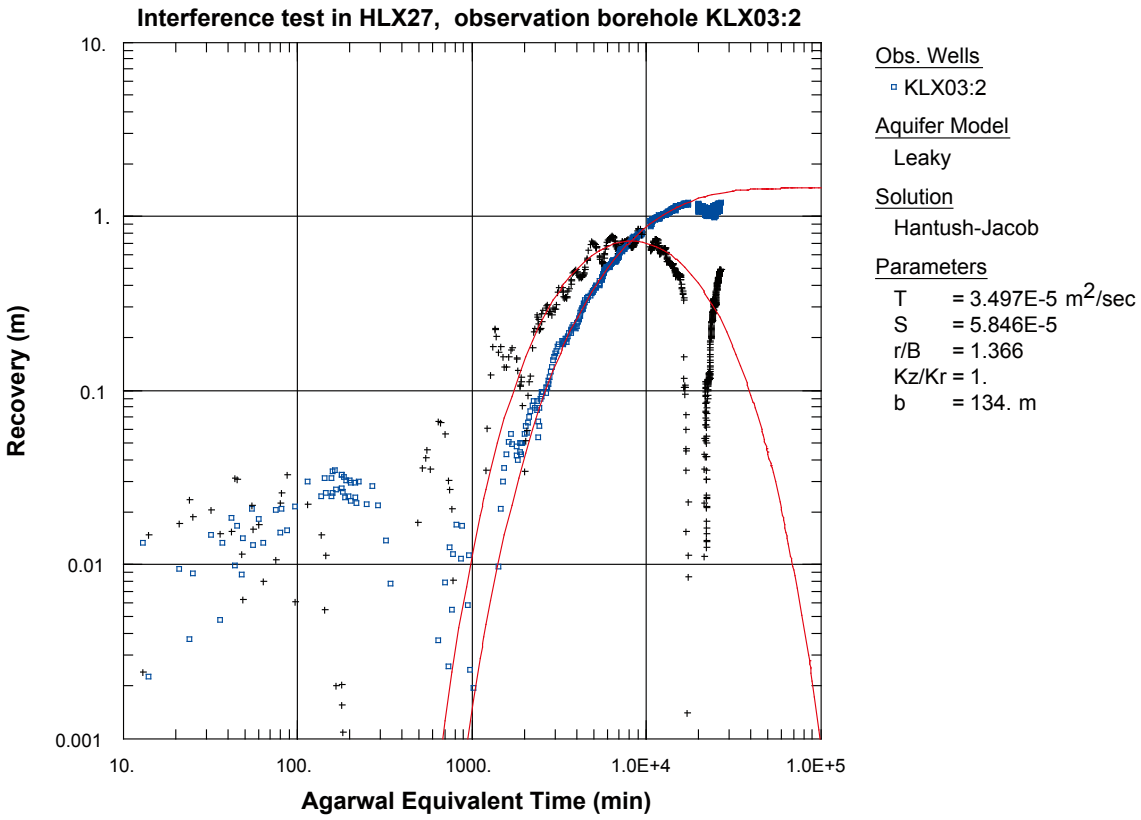

Figure A6-30. *Log-log plot of recovery (▫) and recovery derivative, ds/d(ln t) (+), versus time in KLX03:2 during the interference test in HLX27.*

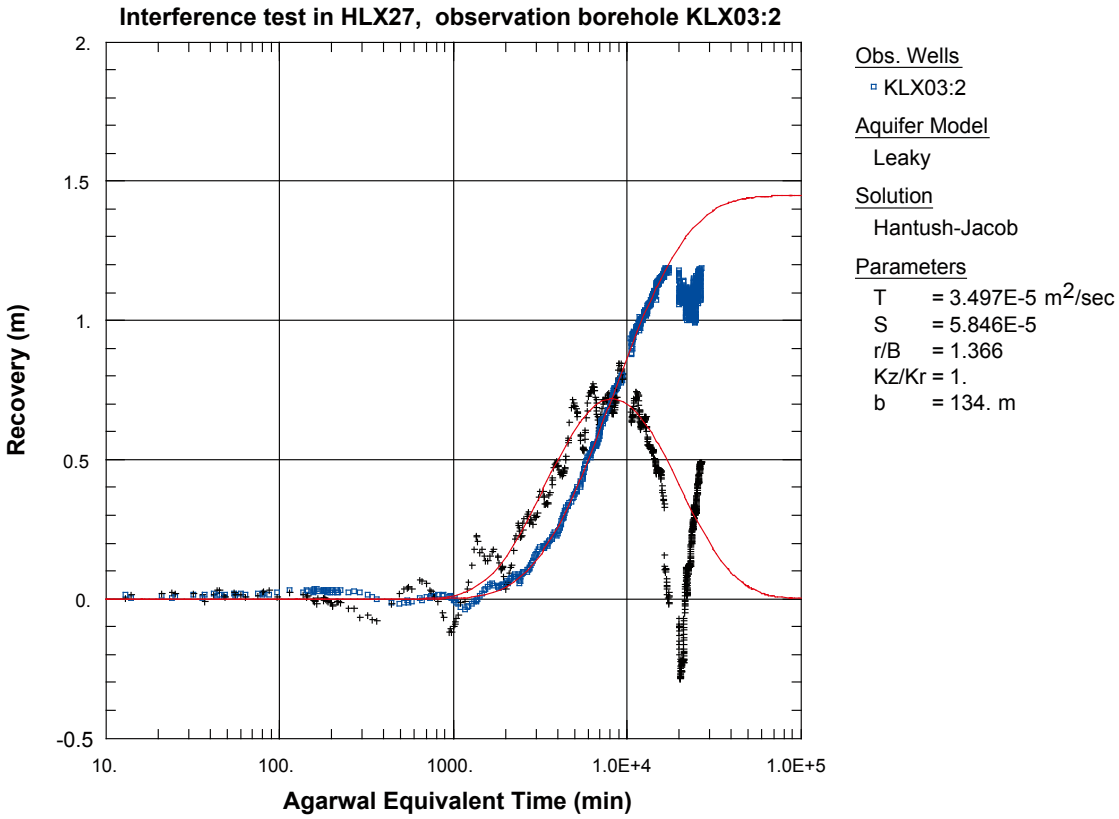

Figure A6-31. *Lin-log plot of recovery (▫) and recovery derivative, ds/d(ln t) (+), versus time in KLX03:2 during the interference test in HLX27.*

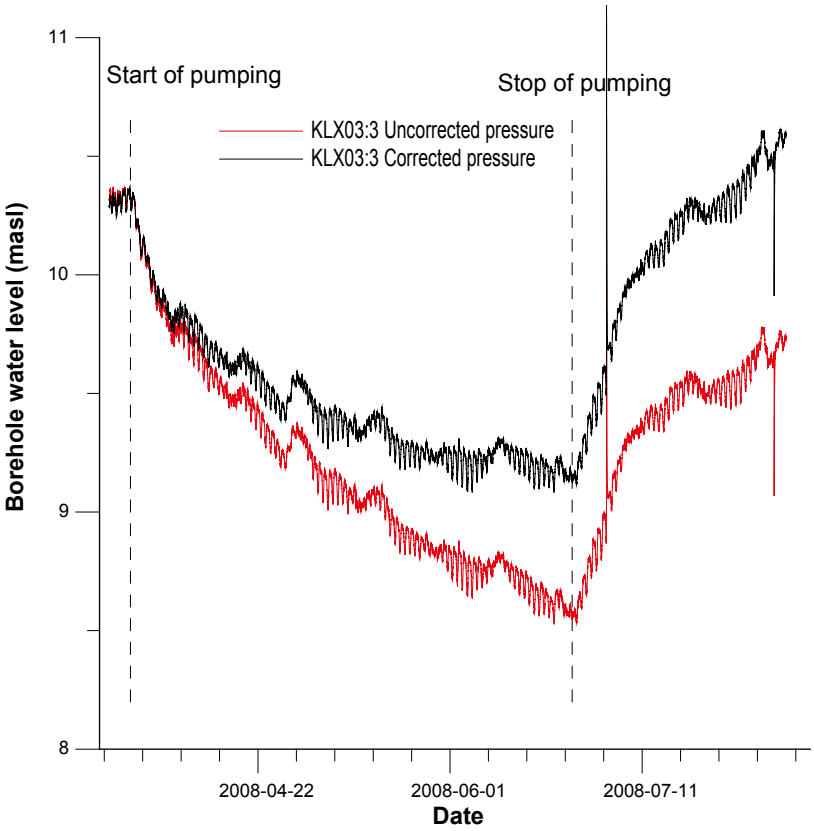

Figure A6-32. *Linear plot of pressure and pressure corrected for the natural decreasing pressure trend versus time in the observation section KLX03:3 during pumping in HLX27.*

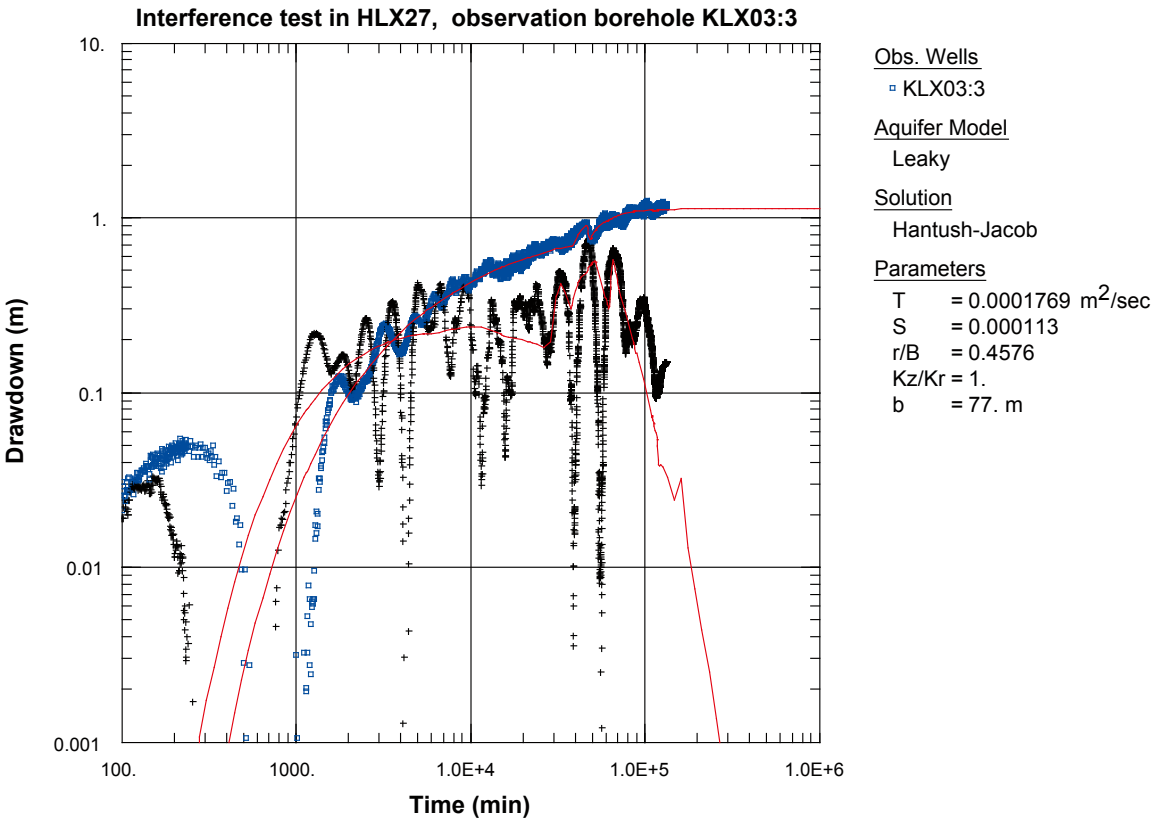

Figure A6-33. *Log-log plot of drawdown (▫) and drawdown derivative, ds/d(ln t) (+), versus time in KLX03:3 during the interference test in HLX27.*

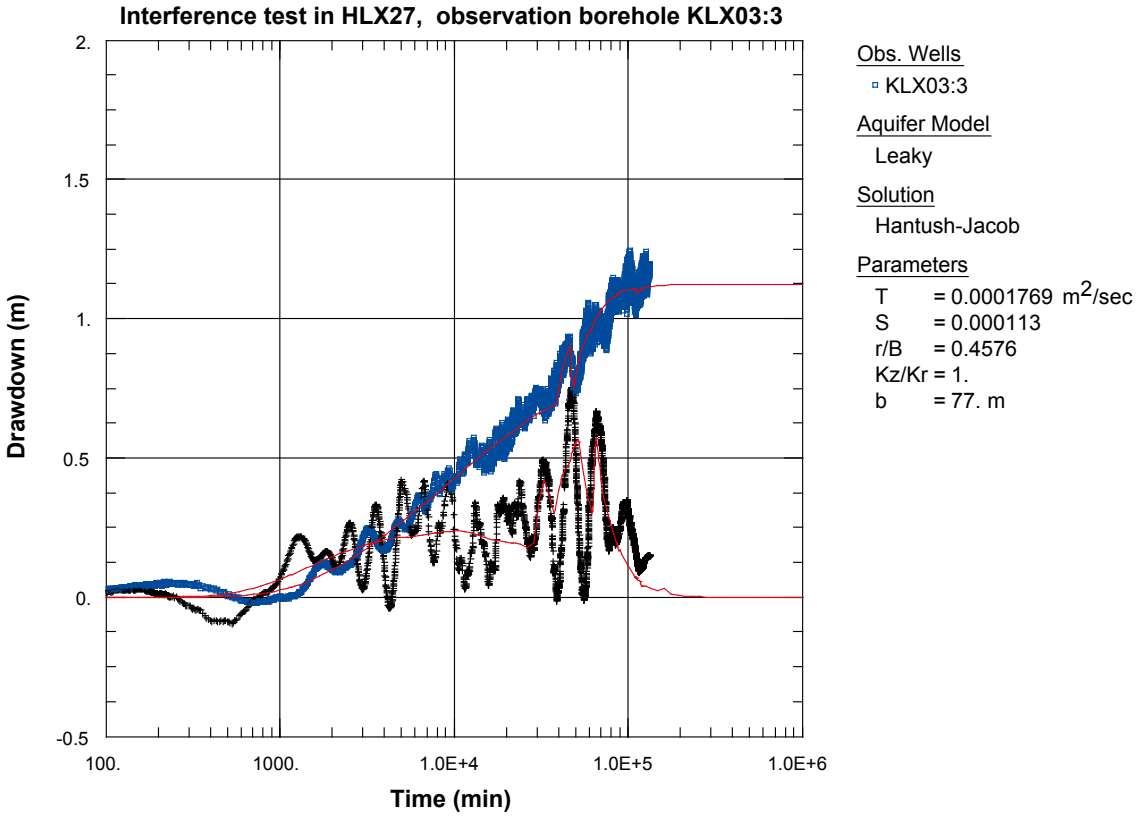

Figure A6-34. *Lin-log plot of drawdown (▫) and drawdown derivative, ds/d(ln t) (+), versus time in KLX03:3 during the interference test in HLX27.*

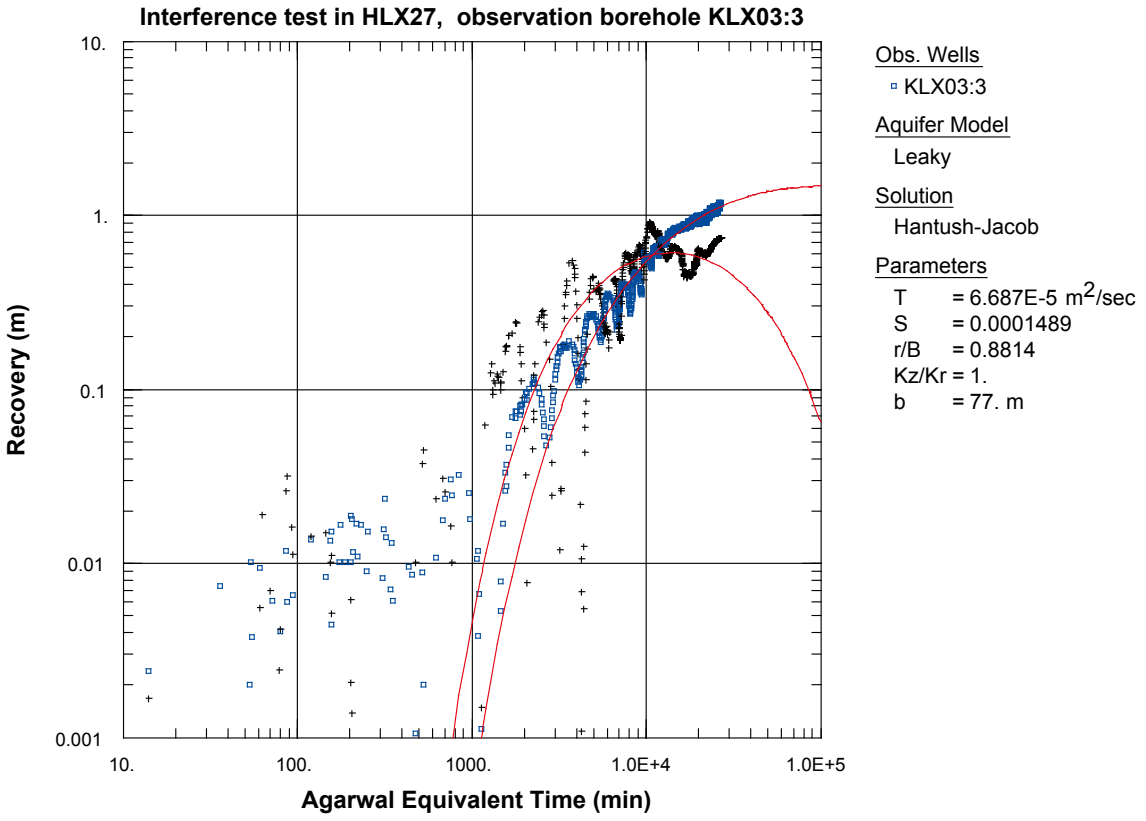

Figure A6-35. *Log-log plot of recovery (▫) and recovery derivative, ds/d(ln t) (+), versus time in KLX03:3 during the interference test in HLX27.*

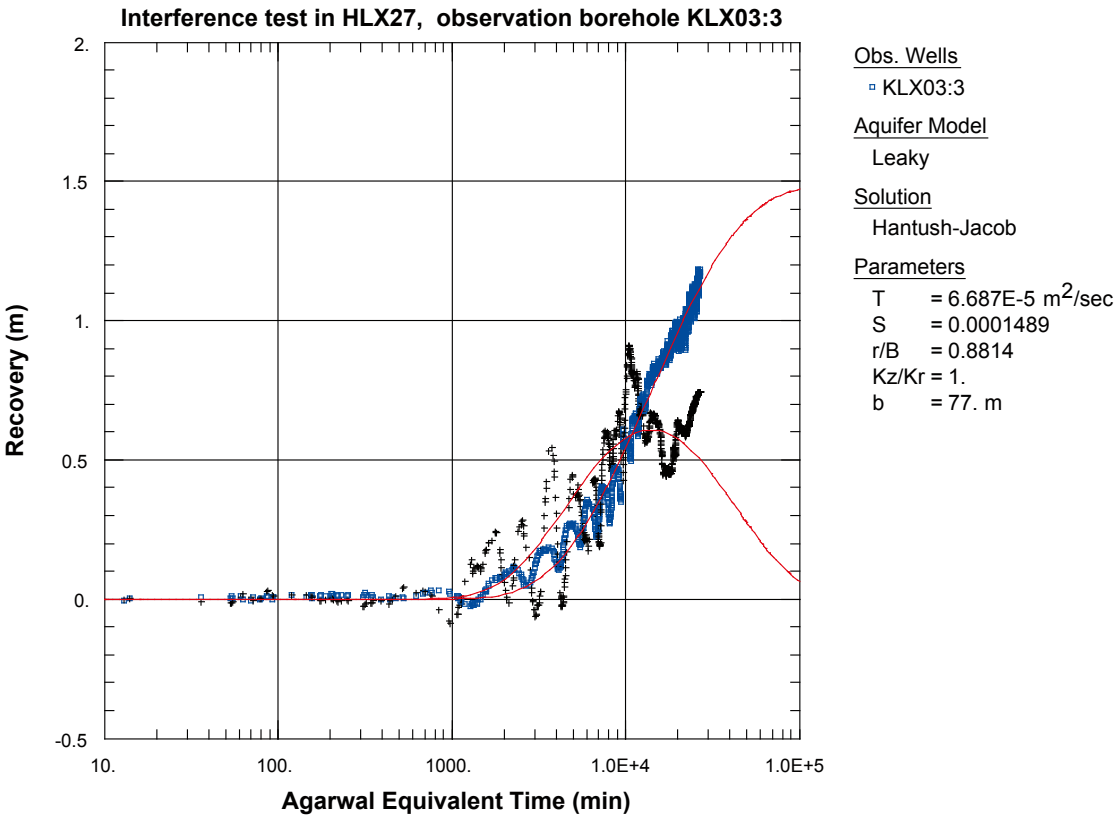

Figure A6-36. *Lin-log plot of recovery (▫) and recovery derivative, ds/d(ln t) (+), versus time in KLX03:3 during the interference test in HLX27.*

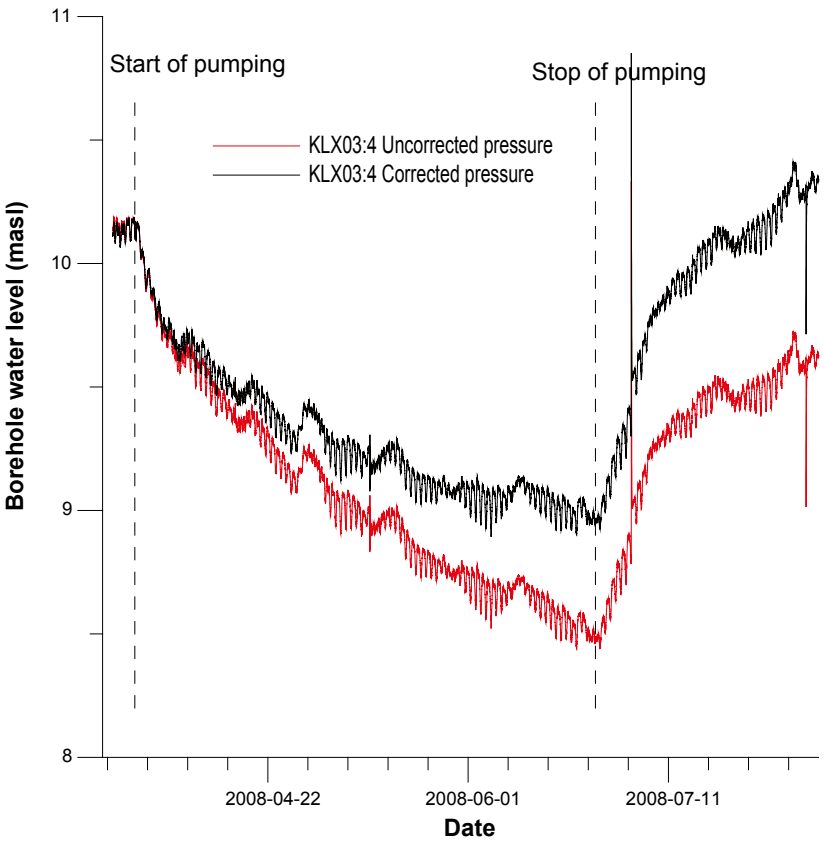

Figure A6-37. *Linear plot of pressure and pressure corrected for the natural decreasing pressure trend versus time in the observation section KLX03:4 during pumping in HLX27.*

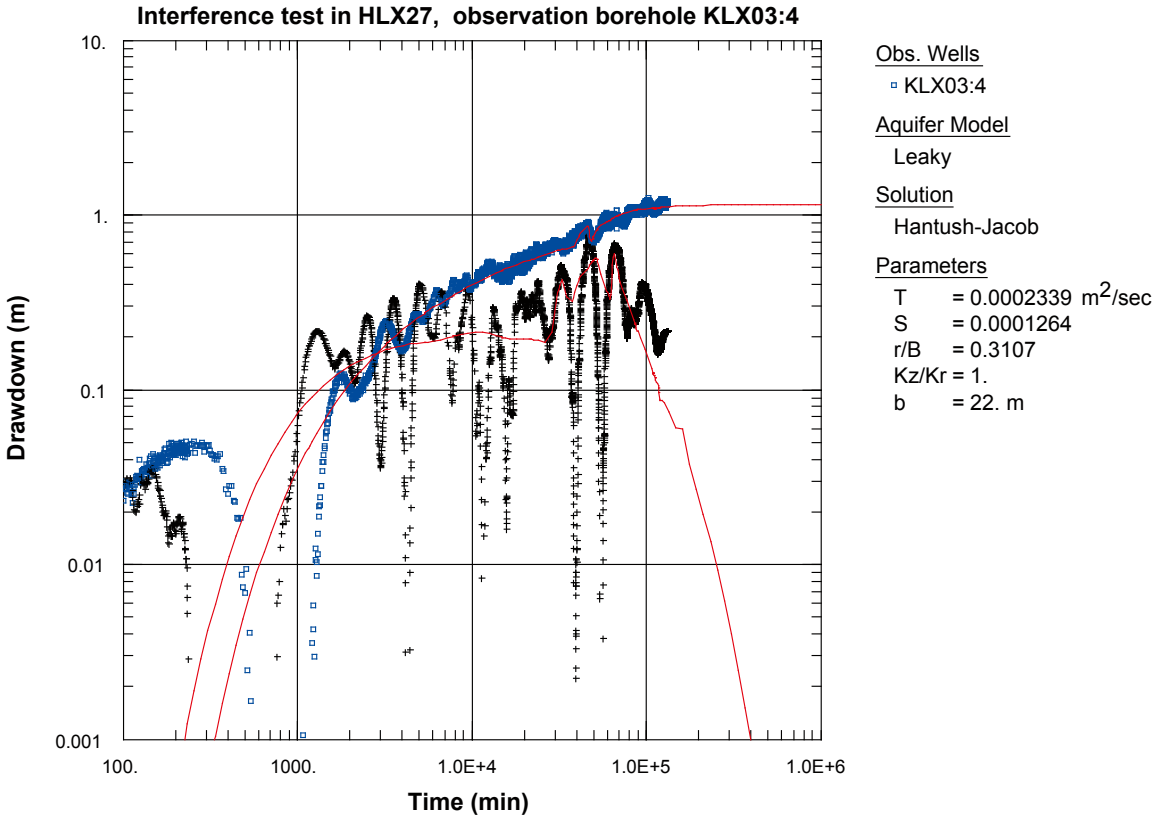

Figure A6-38. *Log-log plot of drawdown (▫) and drawdown derivative, ds/d(ln t) (+), versus time in KLX03:4 during the interference test in HLX27.*

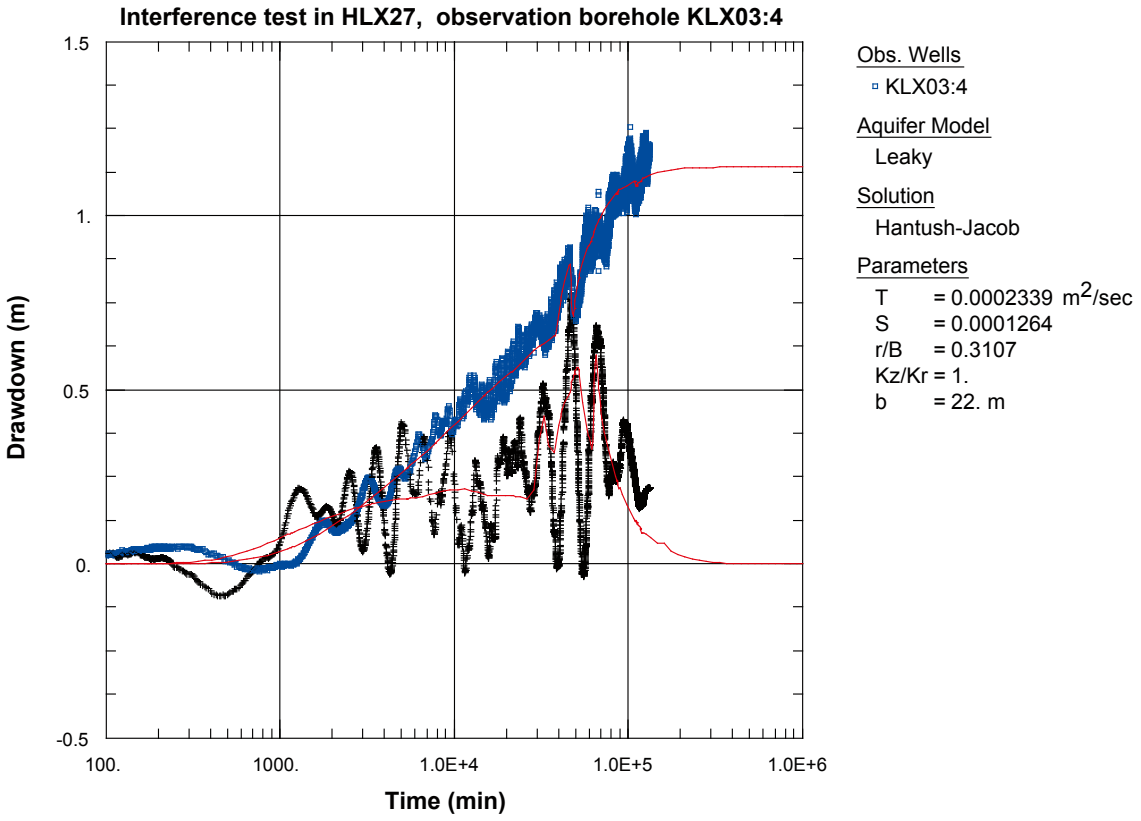

Figure A6-39. *Lin-log plot of drawdown (▫) and drawdown derivative, ds/d(ln t) (+), versus time in KLX03:4 during the interference test in HLX27.*

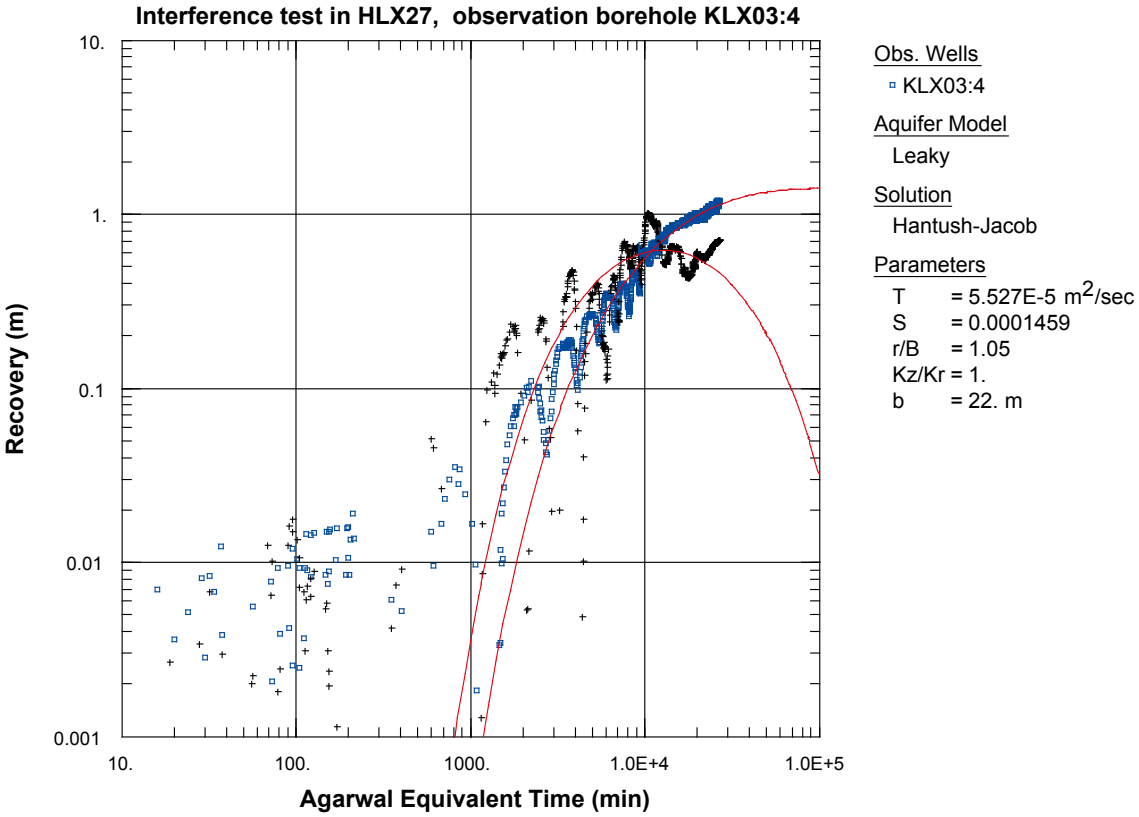

Figure A6-40. *Log-log plot of recovery (▫) and recovery derivative, ds/d(ln t) (+), versus time in KLX03:4 during the interference test in HLX27.*

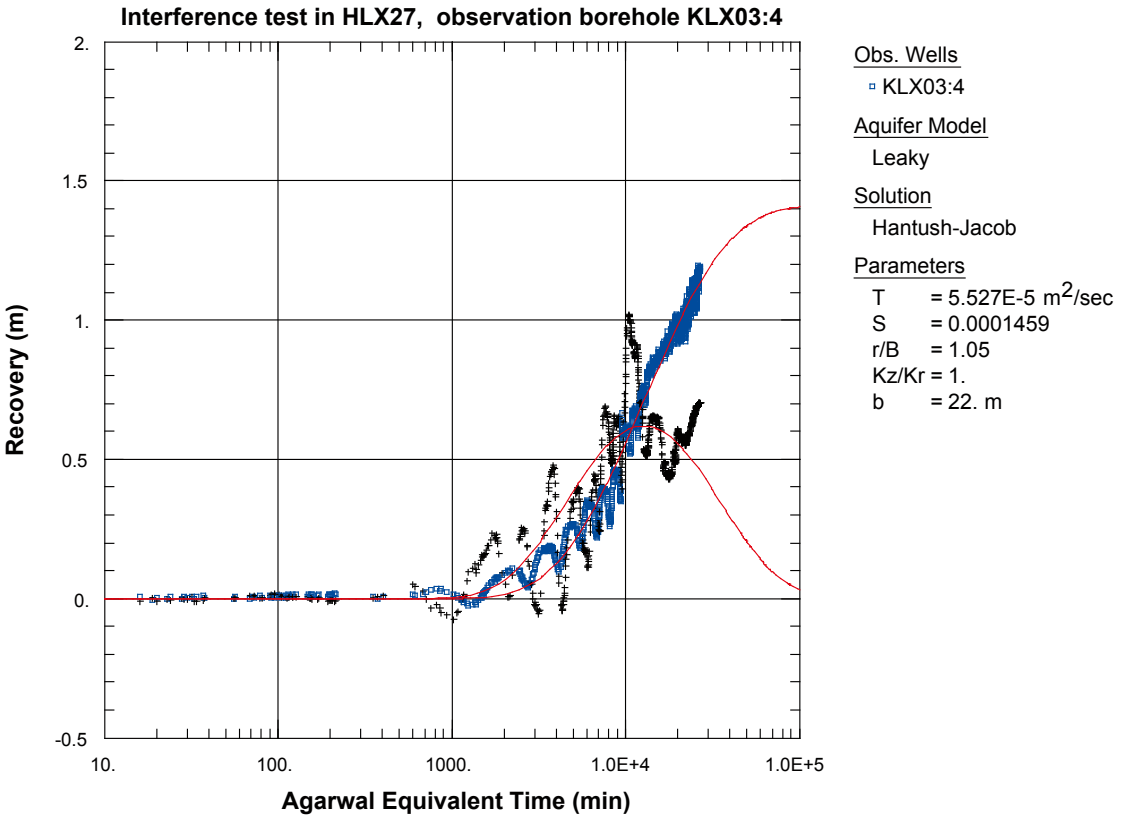

Figure A6-41. *Lin-log plot of recovery (▫) and recovery derivative, ds/d(ln t) (+), versus time in KLX03:4 during the interference test in HLX27.*

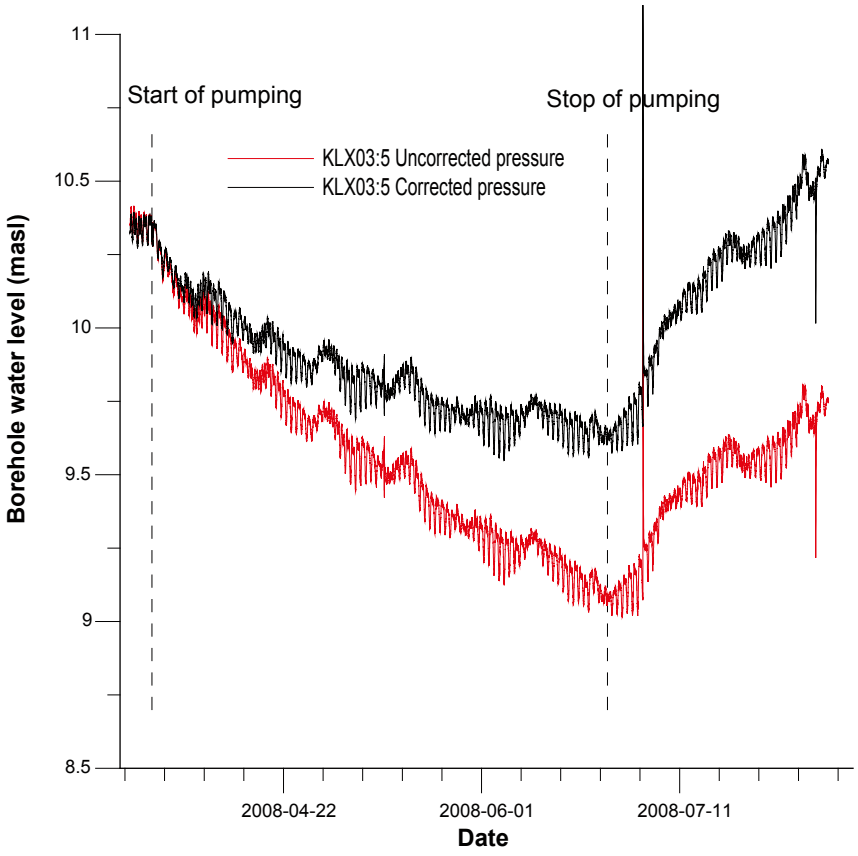

Figure A6-42. *Linear plot of pressure versus time in the observation sections in KLX03:5 during pumping in HLX27.*

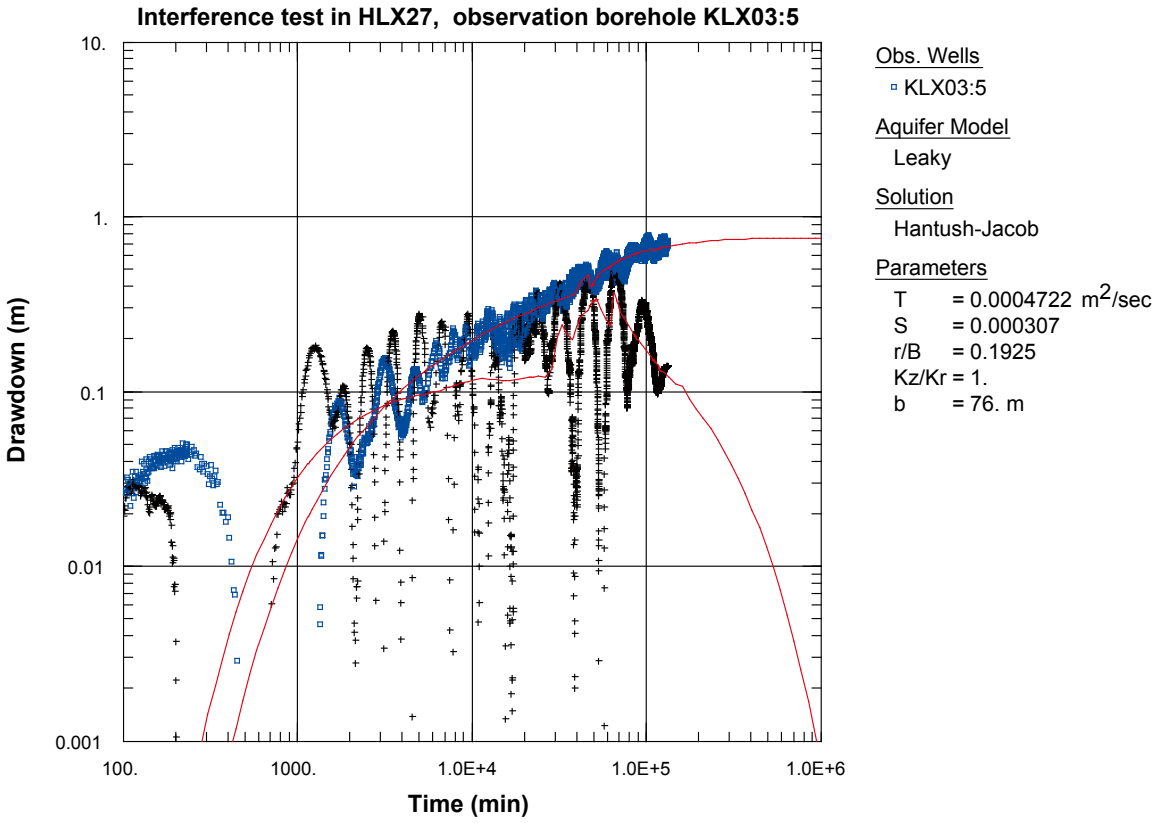

Figure A6-43. *Log-log plot of drawdown (▫) and drawdown derivative, ds/d(ln t) (+), versus time in KLX03:5 during the interference test in HLX27.*

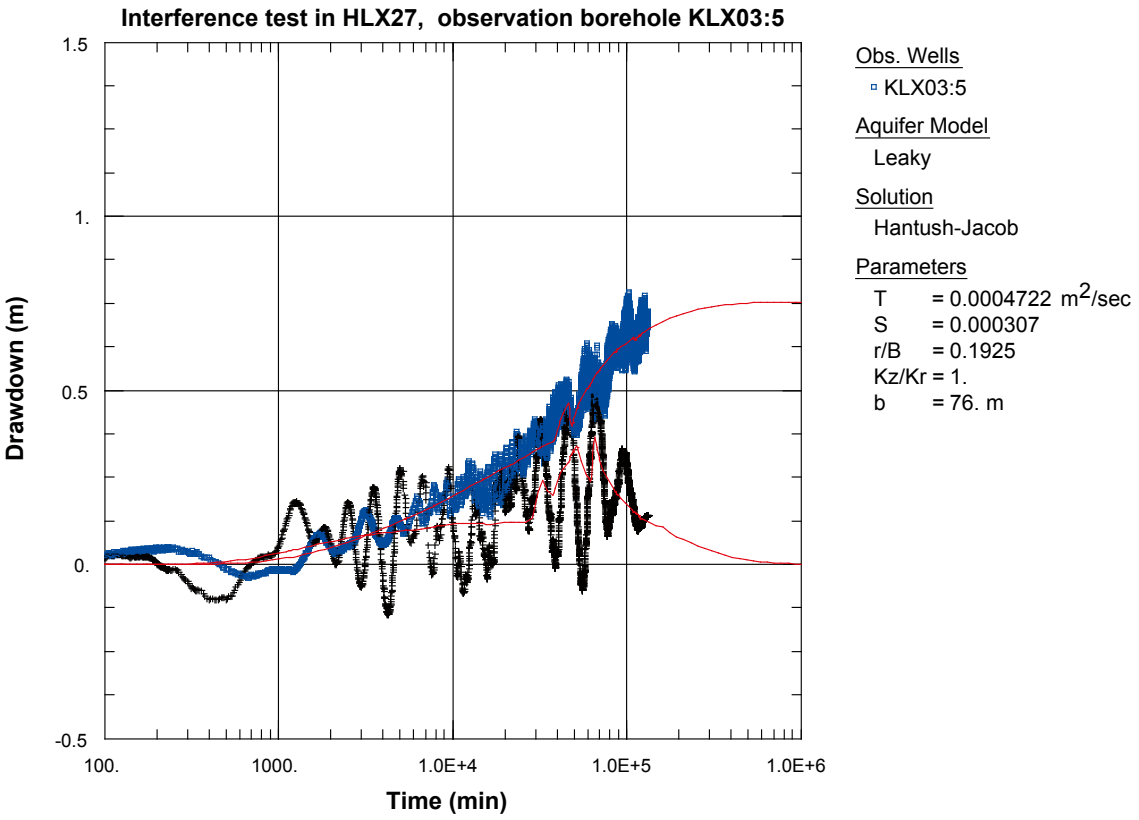

Figure A6-44. *Lin-log plot of drawdown (▫) and drawdown derivative, ds/d(ln t) (+), versus time in KLX03:5 during the interference test in HLX27.*

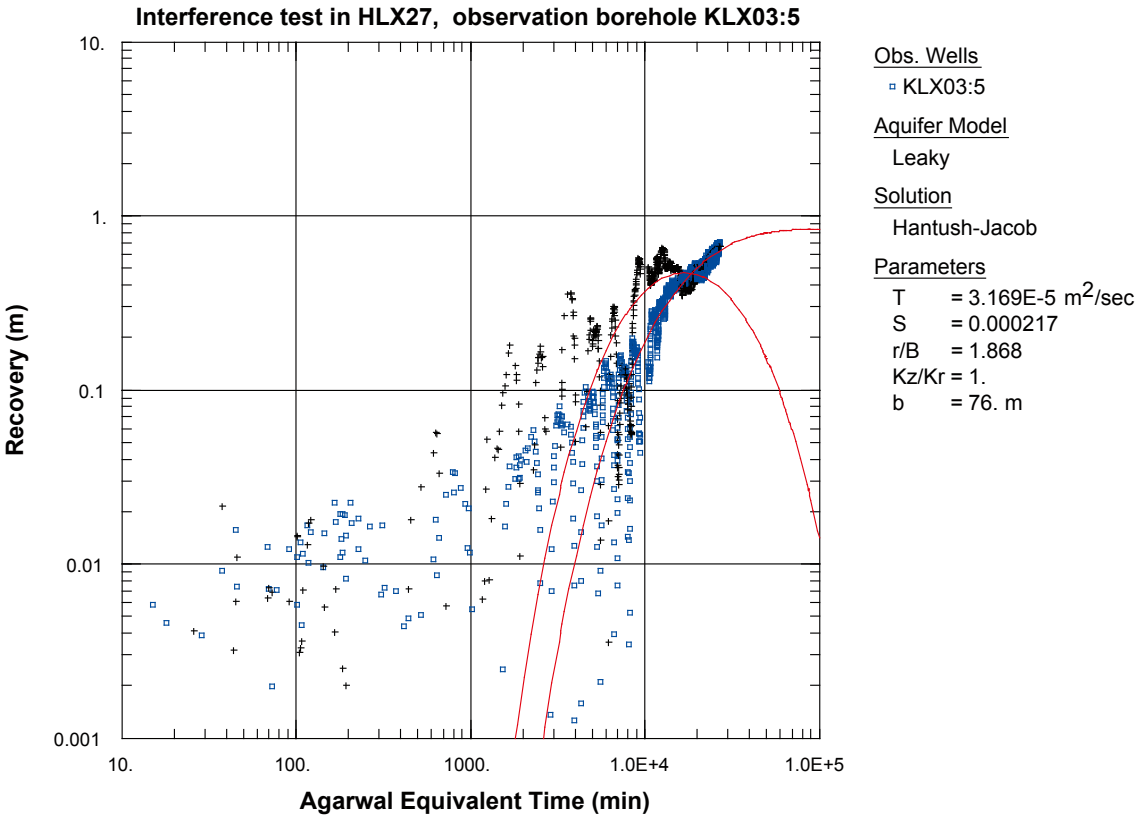

Figure A6-45. *Log-log plot of recovery (▫) and recovery derivative, ds/d(ln t) (+), versus time in KLX03:5 during the interference test in HLX27.*

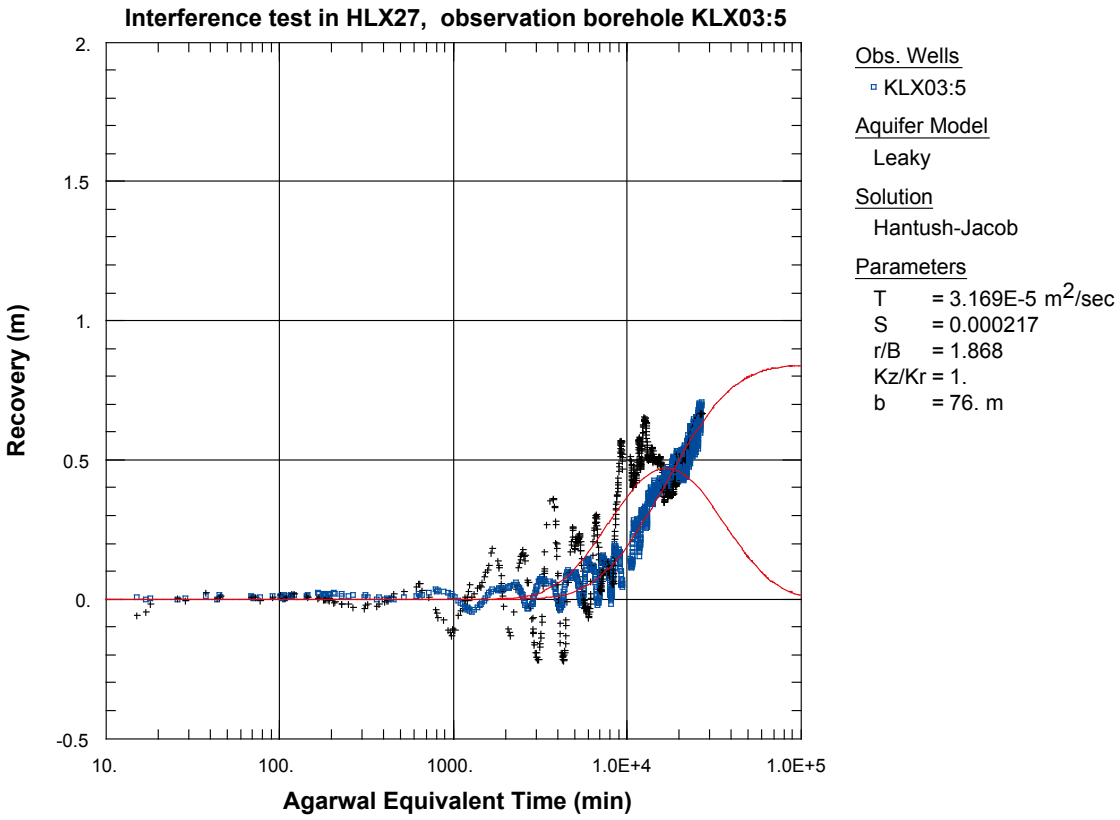

Figure A6-46. *Lin-log plot of recovery (▫) and recovery derivative, ds/d(ln t) (+), versus time in KLX03:5 during the interference test in HLX27.*

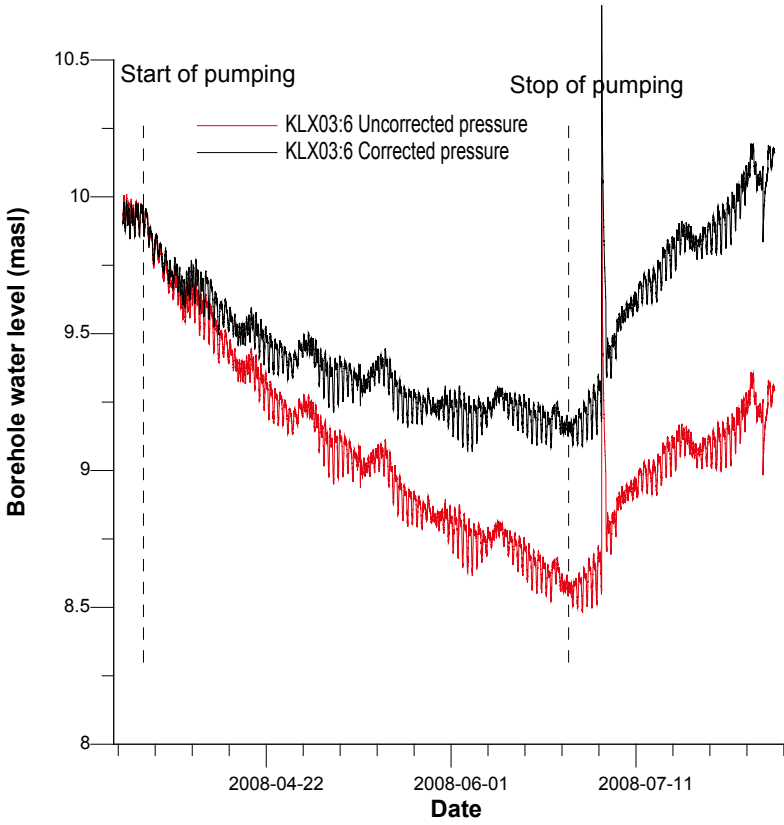

Figure A6-47. *Linear plot of pressure versus time in the observation sections in KLX03:6 during pumping in HLX27.*

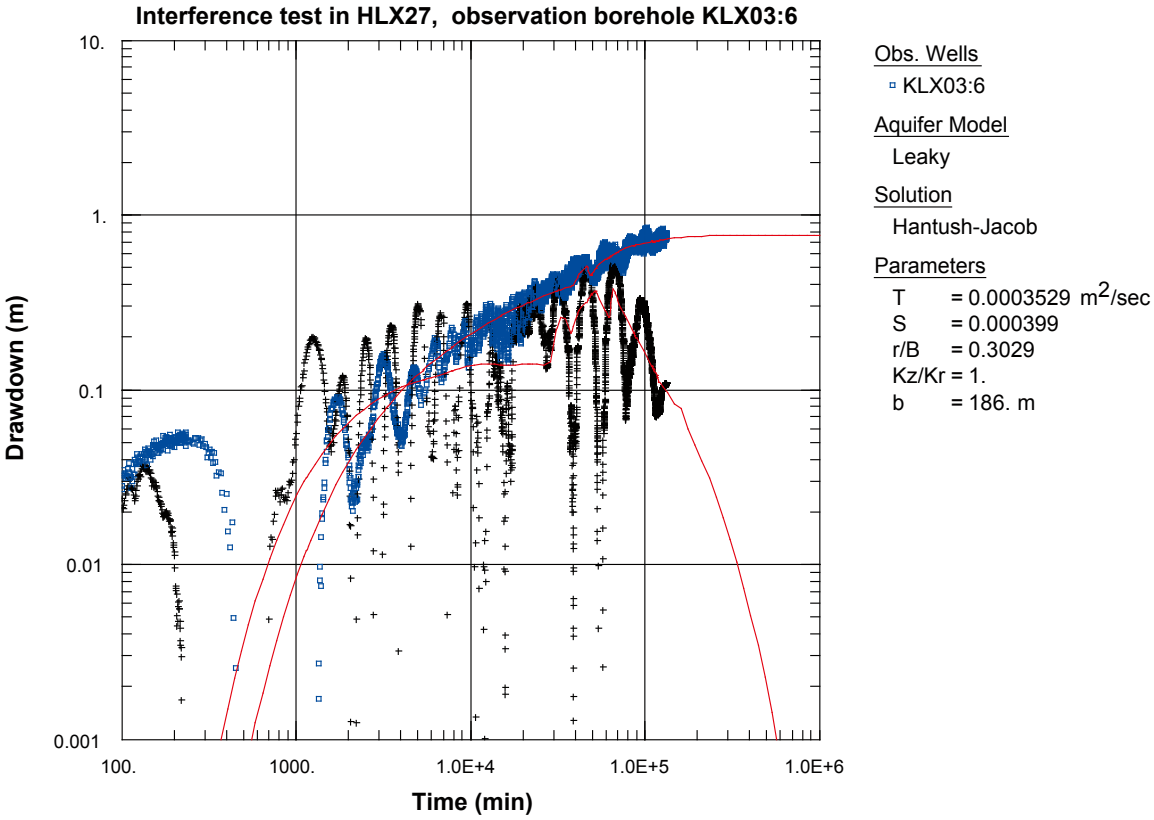

Figure A6-48. *Log-log plot of drawdown (▫) and drawdown derivative, ds/d(ln t) (+), versus time in KLX03:6 during the interference test in HLX27.*

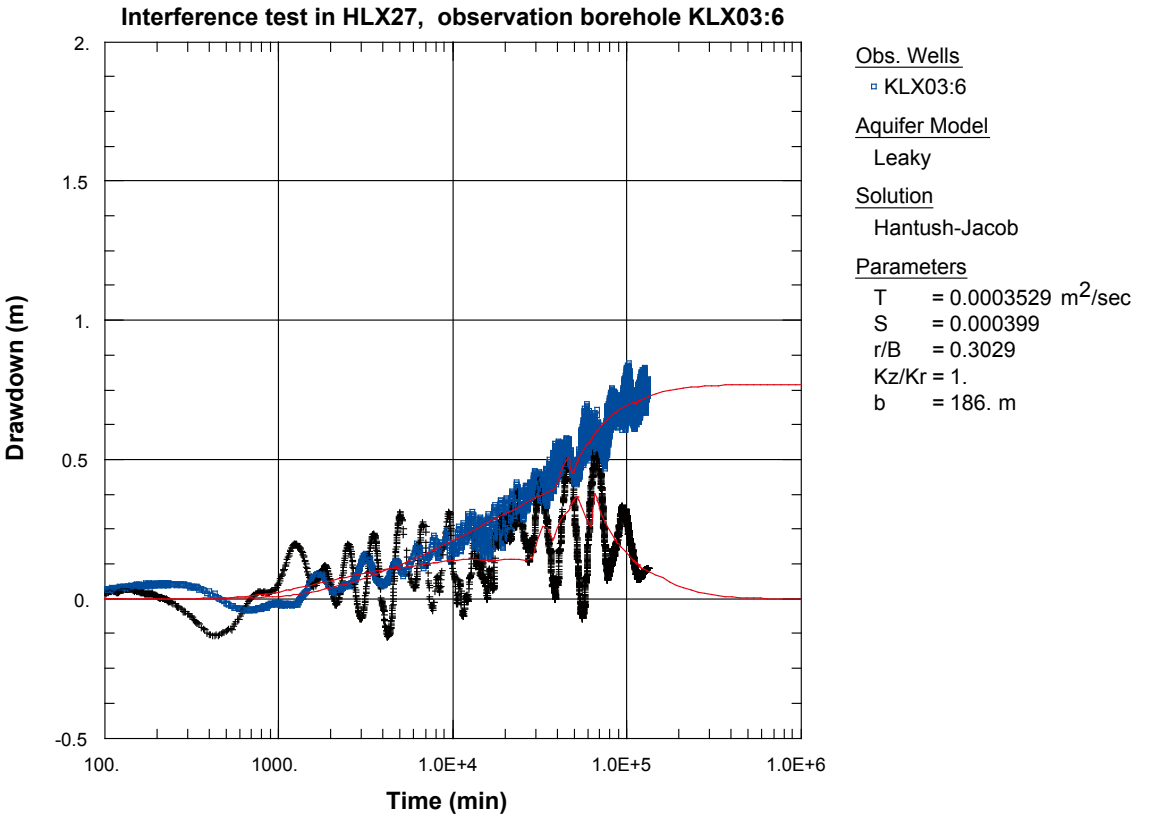

Figure A6-49. *Lin-log plot of drawdown (▫) and drawdown derivative, ds/d(ln t) (+), versus time in KLX03:6 during the interference test in HLX27.*

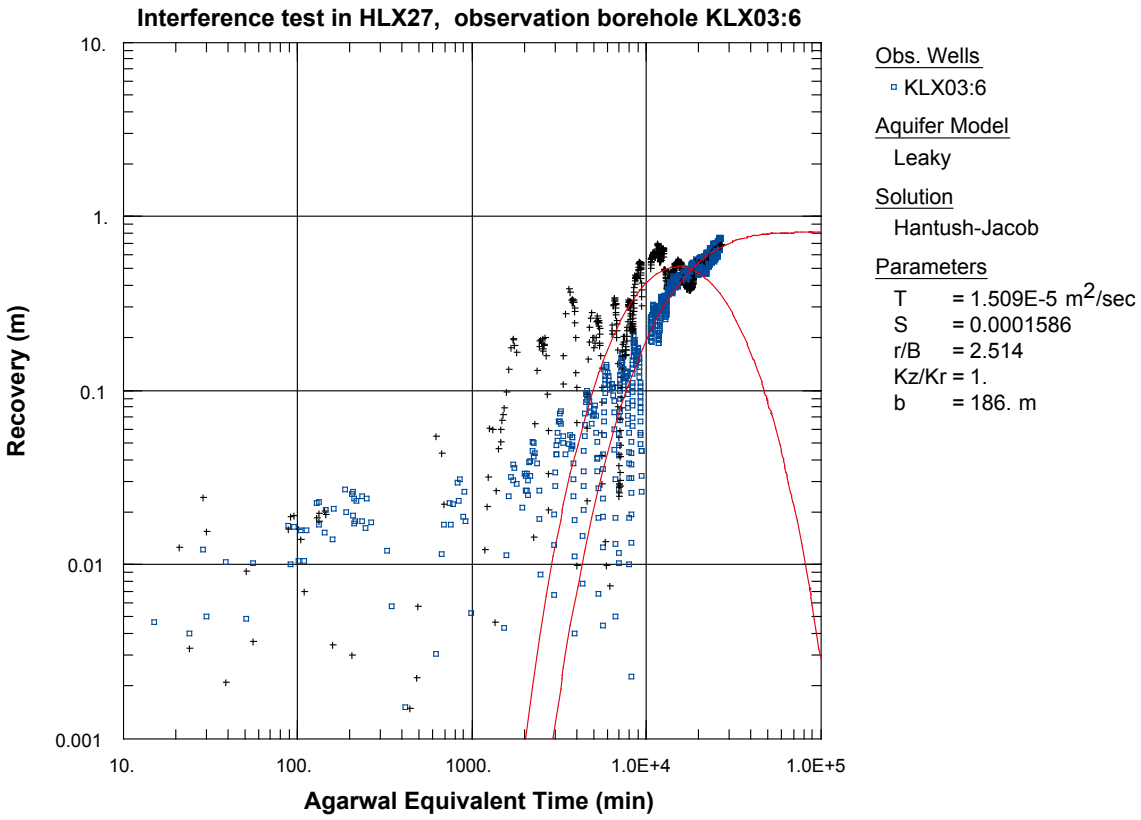

Figure A6-50. *Log-log plot of recovery (▫) and recovery derivative, ds/d(ln t) (+), versus time in KLX03:6 during the interference test in HLX27.*

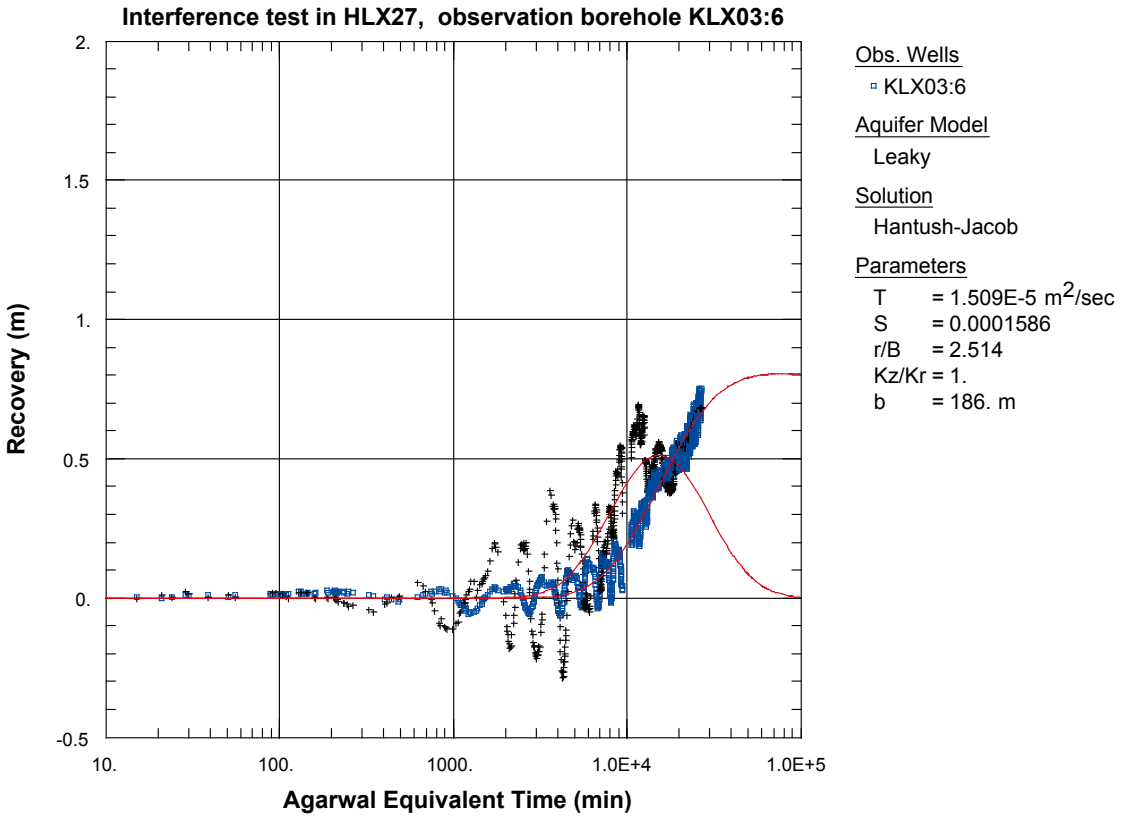

Figure A6-51. *Lin-log plot of recovery (▫) and recovery derivative, ds/d(ln t) (+), versus time in KLX03:6 during the interference test in HLX27.*

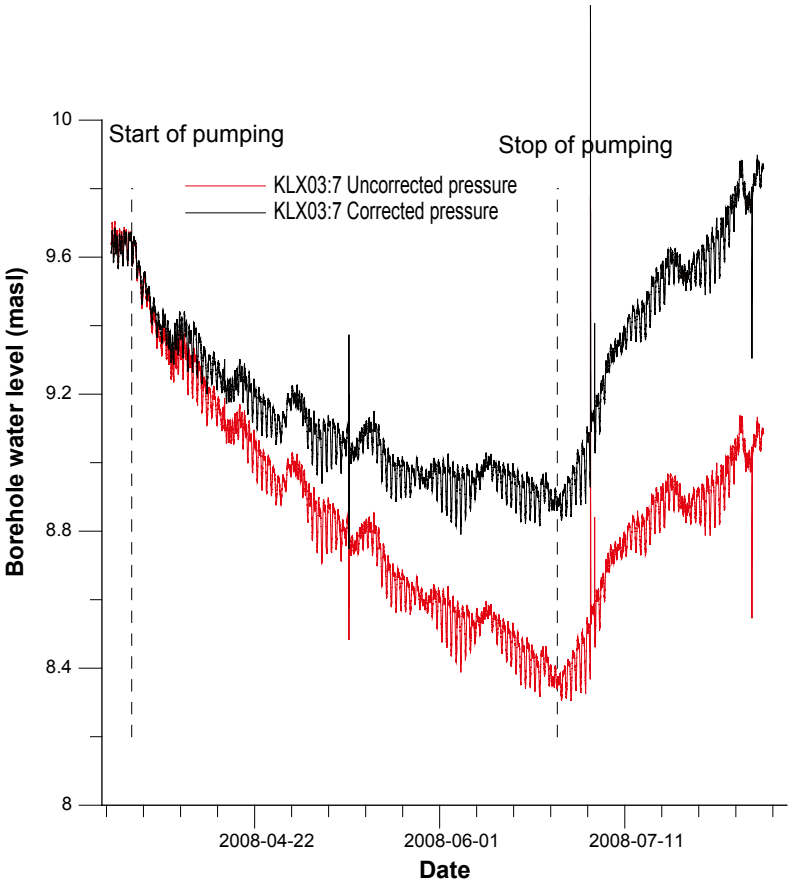

Figure A6-52. *Linear plot of pressure versus time in the observation section KLX03:7 during pumping in HLX27.*

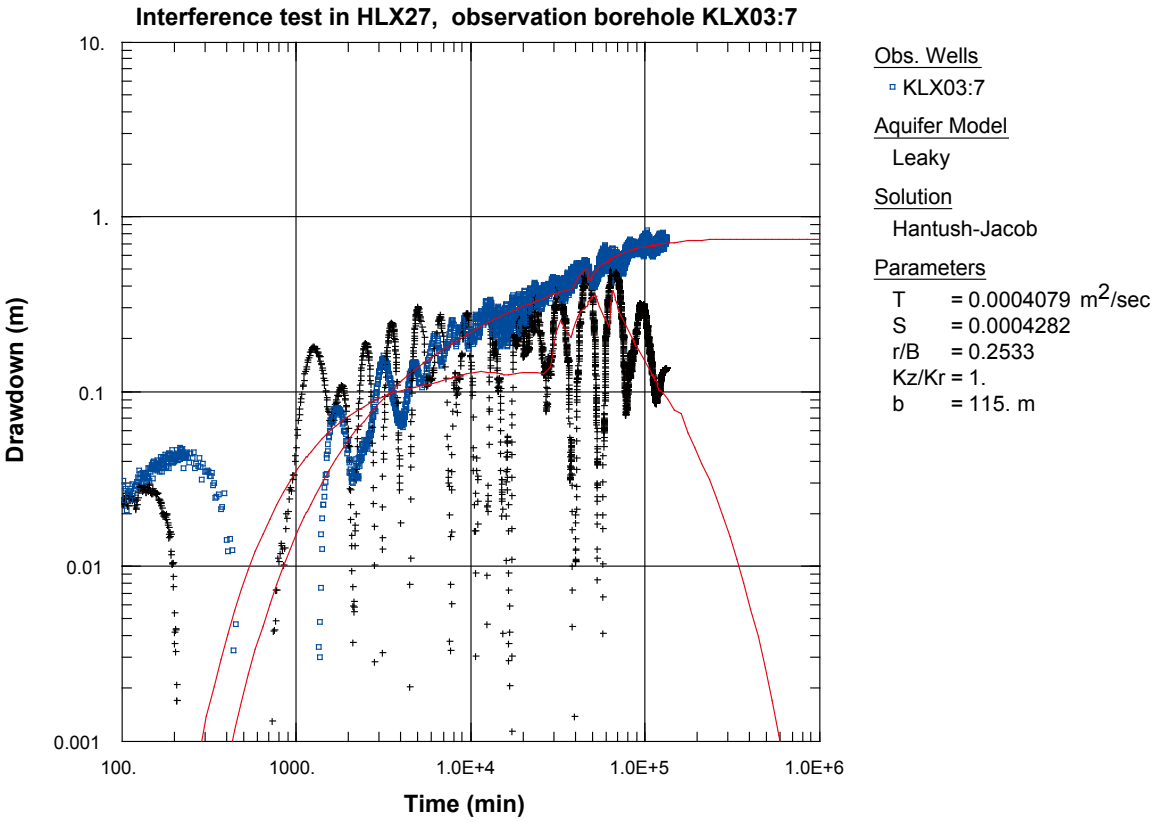

Figure A6-53. *Log-log plot of drawdown (▫) and drawdown derivative, ds/d(ln t) (+), versus time in KLX03:7 during the interference test in HLX27.*

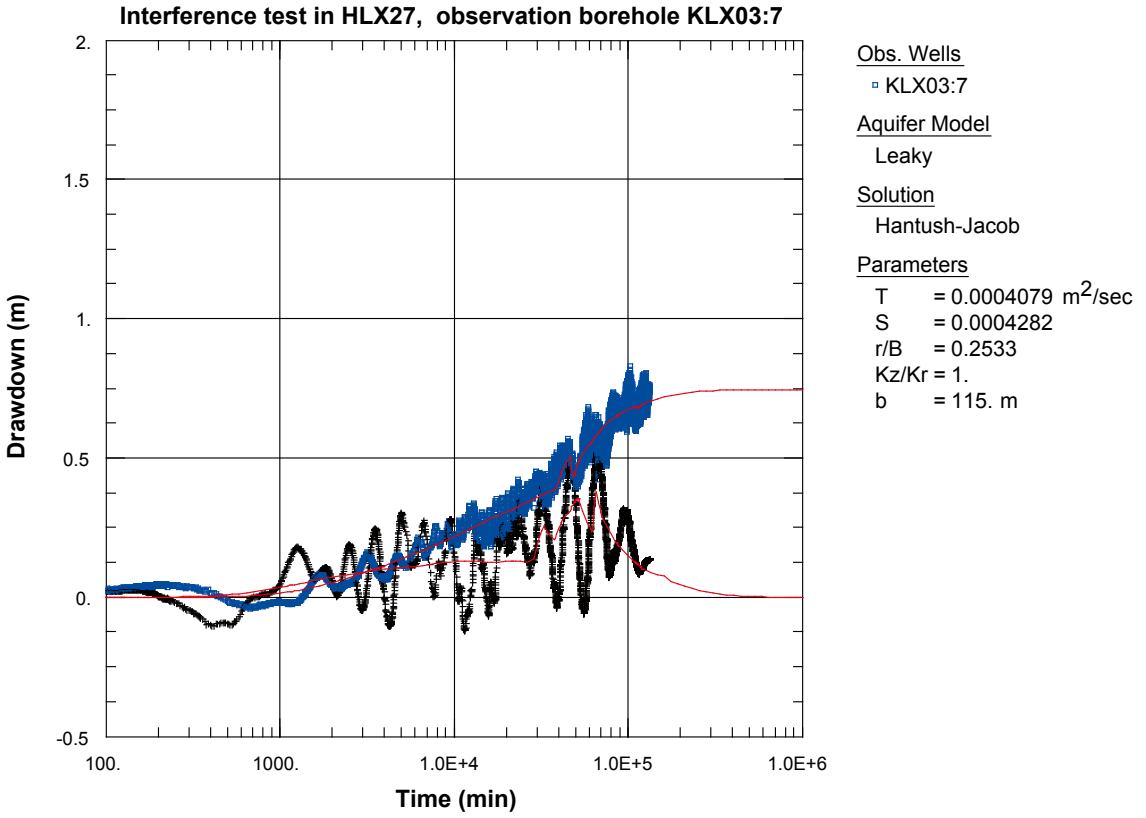

Figure A6-54. *Lin-log plot of drawdown (▫) and drawdown derivative, ds/d(ln t) (+), versus time in KLX03:7 during the interference test in HLX27.*

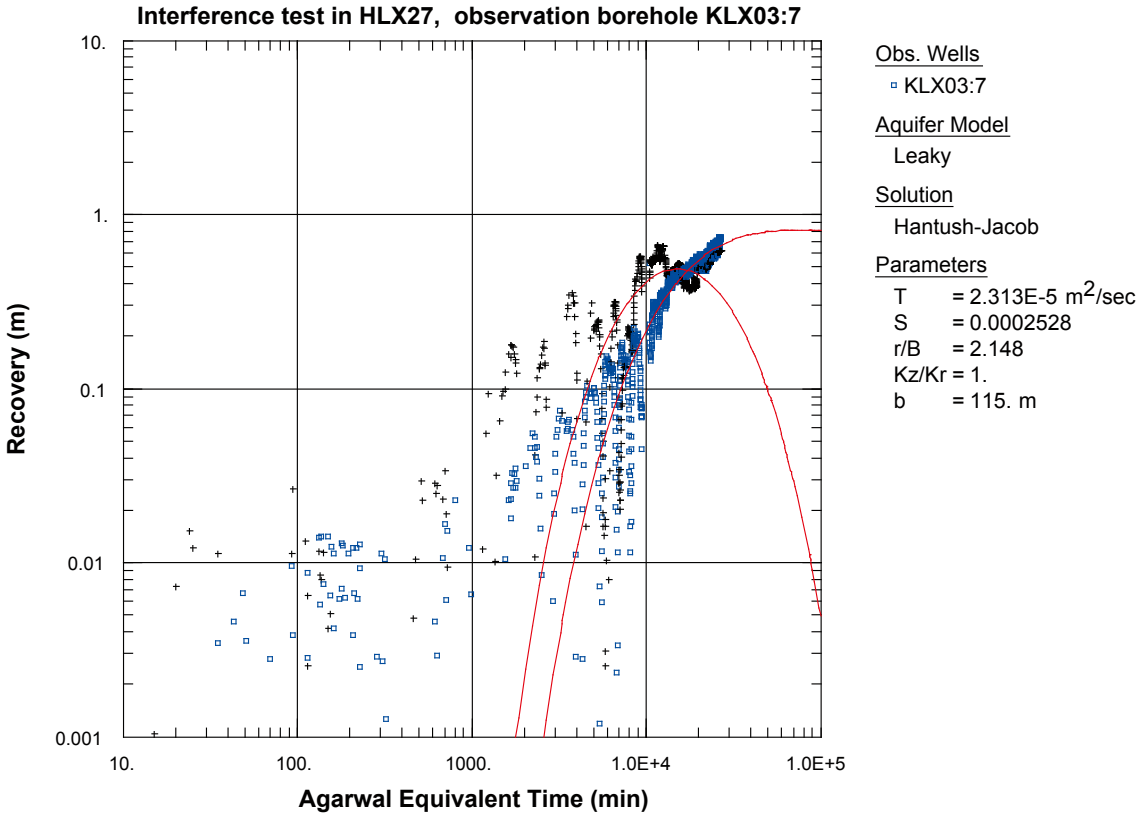

Figure A6-55. *Log-log plot of recovery (▫) and recovery derivative, ds/d(ln t) (+), versus time in KLX03:7 during the interference test in HLX27.*

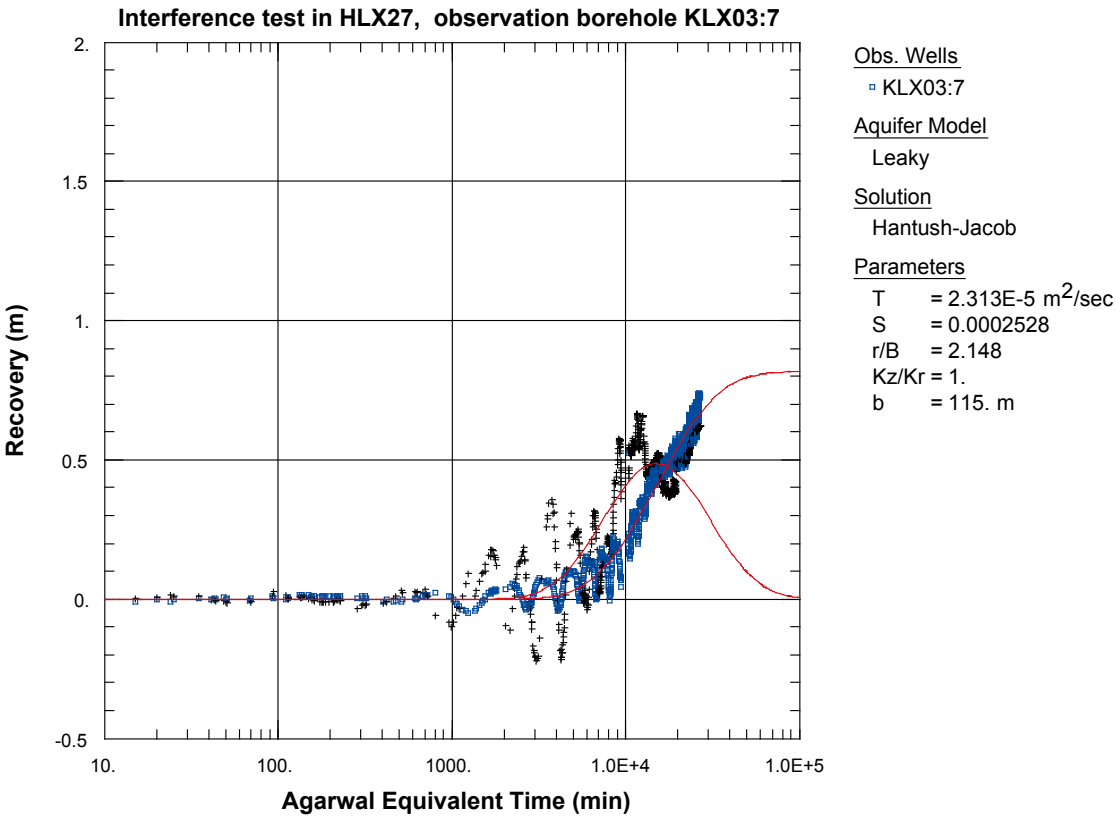

Figure A6-56. *Lin-log plot of recovery (▫) and recovery derivative, ds/d(ln t) (+), versus time in KLX03:7 during the interference test in HLX27.*

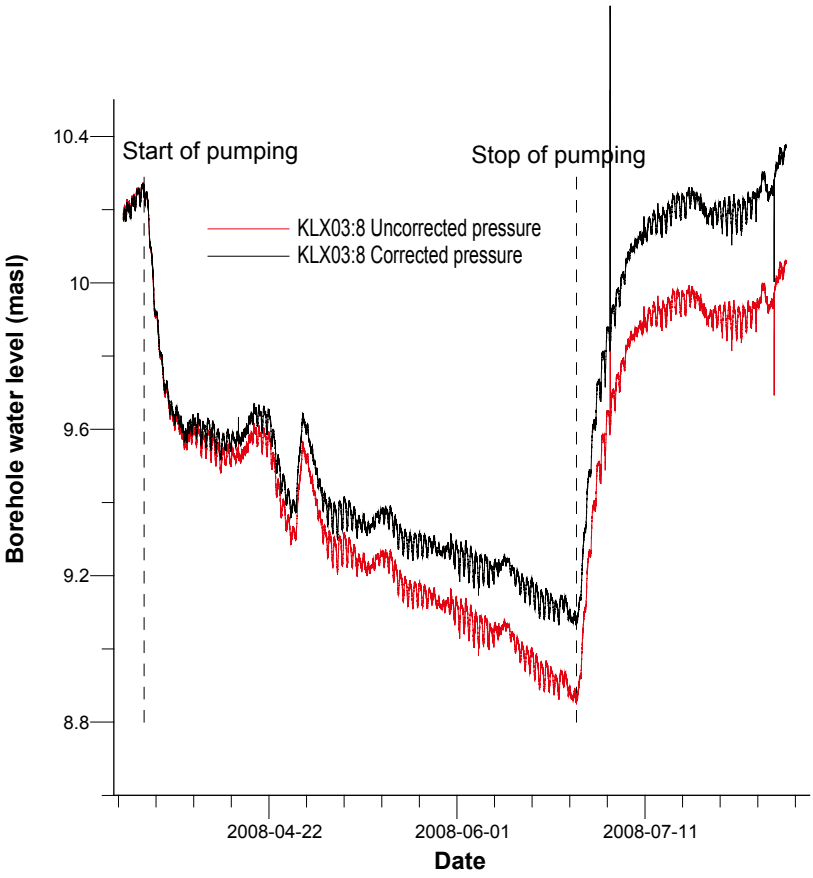

Figure A6-57. *Linear plot of pressure versus time in the observation sections in KLX03:8 during pumping in HLX27.*

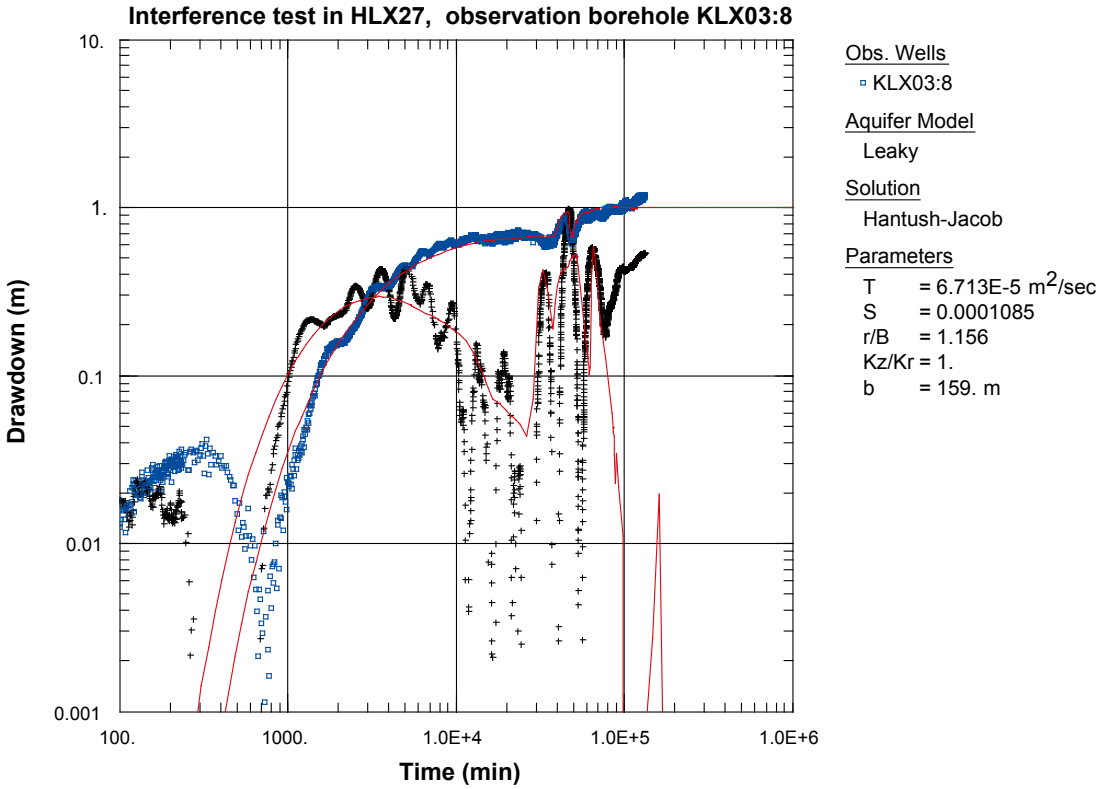

Figure A6-58. *Log-log plot of drawdown (▫) and drawdown derivative, ds/d(ln t) (+), versus time in KLX03:8 during the interference test in HLX27. Transient evaluation is based on the first part of the drawdown period.*

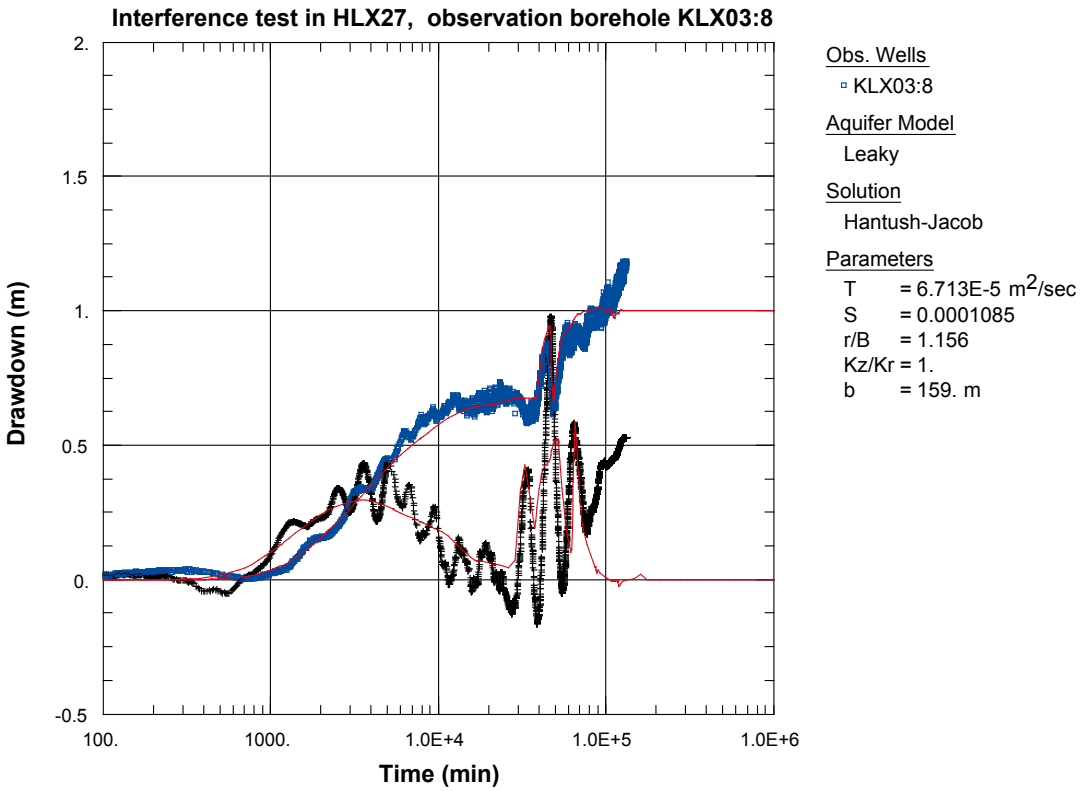

Figure A6-59. *Lin-log plot of drawdown (▫) and drawdown derivative, ds/d(ln t) (+), versus time in KLX03:8 during the interference test in HLX27. Transient evaluation is based on the first part of the drawdown period.*

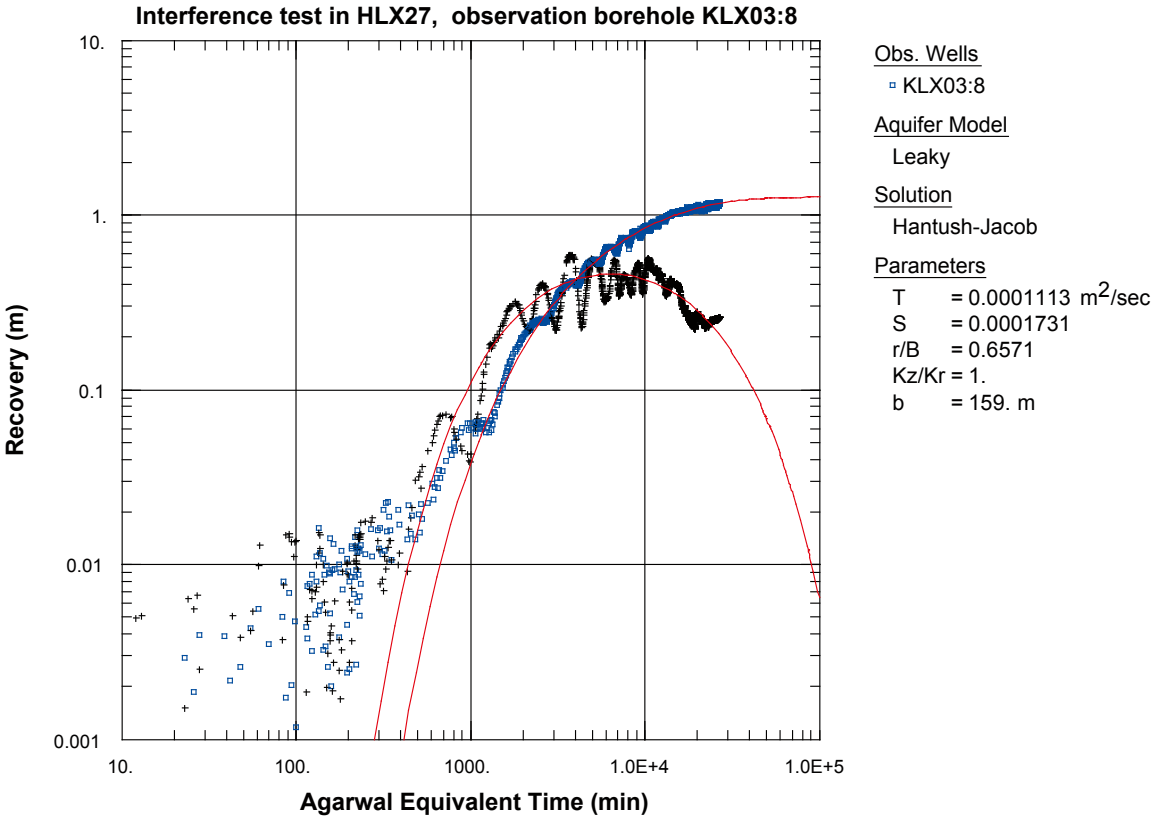

Figure A6-60. *Log-log plot of recovery (▫) and recovery derivative, ds/d(ln t) (+), versus time in KLX03:8 during the interference test in HLX27.*

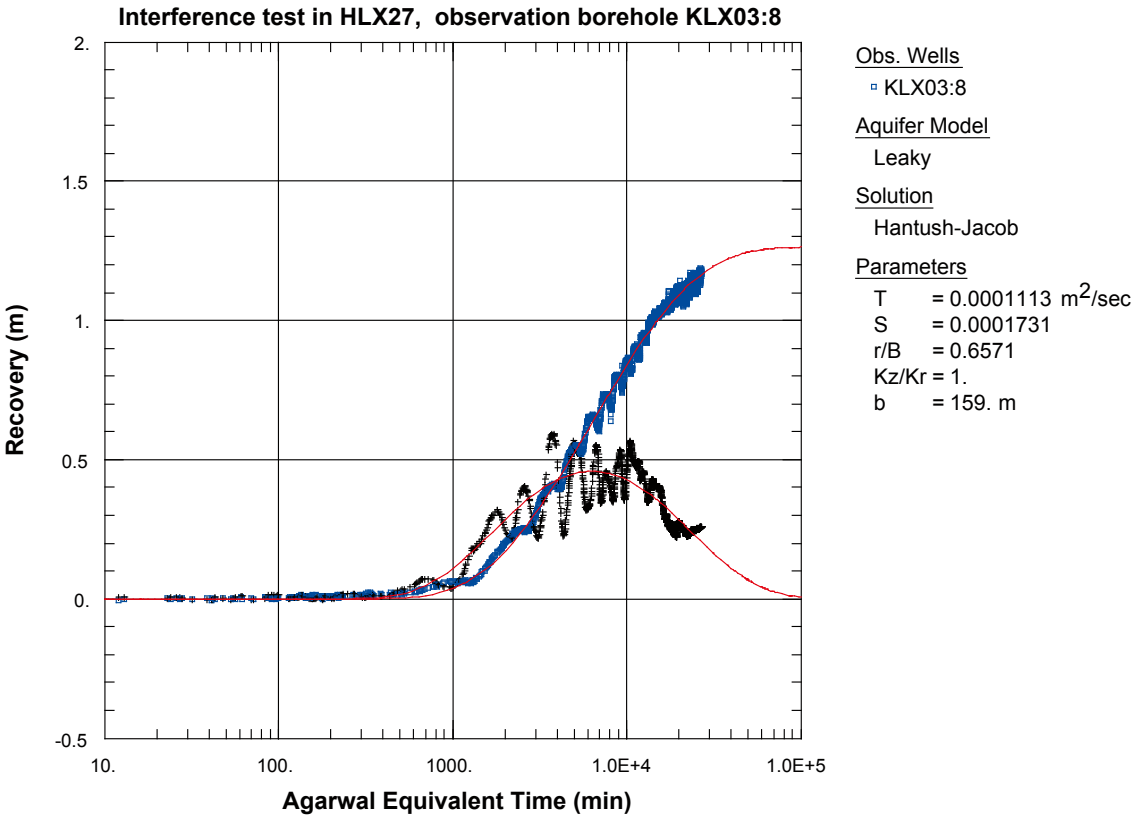

Figure A6-61. *Lin-log plot of recovery (▫) and recovery derivative, ds/d(ln t) (+), versus time in KLX03:8 during the interference test in HLX27.*

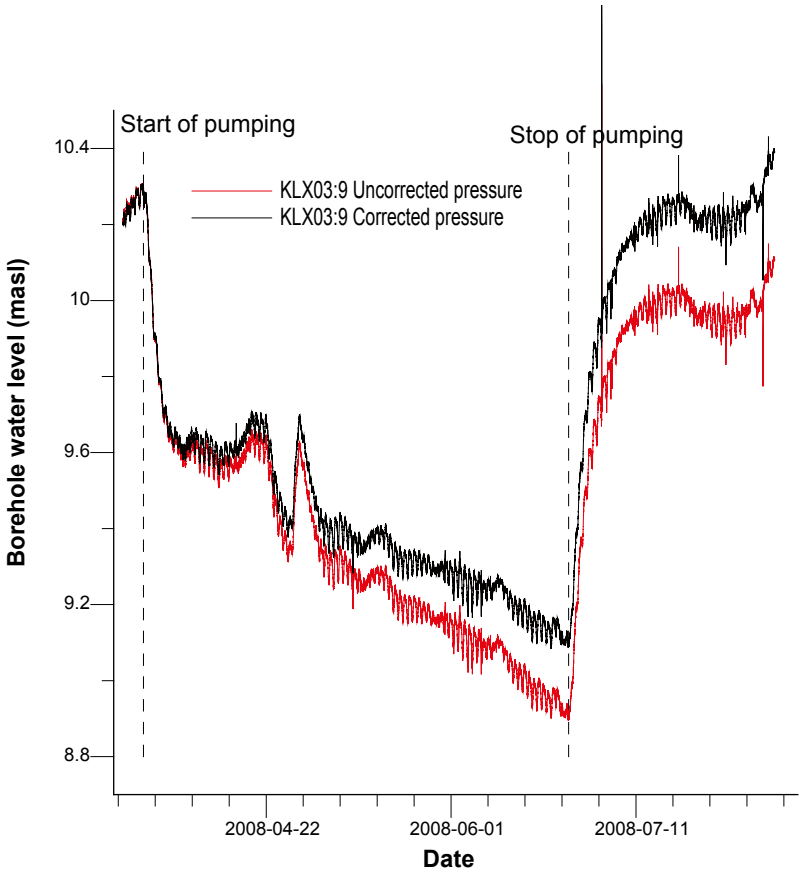

Figure A6-62. *Linear plot of pressure versus time in the observation sections in KLX03:9 during pumping in HLX27.*

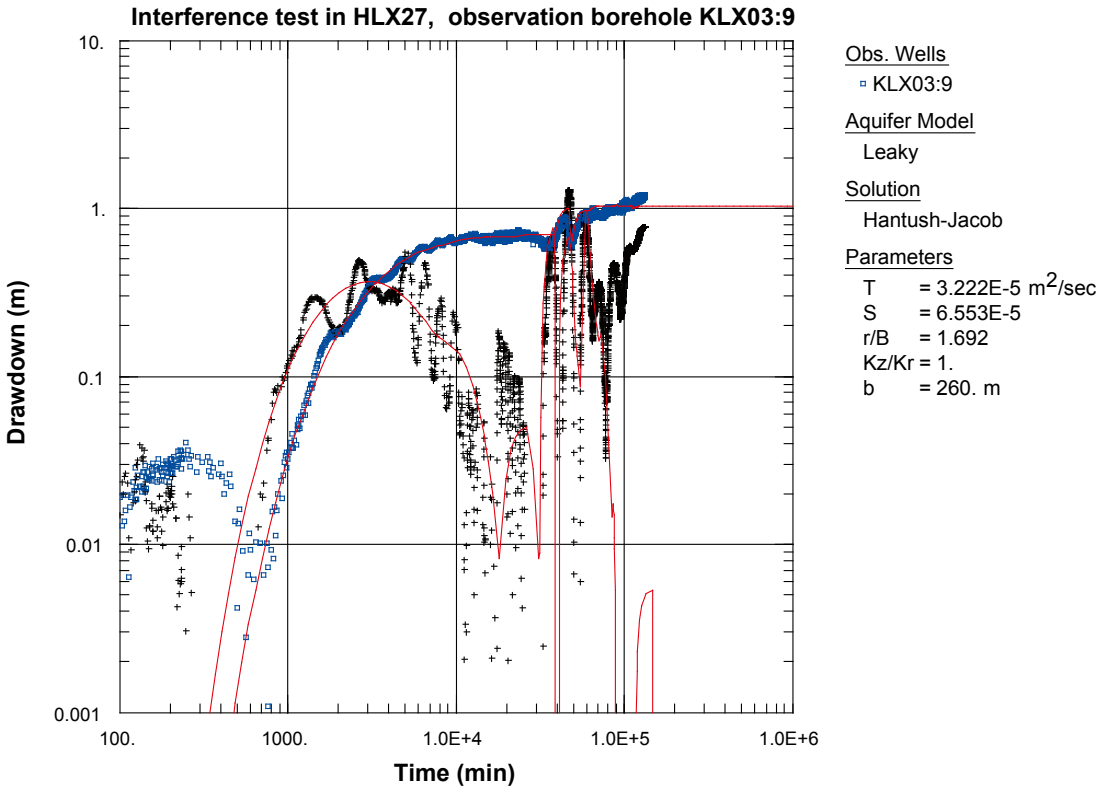

Figure A6-63. *Log-log plot of drawdown (▫) and drawdown derivative, ds/d(ln t) (+), versus time in KLX03:9 during the interference test in HLX27. Transient evaluation is based on the first part of the drawdown period.*

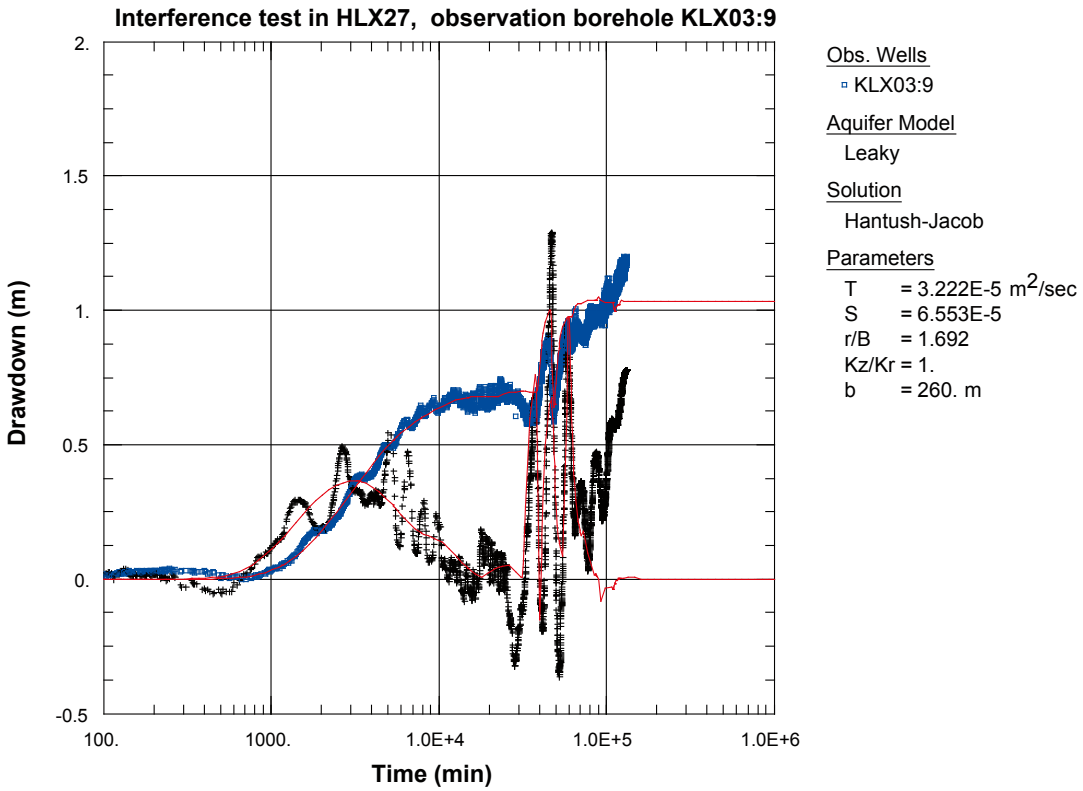

Figure A6-64. *Lin-log plot of drawdown (▫) and drawdown derivative, ds/d(ln t) (+), versus time in KLX03:9 during the interference test in HLX27. Transient evaluation is based on the first part of the drawdown period.*

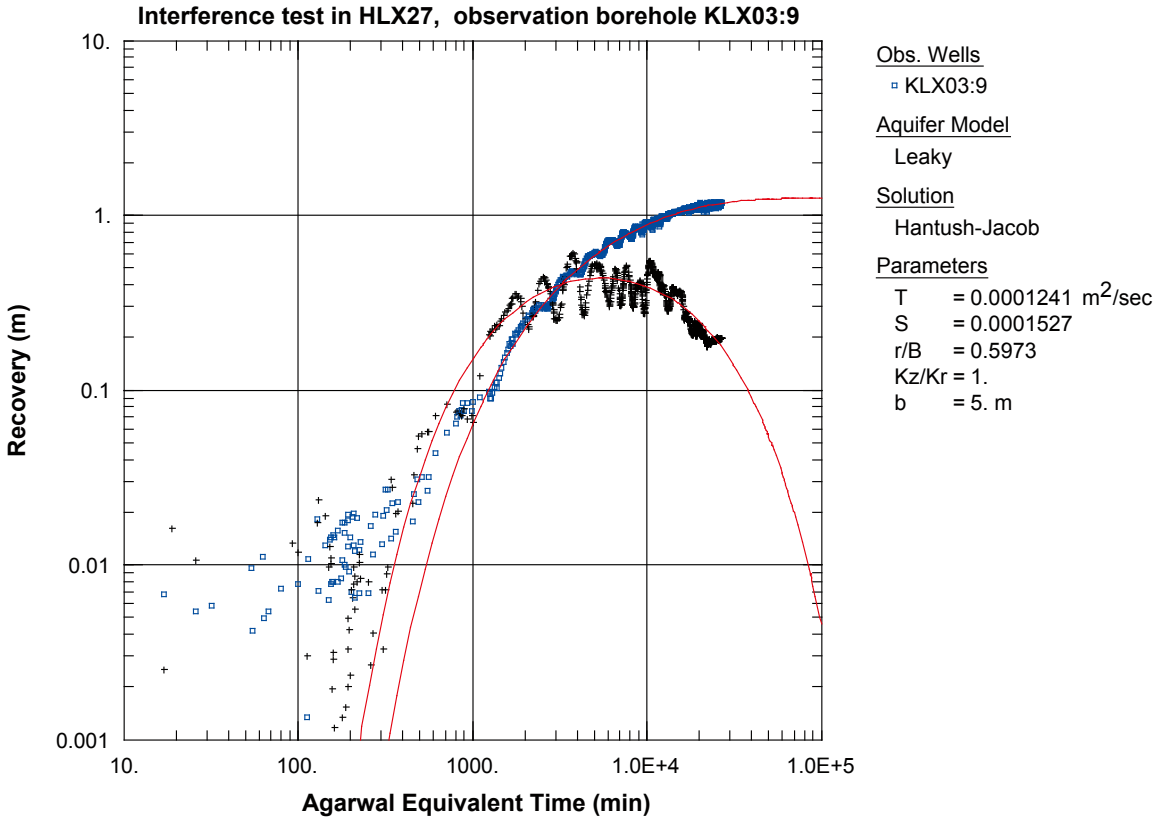

Figure A6-65. *Log-log plot of recovery (▫) and recovery derivative, ds/d(ln t) (+), versus time in KLX03:9 during the interference test in HLX27.*

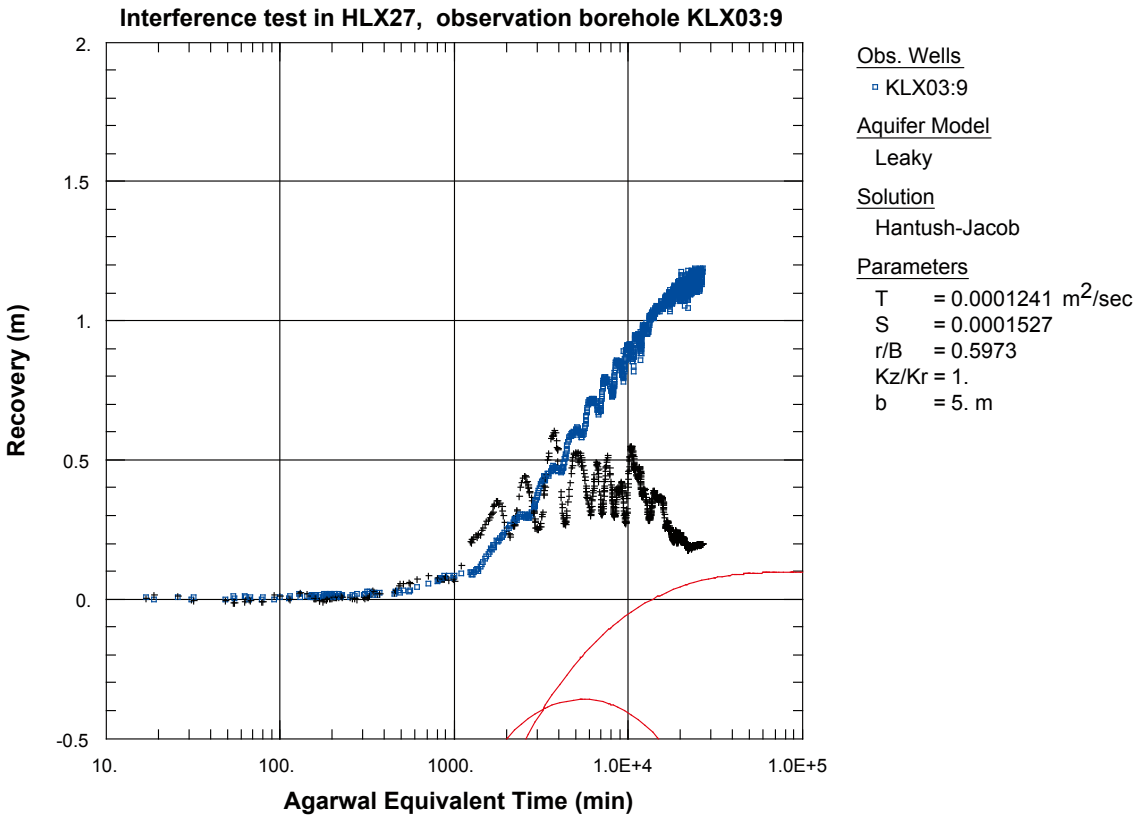

Figure A6-66. *Lin-log plot of recovery (▫) and recovery derivative, ds/d(ln t) (+), versus time in KLX03:9 during the interference test in HLX27.*

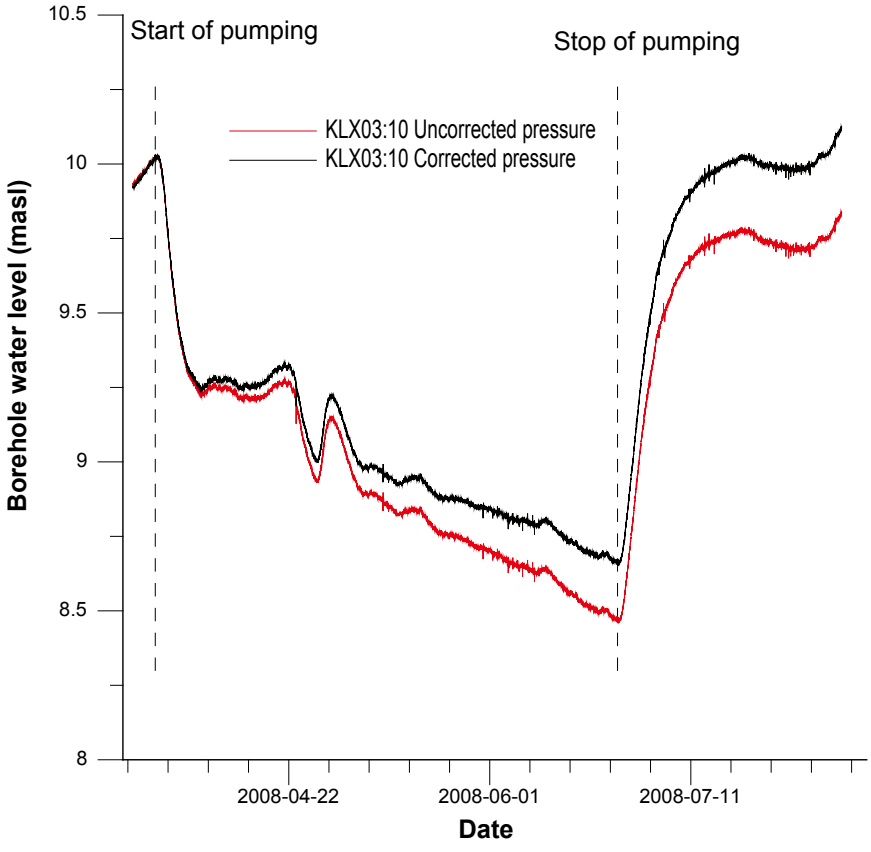

Figure A6-67. *Linear plot of pressure and pressure corrected for the natural decreasing pressure trend versus time in the observation section KLX03:10 during pumping in HLX27.*

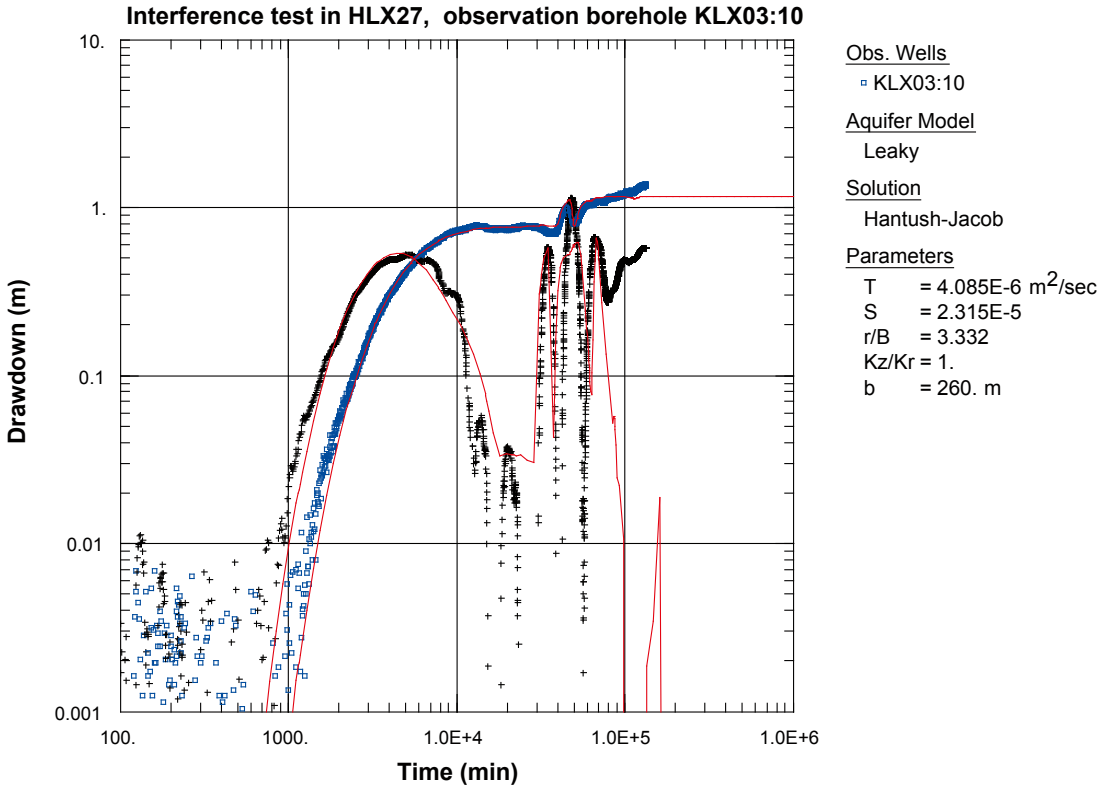

Figure A6-68. *Log-log plot of drawdown (▫) and drawdown derivative, ds/d(ln t) (+), versus time in KLX03:10 during the interference test in HLX27. Transient evaluation is based on the first part of the drawdown period.*

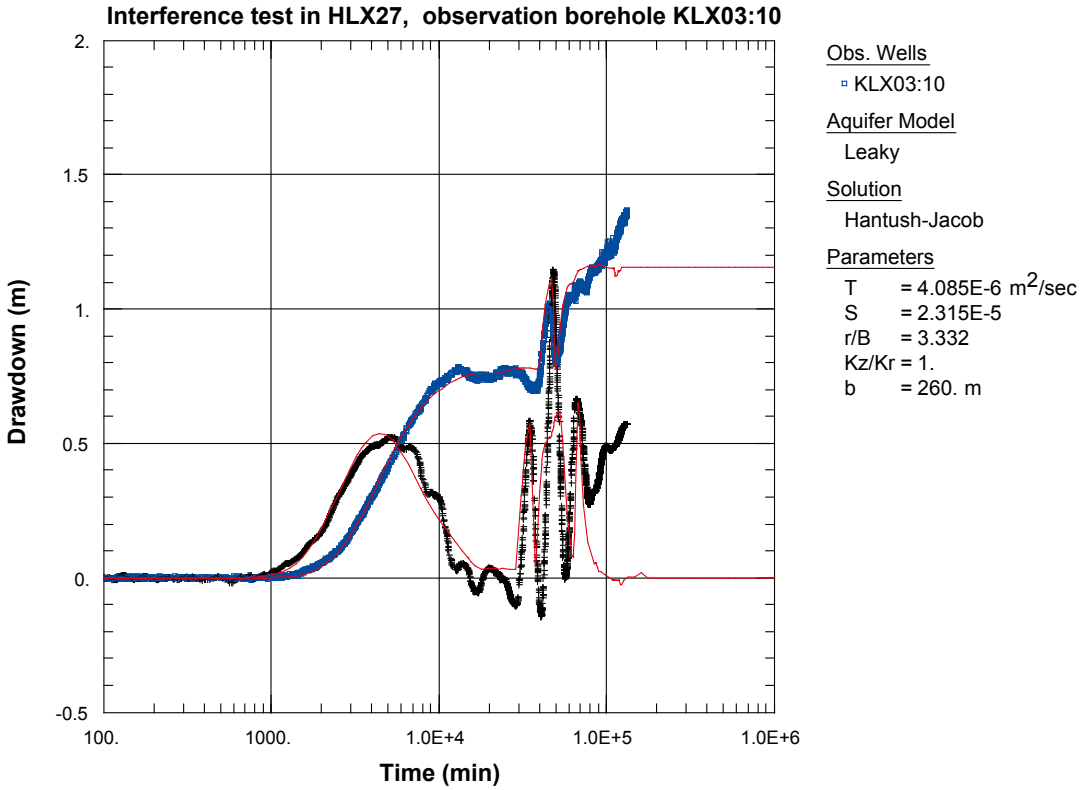

Figure A6-69. *Lin-log plot of drawdown (▫) and drawdown derivative, ds/d(ln t) (+), versus time in KLX03:10 during the interference test in HLX27. Transient evaluation is based on the first part of the drawdown period.*

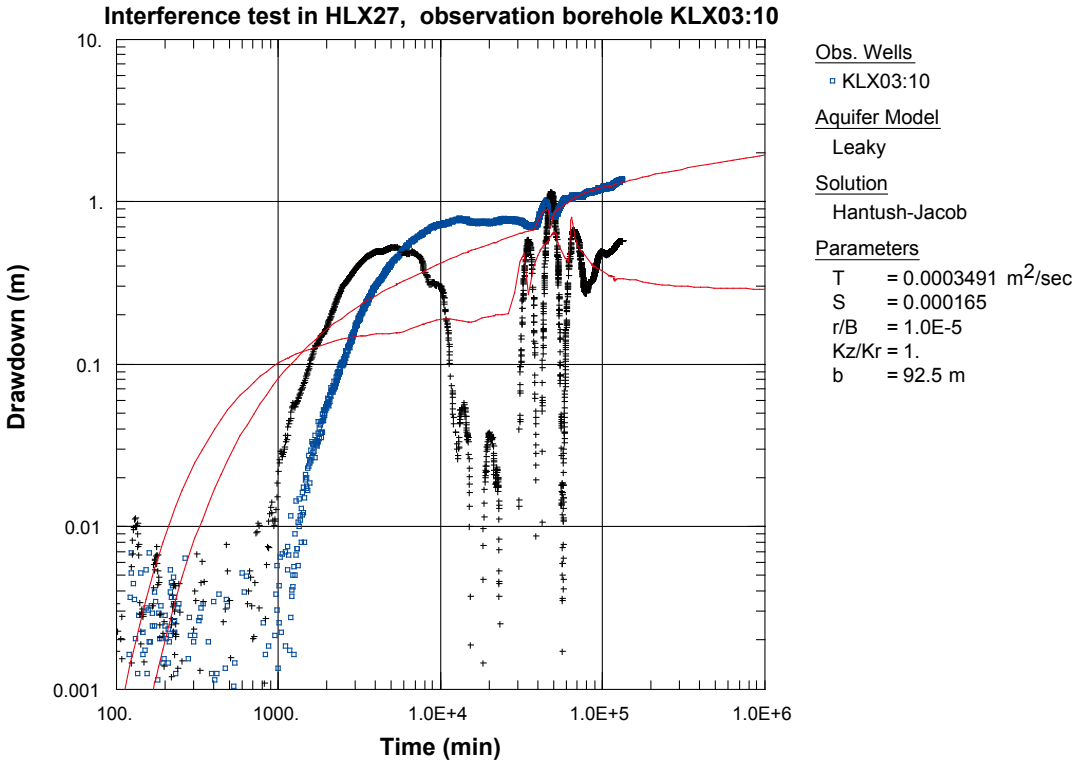

Figure A6-70. *Log-log plot of drawdown (▫) and drawdown derivative, ds/d(ln t) (+), versus time in KLX03:10 during the interference test in HLX27. Transient evaluation is based on the later part of the drawdown period.*

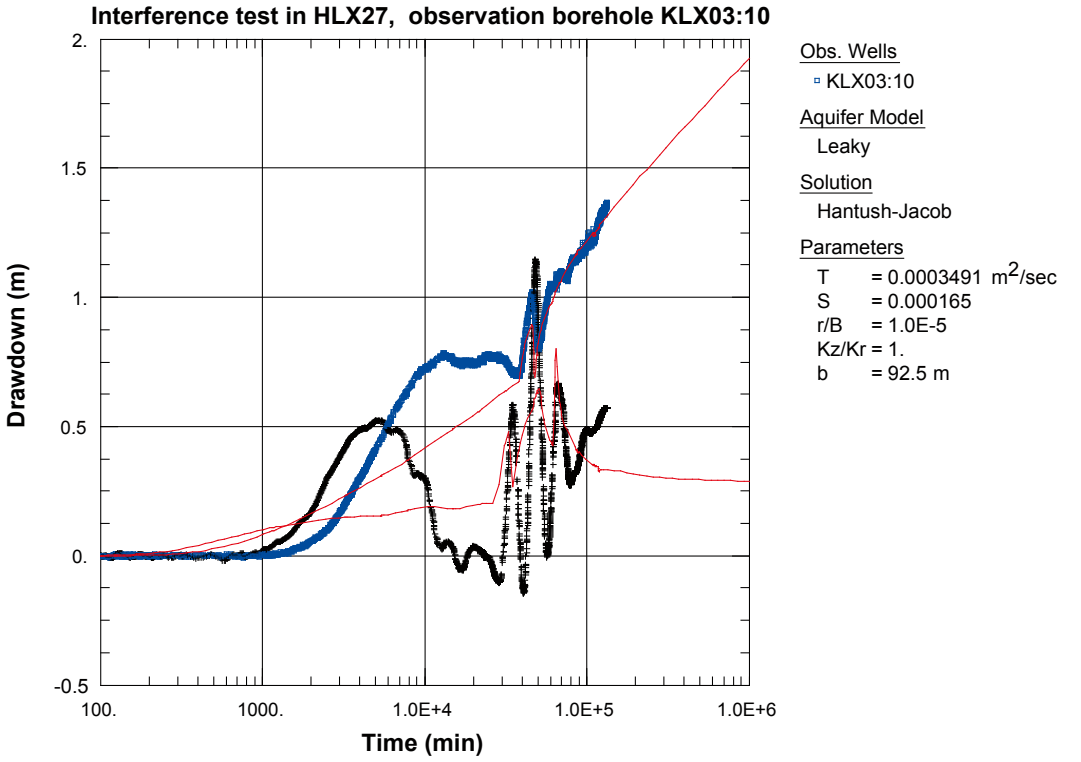

Figure A6-71. *Lin-log plot of drawdown (▫) and drawdown derivative, ds/d(ln t) (+), versus time in KLX03:10 during the interference test in HLX27. Transient evaluation is based on the later part of the drawdown period.*

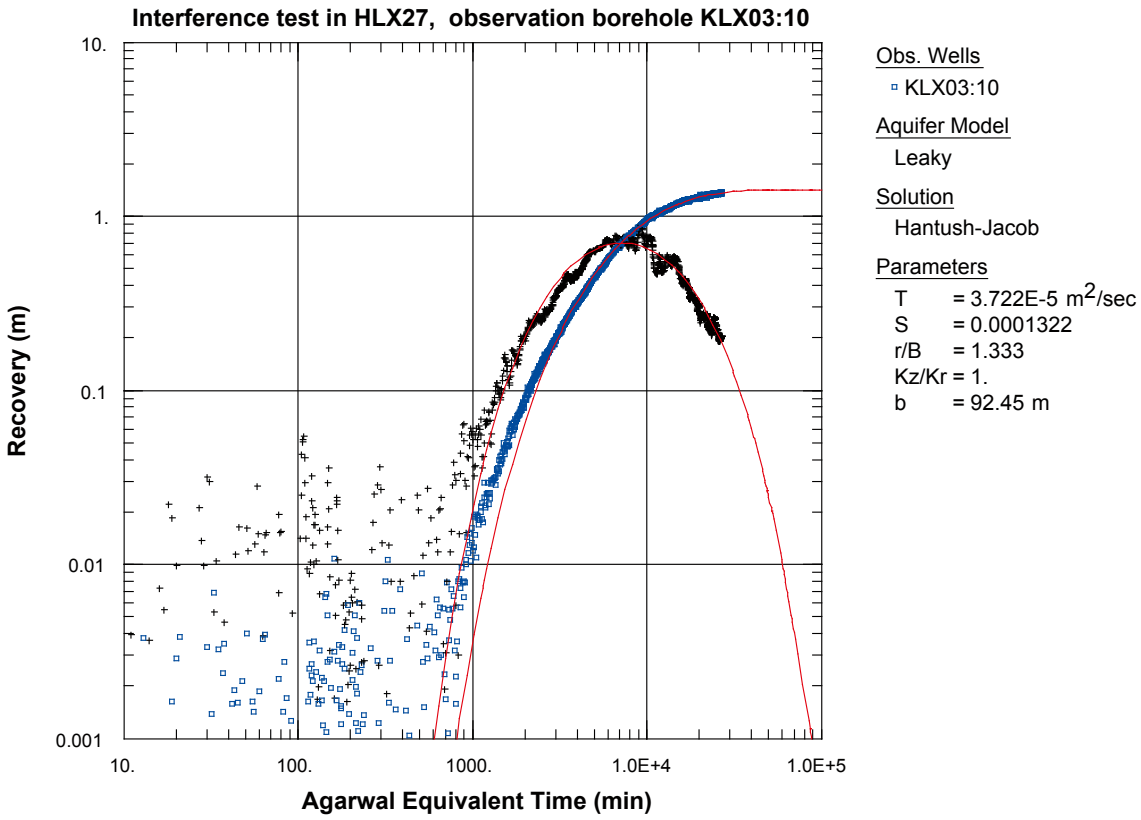

Figure A6-72. *Log-log plot of recovery (▫) and recovery derivative, ds/d(ln t) (+), versus time in KLX03:10 during the interference test in HLX27.*

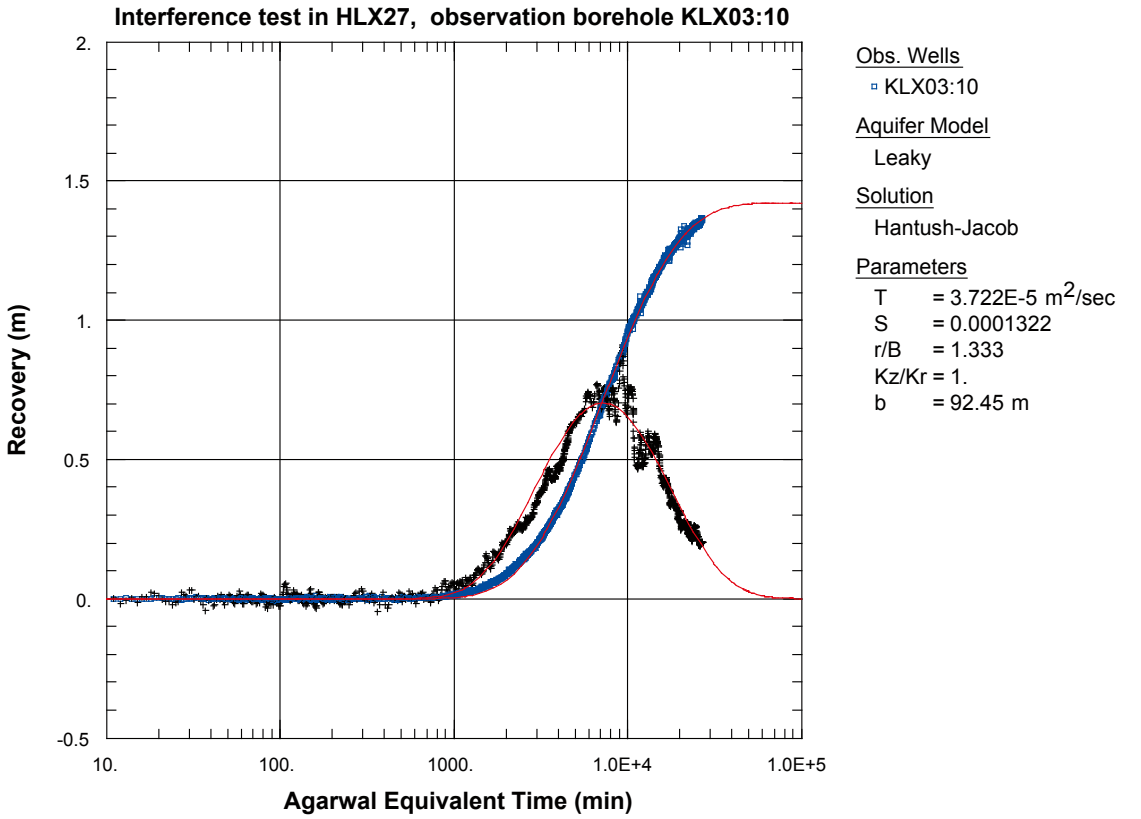

Figure A6-73. *Lin-log plot of recovery (▫) and recovery derivative, ds/d(ln t) (+), versus time in KLX03:10 during the interference test in HLX27.*

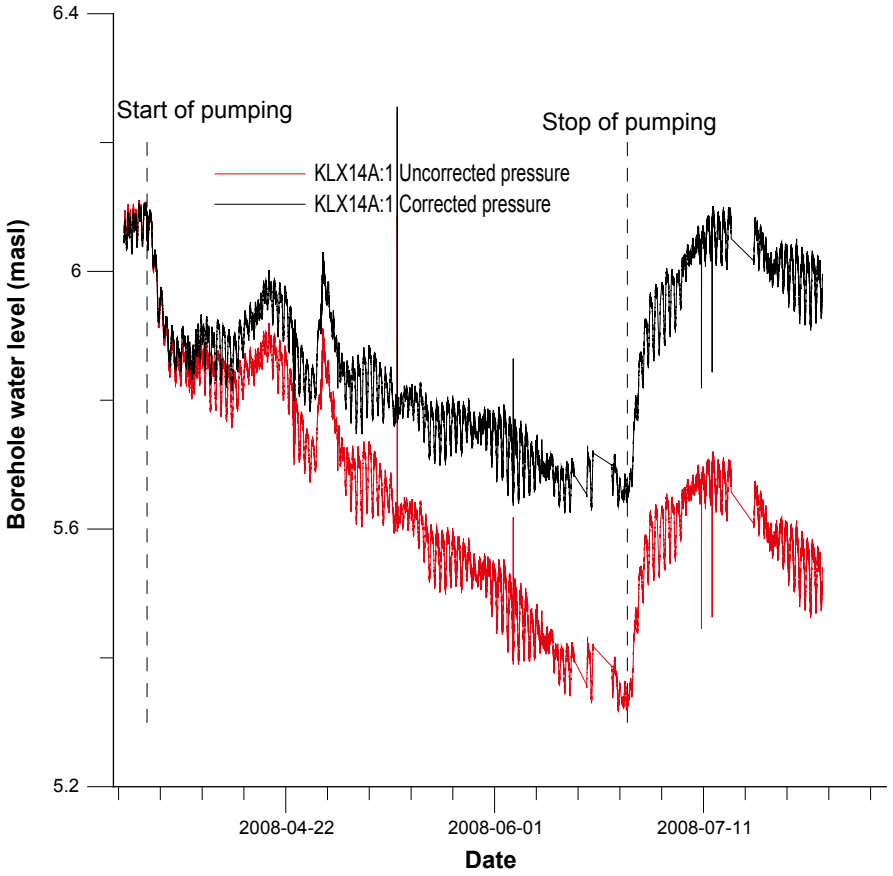

Figure A6-74. *Linear plot of pressure and pressure corrected for the natural decreasing pressure trend versus time in the observation section KLX14A:1 during pumping in HLX27.*

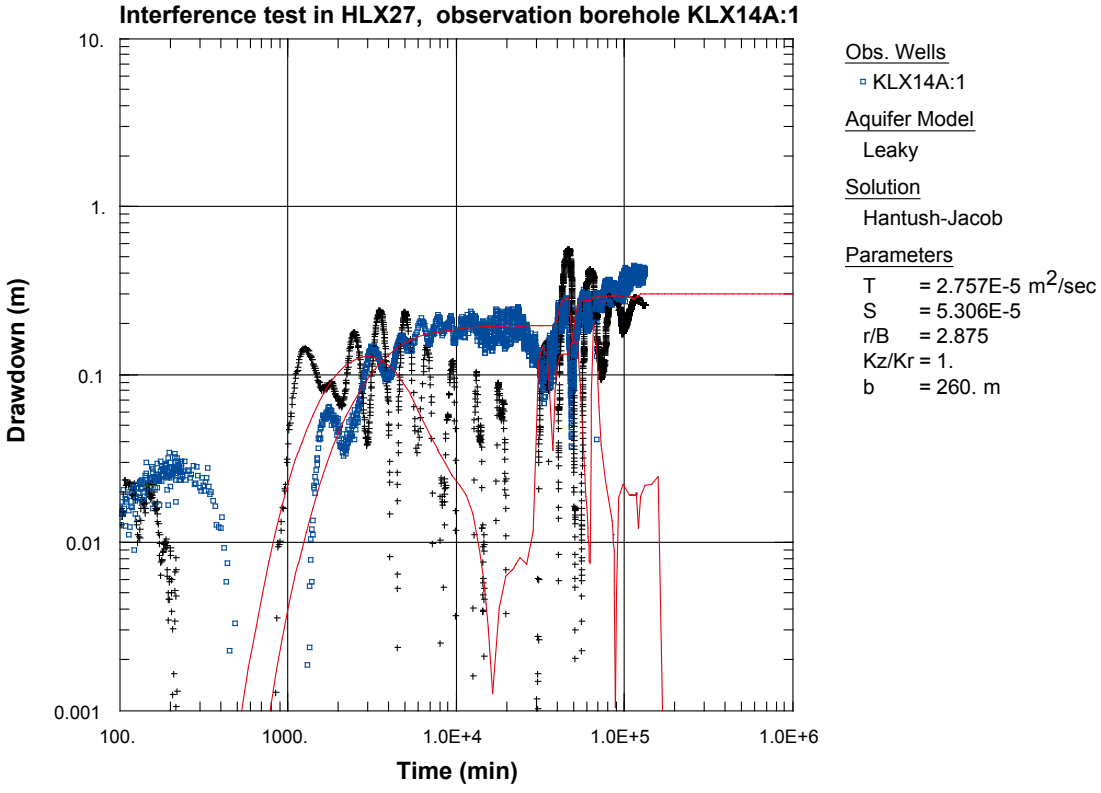

Figure A6-75. *Log-log plot of drawdown (▫) and drawdown derivative, ds/d(ln t) (+), versus time in KLX14A:1 during the interference test in HLX27. Transient evaluation is based on the first part of the drawdown period.*

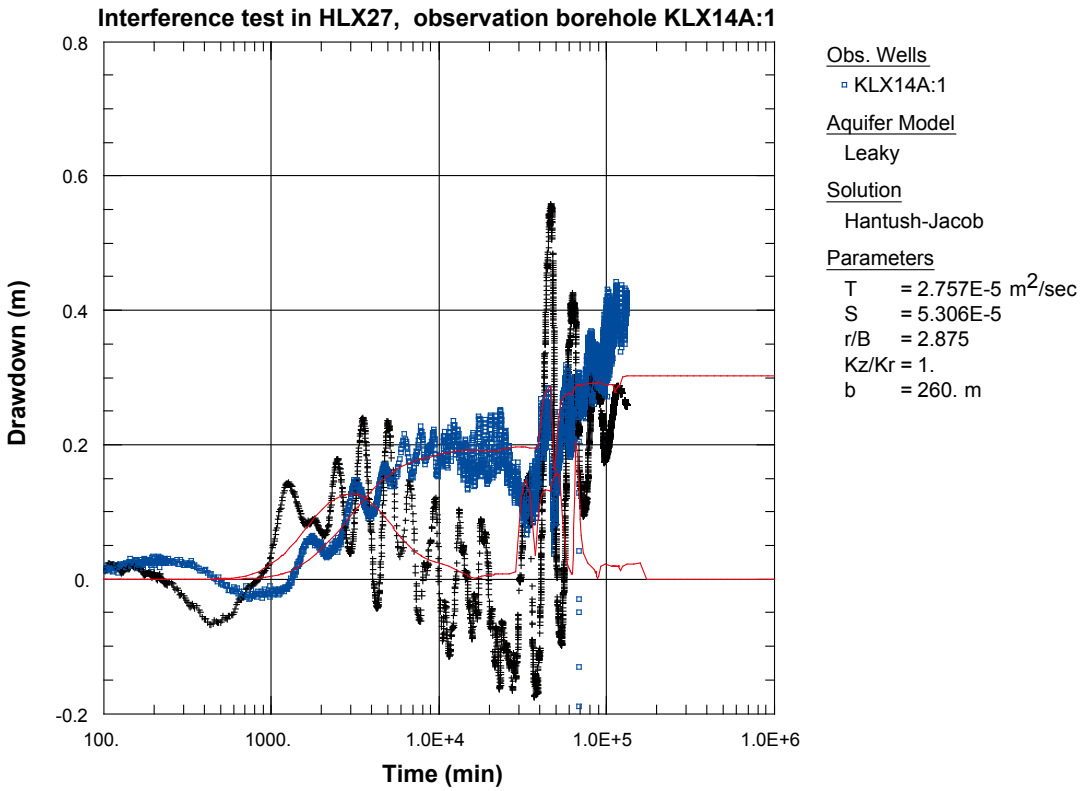

Figure A6-76. *Lin-log plot of drawdown (▫) and drawdown derivative, ds/d(ln t) (+), versus time in KLX14A:1 during the interference test in HLX27. Transient evaluation is based on the first part of the drawdown period.*

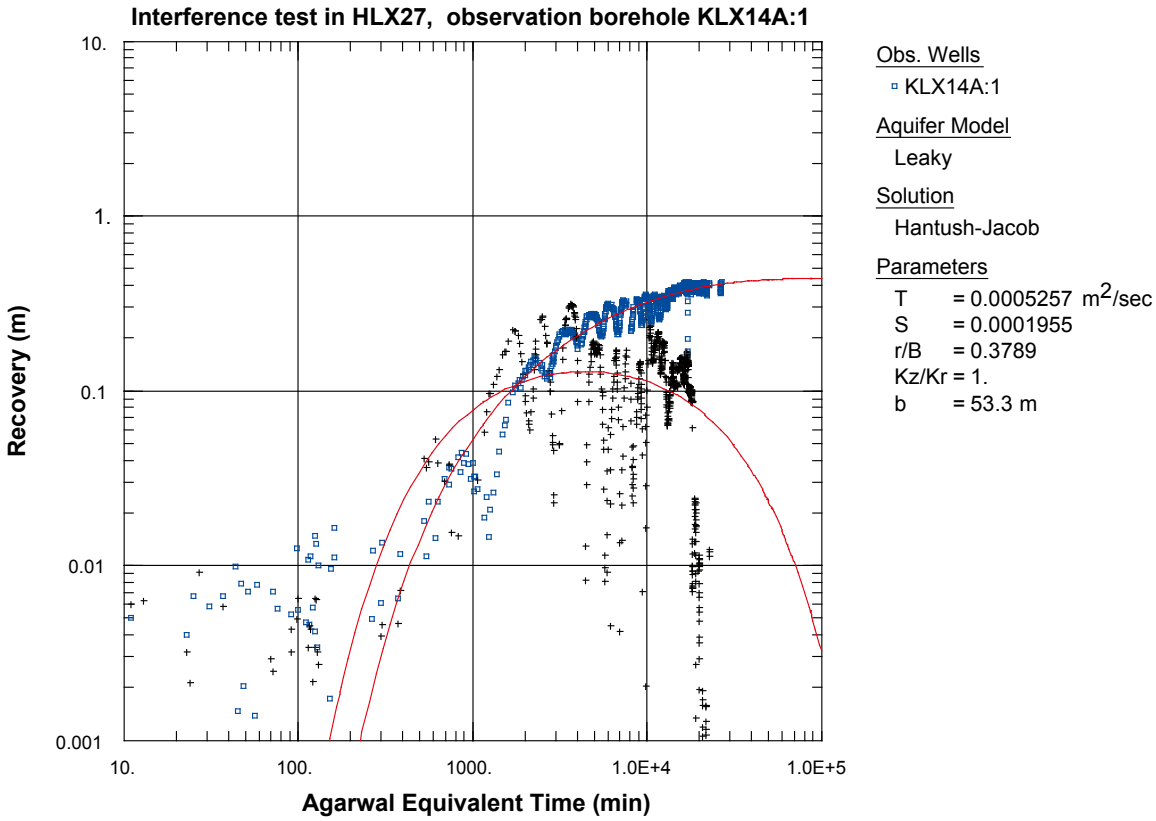

Figure A6-77. *Log-log plot of recovery (▫) and recovery derivative, ds/d(ln t) (+), versus time in KLX14A:1 during the interference test in HLX27.*

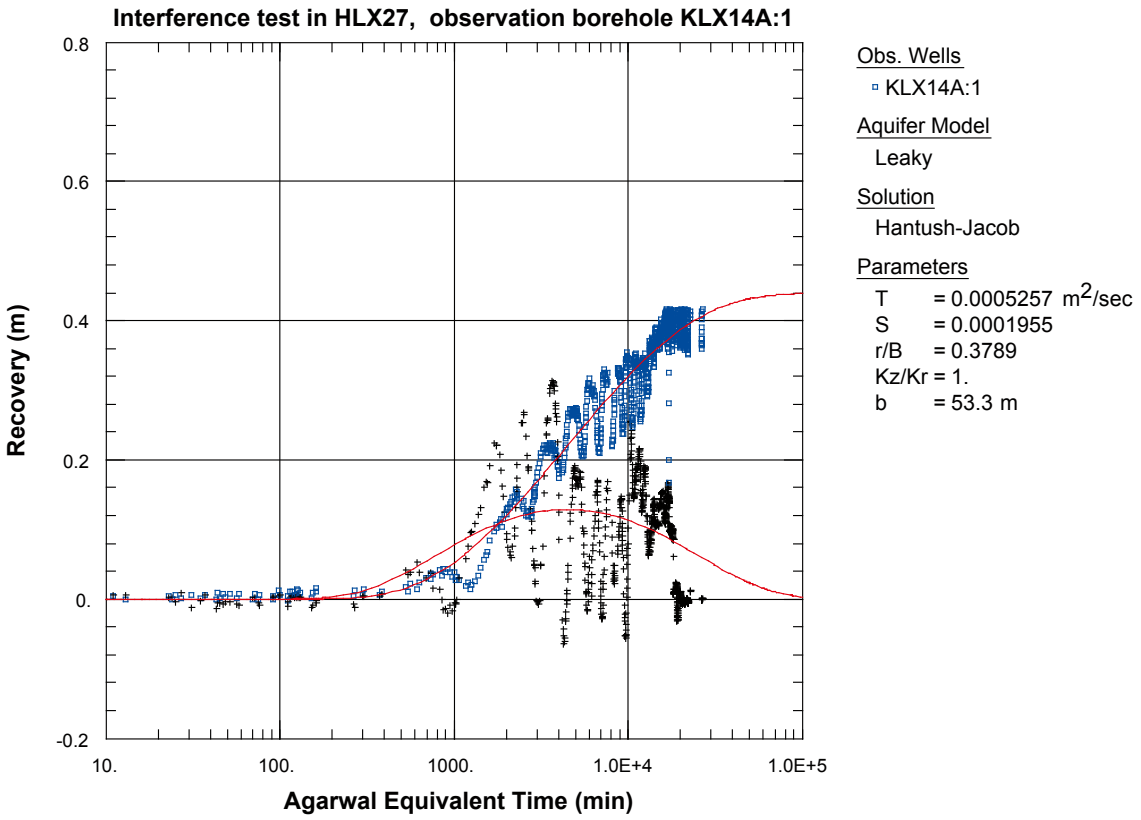

Figure A6-78. *Lin-log plot of recovery (▫) and recovery derivative, ds/d(ln t) (+), versus time in KLX14A:1 during the interference test in HLX27.*

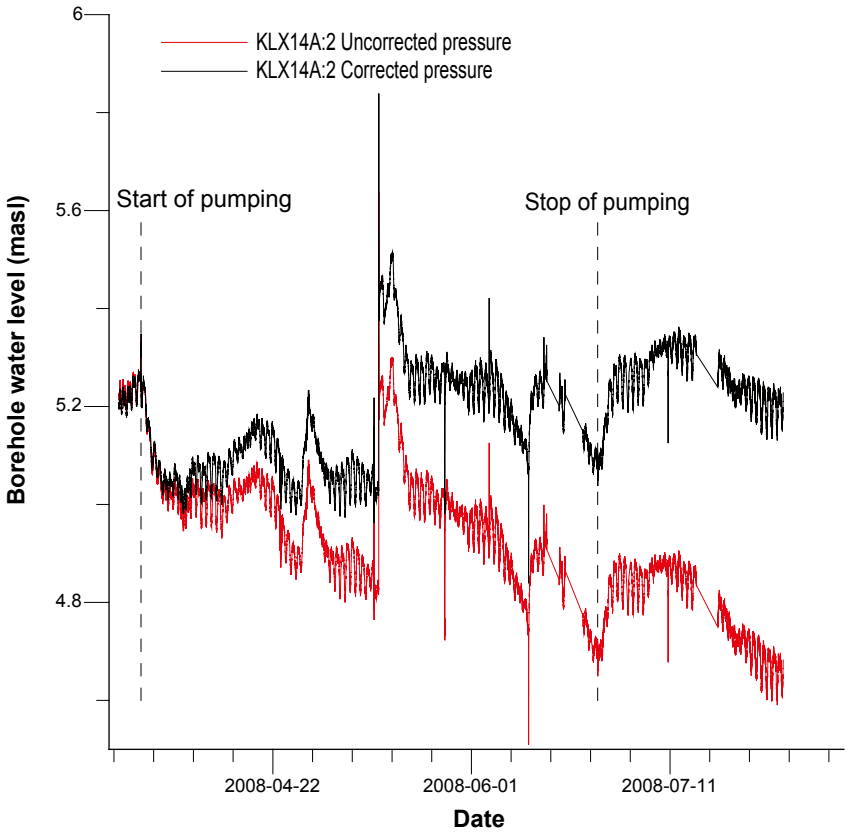

Figure A6-79. *Linear plot of pressure and pressure corrected for the natural decreasing pressure trend versus time in the observation section KLX14A:2 during pumping in HLX27.*

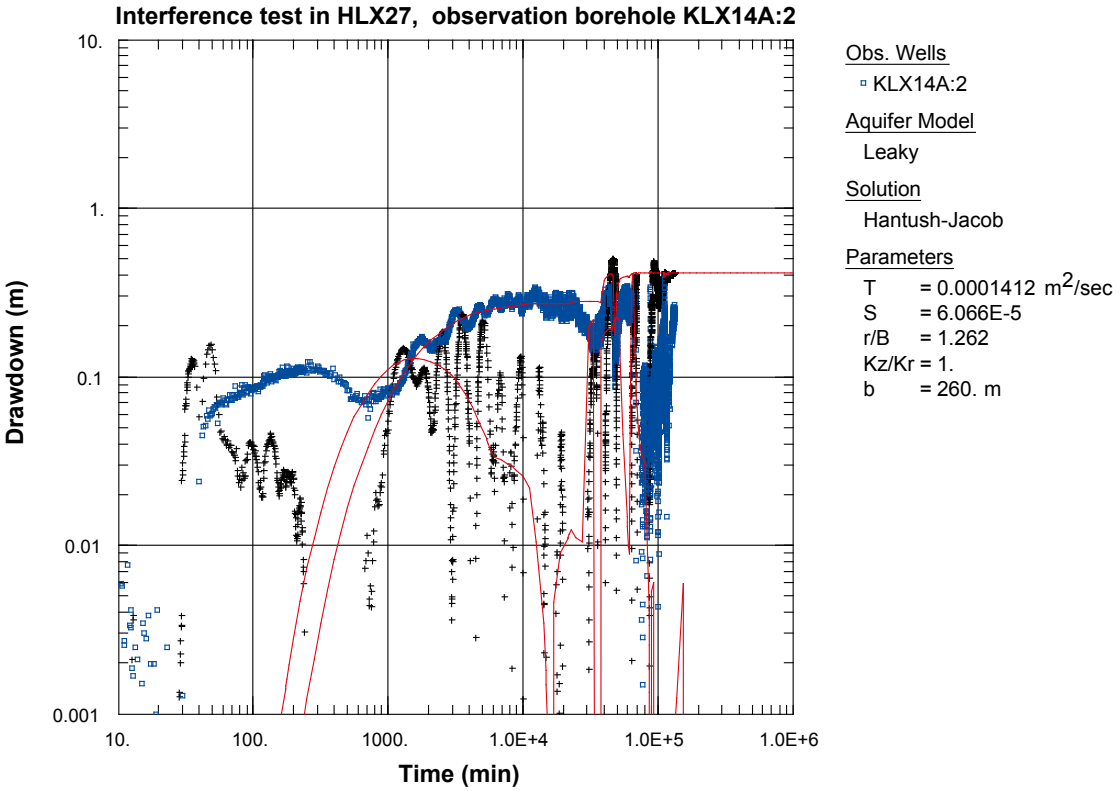

Figure A6-80. *Log-log plot of drawdown (▫) and drawdown derivative, ds/d(ln t) (+), versus time in KLX14A:2 during the interference test in HLX27. Transient evaluation is based on the first part of the drawdown period.*

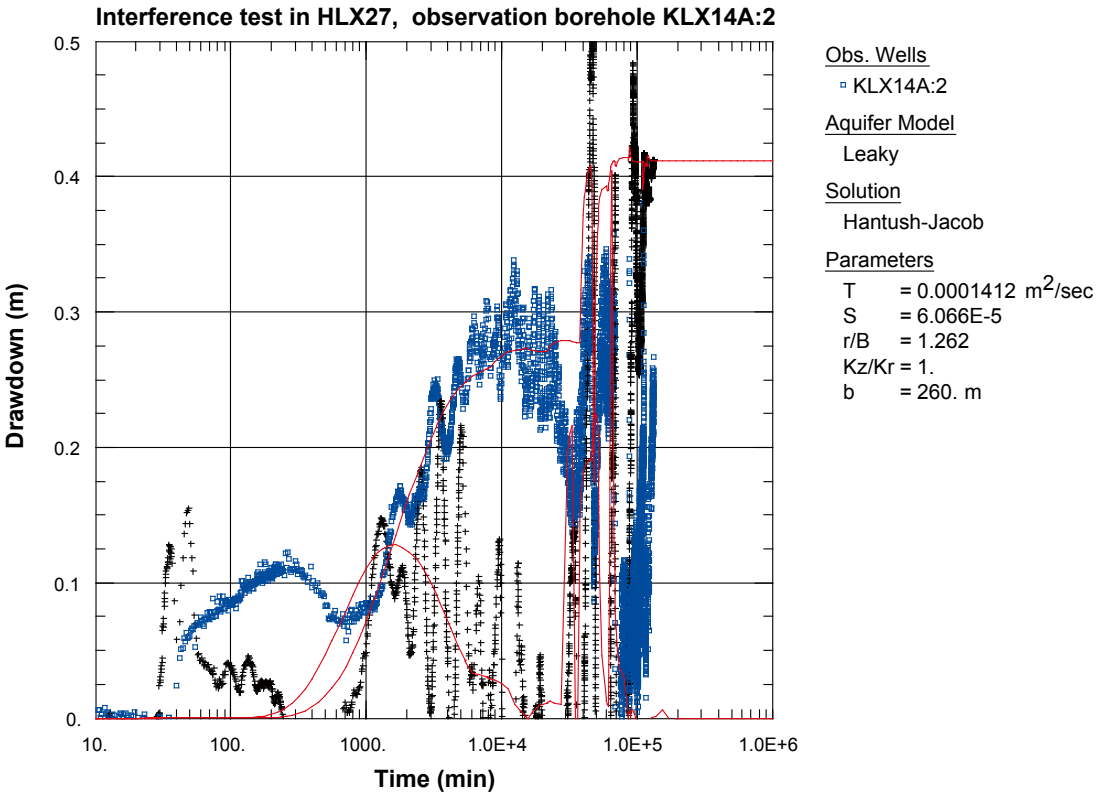

Figure A6-81. *Lin-log plot of drawdown (▫) and drawdown derivative, ds/d(ln t) (+), versus time in KLX14A:2 during the interference test in HLX27. Transient evaluation is based on the first part of the drawdown period.*

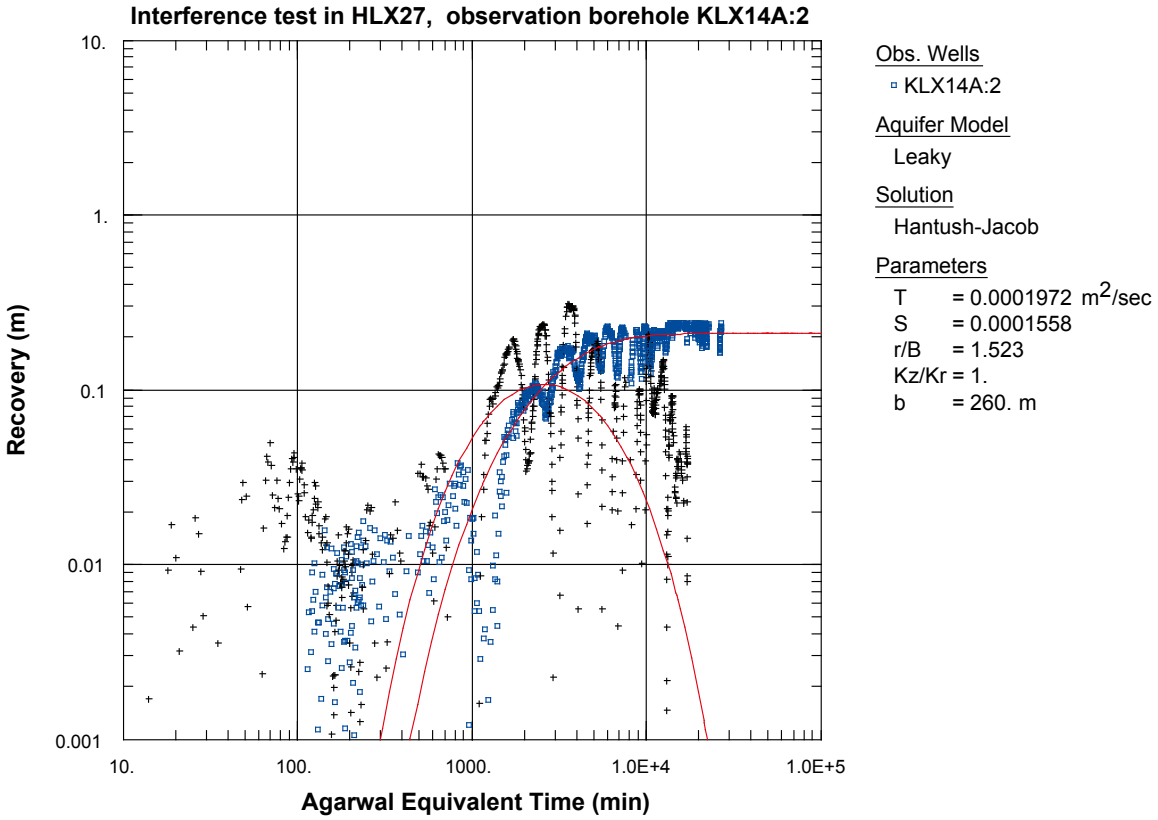

Figure A6-82. *Log-log plot of recovery (▫) and recovery derivative, ds/d(ln t) (+), versus time in KLX14A:2 during the interference test in HLX27.*

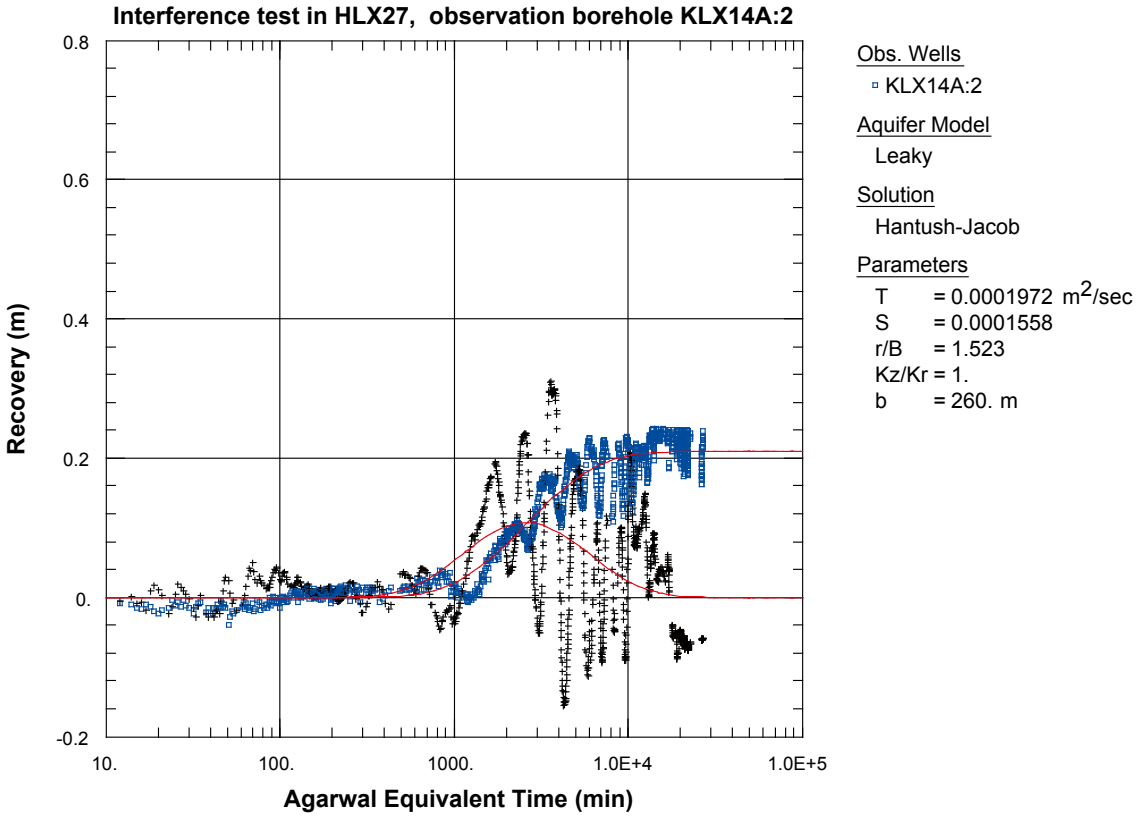

Figure A6-83. *Lin-log plot of recovery (▫) and recovery derivative, ds/d(ln t) (+), versus time in KLX14A:2 during the interference test in HLX27.*

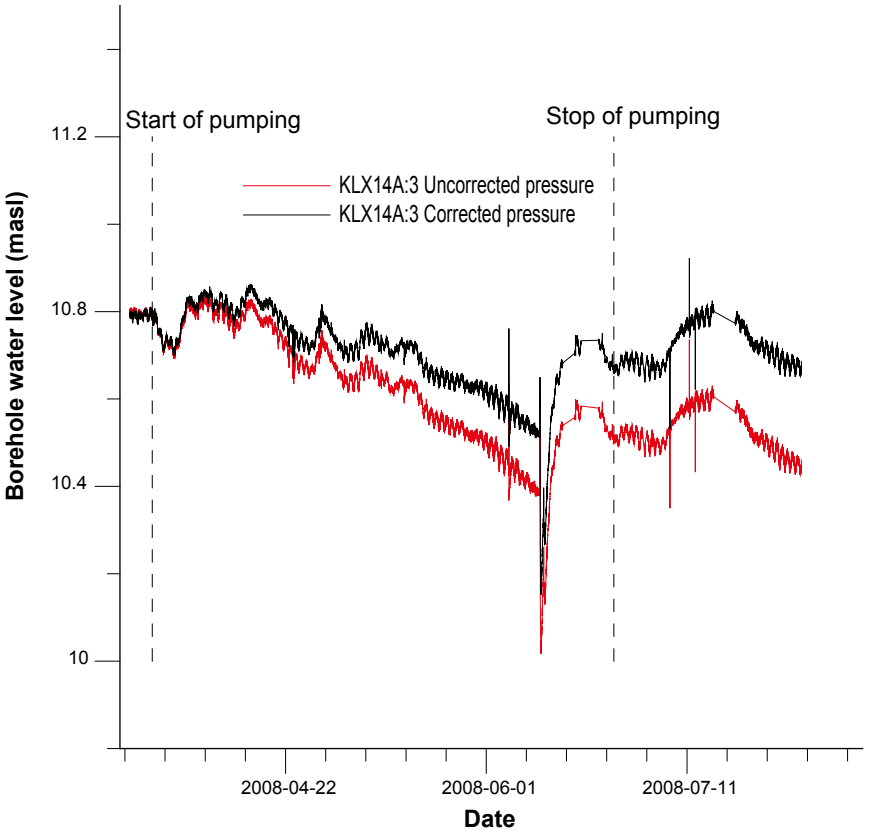

Figure A6-84. *Linear plot of pressure versus time in the observation sections in KLX14A:3 during pumping in HLX27.*

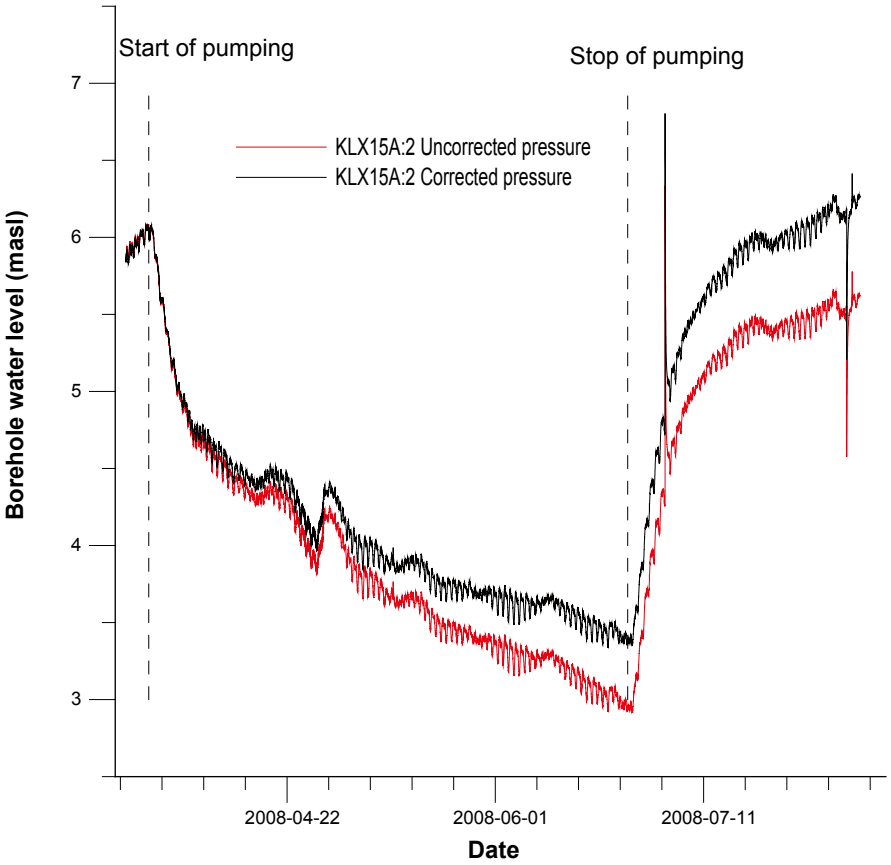

Figure A6-85. *Linear plot of pressure versus time in the observation sections in KLX15A:2 during pumping in HLX27.*

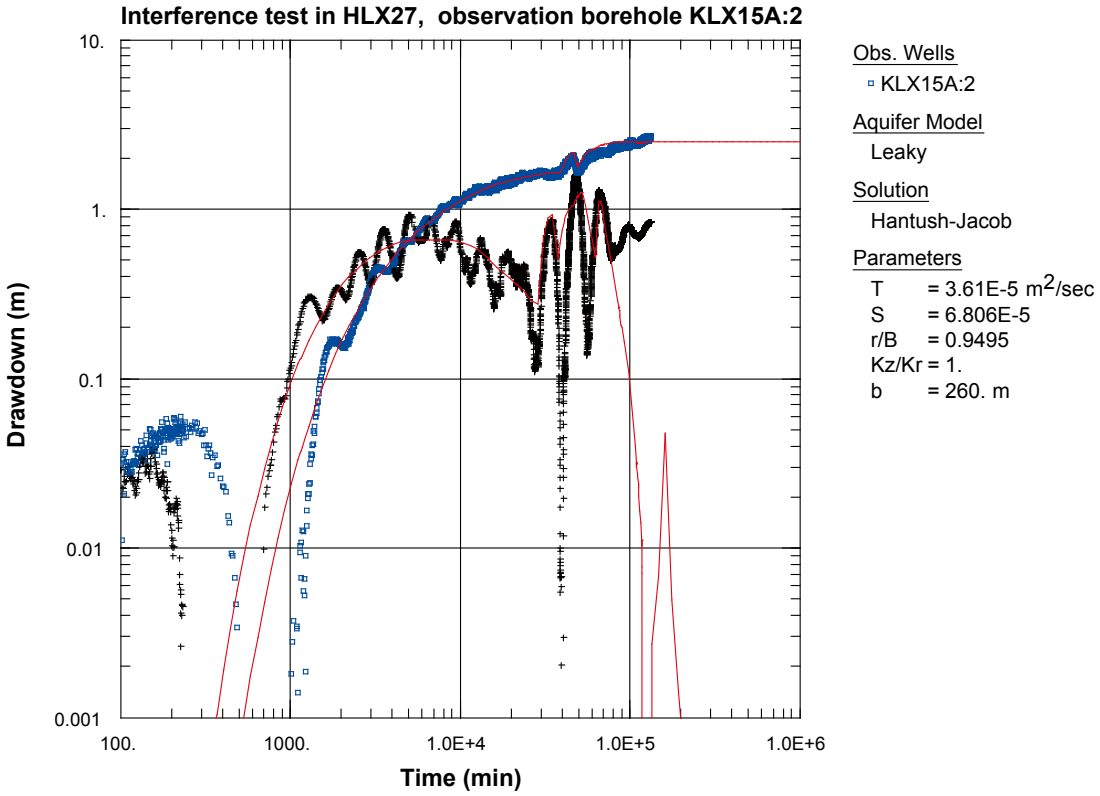

Figure A6-86. *Log-log plot of drawdown (▫) and drawdown derivative, ds/d(ln t) (+), versus time in KLX15A:2 during the interference test in HLX27. Transient evaluation is based on the first part of the drawdown period.*

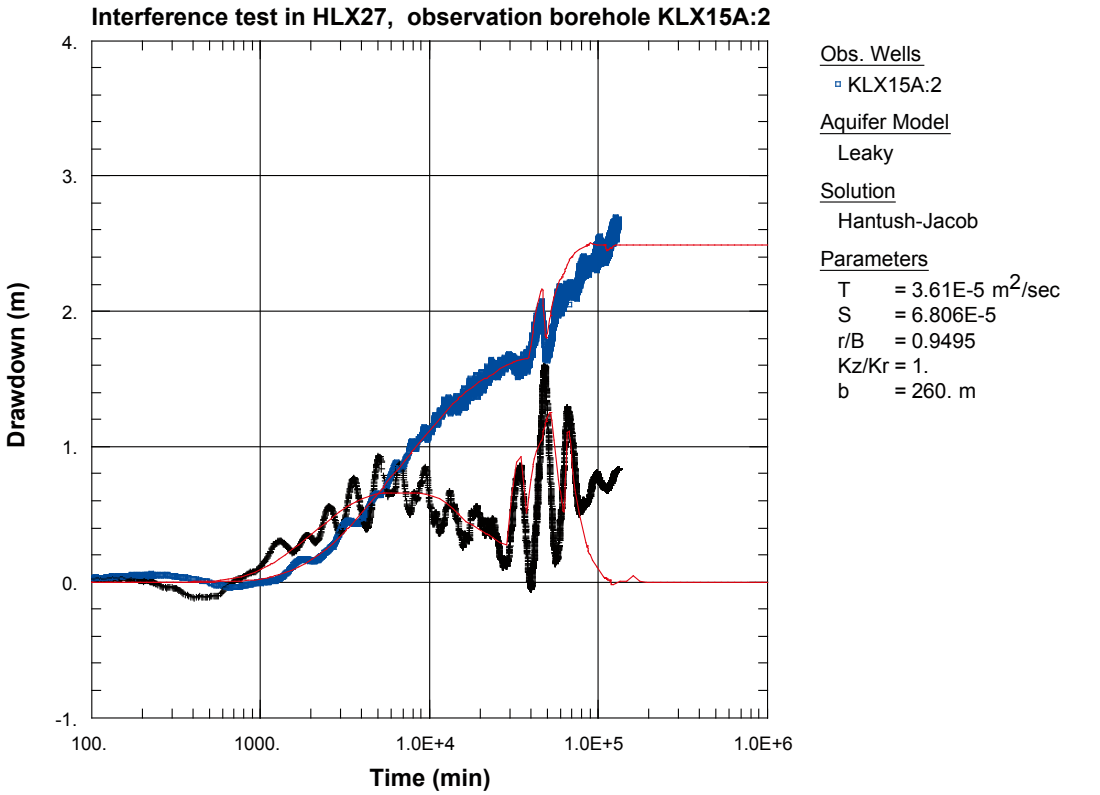

Figure A6-87. *Lin-log plot of drawdown (▫) and drawdown derivative, ds/d(ln t) (+), versus time in KLX15A:2 during the interference test in HLX27. Transient evaluation is based on the first part of the drawdown period.*

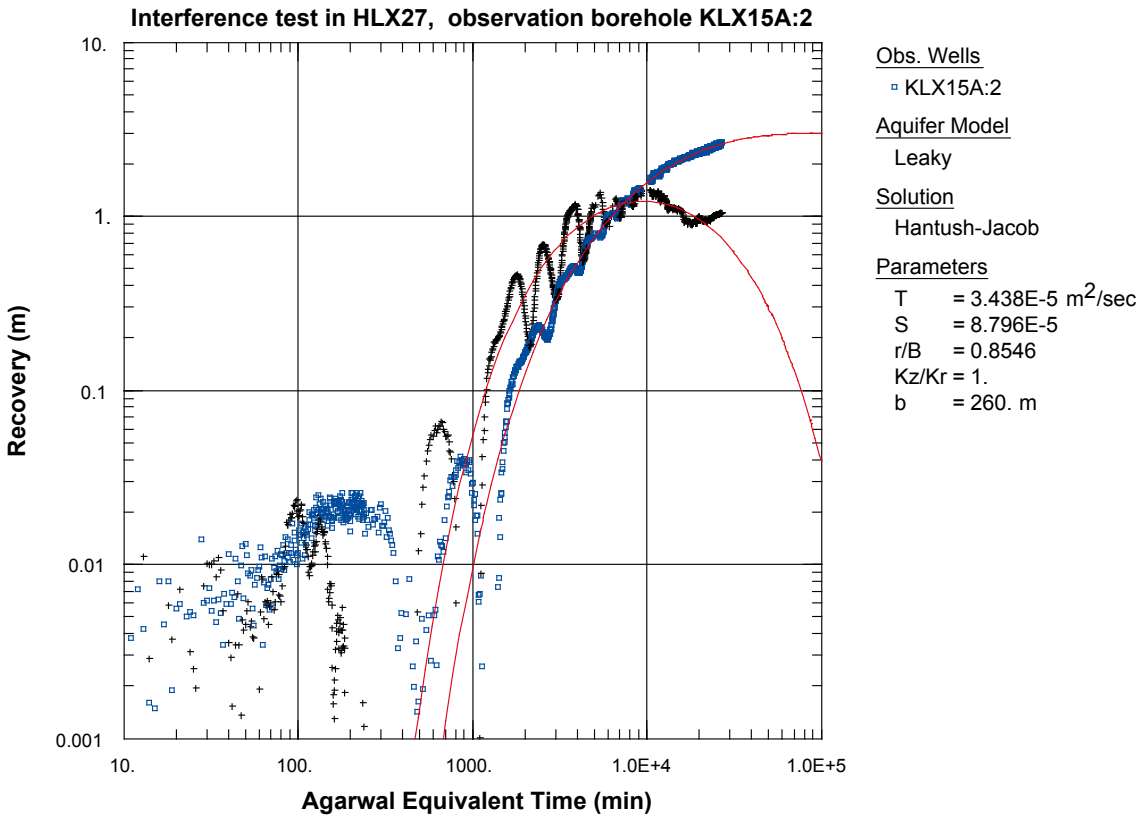

Figure A6-88. *Log-log plot of recovery (▫) and recovery derivative, ds/d(ln t) (+), versus time in KLX15A:2 during the interference test in HLX27.*

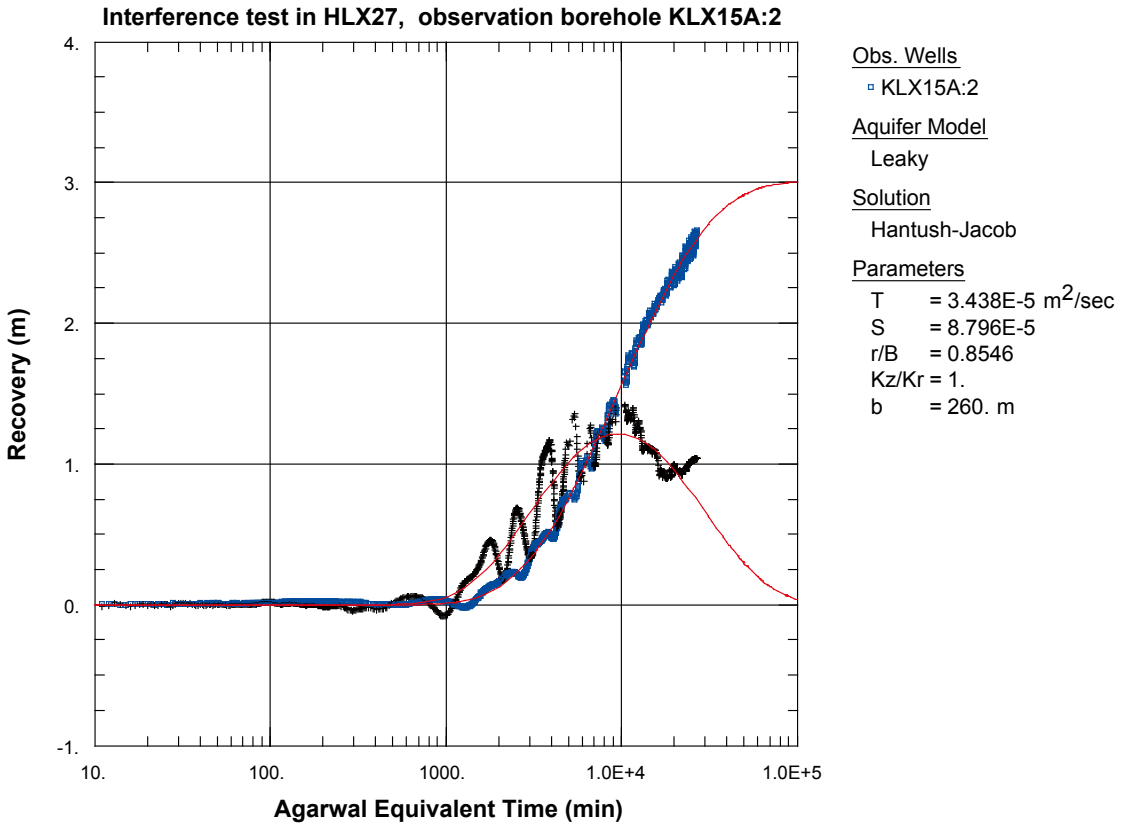

Figure A6-89. *Lin-log plot of recovery (▫) and recovery derivative, ds/d(ln t) (+), versus time in KLX15A:2 during the interference test in HLX27.*

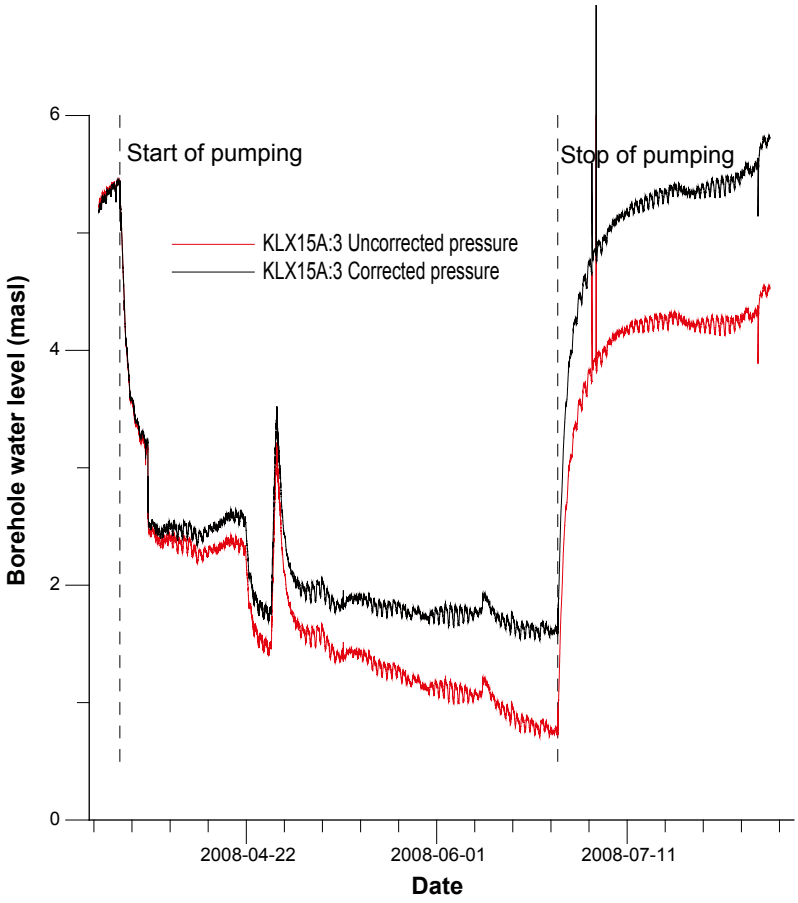

Figure A6-90. *Linear plot of pressure versus time in the observation sections in KLX15A:3 during pumping in HLX27.*

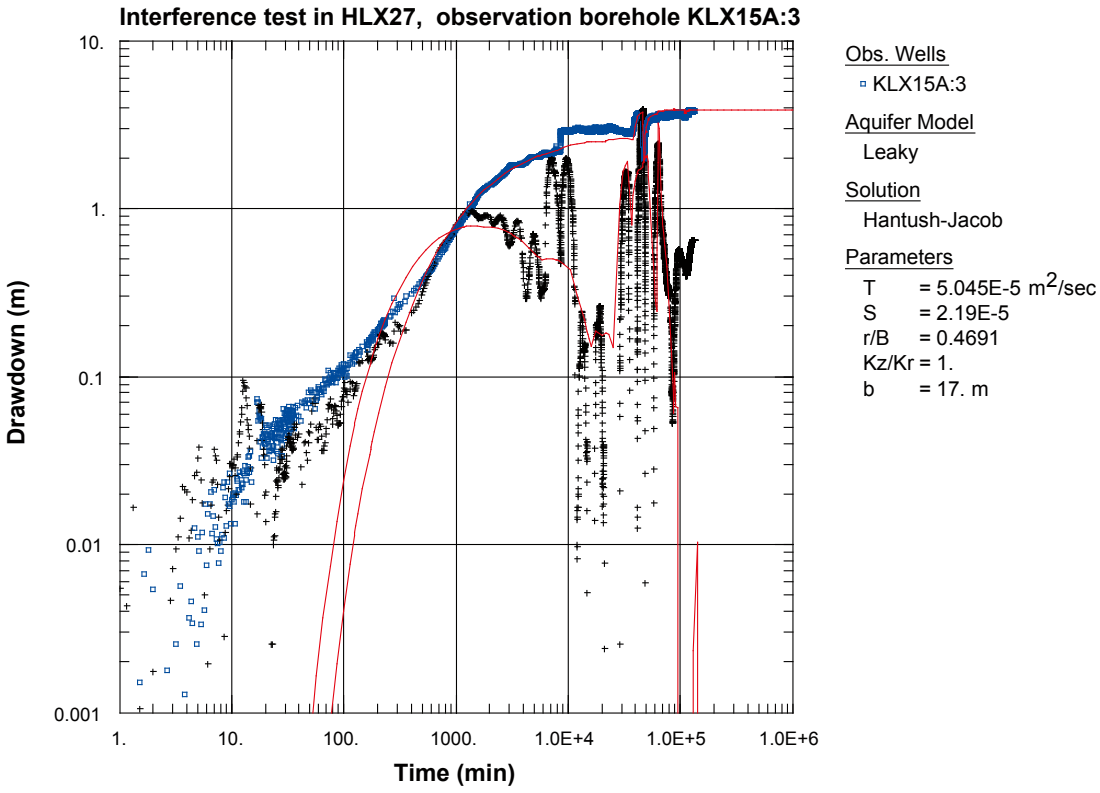

Figure A6-91. *Log-log plot of drawdown (▫) and drawdown derivative, ds/d(ln t) (+), versus time in KLX15A:3 during the interference test in HLX27. Transient evaluation is based on the first part of the drawdown period.*

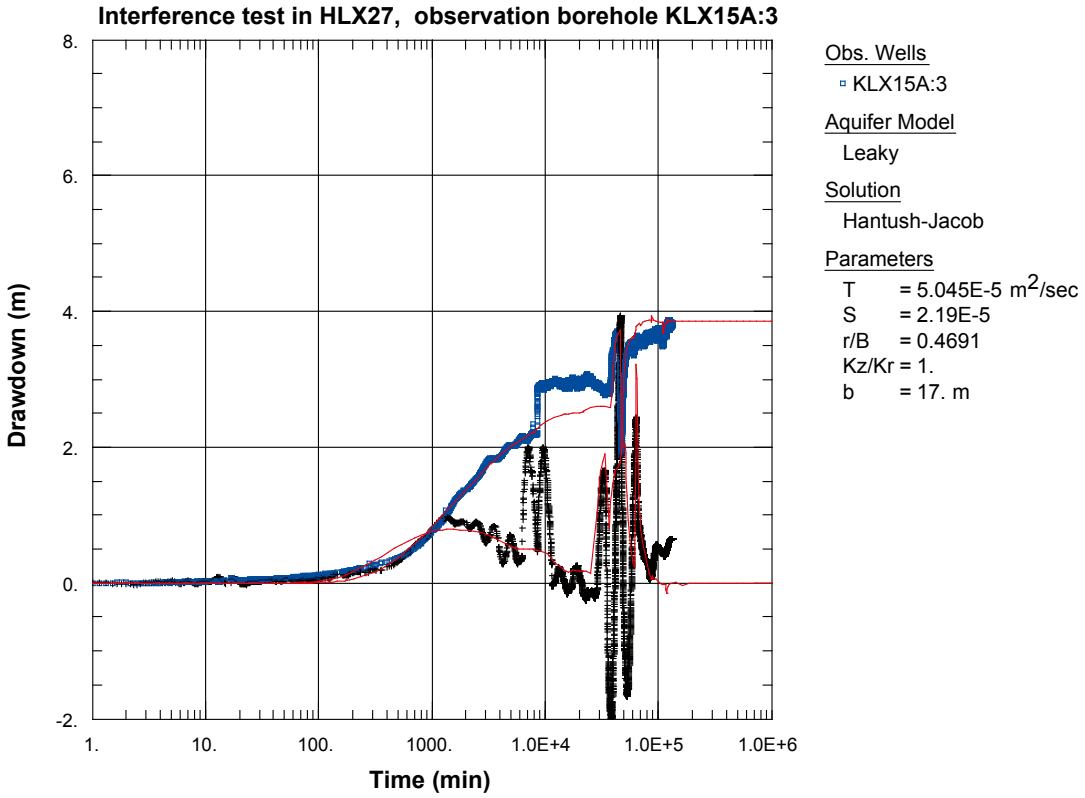

Figure A6-92. *Lin-log plot of drawdown (▫) and drawdown derivative, ds/d(ln t) (+), versus time in KLX15A:3 during the interference test in HLX27. Transient evaluation is based on the first part of the drawdown period.*

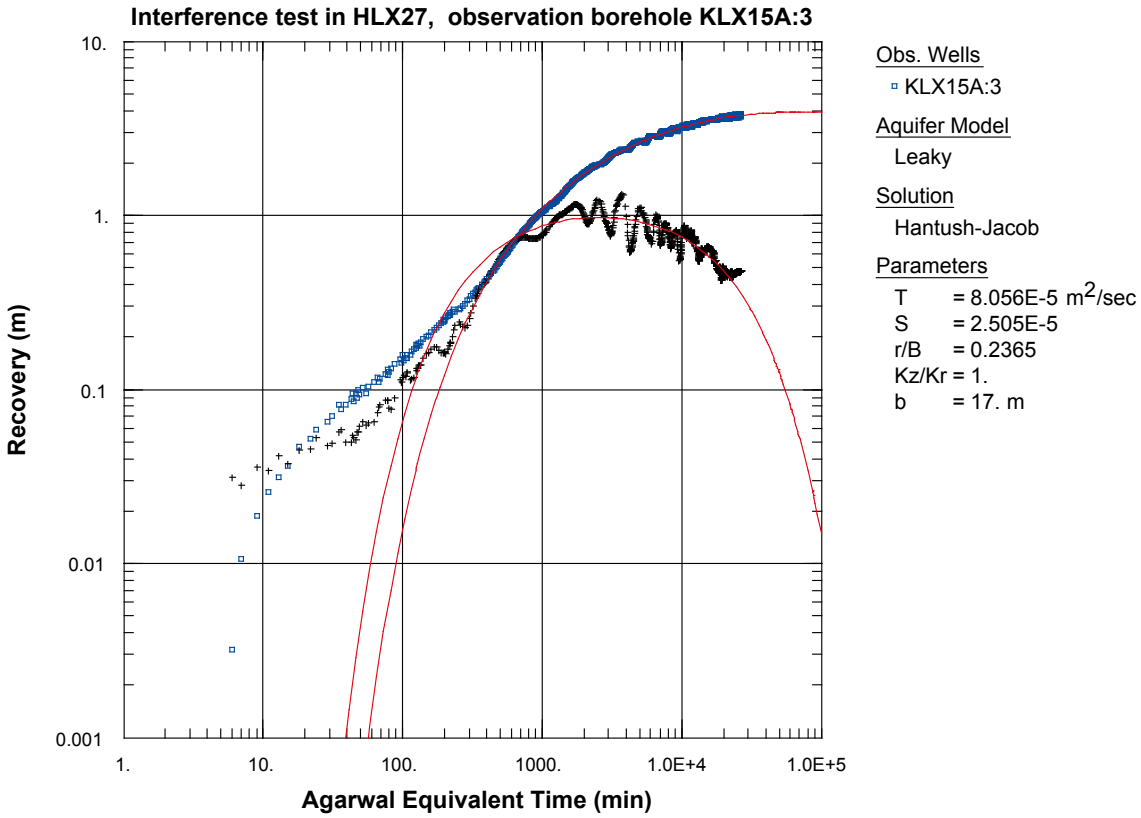

Figure A6-93. *Log-log plot of recovery (▫) and recovery derivative, ds/d(ln t) (+), versus time in KLX15A:3 during the interference test in HLX27.*

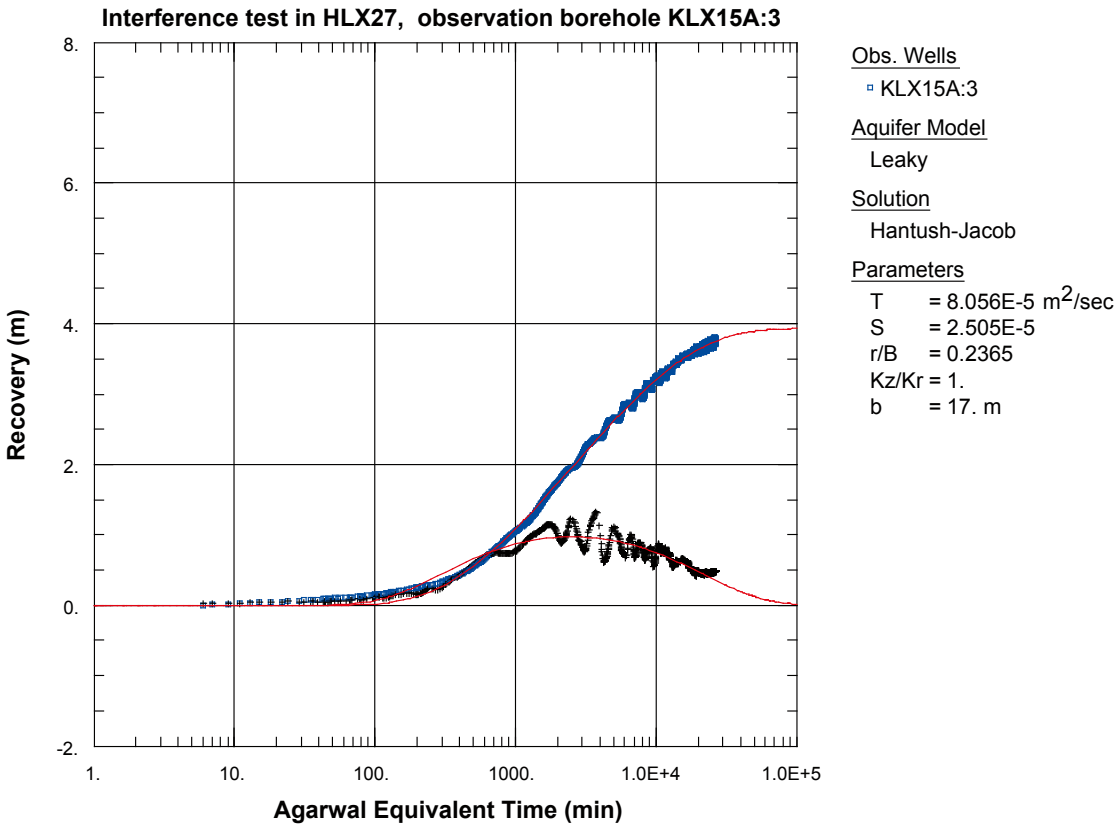

Figure A6-94. *Lin-log plot of recovery (▫) and recovery derivative, ds/d(ln t) (+), versus time in KLX15A:3 during the interference test in HLX27.*

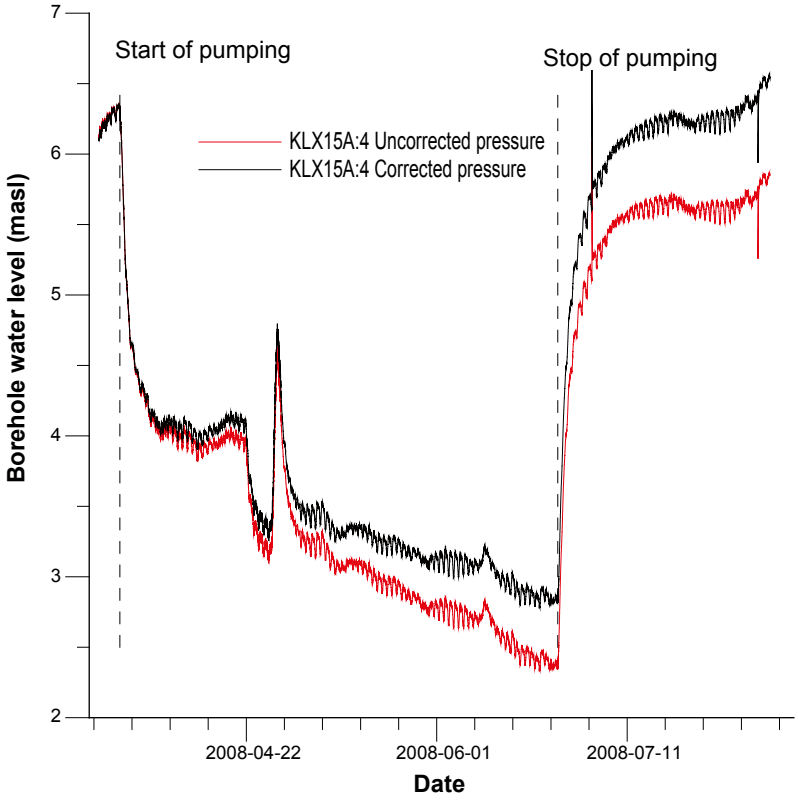

Figure A6-95. *Linear plot of pressure versus time in the observation sections in KLX15A:4 during pumping in HLX27.*

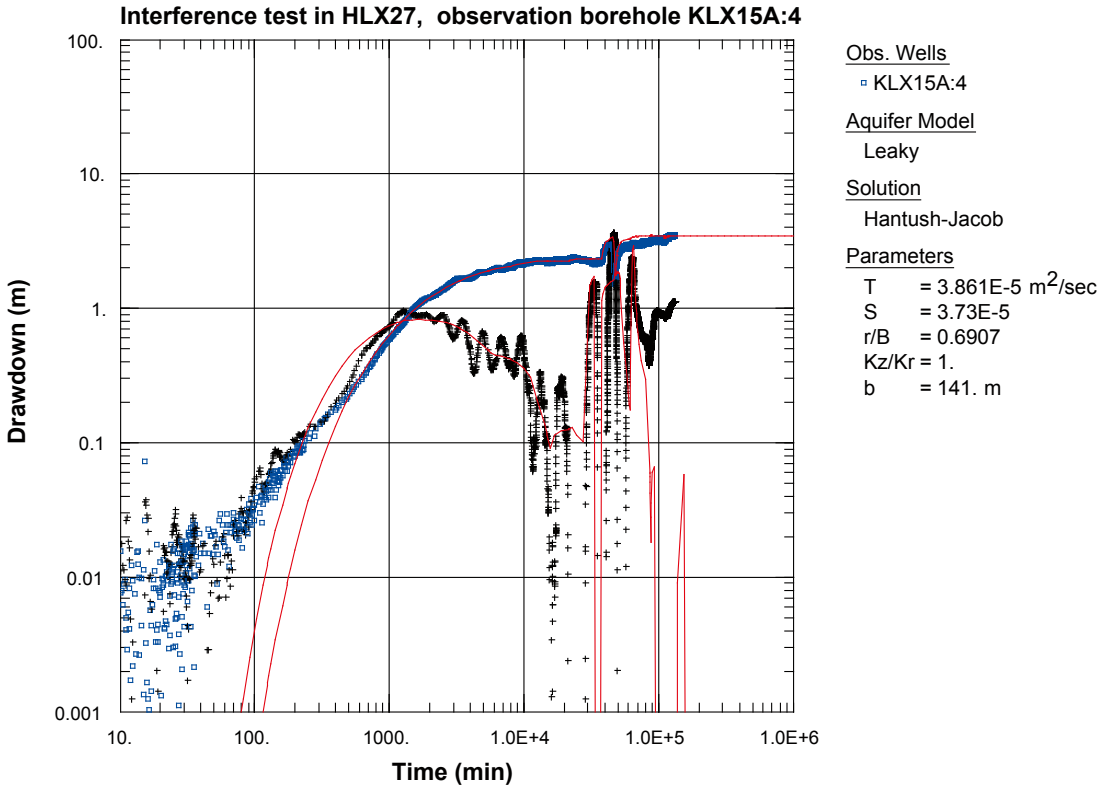

Figure A6-96. *Log-log plot of drawdown (▫) and drawdown derivative, ds/d(ln t) (+), versus time in KLX15A:4 during the interference test in HLX27. Transient evaluation is based on the first part of the drawdown period.*

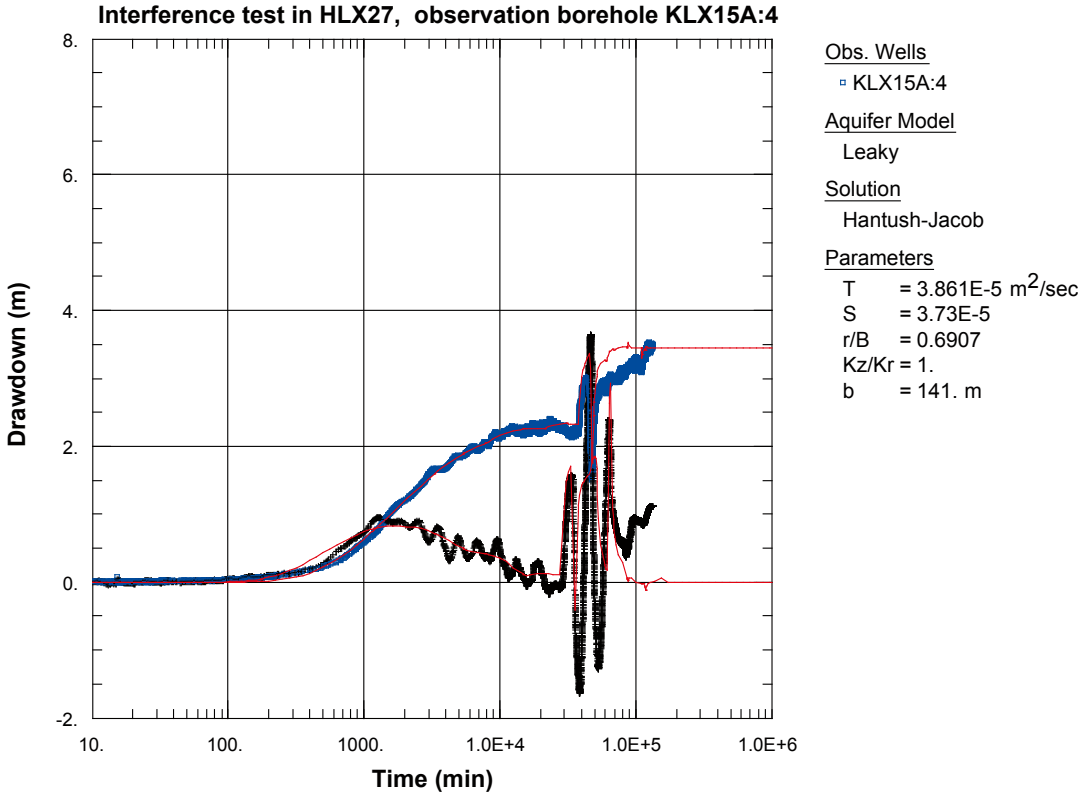

Figure A6-97. *Lin-log plot of drawdown (▫) and drawdown derivative, ds/d(ln t) (+), versus time in KLX15A:4 during the interference test in HLX27. Transient evaluation is based on the first part of the drawdown period.*

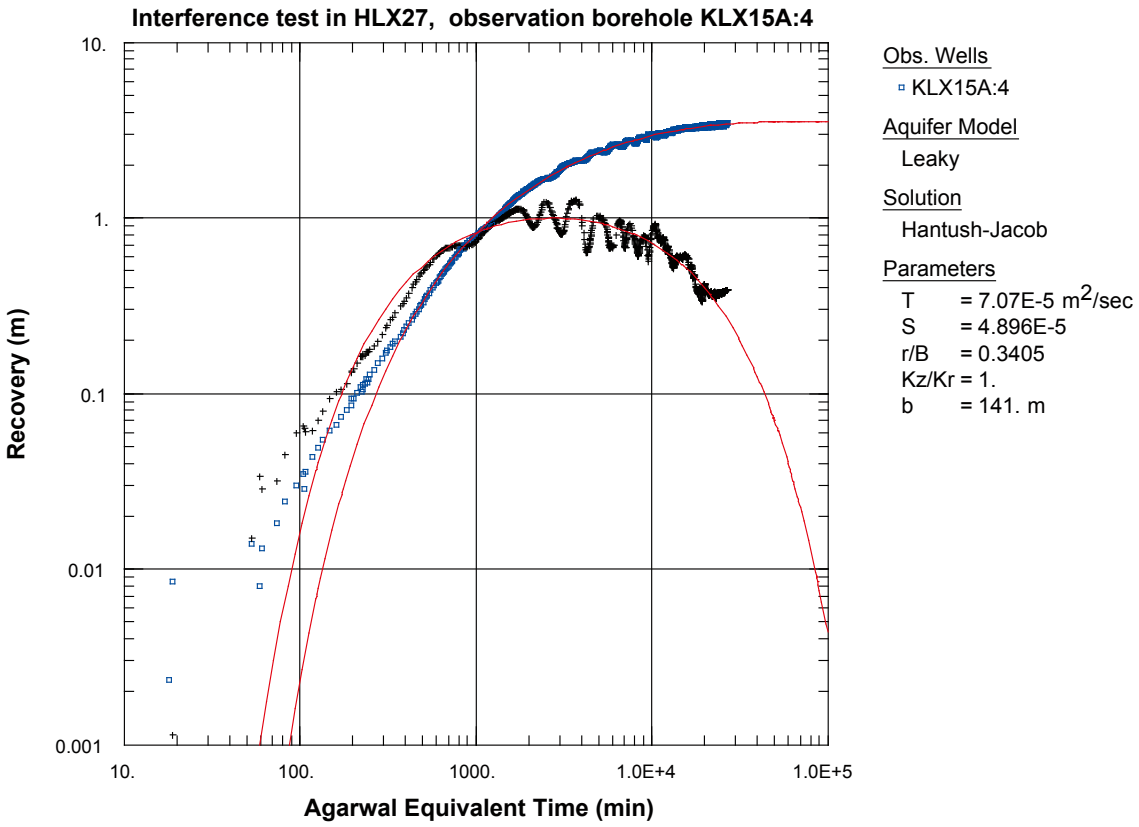

Figure A6-98. *Log-log plot of recovery (▫) and recovery derivative, ds/d(ln t) (+), versus time in KLX15A:4 during the interference test in HLX27.*

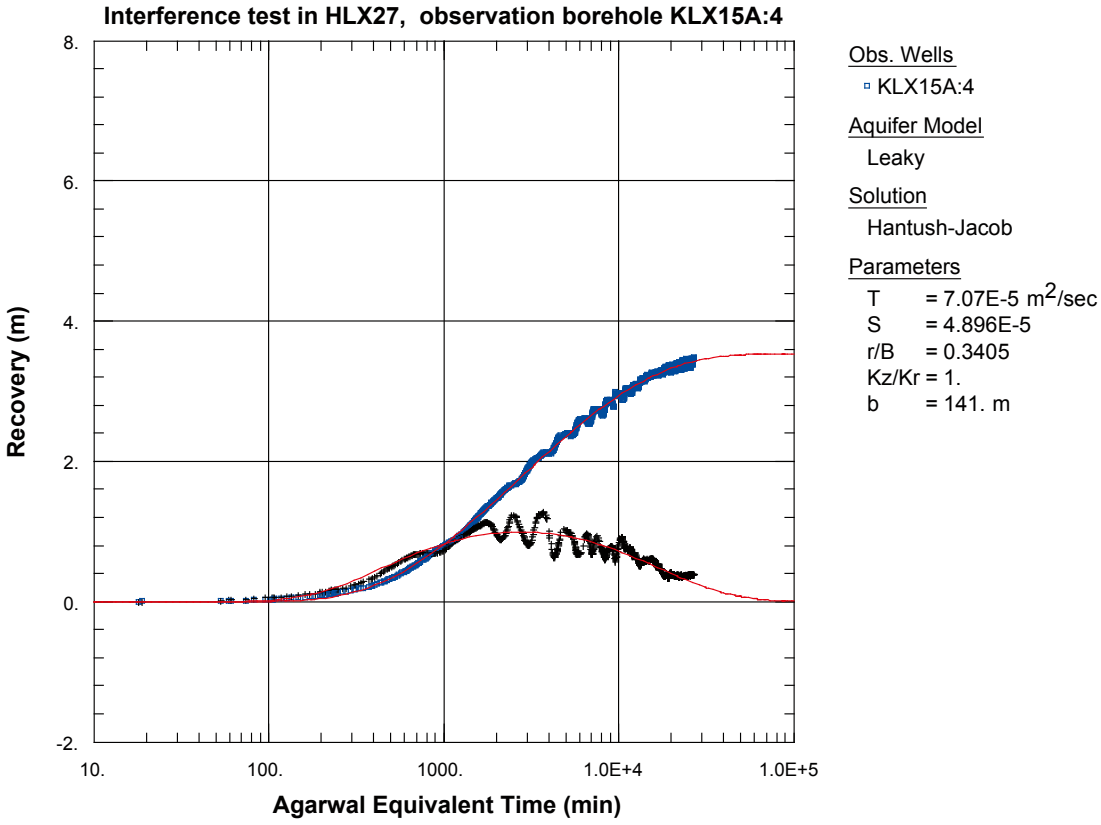

Figure A6-99. *Lin-log plot of recovery (▫) and recovery derivative, ds/d(ln t) (+), versus time in KLX15A:4 during the interference test in HLX27.*

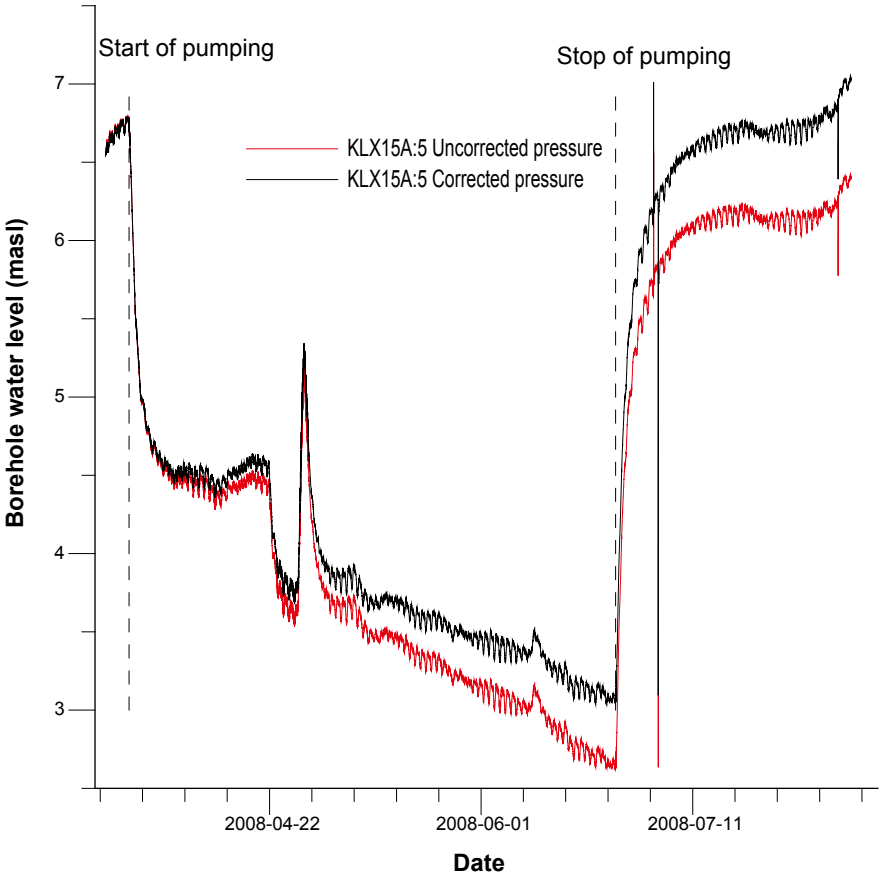

Figure A6-100. *Linear plot of pressure versus time in the observation sections in KLX15:5 during pumping in HLX27.*

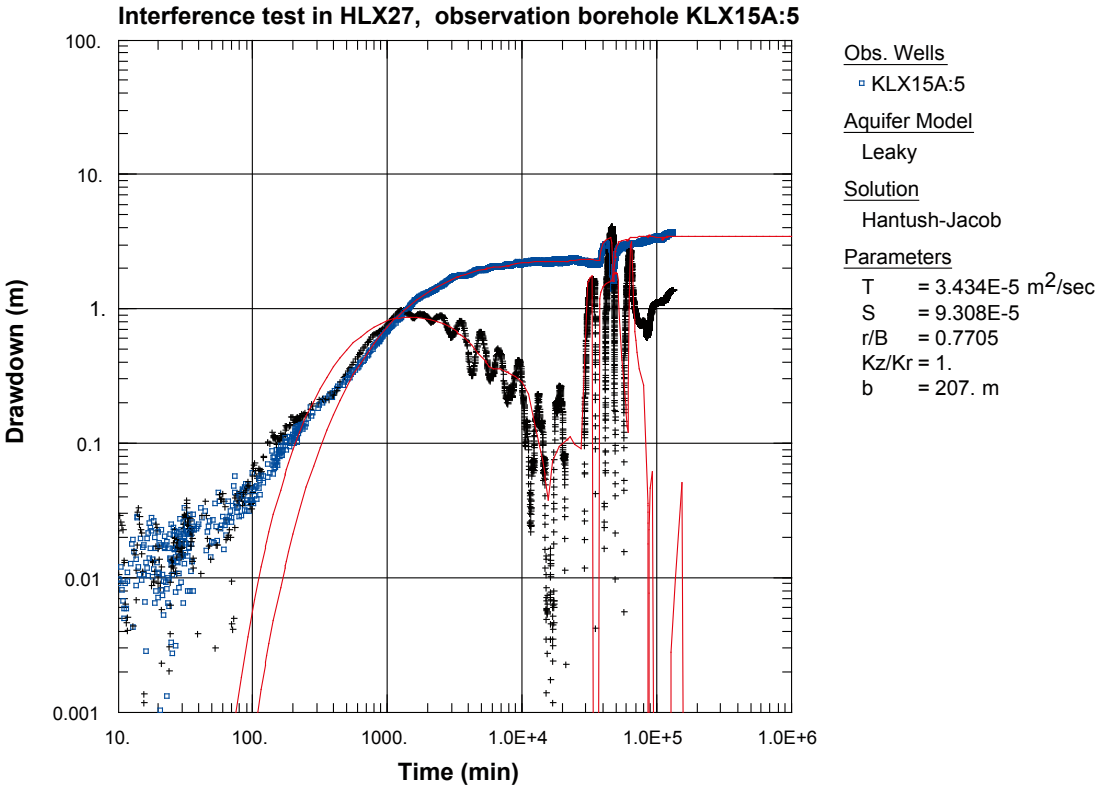

Figure A6-101. *Log-log plot of drawdown (▫) and drawdown derivative, ds/d(ln t) (+), versus time in KLX15A:5 during the interference test in HLX27. Transient evaluation is based on the first part of the drawdown period.*

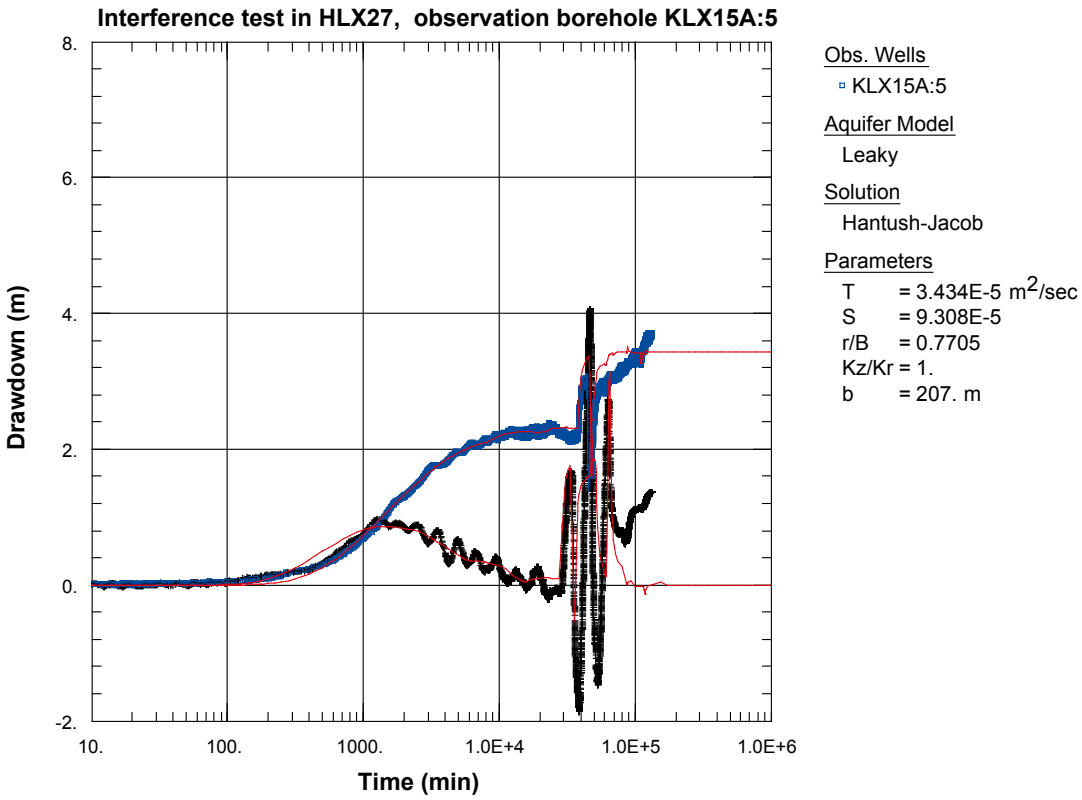

Figure A6-102. *Lin-log plot of drawdown (▫) and drawdown derivative, ds/d(ln t) (+), versus time in KLX15A:5 during the interference test in HLX27. Transient evaluation is based on the first part of the drawdown period.*

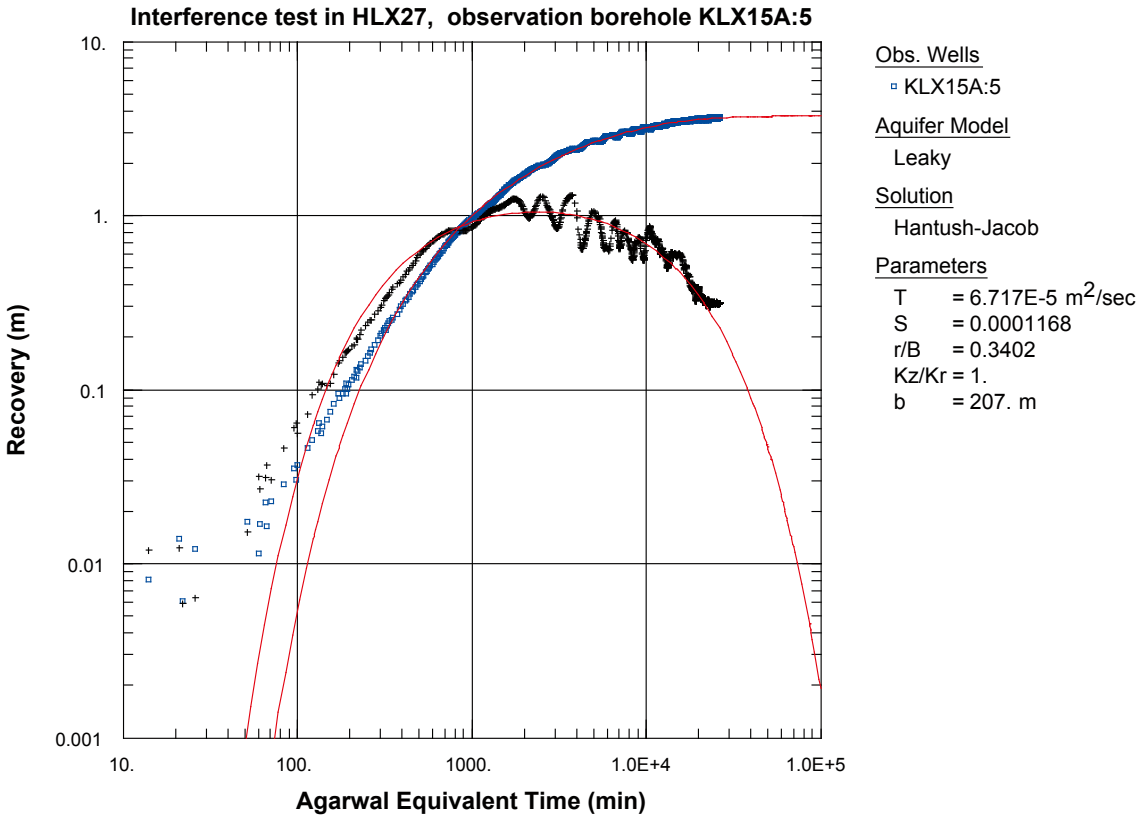

Figure A6-103. *Log-log plot of recovery (▫) and recovery derivative, ds/d(ln t) (+), versus time in KLX15A:5 during the interference test in HLX27.*

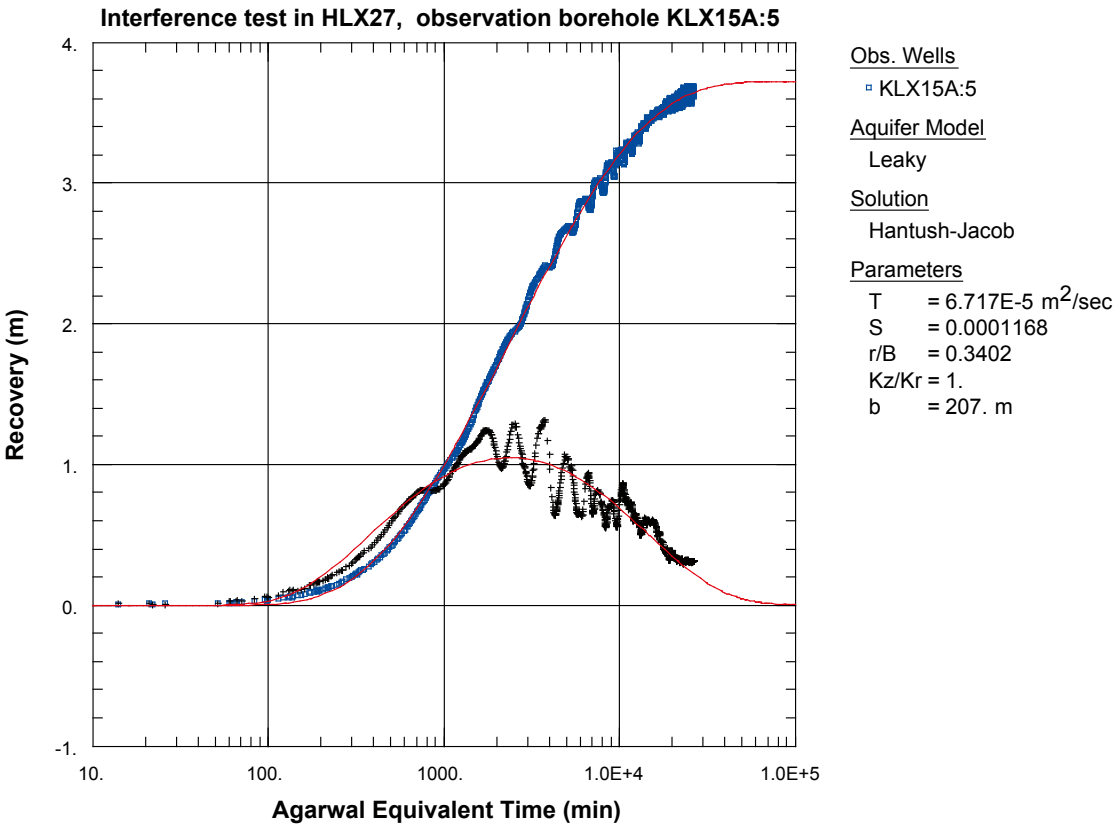

Figure A6-104. *Lin-log plot of recovery (▫) and recovery derivative, ds/d(ln t) (+), versus time in KLX15A:5 during the interference test in HLX27.*

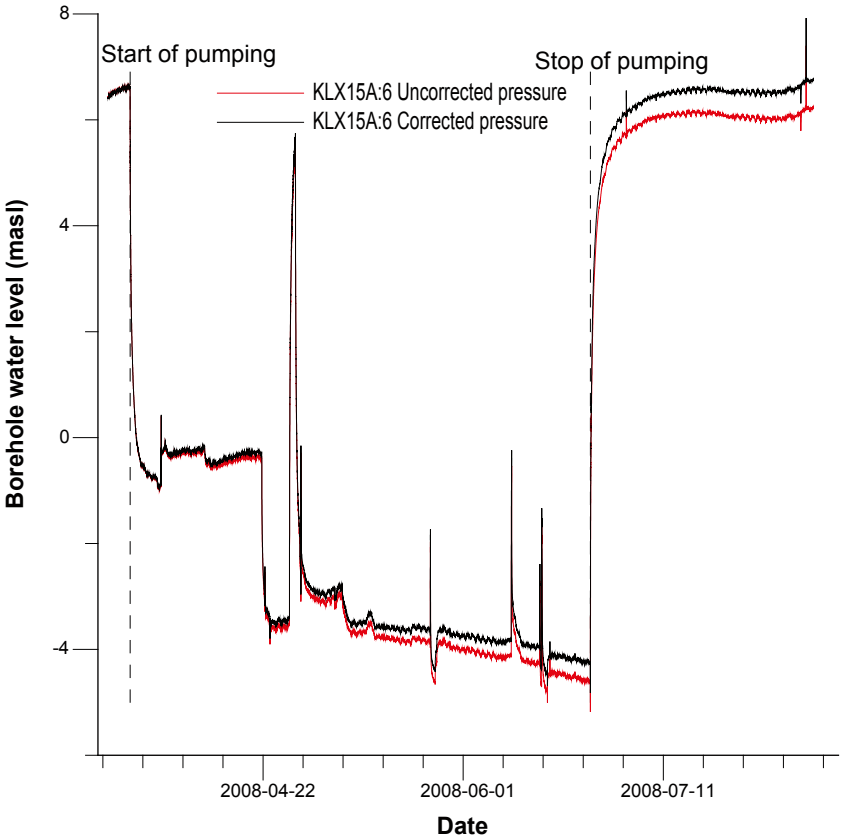

Figure A6-105. *Linear plot of pressure versus time in the observation sections in KLX15A:6 during pumping in HLX27.*

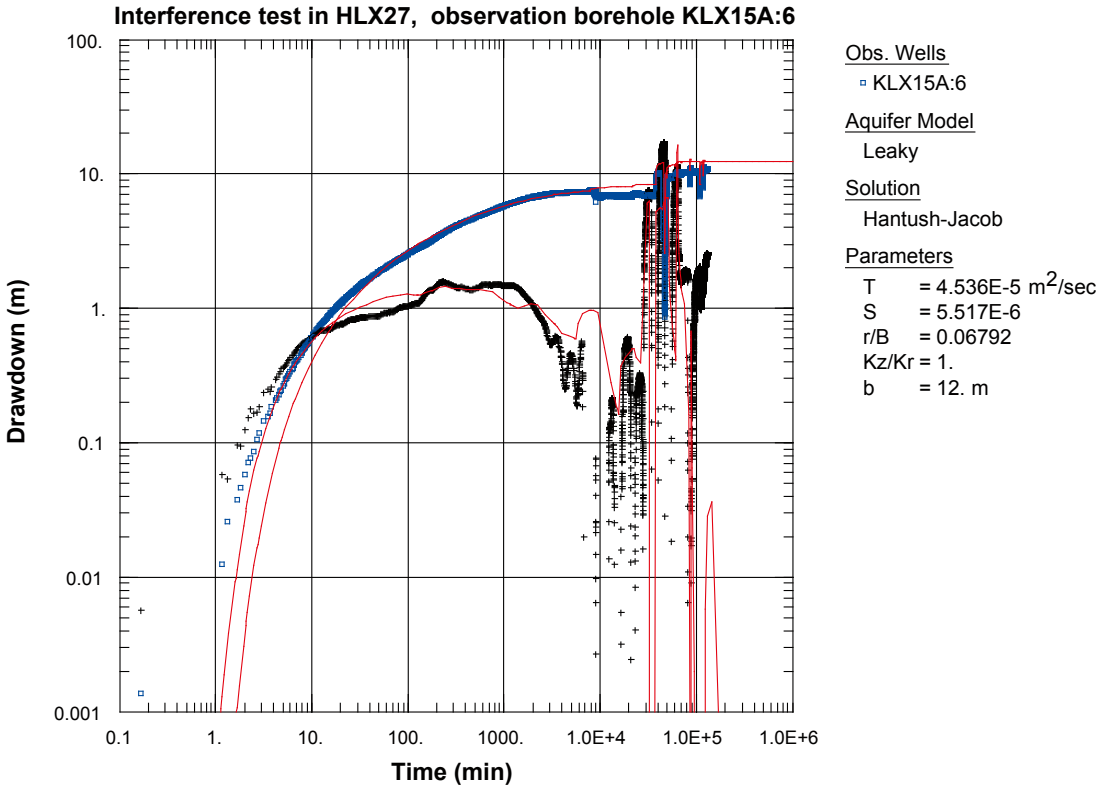

Figure A6-106. *Log-log plot of drawdown (▫) and drawdown derivative, ds/d(ln t) (+), versus time in KLX15A:6 during the interference test in HLX27. Transient evaluation is based on the first part of the drawdown period.*

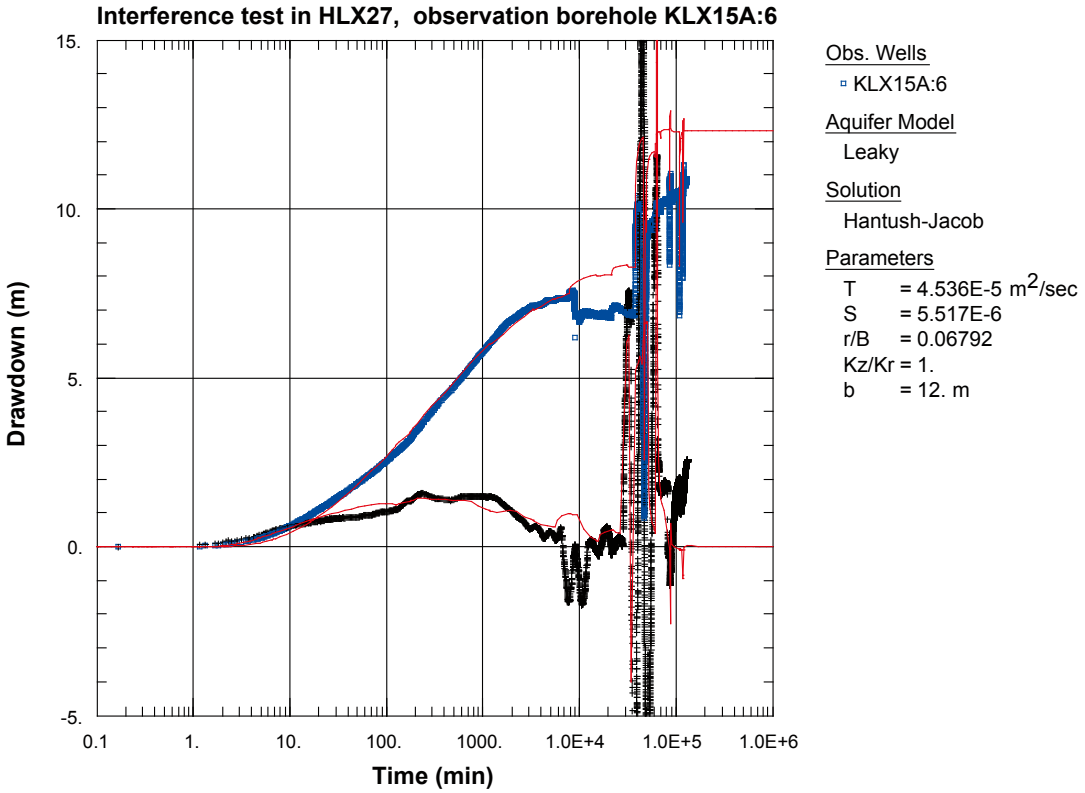

Figure A6-107. *Lin-log plot of drawdown (▫) and drawdown derivative, ds/d(ln t) (+), versus time in KLX15A:6 during the interference test in HLX27. Transient evaluation is based on the first part of the drawdown period.*

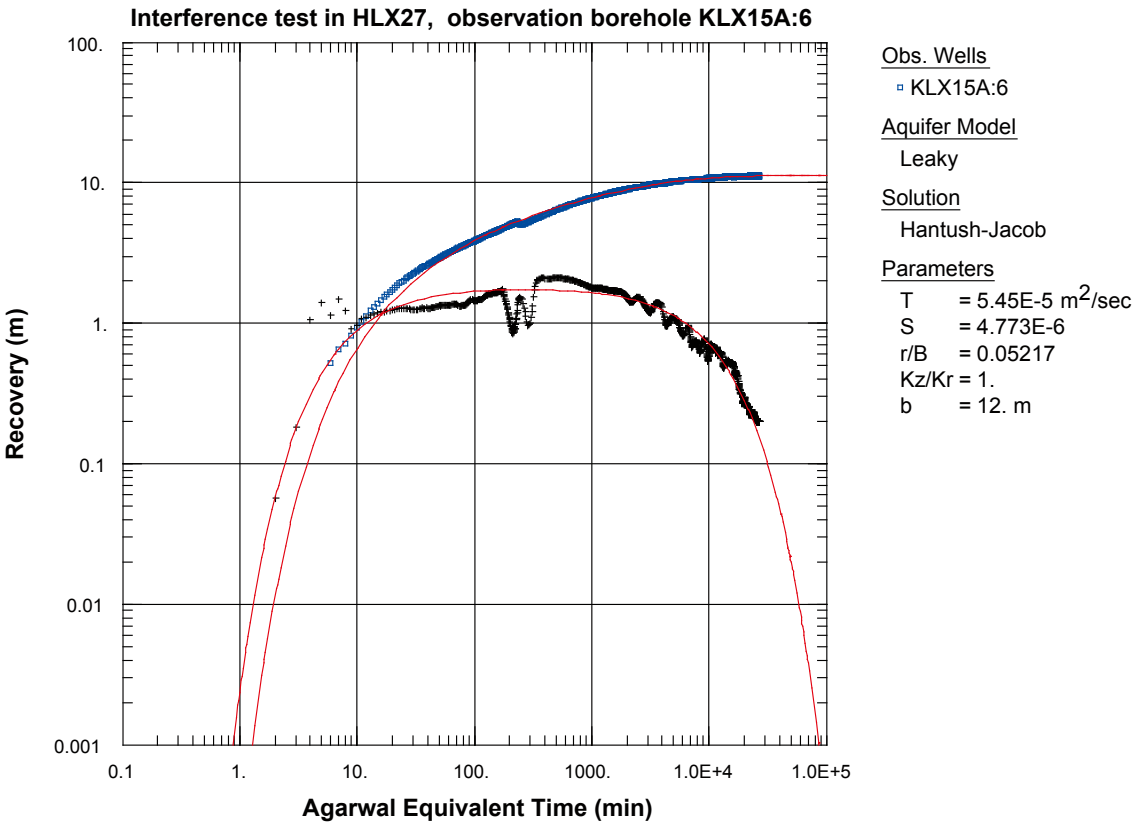

Figure A6-108. *Log-log plot of recovery (▫) and recovery derivative, ds/d(ln t) (+), versus time in KLX15A:6during the interference test in HLX27.*

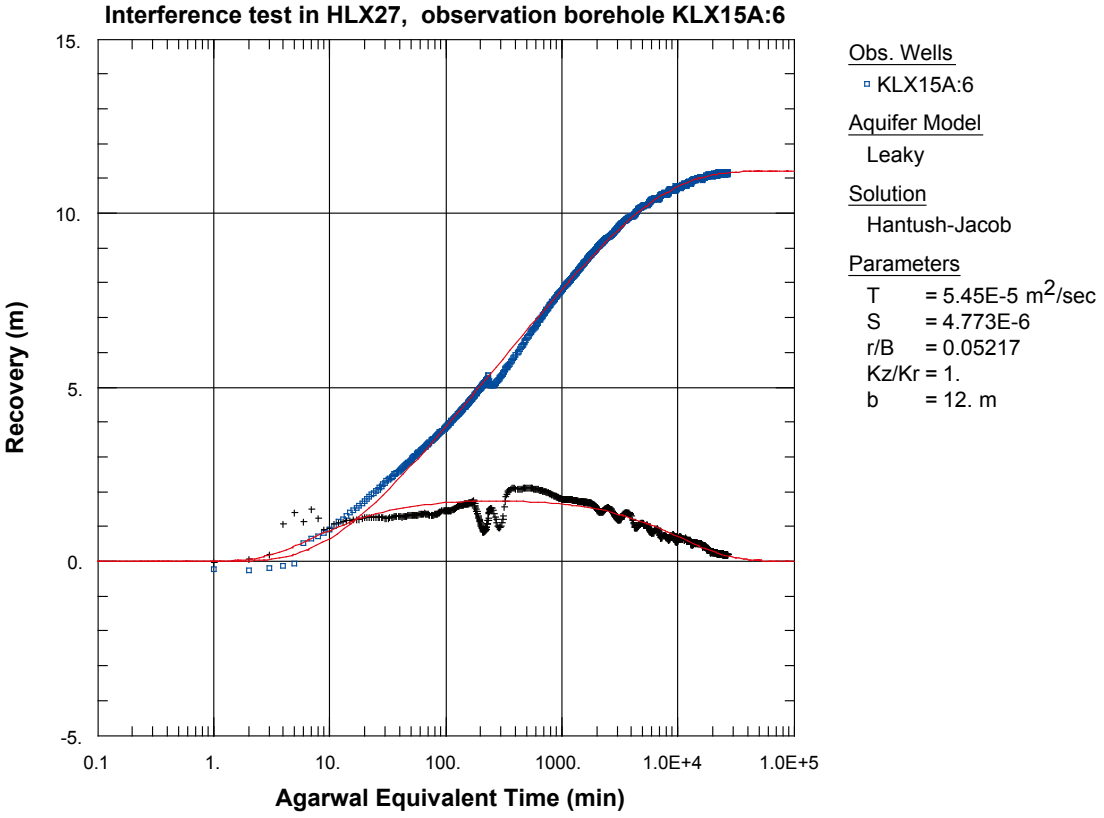

Figure A6-109. *Lin-log plot of recovery (▫) and recovery derivative, ds/d(ln t) (+), versus time in KLX15A:6 during the interference test in HLX27.*

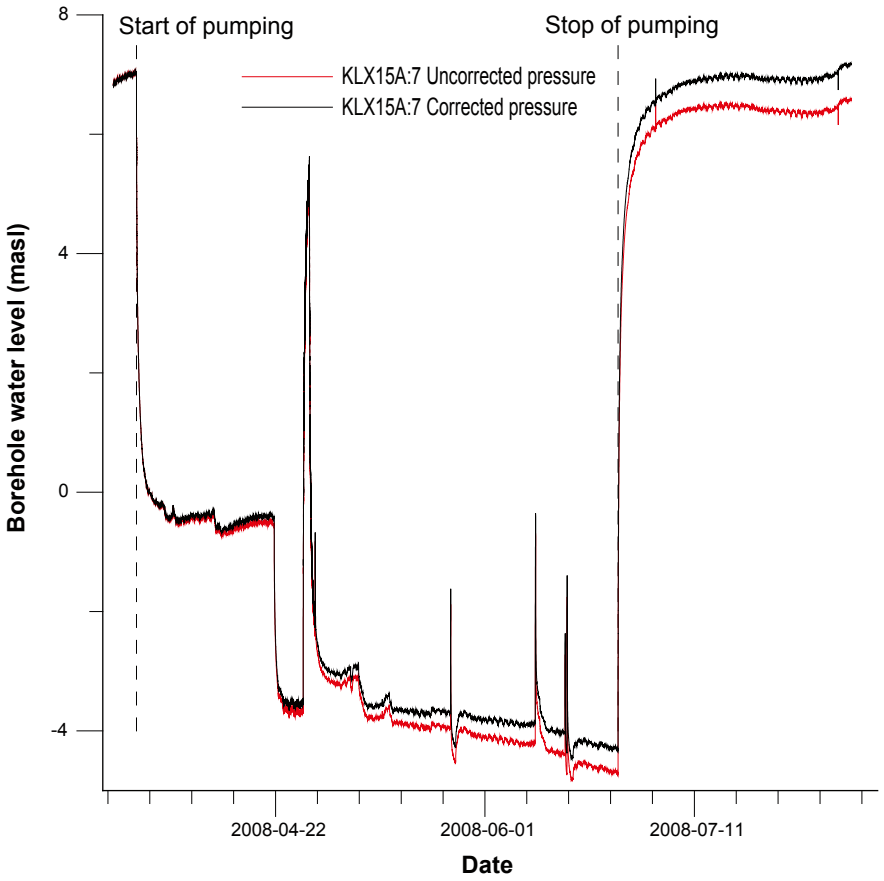

Figure A6-110. *Linear plot of pressure versus time in the observation sections in KLX15A:7 during pumping in HLX27.*

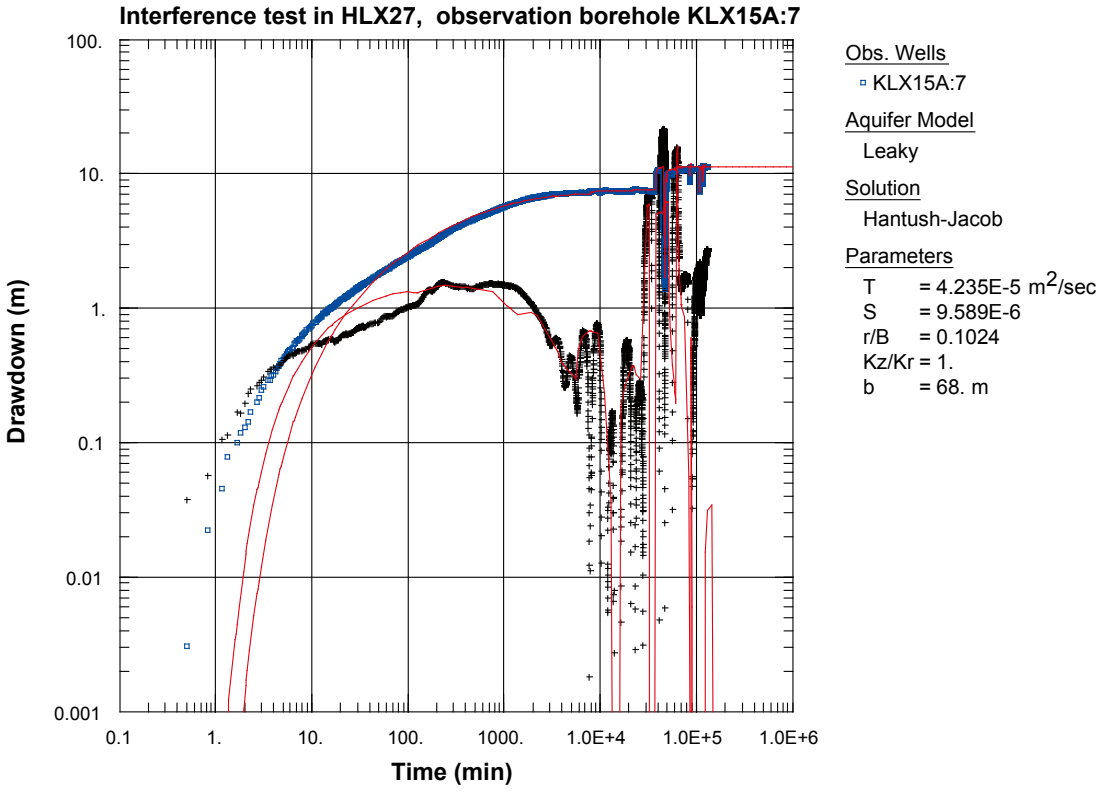

Figure A6-111. *Log-log plot of drawdown (▫) and drawdown derivative, ds/d(ln t) (+), versus time in KLX15A:7 during the interference test in HLX27. Transient evaluation is based on the first part of the drawdown period.*

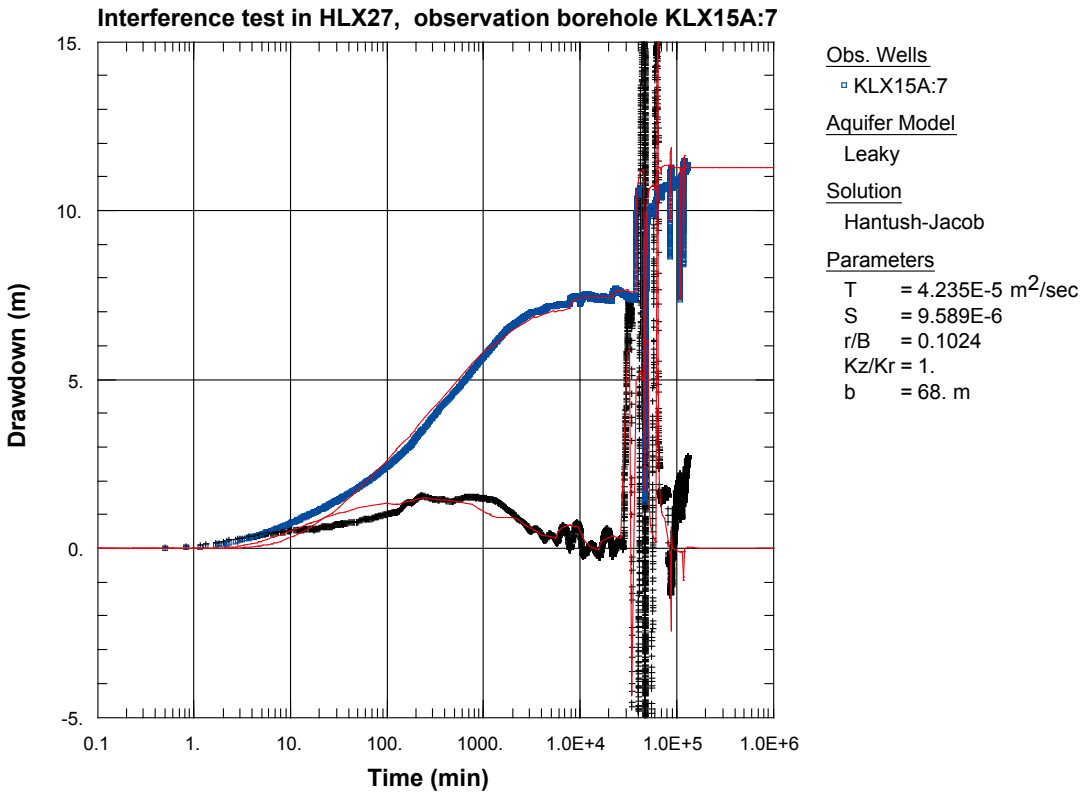

Figure A6-112. *Lin-log plot of drawdown (▫) and drawdown derivative, ds/d(ln t) (+), versus time in KLX15A:7 during the interference test in HLX27. Transient evaluation is based on the first part of the drawdown period.*

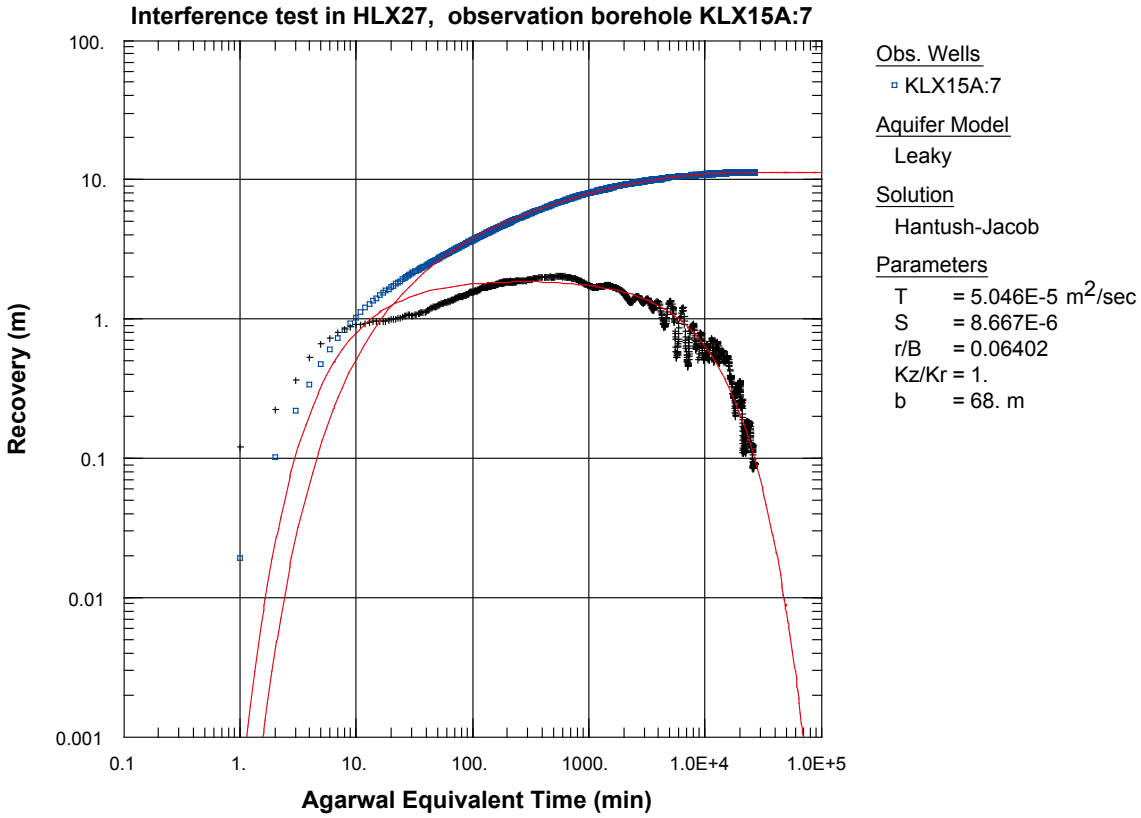

Figure A6-113. *Log-log plot of recovery (▫) and recovery derivative, ds/d(ln t) (+), versus time in KLX15A:7 during the interference test in HLX27.*

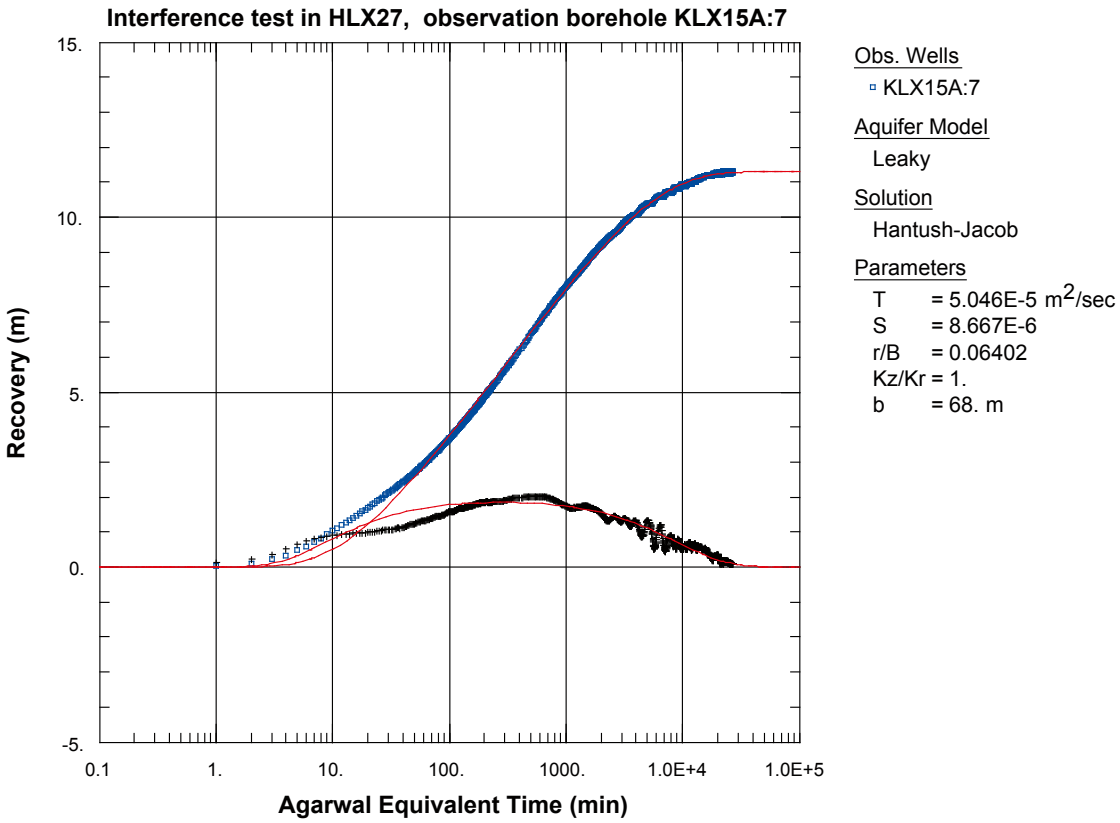

Figure A6-114. *Lin-log plot of recovery (▫) and recovery derivative, ds/d(ln t) (+), versus time in KLX15A:7 during the interference test in HLX27.*

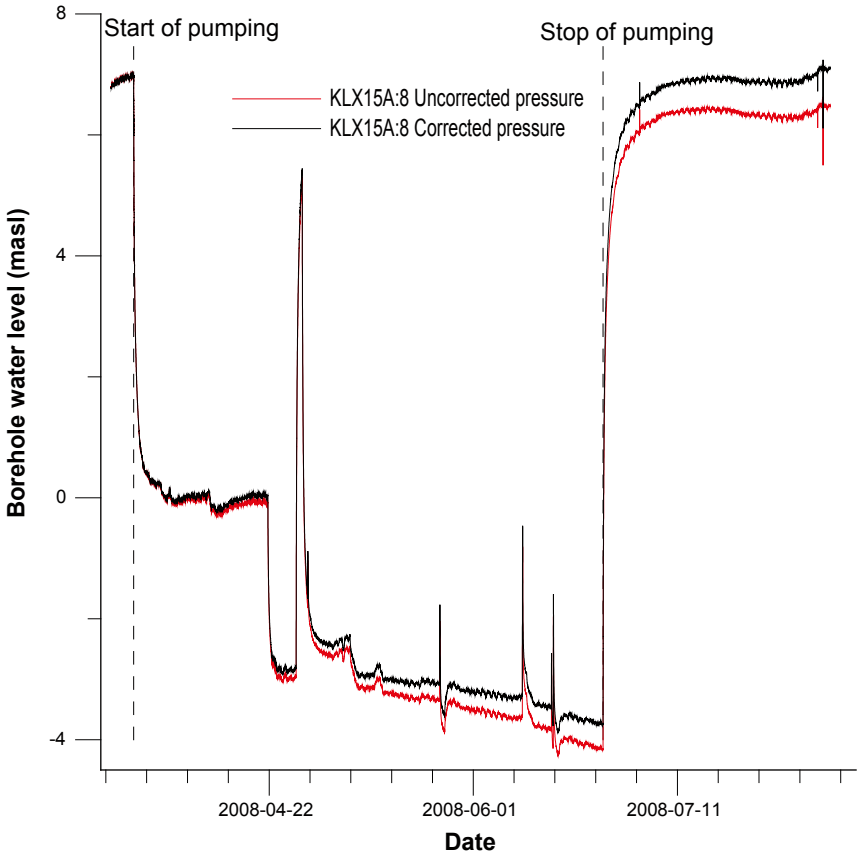

Figure A6-115. *Linear plot of pressure versus time in the observation sections in KLX15A:8 during pumping in HLX27.*

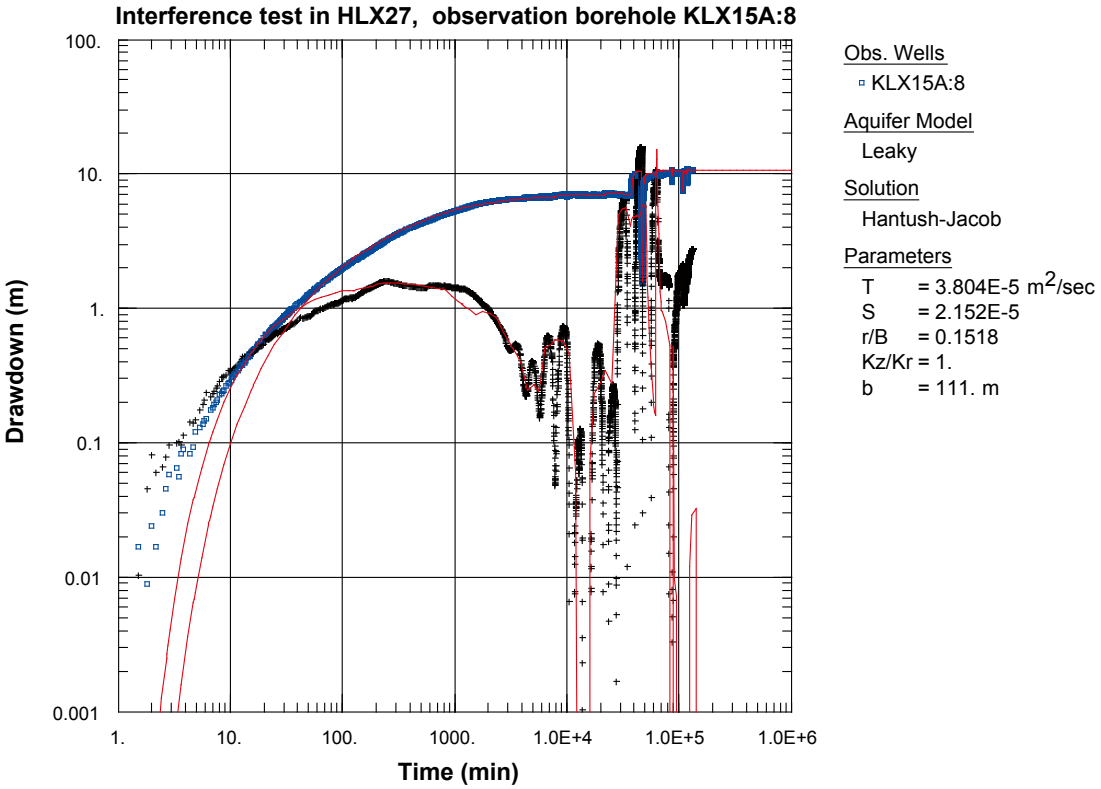

Figure A6-116. *Log-log plot of drawdown (▫) and drawdown derivative, ds/d(ln t) (+), versus time in KLX15A:8 during the interference test in HLX27. Transient evaluation is based on the first part of the drawdown period.*

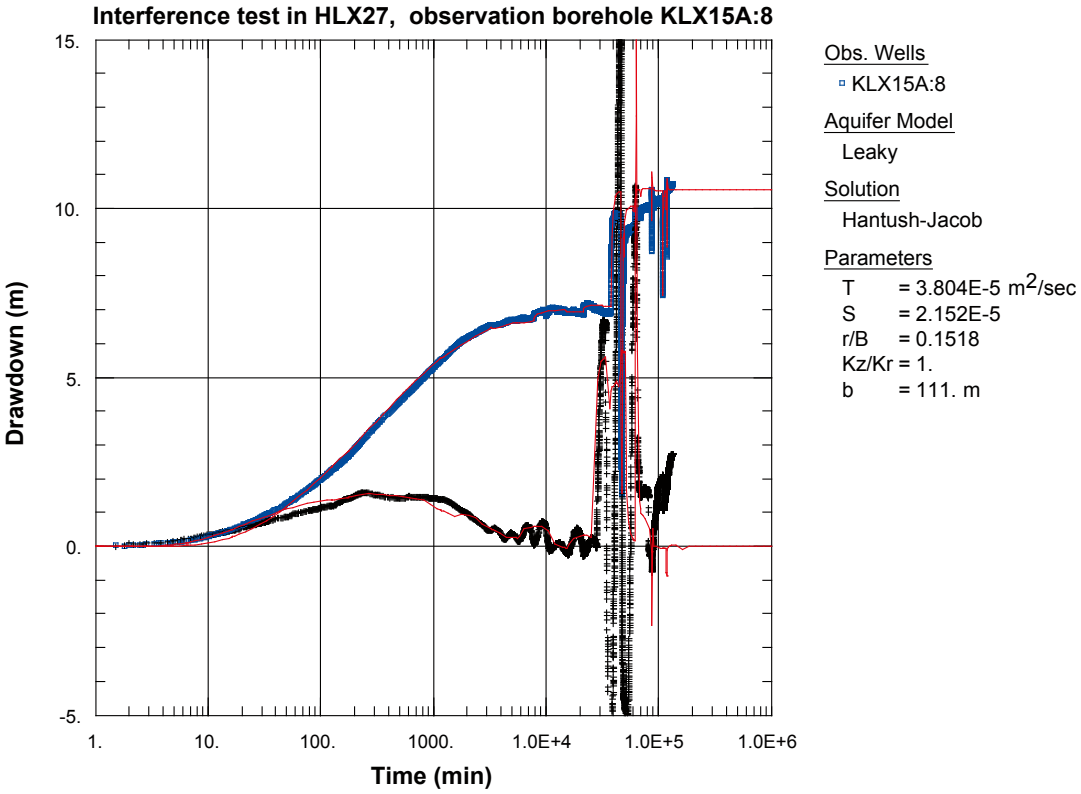

Figure A6-117. *Lin-log plot of drawdown (▫) and drawdown derivative, ds/d(ln t) (+), versus time in KLX15A:8 during the interference test in HLX27. Transient evaluation is based on the first part of the drawdown period.*

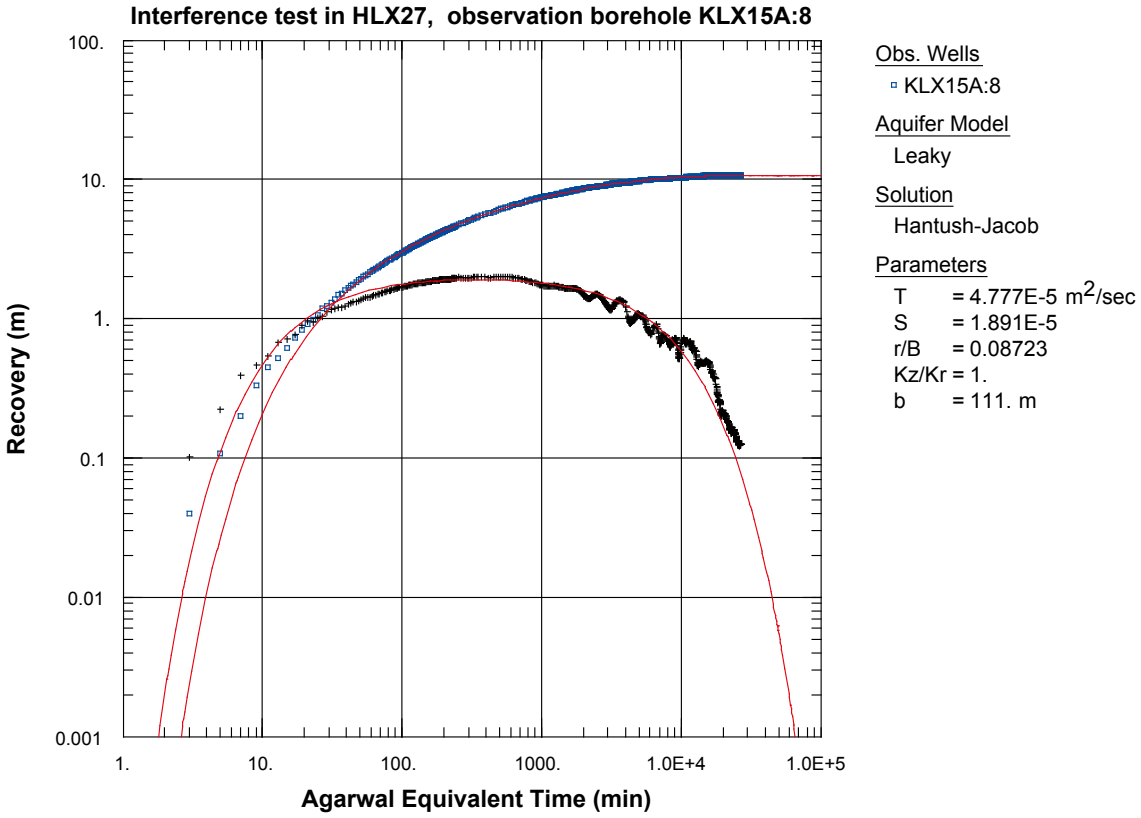

Figure A6-118. *Log-log plot of recovery (▫) and recovery derivative, ds/d(ln t) (+), versus time in KLX15A:8 during the interference test in HLX27.*

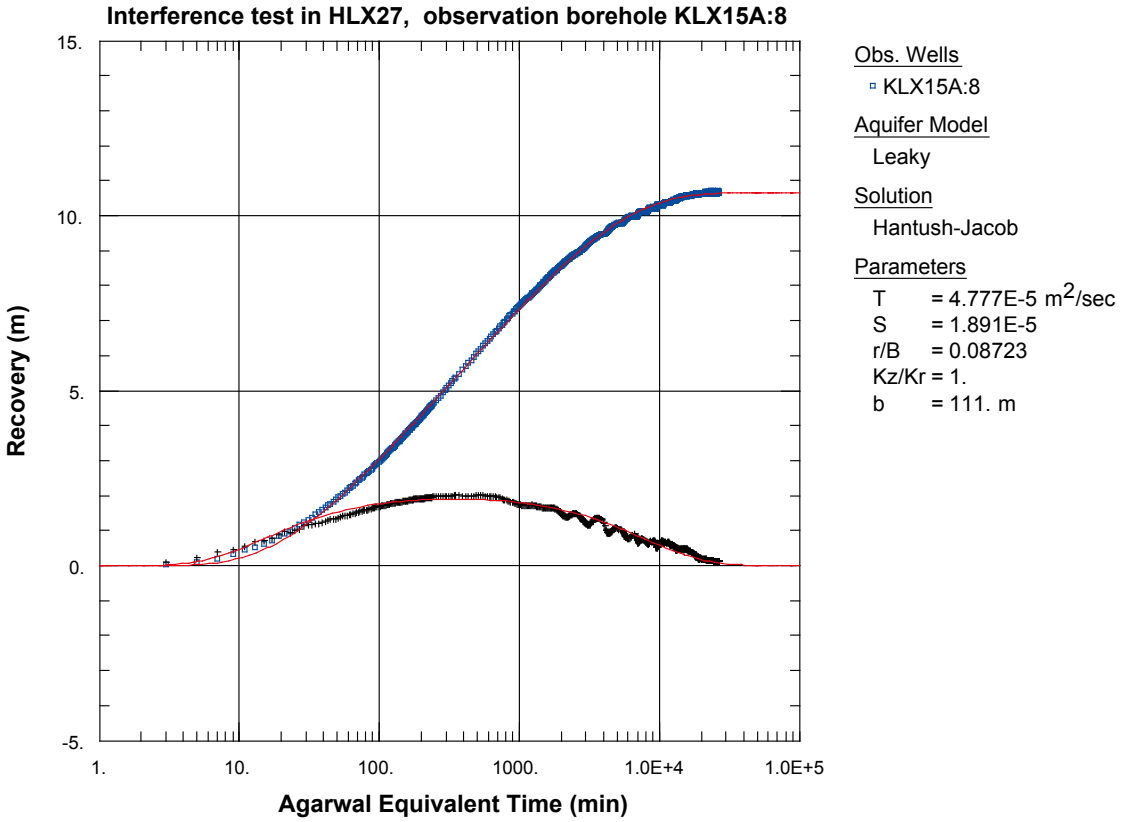

Figure A6-119. *Lin-log plot of recovery (▫) and recovery derivative, ds/d(ln t) (+), versus time in KLX15A:8 during the interference test in HLX27.*

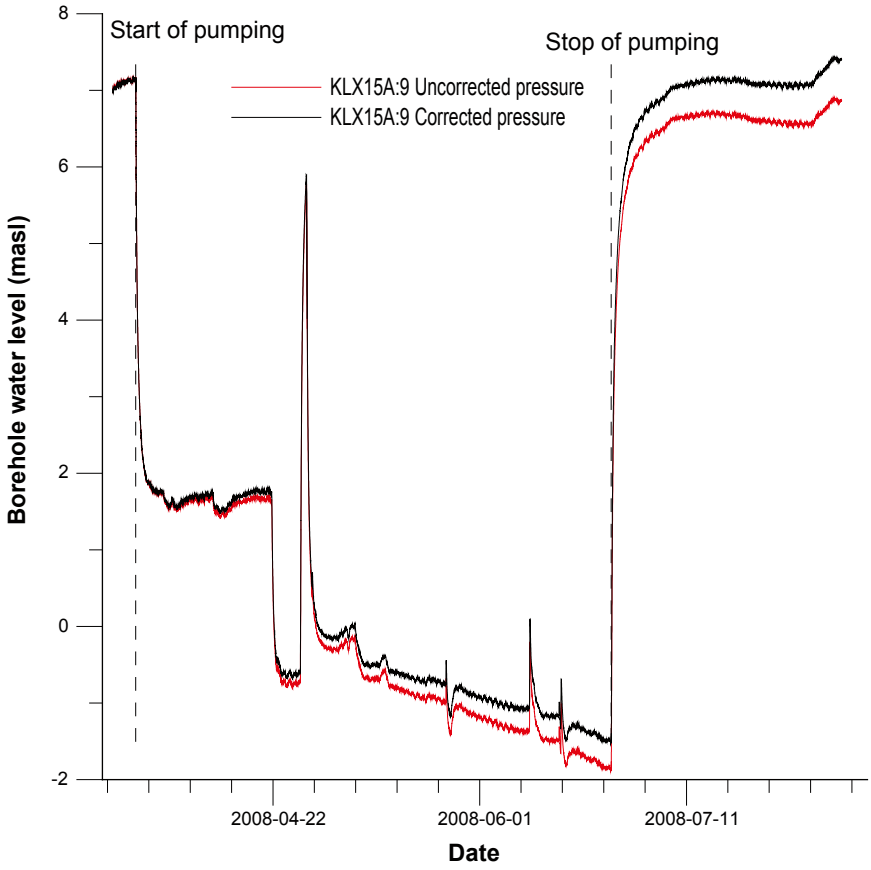

Figure A6-120. *Linear plot of pressure versus time in the observation sections in KLX15A:9 during pumping in HLX27.*

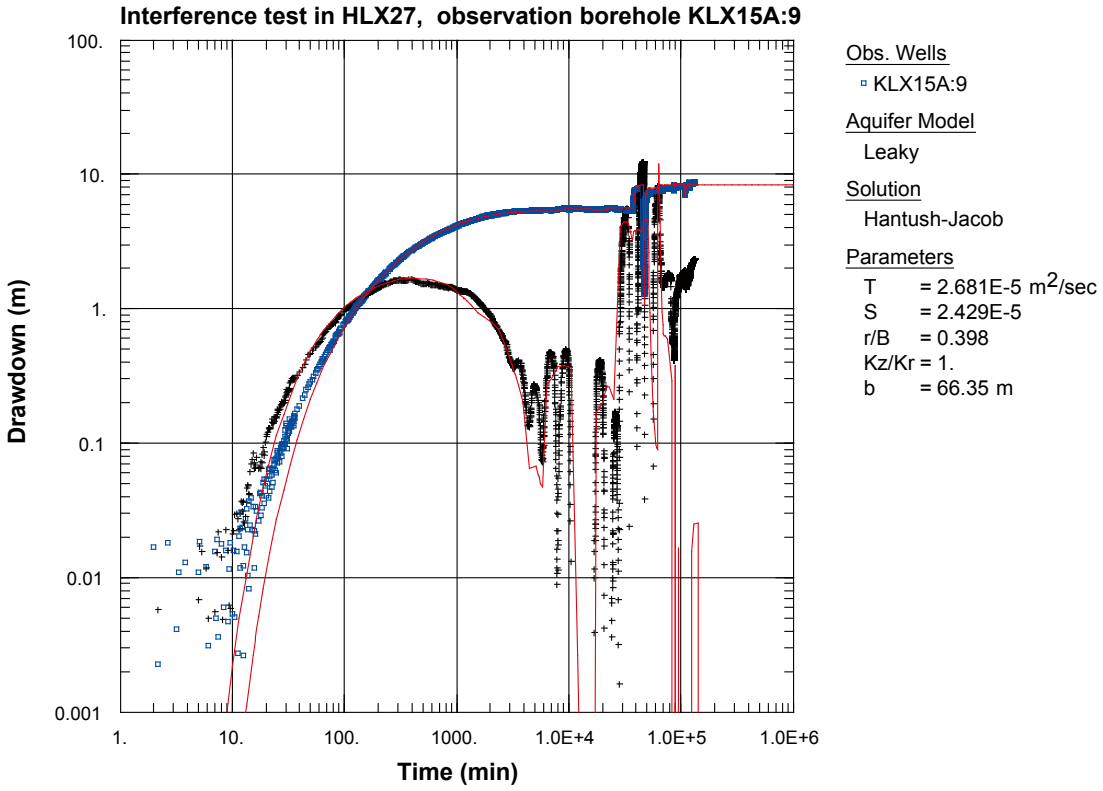

Figure A6-121. *Log-log plot of drawdown (▫) and drawdown derivative, ds/d(ln t) (+), versus time in KLX15A:9 during the interference test in HLX27. Transient evaluation is based on the first part of the drawdown period.*

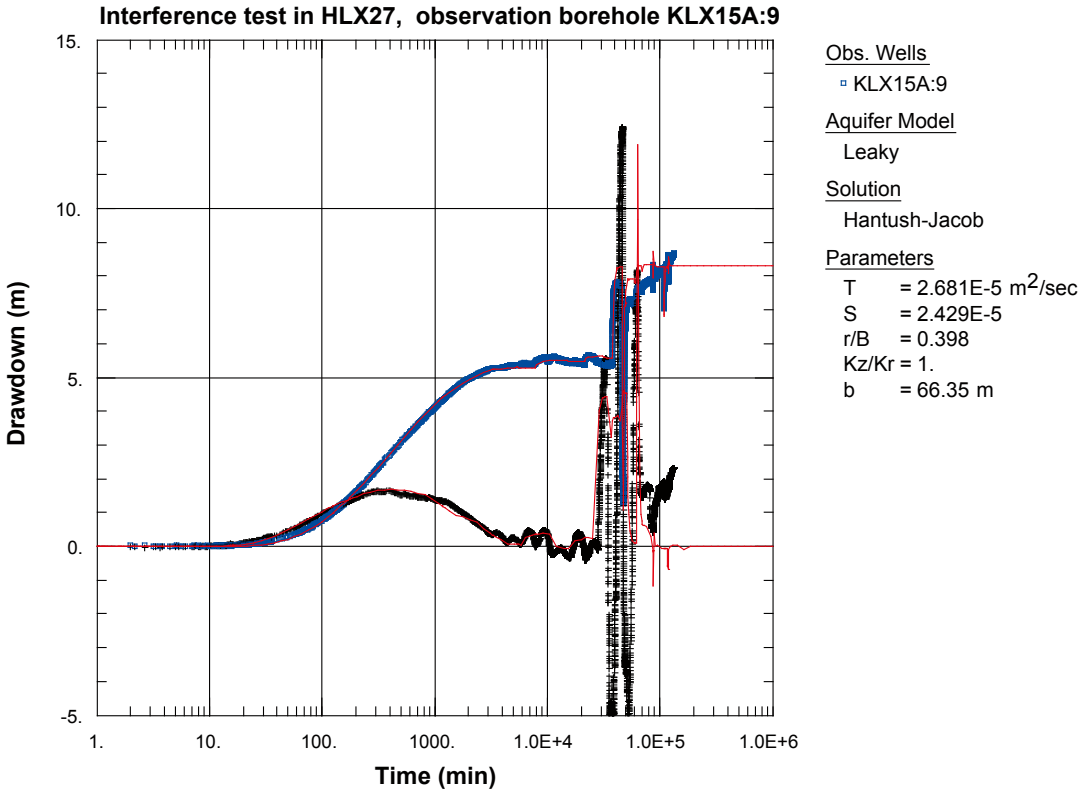

Figure A6-122. *Lin-log plot of drawdown (▫) and drawdown derivative, ds/d(ln t) (+), versus time in KLX15A:9 during the interference test in HLX27. Transient evaluation is based on the first part of the drawdown period.*

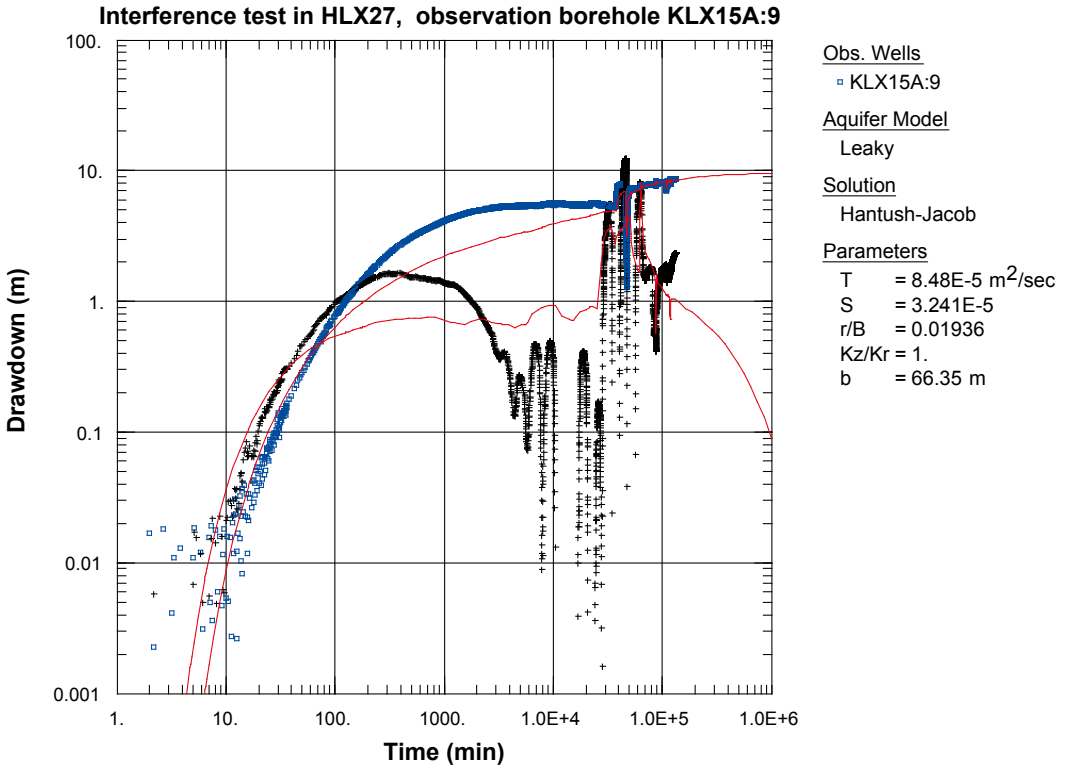

Figure A6-123. *Log-log plot of drawdown (▫) and drawdown derivative, ds/d(ln t) (+), versus time in KLX15A:9 during the interference test in HLX27. Transient evaluation is based on the late part of the drawdown period.*

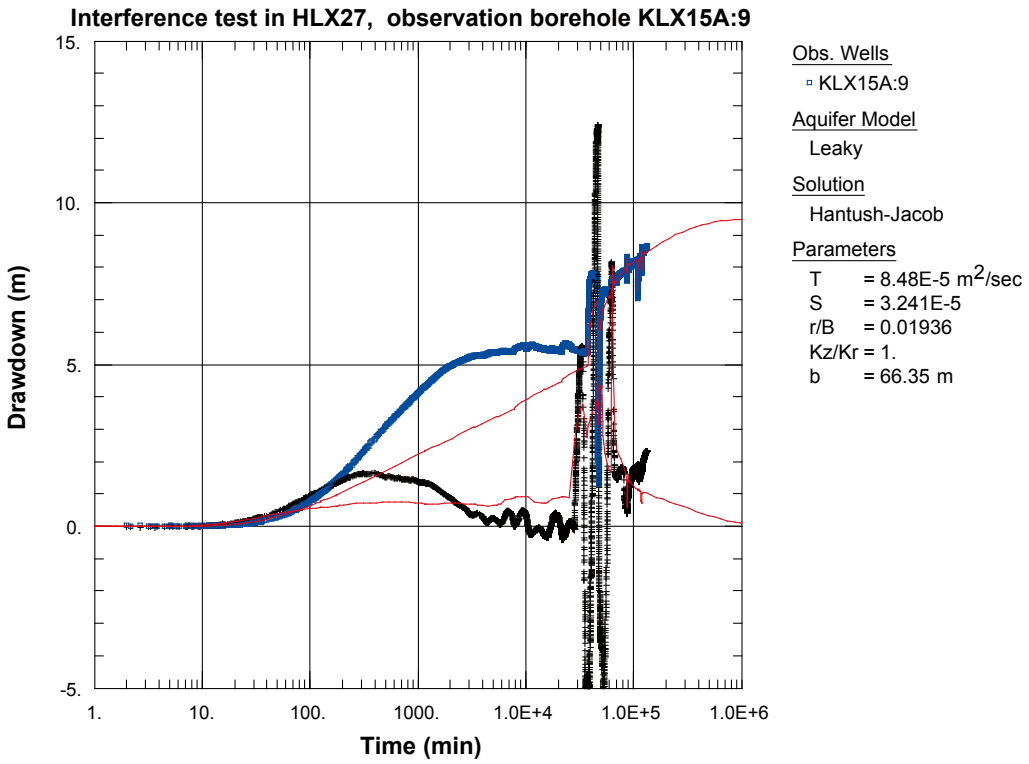

Figure A6-124. *Lin-log plot of drawdown (▫) and drawdown derivative, ds/d(ln t) (+), versus time in KLX15A:9 during the interference test in HLX27. Transient evaluation is based on the late part of the drawdown period.*

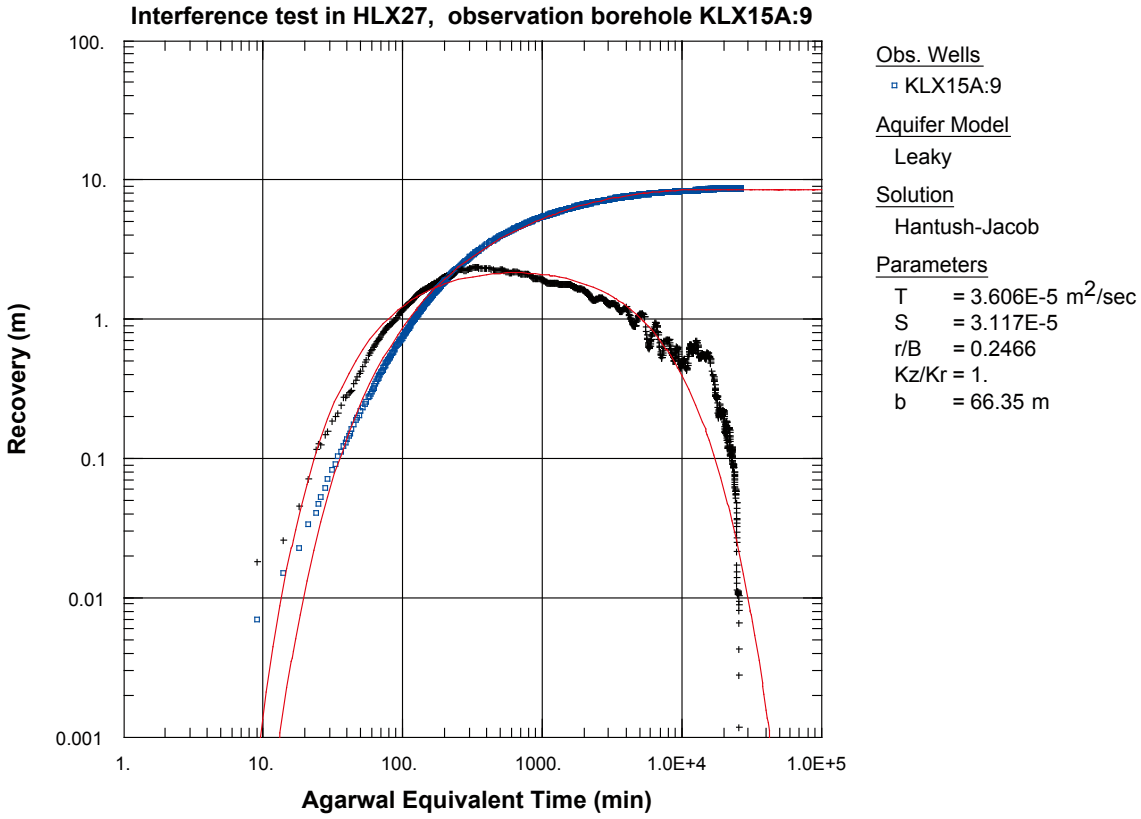

Figure A6-125. *Log-log plot of recovery (▫) and recovery derivative, ds/d(ln t) (+), versus time in KLX15A:9 during the interference test in HLX27.*

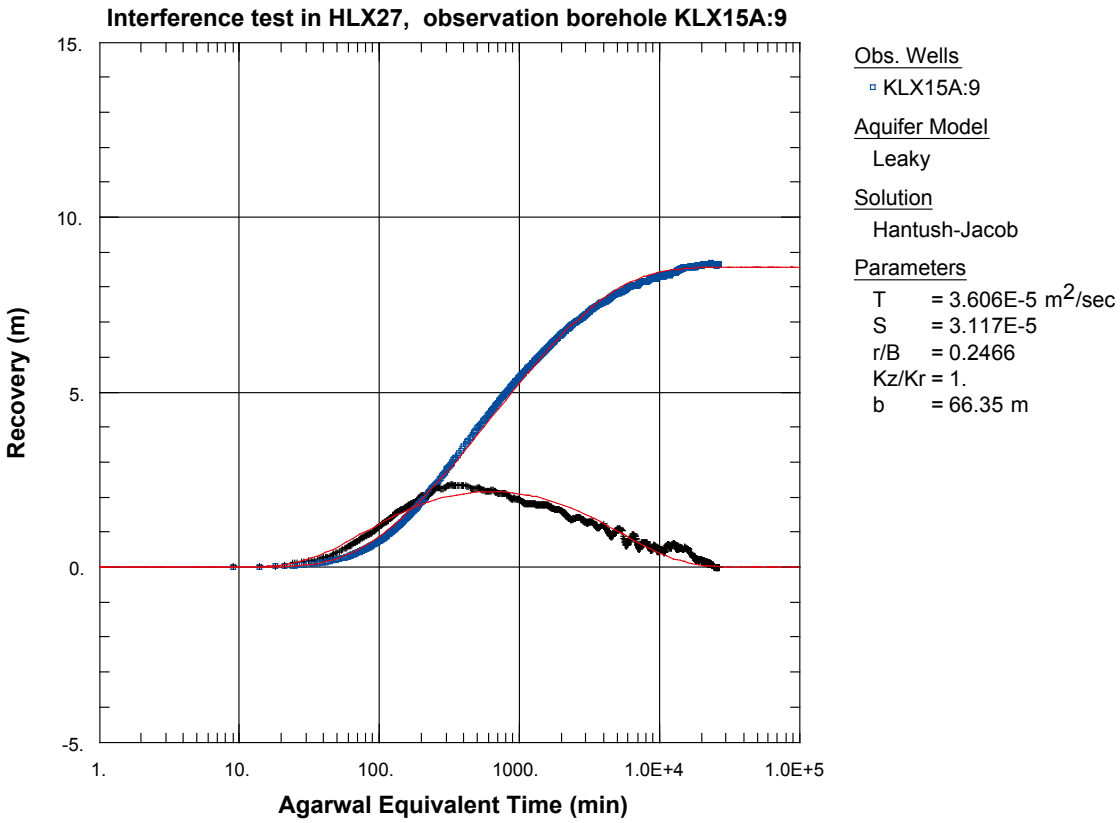

Figure A6-126. *Lin-log plot of recovery (▫) and recovery derivative, ds/d(ln t) (+), versus time in KLX15A:9 during the interference test in HLX27.*

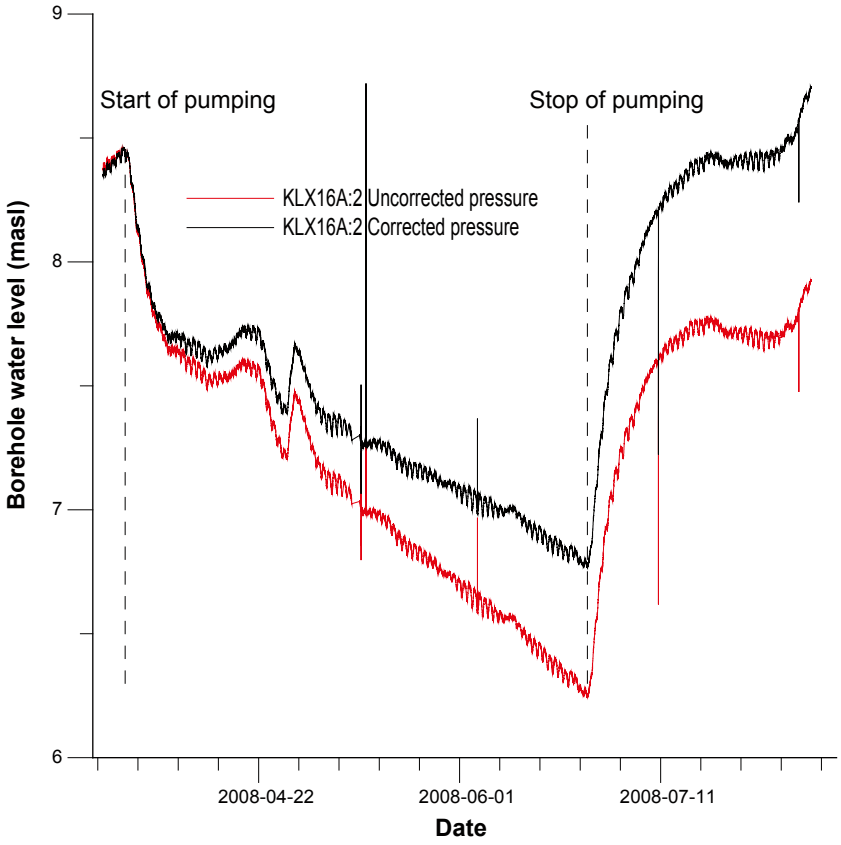

Figure A6-127. *Linear plot of pressure versus time in the observation sections in KLX16A:2 during pumping in HLX27.*

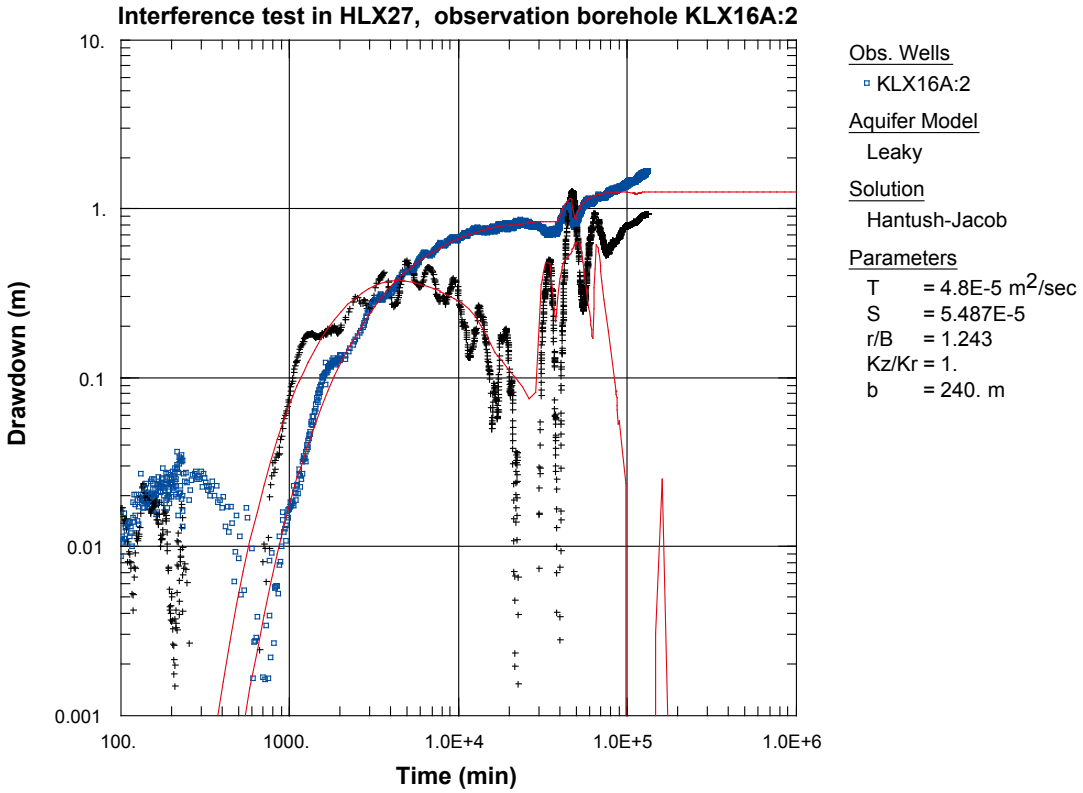

Figure A6-128. *Log-log plot of drawdown (▫) and drawdown derivative, ds/d(ln t) (+), versus time in KLX16A:2 during the interference test in HLX27. Transient evaluation is based on the first part of the drawdown period.*

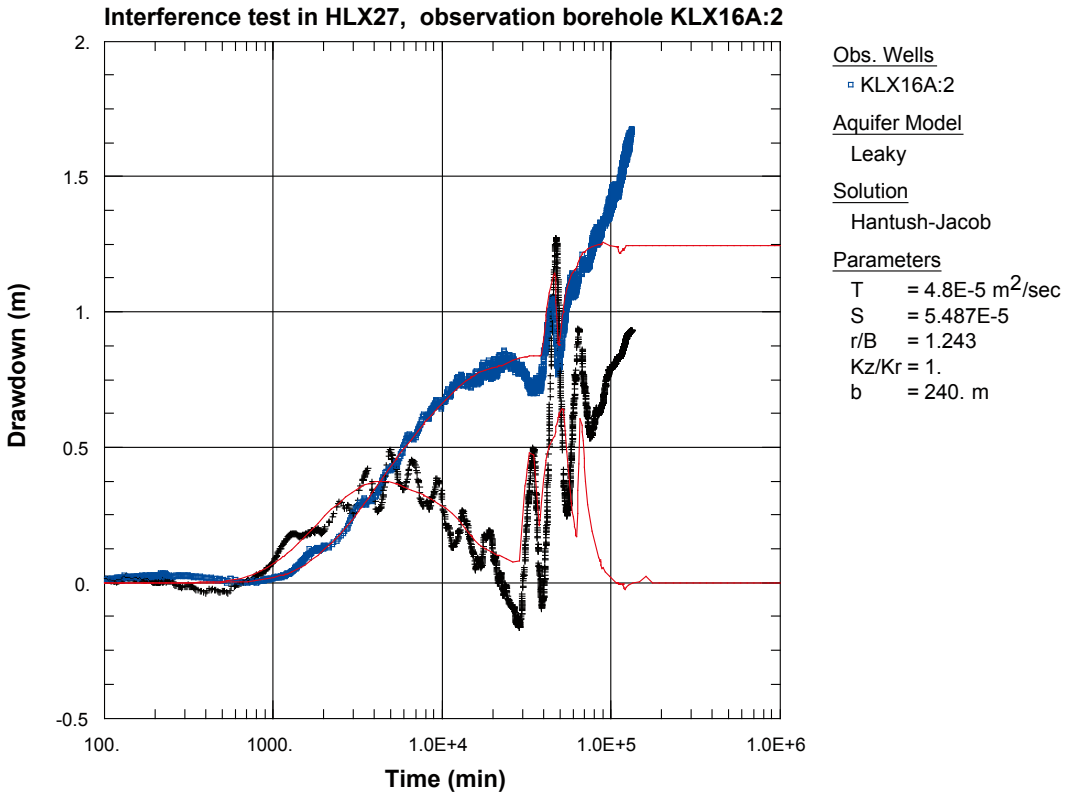

Figure A6-129. *Lin-log plot of drawdown (▫) and drawdown derivative, ds/d(ln t) (+), versus time in KLX16A:2 during the interference test in HLX27. Transient evaluation is based on the first part of the drawdown period.*

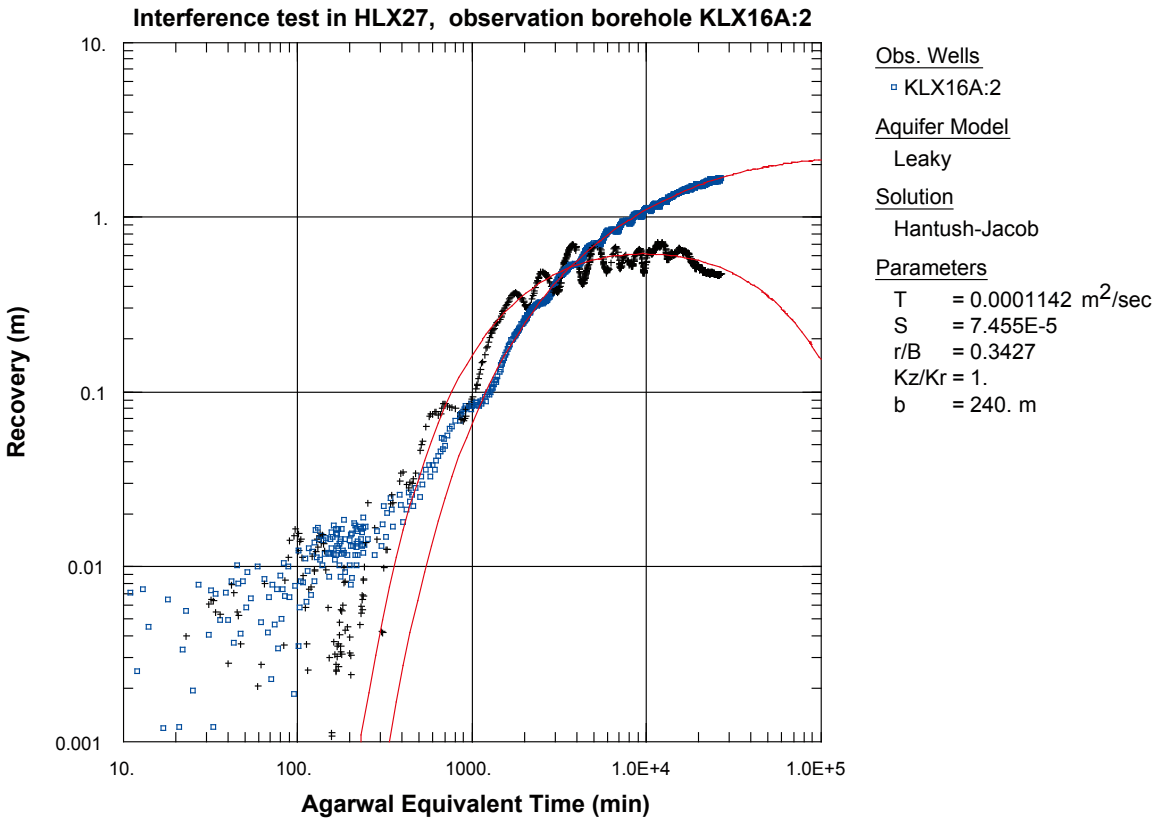

Figure A6-130. *Log-log plot of recovery (▫) and recovery derivative, ds/d(ln t) (+), versus time in KLX16A:2 during the interference test in HLX27.*

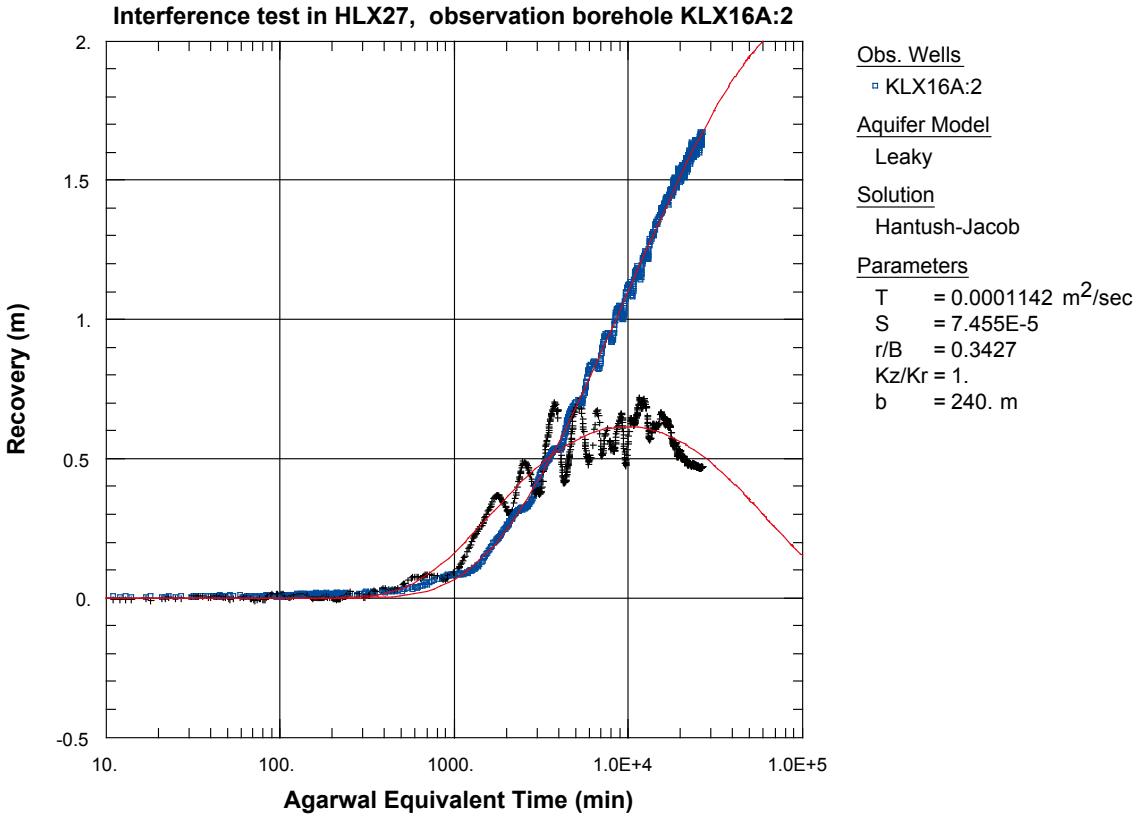

Figure A6-131. *Lin-log plot of recovery (▫) and recovery derivative, ds/d(ln t) (+), versus time in KLX16A:2 during the interference test in HLX27.*

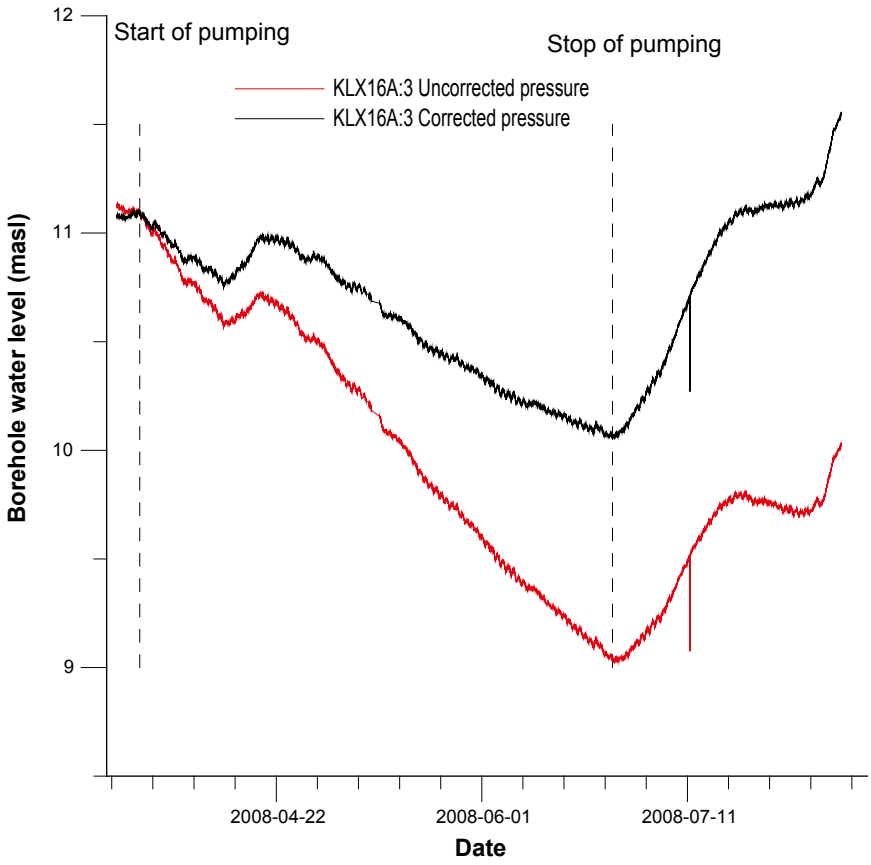

Figure A6-132. *Linear plot of pressure versus time in the observation sections in KLX16A:3 during pumping in HLX27.*

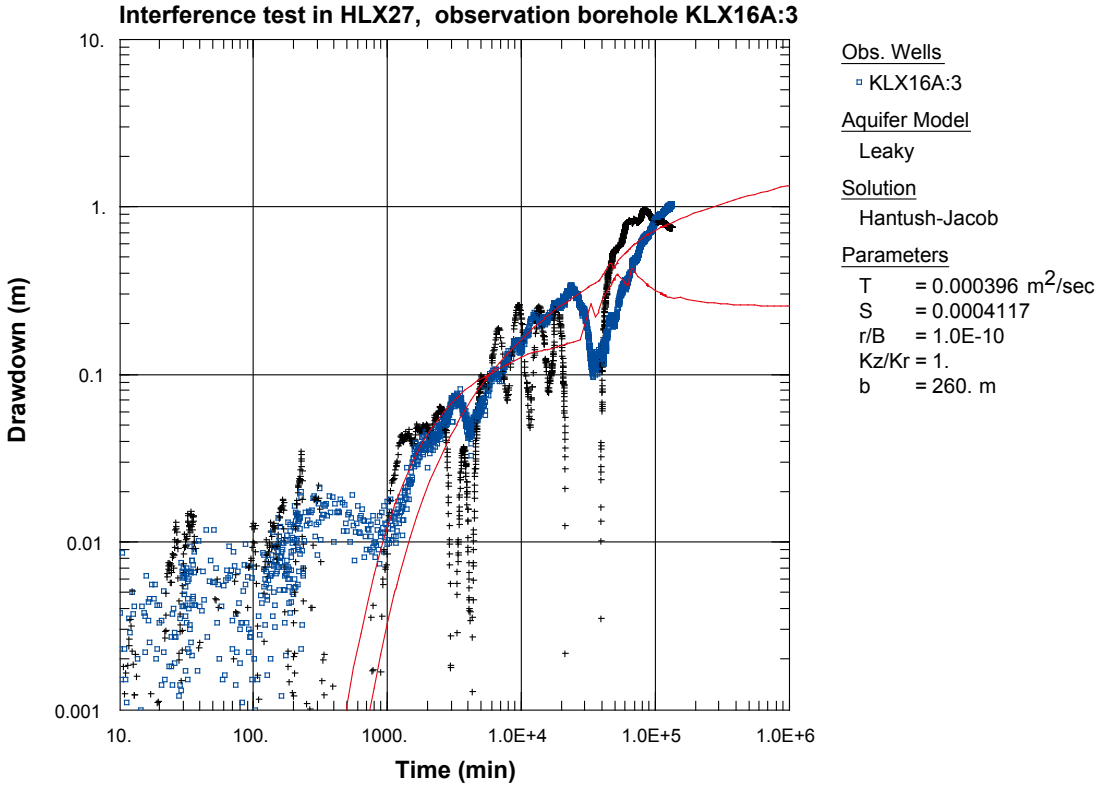

Figure A6-133. *Log-log plot of drawdown (▫) and drawdown derivative, ds/d(ln t) (+), versus time in KLX16A:3 during the interference test in HLX27. Transient evaluation is based on the first part of the drawdown period.*

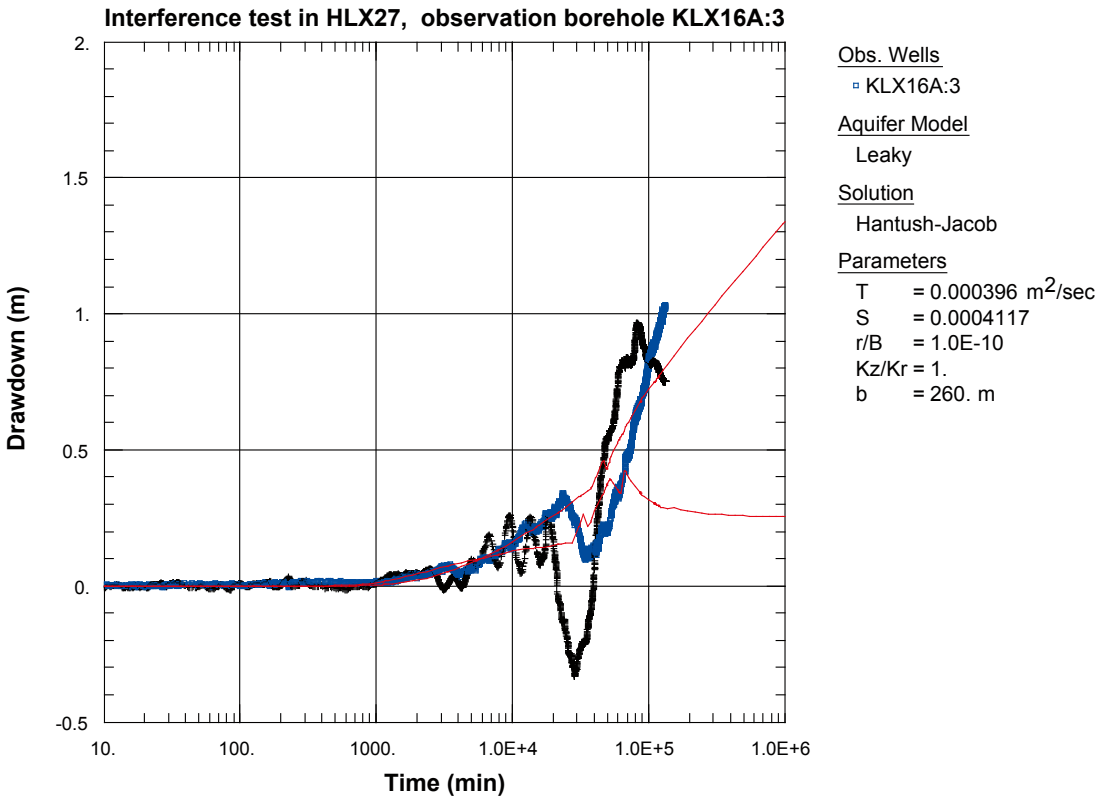

Figure A6-134. *Lin-log plot of drawdown (▫) and drawdown derivative, ds/d(ln t) (+), versus time in KLX16A:3 during the interference test in HLX27. Transient evaluation is based on the first part of the drawdown period.*

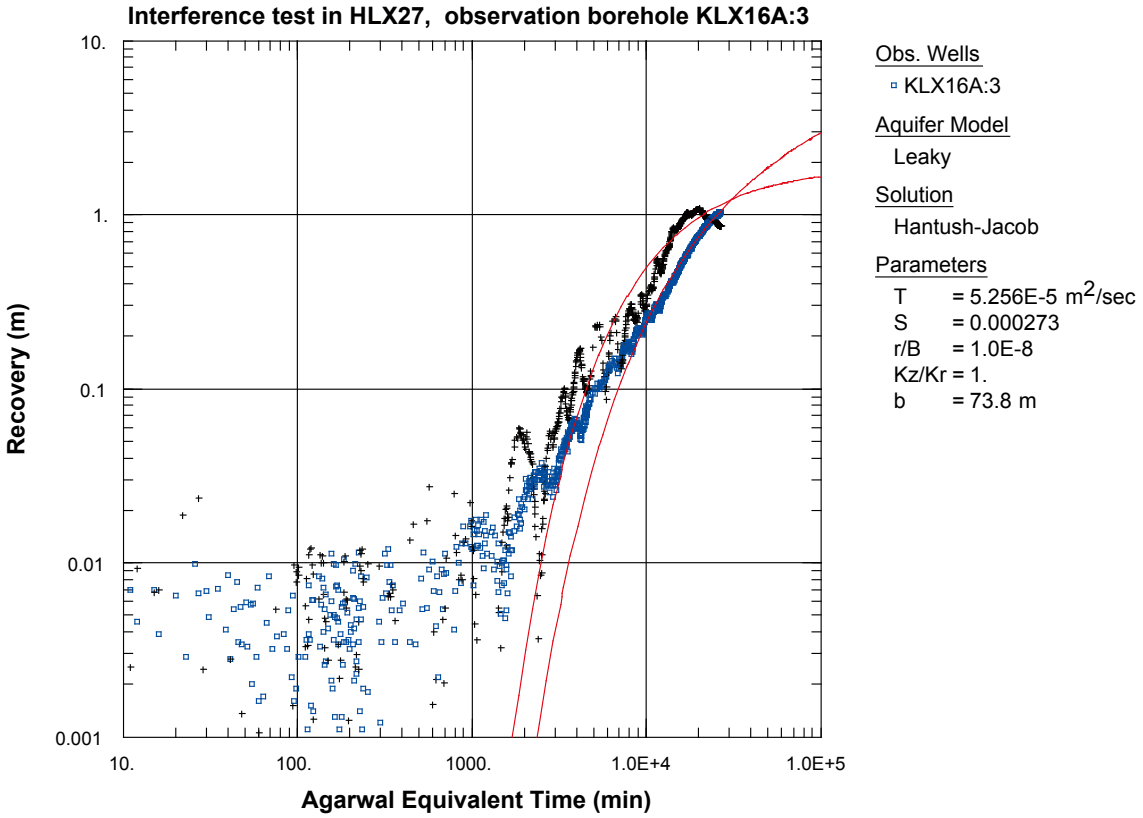

Figure A6-135. *Log-log plot of recovery (▫) and recovery derivative, ds/d(ln t) (+), versus time in KLX16A:3 during the interference test in HLX27.*

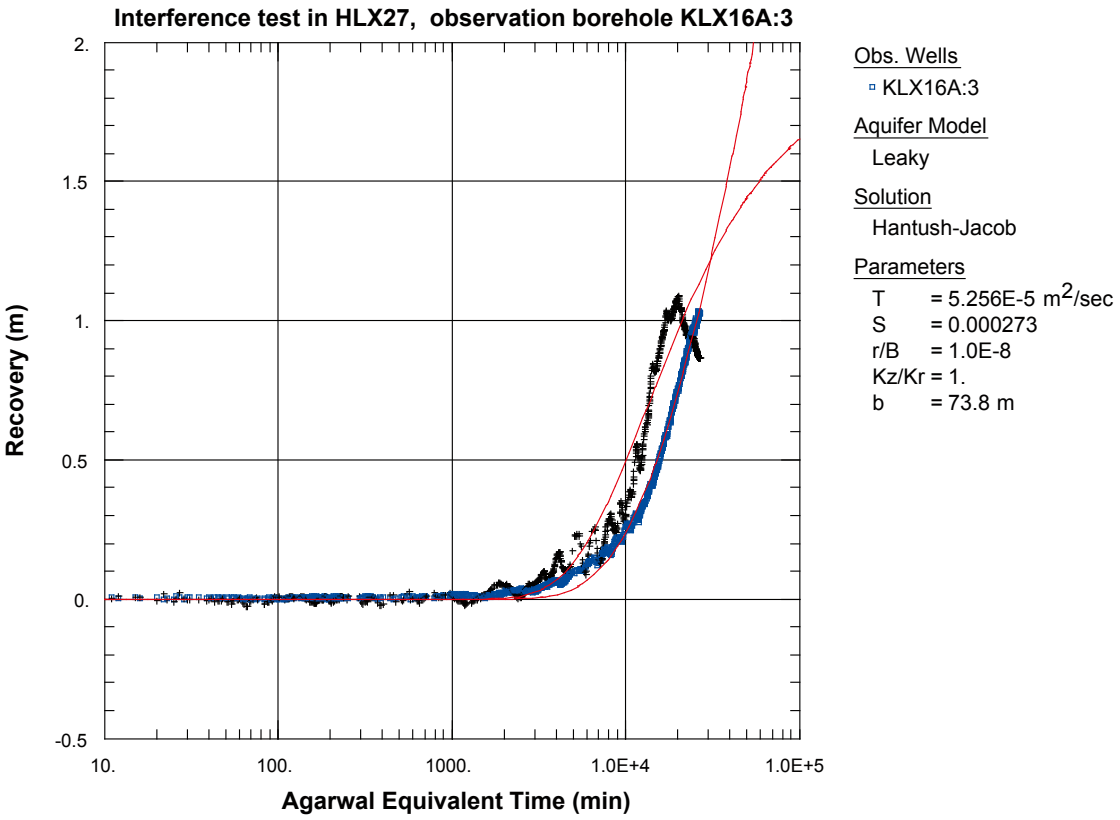

Figure A6-136. *Lin-log plot of recovery (▫) and recovery derivative, ds/d(ln t) (+), versus time in KLX16A:3 during the interference test in HLX27.*

Appendix 7

Correction of head and drawdown for natural decreasing trend

As can be seen from Figure A7-1, a natural, decreasing head trend was ongoing during the entire period of the interference test in HLX27. Even though the section KLX16A:1 is unaffected by the pumping, the pressure slowly drops during the entire period. The data from the test period were corrected for the natural trend using the graphical technique described in Figure A7-2. The difference between the head at start of pumping and the head at maximal pressure recovery after stop of pumping was assumed to represent the existing natural head trend during the entire test period.

A linear trend correction with time was determined individually for all responding observation sections according to Equation A7-1 and applied to the drawdown and recovery period. The total correction at stop of pumping is denoted $corr(t_p)$. The corrected drawdown $s(t)_{corr}$ at time t is calculated according to Equation A7-2.

$$corr(t) = [corr(t_p)/t_p] \cdot t \qquad \text{(A7-1)}$$

$$s(t)_{corr} = s(t) - corr(t) \qquad \text{(A7-2)}$$

$s(t)_{corr}$ = corrected drawdown at time t after start of pumping (m)

$s(t)$ = measured drawdown at time t after start of pumping (m)

$corr(t)$ = applied correction at time t after start of pumping (m)

$corr(t_p)$ = applied correction at time t_p at stop of pumping (m)

t_p = duration of drawdown period (s)

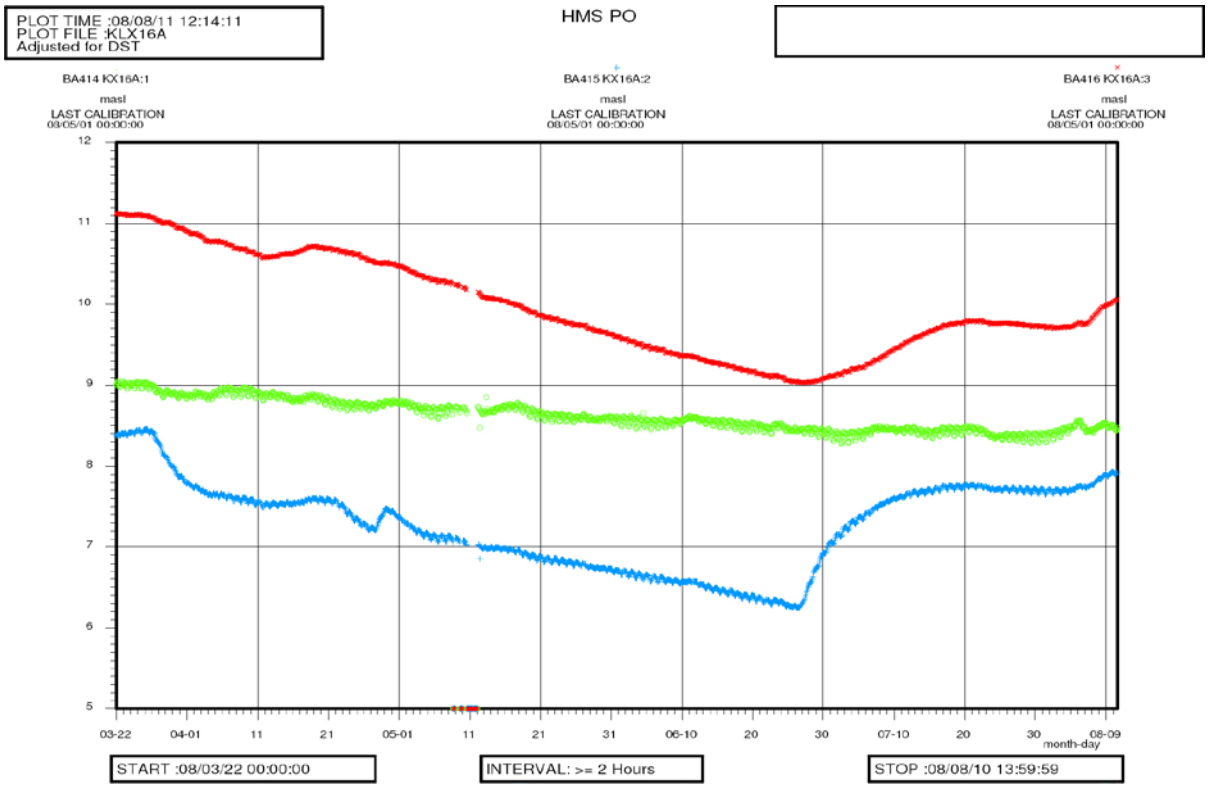

Figure A7-1. *Linear plot of head versus time in observation section KLX16A during the interference test in HLX27. Section KLX16A:1 (middle curve) is assumed to represent the natural trend.*

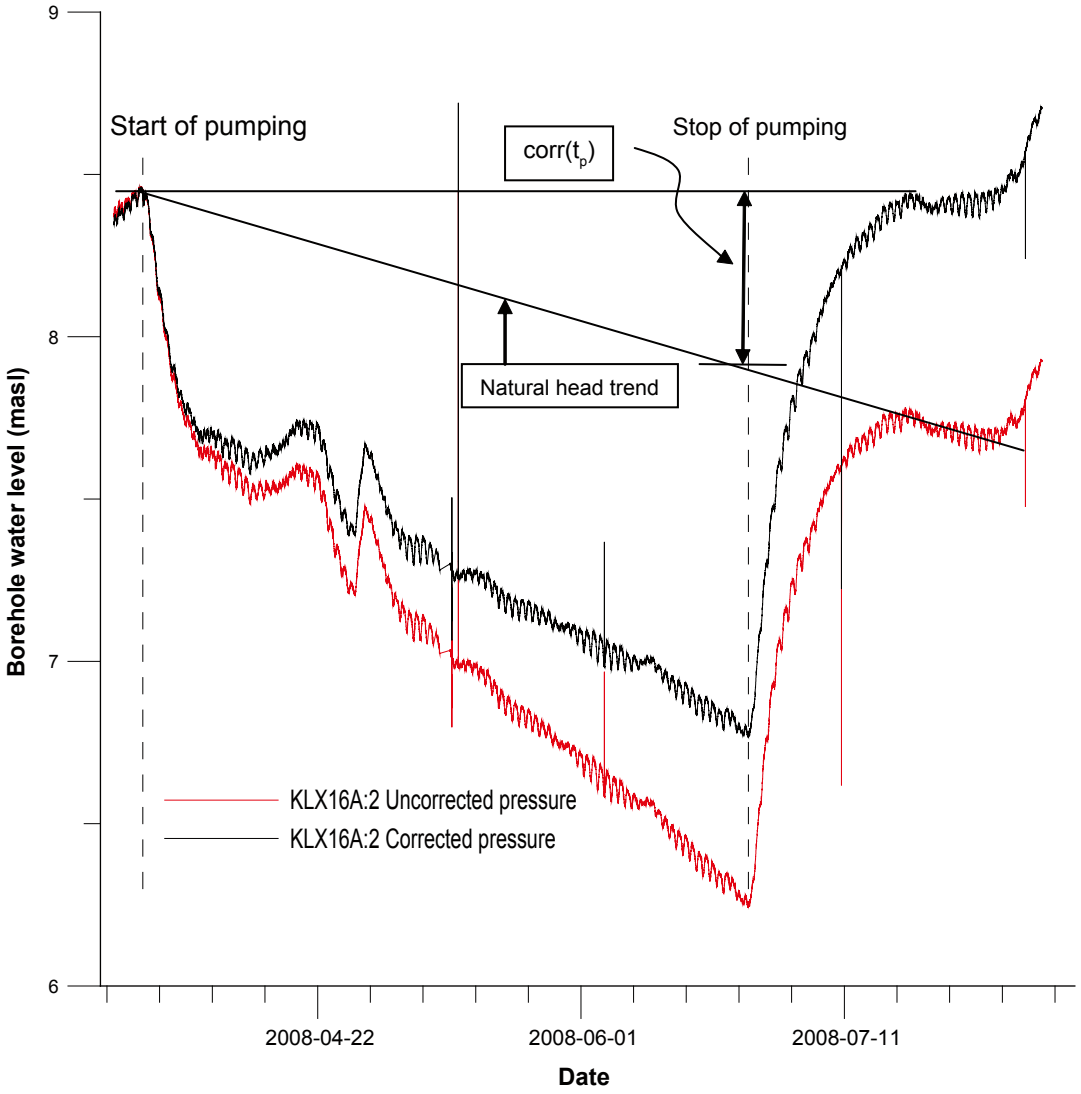

Figure A7-2. *Example of the applied correction technique for the natural decreasing head trend in observation section KLX16A:2 during the interference test in HLX27. The final drawdown correction at stop of pumping is denoted corr(t_p).*

Data files with time and corrected head and drawdown for all responding observation sections were prepared and stored in Sicada. In borehole HLX38 with no registration of the pressure recovery, the correction was based on the observed head trend in surrounding boreholes.

In order to investigate the effect of the applied trend correction on the estimated hydraulic parameters, examples of transient analyses from section KLX16A:2 (same section as in Figure A7-2) using corrected and uncorrected head data respectively are shown in Figures A7-3a-b and A7-4a-b. The evaluation is made on the first part of the flow period (which was normally analyzed in this test) and of the recovery period (which was normally selected as representative). The figures show that the effect of the trend correction on the estimated parameters is not very substantial on the actual analyses. The effect is lower on the analysis of the recovery period.

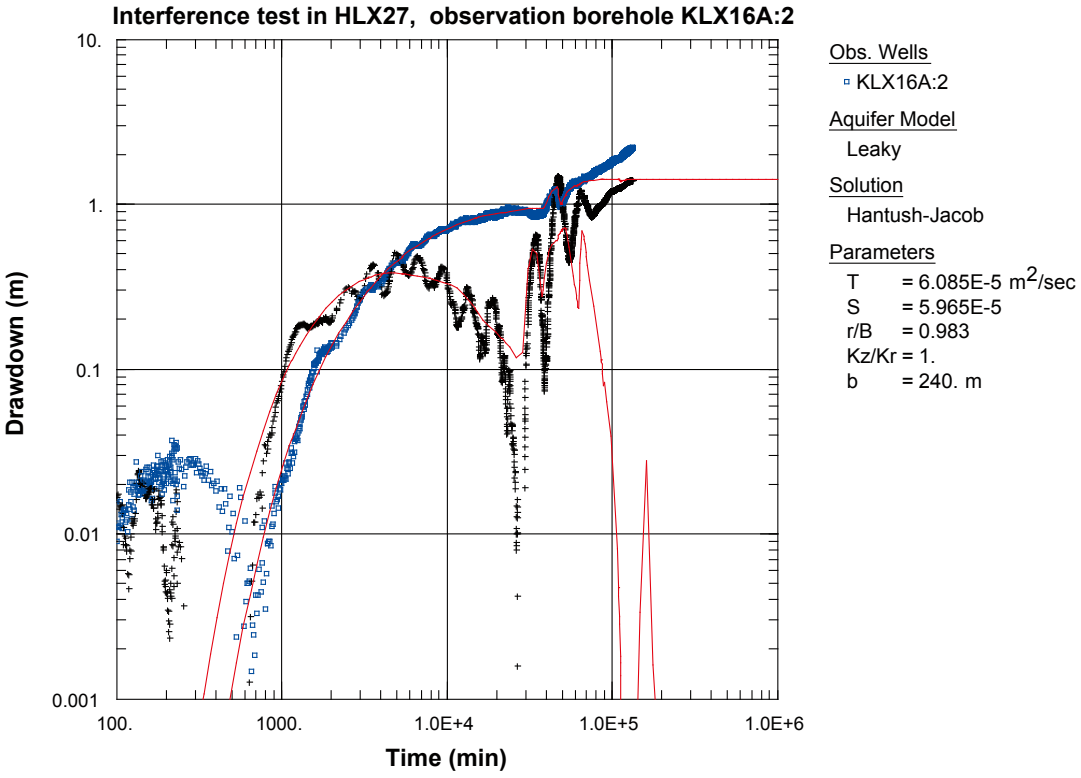

Figure A7-3a. *Transient analysis of the first part (up to 2.5E+4 min) of the flow period in KLX16A:2 during pumping in HLX27 using uncorrected head data for natural trend.*

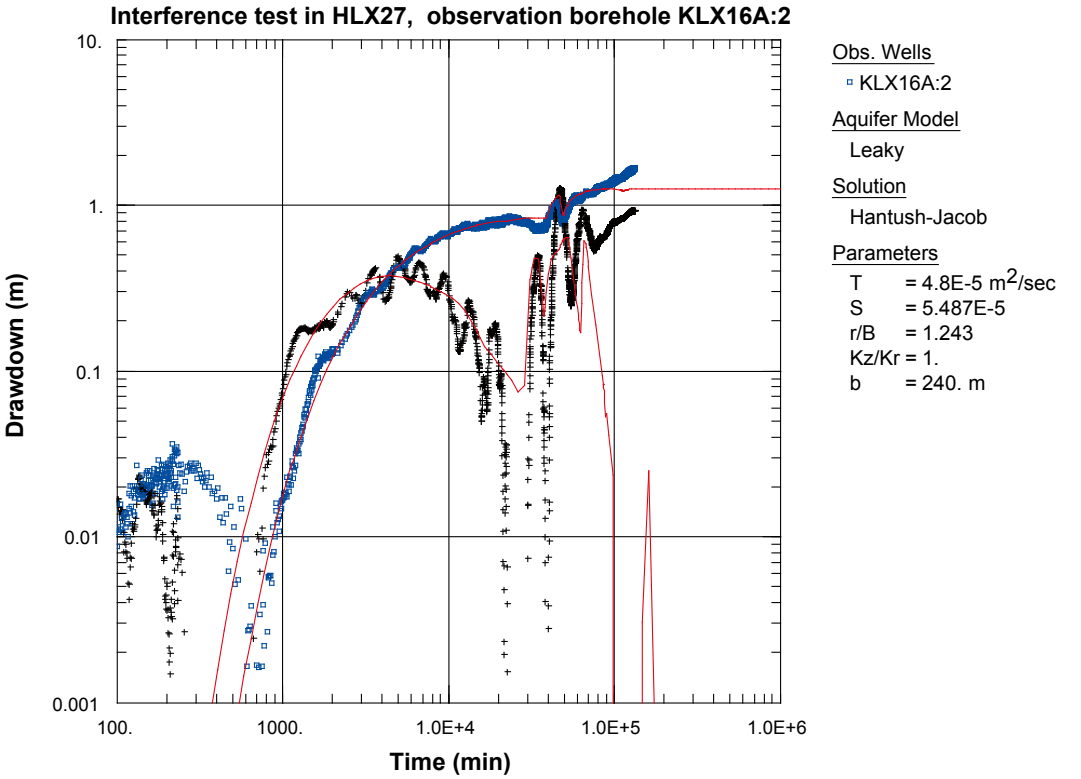

Figure A7-3b. *Transient analysis of the first part (up to 2.5E+4 min) of the flow period in KLX16A:2 during pumping in HLX27 using corrected head data for natural trend.*

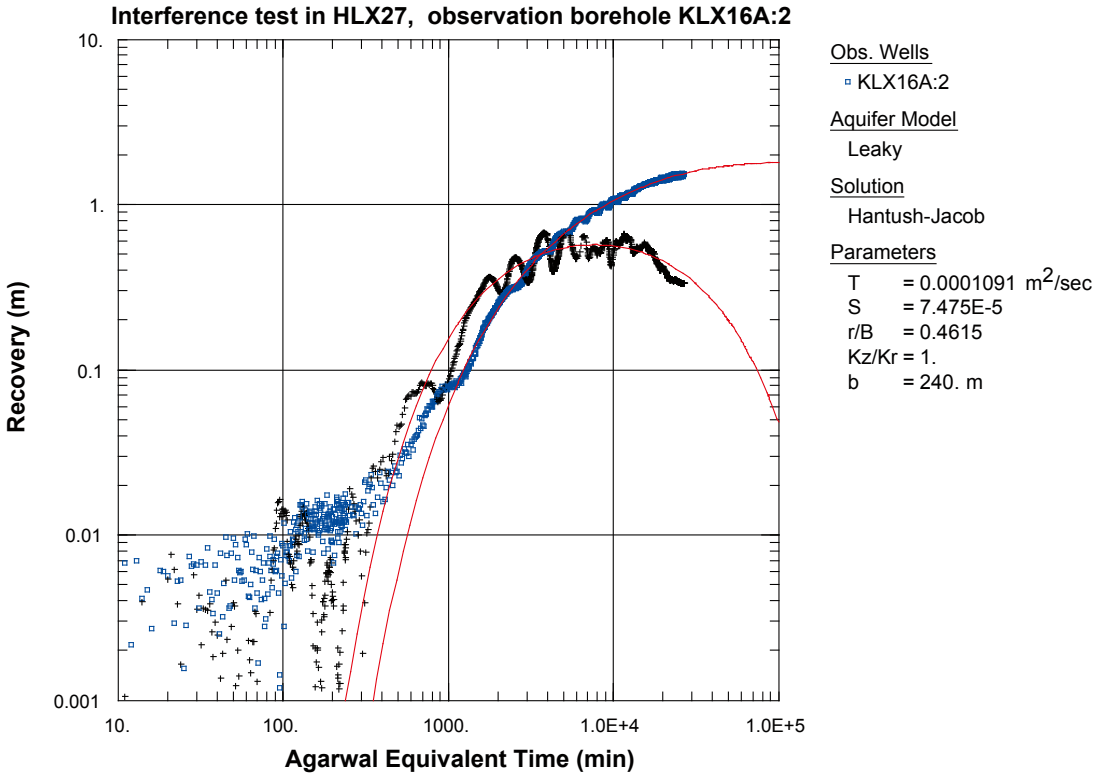

Figure A7-4a. *Transient analysis of the recovery period in KLX16A:2 during pumping in HLX27 using uncorrected head data for natural trend.*

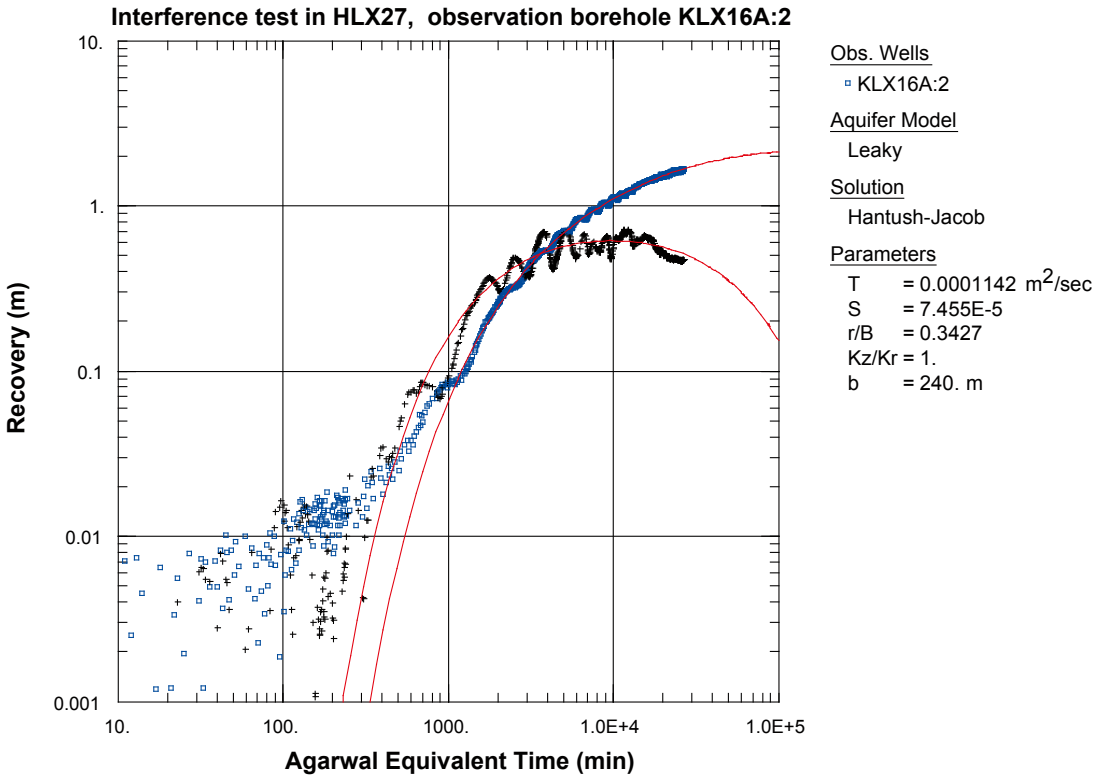

Figure A7-4b. *Transient analysis of the recovery period in KLX16A:2 during pumping in HLX27 using corrected head data for natural trend.*

Appendix 8

Chemical composition of groundwater from HLX27. Samples taken during the tracer test

Table A8-1. Chemical composition of the groundwater in the pumping borehole HLX27.

	HLX27	HLX27	HLX27	HLX27
SKB sample no.	**15484**	**15485**	**15486**	**15487**
Date	**2008-03-18**	**2008-03-27**	**2008-05-21**	**2008-06-26**
pH (pH unit)	7.85	7.87	7.87	7.86
Conductivity (mS/m)	489	485	441	444
Constituent	**(mg/l)**	**(mg/l)**	**(mg/l)**	**(mg/l)**
Na	657	651	600	605
K	8.46	8.52	7.22	7.51
Ca	254	258	229	230
Mg	42.1	41.9	34.7	34.8
HCO_3	147.3	149.1	166	168
Cl	1,497	1,487	1,311	1,410
SO_4_S	26.8	28.1	34.9	37
Br	5.90	6.18	3.0	5.72
F	2.15	2.15	2.60	2.45
Fe	0.112	0.122	0.131	0.133
Mn	0.488	0.448	0.370	0.361
Li	0.0656	0.0673	0.144	0.0905
Sr	4.50	4.52	3.99	3.93
Cs	0.000975	0.00101	0.000912	0.00102
Rb	0.0146	0.0156	0.0143	0.0127

Appendix 9

Injection functions and breakthrough curves

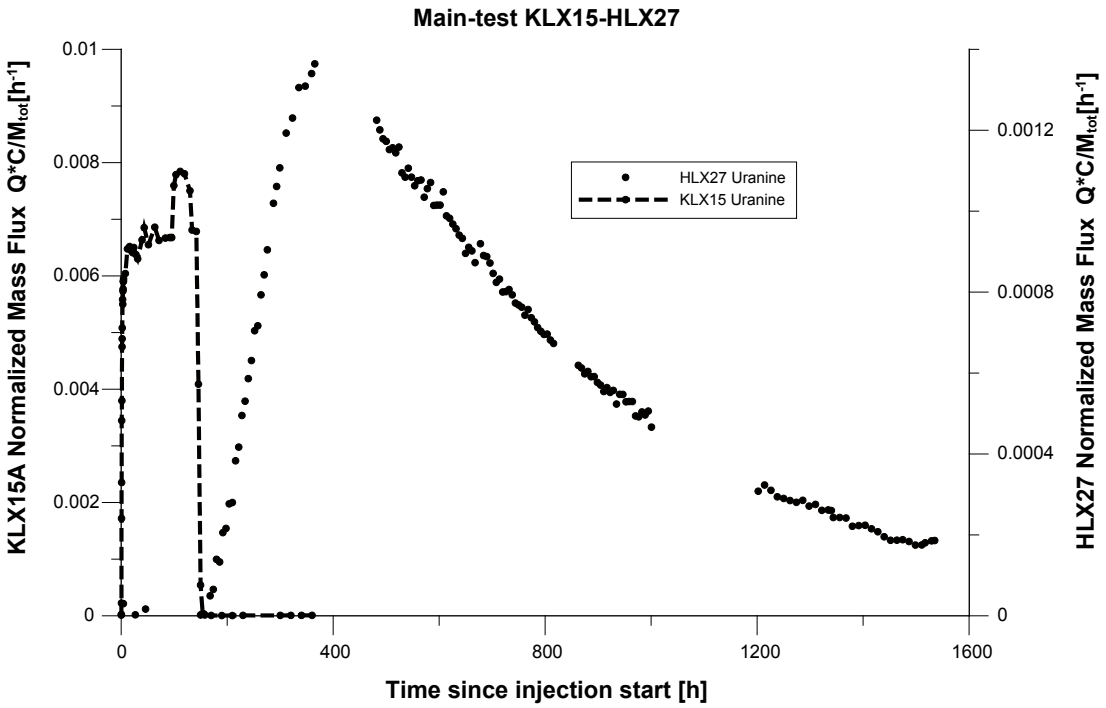

Figure A9-1. *Uranine in injection section in KLX15A and breakthrough curve in HLX27 from the main tracer test. Normalized mass flux against elapsed time.*

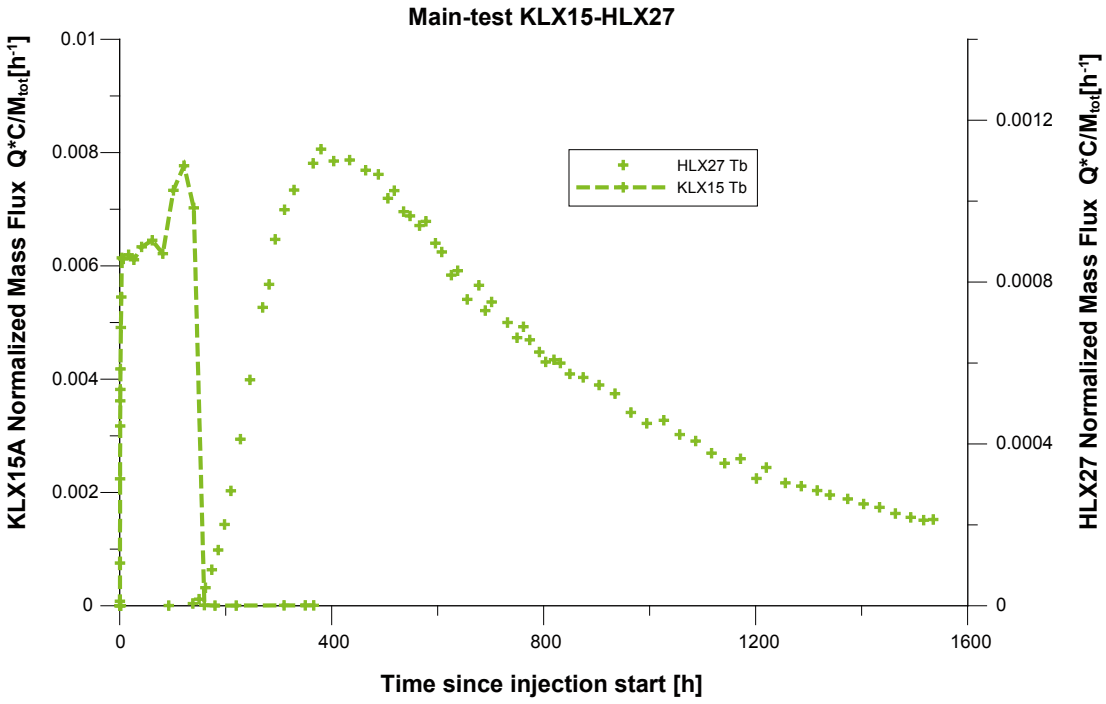

Figure A9-2. *Terbium in injection section in KLX15A and breakthrough curve in HLX27 from the main tracer test. Normalized mass flux against elapsed time.*

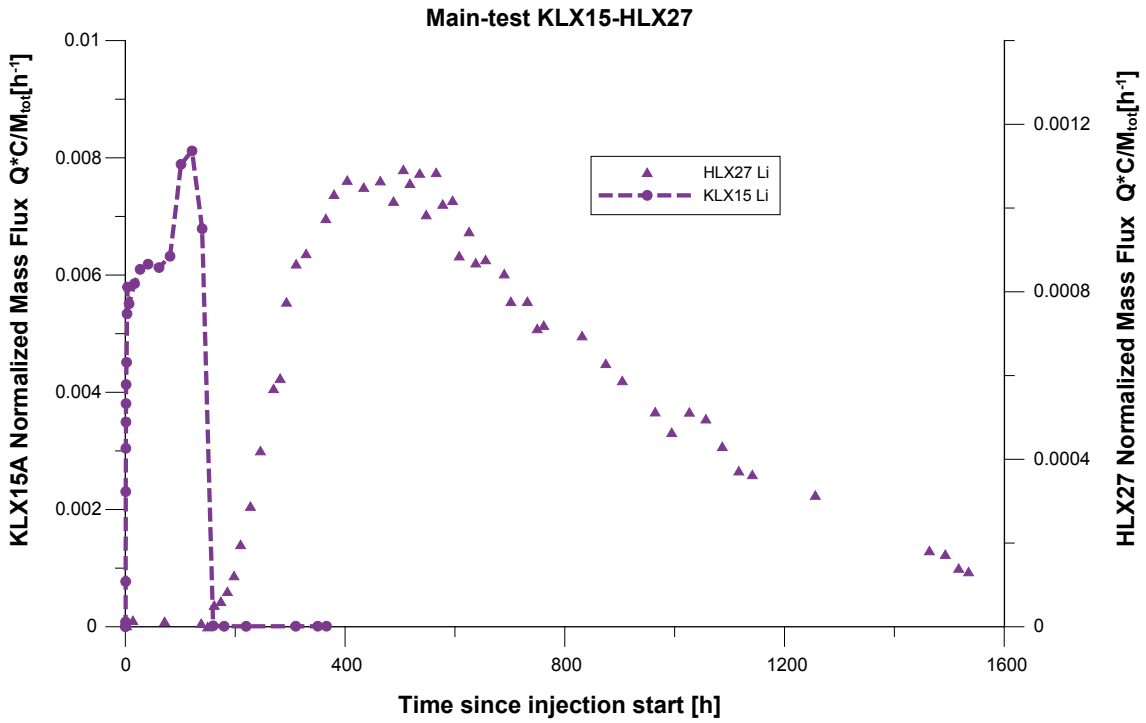

Figure A9-3. *Lithium in injection section in KLX15A and breakthrough curve in HLX27 from the main tracer test. Normalized mass flux against elapsed time.*

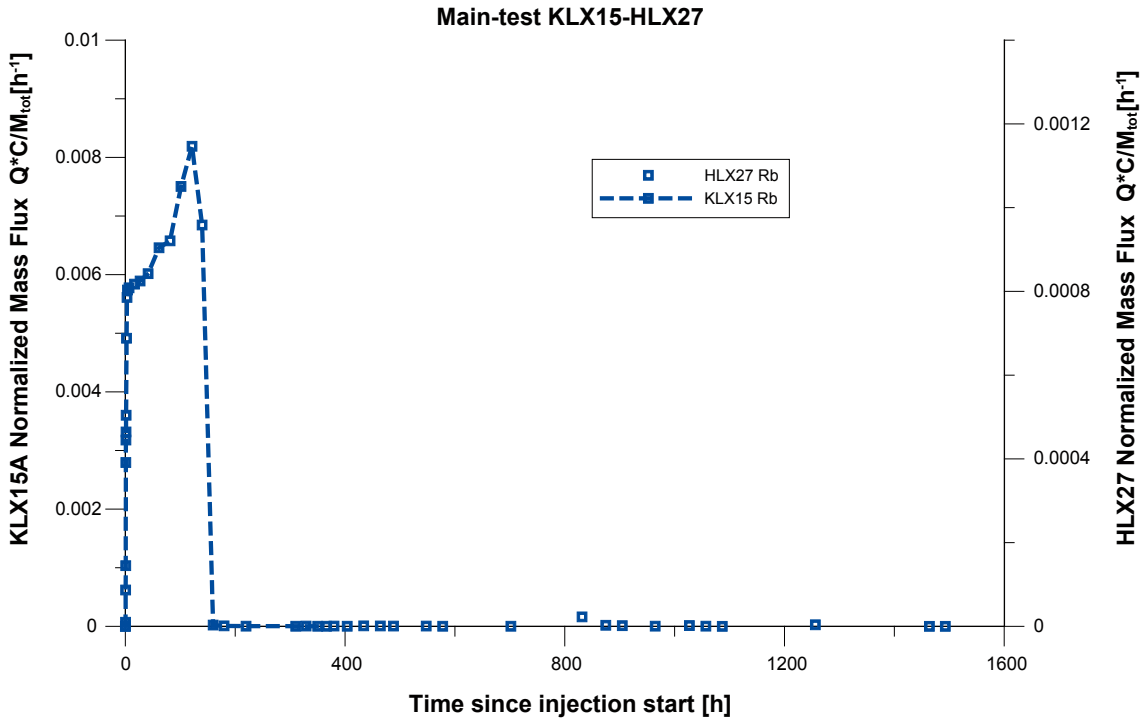

Figure A9-4. *Rubidium in injection section in KLX15A and breakthrough curve in HLX27 from the main tracer test. Normalized mass flux against elapsed time.*

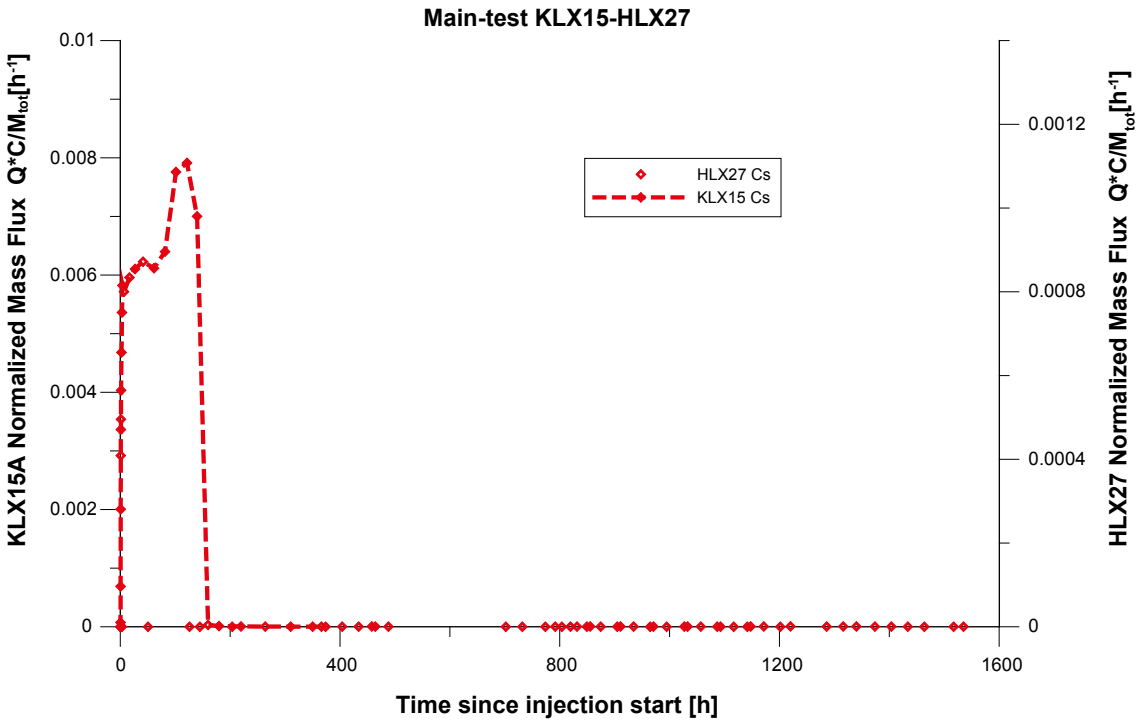

Figure A9-5. *Cesium in injection section in KLX15A and breakthrough curve in HLX27 from the main tracer test. Normalized mass flux against elapsed time.*